Progress in Landslide Research and Technology



Biljana Abolmasov
Irasema Alcántara-Ayala
Željko Arbanas
David Huntley
Kazuo Konagai
Matjaž Mikoš
Kyoji Sassa
Shinji Sassa
Binod Tiwari
Editors

Progress in Landslide Research and Technology, Volume 3 Issue 2, 2024

OPEN ACCESS

Springer

Progress in Landslide Research and Technology

Series Editors

Kyoji Sassa, International Consortium on Landslides, Kyoto, Japan
Kazuo Konagai, International Consortium on Landslides, Kyoto, Japan
Shinji Sassa, International Consortium on Landslides, Kyoto, Japan

The Open Access book series of the International Consortium on Landslides (ICL) aims to be the common platform for the publication of recent progress in landslide research and technology for practical applications and the benefit of society contributing to the Kyoto Landslide Commitment 2020, which is expected to continue up to 2030 and even beyond for the global promotion of understanding and reducing landslide disaster risk as well as the 2030 Agenda Sustainable Development Goals. The contributions include original and review articles, case studies, activity reports and teaching tools for the promotion of understanding and reducing landslide disaster risks.

Biljana Abolmasov • Irasema Alcántara-Ayala
Željko Arbanas • David Huntley
Kazuo Konagai • Matjaž Mikoš
Kyoji Sassa • Shinji Sassa • Binod Tiwari
Editors

Progress in Landslide Research and Technology, Volume 3 Issue 2, 2024

Springer

Editors
Biljana Abolmasov
Faculty of Mining and Geology
University of Belgrade
Belgrade, Serbia

Željko Arbanas
Faculty of Civil Engineering
University of Rijeka
Rijeka, Croatia

Kazuo Konagai
International Consortium on Landslides
Kyoto, Japan

Kyoji Sassa
International Consortium on Landslides
Kyoto, Japan

Binod Tiwari
Civil & Environmental Engineering
California State University, Fullerton
Fullerton, CA, USA

Irasema Alcántara-Ayala
Institute of Geography
Natl Autonomous University of Mexico
Ciudad De Mexico, Estado de México, Mexico

David Huntley
Geological Survey of Canada
Vancouver, BC, Canada

Matjaž Mikoš
Faculty of Civil & Geodetic Engineering
University of Ljubljana
Ljubljana, Slovenia

Shinji Sassa
National Institute of Maritime, Port and Aviation Technology
Port and Airport Research Institute
Yokosuka, Japan



ISSN 2731-3794 ISSN 2731-3808 (electronic)
Progress in Landslide Research and Technology
ISBN 978-3-031-72735-1 ISBN 978-3-031-72736-8 (eBook)
https://doi.org/10.1007/978-3-031-72736-8

© International Consortium on Landslides 2025. This book is an open access publication.

Open Access This book is licensed under the terms of the Creative Commons Attribution 4.0 International License (http://creativecommons.org/licenses/by/4.0/), which permits use, sharing, adaptation, distribution and reproduction in any medium or format, as long as you give appropriate credit to the original author(s) and the source, provide a link to the Creative Commons license and indicate if changes were made.
The images or other third party material in this book are included in the book's Creative Commons license, unless indicated otherwise in a credit line to the material. If material is not included in the book's Creative Commons license and your intended use is not permitted by statutory regulation or exceeds the permitted use, you will need to obtain permission directly from the copyright holder.
The use of general descriptive names, registered names, trademarks, service marks, etc. in this publication does not imply, even in the absence of a specific statement, that such names are exempt from the relevant protective laws and regulations and therefore free for general use.
The publisher, the authors and the editors are safe to assume that the advice and information in this book are believed to be true and accurate at the date of publication. Neither the publisher nor the authors or the editors give a warranty, expressed or implied, with respect to the material contained herein or for any errors or omissions that may have been made. The publisher remains neutral with regard to jurisdictional claims in published maps and institutional affiliations.

Cover illustration: Brienz/Brinzauls rockslide occurred on June 15, 2023 in the Canton of Grisons, Switzerland. The total volume of this rockslide is estimated to be 1.2 million m3. (Photograph taken by Andrea Mancon)

This Springer imprint is published by the registered company Springer Nature Switzerland AG
The registered company address is: Gewerbestrasse 11, 6330 Cham, Switzerland

If disposing of this product, please recycle the paper.

Foreword by Celeste Saulo

As Secretary-General of the World Meteorological Organization (WMO), it is my great pleasure to introduce Volume 3, Issue 2 of the Progress in Landslide Research and Technology. This issue marks a significant milestone as we gather insights and research at the intersection of hydrology, meteorology, and landslide science.

Landslides, triggered by various factors including heavy rainfall, glacial lake outbursts, floods, earthquakes, and volcanic activity, pose a substantial threat to communities worldwide. The impact of these events is profound, leading to loss of life, property damage, and the destruction of critical infrastructure. This year itself, approximately 240 fatal landslides were reported, including in India, Indonesia, Papua New Guinea, and Viet Nam.

Disaster risk reduction has been a cornerstone of WMO's mission for over 150 years. As the specialized UN agency focused on weather, climate, and water, WMO plays a pivotal role in strengthening early warning services globally, regionally, and at national level. The flagship Early Warnings for All initiative aims to ensure that everyone on the planet is protected by people centered, actionable multi-hazard early warning systems.

WMO is leveraging its expertise in rainfall monitoring and forecasting, recognizing that heavy rainfall is a significant trigger for landslides. By continuously monitoring and analyzing meteorological data such as precipitation patterns and intensity, we can identify regions at increased risk of landslides. This critical data is shared among nations to support multi-hazard early warning systems and initiatives such as the Flash Flood Guidance System.

Hydrological data, including river flow measurements and soil moisture content, is equally vital for landslide risk assessment. By monitoring soil saturation levels and water flow in rivers and streams, experts can predict when conditions are ripe for landslides. However, there is currently no operational global system capable of assessing and predicting the status of surface and groundwater hydrological systems comprehensively. To address this, WMO has established the Global Cryosphere Watch and the Global Hydrological Status and Outlook System, which work toward closing this gap in our knowledge.

Integration of data is a key aspect of effective landslide risk management. WMO promotes the development of multi-hazard early warning systems that combine meteorological and hydrological data with geospatial information, topography, and geological data. These comprehensive risk assessment tools provide timely alerts to authorities and communities, enabling them to take preventive measures.

Climate change further complicates this landscape, influencing rainfall patterns and hydrological conditions. As climate change intensifies extreme weather events, including heavy rainfall, it is imperative to continuously monitor and assess these changes.

WMO contributes to this effort through the annual State of the Global Climate report and regional climate reports, which help to understand and mitigate these evolving risks. WMO also publishes The State of Global Water Resources report series, which offers a comprehensive and consistent overview of water resources worldwide, highlighting the influence of climatic, environmental, and societal changes on the hydrological variables. Such technical reports help researchers and practitioners place local and regional landslide risks within a broader context, understanding how global changes might influence local hazards.

WMO remains steadfast in its commitment to the Kyoto Landslide Commitment 2020 and is eager to advance progress through the Early Warning for All initiative.

Thank you very much.



Celeste Saulo
Secretary General, World Meteorological Organization
Genève, Switzerland

Editorial Board of the Book Series

Editor-in-Chief
Kyoji Sassa, International Consortium on Landslides, Japan

Assistant Editors-in-Chief
Kazuo Konagai, International Consortium on Landslides, Japan
Binod Tiwari, California State University, Fullerton, USA
Željko Arbanas, University of Rijeka, Croatia

Editors
Biljana Abolmasov, University of Belgrade, Republic of Serbia
Beena Ajmera, Iowa State University, USA
Irasema Alcántara-Ayala, National Autonomous University of Mexico, Mexico
Netra Prakash Bhandary, Ehime University, Japan
Sabatino Cuomo, University of Salerno, Italy
Yasser Elshayeb, Cairo University, Egypt
Xuanmei Fan, Chengdu University of Technology, China
Faisal Fathani, University of Gadjah Mada, Indonesia
Louis Ge, National Taiwan University, Chinese Taipei
Ivan Gratchev, Griffith University, Australia
David Huntley, Geological Survey of Canada, Canada
Claudio Margottini, IAEG Italian National Group, Italy
Snježana Mihalić-Arbanas, University of Zagreb, Croatia
Matjaž Mikoš, University of Ljubljana, Slovenia
Maneesha Ramesh, Amrita University, India
Paola Reichenbach, Research Institute for Geo-Hydrological Protection, CNR, Italy
Shinji Sassa, Port and Airport Research Institute, Japan
Wei Shan, Northeast Forestry University, China
Josef Stemberk, Institute of Rock Structure and Mechanics, CAS, Czech Republic
Alexander Strom, Geodynamic Research Center, Russia
Huiming Tang, China University of Geosciences, Wuhan, China
David Tappin, British Geological Survey, UK
Veronica Tofani, University of Florence, Italy
Vít Vilímek, Charles University, Czech Republic
Fawu Wang, Tongji University, China

KLC2020 Managing Committee
Kyoji Sassa (Chairman), Secretary General, Secretariat of the Kyoto Landslide Commitment 2020
Kaoru Takara, Managing Director, Secretariat of the Kyoto Landslide Commitment 2020
Matjaž Mikoš, Chair of the Global Promotion Committee of the International Programme on Landslides and Kyoto Landslide Commitment 2020

Qunli Han, Co-chair of the Global Promotion Committee of the International Programme on Landslides and Kyoto Landslide Commitment 2020
Nicola Casagli, Immediate Past President of the International Consortium on Landslides
Peter Bobrowsky, Past President of the International Consortium on Landslides

Advisory Members for KLC2020
Abou Amani, Director, Division of Water Sciences, Secretary, Intergovernmental Hydrological Programme (IHP), UNESCO
Soichiro Yasukawa, Chief of Disaster Risk Reduction Unit, UNESCO
Sonia Talwar, Director General, Geological Survey of Canada, Natural Resources Canada, Canada
Hassina Mouri, President of the International Union of Geological Sciences (IUGS)
John LaBrecque, Chair of IUGG GeoRisk Commission, Center for Space Research, University of Texas at Austin, USA
Vassilis Marinos, President of the International Association for the Engineering Geology and the Environment (IAEG)
Paolo Canuti, past president of the International Consortium on Landslides (ICL), Italy
Sảlvano Briceño, First chair of the Global Promotion Committee of the International Programme on Landslides
Badaoui Rouhban, IPL Advisor and Moderator of ISDR-ICL Sendai Landslide Partnerships 2015–2025 Session of third WCDRR in 2015

KLC2020 Official Promoters
Host Organization
International Consortium on Landslides (ICL)/Željko Arbanas

Public Sectors: KLC2020 Official Promoters-Public
International Unions/Associations, Governmental Organizations, Universities and Research Institutes
- The International Union of Geological Sciences (IUGS)/Hassina Mouri
- The International Union of Geodesy and Geophysics (IUGG)/Chris Rizos
- The International Association for the Engineering Geology and the Environment/Vassilis Marinos
- International Geosynthetics Society (IGS)/John Kraus
- Geological Survey of Canada, Natural Resources Canada, Canada/Sonia Talwar
- Faculty of Civil and Geodetic Engineering, University of Ljubljana, Slovenia/Matjaž Mikoš
- China University of Geosciences, Wuhan, China/Huiming Tang
- The State Key Laboratory of Geohazard Prevention and Geoenvironment Protection, Chengdu University of Technology, Sichuan, China/Qiang Xu
- Department of Civil Engineering, National Taiwan University, Chinese Taipei/Louis Ge
- Institute of Rock Structure and Mechanics, the Czech Academy of Sciences/Josef Stemberk
- Institute of Cold Regions Science and Engineering, Northeast Forestry University, China/Wei Shan

Private Sectors: KLC2020 Official Promoters-Private
Companies and Corporation
- Marui & Co. Ltd, Japan
- Nippon Koei Co., Ltd, Japan
- Ellegi srl, Italy
- Chuo Kaihatsu Corporation, Japan
- Godai Kaihatsu Corporation, Japan

- Kiso-Jiban Consultants Co., Ltd, Japan
- Kokusai Kogyo Co., Ltd., Japan
- OSASI Technos, Inc., Japan

Standing Editors for KLC2020 Book Series
Kyoji Sassa, International Consortium on Landslides, Kyoto, Japan
Kazuo Konagai, International Consortium on Landslides, Kyoto, Japan
Binod Tiwari, California State University, Fullerton, USA
Željko Arbanas, University of Rijeka, Croatia
Paola Reichenbach, Research Institute for Geo-Hydrological Protection, CNR, Italy
Shinji Sassa, Port and Airport Research Institute, Yokosuka, Japan
Fawu Wang, Tongji University, Shanghai, China
Khang Dang, VNU University of Science, Vietnam National University, Vietnam
Beena Ajmera, Iowa State University, USA

Editorial Office
Secretariat of the Kyoto Landslide Commitment 2020
International Consortium on Landslides (ICL)
138-1 Tanaka-Asukai cho, Sakyo-ku, Kyoto 606-8226, Japan E-mail: klc2020@landslides.org

Global Promotion Committee of the International Programme on Landslides and Kyoto Landslide Commitment 2020

A Commitment to the Sendai Framework and the Sustainable Development Goals

Chair
Matjaž Mikoš (Faculty of Civil and Geodetic Engineering, University of Ljubljana)

Co-chairs
Qunli Han (Integrated Research on Disaster Risk, IRDR)
Soichiro Yasukawa (Programme Specialist on Disaster Risk Reduction, UNESCO, Paris)
Hiroshi Kitazato (International Union of Geological Sciences, IUGS)
John LaBrecque (Chair of IUGG GeoRisk Commission)

Secretary
Kyoji Sassa (IPL World Centre, Director)

Members of the IPL-KLC Global Promotion Committee

ICL Full Members
Geotechnical Engineering Office, Hong Kong, China; The State Key Laboratory of Geohazard Prevention and Geoenvironment Protection (SKLGP), Chengdu University of Technology, China, UNESCO Chair for the Prevention and the Sustainable Management of Geo-hydrological Hazards—University of Florence, Italy; Faculty of Civil and Geodetic Engineering, University of Ljubljana (ULFGG), Slovenia; and other members (total 59 members from 27 countries/regions).

ICL Supporting Organizations
UNESCO, UNDRR, WMO, FAO, UNU, ISC, WFEO, IUGS, IUGG

KLC2020 Official Promoters Host Organization
Host Organization
International Consortium on Landslides (ICL)/Željko Arbanas

Public Sectors: KLC2020 Official Promoters—Public

- The International Union of Geological Sciences (IUGS)/Hassina Mouri
- The International Union of Geodesy and Geophysics (IUGG)/Chris Rizos
- The International Association for the Engineering Geology and the Environment (IAEG)/Vassilis Marinos
- International Geosynthetics Society (IGS)/John Kraus
- Geological Survey of Canada, Natural Resources Canada, Canada/Sonia Talwar
- Faculty of Civil and Geodetic Engineering, University of Ljubljana, Slovenia/Matjaž Mikoš

- China University of Geosciences, Wuhan, China/Huiming Tang
- The State Key Laboratory of Geohazard Prevention and Geoenvironment Protection (SKLGP), Chengdu University of Technology, China/Qiang Xu
- Department of Civil Engineering, National Taiwan University, Chinese Taipei/Louis Ge
- Institute of Rock Structure and Mechanics, the Czech Academy of Sciences/Josef Stemberk
- Institute of Cold Regions Science and Engineering, Northeast Forestry University, China/Wei Shan

Private Sectors: KLC2020 Official Promoters—Private

- Marui & Co. Ltd, Japan
- Nippon Koei Co., Ltd, Japan
- Ellegi srl, Italy
- Chuo Kaihatsu Corporation, Japan
- Godai Kaihatsu Corporation, Japan
- Kiso-Jiban Consultants Co., Ltd, Japan
- Kokusai Kogyo Co., Ltd., Japan
- OSASI Technos, Inc., Japan

IPL World Centre

IPL World Centre (IWC) was established in 2006 by the Tokyo Action Plan to serve, as it does, as the secretariat of IPL,GPC/IPL as well as of UNITWIN UNESCO-KU-ICL Programme. IWC also serves as the secretariat of KLC2020. IWC is a part of the legal body (NPO-ICL registered in Kyoto, Japan) of ICL. The Council of the IWC consists of advisors from Ministry of Education, Sports, Science and Technology, Ministry of Agriculture, Forestry and Fisheries, Ministry of Land, Infrastructure and Tourism of the Government of Japan, UNESCO, and of members from ICL Headquarters, chairs of GPC/IPL-KLC, presidents and officers of ICL.

Secretariat of GPC/IPL-KLC

Secretary

Kyoji Sassa
International Consortium on Landslides
138-1 Tanaka-Asukai cho, Sakyo-ku, Kyoto 606-8226, Japan
Tel: +81 (75) 723 0640
Fax: +81 (75) 950 0910
E-mail: secretariat@landslides.org
URL: https://www.landslides.org/; https://www.landslides.org/ipl-info/

Greetings by Tshilidzi Marwala for Opening Session of the Sixth World Landslide Forum

Good day, ladies and gentlemen. It is my great pleasure to address you all at the opening of the Sixth World Landslide Forum in Florence, Italy in 2023 as a Rector of the United Nations University, as well as Under-Secretary-General of the United Nations. Prior to taking up the role of United Nations University Rector on 1 March, 2023, I served as Vice-Chancellor and Principal of the University of Johannesburg in South Africa.

In April, 2022, South Africa experienced a fluidized landslide disaster in Durban, about 550 km away from Johannesburg. Death, devastation, and destruction are some of the descriptors for the apocalyptic scenes at the time. The unprecedented flood damaged infrastructure and roads, washed away a temple, sunk vehicles, uprooted homes, trapped citizens, and even claimed hundreds of lives.

The moment was described as the most catastrophic natural disaster to have hit that area. Images of people stranded on their roofs awaiting rescue were a grim reminder of the impact of climate change. The late former UN Secretary-General, Kofi Annan, remarked in 2014, "On climate change, we often don't fully appreciate that it is a problem. We think it is a problem waiting to happen." Almost a decade later, we are seeing this problem tangibly and viscerally unfold in front of us, and we have to confront it, or we face a reality far worse than the events in Durban that week. The sheer pace of climate change, coupled with urban development, has increased the risk of landslides and floods, not only in Africa, but throughout many other parts of the world.

In 2021, environmental Professor, Nicholas King, warned that extreme weather events will continuously damage public infrastructures, such as roads, water and sanitation, health education, and electricity services. This is the reality we contend with without taking any action on sustainable development goal 13. Here, the United Nations University certainly has a role to play.

The UNU is a solutions-focused think tank and a research arm of the UN System with an emphasis on providing reliable evidence to support policy development and debates on the world's most urgent challenges. UN University seeks to influence policymaking at national, regional, and international levels, raise awareness about pressing global issues, and contribute to rethinking of existing policies; and assist the Global South in enhancing institutional and individual capacities for research, among other goals. The International Consortium on Landslides (ICL), in particular, was founded in Kyoto in 2002 to promote landslide research for the benefit of society and the environment, and capacity building, including education, notably in developing countries.

This aim is a mandate of the UN University and the consortium has been strongly supported by the University since its inception. UN University has made great strides in this area. For example, in 2006, the UN University hosted a roundtable discussion about 2006 Tokyo Action Plan, which created the triennial World Landslide Forum and the Global Promotion Committee of the International Programme on Landslides, GPC/IPL.

In 2008, the First World Landslide Forum was organized at UNU Headquarters. The ICL and GPC/IPL also established the Sendai Landslide Partnerships 2015–2025 and the Kyoto Landslide Commitment 2020. This is the weight with which we approach this year's forum.

In a matter of moments, the KLC2020 General Conference 2023 and High-Level Panel Discussion entitled KLC2020 Review and way forward will commence. Here, new partners will sign the KLC2020 and the Florence Declaration on Landslide Risk Reduction will be adopted. This is a pivotal moment indeed in the fight against climate change.

As we will undoubtedly be reminded over the course of this forum, landslides and resulting major catastrophes can be managed constructively in ways that safeguard not only human lives, but also whole economies through interventions such as better infrastructure, the careful zoning of housing, and many other measures. This is certainly the sustainable future we have in mind. I look forward to seeing a more climate action forward future emerge in these corridors and beyond.

Thank you very much for your attention.

Arigato gozaimashita.



Tshilidzi Marwala
Under-Secretary-General of the United Nations
Rector of United Nations University
Tokyo, Japan
Video link: https://wlf6.org/opening-plenary-session-video-messages/

Message by QU Dongyu for Opening Session of the Sixth World Landslide Forum

I am pleased to address the Sixth World Landslide Forum. FAO has been associated with the International Consortium on Landslides since its creation and we are pleased to see that the landslide prevention community continues to grow, especially in view of the increasing frequency, severity, and impact of landslides due to the impacts of the climate crisis, ecosystem degradation, and biodiversity loss—and often hitting the poorest and most vulnerable the hardest.

With the focus of this Forum on landslide science for sustainable development, I would like to share a few thoughts with you.

First: As many marginalized people are forced to settle in hazard-prone areas exposing them to landslides, operational programs need to be based on assessments of landslide impacts, disaggregated by social groups.

Second: As landslides are often linked to other hazards and disasters, they should not be considered in isolation, but as part of multi-hazard approaches.

Third: As many human activities, such as inappropriate road construction and the misuse of land resources can trigger landslides, landslide risk management should be an integral part of the overall land-use planning.

And Fourth: As many rural and indigenous communities hold vast experience on the management of their lands, including a deep understanding of hazards such as landslides, this knowledge should be integrated in disaster risk management policies.

FAO supports the International Consortium on Landslides by promoting landslide discussions in the context of livelihoods and food security and by integrating landslide concerns into land management approaches. Hazards in mountains and upland areas are a particular focus for FAO.

FAO hosts the Secretariat of the Mountain Partnership—an international alliance committed to improving the lives of mountain people and protecting mountain environments. The Mountain Partnership is an important platform to share and exchange with a broad range of the partners. FAO is committed to minimizing the danger of landslides, including by transforming agrifood systems to be more efficient, more inclusive, more resilient, and more sustainable.

We must strengthen our efforts in landslide risk assessment, prevention, mitigation, preparedness, and rehabilitation.

Our partnership with the International Consortium on Landslides is a vital part of these efforts.

I wish you a successful Forum. Thank you.



Qu Dongyu
Director-General of the Food and Agriculture Organization (FAO)
Rome, Italy
Video link: https://wlf6.org/opening-plenary-session-video-messages/

Greetings by Mustafa B. Shehu for Opening Session of the Sixth World Landslide Forum

The President International Consortium of Landslides, Professor Nicola Casagli, members of the consortium, members of the organizing team of this forum; signatories to the Kyoto Landslide Commitment 2020, distinguished scholars, ladies and gentlemen, it's indeed a great honor and privilege for me on behalf of the World Federation of Engineering Organizations to address you this morning at the opening session of the Sixth World Landslide Forum with the theme, Landslide Science for Sustainable Development. My preference, of course, was to be here with you in the beautiful city of Florence, in Italy, to attend the conference physically, but other existences of duty did not allow me. However, the chairman of the WFEO Committee on Disaster Risk Management and Mitigation, Professor José Macharé, will be there with you to participate at the proceedings.

The theme Landslide Science for Sustainable Development is carefully selected to serve as a commitment to the Sendai Landslide Partnership 2015–2030, the Sendai Framework for disaster risk reduction, 2015–2030, the United Nations Agenda 2030 for sustainable development, the new Urban Agenda and the Paris Agreement. As one of the signatories to the Kyoto Landslide Commitment 2020, WFEO wish to inform this distinguished gathering of its total commitment to the works and resolutions that will be generated at the end of this conference. We're fully aware of the devastating consequences of landslides on humans, hydrosphere environment, biosphere, as well as economy of any so affected by landslide.

The global community is looking at us expecting solutions to these problems being aligned, congregation of professionals. We have to, or we must live to the, to these expectations, to the expectations of the global community. WFEO on its part will leverage on the skills and competencies of its professionals to spread across the globe, to deliver on its mandate in this regard.

While looking forward to the community or declaration that will be generated at the end of this conference for immediate action from our side, I wish you all a very successful conference and a very happy stay in Florence, Italy.

Thank you very much for listening.



Mustafa B. Shehu
President of the World Federation
of Engineering Organizations WFEO
Paris, France

Video link: https://wlf6.org/opening-plenary-session-video-messages/

Greetings by Chris Rizos for Opening Session of the Sixth World Landslide Forum

Good morning ladies and gentlemen, in particular the distinguished guests, colleagues, members of the organizing committee, and attendees of this World Landslide Forum. My name is Chris Rizos and I'm President of the International Union of Geodesy and Geophysics, IUGG, and it is my honor to have been given the opportunity to say a few words of greeting at the opening ceremony of the Sixth World Landslide Forum here in the beautiful city of Florence. Landslides are one of a number of natural disaster phenomena that society must contend with.

Although heavily local, landslides, when they do occur, can be utterly devastating. The conference technical program comprises a very full 3 days, each with seven parallel sessions or presentations covering a diverse range of topics. Too many for me here to highlight.

Nevertheless, the IUGG, covering many of the geoscience disciplines, and by virtue of the existing commissions, working groups, services, and other entities within its constituent associations, is very interested in landslides as an expression of dynamic earth processes. For example, IUGG associations deal with earth observation, hydrology, geodesy, glaciology, volcanology, seismology, climate, and weather. This World Landslide Forum has as its tagline, Landslide Science for Sustainable Development.

We recognize that society's current development path, particularly of increased urbanization, can often increase the risks of geohazards such as landslides. Risk reduction, including forecasting and early warning, must therefore be one of the highest priorities of scientists, engineers, and public officials engaged in landslide science, engineering, and policy development, as well as implementation, of course. The Florence Declaration on Landslide Risk Reduction is therefore a timely and important reminder of landslide geohazards.

I'm sure that all participants will derive considerable benefit from the presentations on the latest developments in landslide science and engineering made at this World Landslide Forum.

Thank you for your attention, and good morning to you all, and may you have a very enjoyable conference.



Chris Rizos
President of the International Union of Geodesy and Geophysics IUGG
Potsdam, Germany
Video link: https://wlf6.org/opening-plenary-session-video-messages/

Contents

Emergency Response to the 2024 Noto Peninsula Earthquake 1
Takeo Murakami

Part I Original Articles

Understanding Landslide Awareness: Exploring Students' Disaster Risk Perception in Higher Education Institutions 11
Karla M. Hernández-Cadena, Ricardo J. Garnica-Peña, Jorge González-Sánchez, and Irasema Alcántara-Ayala

Analytical Hierarchical Process (AHP) Prioritization of Landslide-Causing Factors 23
A. A. Virajh Dias and A. A. Jagath Gunathilake

The Changing Seismic Site Response of the Brienz/Brinzauls Rock Slope Instability: Insights from 5 Years of Monitoring Before, During and After a Partial Collapse in June 2023 47
Mauro Häusler, Franziska Glueer, and Donat Fäh

Lessons from the Great Gramalote: Colombia Landslide (2010) and its Relocation Process 61
Guillermo Ávila and María Paula Ávila-Guzmán

Challenges of Earthquake and Micro-Earthquake Monitoring in Sri Lanka 73
Koji Matsunami, Kyoji Sassa, Ranjan Weerasinghe, Tania Munasinghe, and Loi Doan

Experiments of Modelling Subaqueous Landslide Susceptibility in Lake Albano of Castel Gandolfo 93
Antonio Patera and Andrea G. Fabbri

An Approach to Rockfall Hazard Scenarios Based on Earthquake Ground Motion 107
Antonella Peresan, Massimiliano Alvioli, Elisa Zuccolo, Franco Vaccari, and Hazem Badreldin

Landslides of Moscow River Valley (Russia): Types and Features of their Origin in Different Geological Conditions 119
Pavel V. Novikov, Oleg V. Zerkal, Olga S. Barykina, and Eugene N. Samarin

High-Resolution Rainfall Simulations for Early Warning of Rain-Induced Rapid Long-Traveling Landslides in Sri Lanka 129
Ryo Onishi, H. A. A. I. S. Bandara, and Koki Matsumoto

Application of Subsurface Drainage for Cost-Effective Mitigation Strategies: A Case Study of Hakgala Landslide, Sri Lanka 135
S. H. S. Jayakody, Buddhika Kumarage, and Asiri Karunawardena

Assessing and Contextualizing Site-Specific Landslide Risk in the Philippines 149
Cathleen Joyce Cordero, Kenneth Gesmundo, and Arturo Daag

The Accuracy of Landslide Susceptibility Mapping in Young Glacial River Valleys 163
Anna Małka, Izabela Laskowicz, and Dariusz Grabowski

Experimental Research on Rain-Induced Landslide Mechanism Using Large-Scale Rainfall Experimental Facility: Findings and Challenges 173
Naoki Sakai, Tomohiro Ishizawa, and Toru Danjo

Part II Review Articles

Landslide Dam Studies in Uttarakhand, India: Past, Present and Future 199
Shivani Joshi and Srikrishnan Siva Subramanian

Risk Identification of Large-Scale Landslides Triggered by Rainfalls and Post-Rainfall Earthquakes in Sri Lanka 207
Kyoji Sassa, Loi Doan, Koji Matsunami, Toyohiko Miyagi, Ranjan Weerasnghe, Tania Munasinghe, Nilmini Thaldena, Asiri Karunawardena, and Kazuo Konagai

Part III IPL Projects, World Centres of Excellence on Landslide Risk Reduction, and Kyoto Landslide Commitment 2020

The 6th World Landslide Forum (WLF6), Florence, 2023 239
Veronica Tofani, Kyoji Sassa, Paolo Canuti, Anna Elisa Bandecchi, Elisa Gargini, and Nicola Casagli

How to Detect the Previous Large-Scale Landslide: Source of Future Landslides by Interpretation of Ground Topography from Digital Maps 261
Toyohiko Miyagi and Doan Huy Loi

LS-RAPID Estimation of the Critical Pore Pressure Able to Initiate (Activate) Landslides Within the Existing Large-Scale Landslides 273
Doan Huy Loi, Pham Van Tien, Khang Dang, and Kyoji Sassa

Part IV ICL Landslide Teaching Tools

MaPLoRds: Mobile Application for Local Road Network Risk Assessment 299
Biljana Abolmasov, Ranka Stanković, Nikola Vulović, Miloš Marjanović, Uroš Đurić, and Nikola Gudžić

Simple Method of Risk Assessment for Landslides: A Case Study of the JICA Project in Honduras 309
Kiyoharu Hirota, Kosuke Uzawa, and Takeshi Kuwano

Part V Technical Notes and Case Studies

Assessing Landslide Disaster Risk Reduction and Resilience: Case Studies and Insights, India 323
Surya Parkash, Ravinder Singh, and Shubham Badola

A Web-GIS for the Analysis of Scientific Literature on Earthquake-Triggered Landslides 341
Federica Fiorucci, Luca Schilirò, Mauro Rossi, Federica Polpetta, Carolina Fortunato, and Paola Reichenbach

Time and Site Prediction of a Potential Large-Scale Landslides and the AR (Augmented Reality) Presentation for Early Warning 347
Koichi Araki, Keisuke Takimoto, Yoichi Yamazaki, Doan Huy Loi, Kazuo Konagai, and Kyoji Sassa

Part VI World Landslide Reports

Characteristics of Landslides Affecting Road Networks in Ethiopia: Evidence from 25 Years Research, Practice and Documentation 359
Kifle Woldearegay

KLC2020 Official Promoters 375

Geological Survey of Canada, Natural Resources Canada 377

Faculty of Civil and Geodetic Engineering, University of Ljubljana 381

China University of Geosciences, Wuhan 385

The State Key Laboratory of Geohazard Prevention and Geoenvironment Protection 391

Department of Civil Engineering, National Taiwan University 397

Institute of Cold Regions Science and Engineering, Northeast Forestry University 401

Marui & Co. Ltd. 403

Nippon Koei Co., Ltd., Geohazard Management Division 407

Ellegi Srl 411

Chuo Kaihatsu Corporation 415

Godai Kaihatsu Corporation 419

Kiso-Jiban Consultants Co. Ltd 423

Kokusai Kogyo Co. Ltd 425

OSASI Technos, Inc. 427

List of ICL Members 431

Emergency Response to the 2024 Noto Peninsula Earthquake

Takeo Murakami

Abstract

The earthquake that struck the Noto region of Ishikawa Prefecture, Japan on 1 January 2024 caused extensive damage to many lives, homes, and lifelines in the region and elsewhere, and the extent of the damage extended as far as Niigata, Toyama and other prefectures. Many victims are still forced to live in evacuation centres, and the government continues to support them under the "Emergency Disaster Headquarters for the 2024 Noto Peninsula Earthquake," which was established on 1 January. The government is also making concerted efforts for recovery and reconstruction of the affected areas under the "Headquarters for Recovery and Reconstruction Support of the 2024 Noto Peninsula Earthquake," established on 31 January. This contribution covers the earthquake and tsunami, the damage caused by these disasters, the initial response after the disaster, and support activities for victims.

Keywords

2024 Noto Peninsula Earthquake · Tsunami · Damages · Government response · Rescue operations · Evacuation centres

1 Overview of the Earthquake

At 16:10 on 1 January 2024, an earthquake of magnitude 7.6 (provisional) on the Richter scale occurred with its epicentre at a depth of 16 km (provisional) in the Noto region of Ishikawa Prefecture, with intensity 7 on the Japanese scale being observed in Wajima City and Shika Town in Ishikawa Prefecture, and intensity 6 to 1 being observed from Hokkaido to Kyushu regions. On the same day, the Japan Meteorological Agency (JMA) designated this earthquake and the series of seismic activities since December 2020 as the "2024 Noto Peninsula Earthquake" (Fig. 1).

Seismic activity in the Noto region has been active since December 2020, and 506 earthquakes of intensity 1 or higher were recorded between 1 December 2020 and 31 December 2023. On 5 May 2023, an earthquake of magnitude 6.5 (provisional) occurred at a depth of 12 km (provisional) in the Noto region of Ishikawa Prefecture, hitting Suzu City, Ishikawa Prefecture, with an intensity of 6 upper, causing human suffering and building damage mainly in Ishikawa Prefecture.

Crustal deformation had been observed since December 2020, but with the occurrence of the earthquake, the Geospatial Information Authority (GSI)'s electronic datum points showed significant crustal deformation mainly in the Noto Peninsula, including a 2.0-meter southwestward shift and a 1.3-meter rise at two observation points in Wajima. In addition, crustal deformation in a northwesterly to northerly direction was observed over a wide area, including the Kanto and Chubu regions, as well as the Sea of Japan side, such as Niigata Prefecture. According to the analysis of synthetic aperture radar images observed by the Advanced Land Observing Satellite "Daichi-2," a maximum uplift of about 4 m and a maximum westward deformation of about 2 m were detected in the western part of Wajima City (Fig. 2). This uplift was confirmed by aerial photographs and field surveys as a landward shift of the coastline over a wide area along the northern coast of the Noto Peninsula. Damage due to liquefaction was also confirmed in a wide range of coastal areas, especially in Ishikawa, Toyama, and Niigata prefectures.

T. Murakami (✉)
Disaster Management Bureau, Cabinet Office (formerly), Tokyo, Japan

Ministry of Land, Infrastructure, Transport and Tourism, Tokyo, Japan
e-mail: murakami-t28f@mlit.go.jp

© The Author(s) 2025

B. Abolmasov et al. (eds.), *Progress in Landslide Research and Technology, Volume 3 Issue 2, 2024*, Progress in Landslide Research and Technology, https://doi.org/10.1007/978-3-031-72736-8_1

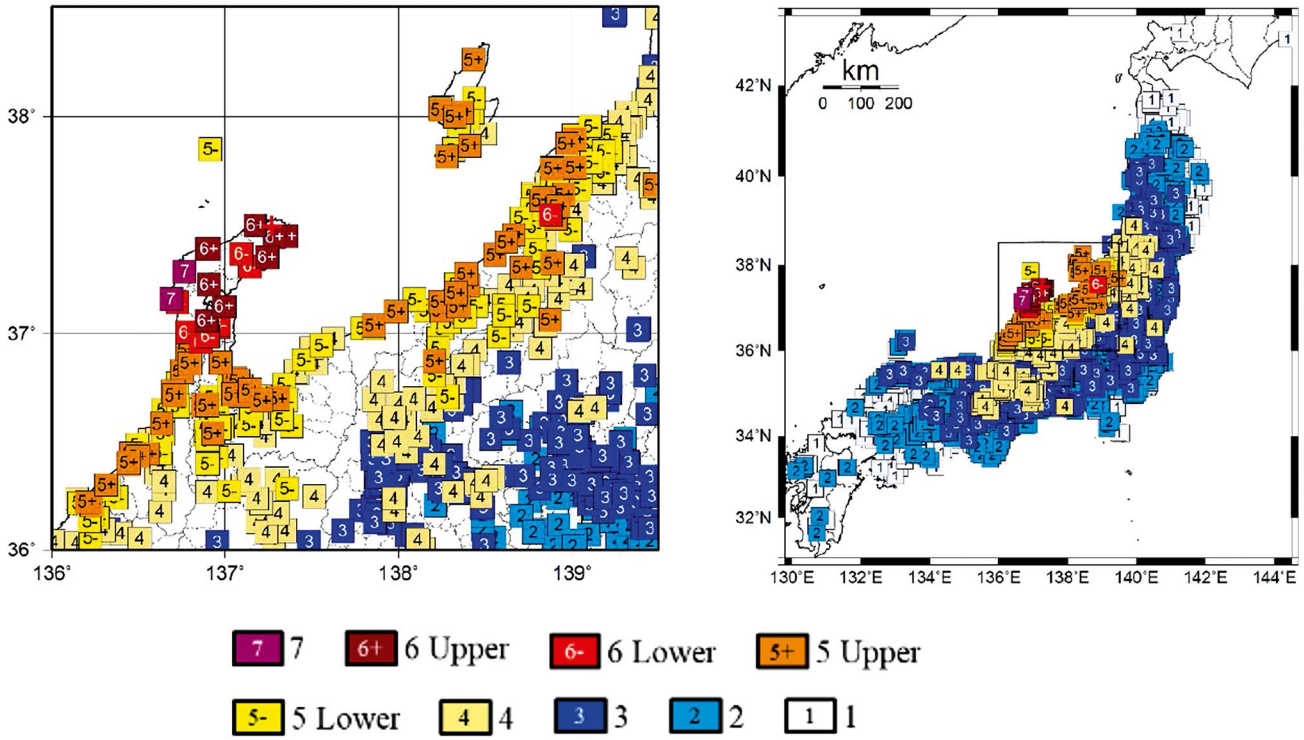


Fig. 1 Distribution map of seismic intensity of the earthquake in Noto, Ishikawa Prefecture at 16:10 on 1 January 2024. Source: Japan Meteorological Agency (2024)

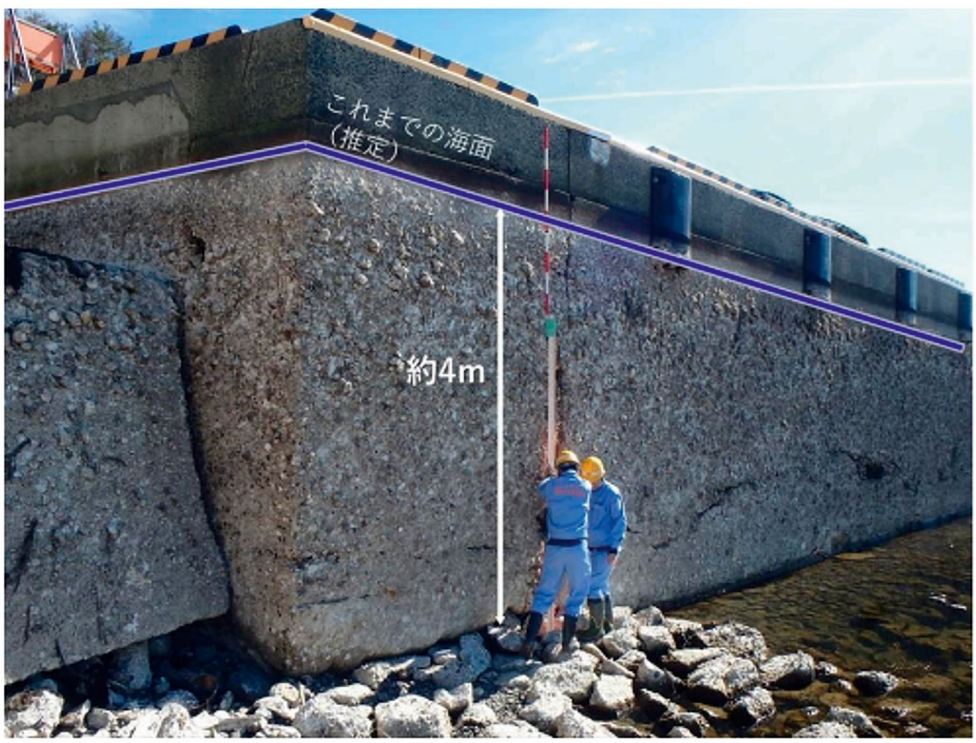


Fig. 2 An uplift of approximately 4-meter was observed at Kaiso fishing port. Source: Geospatial Information Authority (2024)

2 Overview of the Tsunami

A major tsunami warning was issued for Noto, Ishikawa Prefecture, and tsunami warnings were issued from Yamagata Prefecture to Fukui Prefecture and northern Hyogo Prefecture. Tsunamis were observed mainly along the Sea of Japan coast from Hokkaido to the Kyushu region, including 80 cm at the Kanazawa station (Ports and Harbors Bureau) and 0.8 m at the Sakata (JMA) station. In addition, aerial

photographs and field observations indicated that a wide area, including the Noto Peninsula, was inundated by the tsunami. Field surveys also confirmed tsunami inundation heights of 4 m or higher in Noto Town and Suzu City, Ishikawa Prefecture, and a run-up height of 5 m or higher in Joetsu City, Niigata Prefecture.

3 Human Damages

The earthquake caused the collapse of numerous houses, resulting in 248 fatalities and missing persons. The death toll was concentrated in one prefecture, Ishikawa Prefecture, with 106 victims in Wajima City (3 persons missing), 103 in Suzu City, 20 in Anamizu Town, 8 in Noto Town, 5 in Nanao City, 2 in Shika Town, and 1 in Hakui City (8 May).

According to information from the National Police Agency (as 31 March, out of 228 death handled by police), approximately 40% of the deaths were caused by crushing and 20% by suffocation or respiratory failure, and it is believed that many people were trapped under collapsed buildings. "Hypothermia/freezing to death," in which people died as a result of the cold, followed at just over 10%. The number of people in their 70 s was the highest, at 62, followed by 51 in their 80 s and 27 in their 90 s, with those in their 70 s and older accounting for about 60% of the total.

4 Building Damages

Damage to residential buildings occurred in Niigata, Toyama, Ishikawa, Fukui and Nagano prefectures, with 8597 buildings totally destroyed (including 8248 in Ishikawa) and 112,168 partially destroyed or partially damaged (including 70,678 in Ishikawa), for a total of over 120,000 damaged residential buildings in the affected areas (as of 8 May). The number of non-residential houses damaged in Ishikawa Prefecture is estimated to be approximately 25,000 (as of 8 May).

5 Immediate Response and the Establishment of the Disaster Management Headquarters

In response to the occurrence of this earthquake, the government set up a countermeasures office at the Prime Minister's Office at 16:11 on 1 January. At 16:15, Prime Minister Kishida gave the following instructions: (1) Provide the public with timely and accurate information on the tsunami and evacuation, etc., and take thorough measures to prevent damage, including evacuation of residents; (2) Assess the damage as soon as possible; and (3) Work closely with local governments, and under the policy of "human life first," work in unison with the government to make every possible effort to take emergency disaster response measures, including lifesaving and rescue measures for disaster victims. Subsequently, at 17:30, the Specific Disaster Management Headquarters was established, and at 22:40, the Emergency Disaster Response Headquarters was established by upgrading the said Headquarters, due to the need for close coordination among the relevant ministries and agencies, and the first Emergency Disaster Management Headquarters meeting was held at 9:15 on 2 January.

At 20:00 on 1 January, a Cabinet Office investigation team was dispatched to Ishikawa Prefecture Office. Furthermore, at 23:22 on the same day, the On-Site Headquarters for Emergency Disaster Management, headed by Minister of State Koga of the Cabinet Office, was established in the Ishikawa Prefectural Government Building. The On-Site Headquarters formed four teams to work closely with the Ishikawa Prefectural Government on infrastructure restoration, procurement and transportation of supplies, livelihood support, and reconstruction of livelihoods. In particular, with regard to infrastructure restoration, road traffic was disrupted due to collapsed slopes, fallen trees, and fallen utility poles, and lifeline restoration activities were also partially hampered. To address this situation, a team was formed within the On-Site Headquarters consisting of road, electricity, telecommunications, and water supply officials, and restoration work was carried out while clarifying the order of restoration for damaged infrastructure facilities and coordinating efficient road opening. In addition, liaison officers from the Cabinet Office and other related ministries and agencies were dispatched to the six hardest-hit cities and towns in the Noto region (Nanao City, Wajima City, Suzu City, Shika Town, Anamizu Town, and Noto Town) to investigate the situation in the affected areas and coordinate communications with the affected cities and towns.

6 Rescue and Relief Operations

After the earthquake, the police, fire department, Japan Coast Guard, and Self-Defence Forces worked together to carry out large-scale rescue and relief activities, placing the utmost priority on saving lives.

The police dispatched units from all over Japan immediately after the disaster, including a wide-area emergency assistance team (security force), which worked together with the Ishikawa Prefectural Police to conduct various police activities, including rescue and relief activities for disaster victims and searches for missing persons.

By 1 April, a total of 90,000 police personnel had been dispatched to the disaster area, rescuing 114 people from collapsed houses and using police aircraft (helicopters) to perform hoist rescues.

The Fire and Disaster Management Agency dispatched approximately 2000 emergency firefighters immediately

after the disaster, and a total of approximately 70,000 firefighters, including those from local fire departments, were mobilized to assist in the relief efforts. Specifically, firefighters extinguished fires, rescued people from collapsed houses, rescued people from isolated villages by firefighting helicopters, and transported people from hospitals and welfare facilities for the elderly. As a result, 435 people were rescued and 3500 people were transported to emergency medical services (cumulative total from the earthquake on 1 January to 5 March, as of 1 April).

The Japan Coast Guard had a total of 1453 patrol boats, 306 aircraft, 18 special rescue teams, and 316 mobile rescue officers on the ground by 1 April, transporting first aid and searching for missing persons.

The Ministry of Defence began collecting damage information and conducting search and rescue operations by aircraft in the peninsula area, where the road network was cut off, immediately after the disaster. On 2 January, a joint task force was formed with up to 14,000 personnel to respond to the disaster. From the beginning, helicopters were intensively operated to save lives, while offshore vessels were used as bases to transport heavy machinery, vehicles, and equipment necessary for transporting supplies and opening roads. As of 1 April, approximately 1040 people had been rescued (including transportation of evacuees) by maximizing the capabilities of the Ground, Maritime, and Air Self-Defence Forces.

7 Fire Outbreak and Extinguishing Activities

Eleven fires broke out in Ishikawa Prefecture, five in Toyama Prefecture, and one in Niigata Prefecture, and local fire departments and fire brigades were engaged in firefighting activities. In particular, a fire broke out immediately after the earthquake in Wajima City, Ishikawa Prefecture, destroying approximately 240 buildings and covering an area of 49,000 square meters in Wajima Asaichi, one of the three largest morning markets in Japan. The fire occurred in a densely wooded area where fire spreads easily, and the local fire department and fire brigade extinguished it at 7:30 a.m. on 2 January and extinguished it at 5:10 p.m. on the sixth under difficult conditions, as fire hydrants could not be used due to water cutoff and some fire prevention tanks were not available due to collapsed buildings (Figs. 3 and 4).



Fig. 3 Fire at Wajima Asaichi morning market. Source: Kyodo News 2024



Fig. 4 Ruins after the Fire at Wajima Asaichi morning market. Source: Kyodo News 2024

8 Emergency Medical Care

After the disaster, many medical institutions in the affected areas were damaged. Even medical institutions that sustained only minor building damage or were not completely or partially destroyed experienced difficulties in getting staff to work, transporting patients, and transporting medicines and other supplies. Therefore, in order to provide medical support to disaster victims, the Disaster Medical Assistance Team (DMAT), the Disaster Psychiatric Patient Assistance Team (DPAT), the Japan Medical Association Disaster Medical Team (JMAT), and Disaster Support Nurses were dispatched from all over Japan to medical

institutions and evacuation centres. In addition to lifesaving measures and other emergency medical activities by these teams, medical support teams consisting of SDF medical officers and nurses provided traveling medical services mainly in isolated areas.

To date (as of 1 April), 1139 DMAT teams have been dispatched to transport wounded and sick, assist in the evacuation of hospitalized patients, and provide hospital support. DPAT, which provides mental health care for evacuees by patrolling evacuation centres, has dispatched 196 teams. 1008 JMAT teams were dispatched to provide medical support in affected cities, towns, and secondary evacuation centres. A total of 2982 Disaster Support Nurses from the Japan Nurses Association were dispatched to evacuation centres and medical institutions in the affected areas.

In addition, infectious disease specialists and others provided advice on infection control at evacuation centres and other facilities. The Disaster Health Emergency Assistance Team (DHEAT) dispatched by prefectures and designated cities other than the disaster-stricken prefectures provided support for the command and coordination functions of health centres and other facilities. Public health nurses dispatched by local governments made rounds based on the list of residents prepared by each municipality, and conducted health management for evacuees living in evacuation centres and at home.

9 Procurement and Transportation of Daily Necessities

Immediately after the disaster, under the instruction of the Prime Minister, the government began "push-type support" to provide essential supplies for the lives and living environment of disaster victims without waiting for requests from the affected areas, and the first shipment of relief supplies arrived at a wide-area goods transportation base in Ishikawa Prefecture on the following day.

The relief supplies included food, drinking water, powdered and liquid infant formula, blankets, portable toilets, and other urgently needed supplies. Warm clothing, heaters and fuel needed to combat the cold, sanitary products, wipes, and infant diapers were also supplied from the perspective of women and those raising children in evacuation centres. In addition, support was provided based on the needs of the affected areas, including elastic stockings to ensure the health of disaster victims, cardboard beds needed to improve the environment of evacuation centres, and supplies such as portable laundry kits and washing machines to meet laundry needs in the face of prolonged water outages. With the cooperation of private logistics providers, transportation from the wide-area goods transportation bases to the affected local governments was mainly handled by the Self-Defence Forces and the Ishikawa Prefecture Truck Association (Fig. 5). In addition, at the goods transportation bases in each affected



Fig. 5 Transportation of relief items by a helicopter of the Self-Defence Forces. Source: Ministry of Defence (2024)

city and town, logistics companies were in charge of terminal transportation to evacuation centres, etc. for each city and town, while specialized volunteer groups and others handled the sorting work.

10 Evacuation Life

More than 110,000 houses were damaged in the affected areas, and many disaster victims had to live in evacuation centres for a long period of time after the disaster struck. Immediately after the disaster (as of 5:00 a.m. on 2 January), approximately 1300 evacuation centres were opened in one province and nine prefectures, and the number of evacuees exceeded 50,000. As of 6:00 a.m. on the following day, 3 January, approximately 480 evacuation centres were open in Niigata, Toyama, and Ishikawa prefectures, sheltering approximately 30,000 people (according to the Cabinet Office). The evacuation centres received "push-type support" on food, clothing, and other daily necessities, as well as materials necessary to improve the evacuation centre environment, such as cardboard beds, partitions, and temporary toilets (Figs. 6 and 7). Due to the water supply being cut off, toilet trailers were dispatched and water-circulating shower facilities, etc. were installed. In addition, welfare shelters were opened to accommodate the elderly, handicapped, infants, and other people requiring special consideration who might have difficulty living in ordinary shelters.

In addition to local government officers of the affected area, local government officials dispatched from across Japan and NPOs and other specialized volunteer groups that entered the affected areas provided support for shelter operations. A large number of trailer houses and container houses were delivered to the affected areas to improve the accommodation environment for relief workers, including the operation of evacuation centres. In Ishikawa Prefecture, the hardest-hit area, approximately 30,000 people were evacuated immediately after the disaster, but the number has since decreased, and as of May 8, approximately 4000 people are still living in 275 evacuation centres in Ishikawa Prefecture.



Fig. 6 Living zone in an evacuation centre (Suzu City) Source: Cabinet Office



Fig. 7 Setting up partition (Noto Town) Source: Cabinet Office

11 Secondary Evacuation

In the affected areas in the Noto region, many isolated settlements occurred due to the disruption of roads, and even in non-isolated areas, it was difficult to lead a daily life due to damage to lifelines such as water, sewerage and electricity. Disaster-related deaths, particularly among the elderly, were also a concern. For these reasons, Ishikawa Prefecture decided to evacuate the affected people (i.e. to conduct secondary evacuation) to hotels and ryokans that were in good condition. In order to secure hotels and ryokans to receive the evacuees, the Japan Tourism Agency took the lead in coordinating with the travel industry, and on 9 January, accommodation for approximately 5000 people was secured, and by the end of February, accommodation for approximately 31,000 more people had been secured nationwide. The standard rate per night for hotel evacuation for the use of disaster relief funds was raised from 7000 yen to 10,000 yen on a special basis in order to quickly secure accommodation facilities. In addition, temporary evacuation centres (pre-secondary evacuation centres) were opened at the Ishikawa Sports Centre (Kanazawa City) and other locations, which accepted up to 367 evacuees (on 21 January), mainly the elderly and other persons requiring special care.

As for evacuation to secondary evacuation centres, 196 people were evacuated to such centres in Komatsu City and other cities by 8 January, using airlift support by Self-

Defence Force helicopters and buses and taxis secured by the Ministry of Land, Infrastructure, Transport and Tourism. Subsequently, up to 5275 people (16 February) were evacuated to hotels, ryokans and other secondary evacuation centres in and outside the prefecture.

In the pre-secondary evacuation centres, a medical treatment system, the dispatch of nursing staff, the provision of livelihood counselling services such as loans for livelihood welfare funds, and the coordination of the admission of the elderly to welfare facilities in and outside the prefecture have been provided to ensure that the elderly, disabled persons and other persons requiring assistance can spend their time with peace of mind.

The number of evacuees has been decreasing as lifelines are being restored and temporary housing is being constructed in the affected areas, and as of 8 May, 64 people (1495 in total) were still living in the pre-secondary evacuation centres and 1729 people (10,999 in total) in the secondary evacuation centres.

12 Towards Future Disaster Risk Reduction Policy

Support for recovery and reconstruction of the areas affected by the 2024 Noto Peninsula Earthquake is still ongoing, and we must continue our efforts in the future. At the same time, it is important to constantly review the disaster response based on the experiences and lessons learned from this disaster. It is necessary to identify measures to overcome the issues that emerged in the course of the disaster response, new technologies that can be effective in disaster response, and other measures to strengthen initial response and emergency measures, and to reflect these measures in future countermeasures.

For this purpose, the "Verification Team for the 2024 Noto Peninsula Earthquake" was convened, chaired by the Deputy Chief Cabinet Secretary and composed of senior officials from the relevant ministries and agencies. The team will gather and organize the experiences of officials who were involved in the response to the recent earthquake with regard to post-disaster emergency response, including support for local governments, evacuation centre management, and procurement and transportation of supplies.

This verification team will identify areas that can be evaluated and areas that need improvement in the disaster emergency response. The team will then conduct the verification work with the aim of applying the findings to future disaster responses, including those in the affected areas where restoration efforts are still underway. Three areas were selected for verification: support for local governments, evacuation centre management, and procurement and transportation of supplies, for which the "Support Team for Reconstruction of Livelihoods and Livelihoods of the Victims of the 2024 Noto Peninsula Earthquake" was established and all government ministries and agencies collaborated. The report also focuses on new start-up technologies that made a significant contribution to initial response and emergency measures under the geographical constraints of the peninsula, a situation that was more difficult than in previous disaster response efforts.

The experiences and lessons learned from the 2024 Noto Peninsula Earthquake will be examined with experts in addition to the verification results of this verification team to improve institutional and operational aspects, and will be applied to future disaster response.

References

Geospatial Information Authority (2024) Uplift hight at the kaiso fishing port (in Japanese). https://www.gsi.go.jp/BOUSAI/20240101_noto_earthquake.html#8-2. Last access on 19 May 2024

Japan Meteorological Agency (2024) The evaluation of the 2024 Noto peninsula earthquake (in Japanese). https://www.static.jishin.go.jp/resource/monthly/2024/20240101_noto_3.pdf. Last access on 19 May 2024

Ministry of Defence (2024) Disaster dispatch for the 2024 Noto peninsula earthquake (in Japanese). https://www.mod.go.jp/js/activity/domestic/2024notohantou.html. Last access on 19 May 2024

Open Access This chapter is licensed under the terms of the Creative Commons Attribution 4.0 International License (http://creativecommons.org/licenses/by/4.0/), which permits use, sharing, adaptation, distribution and reproduction in any medium or format, as long as you give appropriate credit to the original author(s) and the source, provide a link to the Creative Commons license and indicate if changes were made.

The images or other third party material in this chapter are included in the chapter's Creative Commons license, unless indicated otherwise in a credit line to the material. If material is not included in the chapter's Creative Commons license and your intended use is not permitted by statutory regulation or exceeds the permitted use, you will need to obtain permission directly from the copyright holder.



Part I

Original Articles

Understanding Landslide Awareness: Exploring Students' Disaster Risk Perception in Higher Education Institutions

Karla M. Hernández-Cadena, Ricardo J. Garnica-Peña, Jorge González-Sánchez, and Irasema Alcántara-Ayala

Abstract

Understanding how individuals perceive and respond to the impact of diverse hazards such as landslides is crucial in effective disaster risk management. This is particularly significant in areas like Teziutlán, Puebla, Mexico, where landslides have historically occurred. This study aimed to understand the perception of landslide risk among students in this area. The research methodology involved identifying a school near landslide-prone areas and conducting a risk perception survey. The survey assessed students' perceptions of landslide risk, knowledge of hazards and exposure, previous experience with landslides, information and media, landslide preparedness, and communication. The data was collected through paper-and-pencil surveys. The study results can be used to improve disaster awareness and preparedness, reduce disaster risk and mitigate the impact of landslide disasters in the municipality of Teziutlán and similar mountain regions. This study is a valuable contribution to disaster risk perception and awareness literature, focusing specifically on higher education students in areas susceptible to landslides.

Keywords

Landslides · Rainfall-induced · Landslide exposure · Landslide risk perception · Disaster risk · Disaster risk communication · Landslide preparedness · Disaster risk awareness · Disaster risk reduction.

K. M. Hernández-Cadena
Postgraduate Programme in Geography, National Autonomous University of Mexico (UNAM), Mexico City, Mexico
e-mail: jorgos@unam.mx; ialcantara@geografia.unam.mx

R. J. Garnica-Peña · J. González-Sánchez · I. Alcántara-Ayala (✉)
National Autonomous University of Mexico (UNAM), Institute of Geography, Mexico City, Mexico
e-mail: garnica@geografia.unam.mx

1 Introduction

Education, constant learning, and human experience are essential in forming cognition, thoughts, judgments, and behaviours. In disaster risk research, education is considered one of the fundamental axes for continuing to work on the substantial reduction and possible emergence of new risks through inclusive policies to reduce risk and measures that increase preparation for response and recovery in the event of a disaster (UNISDR 2015).

The presence of a community or population that is consistently engaged in preparing for the hazards of their locality indicates a confluence of social, educational, cultural, institutional, and economic factors that cannot operate in isolation. This way, materials, preparation measures, mitigation, and action policies must be created through agreements and shared responsibilities between the different management actors, such as the community, institutional authorities, researchers, experts, and educational authorities.

Decision-making in disaster risk reduction and management requires more flexible, hybrid, accessible, adaptive, integrative, and collaborative forms of governance that can overcome some of the challenges experienced by stakeholders working in isolation, such as conflict resolution, uncertainty and social legitimacy (Van der Molen 2018).

The literature provides examples of the importance of preparedness for disaster risk education at a global level (O'Donnell et al. 2018; Brilly and Polic 2005; Muttarak and Lutz 2014).

Evidence shows that society's mechanisms, including experience, decision-making, risk perception, and educational level, are crucial in developing preparedness capabilities. These mechanisms can help prevent and reduce the impact of disaster risk well before it materialises into disasters (O'Donnell et al. 2018).

Adopting an interdisciplinary approach involving the community and authorities in disaster risk management can

© The Author(s) 2025

B. Abolmasov et al. (eds.), *Progress in Landslide Research and Technology, Volume 3 Issue 2, 2024*, Progress in Landslide Research and Technology, https://doi.org/10.1007/978-3-031-72736-8_2

improve the effectiveness of warning systems and bring about positive social changes (Brilly and Polic 2005).

It has also been sought that education serves as a fundamental tool for the population to develop strategies that allow them to understand the potential consequences of hazards better, strengthening the capacity for preparation, response and recovery (Muttarak and Lutz 2014).

Research has been conducted in Latin America to determine the significance of disaster risk education preparedness. This method regards education as a social tool that enables communities to prepare and gain knowledge about the environment and its connection to socio-economic systems. This ultimately lessens the chances of disasters and reduces disaster risks (Amaya et al. 2024; DiBella and Burch 2023; Börner 2023; Hlekiwe et al. 2022).

According to Amaya et al. (2024), how inhabitants of countries like Colombia and Ecuador behave and respond to hazards is significantly influenced by various factors such as the presence of risks, their level of preparedness, their perception of risk, and their trust in management authorities. To ensure faster and more effective recovery from disasters, it is crucial that the local population actively participates in improving their preparedness and perception of risk. This will benefit the overall understanding of the risks and improve disaster responses.

Communities can reduce the risk of disasters by utilising their capabilities and experiences. In Sao Paulo, young people are being considered for their participation in the community during hazardous situations. This allows educational strategies to be developed based on their experiences and perceptions of recurring disaster risk situations. By understanding the emotions of young people in disasters, preparedness measures can be designed to improve individual coping behaviours while acknowledging the risk and the individuals' experiences (Börner 2023).

Nonetheless, disaster risk reduction preparedness strategies may not be practical in some countries due to a lack of collaboration and inclusivity. This happens when measures and policies are developed without input from the community, authorities, researchers, and decision-makers. As a result, confusing strategies with different visions and perceptions of the world are generated, leading to ineffective disaster preparedness (DiBella and Burch 2023).

Improved collaboration among countries can enhance disaster preparedness and response by exchanging resources and information (Hlekiwe et al. 2022).

In Mexico, various studies have highlighted the importance of early preparedness to minimise the negative impacts of hazards. However, it is still essential to understand how the population copes with risks or deals with disasters to develop effective disaster management strategies (Atreya et al. 2017; Cohen-Salgado et al. 2021).

The community should adopt essential strategies to prepare for hazards, including accessing risk maps, sharing experiences and early warning systems, and having shelters available (Atreya et al. 2017).

Social capital and a sense of belonging are crucial short-term tools for preparing the population for hazards. In the long run, collaborative relationships between management actors are essential for achieving diverse and productive planning (Cohen-Salgado et al. 2021). However, the literature has also demonstrated that various difficulties and underlying causes hinder the effective implementation of risk-reduction strategies. These include the lack of verification of compliance with standards, the discontinuation of disaster financial mechanisms, the rapid growth of population linked to economic activities like tourism, the absence of territorial planning programs, inadequate information and knowledge among the population, the lack of agreements between authorities and the community, and limited economic, political and institutional resources (Travieso et al. 2023).

Improving disaster risk preparedness and mitigation strategies involves considering fundamental elements such as a community's education, experience, and risk perception concerning potential hazards. Additionally, authorities must understand their capabilities and limitations in promoting preparation, action, response measures, and policies before a hazardous event occurs. By committing these efforts, communities can work towards better disaster risk management (Brilly and Polic 2005; Muttarak and Lutz 2014; DiBella and Burch 2023; Börner 2023).

2 Importance of Landslide Risk Perception Studies

Risk perception is a mental process that involves various cognitive factors, such as selecting, organising, and interpreting information. It can be assessed and described through psychometric analysis because it comprises heuristics and cognitive biases that affect how we think, understand risk, and create meaning in uncertain situations (Slovic 2000).

Risk perception involves individual and collective perspectives, which work together to interpret and assign meaning to a potential hazard. This approach identifies nine dimensions that shape risk perception: whether the risk is voluntary or involuntary, how immediate the risk's effects are, the degree of personal knowledge about the risk, the level of scientific understanding of the risk, the potential of the risk, the type of risk (and the degree of fear it inspires), the perceived severity or potential of disaster, the amount of exposure to the risk, and the novelty of the risk (Fischhoff et al. 1978).

Culture can be defined as a collection of norms, values, and practices that a particular social group commonly adopts. On the other hand, the perception of risk is shaped by how individuals from different cultural groups interpret and incorporate their beliefs and practices related to risk in a given historical context (Douglas and Wildavsky 1982).

Risk perception is crucial in comprehending hazards like landslides, as it is based on a set of definitions and axes that revolve around disaster risk. Understanding risk perception can better assess potential hazards from such events. Incorporating risk perception into disaster studies allows for shedding light on the constraints of disaster risk management and pinpointing shortcomings in how society and governing bodies perceive risk. This knowledge can then inform the development of more effective mitigation and prevention strategies to mitigate the impact of disasters.

More minor recurrent disasters like floods and landslides can cause systemic hazards, resulting in significant economic losses, accounting for up to 50% of global disaster losses (UNISDR 2015).

Research has been improved by considering the community's perception of risk, enabling the development of preparedness and prevention strategies tailored to the community's needs (Finlay and Fell 1996).

One of the primary objectives of research on risk perception is to adopt an interdisciplinary approach to comprehensively understand how people form a social and cultural perception of risk based on their experiences with hazards. This perception influences decision-making during such events (Calvello et al. 2016).

In Mexico, ongoing research efforts have examined how individuals perceive landslide risks. The primary objective of these studies has been to explore the various components that contribute to people's perception of risk, including their personal experiences and commitment to reducing disaster risk and mitigating the impact of disasters. By gaining a deeper understanding of these factors, researchers have developed more effective strategies for communicating and managing landslide risks (Landeros-Mugica et al. 2016; Alcántara-Ayala and Moreno 2016).

Extensive research has been carried out over the years in the state of Puebla in the municipality of Teziutlán since this area is considered highly susceptible to landslides. In one of the studies, risk perception was investigated based on the social construction and cognition of risk, using a mixed method with ten in-depth interviews and a questionnaire on risk perception appropriate to the population of Teziutlán, Puebla (Landeros-Mugica et al. 2016).

A study of 206 individuals analysed their perception of the risk associated with landslides. The findings showed inadequate information and a lack of urban planning, reducing accessibility and multi-sectoral coordination (Alcántara-Ayala and Moreno 2016). Another research concerning landslide awareness found that inhabitants were knowledgeable about landslide risk. Houses in the city centre were considered the safest, while those on edge were exposed. The study revealed a need for initiatives to reduce disaster risk in the community (Hernández-Moreno and Alcántara-Ayala 2017).

3 Studied Area

The municipality of Teziutlán is situated in the northeast of the State of Puebla, within the northeastern Sierra (Fig. 1) (INEGI 2020). Gentle slopes characterise the southern part of the municipality, while the northern areas exhibit a terrain with more pronounced and contrasting mountainous elevations (Alcántara-Ayala et al. 2018).

According to studies conducted in this municipality, Teziutlán is predominantly composed of volcanic material belonging to the Transversal Volcanic Belt. The decomposition of loosely consolidated rock materials with high clay content has formed residual soils. These components greatly influence the soil type, resulting in very light soil with steep slopes (INEGI 2010) and a high capacity for retaining water and nutrients, subjecting the area to mass movement processes.

The eastern region of Teziutlán is characterised by valleys that exhibit intense erosion. These valleys present slopes that are steeper than 20°, which are home to various residential neighbourhoods such as Manuel Ávila Camacho, Juárez, Xoloco, La Aurora, Lindavista, El Calvario, La Gloria and Siete Sabios (Murillo-García et al. 2017).

Based on a multi-temporal landslide inventory map (1:25,000) created by field observation, aerial photographs, and satellite images, Murillo-García et al. (2017) argued that the most frequent types of landslides are flows and complex movements. Significant landslide events have extraordinary rainfall episodes, while small and medium-sized events occur during the rainy season. Their study also highlighted the importance of considering human activities on the slopes in addition to precipitation.

Over the years, rainfall-induced landslides have occurred in the municipality, coupled with the existing conditions of vulnerability and exposure, which have shaped disaster risk and led to significant human, material, and environmental losses.

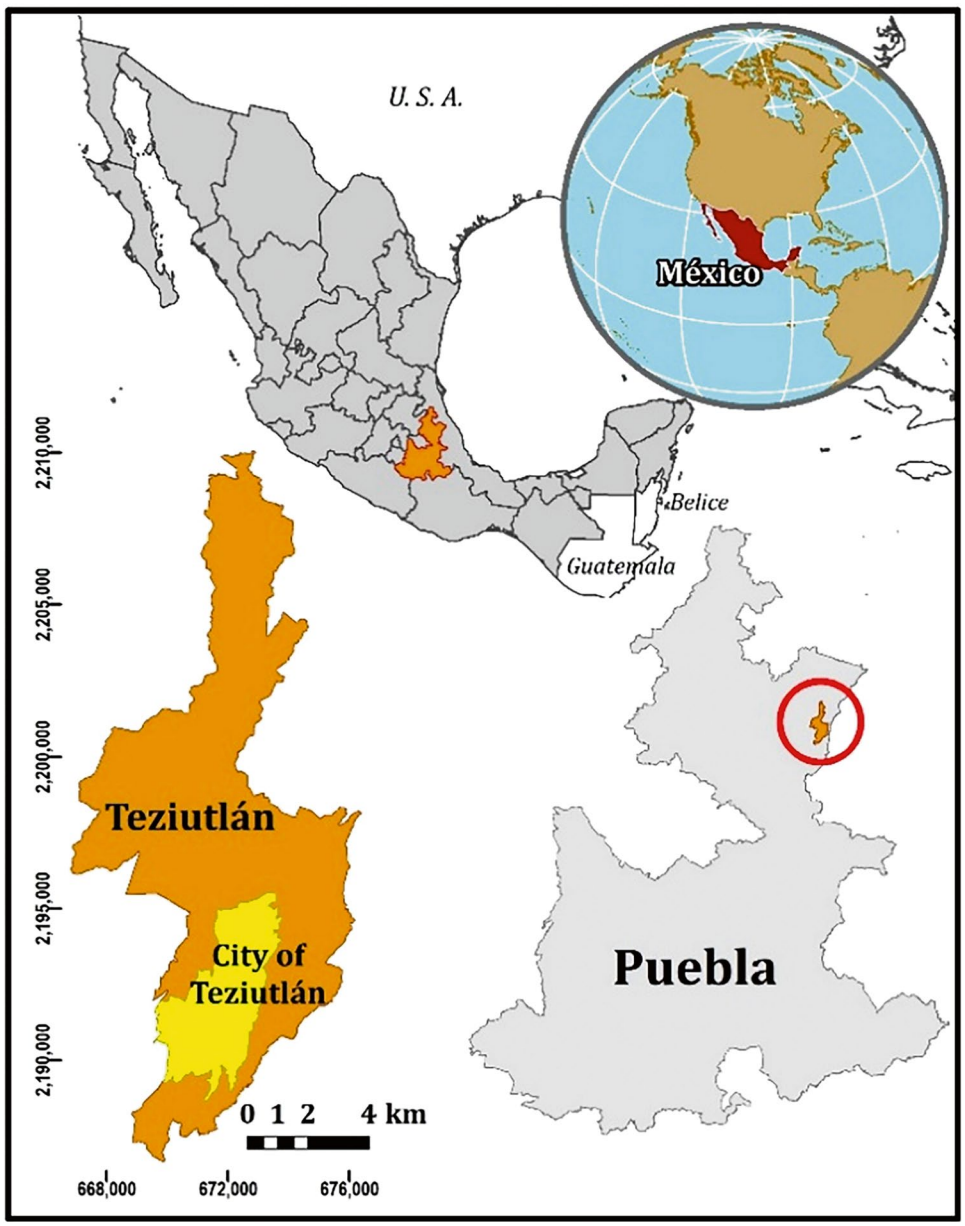


Fig. 1 Location of the studied area

4 Methodology

The methodology comprised three main steps. The first one included selecting an educational institution near landslide-affected regions in Teziutlán, Puebla, Mexico. The second part described the chronology of land-use changes in the region of the chosen school. The third stage involved preparing, conducting and analysing a landslide disaster risk perception survey.

4.1 Selection of the Educational Institution for the Survey

Based on the updated landslide inventory of Murillo-García et al. (2017), various areas in Teziutlán that have experienced landslides, including educational institutions ranging from preschool to higher education, were identified. The proximity between these schools and the impacted regions by landslides was estimated. One of the schools closest to landsliding was selected for the study.

4.2 Chronological Land-Use Change

To gain deeper insights into changes in land use patterns in the area surrounding the selected school over the last decade, Google Earth Pro and drone images acquired in 2023 were analysed using ArcMap v10.6, ESRI. This approach enabled the identification and mapping of changes in land use over time, which is crucial in understanding the risks and vulnerabilities associated with landslides.

Table 1 Description of the key elements included in the survey

Survey key sections	Focus of questions	Risk perception scale
Sociodemographic data	Age	***Open answer***
	Occupation (employee or student only)	
	School grade	
Knowledge and risk identification	Knowledge about the most frequently occurring hazards	***Multiple choice*** Earthquakes, landslides, floods, Forest fires Soft soils, earthquakes, precipitation
	Situations that could trigger a landslide	
	Neighbourhood that is considered to be the highest risk	***Open answer***
Experience with landslides	Personal experiences with landslides during the COVID-19 pandemic	***Dichotomous scale*** Yes, no
	Indirect experiences with landslides during the COVID-19 pandemic	
Landslide exposure	Perception of the degree of risk that homes have in the face of landslides	***Likert scale*** High risk, moderate risk, low risk, very low risk
	Perception of the degree of risk that students and others have in the face of landslides	
Landslide preparedness	Maintenance and inspection actions for a home before and during the pandemic	***Likert scale*** Never, sometimes, almost always, daily
	Perception of the possibility of being affected in the event of a landslide during the pandemic	
	Perception of preparation for the possible occurrence of a landslide	
Information and media	Frequency of receiving information on action and prevention measures against various hazards before and during the pandemic	***Likert scale*** Never, sometimes, almost always, daily
Communication of the population with stakeholders	Perception of the degree of responsibility of the actions of authorities in case of landslides	***Likert scale*** Never, sometimes, almost always, daily
	Perception of the action response of authorities and the community to the possibility of a landslide occurring before and after the COVID-19 pandemic	

4.3 Landslide Disaster Risk Perception Survey

The study was an in-person survey, with data gathered via paper and pencil. An experienced team of interviewers conducted the survey in Spanish, which included 72 questions. Responses were measured using a Likert scale, and the time taken to answer questions ranged from 25 to 35 min. Of the study population, 28 individuals completed and returned the questionnaire.

The initial contact with the participants was arranged through the school authorities and researchers. The meeting occurred at the selected school before the instrument was administered.

The proposed study methodology entailed several key steps: (1) The survey was prepared by adapting the procedure used by Hernández-Moreno and Alcántara-Ayala (2017); (2) Conducting a questionnaire with students at the London University Institute in January 2023; (3) Providing students with informed consent and explaining the study's objectives; (4) Ensuring voluntary participation of participants in the research; and (5) Analysing data using the statistical package SPSS 21.

The questionnaire comprised six sections assessing knowledge, experience, risk information, action measures, prevention, exposure, preparation, and communication among the public and disaster risk management actors (Table 1).

5 Results

5.1 Educational Institutions Located in the Area Affected by Landslides

e study analysed 113 educational institutions, from kindergarten to further education, through a mapping process that overlapped the updated landslide inventory (Murillo-García et al. 2017). The study further estimated the distance of each educational institution to the nearest landslide, thus contributing to a better understanding of the potential risks and hazards associated with landslides in the surrounding areas (Fig. 2).

Nearby schools to the landslide-affected area include Adolfo López Mateos Kindergarten, primary, and secondary schools. The Business Cultural Centre of Puebla is the closest high school. The nearest higher education institutions are the University of Puebla at Teziutlán and London University. London University was chosen for the survey as both authorities and students showed willingness to participate (see Fig. 4).

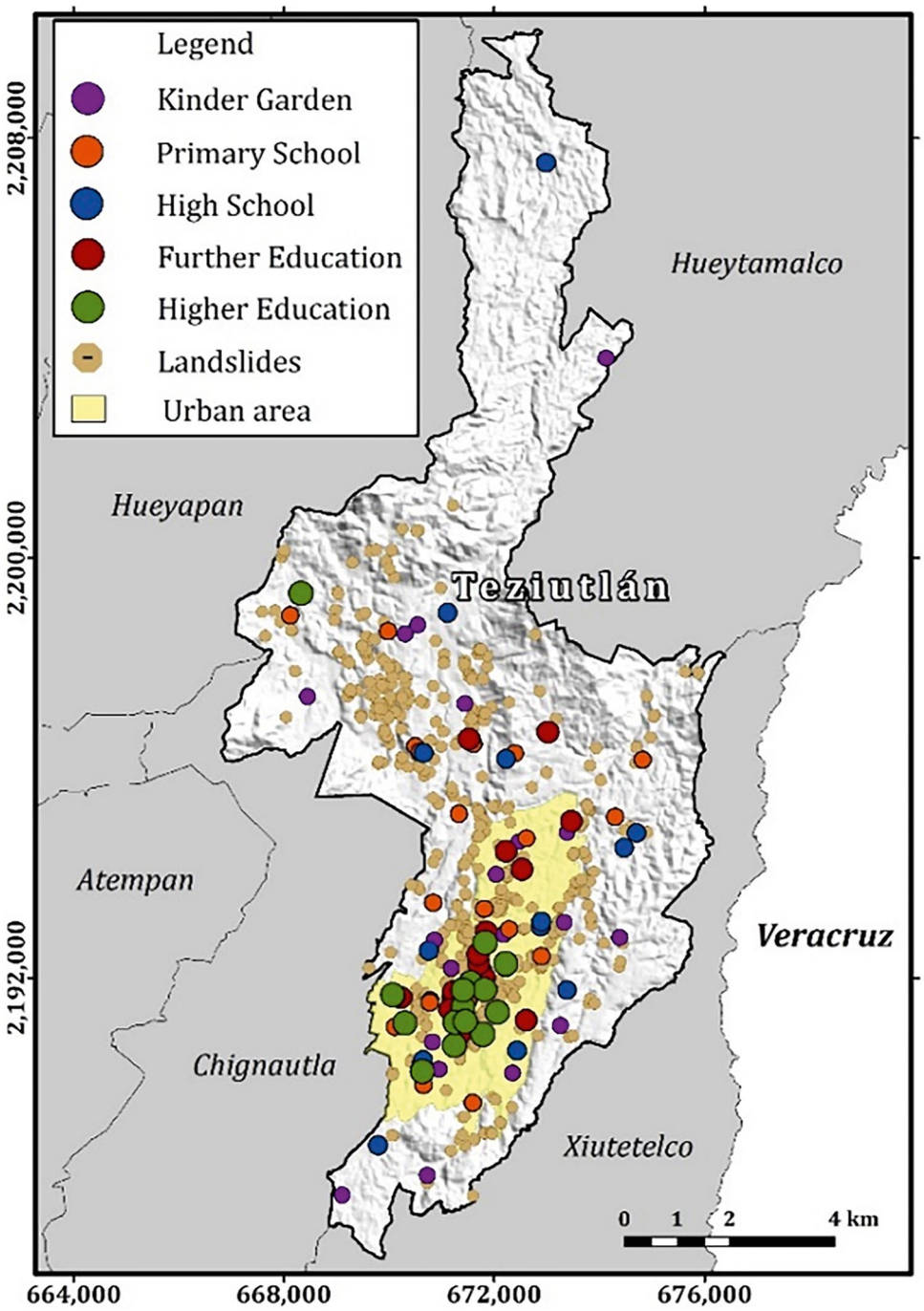


Fig. 2 Location map of schools and areas affected by landslides

5.2 Land-Use Change

Understanding the evolving land-use patterns at the local level in landslide-prone areas is essential for building community awareness and preparedness, implementing accurate risk assessments, planning infrastructure, conserving the environment, and implementing effective mitigation efforts. Through vigilant monitoring and management of land-use dynamics, governing bodies can significantly reduce the people and infrastructure's exposure to the impact of landslide disasters.

Findings revealed that the total area of land modified for development in 2021 was 21,092.89 m, representing a substantial increase compared to previous years. Conversely, 2013 witnessed the slightest land modification, with a mere 572.89 m of area (Table 2, Figs. 3 and 4).

Table 2 Land use changes from 2012 to 2023

Year	Area annual surface development (m)	Accumulated area (m)
2012	2689.58	2689.58
2013	572.89	3262.47
2016	3739.58	7002.05
2018	1754.19	8756.24
2019	972.10	9728.34
2020	925.49	10,653.83
2021	21,092.89	31,746.72
2022	2221.95	33,968.67
2023	5141.35	39,110.02

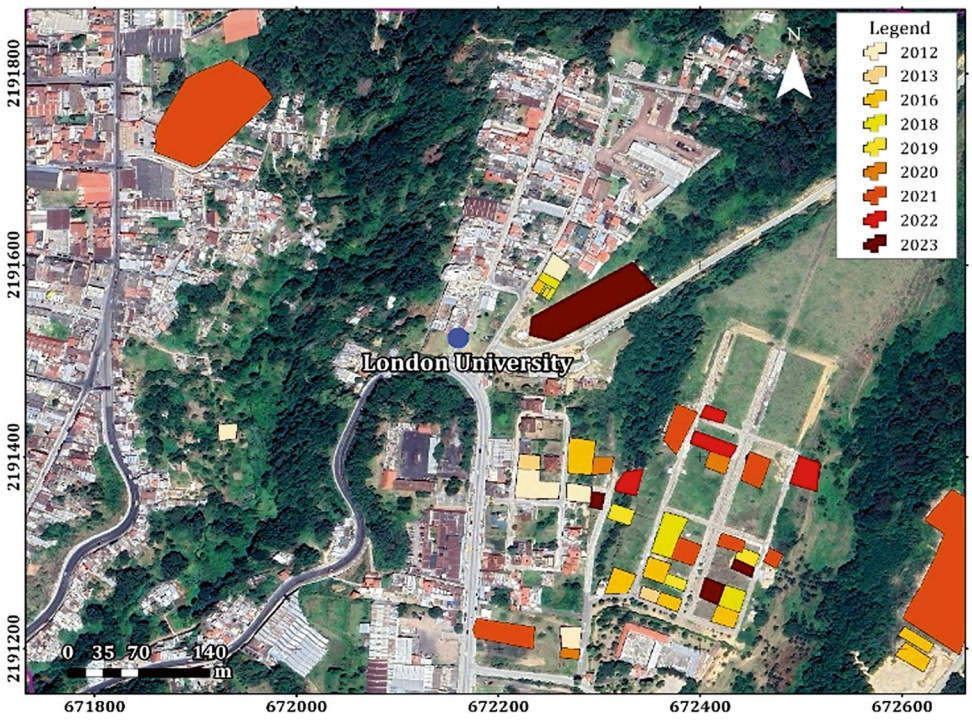


Fig. 3 Location of the University of London and development areas and land use changes from 2012 to 2023

5.3 Landslide Risk Perception Survey

The study involved 28 students from the Institute of London University, 22 of whom were young adults aged 18 to 24 and six of whom were between 25 and 38.

(a) *Knowledge and risk identification*

According to the survey results, out of the 28 students who participated, 89.3% reported being knowledgeable about the potential hazards in their area. Among them, 42.9% identified landslides as the most common hazard, followed by 21.4% who cited earthquakes, 17.9% mentioned forest fires, and 10.7% specified floods as the most frequent hazard. Three primary factors were identified as potential triggers for landslides. Of those factors, 71.4% of respondents pointed to heavy rainfall as the most significant contributor, while earthquakes were considered the second most crucial factor, with 60.7% of students choosing it. Finally, 32.1% of participants cited rain on unstable or soft soil as a potential cause for landslides. Of the sample, 17% believed Xoloco had the highest risk for landslides, while 25% were unsure of any neighbourhood at risk.

(b) *Experience with landslides*

During the pandemic, it was found that, of the 28 students, 21.4% had a direct experience with a landslide. Likewise, 21.4% of the students had a family member, friend or acquaintance who experienced a landslide-related event.

(c) *Landslide exposure*

According to the findings, 50% of students considered houses low-risk in the city's centre. Sun-dried brick houses were identified as high risk by 32.1% of students, while

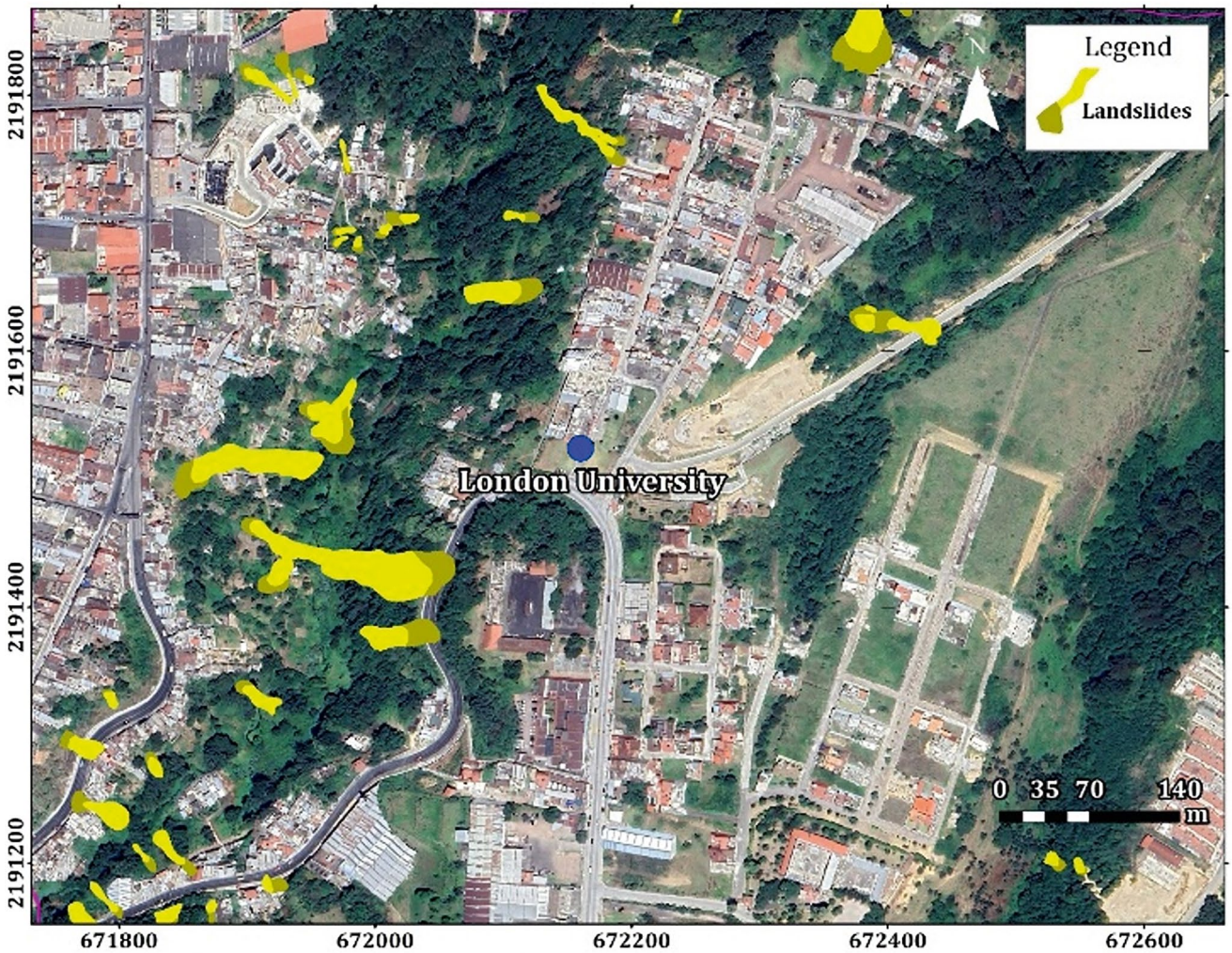


Fig. 4 Location map of the University of London and areas of landslides that have occurred

houses near the river were viewed as high risk by 50%. Government-built houses were seen as somewhat risky by 50% of students. Additionally, houses at the foot of the hillside were deemed high risk (50%), and those in landslide-prone areas were considered high risk by 53.6% of students. Relocated houses were associated with some risk (39.3%), those situated next to the road were perceived as somewhat risky (46.4%), and those surrounded by trees were viewed as somewhat risky (39.3%) (Fig. 5).

According to students' perceptions, the likelihood of experiencing personal damage or loss from landslides is deemed very low to 75%. Similarly, the risk perceived for families was assessed as very low. For those living in the same neighbourhood where the school is located, the risk is believed to be low (39.3%), while for those living in other neighbourhoods of Teziutlán and Puebla, the risk was perceived as moderate.

(d) *Landslide preparedness*

It was found that students were involved in preparedness measures during the COVID-19 pandemic for potential landslides. These measures included observing any ground cracks (53.6%), checking for tilted or leaning trees or poles (46.4%), keeping an eye out for small landslides (50%), checking for accumulated rainwater (50%), relying on government notifications for neighbourhood risk (53.6%), checking for improperly closing doors or windows (53.6%), monitoring for signs of humidity, lumps, or steps forming on the floor, and staying aware of river growth (46.4%) (Fig. 6).

Many students felt there was a low possibility of damage to homes (42.9%) and impact on daily activities (35.7%). In contrast, others perceived health damage (39.3%) and loss of belongings (35.7%) are more likely. Concerns were also expressed about the potential impact on crop areas (39.3%)

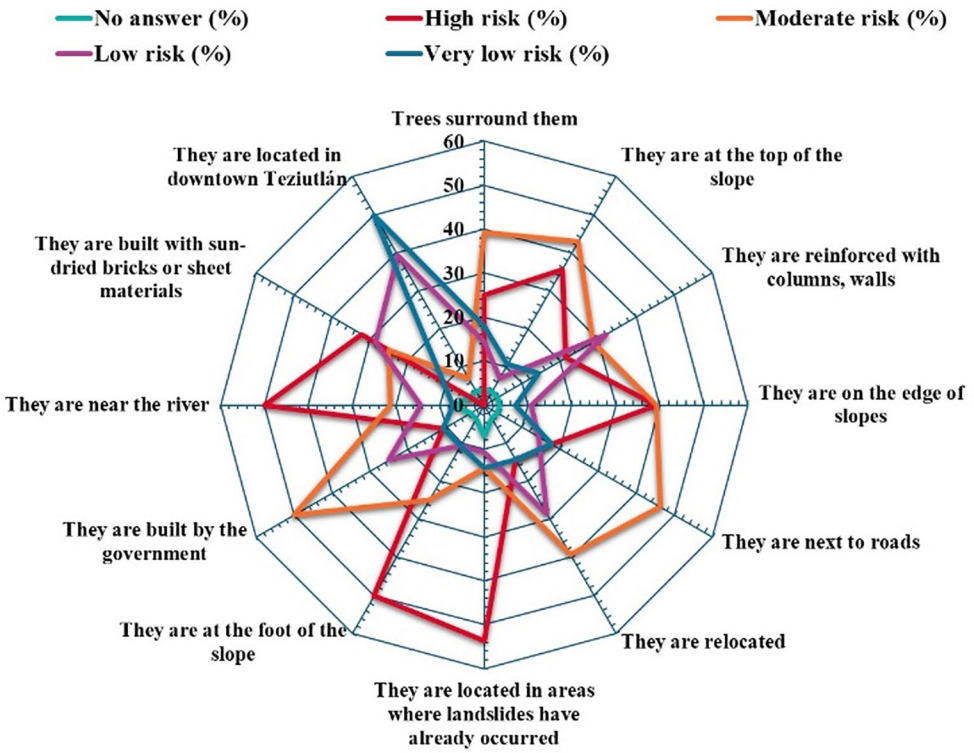


Fig. 5 Perception of the degree of risk homes have of being affected by landslides

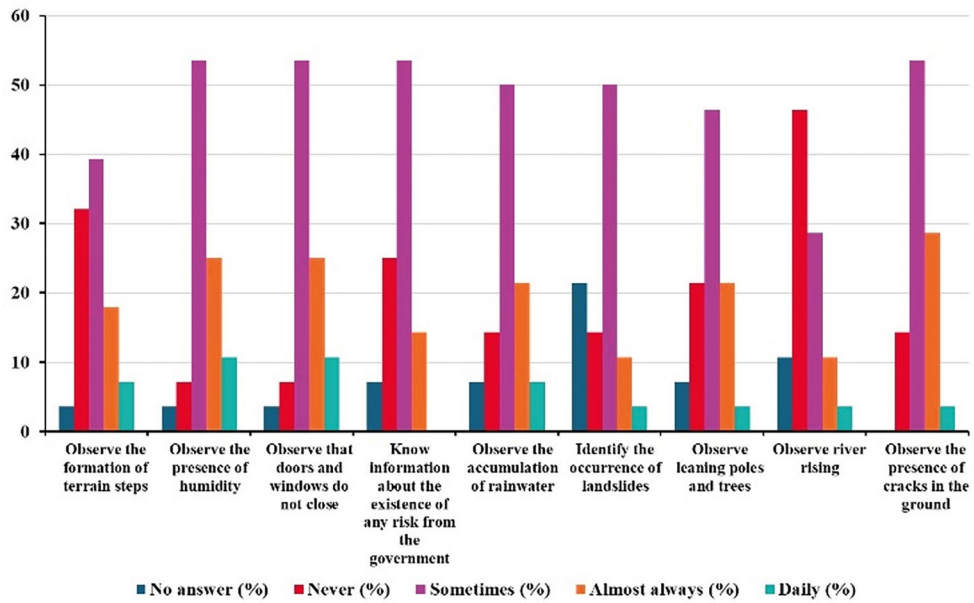


Fig. 6 Frequency with which landslide preparedness actions were undertaken during the pandemic

and the possibility of blocking evacuation routes (32.1%). Interestingly, most students felt that the possibility of a loss of life is low (57.2%) and that their neighbourhood is unlikely to be affected (57.2%). However, some students (35.7%) felt that areas that have experienced landslides could be at risk again. Finally, almost 40% of surveyed students reported believing their homes have not experienced any damage or loss.

Approximately 53.6% of the students felt adequately prepared for a landslide. About 39.3% of the students agreed that their neighbours were participating in protecting the neighbourhood in case of disasters. However, only 32.1% of the students decided that their neighbourhood was prepared for emergencies. In contrast, 32.1% of the students disagreed with this statement. About 57.2% of the students believed

their neighbourhood is well-organized to face disasters that may arise from a landslide.

(e) *Information and media*

According to students' feedback, before the outbreak of the pandemic, the frequency at which they received information regarding preventive measures against potential hazards, namely earthquakes, rains, fires, and landslides, was reported to be 50%, 60.7%, 57.1%, and 64.3%, respectively (see Fig. 7).

During the pandemic, students reported receiving information about COVID-19 prevention measures daily (53.6%), while information about earthquakes (53.6%), rains (50%), landslides (57.1%), and fires (71.4%) was received sometimes.

Since the onset of the pandemic, a discernible decline in the dissemination of information regarding landslides was perceived across various age cohorts. Amongst young adults aged 18–25 years, the proportion of respondents indicating occasional receipt of such information dropped to 46.4%, while those who never received it increased to 21.4%. Similarly, in the adult group aged 26–35, the share of people who occasionally receive information declined to 7.1%, with no change in the proportion of those who never received it. The middle-aged group aged 36–38 also experienced a decrease in the frequency of information receipt, with only 3.6% indicating occasional receipt and none indicating never receiving it (Table 3).

(f) *Communication of the population with stakeholders*

Regarding how responsible the authorities and community were perceived to be in addressing the occurrence of landslides, 57.1% of students believed that Civil Protection held a high level of responsibility. On the other hand, the municipal government (39.3%), health personnel (39.3%), and the community (32.1%) were considered to hold a fair degree of responsibility.

The survey revealed that 42.9% of the respondents considered the municipal government's action response in case of landsliding before the COVID-19 pandemic to be good. In addition, 35.7% of the participants perceived civil protection, the State Government, and the Community to respond well.

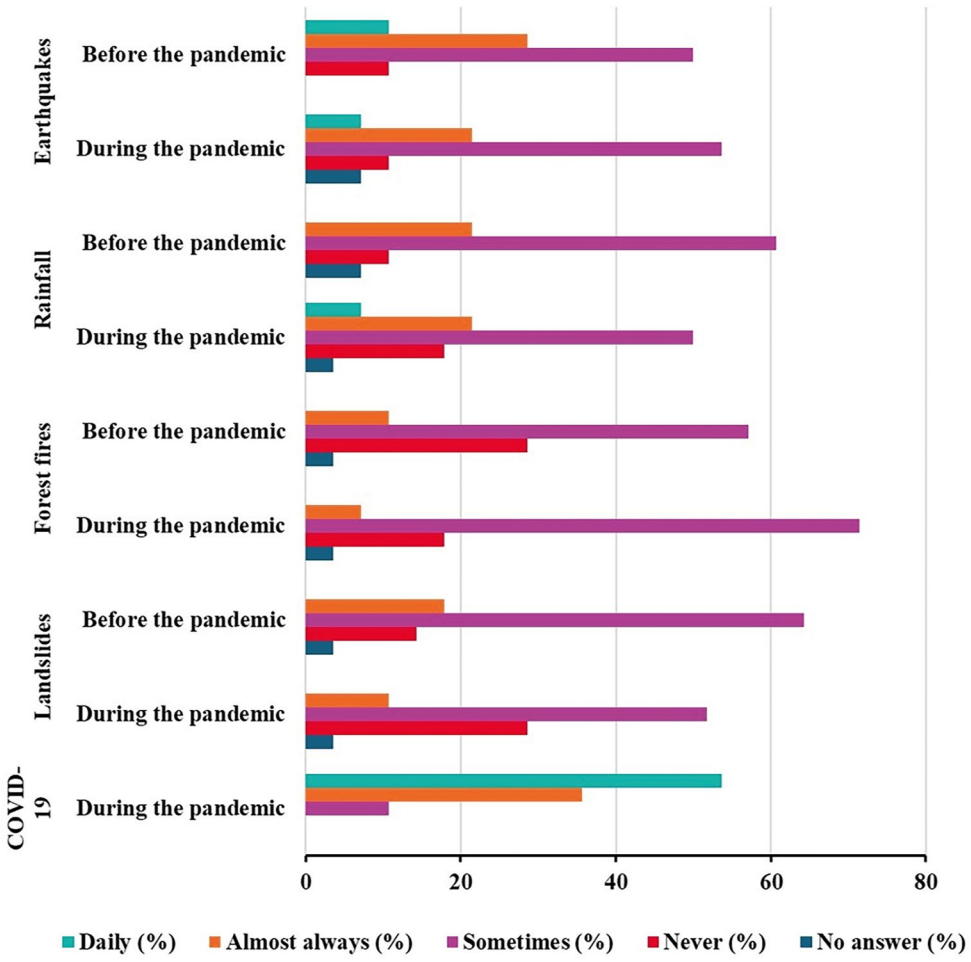


Fig. 7 Perception of the quality of information received from the authorities through the media about hazards that occurred before and during the pandemic

Table 3 Perception of the information received from the authorities about landslides before and during the pandemic

Age (years)	18–25	26–35	36–38
	Before the pandemic		
No answer	3.6%	0.0%	0.0%
Always	0.0%	0.0%	0.0%
Almost always	17.9%	0.0%	0.0%
Sometimes	53.6%	7.1%	3.6%
Never	7.1%	7.1%	0.0%
	After the pandemic		
No answer	3.6%	0.0%	0.0%
Always	0.0%	0.0%	0.0%
Almost always	10.7%	0.0%	0.0%
Sometimes	46.4%	7.1%	3.6%
Never	21.4%	7.1%	0.0%

Meanwhile, 32.1% of the survey participants considered health personnel and the Red Cross satisfactory. The response of civil protection and health personnel to landslides during the pandemic was perceived to be effective.

6 Concluding Remarks

One of the main limitations of this study is that the responses from the London School are not representative of the entire population. Nonetheless, while this type of research may not be statistically generalizable, it complements quantitative research and enriches understanding of landslide risk perception factors. Moreover, non-representative research can provide important insights for larger studies and help refine research questions. Even if the sample size does not represent the entire population, it can offer valuable insights into specific groups or communities. By focusing on a particular geographic location or demographic, such as students, relevant and practical findings can enhance disaster preparedness.

It is important to note that disaster risk perception is influenced by culture, history, and the local environment. This means non-representative research can provide context-specific insights for targeted interventions and policies in specific regions.

Conducting disaster risk perception research has practical implications for disaster management and resilience-building. The findings can aid in creating better risk communication strategies, evacuation plans, and community resilience programs.

To conduct adequate studies on risk perception, a thorough understanding of the approach, objective, and key factors involved is crucial due to multiple theoretical perspectives. This article used the psychometric approach, which offers insight into the mental heuristics and emotional factors that impact risk perception. However, it is essential to note that the data collected from a small sample of young individuals in Teziutlán cannot be generalised to the entire population. These results only represent a small portion of the population and their perceptions of disaster risk associated with landslides. The study considered various factors to understand the participants' perceptions, including experience, preparedness, communication, and trust with management actors.

Recognising that individuals' understandings are influenced by the information they receive from internal and external sources, regardless of age, is crucial. Additionally, the media and emotions play a significant role in shaping these perceptions.

Despite facing challenges during the pandemic, the young scholars of London University felt equipped with the necessary knowledge, assistance, and resources to handle potential hazards like landslides. However, preparedness was primarily focused on disaster response. This emphasises the importance of developing effective disaster risk communication strategies that consider diverse elements to understand the social construction of disaster risk, particularly in areas susceptible to landslides and other hazards, in which vulnerability and exposure conditions are increasing.

Understanding the risks of living near landslides can enable students and school staff to be more aware of potential hazards. This awareness can lead to preparedness measures to reduce disaster risks and prevent disasters.

Landslide risks can be reduced within school communities by educating students about the underlying causes, drivers, warning signs, and preparedness measures. Such education promotes a safety culture and equips students with the knowledge to take appropriate actions to reduce their vulnerability.

Schools serve as community hubs, and educating students about landslide risks can extend this knowledge to families and neighbours. This broader dissemination of information and knowledge can increase community awareness, preparedness, and collective action to address landslide disaster risk.

Students who possess an understanding of the risks associated with living in proximity to landslides have the poten-

tial to act as advocates for policy measures aimed at reducing vulnerability to such hazards. By increasing awareness and advocating for such policies, they can play a crucial role in influencing local authorities to implement zoning regulations, land-use planning, and infrastructure improvements that may help to reduce landslide risks.

Understanding students' perceptions of landslide risk in schools is imperative for fostering a safer environment, building awareness, promoting preparedness, and advocating for measures to mitigate landslide hazards in the community.

Acknowledgements We thank DGAPA-UNAM for providing financial support to conduct landslide risk research through Project PAPIIT IN300823. Thanks to the National Council of Humanities, Sciences, and Technologies (CONAHCYT), who provided a student fellowship for Karla M. Hernández-Cadena.

References

Alcántara-Ayala I, Garnica-Peña R, Murillo-García FG et al (2018) Landslide disaster risk awareness in México: community access to mapping at local scale. Landslides 1-14:1691–1704. https://doi.org/10.1007/s10346-018-1010-4

Alcántara-Ayala I, Moreno AR (2016) Landslide risk perception and communication for disaster risk management in mountain areas of developing countries: a Mexican foretaste. JMtSci 13(12):2079–2093. https://doi.org/10.1007/s11629-015-3823-0

Amaya J, Serrano I, Cantillo V et al (2024) Implications of trust, preparedness, risk perceptions, and local context on deprivation costs and disaster relief planning. Socio-Econ Plann Sci 91:101780. https://doi.org/10.1016/j.seps.2023.101780

Atreya A, Czajkowski J, Botzenb W et al (2017) Adoption of flood preparedness actions: a household level study in rural communities in Tabasco, Mexico. Int J Disaster Risk Reduct 24:428–438. https://doi.org/10.1016/j.ijdrr.2017.05.025

Börner S (2023) Emotions matter: EMPOWER-ing youth by integrating emotions of (chronic) disaster risk into strategies for disaster preparedness. Int J Disaster Risk Reduct 89:1–12. https://doi.org/10.1016/j.ijdrr.2023.103636

Brilly M, Polic M (2005) Public perception of flood risks, flood forecasting and mitigation. Nat Hazards Earth Syst Sci 5:345–355. https://doi.org/10.5194/nhess-5-345-2005

Calvello M, Nicolina M, Pratschke J et al (2016) Landslide risk perception: a case study in southern Italy. Landslides 13:349–360. https://doi.org/10.1007/s10346-015-0572-7

Cohen-Salgado D, García-Frapolli E, Mora F et al (2021) How does social capital shape the response to environmental disturbance at the local level? Evidence from case studies in Mexico. Int J Disaster Risk Reduct 52:101951. https://doi.org/10.1016/j.ijdrr.2020.101951

DiBella J, Burch S (2023) Building parliamentary capacities for advancing the disaster risk reduction agenda: note and reflections from a capacity-building field training for parliamentarians of the Americas and the Caribbean. Int J Disaster Risk Reduct 96(1):103970. https://doi.org/10.1016/j.ijdrr.2023.103970

Douglas M, Wildavsky A (1982) Risk and culture. An essay on the selection of technological and environmental dangers. University of California Press, Berkeley. https://books.google.com.mx/books?id=rXrGbnMg63YC&printsec=frontcover&source=gbs_ge_summary_r&cad=0#v=onepage&q&f=false

Finlay PJ, Fell R (1996) Landslides: risk perception and acceptance. Can Geotech J 34:169–188

Fischhoff B, Slovic P, Lichtenstein S et al (1978) How safe is safe enough? A psychometric study of attitudes toward technological risks and benefits. Policy Sci 9:127–152. https://link.springer.com/article/10.1007/BF00143739

Hernández-Moreno G, Alcántara-Ayala I (2017) Landslide risk perception in Mexico: a research gate into public awareness and knowledge. Landslides 14:351–371. https://doi.org/10.1007/s10346-016-0683-9

Hlekiwe K, Ira H, Rikka-Leena L et al (2022) Are preparedness índices reflective of pandemic preparedness? A COVID-19 reality check. Int J Disaster Risk Reduct 77:1–14. https://doi.org/10.1016/j.ijdrr.2022.103074

INEGI (2010) Compendio de información geográfica municipal de los Estados Unidos Mexicanos. In: Teziutlán: Instituto Nacional de Geografía y Estadística. In Spanish, pp 1–10. https://www.inegi.org.mx/contenidos/app/mexicocifras/datos_geograficos/21/21174.pdf

INEGI (2020) México en cifras. Teziutlán, Puebla. https://www.inegi.org.mx/app/areasgeograficas/?ag=070000210174#collapse-Indicadores

Landeros-Mugica K, Urbina-Soria J, Alcántara-Ayala I (2016) The good, the bad and the ugly: on the interactions among experience, exposure and commitment with reference to landslide risk perception in México. Nat Hazards 80:1515–1537. https://doi.org/10.1007/s11069-015-2037-7

Murillo-García FG, Gárnica RJ, Alcántara-Ayala I (2017) Factores condicionantes de la susceptibilidad a PRM. In: Alcántara-Ayala I, Garnica-Peña RJ, Coll-Hurtado A, MacGregor MT (eds) Inestabilidad de Laderas en Teziutlán, Puebla. Factores inductores del riesgo. UNAM, Instituto de Geografía, pp 1–223

Muttarak R, Lutz W (2014) Is education a key to reducing vulnerability to natural disasters and hence unavoidable climate change? Ecol Soc 19(1):1–9. https://www.jstor.org/stable/26269470

O'Donnell EC, Lamond JE, Thorne CR (2018) Learning and action Alliance framework to facilitate stakeholder collaboration and social learning in urban flood risk management. Environ Sci Policy 80:1–8. https://doi.org/10.1016/j.envsci.2017.10.013

Slovic P (2000) Perception of risk. The perception of risk. 220–231

Travieso AC, Frausto O, Hernández ML et al (2023) Comprehensive risk management of hydrometeorological disaster: a participatory approach in the metropolitan area of Puerto Vallarta, Mexico. Int J Disaster Risk Reduct 87:103578. https://doi.org/10.1016/j.ijdrr.2023.103578

UNISDR (2015) Sendai framework for disaster risk reduction 2015–2030. United Nations international strategy for disaster reduction http://www.wcdrr.org/uploads/Sendai_Framework_for_Disaster_Risk_Reduction_2015-2030.pdf. Accessed Jan 24 2024 (Accessed on 29 February 2024)

Van der Molen F (2018) How knowledge enables governance: the coproduction of environmental governance capacity. Environ Sci Policy 87:18–25. https://doi.org/10.1016/j.envsci.2018.05.016

Open Access This chapter is licensed under the terms of the Creative Commons Attribution 4.0 International License (http://creativecommons.org/licenses/by/4.0/), which permits use, sharing, adaptation, distribution and reproduction in any medium or format, as long as you give appropriate credit to the original author(s) and the source, provide a link to the Creative Commons license and indicate if changes were made.

The images or other third party material in this chapter are included in the chapter's Creative Commons license, unless indicated otherwise in a credit line to the material. If material is not included in the chapter's Creative Commons license and your intended use is not permitted by statutory regulation or exceeds the permitted use, you will need to obtain permission directly from the copyright holder.



Analytical Hierarchical Process (AHP) Prioritization of Landslide-Causing Factors

A. A. Virajh Dias and A. A. Jagath Gunathilake

Abstract

Prioritization of factors responsible for a landslide trigger is an essential process in landslide susceptibility analysis. This allows the researcher to recognize how important each factor is. If time or resources are short, the least important factors may have to be left out. This paper aims to employ Analytical Hierarchical Process (AHP) to prioritize factors responsible for landslide susceptibility analysis. The AHP methodology will be utilized to analyze and rank the relative importance of various factors influencing landslides. This was based on old landslide data and also considering sensitivity of occurrences. The results classifying to five number of classes with the ArcGIS facility and occurrences of landslide under each category. The overall assessment is based with the 39 number of old landslides selected and verified at site. In such situation more than 84.6% of landslides fall in the category of moderate susceptibility to high susceptibility. The results will provide valuable insights into the factors that require immediate attention for mitigating landslide incidences.

Keywords

Landslides · AHP · Geology · Landuse · Hydrology · First order streams · Rainfall · Road buffer · Multi-Criteria Analysis (MCA) · Susceptibility index (SI)

A. A. V. Dias (✉)
Central Engineering Consultancu Bureau, Colombo 7, Sri Lanka

Postgraduate Institute of Science, University of Peradeniya, Peradeniya, Sri Lanka
e-mail: phd23940@pgis.lk

A. A. J. Gunathilake
Post Graduate Institute of Science, Engineering Geology Research Group (EGRG), Department of Geology, University of Peradeniya, Peradeniya, Sri Lanka

1 Introduction

Landslides are a significant natural hazard that poses threats to lives, infrastructure, and the environment. Identifying and understanding the key factors contributing to landslides can aid in better land management and risk reduction strategies.

Predicting potential landslides scientifically involves considering several key factors, including soil density, pore pressure, angle of internal friction, soil properties, geometry, and external triggers (Carrara 1983; Cruden and Varnes 1996).

Unexpected and frequent landslide disaster events have been recorded in the Ratnapura District of Sri Lanka for the past few decades. These events followed the largest disaster ever recorded in the country's history in May, 2003 involving floods and landslides. Heavy rains, accompanied by strong winds, are shown to have set a record for the highest recorded rainfall in the Ratnapura district, as depicted in Fig. 1. This catastrophic event resulted in an estimated 247 casualties, over 200,000 families displaced, thousands of

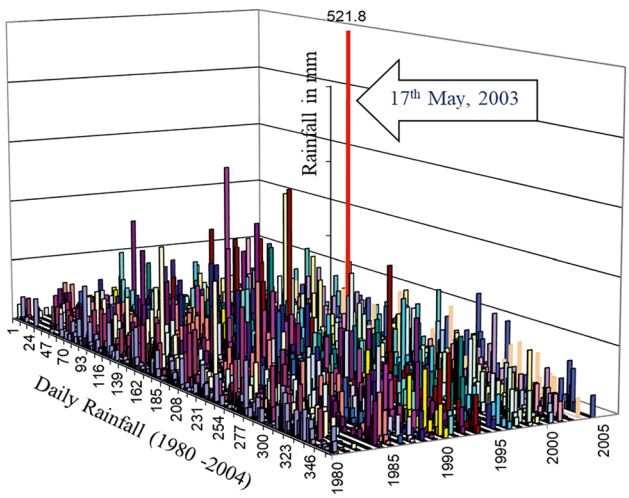


Fig. 1 Daily Rainfall of Kalawana divisional area during the period of 1980–2003. The figure indicates the maximum rainfall of 521.8 mm occurred in 17th May 2003

© The Author(s) 2025

B. Abolmasov et al. (eds.), *Progress in Landslide Research and Technology, Volume 3 Issue 2, 2024*, Progress in Landslide Research and Technology, https://doi.org/10.1007/978-3-031-72736-8_3

houses damaged, and essential infrastructure facilities completely destroyed (CECB Report 2003). The worst affected areas were the Kalawana division of the Ratnapura district and parts of the Galle, Matara, Kalutara, and Hambantota districts. Landslides were reported in villages along the Colombo-Ratnapura Road, including Ratnapura, Elapatha, Thotagamuwa, Hangamuwa, Palawela, Dambuluwana, Karangoda, Muwagama, Godigamuwa, and Getangama. More than 140,000 people were evacuated to schools and temples, and helicopters dropped emergency rations in villages that were cut off from assistance (Dias and Gunathilaka 2014).

2 Judgment Based Direct Evaluations

The catastrophic events resulted in numerous buildings becoming submerged, tragically leading to the burial of several individuals due to landslides (CECB Report 2003). Landslides were widespread and highly variable from one location to another in the Ratnapura District, as shown in Fig. 2. The highest concentration of landslides occurred in the Kalawana division, which includes poorly managed plantation areas, forested regions, highly urbanized areas with unlined roads, and improperly constructed roads on steep slopes (Dias and Gunathilaka 2014).

Notably, a significant response came from a voluntary group of professionals known as the "Operation Professional Combine (OPC)" (CECB Report 2003), who took immediate action to investigate landslide damage. This action was an obligation of the emergency management action plan proposed by the Central Engineering Consultancy Bureau (CECB) at the council meeting of the Disaster Management Committee held in Colombo on May 28, 2003. The OPC consisted of hundreds of academics, professionals, and volunteers from various backgrounds, coming together for the first time in recent history.

The objective of the study is to provide a comprehensive summary of the destruction caused by landslide activities in the Ratnapura District, propose recommendations to mitigate further crises, and establish a foundation for the next costly phases in disaster-prone areas. The assessment focused on a total of 316 reported landslides in the Ratnapura District, Sri Lanka. The field operation was completed within 2 weeks, owing to twenty-four-hour hard work, dedication, and commitment from the members of OPC. It was a truly challenging task under the most difficult terrain and weather conditions. Their dedication in the face of a national disaster is remarkable. The overall study revolved around assessing the geological and geotechnical validity (Dias et al. 2014) and identifying the extent of landslide hazards. Conversely, well-managed areas experienced the least impact (Dias 2018).

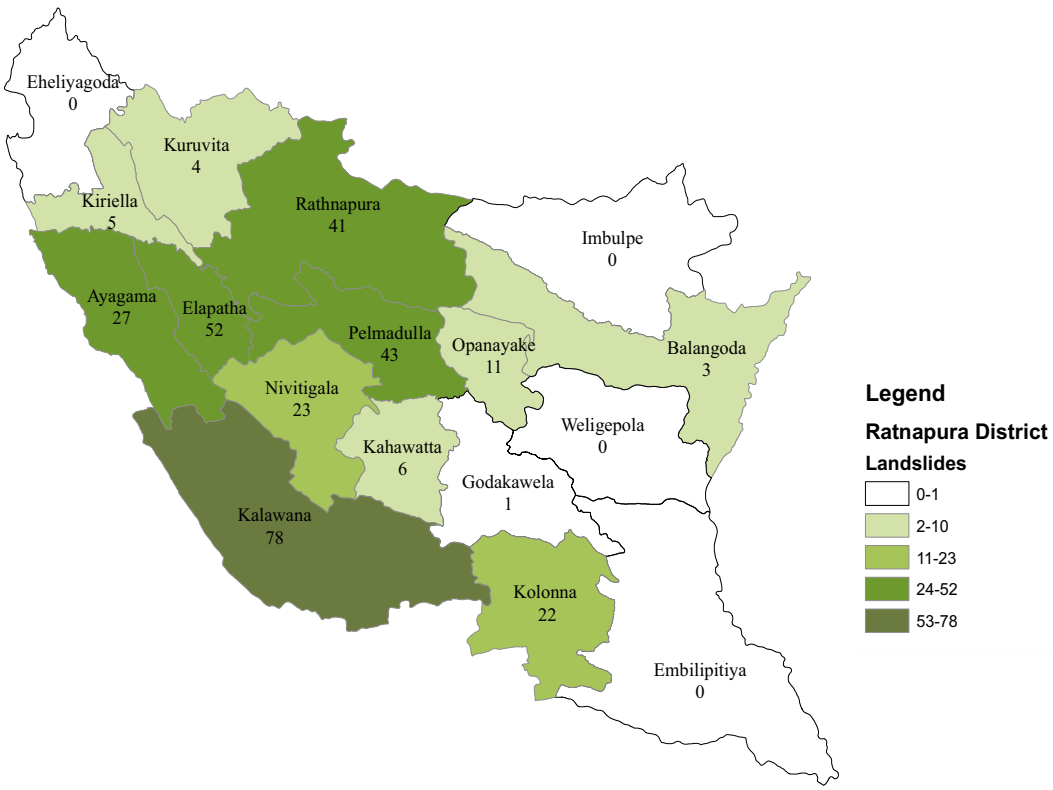


Fig. 2 In May 2003, a landslide vulnerability map of the Ratnapura District was created based on judgments under emergency conditions and the highest count recorded in the Kalawana Division area is prompted further evaluations

2.1 Relative Importance under Emergency

The final report of the OPC provided a summary of categorized judgments made under landslide emergency situations caused by extreme rainfall events. Among the 316 landslide cases examined (Dias and Gunathilaka 2014), 139 were designated as high-risk zones, necessitating the immediate evacuation of 754 families. Additionally, 73 moderate-risk zones prompted warnings for 496 families, while 101 low to very low-risk zones raised awareness of landslide susceptibility among 441 families concerning potential landslide risks (CECB Report 2003), potentially leading to a reconsideration of their original localities as a suitable for resettlements (Dias and Gunathilaka 2014).

3 Use of Multi Criteria Analysis

Multi-Criteria Analysis (MCA) is a widely used methodology in landslide susceptibility assessment (Bhushan and Ria 2004), as depicted in Fig. 3. It is a systematic approach that combines multiple factors or criteria to evaluate the likelihood of landslides occurring in a particular area. Multi-Criteria Assessment (MCA) is a broader framework that encompasses various methods, including the Analytical Hierarchy Process (AHP) (Saaty 1994a, b, 2008), which is one of the techniques used within MCA. The choice between MCA and AHP depends on the specific decision problem, the need for transparency, and the complexity of the criteria and alternatives (Carrara 1983). AHP is particularly well-suited for structuring complex problems and ensuring consistency in decision-making, while MCA offers greater flexibility and comprehensiveness in handling a wide range of decision contexts.

4 Analytic Hierarchy Process (AHP)

Analytic Hierarchy Process (AHP) is a quantitative technique for multiple criteria decision-making (Saaty 1994a, b; Saaty 2000). It provides a convenient way to quantify qualitative aspects, thus eliminating subjectivity in the outcome. AHP includes a process for making pairwise comparisons to determine the relative importance of criteria. This process helps ensure that the judgments made by decision-makers are consistent and free from inconsistencies. This means that the AHP approach is a semi-quantitative method in which decisions are made by applying weightings through relative pairwise comparisons, with inconsistencies in the decision-making process (Saaty 1980).

The process involves the following steps:

- Problems are decomposed into a hierarchy of criteria and alternatives.

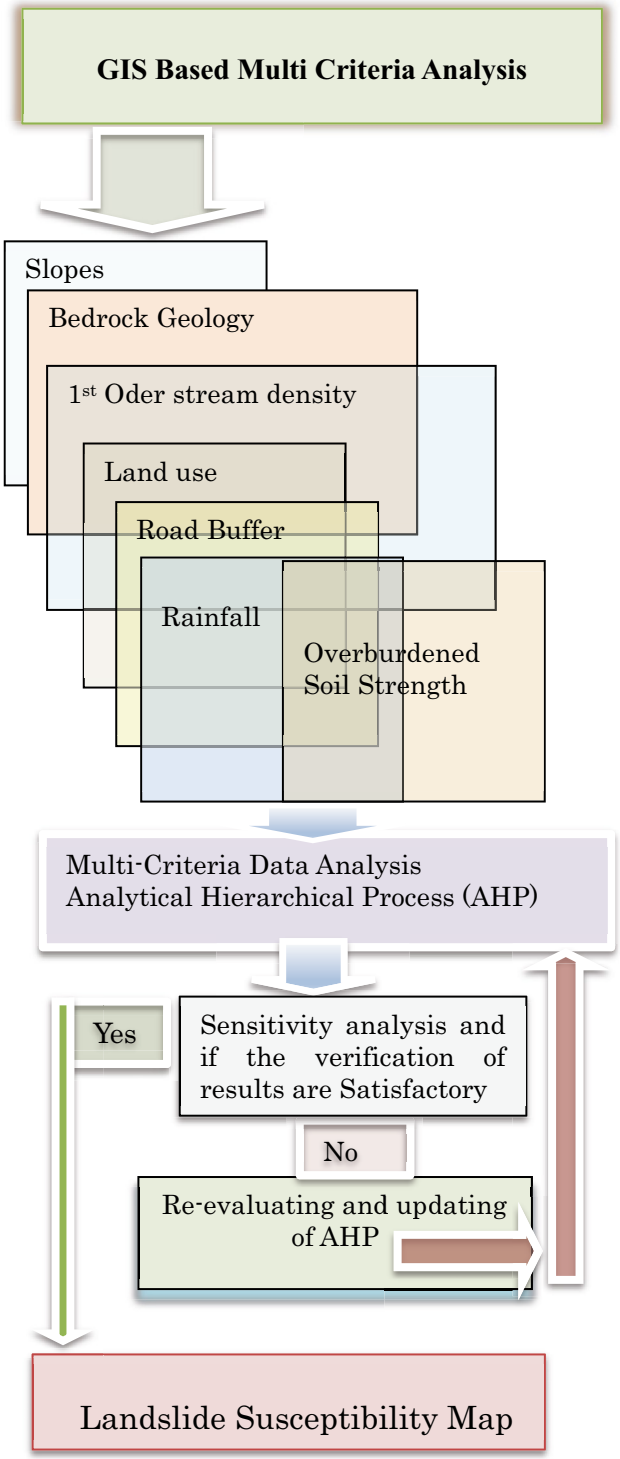


Fig. 3 A schematic diagram illustrates a systematic approach that combines multiple factors or criteria (Multi-Criteria Analysis) with the use of AHP to assess the likelihood of landslides

- Information is then organized in a hierarchical tree, as shown in Table 5, using quantitative values from 1 to 9.
- Assignment of numeric values is carried out to determine the relative importance of each factor according to its subjective relevance.

- Configuration of a comparison matrix.
- Calculation of the normalized main eigenvector, which provides the weight factor up to that point.

The eigenvalue approach investigates the dominance of a solution. It assumes that small perturbations in a consistent matrix induce small changes in the priorities. For each level of the hierarchy, calculate the eigenvector associated with the highest eigenvalue (Saaty 2000). This eigenvector represents the relative priority weights of the criteria or alternatives.

5 Area Selected for Landslide Susceptibility Assessment

The research study area is located in Kalawana sub division (DS division) of the Ratnapura district in Sri Lanka. The selected area lies between 6°35'30" N to 6°22'20" N and 80°38'25" E to 80°17'23"E. The study area belongs to three major perennial watersheds, within the Kalawana Watershed. Geomorphology of the area including many tributaries are illustrated in Fig. 4.

6 Landslide-Causing Factors

The prioritization of factors responsible for triggering landslides is a critical step in landslide susceptibility analysis (Campbell 1975). The computation of slope stability involves a range of intrinsic and extrinsic variables (Dias et al. 2014), which require input from various sources, including geomorphological (rainfall, catchments, streams), geological (rocks and soil), geotechnical (shear strength variables), and land use (social and environmental) data for the evaluation of the factor of safety. These factors encompass slope (S), rainfall and precipitation potential (R), hydrology (H): considering the number of 1st order streams within the selected catchment, road buffer (RB): the boundary demarcating from the center of the road, bedrock geology (BG) : considering dipping and foliation issues, shear strength of the top overburdened soil

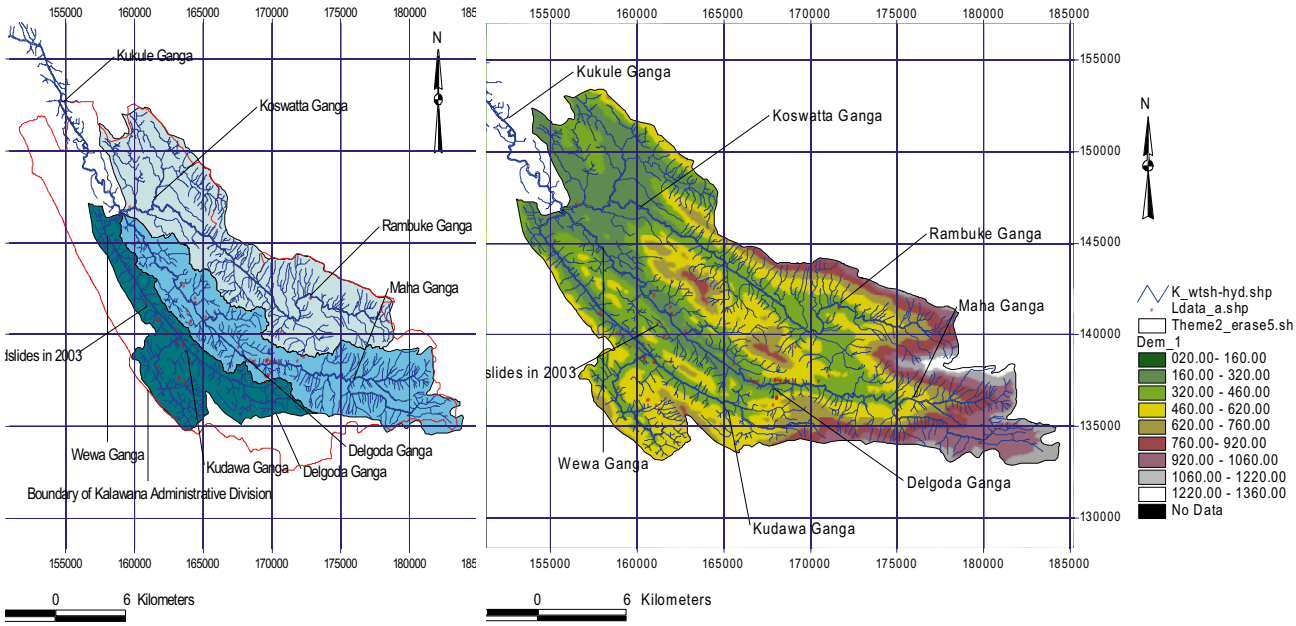


Fig. 4 Geomorphology of the area which shows major tributaries and elevation differences within the study area, Kalawana Division of Rathnapura District, Sri Lanka

(SS), and land use (L) :the most significant social and environmental issues.

7 Geology and Geomorphology

Heavy rain saturates the soil, causing it to become a slurry of water, rocks, and debris, which flows rapidly down slopes, often with devastating consequences (Campbell 1975). The characteristics of the underlying bedrock play a significant role in determining the susceptibility of an area to landslides and the potential for recurrent incidents (Cooray 1994) over time as in the Fig. 5.

In addition, bedrock integrity, orientation and similar key geological factors related to bedrock condition (Dias et al. 2014) are essential for assessing landslide stability and those usually recognized in Table 1.

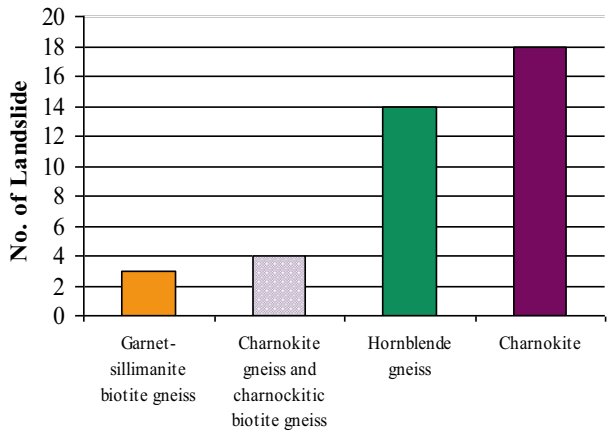


Fig. 5 Statistical interpretation of Bedrock Geology map and significance of Landslide in Kalawana Watershed

8 Critical Slopes and Soil Strength

The occurrence of landslides in relation to slope was studied based on field data collected in the Kalawana administrative division in the Ratnapura district, as presented in Table 2. Understanding the impact of slope class is essential for assessing landslide susceptibility and implementing measures to mitigate landslide risks in vulnerable areas (Dias 2018). The contribution of slope class to the activation of landslides is a crucial factor in comprehending and predicting landslide occurrences. Different slope classes, including gentle slopes, moderate slopes, and steep slopes, significantly influence when and where landslides are more likely to occur. Moderate slopes, typically ranging from 12 to 32 degrees, are statistically more susceptible to landslides due to their composition (Dias et al. 2014), often consisting of colluvium and deposited material. These slopes may appear stable to the human eye but can be easily destabilized by factors such as heavy rainfall or seismic activity (Vitanage 1994).

Table 2 Statistical distribution of landslides occurrence in different Slope Category based on observations, 2003

Slope Category in Degrees	Slope Class	No of Landslides
0–11	1	5
12–21	2	19
22–31	3	11
32–41	4	3

Table 1 Geological factor responsible for destabilization of soil and rock slopes

Sub factor	Description
Bedrock type	Different types of bedrock, have varying degrees of susceptibility to weathering and erosion. Assessing the type of bedrock helps in understanding its resilience to external forces
Bedrock integrity	The structural integrity including presence of fractures, faults, or bedding planes can weaken the bedrock, making it more susceptible to landslides.
Weathering and alteration	The extent of weathering and alteration in the bedrock can greatly affect its stability. Highly weathered or altered bedrock is generally less resistant to landslides.
Bedrock depth	The depth of bedrock beneath the soil and regolith layers is important. Shallow bedrock can increase the likelihood of landslides, especially in areas with heavy rainfall.
Bedrock orientation	The orientation of bedding planes and fractures in the bedrock can influence the direction and type of landslides that may occur.
Hydrogeological conditions	Bedrock can act as an aquifer or a barrier to groundwater flow. Understanding the hydrogeological properties of the bedrock is crucial, as changes in groundwater levels can trigger landslides.
Geotechnical properties	The geotechnical properties of the bedrock, including its strength and deformation characteristics, are essential for assessing landslide potential.

9 Rainfall and Hydrology

One of the challenges in approaching rainfall-triggering relationships (Bhandari and Dias 1996) at a regional scale is that prevailing precipitation regimes are not suitably represented due to limitations in the number of rain gauge data within the study area. As a result, the rainfall intensity-duration threshold representing the landslide triggering relationships across this region did not properly developed for the sensitive areas of the Kalawana Division. The present state of the study considered the statistical distribution of daily rainfall over a 23-year record, to create a precipitation potential and trend that could be compared across morphologies and landslide events.

9.1 Flow Regime of Streams

The general topography is consisting of ridges and valleys with steep slopes. Maha Ganga, Rambuke, Gannga and Kudawa Ganga initiated from this Rakwana Massif which overlook the middle peneplane. A large number of streams arise in the area and drainage occurs in a rectangular "trellis" pattern (Dias and Gunathilaka 2014). The streams on the southern side form the headwaters of the Gin Ganga while those on the Kukulu Ganga, a major tributary of the Kalu Ganga (Cooray 1994). The ridges are heavily dissected by first and second order streams connected to the three major tributaries of Koswatta Ganga, Delgoda Ganga and Wewa Ganga as shown in Figs. 6, 7 and 8 and evaluation is given in the Fig. 9.

9.2 3 Day-Cumulative Rainfall in a Sub Watershed

Establishing threshold values for cumulative rainfall is crucial. Different regions may have different thresholds beyond which the risk of landslides significantly increases (Bhandari and Dias 1996). Historical data and local expertise can help determine appropriate thresholds for triggering landslide events.

The study aims to assess the sensitivity of a 3-day cumulative rainfall, which indirectly influences the potential for ground stability saturation. The project area is situated in intermediate wet zone which receives average annual rainfall of 2564 mm to 5005 mm. Daily rainfall data of 1981–2004

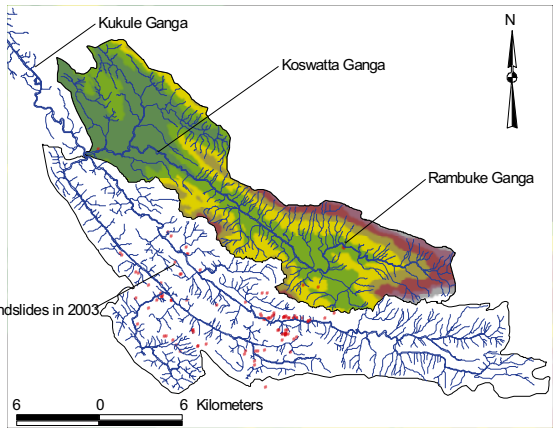


Fig. 7 Geomorphology of the major sub watersheds of the Delgoda Ganga of the Kukuleganga Watershed

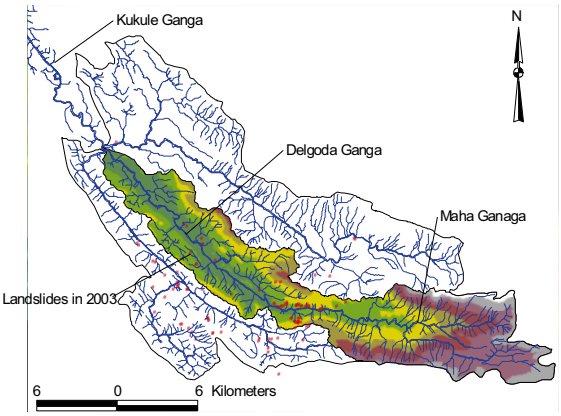


Fig. 6 Geomorphology of the major sub watersheds of the Koswatta Ganga of the Kukuleganga Watershed

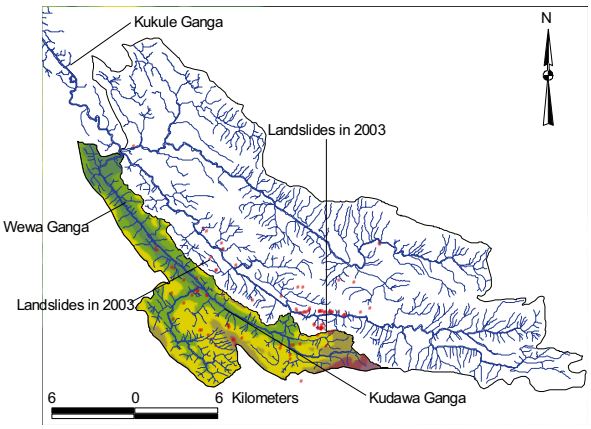
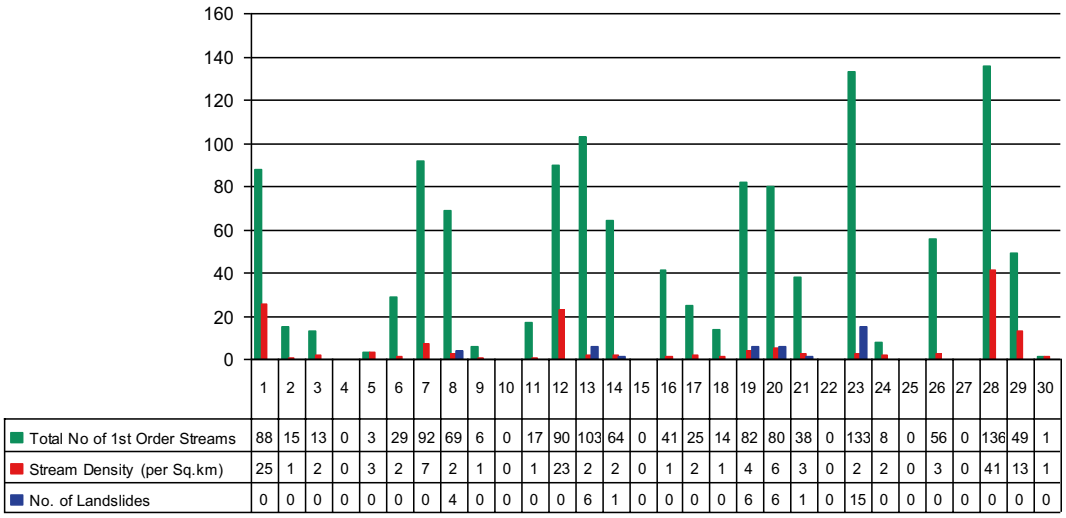


Fig. 8 Geomorphology of the major sub watersheds of the Wewa Ganga of the Kukuleganga Watershed



	1	2	3	4	5	6	7	8	9	10	11	12	13	14	15	16	17	18	19	20	21	22	23	24	25	26	27	28	29	30
Total No of 1st Order Streams	88	15	13	0	3	29	92	69	6	0	17	90	103	64	0	41	25	14	82	80	38	0	133	8	0	56	0	136	49	1
Stream Density (per Sq.km)	25	1	2	0	3	2	7	2	1	0	1	23	2	2	0	1	2	1	4	6	3	0	2	2	0	3	0	41	13	1
No. of Landslides	0	0	0	0	0	0	0	4	0	0	0	0	6	1	0	0	0	0	6	6	1	0	15	0	0	0	0	0	0	0

Fig. 9 Relationship with the first order stream density and landslide occurrence in Kalawana Watershed

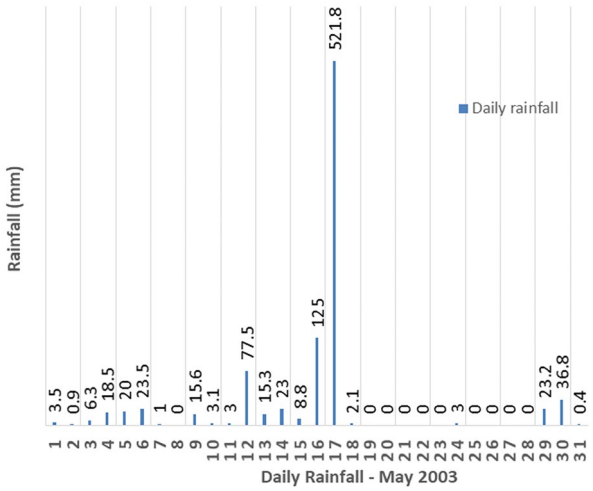


Fig. 10 Daily rainfall in Kalawana area for the month of May 2003

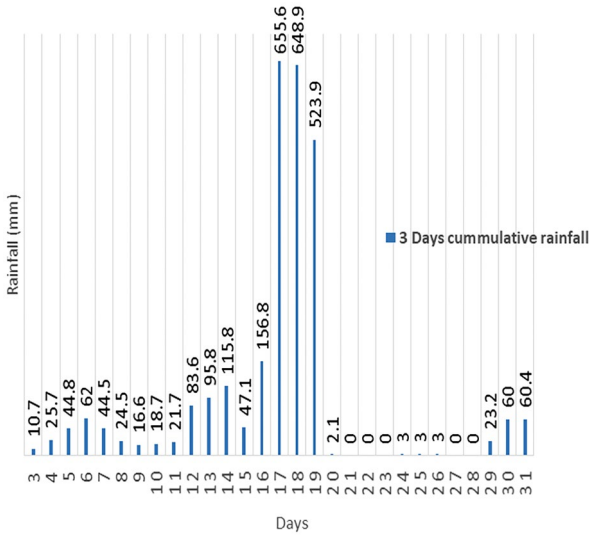


Fig. 11 Three-day antecedent rainfalls (every bar is sum of three-day rainfall) were about 655.6 mm just prior to the landslide event and was the highest since 1947

(i.e. 23 years) at Kudawa gaging station was used for the study area. Evaluation of average daily rainfall, mean monthly rainfall and annual precipitation details are based on Kudawa rainfall data. The mean annual rainfall of the area is 4085 mm. And it indicates the maximum rainfall of 522 mm occurred in May 2003. In the late 1980's when information was scanty, the landslide triggering threshold was placed at 200 mm of rainfall within a 72 h period, provided that the rain in the area continued (Bhandari and Dias 1996). Therefore, maximum of three-day cumulative rainfall distribution patterns are shown in the Figs. 10 and 11. The accumulated rainfall during this event exceeded the threshold limits for shallow landslide triggering (Bhandari and Dias 1996).

Intense rainfall infiltrates the soil, reducing its cohesion, and leads to surface erosion and shallow landslides. Debris flows, also known as mudslides (Cooray 1994), are a common type of landslide in Sri Lanka during heavy rainfall. They often occur in steep terrains with loose soil or unconsolidated materials (Varnes 1978).

Besides cumulative rainfall, the intensity and duration of rainfall events also influence landslide susceptibility. Short-duration, high-intensity rainfall can trigger landslides even with relatively lower cumulative rainfall (Bhandari and Dias 1996), especially in areas with steep slopes and susceptible geology.

The planar failure and circular behavior are prominent in landslides in clay soil and residual soils and depths of failure circles usually do not exceed 4 to 6 M (Bhandari, et al., 1996). Those continue to exhibit intermittent, relatively slow

deformations with limited mobility. The antecedent soil moisture conditions are vital in landslide assessment (IUGS 1997). Heavy rainfall on already saturated or moist soils increases the likelihood of landslides. Therefore, monitoring soil moisture levels before and during rainfall events is essential for accurate assessment.

Incorporating rainfall data into early warning systems can improve landslide risk management. Real-time monitoring of rainfall, coupled with landslide susceptibility models, can help forecast landslide events and trigger timely evacuation or mitigation measure (Dias and Gunathilaka 2014).

A devastated landslide has been reported to be occurred killing 7 people and destroying 8 houses with extremely rapid flow slides having various combination of soils and rock as in the Weddagala, Pothupitiya, occurred in Kalawana division in May, 2003 as shown in the Fig. 12. Rainfall may not be uniformly distributed across a watershed, that leading to variations in landslide susceptibility within the sub watershed and monitoring rainfall distribution using remote sensing techniques can provide insights into localized landslide risk (Bhandari and Dias 1996).

10 Influence of Road Buffers (from Center to Upward Slope Distance) on Landslide Frequency

The "Influence of Road Buffers (from center to upward slope distance) on Landslide Frequency" is a topic of relevance in the field of landslide susceptibility and hazard analysis. Road buffers, which refer to the space or distance between the center of a road and the upward slope, can play a crucial role in landslide occurrences (Dias and Gunathilaka 2014). The relationship between road buffers and landslide occurrences is a critical consideration in regions with hilly terrain (Vitanage 1994). Specifically, when the road buffer boundary distance is reduced to less than 100 meters, there is a noticeable increase in the frequency of landslides, Figs. 13, 14 and 15. This finding is not only based on the 2003 data but is a trend that has been observed in various regions with hilly terrain. Several factors contribute to the increase in landslides when road buffers are minimized. One of the primary factors is the alteration of the natural drainage patterns will increase in-



Fig. 12 Geomorphological, geological and hydrological evidence of slope failure in Pothupitiya Weddagala, Kalawana after the first record event, May 2003

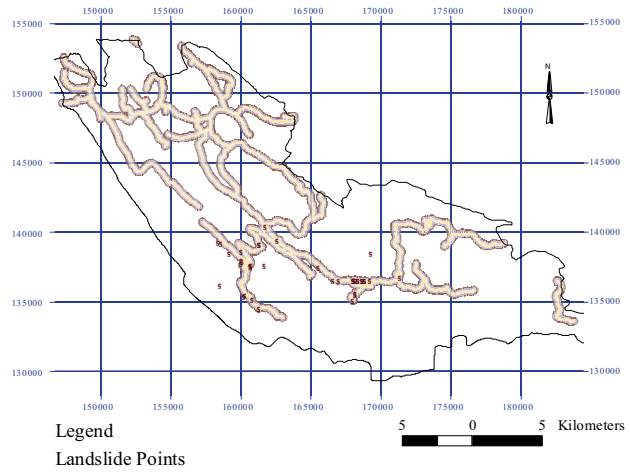


Fig. 13 Landslide occurrence with respect of road buffer boundary distance from the road centre, Kalawana Division, Sri Lanka

situ pore pressure (Bhandari and Dias 1996). Roads, particularly those with steep gradients, will channel rainwater towards the boundaries and increase hydrostatic pressure within the soil, making it more prone to failure (Cooray 1994) (Table 3).



Fig. 14 Landslide observation at the boundary of roadway (measure from center to upward slope distance 100 m)



Fig. 15 Circular failure observation at which extent to 100 m from the roadway

Table 3 Statistical distribution of landslides occurrence in road buffer measured from road centre to upward slope based on observations, 2003

No of Landslides	Road Buffer Distance from Road Center			
	0–100	100–200	200–300	>300
	27	7	2	3

11 Land Use

In the eastern sector of the Kalawana division watershed, there are several prominent peaks, including the 1171 m high Hinipitigala Peak, which stands as the highest point in the Rakwana Mountain (Cooray 1994). From this elevated vantage point, the altitude frequently descends to as low as 90 meters in the valleys (Vitanage 1994). The area is characterized by a relatively undulating topography, featuring a mix of vegetation primarily due to the presence of home gardens (Dias and Gunathilaka 2014). Notably, the predominant land use patterns in the area are tea plantations, abandoned tea fields, homesteads, and scrubland, as depicted in Fig. 19. Observations indicate that a significant portion of the old landslide occurrences are concentrated in the Homestead and Barren land use categories, as shown in Table 4.

11.1 Constructing Decision Hierarchy

This process helps researchers understand the relative importance of each factor, which is particularly valuable when there are constraints on time or resources. Constructing a decision hierarchy in the Analytical Hierarchy Process (AHP) involves breaking down a complex decision problem into a hierarchical structure of criteria and alternatives. All criteria should be mutually exclusive, collectively exhaustive, and relevant to the decision at hand. In the case of the Kalawana watershed in Sri Lanka, this study utilized the Analytic Hierarchy Process (AHP) to prioritize the factors contributing to slope destabilization.

11.2 Reciprocity

- Reciprocity in AHP refers to the pairwise comparisons of factors or criteria, where the relative importance or influence of one factor over another is assessed.
- For example, when comparing two factors such as “slope (gradient)” and “land use” in terms of their influence on

Table 4 Land use area in km^2, recoded number of landslides in different slope category

Land use	Number of Landslides	Area of Land use category in different Slopes (Sq km)						
		0-12 deg	12-22 deg	22-32 deg	32-42 deg	42-52 deg	>52 deg	Area (Sq.km)
Dense Forest	6	67.22	53.32	30.73	10.94	2.77	0.73	165.72
Homestead and Barren	24	64.42	33.6	16.12	3.89	0.82	0.16	119
Plantations	6	21.33	10.18	4.1	0.98	0.22	0.06	36.86
Scrub and Grass	3	7.05	6.18	3.86	1.26	0.3	0.13	18.78

landslide susceptibility, need to assess how much more important one factor is over the other.

- Reciprocity ensures consistency in the judgments made during pairwise comparisons. If factor A is judged to be twice as important as factor B, then factor B should be judged to be half as important as factor A. This ensures logical coherence in the decision-making process.
- Unlikeness in reciprocity occurs when there are inconsistencies or contradictions in the pairwise comparisons. For instance, if in one comparison factor A is considered more important than factor B, but in another comparison, the reverse judgment is made, it indicates unlikeness in reciprocity.
- Unlikeness in reciprocity can lead to biased or unreliable results in landslide susceptibility analysis, as it introduces inconsistency into the decision-making process. Therefore, it's essential to detect and resolve such inconsistencies to ensure the robustness of the analysis.

11.3 Transitivity

- Transitivity in AHP refers to the logical consistency among the pairwise comparisons of factors or criteria. It implies that if factor A is judged to be more important than factor B, and factor B is judged to be more important than factor C, then factor A should also be judged to be more important than factor C.
- In landslide susceptibility analysis, transitivity ensures that the relative importance or influence of factors remains consistent across all pairwise comparisons, thereby maintaining the integrity of the decision-making process.
- Unlikeness in transitivity occurs when inconsistencies arise in the pairwise comparisons that violate the transitive property. For example, if factor A is judged to be more important than factor B, and factor B is judged to be more important than factor C, but then factor C is judged to be more important than factor A, it indicates unlikeness in transitivity.
- Unlikeness in transitivity can lead to logical contradictions and undermine the reliability of the analysis results. Therefore, it's essential to identify and rectify any instances of unlikeness in transitivity to maintain the coherence and validity of the decision-making process.

Table 5 Degree of Importance; Factors preference and conversion into quantitative values from 1 to 9

Preference of a factor as compared with the other	Numerical value
Extremely preferred	9
Very strongly preferred	7
Strongly preferred	5
Moderately preferred	3
Equally preferred	1
Intervals between preferences	2,4,6,8

In summary, both reciprocity and transitivity are fundamental principles in landslide susceptibility analysis using AHP, as they ensure consistency and logical coherence in the pairwise comparisons of factors or criteria. Unlikeness in reciprocity and transitivity can compromise the reliability of the analysis results, highlighting the importance of detecting and addressing such inconsistencies to ensure the robustness of the decision-making process.

11.4 Degree of Relative Importance

The Eigenvalue approach is a mathematical technique used within the Analytical Hierarchy Process (AHP) to determine the relative importance or priority and alternatives in a decision-making process. In this method, at first for the reason of determining different factors preference and conversion into quantitative values, is done with valued judgments. In this case, the preference of a factor as compared with the other factor is taken into as a Table 5, and.

Stage A: Defining a Numerical Matrix

A comparison matrix is consistent if all its elements a_{ij} comparing alternatives i and j, respect the reciprocity [1] and transitivity [2] rules:

Reciprocity

$$a_{ij} = 1 / a_{ji} \tag{1}$$

where i, j are any alternatives of the matrix.

Example: If rainfall is twice as important as hydrology ($a_{1,2} = 2$), then hydrology is half as important as rainfall ($a_{2,1} = 1/2$).

Transitivity

$$a_{i,j} = a_{i,k} \cdot a_{k,j}, \tag{2}$$

where i, j and k are any alternatives of the matrix.

Example: Suppose rainfall is twice as important as hydrology ($a_{1,2} = 2$) and hydrology is four times as important as bedrock geology ($a_{2,3} = 4$). If rainfall is eight times as important as bedrock geology ($a_{1,3} = 8$), the transitivity rule is respected.

A matrix is reciprocal, if it's inferior part is reciprocal to the superior part and all the elements of the principal are equal to 1. Therefore, the transitivity needs to be tested for the upper part of the matrix only:

$$a_{i,j} = a_{i,k} \cdot a_{k,j} \quad \text{, for } j > k > i \tag{3}$$

Hence, for each element $a_{i,j}$ a number of j-(i + 1) eqs. [1] have to be respected.

11.5 Eigenvalue Approach (Normalization Method)

Stage 1

Evaluating the Analytic Hierarchy Process (AHP) using the eigenvalue method involves several steps to determine the priority weights for criteria and alternatives in a decision-making process (Saaty 2006). Simplification is given in the Figs. 16 and 17.

Example: The comparison $a_{2,5}$ has to respect equations $a_{2,5} = a_{2,3} \cdot a_{3,5}$ and $a_{2,5} = a_{2,4} \cdot a_{4,5}$.

These equations can be expressed exclusively in terms of the first diagonal above the principal diagonal (i.e. a_{12}, a_{23}, …, $a_{n\text{-}1n}$):

$$a_{i,j} = a_{i,i+1} \cdot a_{i+1,i+2} \cdot \ldots \cdot a_{j-1,j} \tag{4}$$

All the priorities derivation methods provide the same priorities with consistent matrices. In the case of inconsistencies, they can be arranged in eigenvalue approach (Saaty 1980).

Stage 2: Solve for the Eigenvector

Eigenvectors can assist in approximating a large matrix as a smaller vector. In the context of a linear transformation matrix, eigenvectors represent a set of vectors that undergo stretching without rotation or shearing (Saaty 2006). The eigenvalue quantifies the extent of this stretching, and a simplified approach is illustrated in Fig. 17.

11.6 Defining Reciprocity and Transitivity

In AHP, decision-makers or experts are asked to perform pairwise comparisons of the criteria and alternatives at each level of the hierarchy. They assign relative importance or preference values to indicate how much one criterion or alternative is favored over another. It should be noted that

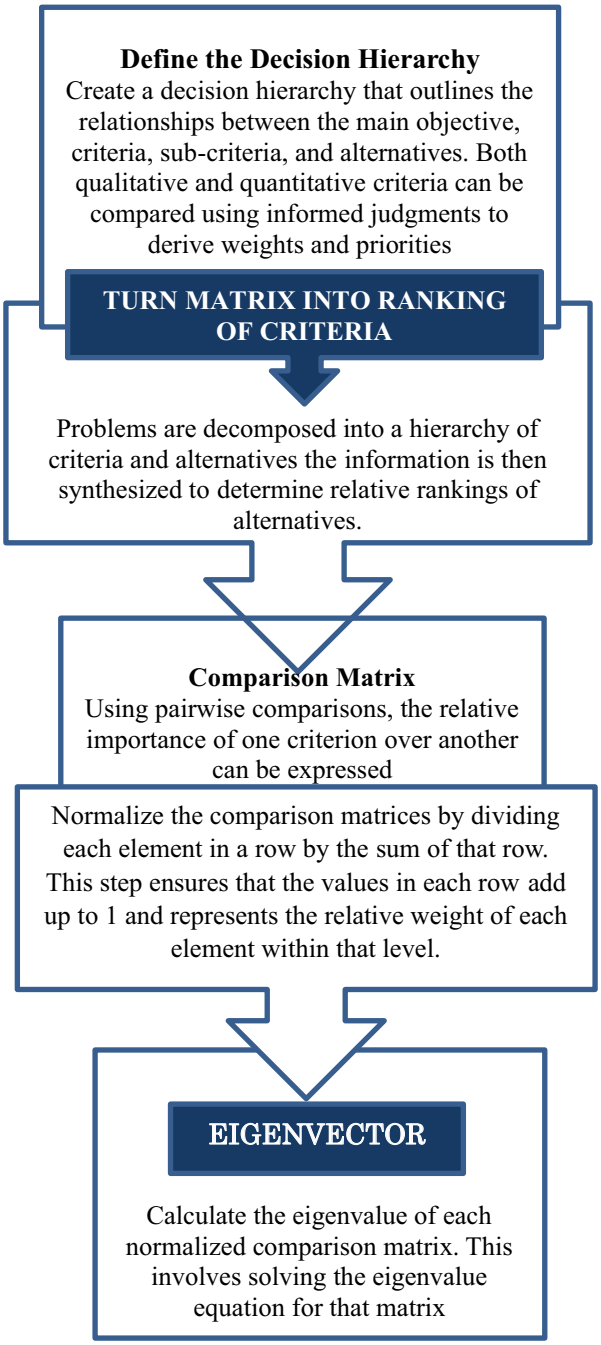


Fig. 16 Stage 1, Establishing a comparison numerical matrix and methodology for eigenvector assessment

pairwise comparisons, the relative importance of one criterion over another can be expressed and showing challenge with each judgement (Dias and Gunathilaka 2014). These comparisons result in a square matrix known as the pairwise comparison matrix. Some representative reciprocity and transitivity factors for the matrix development is given below.

- Soil strength is 1.5 times as important as Landuse
- Rainfall is 6 times as important as Soil Strength

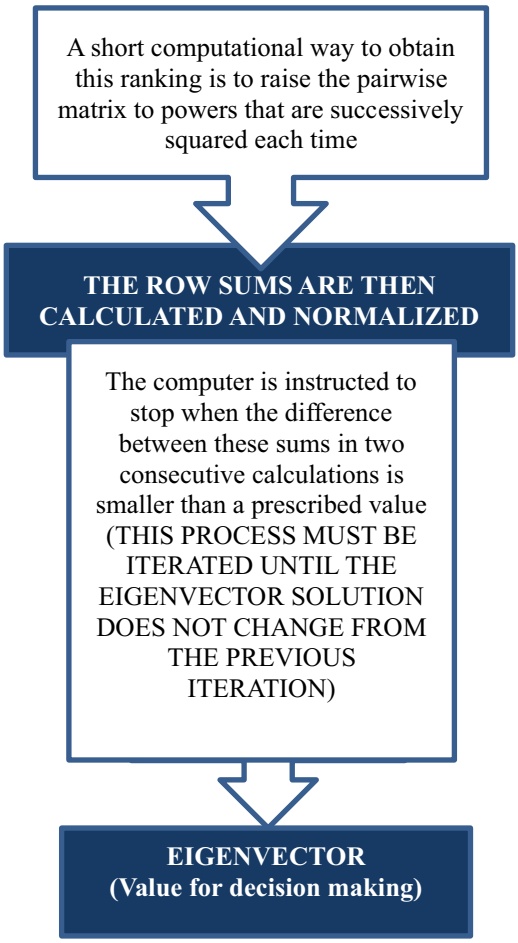


Fig. 17 Stage 2- Computation approach of eigenvector

- Bedrock Geology is 2 times as important as Land use
- Bedrock geology is 1.5 times important as soil strength
- Road buffer is 3 times important as Bedrock Geology
- Rainfall zone is 2.5 times important as first Oder stream Hydrology
- first Oder stream Hydrology is 7 times important as Landuse
- Slope is 3 times important as Landuse
- first Oder stream Hydrology is 5 times important as Soil Strength
- first Oder stream Hydrology is 2 times important as Slopes
- Rainfall zone is 9 times important as Land use
- Rainfall zone is 6 times important as Soil Shear Strength
- Rainfall zone is 4 times important as Bedrock Geology
- Rainfall zone is 2 times important as Road Buffer
- Slope is 3 times important as Land use
- Road buffer is 4 times important as Shear strength
- Rainfall Zone is 2.5 times important as first Oder stream Hydrology

In landslide susceptibility analysis using the Analytical Hierarchical Process (AHP), both reciprocity and transitivity play crucial roles in ensuring the validity and reliability of the results. Recent observations are very much significant of each other and breakdown of each concept and their respective significance according to our categorization is tabulated in Table 6 and computation of eigen vector in eight consecutive steps are shown in the Table 7.

Table 6 Reciprocity and transitivity of factors in landslide susceptibility analysis

Original Decision Hierarchy		L	SS	BG	S	RB	H	R
		Landuse	Soil Shear Strength	Bedrock Geology	Slopes	Road Buffer	Hydrology - first order stream	Rainfall Zones
L	Landuse	1	1/1.5	1/2	1/3	1/5	1/7	1/9
SS	Soil shear strength	1.5	1	1/1.5	1/2	1/4	1/5	1/7
BG	Bedrock geology	2	1.5	1	1/1.5	1/3	1/3.5	1/5
S	Slopes	3	2	1.5	1	1/1.5	1/2	1/3
RB	Road buffer	5	4	3	1.5	1	1/1.5	1/2
H	Hydrology - first order stream	7	5	3.5	2	1.5	1	1/2.5
R	Rainfall zones	9	6	4	3	2	2.5	1

Table 7 Computation of reciprocity and transitivity of factors in landslide susceptibility analysis

Catogary	Eigen Values Stage 1	Eigen Values Stage 2	Eigen Values Stage 3	Eigen Values Stage 4	Eigen Values Stage 5	Eigen Values Stage 6	Eigen Values Stage 7	Eigen Values Stage 8	Value Difference of last two stages
Landuse	0.038528	0.039872	0.040459	0.040877	0.041203	0.041461	0.041666	0.041828	0.000
Soil Strength	0.039272	0.036816	0.035468	0.034545	0.033828	0.033261	0.032811	0.32454	0.000
Bedrock Geology	0.077853	0.080772	0.081952	0.082800	0.083460	0.083983	0.084398	0.084726	0.000
Slope	0.120188	0.124156	0.125969	0.127271	0.128286	0.129090	0.129727	0.130232	0.001
Road Buffer	0.196088	0.202451	0.205524	0.207651	0.209306	0.210618	0.211658	0.212483	0.001
Hydrology 1st Or streams	0.250560	0.257004	0.260929	0.263629	0.265731	0.267397	0.268717	0.269764	0.001
Rainfall	0.277513	0.258928	0.249699	0.243228	0.238186	0.234191	0.231023	0.228512	-0.003

Table 8 Factor weight for the computation of landslide susceptibility analysis

Notation	Factor map category	Factor weight (x)
X1	Landuse	0.02644
X2	Soil strength	0.02226
X3	Bedrock geology	0.06085
X4	Slope	0.11155
X5	Road buffer	0.17267
X6	Hydrology first order streams	0.33050
X7	Rainfall zones	0.27572

The eigenvector evaluation was complted following the procedure outlined in Fig. 6, ensuring accuracy up to nearly 99% in value differences by Stage 8, as depicted in Table 7. Therefore, the reciprocity and transitivity contribution to major vector map weight is given in the Table 8.

12 Evaluation of Consistency of Judgement Matrix

The next step is to calculate the Consistency Ratio (CR) to assess the reliability of the judgments compared to large samples of random judgments (Saaty 1980, 2000). The Consistency Index (CI) measures the deviation from consistency in a pairwise comparison matrix. The consistency ratio is designed such a way that shows a reasonable level of consistency in the pairwise comparisons if CR < 0.10 and ≥ 0.10 CR indicate inconsistent judgments are considered unreliable and invalid. In such situations, the judgment matrix needs to be restructured with expert evaluations until the minimum accuracy and necessitating repetition. The Consistency Ratio (CR) further quantifies how far the matrix is from being consistent. Consistency ratio (CR) is a non-statistic index that is determined by the quotient between the Consistency Index (CI) and the Random Consistency Index (Malczewski 1999, 2006).

$$\mathrm{CRCI}/\mathrm{RI} \tag{5}$$

Han and Tsay (1998) stated that the value of λ_{max} is essential for computing the consistency ratio. This is obtained by calculating matrix product of the pairwise comparison matrix and the weight vectors and then adding all elements of the resulting vector. Consistency Index (CI) is introduced as:

$$\mathrm{CI} = \left(\lambda_{max} - n\right)/\left(n-1\right) \tag{6}$$

Where, n is the number of criteria and λ_{max} is the maximum eigenvalue (Han and Tsay 1998; Malczewski 1999).

In other words, the CR evaluates the consistency of the decision-making process of the operator providing the decision judgement (Saaty 2000). The above approach was used to quantitatively assess the consistency of assigning relative weights to the seven conditioning factors in slope instability,

Table 9 Random consistency index (RI) (Saaty 1980)

n	1	2	3	4	5	6	7	8
RI	0.00	0.00	0.58	0.90	1.12	1.24	1.32	1.41
n	9	10	11	12	13	14	15	
RI	1.45	1.49	1.51	1.48	1.56	1.57	1.59	

as conducted under the original decision hierarchy outlined in Table 6.

n = 7 (conditioning factors in slope instability).

Determination of λ_{max}

- The maximum value of the pairwise comparison matrix was obtained by multiplying the values of the original comparison matrix by the relative weights granted in every row.
- Then determine the consistancy vector by dividing the weighted sum vector by sum of the normalized scores for each raw matrix.
- λ_{max} is the average value of consistency vector

λ_{max} = 7.6126

From the eq. [6] gives,

CI = 0.102

The RI is the random index (Saaty 1980, 2000), the consistency index of a randomly generated pair wise comparison matrix. RI depend on number of elements being compared for the computation of landslide susceptibility analysis as in the Table 9.

Thus,

$$\mathrm{CR} = 0.102/1.32 = 0.077 < 0.1$$

i.e. fulfilled the conditional consistency requirement (Saaty 1980, 2000).

13 Evaluation of Subfactor Map Weights

The factor maps present various sub-factor ratings within the primary factor map, and each factor influencing slope instability is analyzed (Corominas et al. 2014). Therefore, it is imperative to reassess pairwise comparison judgments using available data to compute priority weights for each element at every level of the hierarchy. Constructing a decision hierarchy (Han and Tsay 1998) involves breaking down a complex decision problem into a structured hierarchy of criteria and alternatives, which need to be evaluated using known datasets. Verifying site data for consistency and ensuring data alignment is crucial for accurate subfactor rating.

This study explores the feasibility of integrating historical data from 2003 into the numerical curve fitting process. This integration is illustrated in Fig. 18 for Landuse, 19 for Soil Shear Strength, 20 for Geology, 21 for Slopes, 22 for

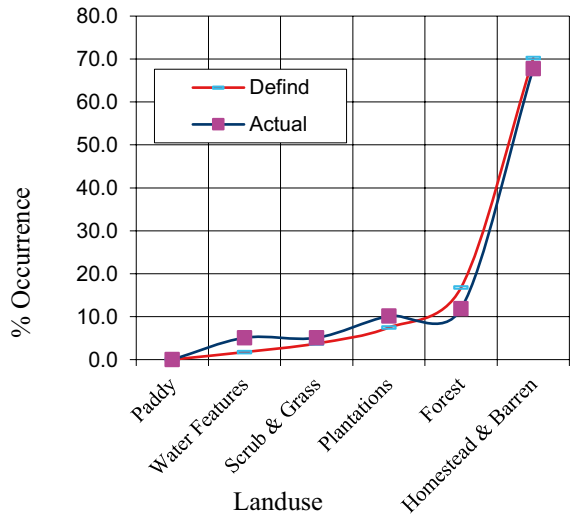


Fig. 18 A Comparison between numerical ratings and Landslide Occurrences prior to finalizing sub-coefficients for the landuse category

Road Buffer, 23 for first Order Streams, and 24 for Rainfall Zones, as defined in the original decision hierarchy in Table 6.

13.1 Sum of Squares, SST

The sum of squares total, denoted SST, is the squared differences between the observed dependent variable (Y_i) and its mean (Y_{mean}).

$$SST = \sum \left(Y_i - Y_{mean} \right)^2 \quad (7)$$

The sum of squares regression, or SSR, is the sum of the differences between the predicted value (Y_{ai}) and the mean of the dependent variable.

$$SSR = \sum \left(Y_{ai} - Y_{mean} \right)^2 \quad (8)$$

It is the explained sum of squares, and tells you how much of the variation in the dependent variable your model explained.

13.2 Sum of Squares Error, SSE

The Sum of Squares Error, or SSE, is the difference between the observed value and the predicted value. It measures dispersion of values around regression line, and is the unexplained variability by the regression.

- The smaller the SEE, the more accurate the regression line to predict the value of the dependent variable.

Table 10 Categories of Landuse map weights

Decision Tree	Landuse	Sub factor weight x	%	Actual Records of landslides	%
Stable	Paddy	0.0001	0.0	0	0.0
Slightly	Water features	0.0175	1.8	3	5.1
Low	Scrub & Grass	0.0376	3.8	3	5.1
Moderate	Plantations	0.0747	7.5	6	10.2
High	Forest	0.1679	16.8	7	11.9
V high	Homestead & Barren	0.7021	70.2	40	67.8

- It is very much like the standard deviation for a single variable, except that it measures the standard deviation of the residual term in the regression.
- If the actual values for the observations are close to the regression line (Corominas et al. 2014), it means that the relationship between the dependent and independent variables are strong. However, it does not tell us how well the independent variable explains variation in the dependent variable.

$$\text{Mathematically}, SST = SSR + SSE \quad (9)$$

13.3 Landuse Map Unit

Landuse assumes a pivotal role, particularly when human activities intensify and contribute to instability. Consequently, this study undertakes an evaluation of diverse landuse patterns, encompassing Paddy, Water, Scrub, Plantations, Forest, and Homesheds. The evaluation is based on the data presented in Table 10 and Fig. 18. The scoring for each factor may vary depending on the sensitivity and judgment of values (Dias and Gunathilaka 2014). The original comparison matrix, which includes the final output for generating the landslide susceptibility index (rating), is presented in Table 16. Factor preferences are organized in ascending order, and the weighted coefficients are computed using the mean of the normalized values method to determine the factor weights.

Although the mean of normalized values lacks a theoretical foundation for inconsistent matrices, reciprocity and transitivity have been identified as criteria for enhancing the factor maps in the Landuse sub category. To quantify the standard error of the qualitative judgment and the actual values, the square root of the sum of squared differences was used to provide a quantifiable measure of the "goodness" of the defined values as shown in the Table 11.

Table 11 Computation of SSE for the Landuse sub category

Sum of Squares (observed/actual dependent variables)			Sum of Squares Regression (predicted variables)			Sum of Squares Error
Y_i	Y_i-Y_{mean}	$(Y_i$-$Y_{mean})^2$	Yai	Y_{ai}-Y_{mean}	$(Y_{ai}$-$Y_{mean})^2$	
0	-0.167	0.028	0.000	-0.167	0.028	-0.04
0.051	-0.116	0.013	0.018	-0.149	0.022	
0.051	-0.116	0.013	0.038	-0.129	0.017	
0.102	-0.065	0.004	0.075	-0.092	0.008	
0.119	-0.048	0.002	0.168	0.001	0.000	
0.678	0.511	0.261	0.702	0.535	0.286	
Total	1.001	0.322			0.361	
Y_{mean}	0.167					

13.4 Soil Strength (Table 12, Fig 19)

Table 12 Categories of Soil Strength map weights

Decision tree	Shear Strength	Sub factor weight x	%	Actual Records of landslides	%
Low	>75	0.0007	0.1	0	0.0
Moderate	51–75	0.1294	12.9	16	27.1
High	0–50	0.8700	87.0	43	72.9

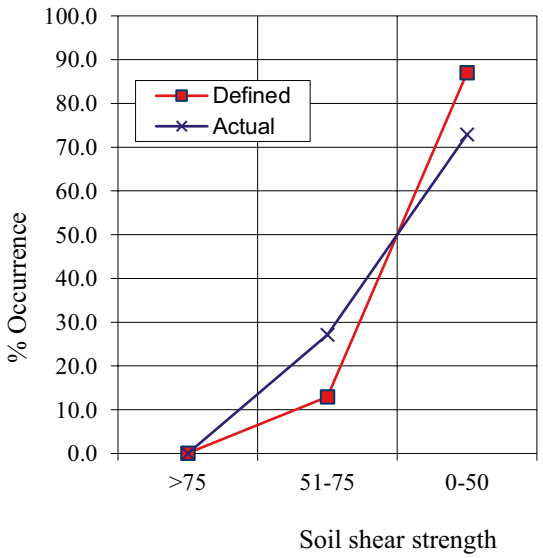


Fig. 19 A Comparison between numerical ratings and Landslide Occurrences prior to finalizing sub-coefficients for the soil shear strength category

13.5 Geology (Table 13, Fig. 20)

Table 13 Categories of Geology map weights

Decision Tree	Geology	Sub factor weight x	%	Actual Records of landslides	%
Slightly	E	0.0017	0.2	0	0.0
Low	D	0.0505	5.0	6	10.2
Moderate	C	0.1528	15.3	11	18.6
High	B	0.2779	27.8	19	32.2
V high	A	0.5171	51.7	23	39.0

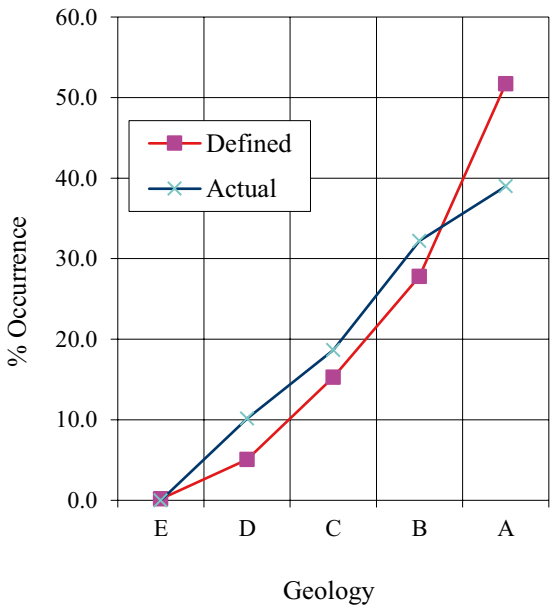


Fig. 20 A Comparison between numerical ratings and Landslide Occurrences prior to finalizing sub-coefficients for the Geology factor

13.6 Slope (Table 14, Fig. 21)

Table 14 Categories of Slope map weights

Decision tree	Slopes	Sub factor weight x	%	Actual Records of landslides	%
Stable	0–12	0.0009	0.1	0	0.0
Slightly	>50	0.0186	1.9	1	1.7
Low	42–52	0.0588	5.9	4	6.8
Moderate	32–42	0.1174	11.7	11	18.6
High	12–22	0.2776	27.8	24	40.7
Extremely high	22–32	0.5266	52.7	19	32.2

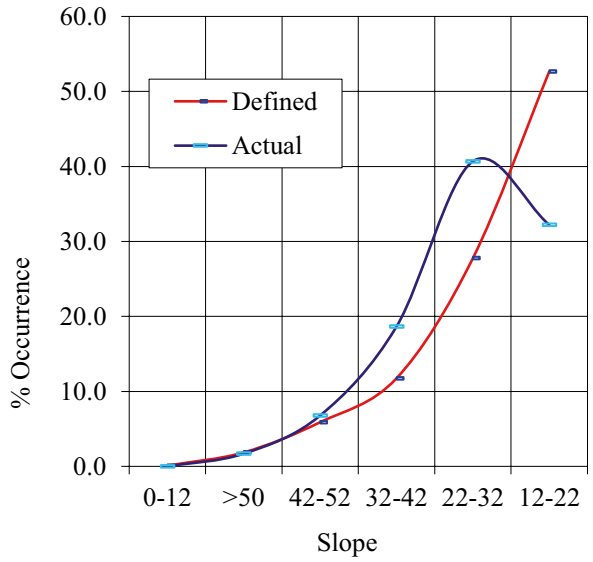


Fig. 21 A Comparison between numerical ratings and Landslide Occurrences prior to finalizing sub-coefficients for the Slope factor

13.7 Road Buffer (Table 15, Fig. 22)

Table 15 Categories of Road Buffer map weights

Decision tree	Buffer distance	Sub factor weight x	%	Actual Records of landslides	%
Slightly	200–300	0.0005	0.1	2	3.4
Low	>300	0.0365	3.7	3	5.1
Moderate	100–200	0.1653	16.3	13	22.0
High	0–100	0.7976	80.0	41	69.5

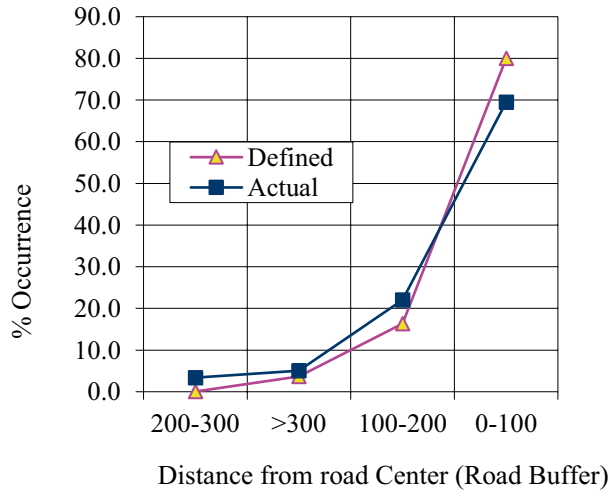


Fig. 22 Comparison of numerical ratings and actual scenarios of landslide occurrences before finalizing of sub coefficients, factor for Road Buffer

13.8 First Order Streams Hydrology

Hydrology becomes particularly critical when the cumulative accumulation over three consecutive days surpasses a certain threshold value for stability. As a result, the study assesses the three-day cumulative rainfall within the following ranges: 500-550 mm, 551-600 mm, 601-625 mm, and 625-650 mm and evaluation of data given in the Table 16 and Fig. 23.

Table 16 Categories of first Order Stream Hydrology map weights

Decision tree	1st Order Stream Hydrology nos	Sub factor weight x	%	Actual Records of landslides	%
Slightly	0–25	0.0008	0.1	1	1.7
Low	26–50	0.0236	2.4	3	5.1
Moderate	51–75	0.0895	9.0	7	11.9
High	76–100	0.2662	26.6	15	25.4
V high	>100	0.6199	62.0	33	55.9

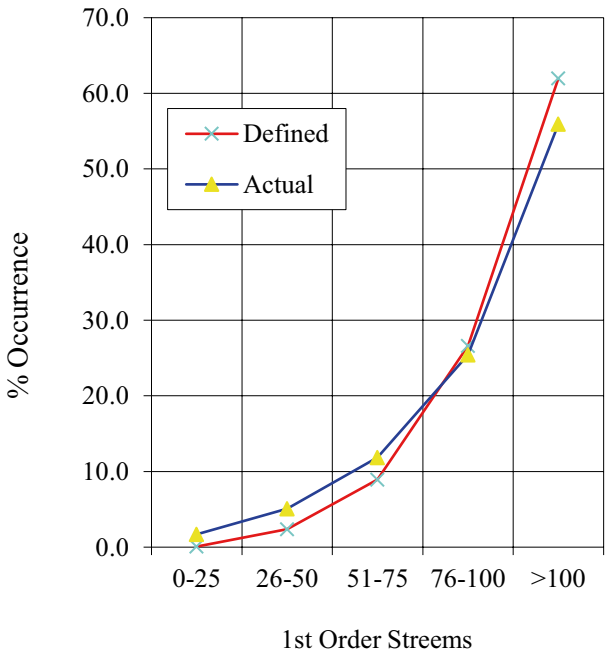


Fig. 23 Comparison of numerical ratings and actual scenarios of landslide occurrences before finalizing of sub coefficients, factor for first order streams

13.9 Rainfall Zones (Tables 17 and 18, Fig. 24)

Using the SSE approach within the AHP (Analytical Hierarchy Process) combines quantitative and qualitative methods to enhance the accuracy of sub-factor weight dependencies. The Sum of Square Errors (SSE) provides maximum likelihood estimation, especially when the errors follow a normal distribution (Stansbury 2020). The estimated SSE loss indicates negative results from the defined scenarios but shows very low significance (Corominas et al. 2014).

Table 17 Categories of Rainfall map weights

Decision tree	Rainfall mm	Sub factor weight x	%	Actual Records of landslides	%
Slightly	500–550	0.0004	0.0	0	0.0
Low	551–600	0.0268	2.7	0	0.0
Moderate	601–625	0.2230	22.3	25	42.4
High	625–650	0.7498	75.0	34	57.6

Table 18 Summary of Sum of Square Error (SSE) of the sub-factor weights, comparing actual values (landslide observations) to the regression line

Sub-Factor category	Sum of Squares Error (SSE)
Landuse	−0.04
Soil strength	−0.17
Bedrock geology	−0.07
Slope	−0.06
Road buffer	−0.13
Hydrology first order streams	−0.07
Rainfall zones	−0.10

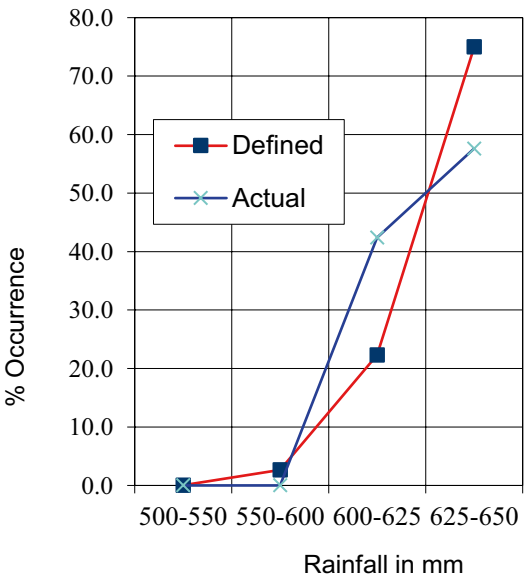


Fig. 24 Comparison of numerical ratings and actual scenarios of landslide occurrences before finalizing of sub coefficients, factor for Rainfall zones

The input parameters of the sub-factor weights improve the accuracy of the susceptibility maps, ranking factors from the most unstable to the most stable variable.

14 Landslide Susceptibility Coefficient

The simplification process involved sub-factor evaluations, leading to the computation of the susceptibility coefficient using eqs. [10]. The Table 08 illustrates the simplification of factor evaluations, including the assessment of reciprocity and transitivity of factors in the landslide susceptibility analysis (eigenvalue) and final computation of weighted maps integrated using the eq. [11].

The weight values in the comparison matrix of each row were calculated according to the evaluation of sub-factor coefficients is presented in Tables 10 through 17. Upon assessing the area with respect to the seven factors, the values of the seven factor classes (X) are now multiplied by their respective individual pixel weights (w1…w7) and subsequently summed together.

This results in the calculation of the total value (M1) for each pixel and the regional model, as shown in the following equation,

$$M1 = w1x1 + w2x2 + w3x3 + w4x4 + w5x5 + w6x6 + w7x7 \quad (10)$$

By substituting the previously estimated combined weights (w1…w7), we arrive at the final model,

$$M = w1X1 + w2X2 + w3X3 + w4X4 + w5X5 + w6X6 + w7X7 \quad (11)$$

where, X1…X7 are the initials that stand for the conditioning factors of landuse, soil strength, bedrock geology, slope, road buffer, hydrology (first order streams), and rainfall and w1…w7 pixel weights associated with each X1…X7 factor.

M = Susceptibility coefficient

The susceptibility coefficient (M) varies between 0 and 1.

In this study, the Kalawana watershed has been divided into five susceptibility classes or ranks, as shown in Table 19. The factors of first Order stream hydrology and rainfall zones have the highest relative weight, indicating that these factors related to topographic and extrinsic variables have a greater impact on slope instability. Relative ranks were assigned to each prediction pattern, and the calculated index

Table 19 Landslide susceptibility class for creating the landslides susceptibility map

Value of Susceptibility Coefficient	Class	Category Name
0.0 M 0.146	1	No susceptibility
0.146 < M 0.256	2	Low susceptibility
0.256 < M 0.365	3	Moderately susceptibility
0.365 < M 0.475	4	High susceptibility
o.475 < M 1	5	Very high susceptibility

values for all cells in the study area were sorted in descending order. These ordered cell values were then divided into 64 classes with logically accumulated intervals, ultimately creating the primary set of susceptibility categories, as quantitatively depicted in Fig. 25.

The final susceptibility map was validated using a landslide inventory map. This simple validation method, based on spatial cross-checking of the mapping results, serves as an initial indicator of the reliability of the landslide susceptibility map. In the final susceptibility map for instability processes in the Kalawana watershed area, the largest areas correspond to degrees 1 (No Susceptibility), 2 (Low Susceptibility), 3 (Moderate Susceptibility), 4 (High Susceptibility), and 5 (Very High Susceptibility). The areas classified as degrees 4 (High) and 5 (Very High) are smaller and some locations are inaccessible due to rock outcrops, but they are still important. The results of the susceptibility mapping to slope instability processes, using the analytic hierarchy process (AHP), are documented in Fig. 28.

15 Results and Discussion

The conventional approach for assessing factor weights and their relative significance in landslide susceptibility mapping involves the utilization of the Multi-Criteria Decision Making (MCDM) method. Specifically, the Analytic Hierarchy Process (AHP) was employed to enhance our understanding of landslide factor significance. This involved factor map overlay criteria and decisions were made, taking into consideration topography and slope with various slope combinations, bedrock geology as a function of slope and rock type (Varnes 1978), first order stream density in relation to sub-catchment, land use as a sensitive factor within a catchment, road buffer or slope distance from the center of the road, precipitation potential based on rainfall zones, and the stability of topsoil cover as a function of combined soil cohesion strength. These factors were identified as primary and secondary contributors to susceptibility. The pairwise comparison judgments to derive priority weights for each element at every level of the hierarchy. Prior to deriving their weights, each factor was compared based on its usage and occurrence frequency. The interpretation of map units was established using class attributes, the number of pixels, pixel area, mean class value, maximum class value, and statistical mean of the class and conclude as in the Table 20. Some significant observations are,

(i) The numerical rating and integration of data only concludes if the reasonable observations of verification data (old landslides).

Table 20 Map pixel count according to classification

Class	Class Label Range	Pixel Count
1	0.036–0.146	1,461,669
2	0.146–0.256	719,978
3	0.256–0.365	861,153
4	0.365–0.475	615,242
5	0.475–0.585 and over	122,367

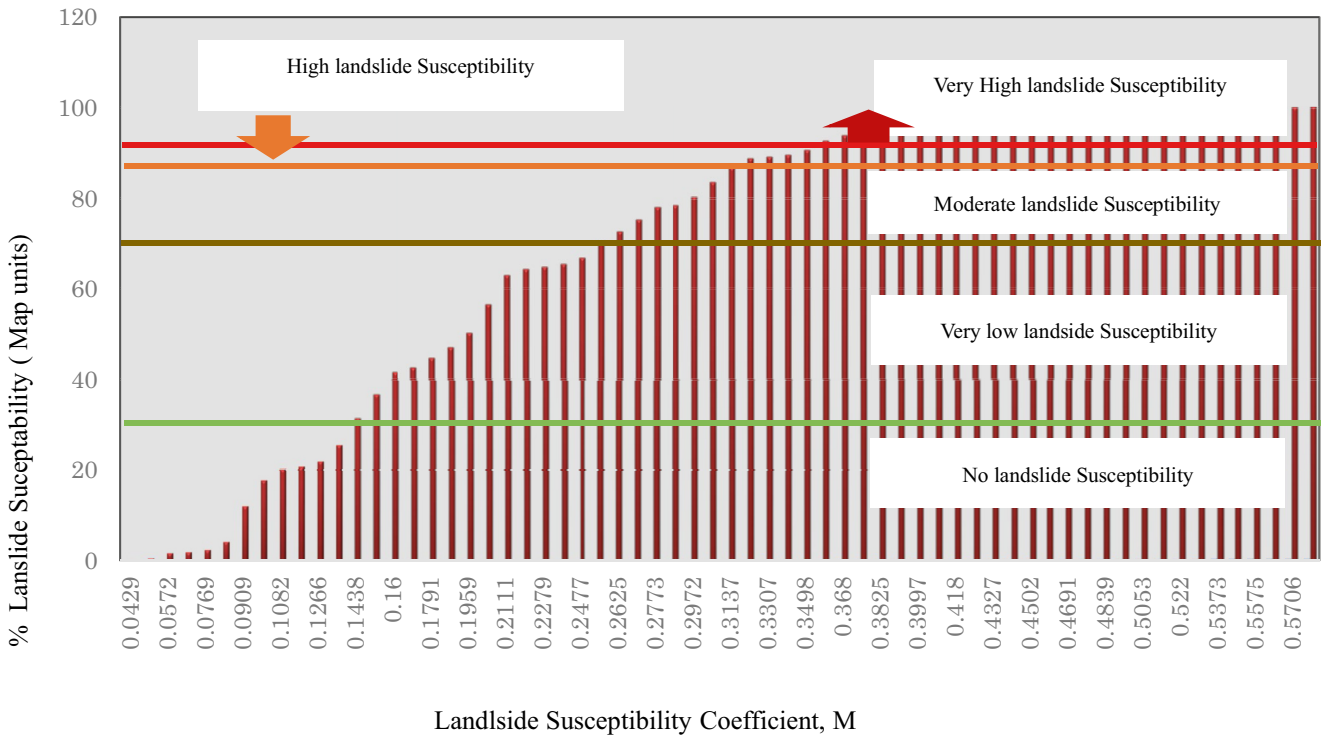


Fig. 25 Landslide Susceptibility Coefficients of 64 map units creating the primary set of susceptibility categories for the Kalawana Division of Rathnapura District, Sri Lanka

(ii) More precise the judgment, the more compatible the produced map is in reality.
(iii) Landslide susceptibility analysis result was validated using known landslide locations. Validation was performed by comparing the known landslide location data with the landslide susceptibility map and method of approach is shown in the Figs. 26 and 27.
(iv) Study has limited data on landslide and therefore accuracy of the observations do not strictly defined the high accurate susceptibility rating.
(v) It is indeed more accuracy can be achieved by editing and creation of factor maps which are satisfactory with numerical logic in AHP.

Additionally, using accurate evidence and developing a value judgment matrix will help improve the accuracy of the AHP methodology. If necessary, decompose the identified criteria into sub-criteria to further refine the decision-making process. Sub-criteria provide more granularity and specificity, enhancing the analysis. Finally, the zoning map of the Kalawana Division watershed was derived using the Analytical Hierarchy Process (AHP) method and is presented as the Landslide Susceptibility Re-Classified Results (standard deviation reduced to 5 classes) in Table 21. The overall assessment of sensitivity is documented in the landslide susceptibility map of the Kalawana Division, Rathnapura District, Sri Lanka, shown in Fig. 28.

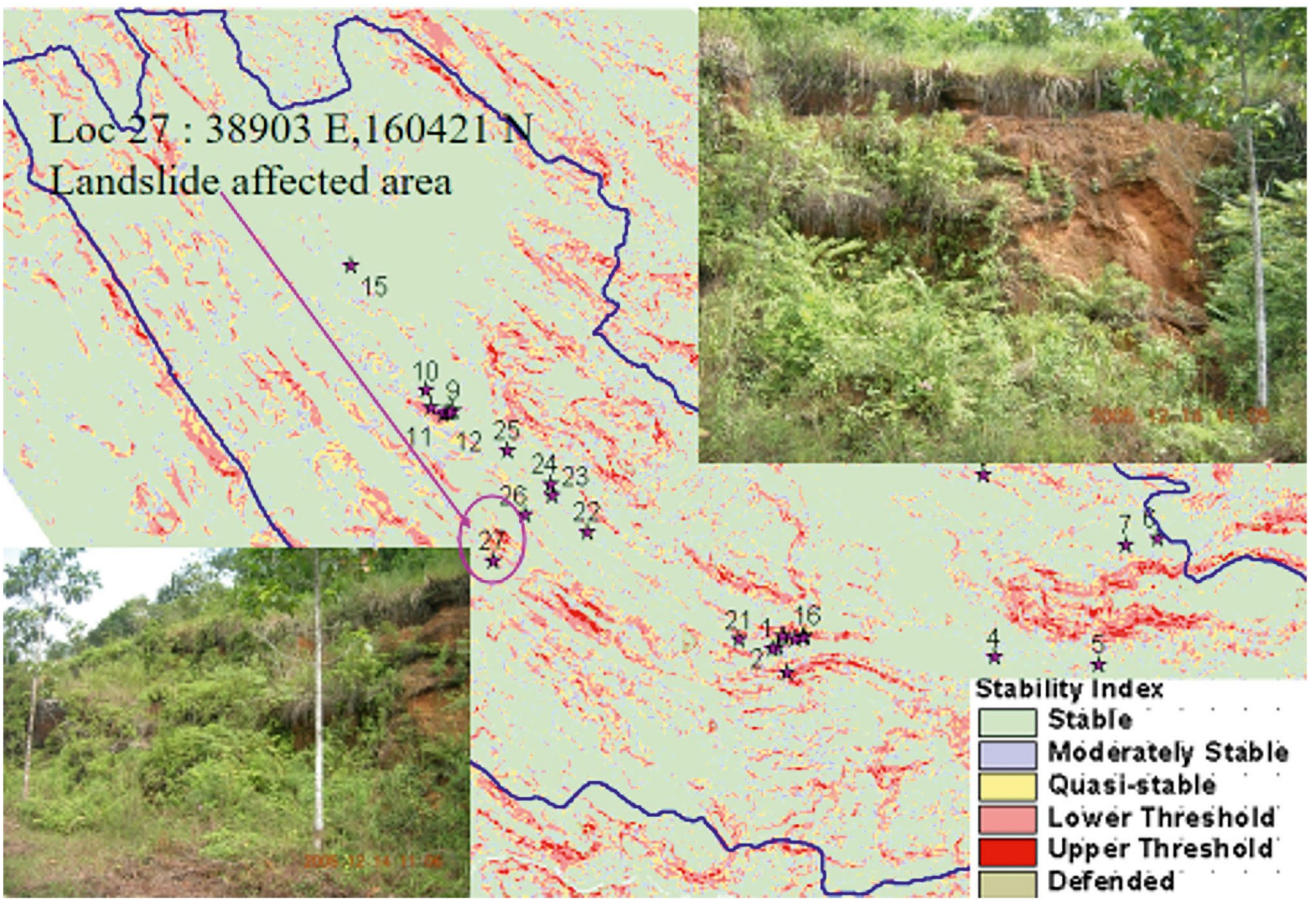


Fig. 26 Field verification of results in minor slides

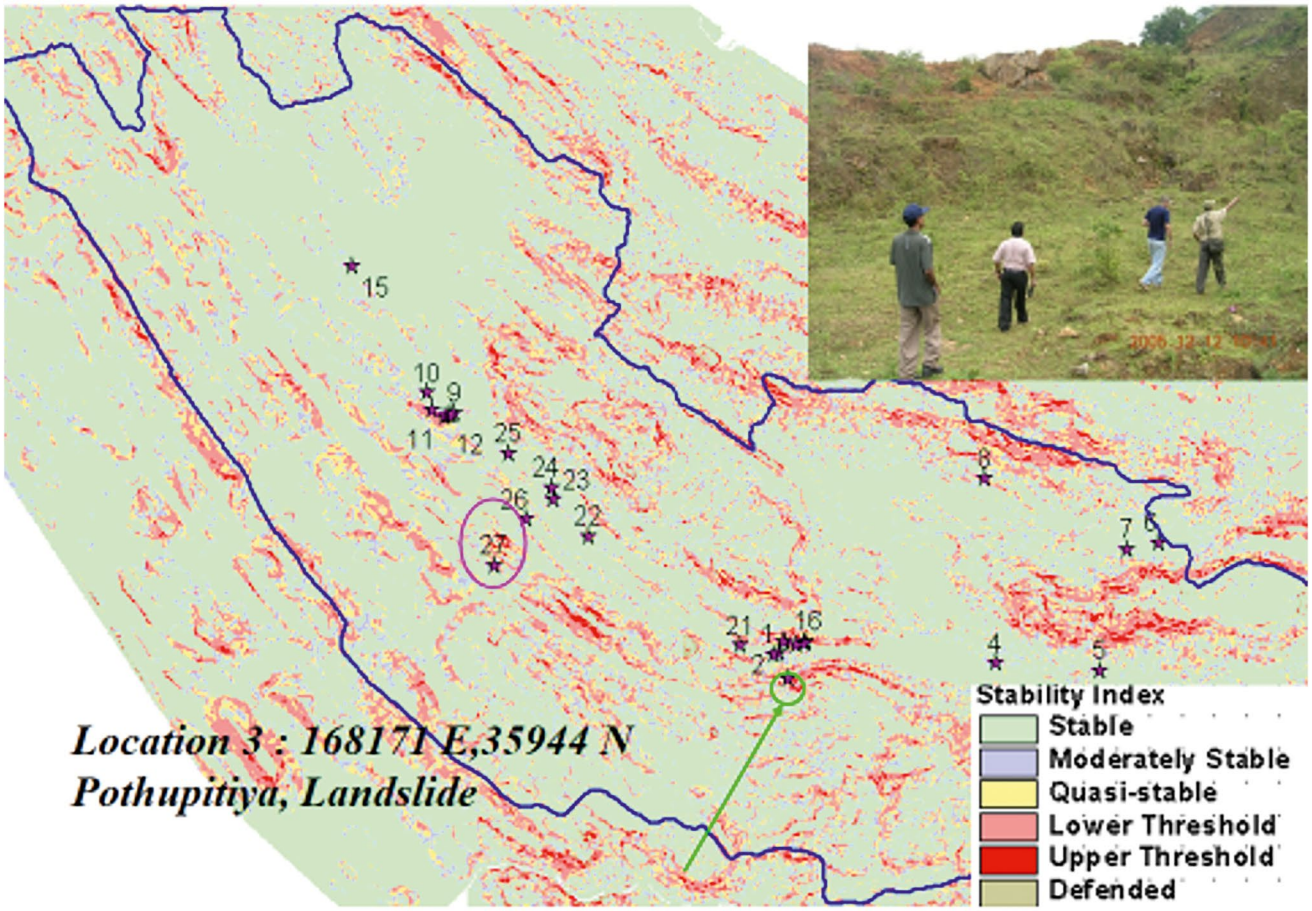


Fig. 27 Field verification of results in major slides

Table 21 Landslide Susceptibility Re-classified Results (Std deviation ½ reduced to 5 classes)

Class	Class Label	Landslide Susceptibility	Count	% Area	Verified Number of Landslides	% Occurrences
1	0.036–0.146	No susceptibility	1,461,669	38.67	4	10.3
2	0.146–0.256	Low susceptibility	719,978	18.99	2	5.1
3	0.256–0.365	Moderately susceptibility	861,153	22.8	12	30.8
4	0.365–0.475	High susceptibility	615,242	16.3	6	15.4
5	0.475–0.585 and over	Very high susceptibility	122,367	3.24	15	38.5
		Total	3,780,409	100	39	

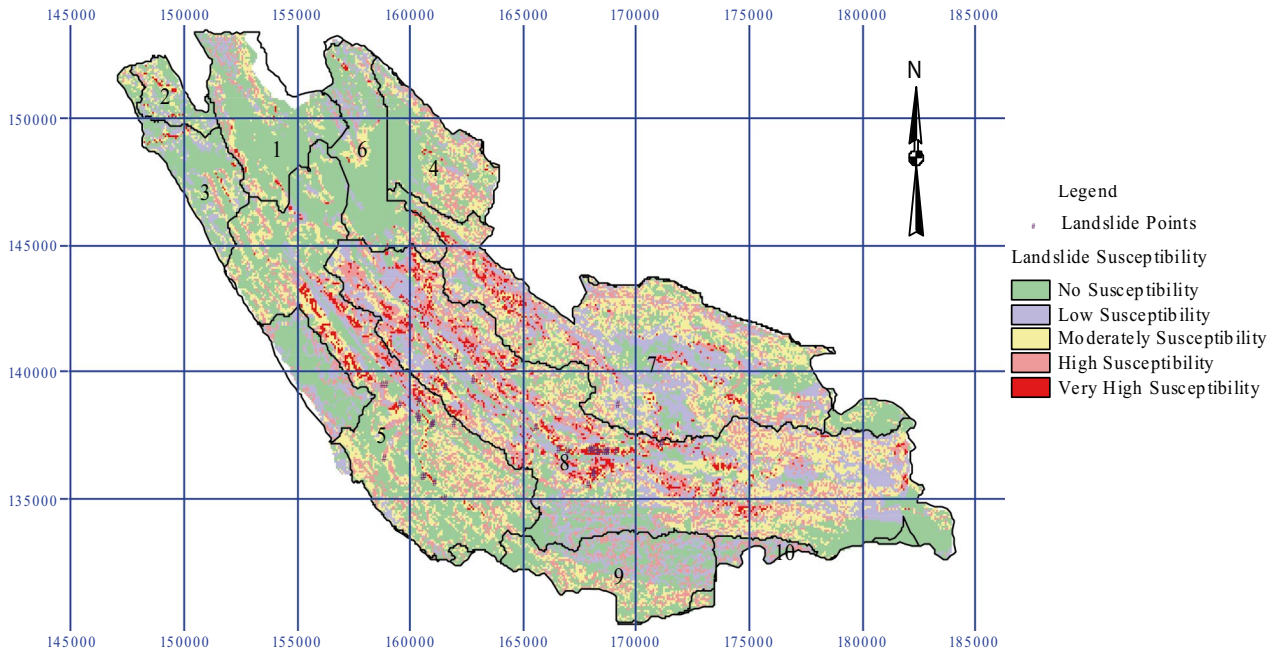


Fig. 28 Landslide Susceptibility Map at the Kalawana Division of Rathnapura District, Sri Lanka

16 Conclusions and Recommendations

Rain-induced landslides in Sri Lanka can vary in pattern and severity, especially during extreme rainfall events. These patterns are influenced by factors such as topography, soil types, vegetation cover, and the intensity and duration of rainfall (Dias et al. 2014). Some different patterns of rain-induced landslides commonly observed during extreme rainfall event in May, 2003, in the Kalawana division of the Ratnpura district.

The landslide susceptibility mapping study in the Kalawana division, Ratnapura, used the Eigenvalue approach technique to establish the susceptibility coefficient.

The computation of landslide susceptibility coefficients constitutes a pivotal phase in the process of landslide susceptibility mapping (Carrara 1983). In this study, we undertook an extensive examination of various geological, geomorphological, climatic, parametric, and land-use factors that contribute to the likelihood of landslides occurring, as previously calculated. The calculated average weights provide insights into how effectively the model statistically estimated the actual state of slope instability (Bhushan and Ria 2004). We used eigenvalue for the major factor criteria and a normalized approach for sub-factor evaluation within the AHP to assess cumulative values of pixel frequencies for landslide susceptibility.

From the comparison of the results obtained with the inventory map, it is observed that 39 instability events have been recorded, coinciding with the highest susceptibility degrees as shown in Table 21. Of these, 38.5% (15 events) correspond to very high susceptibility, 15.4% (6 events) correspond to high susceptibility, 30.8% (12 events) correspond to moderate susceptibility, 5.12% (2 events) correspond to low susceptibility, and 10.3% (4 events) are located on slopes with low or no susceptibility.

The analysis fairly well defines areas that intuitively appear to be susceptible to landslides. It was noted that a few landslides occurred on slopes that would not normally be recognized as susceptible to landslides. This means that the methodology missed classifying several of these sites as being landslide-prone due to the site-specific geologic conditions and inaccurate input parameters of soil. The above finding indicates that the variability of conceptual models and their relative importance with the input databases. Detailed and comprehensive geographical information databases are required to obtain statistical interpretation and calibration of the model. In mountainous regions of Sri Lanka, where rock outcrops are common, heavy rainfall can saturate and weaken the rocks, leading to rockfalls and rockslides (Dias et al. 2014). These events pose a significant risk to people, property, and transportation routes. In addition to natural factors, human activities such as deforestation, construction, and improper land use can exacerbate the susceptibility to landslides during extreme rainfall events.

The topography, geology, vegetation cover, and land use within the sub watershed play significant roles in landslide susceptibility (Varnes 1978). Areas with steep slopes, weak geological formations, sparse vegetation, or human activities such as deforestation or construction are more prone to landslides (Corominas et al. 2014). Therefore, by following such

secondary variable evaluation steps, can effectively construct a decision hierarchy in AHP and facilitate a structured and systematic decision-making process.

Considering the long-term stability of landslides, an in-depth analysis of these bedrock-related factors provides valuable insights into the resilience of a particular area to landslide hazards. By understanding the bedrock's role in landslide initiation and propagation, mitigation strategies can be developed to reduce the risk and impact of landslides in vulnerable regions (Cruden and Varnes 1996). This knowledge is particularly important in areas with a history of landslides or where future landslide risks need to be assessed for sustainable land use and infrastructure development (Bhandari and Dias 1996). Understanding this relationship, implementing responsible road construction practices, and adopting appropriate mitigation measures are essential steps in reducing the impact of landslides on both infrastructure and communities.

Acknowledgments This paper forms an integral part of the research on "Evaluation of Sensitivity of the Combined Hydrological Model for Landslide Susceptibility Risk Mapping in Sri Lanka" being implemented by the Natural Resources Management and Laboratory Services, Central Engineering Consultancy Bureau (CECB) of the Ministry of Irrigation, Sri Lanka. Author would like to acknowledge the financial and technical support originally provided by the Japan Aerospace Exploration Agency (JAXA) and the Dr. L Samarakoon, Director, Geo Informatics Centre (GIC) of the Asian Institute of Technology (AIT) in executing this initial research works. The extensive support provided for collecting necessary digitized data by the Survey Department of Sri Lanka. Also, it was a part of the research leading to MPhil degree which has been registered at the Post Graduate Institute of Science, University of Peradeniya, Sri Lanka and has been granted permission to publish these data. The views expressed in the paper are however those of the authors only. Our grateful thanks are due to the Eng. B.A.S.S. Perera, Chairman and Eng. S.A.U.D.C. Siriwardana, General Manager, Central Engineering Consultancy Bureau for the encouragements.

References

Bhandari RK, Dias AAV (1996) Rain Triggered Slope Movement as Indicators of Landslide Dynamics. Proc. 7th International Symposium on Landslides; 17-21 June 1996, Trondheim, Norway: Balkema. pp. 1515–1520

Bhushan N, Ria K (2004) Strategic decision making: applying the analytic hierarchy process. London, Springer-Verlag London Limited

CECB Report (2003) Landslides case studies at Ratnapura 2003, Operational Professional Combine, CECB, Ministry of Irrigation and Water Management (MIWM)

Carrara A (1983) Multivariate methods for landslide hazard evaluation. Math Geol 15:403–426

Cooray PG (1994) Geological factors affecting landslides in Sri Lanka; Proc. National Symposium of Landslides in Sri Lanka, Colombo 17-19th March, 1994, pp 15–22

Campbell RH (1975) Soil slips, debris flows, and rainstorms in the Santa Monica Mountains and vicinity, southern California. U.S. Geological Survey Prof. Paper 851, pp. 51

Cruden DM, Varnes DJ (1996) Landslide types and processes, in landslides. Investigation and mitigation. In: Turner AK, Schuster RL (eds) Special report 247, transport research board. National Research Council, Washington D.C., pp 36–75

Corominas J, Van Westen C, Frattini P, Cascini L, Malet JP, Fotopoulou S, Catani F, Van Den Eeckhaut M, Mavrouli O, Agliardi F, Pitilakis K, Winter MG, Pastor M, Ferlisi S, Tofani V, Hervás J, Smith JT, Pitilakis K (2014) Recommendations for the quantitative analysis of landslide risk. Bull Eng Geol Environ 73(2):209–263. https://doi.org/10.1007/s10064-013-0538-8

Dias AAV, Gunathilaka AAJK (2014) Evaluation of sensitivity of the WAA and SINMAP models for landslide susceptibility risk mapping in Sri Lanka, Proceeding of the World Landslide Forum3 (WLF3), Beijing, China, 2-6 June 2014; Volume 2, Landslide Science for a Safer Geoenvironment, pp 167–173; Springer

Dias AAV, Abayakoon SBS, Bhandari RK (2014) Discrete boundary shear strength of a landslide at high rainfall precipitation zone in Sri Lanka; World Landslide Forum 3; Beijing, China, China, 2-6 June 2014; Volume 1, Landslide Science for a Safer Geoenvironment, pp 101–106; Springer

Dias AAV (2018) Spatial analysis and modelling for landslide susceptibility mapping in Kalawana, Sri Lanka. MPhil thesis, Post Graduate Institute of Science, University of Peradeniya, Peradeniya, Sri Lanka

Han WJ, Tsay WD (1998) Formulation of quality strategy using analytic hierarchy process, Twenty-Seven Annual Meeting of the Western Decision Science Institute. University of Northern, Colorado, USA, pp 580–583

IUGS (1997) Working group on landslides, committee on risk assessment: quantitative risk assessment for slopes and landslides—the state of the art. In: Cruden D, Fell R (eds) Landslide risk assessment. Balkema, Rotterdam, pp 3–12

Malczewski J (1999) GIS and multicriteria Desision analysis. John Willey and Sons, Inc, New York

Malczewski J (2006) GIS-based multicriteria decision analysis: a survey of the literature. International Journal of Geographical Information Science 20(7):703–726

Saaty LT (1980) The analytic hierarchy process. McGraw-Hill International, New York

Saaty LT (1990) How to make a decision: the analytic hierarchy process. Eur J Oper Res 48:9–26

Saaty TL (1994a) The fundamentals of decision making and priority theory with the analytic hierarchy process, the analytic hierarchy process series, vol VI. RWS Publications, Pittsburgh

Saaty TL (1994b) How to make a decision: the analytic hierarchy process. Interfaces 24(6):19–43

Saaty TL (2000) The fundamentals of decision making and priority theory with the analytic hierarchy process, 2nd edn. RWS Publications, Pitsburg, p 478

Saaty LT (2006) Rank from comparisons and from ratings in the analytic hierarchy/network processes. Eur J Oper Res 168:557–570

Saaty TL (2008) Decision making with the analytic hierarchy process. Int J Ser Sci 1(1):83–98

Stansbury D (2020) Cutting your losses: loss functions & the sum of squared errors loss; https://dustinstansbury.github.io/theclevermachine/cutting-your-losses

Varnes DJ (1978) Slope movement types and processes. In: Schuster RL, Krizek RJ (eds) Special Report 176: landslides: analysis and control. TRB, National Research Council, Washington, D.C., pp 11–33

Vitanage PW, (1994) Seismicity-neglected aspects of Sri Lankan landslide studies; proc. National Symposium of landslides in Sri Lanka, Colombo 17-19th march, 1994, pp 31-40

Open Access This chapter is licensed under the terms of the Creative Commons Attribution 4.0 International License (http://creativecommons.org/licenses/by/4.0/), which permits use, sharing, adaptation, distribution and reproduction in any medium or format, as long as you give appropriate credit to the original author(s) and the source, provide a link to the Creative Commons license and indicate if changes were made.

The images or other third party material in this chapter are included in the chapter's Creative Commons license, unless indicated otherwise in a credit line to the material. If material is not included in the chapter's Creative Commons license and your intended use is not permitted by statutory regulation or exceeds the permitted use, you will need to obtain permission directly from the copyright holder.



The Changing Seismic Site Response of the Brienz/Brinzauls Rock Slope Instability: Insights from 5 Years of Monitoring Before, During and After a Partial Collapse in June 2023

Mauro Häusler, Franziska Glueer, and Donat Fäh

Abstract

Unstable rock slopes pose significant hazards, requiring reliable monitoring for effective mitigation. However, existing methods often struggle to capture the dynamic nature of these environments, highlighting the need for enhanced monitoring techniques. This study investigates the Brienz/Brinzauls landslide in Switzerland to deepen our understanding through passive seismic techniques. The objective is to gain insights into the evolving seismic response of active slopes before, during and after collapse events, thus, filling gaps in our understanding of the dynamics of the seismic response of landslides. We deployed automated tracking of seismic parameters spanning 5 years (2018–2023) and covering a partial collapse of the landslide, and tracked resonance frequencies, seismic amplitudes, wavefield polarization, and seismic event occurrences. In addition, we compared the seismic parameters with geodetic surface displacement rates. Over the 5 years, significant seismic parameter shifts were observed associated with increased rock fall events, resonance frequency reductions, and changes in wavefield polarization. Immediate seismic responses during and post-collapse in June 2023 gradually reverted to pre-event conditions within 2 weeks. This study provides new data-driven insights into unstable rock slope behavior, potentially contributing to the development of new ways of seismic early-warning systems. It emphasizes the necessity of ongoing and future monitoring efforts to accurately anticipate future landslide incidents, given the degree of uncertainties in the parameters monitored, for example, caused by transient seismic signals.

Keywords

Seismic noise · Site effects · Landslide analysis · Rock slope instability · Seismic monitoring · Rock slope failure

1 Introduction

The Brienz/Brinzauls region in the Canton of Grisons, Switzerland, experienced a significant landslide event on June 15, 2023, involving a mass movement of 1.2 million cubic meters. This event resulted in damage to infrastructure and surrounding areas, gaining widespread public attention, particularly due to the proactive evacuation measures of the village of Brienz/Brinzauls (Gartmann 2023). While Häusler et al. (2022) conducted a comprehensive study analyzing passive seismic data related to the rock slope instability of Brienz/Brinzauls until 2022, the recent landslide event underscores the necessity for further investigation, extending the analysis and data availability until 2024. Passive seismic techniques have proven valuable in characterizing and monitoring landslides, offering insights into the dynamic behavior of slopes (Bessette-Kirton et al. 2022; Bontemps et al. 2020; Bottelin et al. 2017; Burjanek et al. 2018; Colombero et al. 2021; Fiolleau et al. 2020; Geimer et al. 2022; Häusler et al. 2021; Kleinbrod et al. 2019; Larose et al. 2015; Le Breton et al. 2021; Levy et al. 2010). However, there is a limited number of studies that have observed passive seismic signals during partial or complete failures (Levy et al. 2010; Taruselli et al. 2020).

Understanding the June 2023 landslide event in Brienz/Brinzauls requires contextualizing the geological setting of the Brienz/Brinzauls Deep-Seated Gravitational Slope Deformation (DSGSD). Spanning approximately 10 km^2, this area has distinct boundaries and geological features, including a lower domain composed of Flysch near the Brienz/Brinzauls village with a flat basal sliding plane (BTG

M. Häusler · F. Glueer (✉) · D. Fäh
Swiss Seismological Service, ETH, Zurich, Zurich, Switzerland
e-mail: mauro.haeusler@sed.ethz.ch; franziska.glueer@sed.ethz.ch; donat.faeh@sed.ethz.ch

© The Author(s) 2025

B. Abolmasov et al. (eds.), *Progress in Landslide Research and Technology, Volume 3 Issue 2, 2024*, Progress in Landslide Research and Technology, https://doi.org/10.1007/978-3-031-72736-8_4

2021), and an upper domain characterized by rock formations such as dolomites, rauhwackes, and marly schists (Kenner et al. 2022; Krähenbühl and Nänni 2017). The DSGSD exhibits various kinematic mechanisms, including sliding and toppling (Loew et al. 2023). The DSGSD, with a volume ranging from 100 to 200 million cubic meters, initiated sliding in prehistoric times, possibly triggered by glacial retreat after the last glacial maximum. Historical records indicate lateral landslides in the region (Igl Rutsch), suggesting a recurring geological phenomenon (Heim 1932). The June 15, 2023 landslide occurred in the upper domain from a sub-volume named "Insel" (island, Fig. 1), with an accelerated phase marked by increased rock fall incidents in the week leading up to the event (Manconi et al. 2023). Proactive evacuation measures were undertaken in response to the escalating landslide activity (Gartmann 2023).

This study presents seismic data associated with the Brienz/Brinzauls landslide, comparing data collected before, during, and after the recent partial collapse with long-term information dating back to June 2018. While this study does not introduce new methods, it presents new data following a significant landslide event (partial collapse), contributing to our understanding of ambient seismic data linked to landslides, aiming for improving prediction and mitigation of

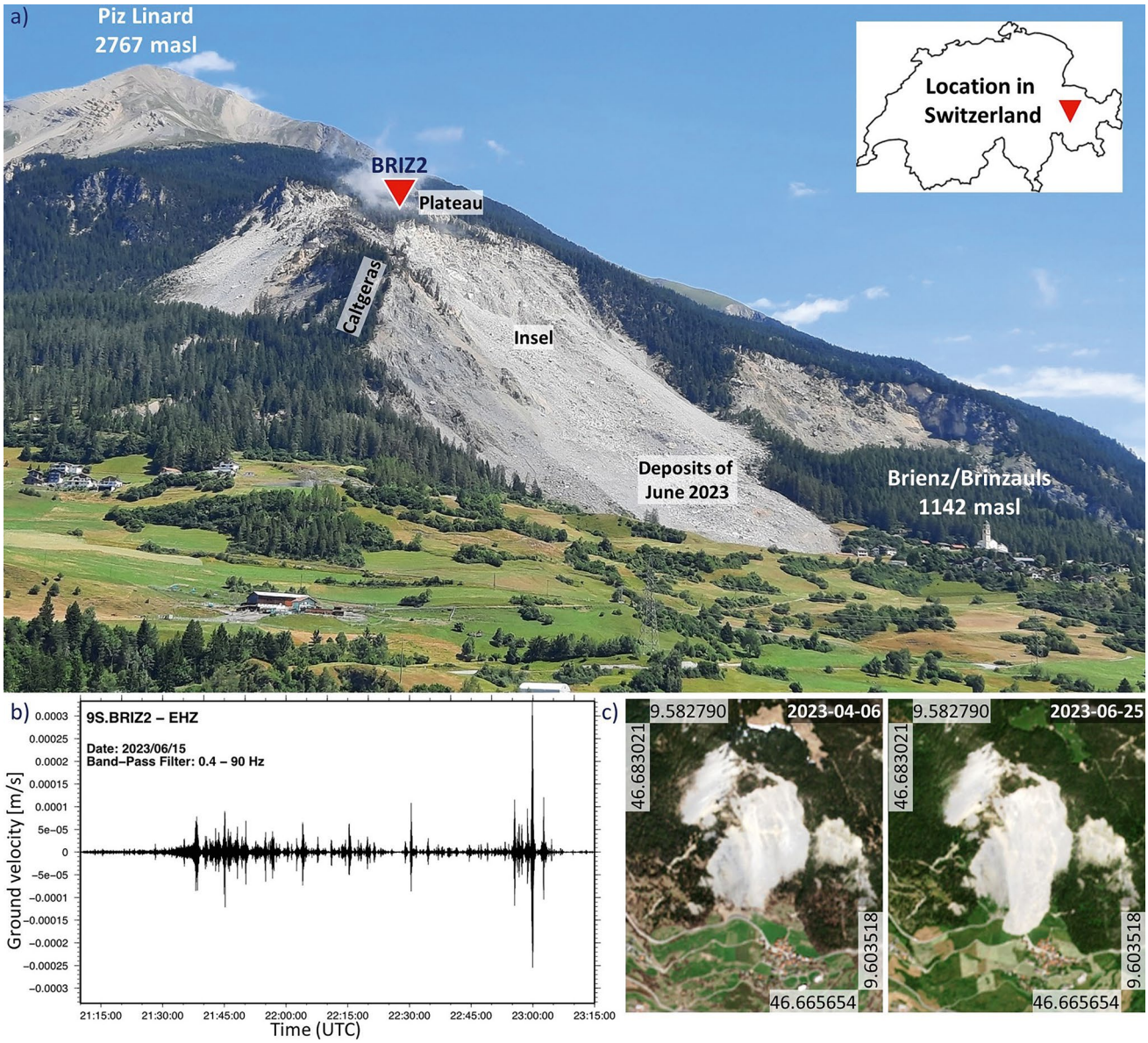


Fig. 1 Overview of the slope instability at Brienz/Brinzauls; (**a**) Photograph of the Brienz/Brinzauls rock slope instability looking in direction NE (Photo by Andrea Manconi, SLF, July 12, 2023) with location of seismometer BRIZ2; the inset shows the location in Switzerland; (**b**) Seismogram of the station BRIZ2 between 21:15 and 23:15 UTC on June 15, 2023, showing the collapse of the "Insel" compartment; (**c**) Sentinel-2 images from April 6, 2023 (left) and June 25, 2023 (right), coordinates in WGS84, EO Browser (2023)

future occurrences. Furthermore, this study highlights the susceptibility of automated passive seismic monitoring of landslides to increased occurrences of seismic events, emphasizing the need for ongoing research and development.

2 Data and Methods

Our investigation focuses on ambient vibration data collected at the permanent seismic station BRIZ2 (WGS84: 46.67868, 9.59269). The continuous data stream of seismic data, available from May 2018 to January 2024, was acquired using a Lennartz LE-3Dlite/1 s short-period seismometer recording at 200 Hz. This seismometer is coupled with a solar-powered Nanometrics Taurus digitizer and data transmission through mobile phone network. For automated signal processing, we employed normal mode analysis (Häusler et al. 2021) and wavefield polarization analysis (Koper and Hawley 2010) at intervals of 60 min across two frequency bands.

Band A, which is presumed to represent the entire slope stability or a large part of it (Häusler et al. 2022), covers the frequencies 1.6–2.2 Hz for normal mode analysis and 1.0–2.3 Hz for polarization analysis. In contrast, Band B is supposed to represent a sub-volume within the "Plateau" domain (second resonance frequency; Figs. 1a, and 2) and covers the frequencies 2.3–3.05 Hz for normal mode analysis and polarization analysis.

The selection of these bands was guided by assessments of results from frequency domain decomposition (FDD) modal analysis, as depicted in Fig. 5, and the passive seismic mapping presented by Häusler et al. (2022). We implemented a concept of automated signal processing, following Häusler et al. (2021). This approach enhances efficiency and objectivity by automating routine tasks such as frequency selection, parameter extraction, and noise reduction. Real-time automated processing enables the timely detection of changing seismic site response and associated structural dynamics. Six parameters were automatically monitored: resonance frequency [Hz], power [dB] of the selected resonance frequency, principal polarization azimuth of the wavefield [°N], dip of the wavefield polarization [°] and number of seismic events per hour. For post-processing analyses, these data were compared with surface displacement [m/year], and relative geodetic azimuthal direction [°N] from GNSS measurements.

The resonance frequency [Hz], a fundamental property of structural systems, is determined by the mass and stiffness matrices. Analyzed through the frequency domain decomposition (FDD) technique for normal mode analysis (Bottelin et al. 2017; Brincker and Ventura 2015; Häusler et al. 2021; Mercerat et al. 2020; Michel et al. 2010; Poggi and Fäh 2010), variations in resonance frequency indicate changes in the stiffness of the rock mass, potentially signaling progressive failure, accumulation of damage, or alterations in mass (Colombero et al. 2021; Levy et al. 2010). FDD employs singular value decomposition to reveal principal components of vibration data, consolidating input traces into a unified plot for a comprehensive view. The power parameter [dB] quantifies the magnitude of the first singular value at the selected resonance frequency and correlates with signal strength of the vibration data. Using the polarization analysis as introduced by Koper and Hawley (2010), we calculate the coherency matrix across all three components and evaluate the directionality of the seismic signal through eigenvalue decomposition. Unlike FDD, the polarization analysis provides polarization information averaged within a defined frequency band rather than at a given frequency (e.g., the tracked resonance frequency). The algorithm provides the azimuth parameter (°N), which denotes the wavefield's orientation from North and the dip parameter [°] representing the wavefield's inclination relative to the horizontal plane. Additionally, ellipticity describes the degree of polarization of the wavefield, indicating circular (0) to linear (1) particle motion. We integrated a seismic event counter using the 'short-time-average through long-time-average trigger' (STA/LTA) algorithm (e.g., Trnkoczy 2009). This STA/LTA ratio is then compared to a user-selected threshold value. Employing a 20-second short-time average window (STA) and 180 seconds for the long-time average window (STA), the trigger threshold level is set at 2.25, with a de-trigger threshold at 1.5. Though not employed as a classifier, the STA/LTA filter serves as a useful proxy for identifying potential landslide activity (e.g., rock fall).

However, events not originating from the landslide can distort the result. We compared the seismic parameters to surface displacement data acquired from a permanent GNSS station nearby (station 6003) and a marker that is periodically surveyed with a portable high precision differential GNSS instrument (marker 1007; see Fig. 2). Both methods ensure an accuracy of about 0.02 m in position. In addition, the secondary azimuthal geodetic direction of movement [°N] is calculated based on coordinates from subsequent measurements. To analyze relative secondary displacement vectors, we employed a singular value filter to retrieve and eliminate the principal component of the displacement field, using several GNSS stations and markers spread across the landslide (for a detailed description of the geodetic analysis, see Häusler et al. 2022).

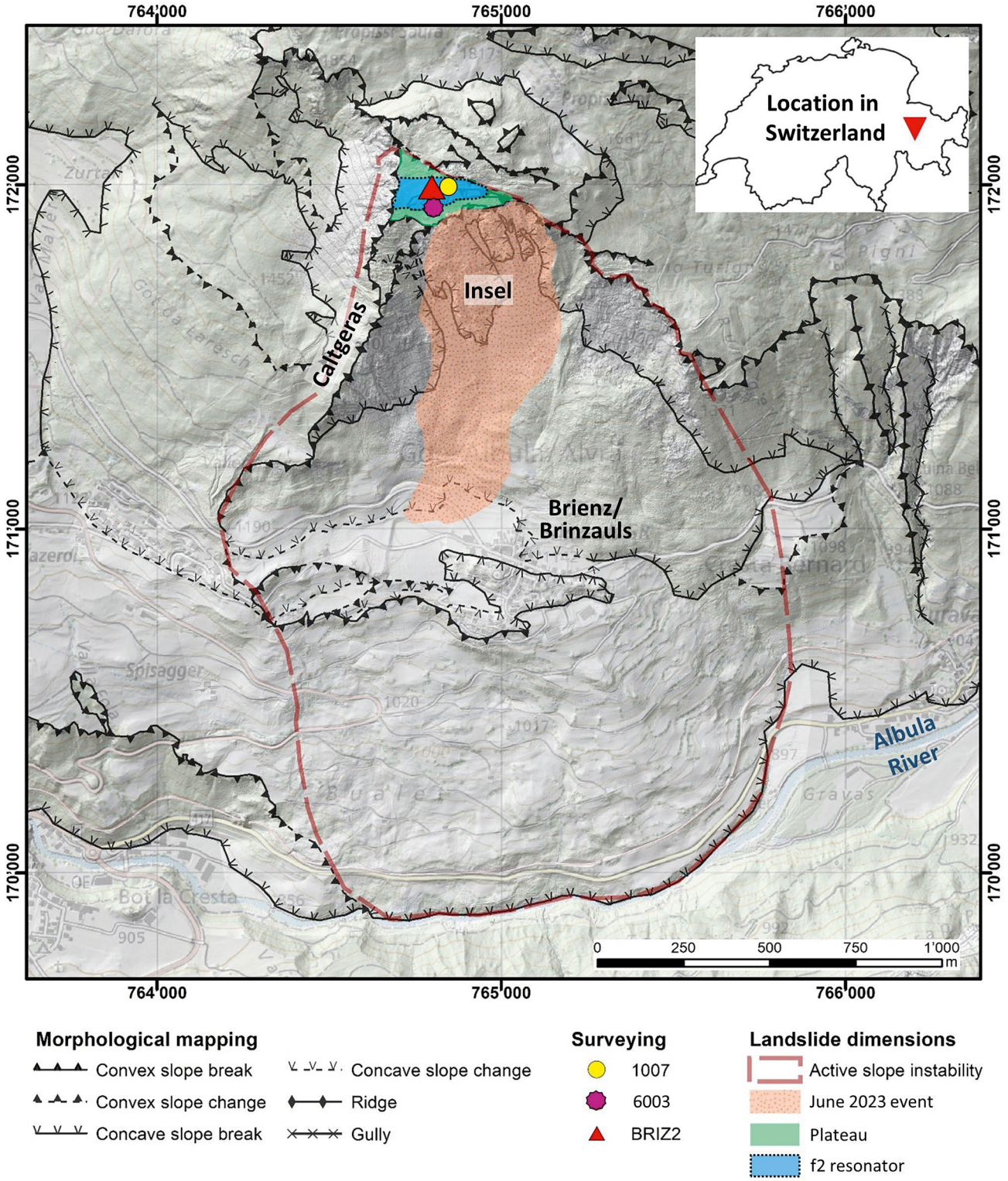


Fig. 2 Geomorphological map of the Brienz/Brinzauls landslide. The landslide event of June 2023, the location of the surveying points of permanent GNSS (6003), differential GNSS (1007) and seismic station BRIZ2, and large-scale geomorphologic features based on aerial photographs and the digital elevation model swissALTI3D (2018) are highlighted. Geodata source: Federal Office of Topography, coordinates in CH1903

3 Results

In this section, we present the results focusing on the second resonance frequency, f_2 (B: 2.3–3.05 Hz), while the findings related to the fundamental mode, f_1 (A: 1.6–2.2 Hz), are detailed in the Electronic Appendix. Based on passive seismic mapping, resonance frequency f1 is assumed to represent the entire unstable volume of the Brienz/Brinzauls rock slope instability (Häusler et al. 2022) with an estimated volume in the range of 10 to 25 million cubic meters. However, the exact spatial extent has not yet been resolved. In addition, the seismic response below 2.2 Hz appears complex and the resonance frequency is not visible consistently. Therefore, we primarily analyze f_2 due to its more pronounced characteristics, which represent a sub-volume in the vicinity of the station with an estimated volume in the range of 1 to 2 million cubic meters.

The monitoring of this sub-volume is providing insights into the local behavior of the slope instability. Over our analysis period, we observed several variations in the seismic parameters of f_2, indicating nine significant changes. To illustrate these changes, we employed two levels of detail: Level A (Fig. 3), covering the long-term period of 5 years (2018–2023) with a centered 14-day running median for visualization purpose and Level B (Fig. 4), spanning the acceleration period from November 2022 to September 2023 with a 7-day running median. The seismic data underwent fully automated processing, eliminating manual intervention but potentially increasing uncertainties due to inappropriate initial parametrization.

1. Mid-May, 2019 (Fig. 3, blue dashed line 1): We observe an initial drop in resonance frequency from 3.0 Hz to 2.8 Hz and back to 2.9 Hz. This is accompanied by an increase in power from −145 dB to −140 dB and back to −150 dB. The dip changes from −4° to −2°, while the ellipticity rises from 0.46 to 0.61 and back again. Displacement rates increases from about 2 to 3 m/yr., and the geodetic azimuth starts to drop from 110°N to 100°N counterclockwise. Since the beginning of the monitoring period, the seismic azimuth changed by 13° from 127°N to 114°N.
2. Mid-August, 2019 (Fig. 3, blue dashed line 2): Seismic events decrease notably from over 10 to less than 2 per hour, accompanied by a reduction in deformation rate (back to 2.5 m/yr). Resonance frequency remains at 2.9 Hz, power increased to −145 dB and the seismic azimuth continues to rotate counterclockwise, from 114°N in June 2019 to 111°N.
3. Mid-May, 2020 (Fig. 3, blue dashed line 3): The ellipticity reaches its minimum value at 0.29, with the resonance frequency starting to decrease on an irregular trajectory. The azimuth continues to decrease, passing 73°N and the dip starts to fluctuate and increase. In the months after, ellipticity slowly increases again.
4. December, 2020 (Fig. 3, blue dashed line 4): After a short period of increased seismic events (up to eight per hour), the resonance frequency starts decreasing, temporarily reaching 2.5 Hz, and power decreases to −150 dB. The seismic azimuth reaches 51°N and, from this point in time, slows down its rotational rate. The dip fluctuates around 0°. Deformation rate increases to 3 m/yr., whereas the geodetic azimuth stabilizes at about 40°N. In the following months, the resonance frequency recovers to 2.8 Hz.
5. May, 2021 (Fig. 3, blue dashed line 5): We observe a surge in seismic events reaching up to 7 events per day, with the resonance frequency and power remaining constant around 2.8 Hz and -147 dB, respectively. The dip shows abrupt fluctuations during this period, shifting from −2 to +5° and back accompanied by a constant geodetic deformation rate of 3 m/yr.
6. August, 2021 (Fig. 3, blue dashed line 6): A significant decrease in seismic activity (<2 events per hour) coincides with a slight decrease in resonance frequency to 2.7 Hz and the seismic azimuth reaching 42°N. The dip now remains at positive values between 0° and 3° and ellipticity starts to increase to reach about 0.6 in mid-2022.
7. November, 2022 (Fig. 3, blue dashed line 7, with more details in Fig. 4): Seismic events increase significantly up to 13 per hour. A drop in resonance frequency from 2.7 Hz in November to 2.6 Hz in January 2023 aligns with a decrease in power to −149 dB. Azimuth, dip, ellipticity and deformation rate show no significant reaction.
8. March, 2023 (Fig. 3, blue dashed line 8, with more details in Fig. 4): Seismic events escalate (up to 18 events per hour), with the resonance frequency increasing to 2.9 Hz in the following months. At the same time, power and ellipticity start to increase with significant scatter and reach their peaks at −134 dB and 0.64, respectively, just before the landslide event. Surface deformation rates increased to about 3 m/yr.
9. Mid-June, 2023 (Fig. 3, blue dashed line 9, with more details in Fig. 4): The landslide event on June 15 leads to instant reactions in almost all parameters, returning to their previous values within 2 weeks after failure. Resonance frequency rapidly peaks at 2.9 Hz and decreases post failure back to 2.7 Hz. Power reaches a post-failure level of −146 dB with strong fluctuations. Ellipticity drops to values between 0.3 and 0.5. The number of seismic events slowly reduces but remains higher compared to pre-2023. At the day of the landslide event, surface deformation rates temporarily reach 31 m/yr. (~8.5 cm/day) and subsequently decrease to about 2 m/yr.

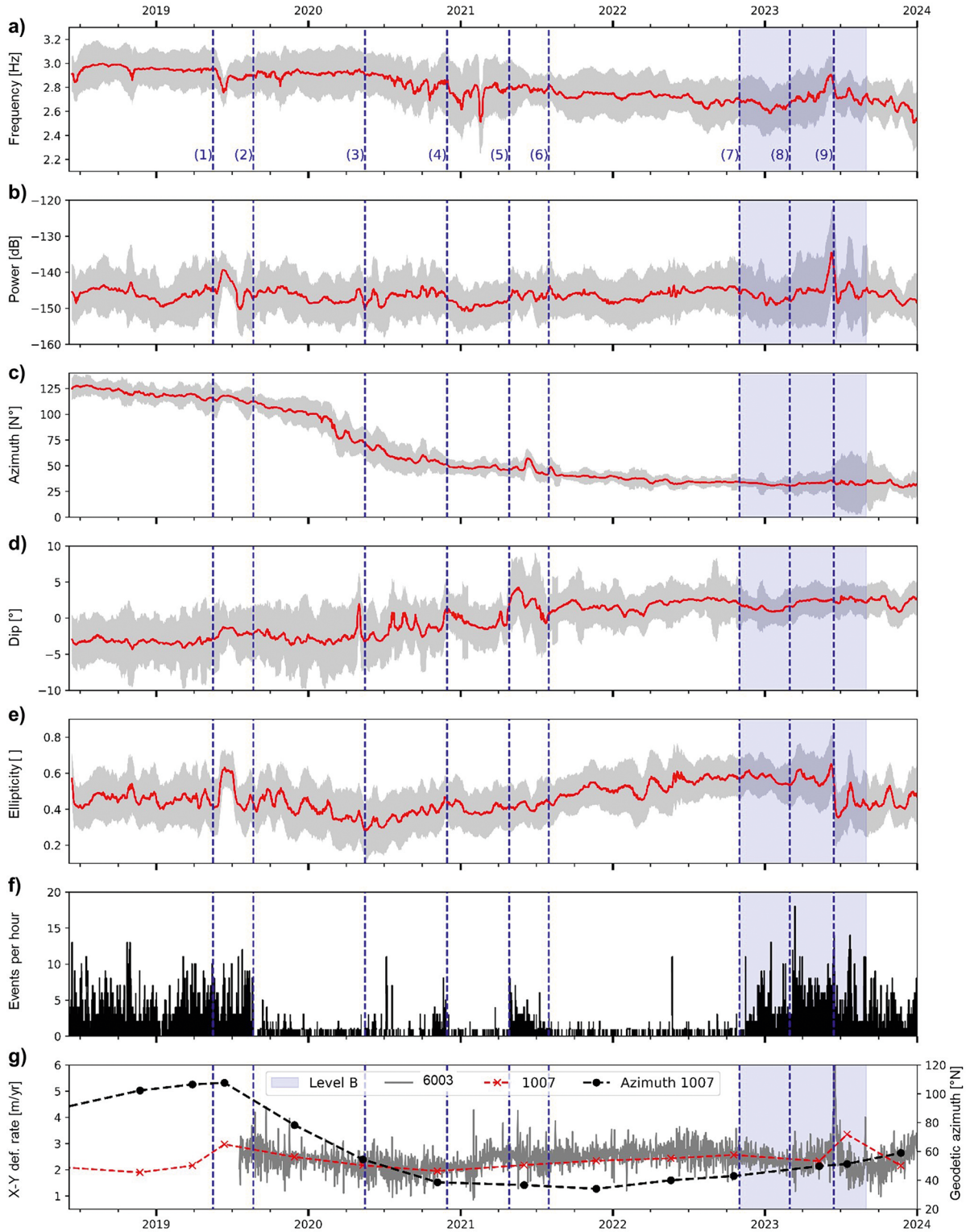


Fig. 3 Resulting parameters from the automated seismic monitoring at Brienz/Brinzauls (BRIZ2) for level A (2018–2023; 5 years, 14-day centered running median) in red solid lines with standard deviation in grey for the seismic parameters. The vertical blue dashed lines labelled 1) to 9) represent the signal changes discussed in the text; the time window of level B is held in transparent blue from 11/2022–09/2023; (**a**) the change in frequency of station BRIZ2 over the course from June 2018 to December 2024; (**b**) the power of the first singular value; (**c**) the azimuth representing the orientation of the wavefield from North; (**d**) the dip representing the inclination of the wavefield to the horizontal plan; (**e**) the ellipticity parameter describing the degree of polarization of the wavefield; (**f**) the seismic event counter using 'short-time-average through long-time-average trigger' (STA/LTA); (**g**) 2D deformation rate calculated from GNSS stations No. 6003 (permanent) and No. 1007 (semi-annually) and for No. 1007 the secondary azimuthal geodetic direction of movement from North

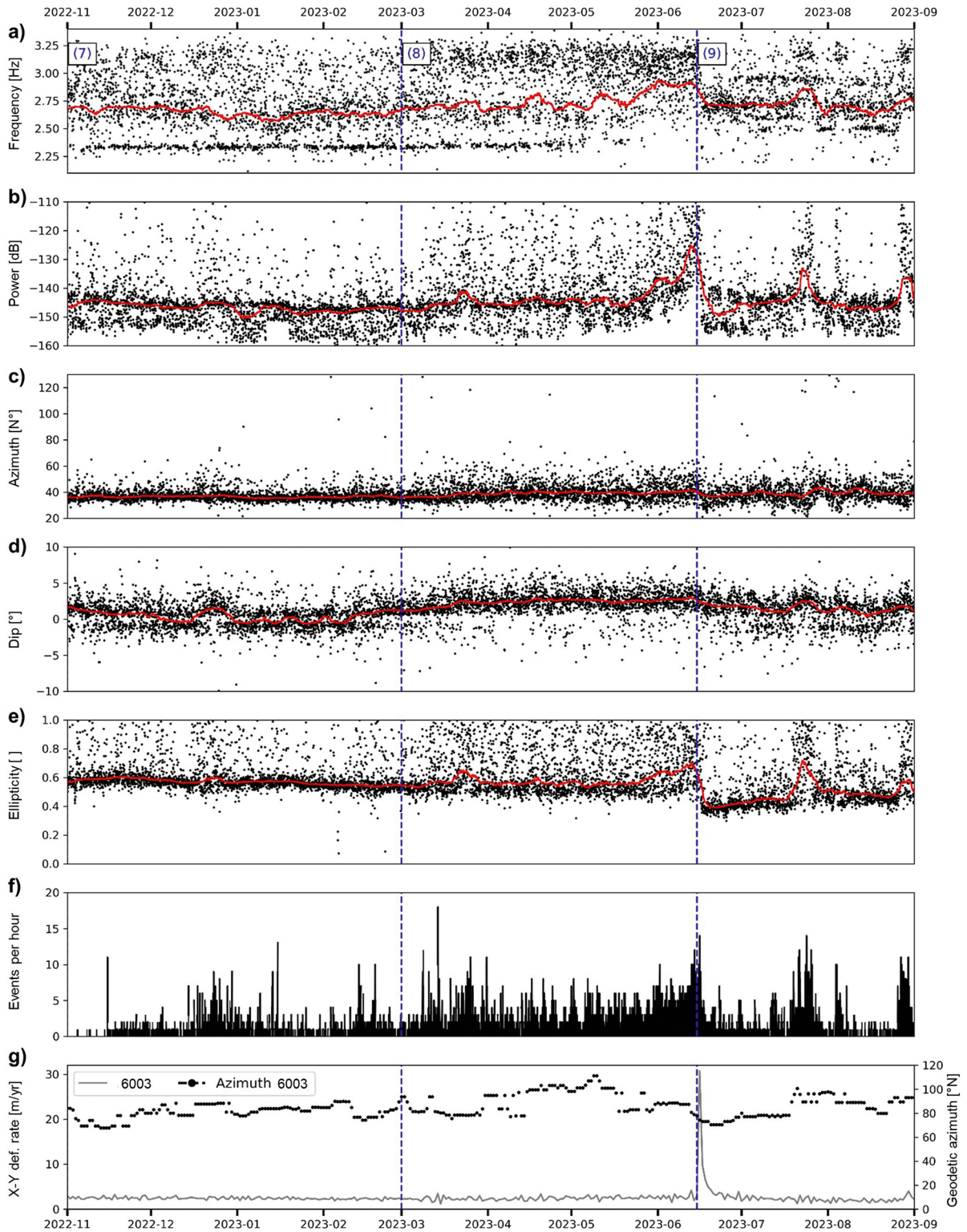


Fig. 4 Resulting parameters from the automated seismic monitoring at Brienz/Brinzauls (BRIZ2) for level B (November 2022—September 2023; 7-day centered running median) in red solid lines with hourly values indicated by black points. The vertical blue dashed lines labelled 7) to 9) represent the significant signal changes discussed in the text; (**a**) the change in frequency of station BRIZ2 over the course from November 2022—September 2023; (**b**) the power of the first singular value, i.d. the power at the resonance frequency; (**c**) the azimuth representing the orientation of the wavefield from north; (**d**) the dip representing the inclination of the wavefield to the horizontal plan; (**e**) the ellipticity parameter describing the degree of polarization of the wavefield; (**f**) The seismic event counter using 'short-time-average through long-time-average trigger' (STA/LTA); (**g**) 2D deformation rate and secondary azimuthal geodetic direction of movement from North calculated from GNSS stations No. 6003 (permanent)

In summary, our analysis from 2018 to early 2024 of seismic parameters related to the second resonance frequency f2 revealed significant variations. Apart some shorter-term changes, the signal power shows a seasonal variation with minima in winter. For the seismic parameters we observed nine notable changes during the observation period. Noteworthy events included decreases and subsequent recoveries in resonance frequency and power levels, shifts in azimuthal orientation, and fluctuations in seismic event rates.

The most prominent event was the landslide occurrence in mid-June 2023, which triggered instant reactions across multiple parameters, reverting to pre-event conditions within 2 weeks post-failure. To this point in time (January 2024), resonance frequency is on a decreasing branch (2.5 Hz), azimuth is slightly decreasing (32°N), dip is levelled around 3°, and ellipticity shows a scatter between 0.4 and 0.5.

Similar observations can be done for the presumed fundamental frequency of resonance f_1 of the instability at about 2 Hz (Figs. S1 and S2 in the Electronic Appendix). Since this resonance frequency is less pronounced, uncertainties are larger than for the sub-volume described before. The fundamental frequency of resonance changed from about 2.1 Hz to 1.8 Hz. For the signal power, we observe three strong increases between events (1) and (2), between (5) and (6), and before the collapse in June 2023 (9). The wavefield polarization changed from about 130° in 2018 to 20° in 2023. The associated dip changed from −5° in 2018 to about +3° in 2023. Ellipticity values increase from about 0.3 in 2018 to about 0.45 before the rock failure and decrease to about 0.4 after the failure. In January 2024, the fundamental frequency f_1 and wavefield polarization show a similar trend as observed for the resonance frequency f_2.

4 Discussion

The research provides insights into the dynamic behavior of the Brienz/Brinzauls rock slope instability, particularly focusing on seismic parameters such as resonance frequency, seismic power, wavefield polarization, dip, and ellipticity compared to surface displacement measurements. Over the monitoring period from 2018 to early 2024, we observed distinct variations in these parameters, which were closely associated with the evolving instability dynamics. Notably, the decrease in resonance frequency, particularly after December 2020 and November 2022, is interpreted as a reduction in material stiffness attributed to the disintegration of landslide material.

Our research contributes to the existing literature of how seismic parameters reflect underlying processes within the unstable mass, thus how landslide kinematics and wavefield polarization are linked (Burjanek et al. 2010; Burjanek et al. 2018; Häusler et al. 2022; Häusler et al. 2021; Kleinbrod et al. 2019). We hypothesize that polarization follows direction of minimum stress (σ3), similarly to what is observed in large tectonic regimes (Pischiutta et al. 2012). However, such physical relations are yet to be proven by physical or numerical models. In line with earlier research findings on Brienz/Brinzauls, our study adds additional data regarding the temporal development of seismic parameters preceding and succeeding partial failure.

Unexpectedly, we observed a remaining low level of ellipticity and no immediate persistent change in resonance frequency f2 following the collapse of the "Insel" compartment, contrary to the anticipated change in stress regime in the larger mass. This supports the hypothesis that the resonance frequency f2 represents a rather local feature and is not sensitive to actions in other compartments. This finding underscores the complex interplay between seismic parameters and the structural integrity of different compartments within the instability. Due to higher uncertainty in monitoring the fundamental frequency f1 and the large volume related to it, we cannot expect to detect potential changes due to the partial collapse with a volume of only 1.2 million cubic meters.

A key limitation of our monitoring system lies in the inability to precisely identify the sources of seismic events, particularly transient signals originating from rock fall or rupture processes within the unstable mass. While our event detection algorithm captured a significant number of seismic events, it is possible that some events went undetected, leading to incomplete data interpretation and, at the same time, erroneously count events not related to the landslide. Additionally, the auto-picking algorithm for resonance frequencies may introduce uncertainties, particularly during periods of high seismic activity. We observed an immediate decrease in resonance frequency, amplitude and ellipticity right after the collapse of the "Insel" compartment, synchronously with the rapid reduction in the number of seismic events. We interpret that before failure of the "Insel", a large portion of the ambient vibration wavefield was constituted by energy emitted by rock fall events and ruptures within the landslide mass. Such signals show high power towards higher frequencies and are heavily directional, leading to high ellipticity values and ill-picked resonance frequencies in the automatic monitoring procedure (Fig. 5). Such signals should be treated as transient signals to be omitted in ambient vibration analysis and a refined picking algorithm might reduce their influence. In order to separate the ambient vibration wavefield from the transient signals, we tested different anti-trigger parametrizations for the implemented STA/LTA filter. However, the results remained unsatisfactory, most probably due to too many transient signals in particular such with small amplitudes not detected by the filter. Therefore, more advanced event detectors should be implemented. The current setup of the monitoring system uses static sets of

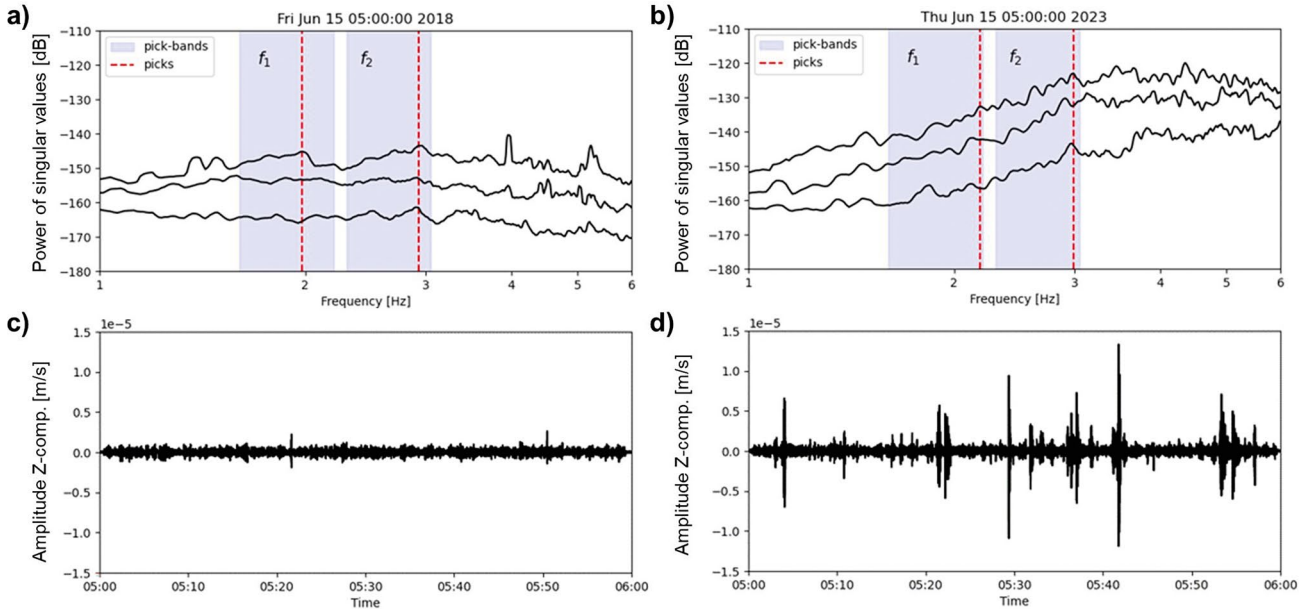


Fig. 5 Singular values of the FDD modal analysis with pick bands in light blue of f1 (1.6–2.2 Hz) and f2 (2.3–3.05 Hz) and selected resonance frequency (red dashed line) for two different points in time without and with seismic events (presumably rock fall); (**a**) power of singular values from June 15 2018; (**b**) power of singular values for June 15, 2023; (**c**) amplitude of the Z-component for June 15, 2018; (**d**) amplitude of the Z-component for June 15, 2023

parameters. However, in case of irreversible frequency changes, the resonance frequency might wander out of the predefined frequency band. Therefore, more dynamic system parametrizations could improve the monitoring performance, for example, by using frequency bands based on most recent past data.

Future studies should focus on refining monitoring techniques to better differentiate between ambient vibration signals and transient seismic events. Incorporating dynamic system parameters, which adjust frequency bands based on real-time data, could improve the accuracy of resonance frequency tracking.

Furthermore, investigating the relationship between seismic parameters and external factors such as weather conditions and seasonal variations may provide further insights into the underlying mechanisms driving instability dynamics.

5 Conclusion

The landslide event on June 15, 2023 at Brienz/Brinzauls in Switzerland had significant consequences, including infrastructure damage and the evacuation of nearby residents. In this study, we examined ambient vibration data collected from a permanent seismic station located on top of a partially collapsed instability. Our analysis focused on tracking resonance frequencies using automated techniques to study normal modes and wavefield polarization, with the aim to detect precursory signals preceding the collapse. Our observations from June 2018 to June 2023 revealed a notable decrease in resonance frequencies, from 3 Hz to 2.5 Hz for f_2 and 2.1 to 1.8 for f_1, indicating a reduction in bulk stiffness attributed to ongoing disintegration. We also observed similar counterclockwise rotations in wavefield polarization for the two resonance frequencies, with 95° for f_2 coinciding with changes in secondary surface deformation vectors. In the weeks preceding the partial collapse, no clear and irreversible precursory signals could be detected, which could have been interpreted as an indication of the imminent failure of the "Insel" compartment. In contrast, the observed permanent changes are attributed to changes in the neighboring landslide compartment, where the monitoring station is located on. Following the event, most parameters quickly returned to pre-acceleration values within 2 weeks, suggesting that the structural integrity of the monitored rock volume of the sub-compartment within the "Plateau" sector was likely not immediately and severely affected by the partial collapse of 1.2 million m^3. However, continued monitoring is essential to understand how the remaining volume responds to the recent failure event. Here, particularly phases of dropping resonance frequency and elevated ellipticity as an indicator for the activation of the landslide mass shall be looked at.

Our study highlights the challenges of automated passive seismic monitoring in landslide-prone areas, particularly due to high rates of seismic events such as rock falls or sliding events. These transient signals pose a challenge by increas-

ing wavefield ellipticity and disrupting stable resonance frequency tracking. To overcome this challenge, future advancements in monitoring systems should integrate effective anti-trigger filters and dynamic monitoring parameters tailored to sites with rapidly changing site responses. Despite these challenges, our findings indicate a promising direction for improving the method towards a novel early-warning system. A deeper understanding of structural changes preceding surface deformations could improve the reliability and effectiveness of landslide prediction and mitigation efforts.

Acknowledgments We thank A. Huwiler (office for forest and natural hazards, Canton of Grisons) and the commune Albula/Alvra for their collaboration, shared data, and unrestricted access to the site. We thank Andrea Manconi for the picture of the Landslide and Tobias Diehl for the seismogram both used in Fig. 1. We thank the Swiss National Science Foundation and the Swiss Federal Office for the Environment for their support.

This research was funded by the projects "4D seismic response and slope failure" Swiss National Science Foundation SNF (200021E 177586), "Skyfall" ETHZ 0-20361-17, "Quantification of the seismic response of instable slopes and its time variability: an important indicator for potential mass movements" SNF 200020_214916, and "Erkennung, Charakterisierung und Überwachung von Instabilitäten mit seismischen Technologien" Swiss Federal Office for the Environment FOEN 00.5032.PZ/ EC049A5A7.

All authors contributed to the study conception and design. Material preparation and data collection were performed by Mauro Häusler. Data analysis was performed by all authors. The manuscript was written by Franziska Glueer and all authors commented on previous versions of the manuscript. All authors read and approved the final manuscript.

Appendix

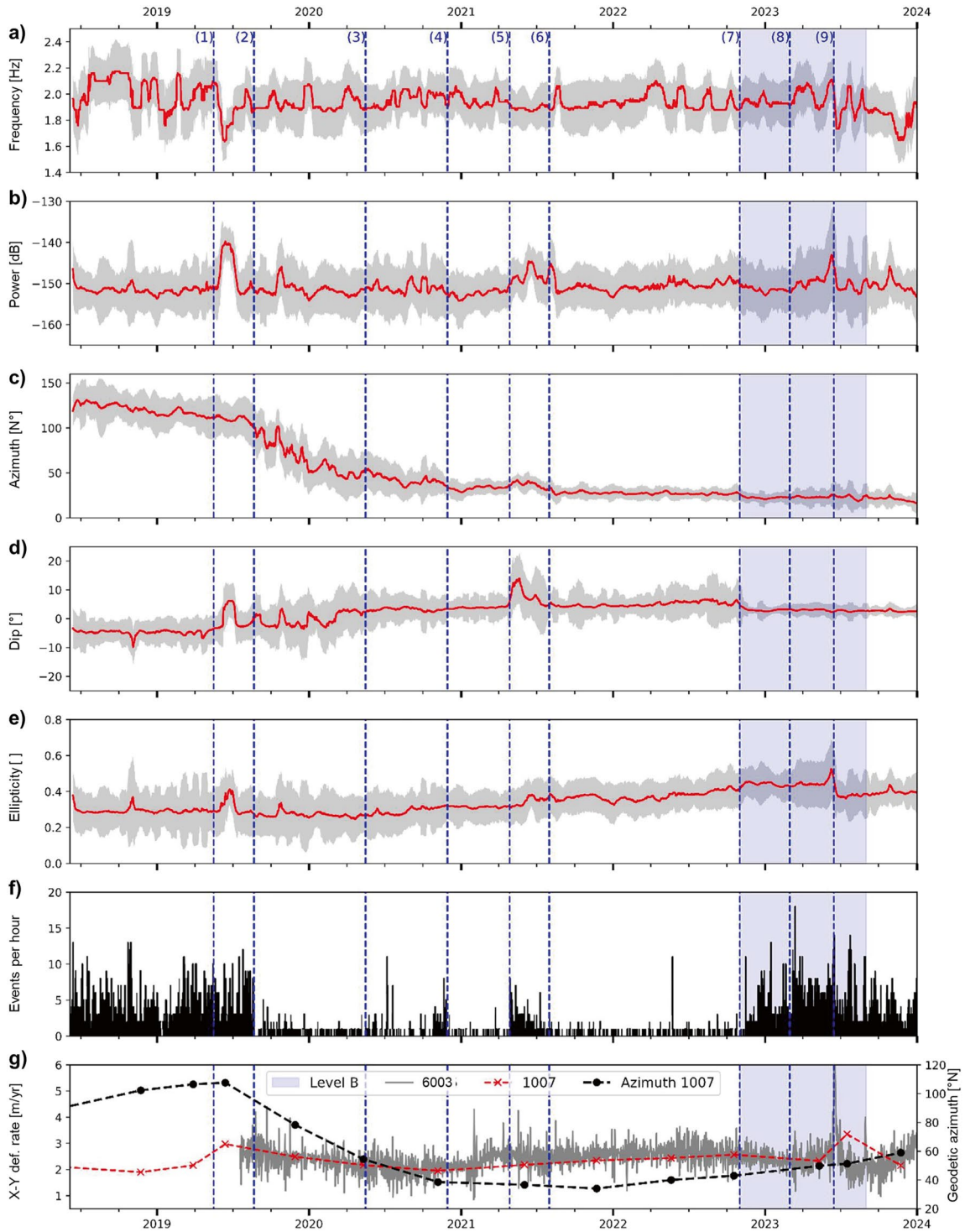


Fig. S1 Parameters for f_1 from the seismic monitoring at Brienz/Brinzauls (BRIZ2) for level A (2018 – 2023, 14-day centered running median) in red solid lines with standard deviation in grey for the seismic parameters. The vertical blue lines labelled (1 to 9) represent the signal changes; the time window of level B is held in transparent blue from 11/2022 – 09/2023; (**a**) resonance frequency of station BRIZ2; (**b**) power of the first singular value; (**c**) azimuth, representing the orientation of the polarization from North; (**d**) dip, representing the inclination of the polarization to the horizontal plan; (**e**) ellipticity, describing the degree of polarization; (**f**) number of seismic events using a 'short-time-average through long-time-average' trigger; (**g**) 2D deformation rate calculated from GNSS stations No. 6003 (permanent) and No. 1007 (semi-annually) and for No. 1007 the secondary azimuthal geodetic direction of movement from North

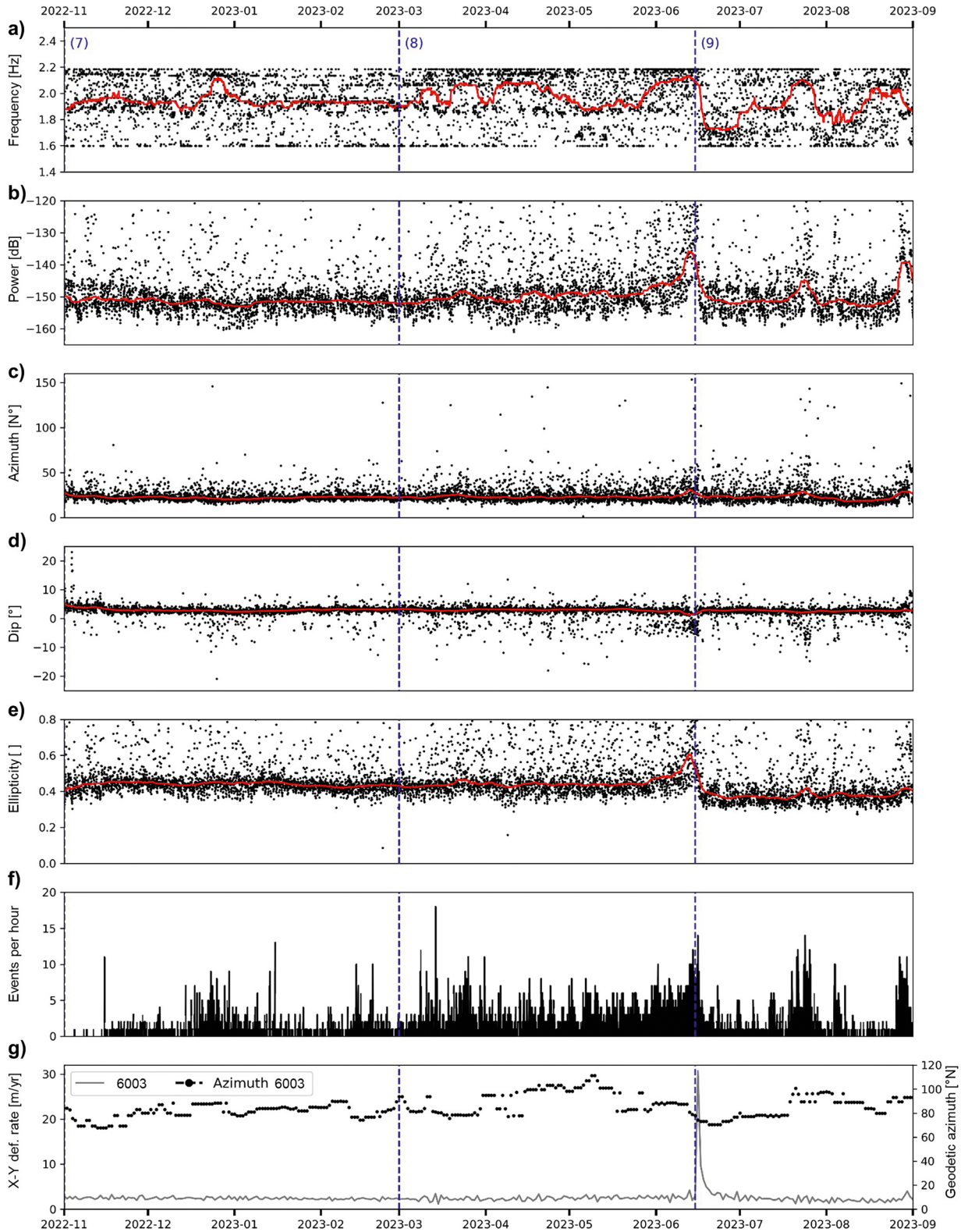


Fig. S2 Parameters for f_1 from the seismic monitoring at Brienz/Brinzauls (BRIZ2) for level B (November 2022 – September 2023; 7-day running centered median) in red solid lines with hourly values indicated by black points. The vertical blue lines labelled (1 to 9) represent the signal changes; (**a**) resonance frequency of station BRIZ2; (**b**) power of the first singular value; (**c**) azimuth, representing the orientation of the polarization from North; (**d**) dip, representing the inclination of the polarization to the horizontal plan; (**e**) ellipticity, describing the degree of polarization; (**f**) number of seismic events using a 'short-time-average through long-time-average' trigger; (**g**) 2D deformation rate and secondary azimuthal geodetic direction of movement from North calculated from GNSS stations No. 6003 (permanent)

References

Bessette-Kirton EK, Moore JR, Geimer PR, Finnegan R, Häusler M, Dzubay A (2022) Structural characterization of a toppling rock slab from Array-based ambient vibration measurements and numerical modal analysis. JGR Earth Surface 127(8):13. https://doi.org/10.1029/2022JF006679

Bontemps N, Lacroix P, Larose E, Jara J, Taipe E (2020) Rain and small earthquakes maintain a slow-moving landslide in a persistent critical state. Nat Commun 11(1):10. https://doi.org/10.1038/s41467-020-14445-3

Bottelin P, Baillet L, Larose E, Jongmans D, Hantz D, Brenguier O, Cadet H, Helmstetter A (2017) Monitoring rock reinforcement works with ambient vibrations: La Bourne case study (Vercors, France). Eng Geol 226:136–145. https://doi.org/10.1016/j.enggeo.2017.06.002

Brincker R, Ventura C (2015) Frequency-domain identification. In: Introduction to operational modal analysis, pp 261–280. https://doi.org/10.1002/9781118535141.ch10

BTG (2021) Rutschung Brienz/Brinzauls GR, Geologische Detailuntersuchungen 2018 bis 2021, Sondierbohrungen. Report 5897–5813

Burjanek J, Gassner-Stamm G, Poggi V, Moore JR, Fäh D (2010) Ambient vibration analysis of an unstable mountain slope. Geophys J Int 180(2):820–828. https://doi.org/10.1111/j.1365-246X.2009.04451.x

Burjanek J, Gischig V, Moore JR, Fah D (2018) Ambient vibration characterization and monitoring of a rock slope close to collapse. Geophys J Int 212(1):297–310. https://doi.org/10.1093/gji/ggx424

Colombero C, Jongmans D, Fiolleau S, Valentin J, Baillet L, Bièvre G (2021) Seismic noise parameters as indicators of reversible modifications in slope stability: a review. Surv Geophys 42(2):339–375. https://doi.org/10.1007/s10712-021-09632-w

EO Browser (2023) Modified copernicus sentinel data *Sentinel Hub*. https://apps.sentinel-hub.com/eo-browser/, Sinergise Ltd.

Fiolleau S, Jongmans D, Bièvre G, Chambon G, Baillet L, Vial B (2020) Seismic characterization of a clay-block rupture in Harmalière landslide, French Western Alps. Geophys J Int 221(3):12–1788. https://doi.org/10.1093/gji/ggaa050

Gartmann C (2023) Brienz/Brinzauls muss evakuiert werden. Informationen zum Brienzer Rutsch, 46. Bulletin vom 9. Mai 2023 Gemeinde Albula Cumegn Alvra, 7. http://www.albula-alvra.ch/files/BXMediaPlusDocument6388file.pdf

Geimer PR, Finnegan R, Moore JR (2022) Meteorological controls on reversible resonance changes in natural rock arches. J Geophys Res Earth Surf 127(10):19. https://doi.org/10.1029/2022JF006734

Häusler M, Gischig V, Thöny R, Glueer F, Fäh D (2022) Monitoring the changing seismic site response of a fast-moving rockslide (Brienz/Brinzauls, Switzerland). Geophys J Int 229:310–310. https://doi.org/10.1093/gji/ggab473

Häusler M, Michel C, Burjánek J, Fäh D (2021) Monitoring the Preonzo rock slope instability using resonance mode analysis. J Geophys Res Earth 126(4):e2020JF005709. https://doi.org/10.1029/2020JF005709

Heim A (1932) Bergsturz und Menschenleben. Beiblatt zur Vierteljahrsschrift der Naturforschenden Gesellschaft in Zürich No 20. https://doi.org/10.5169/seals-9840

Kenner R, Gischig V, Gojcic Z, Quéau Y, Kienholz C, Figi D, Thöny R, Bonanomi Y (2022) The potential of point clouds for the analysis of rock kinematics in large slope instabilities: examples from the Swiss Alps: Brinzauls, Pizzo Cengalo and Spitze Stei. Landslides 19(6):1357–1377. https://doi.org/10.1007/s10346-022-01852-4

Kleinbrod U, Burjanek J, Fah D (2019) Ambient vibration classification of unstable rock slopes: a systematic approach. Eng Geol 249:198–217. https://doi.org/10.1016/j.enggeo.2018.12.012

Koper KD, Hawley VL (2010) Frequency dependent polarization analysis of ambient seismic noise recorded at a broadband seismometer in the Central United States. Earthq Sci 23(5):439–447. https://doi.org/10.1007/s11589-010-0743-5

Krähenbühl R, Nänni C (2017) Ist das Dorf Brienz-Brinzauls Bergsturz gefährdet? Swiss Bull angew Geol 22(2):15. https://doi.org/10.5169/seals-738126

Larose E, Carrière S, Voisin C, Bottelin P, Baillet L, Guéguen P, Walter F, Jongmans D, Guillier B, Garambois S, Gimbert F, Massey C (2015) Environmental seismology: what can we learn on earth surface processes with ambient noise? J Appl Geophys 116:13–74. https://doi.org/10.1016/j.jappgeo.2015.02.001

Le Breton M, Bontemps N, Guillemot A, Baillet L, Larose É (2021) Landslide monitoring using seismic ambient noise correlation: challenges and applications. Earth Sci Rev 216:26. https://doi.org/10.1016/j.earscirev.2021.103518

Levy C, Baillet L, Jongmans D, Mourot P, Hantz D (2010) Dynamic response of the Chamousset rock column (Western Alps, France). J Geophys Res Earth Surf 115:13. https://doi.org/10.1029/2009jf001606

Loew S, Huwiler A, Schneider S, Largiader A, Nänni C, Figi D, Thöny R, Josuran M (2023) Summary of the 15 June 2023 Brienz/Brinzauls rockslide collapse in the Swiss Alps. Retrieved from https://blogs.agu.org/landslideblog/2023/06/21/brienz-brinzauls-rockslide:

Manconi A, Jones N, Loew S, Strozzi T, Caduff R, Wegmueller U (2023) Monitoring surface deformation with spaceborne radar interferometry in landslide complexes: insights from the Brienz/Brinzauls slope instability, Swiss Alps https://doi.org/10.31223/X5PQ30

Mercerat ED, Payeur JB, Bertrand E, Malascrabes M, Pernoud M, Chamberland Y (2020) Deciphering the dynamics of a heterogeneous sea cliff using ambient vibrations: case study of the Sutta-Rocca overhang (southern Corsica, France). Geophys J Int 224(2):813–824. https://doi.org/10.1093/gji/ggaa465

Michel C, Guéguen P, El Arem S, Mazars J, Kotronis P (2010) Full-scale dynamic response of an RC building under weak seismic motions using earthquake recordings, ambient vibrations and modelling. Earthq Eng Struct Dyn 39(4):419–441. https://doi.org/10.1002/eqe.948

Pischiutta M, Salvini F, Fletcher J, Rovelli A, Ben-Zion Y (2012) Horizontal polarization of ground motion in the Hayward fault zone at Fremont, California: dominant fault-high-angle polarization and fault-induced cracks. Geophys J Int 188(3):1255–1272. https://doi.org/10.1111/j.1365-246X.2011.05319.x

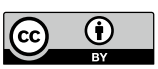
Poggi V, Fäh D (2010) Estimating Rayleigh wave particle motion from three-component array analysis of ambient vibrations. Geophys J Int 180(1):251–267. https://doi.org/10.1111/j.1365-246X.2009.04402.x

Taruselli M, Arosio D, Longoni L, Papini M, Zanzi L (2020) Seismic noise monitoring of a small rock block collapse test. Geophys J Int 224(1):9–215. https://doi.org/10.1093/gji/ggaa447

Trnkoczy A (2009) Understanding and parameter setting of STA/LTA trigger algorithm. New manual of seismological observatory practice (NMSOP), 1-20. https://doi.org/10.2312/GFZ.NMSOP-2_IS_8.1

Open Access This chapter is licensed under the terms of the Creative Commons Attribution 4.0 International License (http://creativecommons.org/licenses/by/4.0/), which permits use, sharing, adaptation, distribution and reproduction in any medium or format, as long as you give appropriate credit to the original author(s) and the source, provide a link to the Creative Commons license and indicate if changes were made.

The images or other third party material in this chapter are included in the chapter's Creative Commons license, unless indicated otherwise in a credit line to the material. If material is not included in the chapter's Creative Commons license and your intended use is not permitted by statutory regulation or exceeds the permitted use, you will need to obtain permission directly from the copyright holder.



Lessons from the Great Gramalote: Colombia Landslide (2010) and its Relocation Process

Guillermo Ávila and María Paula Ávila-Guzmán

Abstract

Colombia is located in a tropical zone periodically affected by El Niño Southern Oscillation (ENSO), which in the wet phase is called La Niña, characterized by rain values over the historical average. The last important La Niña event occurred in 2010–2011 and produced generalized floods and many landslides around the country, with important human and material losses. One of the most significant landslides triggered in this period was the Gramalote landslide, which destroyed a town of 3000 people, located in the northeast of the country and made it necessary to evacuate all the population and construct a new village 3.5 km north of the affected site. This article presents a general framework of the 2010–2011 La Niña effects in Colombia as a main cause of the Gramalote Landslide, the description of the instability problem, considering the stages previous, during, and after the landslide, as well as a back data vulnerability analysis and a review regarding the relocation process and its results after more than 13 years of the landslide occurrence. Important lessons can be learned about this complex risk management process, as a) the geological and geotechnical conditions in which the landslide occurred and the identification of the main triggering factors, b) the necessity of confident technical information about the local risk condition that takes into account extreme climate events c) the importance of such information being known and understood by local authorities and the population, d) the difficulties that arise under massive evacuation when a detailed emergency plan is not available (no one expected that there would be a landslide of the magnitude that occurred, much less that they would have to permanently evacuate all the homes), e) the complexities associated to the selection of a new site for relocation, considering not only technical aspects but social, economic, cultural and political elements that play a relevant role in the governance and success of the process, f) the back analysis of the structural vulnerability showed similar results as observed in place, but human susceptibility was much lower than the estimated on the model, and g) the positive and negative aspects of a big and long-time relocation project that may be of interest for similar cases, considering that the frequency and magnitude of future events due to climate change may produce large population migrations and the necessity to find new places to relocate these people.

Keywords

Gramalote · Landslide · Relocation · La Niña · Vulnerability · Risk

1 Introduction

One of the landslides that has had the greatest impact in Colombia in recent years is the one that occurred in the municipality of Gramalote, Norte de Santander department, on December 16 and 17, 2010, during a very intense La Niña event, which, despite not causing fatalities, destroyed the entire urban area, affecting about 3000 people, and considered one of the eight greater people displacements caused by natural disasters in the world from 2005 and 2015 (Norwegian Refugee Council and International Displacement Monitoring Centre, 2015) and producing damage of 974 houses (Fondo de Adaptación 2015). Due to the landslide, the town had to be moved to another site, located 3.5 km N-E from the original one, specifically constructed to receive all the affected people.

According to the Economic Commission for Latin America and the Caribbean- CEPAL (2012) La Niña event of 2010–2011 was the second hydrometeorological event that

G. Ávila (✉) · M. P. Ávila-Guzmán
Universidad Nacional de Colombia, Department of Civil and Agricultural Engineering, Bogotá, Colombia
e-mail: geavilaa@unal.edu.co; mpavilag@unal.edu.co

© The Author(s) 2025

B. Abolmasov et al. (eds.), *Progress in Landslide Research and Technology, Volume 3 Issue 2, 2024*, Progress in Landslide Research and Technology, https://doi.org/10.1007/978-3-031-72736-8_5

generated the greatest losses in the history of Colombia after the Eje Cafetero earthquake. Affecting more than 3.2 million people of which 243.127 were related to avalanches and landslides. The total cost was estimated at 6.052 million US dollars.

A relocation process most of the time is the last option for risk reduction due to the high complexity that this implies, however, sometimes it is the only option, like in the Gramalote case, where stabilization and reconstruction works after the landslide were not viable due to generalized destruction of the whole town and the prevalent instability conditions. Many cases of relocation due to natural hazards have been well documented in the last 20 years. For example, Luchi and Mutter (2020) analyzed three cases: The tsunami in Japan in 2011, the storm surge in Leyte (the Philippines) in 2013, and the volcanic eruption in Yogyakarta (Indonesia). Matti et al. (2023) analyzed two planned relocation projects in south-east Iceland and north-west Greenland. In North America, one important relocation project is the Isle de Jean Charles Resettlement in Louisiana (USA) affected by severe coastal erosion (Louisiana Office of Community Development 2021), and in South America cases of resettlement due to recurrent flood events in areas of Sao Paulo, Brazil and seven provinces in Argentina are presented by the World Bank (2016).

In the Colombian context, certain urban areas had to be relocated due to landslide risk. For example, in 1999, the municipality of San Cayetano, Cundinamarca was evacuated from a big landslide that caused the relocation of the town. Similarly, in the neighborhoods, Altos de la Estancia and Nueva Esperanza in Bogotá city 5259 and 1120 families respectively were relocated (World Bank 2016) also caused by landslides.

This document has three main purposes. The first is compiling and analyzing, from the available information, the most relevant geological and geotechnical aspects that gave rise to the landslide, focusing on the alert signs reported by the community as crack opening, water infiltration, and small landslides in the upper part of the mountain some months before the event. If these warning signs had been addressed on time by doing mitigation works, the impact could have been less, or eventually, the town would not have to be totally relocated. Second, analyze the risk management process in the different stages: previously, during, and after the landslide, and third, explore the most important lessons from the relocation process 13 years after the landslide occurrence.

2 Study Area and Landslide Effects

The municipality of Gramalote is located in the eastern mountain range of the Colombian Andes, in the department of Norte de Santander (Fig. 1), at a height of 1044 meters above sea level, with an average temperature of 23 ° C. In 2010 the population of the entire municipality was 5968 inhabitants and around 3000 people lived in the urban area (DANE 2010). The main economic source was agriculture, especially coffee cultivation, in addition to livestock, artisanal mining, and to a lesser extent tourism (Fondo de Adaptación 2015).

The urban area consisted mainly of 1 and 2-story houses, although it had some taller buildings such as the 5-story school and the church with towers of approximately 20 meters high.

On December 16, 2010, after a very intense and prolongated rain period caused by the La Niña event, a rotational landslide generated at the western side of the municipality of Gramalote produced the complete destruction of the urban area and some peripherical rural areas. Figure 2 shows a pan-

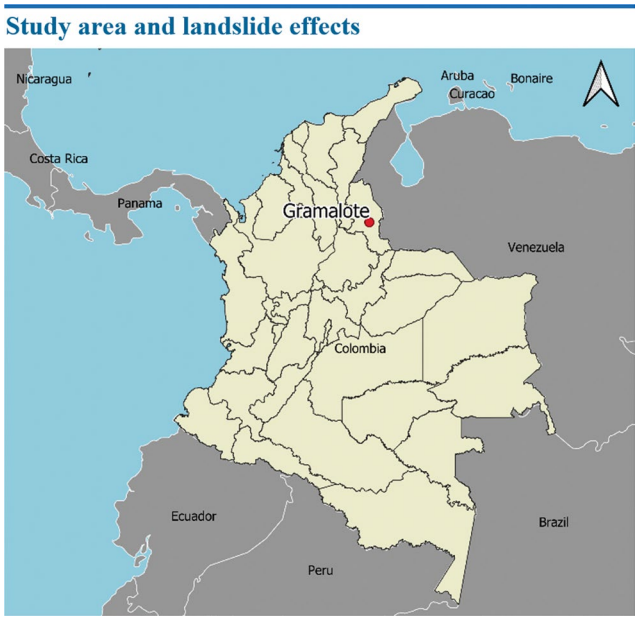


Fig. 1 Location map of Gramalote town

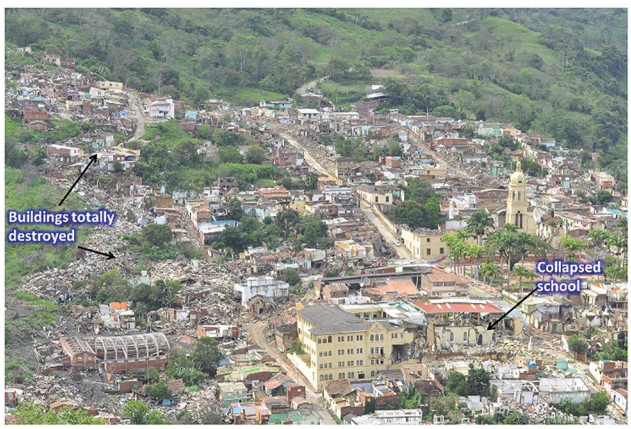


Fig. 2 Panoramic view of Gramalote town after 2010 Landslide. Source: (Iannini and Romero 2020)

oramic photograph of the urban area after the landslide, evidencing the devastation of most of the constructions.

Figure 3 shows the central plaza after the landslide where is clear the presence of many cracks 1 to 2 m wide, across the whole plaza, and Fig. 4 presents detailed photographs of the church, before and after the landslide showing the collapse produced by horizontal and vertical ground displacements.

Due to the landslide and the generalized destruction, all the residents had to be evacuated. Figure 5 shows two Google Earth images. (a) is from the year 2002 (before the landslide) where all the constructions may be observed and (b) was taken in 2014 (4 years after the landslide) where there are no buildings because the landslide destroyed them, and people had been permanently evacuated. Only the roads and the ruins reveal the existence of the ancient town.



Fig. 3 Crack crossing the Central Plaza of Gramalote Town (Pedroza 2012)



Fig. 4 Church of Gramalote town a) before (Pedroza 2012) and b) after the 2010 landslide (Torres 2012)



Fig. 5 Satellite image of Gramalote before and after 2010. (Google Earth Pro and Maxar Technologies 2024)

The geology of the area is composed of igneous and metamorphic basement rocks and a sedimentary sequence ranging in age from Pre-Mesozoic to Upper Cretaceous. Regional geology shows the presence of a geological reverse fault called the Gramalote fault, which crosses the landslide in the North-South direction (SGC 2012).

Two main formations are present: the Uribante Formation (Kmc) and the Cogollo Formation (Kmu) divided by the mentioned fault. Uribante formation (Kmc) is composed of feldspathic sedimentary arenites deposited in a marine environment from the Lower Cretaceous Era. The Cogollo Formation (Kmu) is made of sedimentary shales, limestones, arenites, cherts, and phosphorites deposited in a transitional marine environment from the Upper Cretaceous Era (Camargo et al. 2011). These formations have a structural orientation opposite to the land slope, which could be considered favorable for stability conditions. On the surface, there are clastic-supported colluvial deposits, made up of large blocks of sandstone and limestone embedded in a

sandy clay matrix. Due to the geological environment, the material presents severe rock fracturing, allowing water infiltration to the rock strata.

Regarding the hydrography, two small cricks called El Palo and Laguneta come from the upper part of the town and cross it until they flow into a bigger crick called Calderero (see Fig. 5). Between the two small cricks the landslide occurred.

3 Landslide Description and Triggering Factors

Gramalote town was located in a medium slope area (varying between approximately 15° and 25°). A schematic view of the process is shown in Fig. 6. According to the SGC (2012) report, due to the intensive rain, many landslides and earthflows occurred in the upper part of the village, the most important of these flows was a debris flow, that initiated in the road that connected Gramalote to a small place called San Isidro. This debris flow did not cause any damage but could have generated an overload that contributed to the main landslide initiation. As mentioned before, the landslide that destroyed Gramalote Town started on December 16, 2010, but the earth continued moving significantly for nearly one more day.

The main landslide is a rotational slide following the classification of Cruden and Varnes (1996) of approximately 600 m. long, variable width between 200 and 400 m, and depth between 15 to 20 m. Based on local people versions, the mean landslide speed was about 4 m/h (Pedroza 2012) classified in category 5 (rapid). The surface area was approximately 16 ha and the estimated landslide volume is about 1.8 million cubic meters.

The trigger factor was rain because a strong rainy season had occurred throughout the year due to the La Niña phenomenon. Figure 7 shows the precipitation comparison between mean monthly precipitation records from 1987 to 2009 and rain records of the year 2010 (until the landslide's day). There is a notorious difference in the antecedent months, especially September and November 2010 compared to the mean monthly multiannual records.

Specifically for December 2010, before the occurrence of the Great Landfall, some rain events were recorded until the day of the event (Fig. 8), when the station was disrupted. For the seventh day of December, the cumulative rainfall already

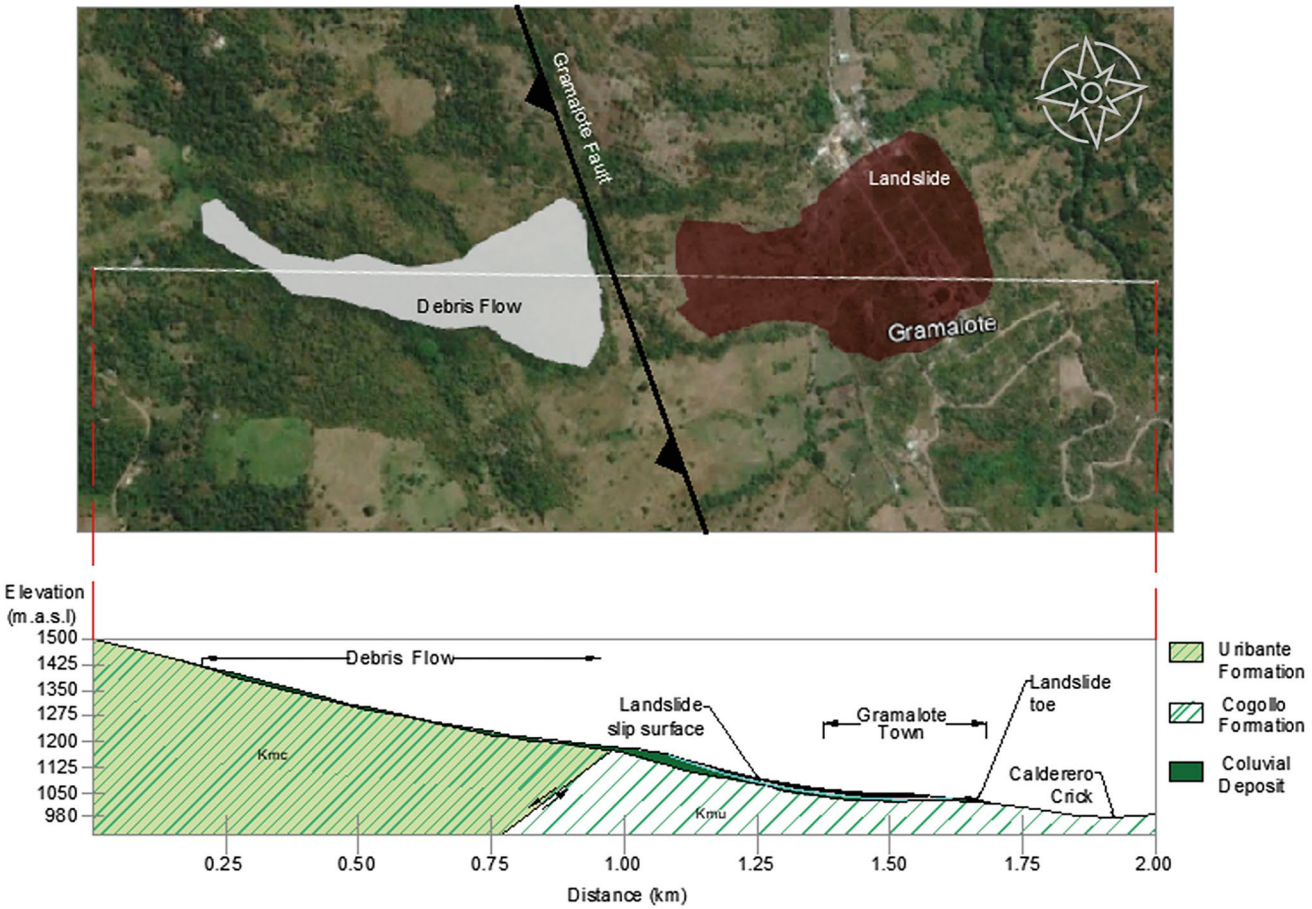


Fig. 6 Plan view and cross section of the Gramalote landslide

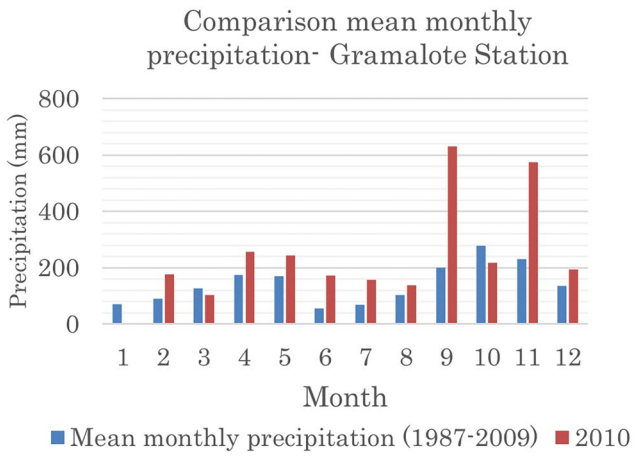


Fig. 7 Mean monthly multiannual precipitation compared with monthly precipitation of 2010 (La Niña event) in Gramalote Station. Source: (IDEAM 2024)

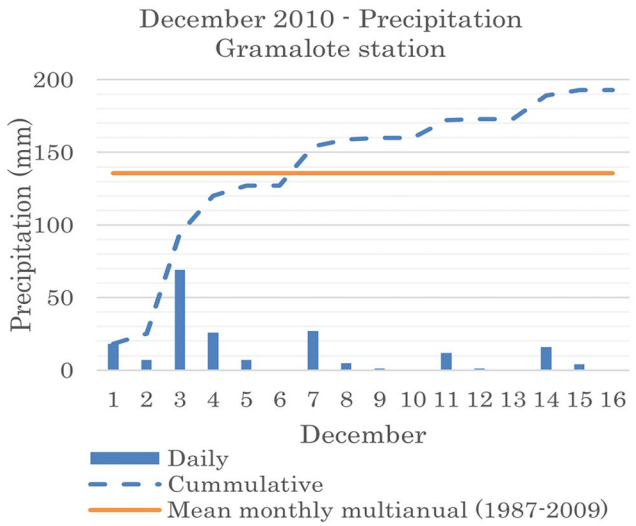


Fig. 8 Precipitation in December 2010 until the day of the event at Gramalote station. Source: (IDEAM 2024)

exceeded the mean monthly multiannual rainfall. This cumulative rainfall is a key point because when it infiltrates, it might generate internal erosion and the presence of water for long periods can cause the degradation of the resistance of materials. Also, high hydraulic gradients may reduce effective stresses that contribute to slope instability.

According to versions of the residents of the Jácome village, located in the upper part of the western mountain (Cerro de La Cruz) that limits the town, since 2008 there were already surface soil cracks and damages in rural houses that were accentuated periodically when there were heavy rains, but during 2010 the problem increased notoriously and one month before the landslide, on November 16, 2010, people were perceiving a significant increase in the presence of cracks in the ground, minor landslides in several places, earth movements that affected some houses and also the sounds of water infiltration and underground water flow in the downslope direction for which they were very concerned and requested attention from the risk prevention authorities (Figueroa 2011).

The saturation of the geologically fractured mass produced by the extraordinary rainy season may be considered the main cause of the landslide. The presence of a relatively permeable colluvial deposit allowed the infiltration of rainwater and its arrival to the rock units, generating unfavorable pore pressures and reduced resistance of the materials due to the effect of the softening associated with the permanent presence of water, especially on the contact surface between the colluvial deposit and the rock.

The contributing causes were the high degree of inclination of the slope, the overload produced by the debris flow, and the changes in land use for example secondary road construction, artisanal mining, and the agricultural activities associated with the process of deforestation. Landslide displacements after the initiation could have been increased by the occurrence of a series of small earthquakes registered by the National Seismological Network (SGC, 2012) being the most important the one with the epicenter in the municipality of Salazar, 13 km from Gramalote, (3.8 on the Richter scale).

4 Landslide Effects, Evacuation, and Relocation Processes

The numerous instability problems affected the surface soils of about 100 ha around the village and left more than 1000 families homeless. According to Fondo de Adaptación (2015), there were no fatalities nor injuries, but there was big damage to properties (Table 1).

The reason for which there were no fatalities may be attributed to two factors. Firstly, although the velocity of the landslide of about 4 m/h is classified as rapid (Cruden and Varnes 1996), it allowed people to evacuate safely, after the evacuation order given by the authorities. Secondly, the instability signs perceived by local people in the upper part of the mountain and in the town itself, after about 1 year of extraordinary rains, permitted the people to be aware of the problem, facilitating the evacuation process.

Once the people were evacuated, most of the families went to Cucuta, the capital of the department, located 45 km to the East of Gramalote, and others went to temporary shelters or relative's houses in nearby towns. Authorities helped with humanitarian aid such as food and temporary rent payments, however, the social and economic impact was devastating because people lost everything, including houses, jobs, means of production, and schools. Considering the magnitude of the landslide, the stabilization process was too difficult and expensive, the only alternative was to relocate

Table 1 Damages produced by the 2010 Gramalote Landslide (Fondo de Adaptación 2015)

Consequences	Count
Fatalities	0
Public facilities destroyed	29
Private facilities destroyed	63
Affected properties	3.64
Damaged houses	974

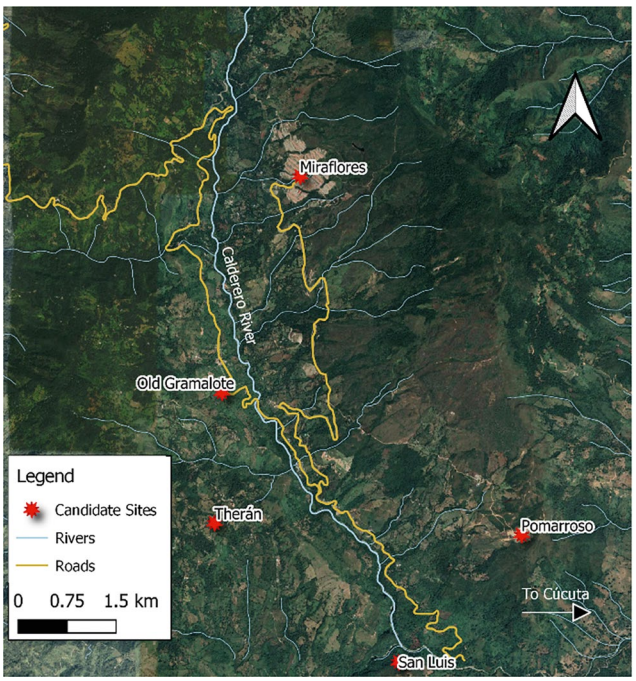


Fig. 9 Candidate places for Gramalote relocation

the town. The selection of the new site was not easy because many factors had to be considered: geological stability, favorable geomorphological conditions to urban development, regional articulation, similar climate conditions, access roads, water sources, public aqueduct, and sewerage services, construction time, etc. (Fondo de Adaptación 2015).

Initially, four sites were preselected for relocation: Pomarroso, Miraflores Teherán, and San Luis (Fig. 9). Teheran place was discarded after evidence of possible affectation for geological faults, and San Luis was discarded because it was too far and outside of the municipal jurisdiction of Gramalote, so the other two were the final candidates for relocation. Pomarroso place is located 6 km SE and Miraflores 3 km NE from Gramalote town respectively. Initially, the selected place was Pomarroso. However, after more detailed technical, economic, and socio-political processes, including residents' opinions, the final selected place for the construction of New Gramalote village was Miraflores.

The selected place has an average altitude of 1480 m and similar environmental conditions to the former municipality.



Fig. 10 New Gramalote at Miraflores sector. (Fondo de Adaptación 2015)

The selection took about 2 years from the occurrence of the landslide event and during this time, people were in an uncertain condition, most of them living under difficult economic conditions.

The technical studies for the selection of the new site consisted of a regional geological and geomorphological survey, at a scale of 1: 25.000 and later a detailed landslide hazard assessment for the two candidate places, using deterministic methods at a scale of 1: 5.000. This process included direct and indirect soil and rock exploration, soil and rock sampling, geotechnical laboratory testing (density, simple compression, direct shear and point load tests on rock specimens and soil classification, unconfined compression, direct shear and triaxial tests for soil specimens), slope stability analysis and landslide hazard modeling and mapping (SGC 2012).

The construction process of the New Gramalote had several stages. In the first stage, socio-demographic studies and technical studies were conducted for the development of the municipal infrastructure for the aqueduct, sewerage, communication routes, and adaptation of the land. In addition, the land for the relocation of the new homes had to be purchased. This first stage lasted approximately 3 years (plus the 2 years for the site selection) so the second stage, the construction, could only be started in 2015, 5 years after the event. On December 20, 2016 (6 years after the landslide) the first 189 homes were delivered to the community and also the central plaza, the town hall facilities, and the marketplace (see Fig. 10), but on 20 December 2020 (10 years after the landslide) of the 988 projected homes only 860 had been delivered, resting to deliver 128 homes (Cotamo 2020). The total cost of the project, according to the World Bank (2016) was 374.729 million Colombian pesos (about 136 million U.S dollars) representing 0.05% of the Colombian annual GDP for that year.

Arenas and Oliver-Smith (2017) present an analysis of the social aspects of the relocation of the affected community and indicate that despite the delays, the multiple problems that arose, and the cost overruns of the works, in general, the

resettlement project leaves some favorable lessons such as a flexible, participatory administration was carried out that could be adjusted according to the circumstances; the size of the houses and the way they were selected were generally well accepted by the community; the family assistance program has assisted in legal and operational processes for the transfer of families.

5 Semiquantitative Back-Analysis Vulnerability Assessment Based on the Du Et al. Model (2013)

The evaluation is based on the model proposed by Du et al., (2013), which in turn uses concepts proposed by Uzielli et al. (2008) and Li et al. (2010). In this model, vulnerability is calculated as a function of two parameters, the landslide intensity (I) and the element susceptibility (S). as indicated in Eq. 1

$$For\ I \le 1-SV = 1/2\left[I/(1-S)\right]^2$$
$$For\ I > 1-SV = 1-1/2\left[I/(1-S)\right]^2 \quad (1)$$

5.1 Intensity Parameters

Landslide intensity varies from 0 to 1. I = 1 means that the structure is completely destroyed and I = 0 means that the structure is not affected. Susceptibility also varies from 0 to 1. If S = 0 the structure is very strong and will resist landslide impacts. To account for the landslide impact, two landslide velocity stages are considered: slow stage and fault or rapid stage.

For the conditions observed in the Gramalote landslide, the intensity may be evaluated under a slow deformation stage, characterized by horizontal movements, settlements, and the presence of cracks and tilting of the structures located on the landslide. The intensity factor (I) includes three parameters, as indicated in Eq. 2: deformation parameter (Id-def), velocity parameter (Id-vel), and depth parameter (Id-dep)

$$I = 1-\left(1-I_{d-def}\right)\left(1-I_{d-vel}\right)\left(1-I_{d-dep}\right) \quad (2)$$

Id-def is calculated as the ratio of deformation to an allowable threshold. In this case, most of the structures overpassed the allowable threshold, then according to the methodology Id-def = 1. With this parameter equal to 1, the first term in parenthesis in Eq. 2 becomes zero, and then Idef = 1.

To have an estimation of the other two parameters (even though they no longer have a role in Eq.2, the velocity parameter is calculated as a function of the maximum estimated velocity of the landslide. In this case, maximum velocity was estimated at about 11 x 10–1 mm/s. The parameter is calculated according to Eq. 3 (Li et al. 2010) and in this case, for v > = 5x10–1 mm/s, the parameter Id-vel =1.

$For\ v \le 5x10^{-7}$	$I_{d-vel} = 0$	
$For\ 5x10^{-7} \le v \le 5x10^{-1}$	$I_{d-vel} = 1/36[log_{10}v + 6.30]^2$	
$For\ v \ge 5x10^{-1}$	$I_{d-vel} = 1$	(3)

The deep parameter Id-dep is calculated as a function of the relation d/h, as indicated in Eq. 4 from where d (m) is the predicted landslide depth and h (m) is the foundation depth. It is estimated that most of the structures in Gramalote had surface foundations, and assuming a mean value of h = 1 m, different values of d/h occur throughout the landslide, as observed in Fig. 11 for a structure A, the relation d/h is greater than one whereas for the structure B, the relation d/h is less than one considering that the depth of the foundation is less than 1 m. In Gramalote, for case A structures, mean landslide depth is estimated as d = 15 m, then d/h = 15, and according to Eq. 4 for d/h > 1.2, Id-dep = 0.006. For case B structures, d/h = 0.5 m then using the first condition of eq. (5), for h/h < 0.8, Id-dep = 0.85. It is observed that the value in B is higher than in A, indicating that structures may be more affected when the slip surface is near the foundation deep, as observed in the structures located near the Central Plaza.

$For\ d/h < 0.8$	$I_{d-dep} = (1.25 * d/h)^{1/3}$	
$For\ 0.8 \le d/h \le 1.2$	$I_{d-dep} = 1$	
$For\ d/h \ge 1.2$	$I_{d-dep} = 1.44(d/h)^{-2}$	(4)

5.2 Structural Susceptibility Parameters

According to Du et al. (2013), four parameters should be considered to calculate structural susceptibility: structure type (S_{str}) maintenance state (S_{mai}), the ratio of service years to design service life (S_{ser}), and the difference in the directionality of landslide movement and the principal longitudinal direction of the structure (S_{dir}), as indicated in Eq. 5.

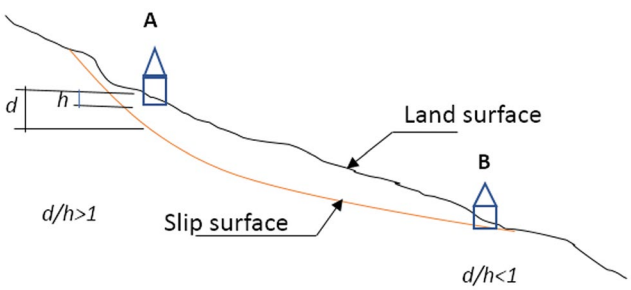


Fig. 11 Schematic representation of the d/h relation depending on the position over the landslide

$$S = 1-(1-s_{str})(1-s_{mai})(1-s_{ser})(1-s_{dir}) \quad (5)$$

Many of the structures in Gramalote were predominantly light structures of one or two stories, then, according to the methodology, this parameter should be $S_{str} = 0.9$. Some other structures as the school and public offices, may be classified in the category of rock masonry and concrete ($S_{str} = 0.7$). A mean value of Sstr = 0.8 is adopted for the present analysis.

The maintenance state susceptibility parameter is calculated for the typical conditions before the landslide. Considering that no significant deformations or damages were reported in the urban area before the landslide occurrence, this parameter corresponds to a slight deformation for what $S_{mai} = 0.2$.

The service parameter is calculated as the ratio of the service year to the design service life. Most of the structures in Gramalote did not have a formal service life design but it may be assumed that the service year at the moment of the landslide was close or greater than the service life (1.0–1.2), then, according to the values proposed by Du et al. (2013), $S_{ser} = 0.8$.

Finally, the directional parameter considers the difference in the directionality of landslide movement and the principal longitudinal direction of the structure (S_{dir}). In Gramalote two main directions of structures were present, oriented parallel and perpendicular to the two main roads. For the first case, the angle between the landslide direction and the structure direction is 10° to 15°, then according to the used methodology the directional parameter corresponds to a value between 0.6 and 0.4, and the adopted parameter Sdir is 0.5. For the second case, the difference in the direction is between 80° and 85°, values that are higher than those proposed by Du et al. (2013) for which the maximum angle difference is 45°, then the minimum value Sdir = 0 is adopted.

Table 2 presents the synthesis of the intensity and structural susceptibility parameters previously calculated for slow movement landslide in Gramalote.

Table 2 Final parameters of intensity and structural susceptibility calculated for the Gramalote landslide

Summary Of Parameters	
Intensity	
$I_{d\text{-}def}$	1.00
$I_{d\text{-}vel}$	1.00
$I_{d\text{-}dep}$	0.85
Intensity (I)	1.00
Susceptibility	
S_{str}	0.80
S_{mai}	0.25
S_{ser}	0.80
S_{dir}	0.50
Susceptibility (S)	0.99

Replacing the values of I and S in Eq. 1 for I > (1-S), vulnerability V = 1, a value that is consistent with the total destruction conditions observed in Gramalote after the landslide.

5.3 Susceptibility of Persons

Du et al. model (2013) also estimate the susceptibility of persons to be hurt or killed by a landslide. They estimate this susceptibility from three parameters: health condition parameter (S_{hel}), age parameter (S_{age}), and the existence of warning systems parameter (S_{war}), according to Eq. 6.

$$S_p = 1-(1-s_{hel})(1-s_{age})(1-s_{war}) \quad (6)$$

Reviewing the population situation no critical health conditions are reported and a generally healthy condition may be assumed, then the health condition parameter is adopted as $S_{hel} = 0.1$.

The age parameter (S_{age}) is calculated in Du et al. (2013) based on Eq. 7 proposed by Li et al. (2010).

$$s_{age} = 0.95 - 0.00486\left[INT(a/5)-5\right]^2 \quad (7)$$

Where INT() is the downward-rounded integer function and a is the mean age (in years). According to the national census (DANE, 2010), most of the population was younger than 50 years. However, a conservative mean age value of 50 years is adopted, then following Du et al. (2013), Sage = 0.82.

The early warning system parameter gives a value of $S_{war} = 1$ when this type of system is not present, and this is the case of Gramalote.

Computing Eq. 6, the susceptibility of persons Sp = 1. It is observed that the calculated susceptibility is controlled by the absence of any early warning system, because the third term in parenthesis becomes zero, however, as it was previously explained, in the Gramalote landslide no one was injured nor killed, probably because people were attentive given the heavy rains of the previous days, the presence of cracks in the ground, the occurrence of some small landslides in the upper part and the noises that were felt due to the movement of the ground. Then we may conclude that for slow velocity landslide, early warning systems are not as decisive as they can be in a fast landslide because people have time to evacuate, but it is very difficult to estimate a priori if the landslide is going to be rapid or slow, so always is recommendable to have at least an incipient early warning system.

The final parameter that is calculated from the methodology of Du et al. (2013) is the vulnerability of persons in structures but in Gramalote's case, this parameter was not

calculated because no one was trapped in the debris or in the collapsed buildings. Again, this result may be associated with the slow landslide movement and to the previous instability signs that alerted local authorities and the general population.

6 Lessons Learned from the Different Phases of the Event

6.1 The Situation before the Landslide

The territorial planning scheme is a technical document that all municipalities in Colombia must have up to date with clear identification of all potential geological and hydrometeorological hazards that may affect the community or their properties. According to the Gramalote territorial planning plan, 71% of the area was classified as low landslide risk and only 17% as high landslide risk (Fondo Adaptación, 2015). Strictly speaking, the previous studies did not correspond to a landslide risk analysis but a susceptibility analysis, that identified some possible unstable areas but they did not identify the possible occurrence of a landslide as large as the one that occurred. This highlights the need to carry out more detailed and comprehensives studies that allow for the identification of possible risk scenarios, considering extreme probable conditions as intensive and prolonged rain periods or seismic effects, because if the imminence of the Gramalote situation had been warned, at least, certain measures could had been adopted aimed at mitigating the extensive effects, which indeed could be profitable in the medium and long term.

Changes in land use were identified as one of the contributing factors to the instability processes, as they went from natural covers to pastures. In addition, there was high deforestation, both surface and underground mining, and the construction of several secondary roads (Pedroza, 2012). These factors favored the infiltration of water into the ground, reaching the contact between the surface colluvial material and the underlying rock, which facilitated the occurrence of the landslide. Here it is necessary to highlight how water management can play a decisive role in the conditions of land stability.

The La Niña event significantly increased rainfall throughout the year, particularly in November and December 2010, exceeding historical averages and highlighting the need to consider critical scenarios for stability analysis that might be increased by climate change. Additionally, prior heavy rains led to small landslides, ground cracks, and infiltration, reported by the population to authorities but this situation tends to be minimized due to a lack of formal studies indicating the potential for a major event.

6.2 During the Event

It should be noted that despite it was a landslide that caused great destruction of housing and infrastructure, in Gramalote there were no dead or injured people. This was because the process gave some clues about what was happening and when people noticed it, they were able to identify the dangerous situation, especially by evacuating the area in which the initial debris flow occurred. Additionally, the main landslide had a speed of around 4 m/h, which despite being classified as fast (according to Cruden and Varnes, 1996) allowed people to evacuate safely, following the order issued promptly by the municipal authorities. This is a positive aspect since pertinent actions were taken that prevented damage to the population, which does not always happen.

Just after the initiation of the landslide, local authorities responded timely to the emergency, since they first gave rise to an evacuation order, and then the protocols for identifying affected people were advanced, humanitarian aid was delivered, support was given for the search for temporary shelters, etcetera.

It is highlighted that during the event there was great social solidarity as many people who lost their homes stayed for several days and weeks in the homes of relatives and known people. Many aids were also received from different cities in the country and abroad and the national government established a unified command post to attend and coordinate the emergency.

6.3 After the Event

Given the magnitude of the destruction caused by the landslide, practically the entire town was destroyed and therefore it was necessary to define what could be done with the affected population. Given the multiple events of landslides, floods, and torrential flows that occurred in Colombia due to the La Niña phenomenon of 2010 and 2011 and especially in the case of Gramalote, in 2011 an entity called the Adaptation Fund was created whose purpose was to execute comprehensive risk management and adaptation projects to climate change with a multisectoral and regional approach (Fondo Adaptación, 2015).

The reconstruction project of Nuevo Gramalote, after approximately 13 years, presents several positive aspects, but also other negative ones. Among the positive ones, we can mention: a) a solution for housing and maintaining social and cultural cohesion was provided to a large part of the affected population. b) a technical and participatory process was carried out by the community and local and national authorities for the selection of the new location of the urban area, c) an urban environment was generated that has been

well valued by the population, with environmental conditions similar to those of the original municipality and with new road infrastructure facilities, schools, municipal dispatch offices, commerce, etc., which allow a harmonious development of the new urban environment. As negative aspects, we can mention: a) Not all the planned houses have yet been delivered, since there are still 183 that have not been built and this has generated the discomfort of many of the victims, b) The total cost of moving the municipality has been 136 million U.S dollars (World Bank 2016) which represent 0.05% of the country's GDP, c) even there was a similar environment in the New Gramalote local people had a feeling of uncertainty due to the changes in the selected site that were made, delays in the process and political interest around this process (Rojas and Durán 2022).

7 Conclusions

Large landslides that require the relocation of entire populations are not very frequent and, considering the strong economic, social, and political implications of a massive relocation process, it is important to document, in detail, the different stages of the process. This includes identifying the conditions that gave rise to the great landslide, the available previous studies, the actions of local and national authorities in managing the emergency, and the complex process of relocating the population.

The Gramalote landslide in 2010 covered a surface area of approximately 16 ha, and was predominantly of rotational type, with a slip surface identified at depths between 15 and 20 m. The landslide occurred on a superficial colluvial deposit that rested on sedimentary rocks whose orientation was almost normal to the plane of the slope of the terrain. Despite the favorable orientation of the rock strata, the presence of the Gramalote geological fault produced high rock fracturing that favor infiltration and reduced the mechanical strength. The maximum speed of movement was approximately 4 m/h, which is classified, according to Cruden and Varnes (1996), as a rapid landslide, but which still allowed the evacuation of the entire population without any deaths nor injured.

The main triggering factor for the landslide was the heavy and prologued rains that occurred throughout 2010 due to the so-called La Niña phenomenon, with rainfall well above historical averages. The contributing factors were the steep slopes, the overload produced by a debris flow in the upper part of the hill, and the changes in land use that caused deforestation and soil degradation.

At the site, there were studies of susceptibility to landslides on a regional scale that indicated that only a small proportion of the urban area was in a high landslide hazard condition. However, there were not detailed risk studies that specified about the geotechnical stability conditions, considering critical rain scenarios like the one that occurred in Gramalote. This implies that landslide risk studies must have a greater level of detail and the analysis of multiple possible scenarios, in order for them to be truly useful for making timely decisions.

The semi quantitative back vulnerability analysis using Du et al., model (2013) gave a result of structural vulnerability equal to one, which matches well with the total destruction observed onsite. Instead, the evaluation of human susceptibility predicted by the model was much higher than the observed after the event, considering that everybody could evacuate safely and no deaths or injured were reported.

The urban relocation project was carried out technically, considering different possible sites and analyzing multiple variables that incorporated community participation. The process was not simple because there were social, political, and economic interests, however, the project was executed. The New Gramalote project contemplated the construction of 998 houses, road and public services infrastructure, community buildings, a school, etc. So far, 13 years from the event, most of the works have been carried out, although the construction of 128 houses is still in process due to contract difficulties and the pandemic. The perception of the relocation project by residents has been variable. Initially, there was a lot of confusion because one relocation site was selected but then changed, also, the construction in the new site lasted to begin almost 5 years after the landslide occurrence, nonetheless, when the works began, people had a more positive view of the project and currently many families live on the site and consider that the community identity has been maintained and productive projects are starting to give results.

References

Arenas C, Oliver-Smith A (2017) Gramalote, Colombia: A displaced community in transition

Camargo G, Morales C, Veloza J (2011) MEMORIA TÉCNICA PLANCHA 5-09 MAPA DE PERMEABILIDADES DE Colombia ESCALA 1:500.000. VERSION 1. Bogotá

Comisión Económica para América Latina y el Caribe (CEPAL) (2012) Valoración de daños y pérdidas. Ola invernal en Colombia, 2010–2011. Bogotá

Cotamo O (2020) Colombia Diez años después de destrucción de Gramalote, aún faltan obras por entregar. RCN Radio

Cruden DM, Varnes DJ (1996) Landslide types and processes, Transportation Research Board. In: U.S. National Academy of Sciences-Special Report, pp 36–75

DANE (2010) Proyecciones de población municipales 2005-2020

Du J, Yin K, Nadim F, Lacasse S (2013) Quantitative vulnerability estimation for individual landslides. In: proceedings of the 18th international conference on soil mechanics and geotechnical engineering. Paris

Fondo de Adaptación (2015) Plan De Reasentamiento De La Población Habitante Del Casco Urbano De Gramalote. Bogotá

Google Earth Pro, Maxar Technologies (2024) Gramalote, Colombia (2002, 2013)

Iannini D, Romero F (2020) La maldición de Gramalote (I): una tragedia muy anunciada. El Espectador newspaper

IDEAM (2024) Banco de datos hidrometeorológicos. http://dhime.ideam.gov.co/atencionciudadano/. Accessed 7 Mar 2024

Li Z, Nadim F, Huang H et al (2010) Quantitative vulnerability estimation for scenario-based landslide hazards. Landslides 7:125–134. https://doi.org/10.1007/s10346-009-0190-3

Louisiana Office of Community Development (2021) Community master planning and program development for the isle de Jean Charles resettlement. Phase 2

Luchi K, Mutter J (2020) Governing community relocation after major disasters: an analysis of three different approaches and its outcomes in Asia. Prog Disaster Sci 6:100071. https://doi.org/10.1016/j.pdisas.2020.100071

Matti S, Cullen M, Reichardt U, Vigfúsdóttir A (2023) Planned relocation due to landslide-triggered tsunami risk in recently deglaciated areas. Int J Disaster Risk Reduct 86:103536. https://doi.org/10.1016/j.ijdrr.2023.103536

Norwegian Refugee Council, International Displacement Monitoring Centre (2015) People displaced by disasters - Global Estimates 2015

Pedroza Á (2012) ¿Por qué se cayó Gramalote? In: Primer Simposio Geotécnico De Ingeniería Geológica Sociedad Santandereana De Geotecnia. Bucaramanga, Colombia

Rojas S, Durán H (2022) Entre dos pueblos. Desastre, desplazamiento ambiental y reasentamiento en Gramalote, Norte de Santander. Colección de Justicia

SGC (2012) Informe Final Del Estudio De Prefactibilidad De Sitios Para Reubicacion Del Casco Urbano Del Municipio De Gramalote, Departamento Norte De Santander. Bogotá

Torres G (2012) Gramalote tiene que aprender a florecer en el desierto. Semana Magazine

Uzielli M, Nadim F, Lacasse S, Kaynia AM (2008) A conceptual framework for quantitative estimation of physical vulnerability to landslides. Eng Geol 102:251–256. https://doi.org/10.1016/j.enggeo.2008.03.011

World Bank (2016) La experiencia de intervención en Gramalote: Un caso de reasentamiento en Colombia, Sur América. Bogotá

Open Access This chapter is licensed under the terms of the Creative Commons Attribution 4.0 International License (http://creativecommons.org/licenses/by/4.0/), which permits use, sharing, adaptation, distribution and reproduction in any medium or format, as long as you give appropriate credit to the original author(s) and the source, provide a link to the Creative Commons license and indicate if changes were made.

The images or other third party material in this chapter are included in the chapter's Creative Commons license, unless indicated otherwise in a credit line to the material. If material is not included in the chapter's Creative Commons license and your intended use is not permitted by statutory regulation or exceeds the permitted use, you will need to obtain permission directly from the copyright holder.



Challenges of Earthquake and Micro-Earthquake Monitoring in Sri Lanka

Koji Matsunami, Kyoji Sassa, Ranjan Weerasinghe, Tania Munasinghe, and Loi Doan

Abstract

Site amplification effects of Aranayake landslide area in Sri Lanka are analyzed using records observed by a wide dynamic-range earthquake motion array with soil- and rock-site stations. We find that the rock site on the mountain ridge does not have the same response as the rock site at the foot of mountain, which has a characteristic frequency-dependent site effect. The relative amplification of the mountain ridge rock site to the mountain foot rock site is nearly 1.0 at frequencies of $2 < f < 6$ Hz, having a peak of 2 or more at 6 to 8 Hz, that gradually decreases with increasing frequency, and becomes less than 1 above 10 Hz. On the land slide slope in Aranayake, clear resonant vibration with a frequency of nearly 12 Hz and an amplification of about 20 times is found from the amplification analysis of the main part of the S-wave. The vibration is excited immediately after P-wave arrival and continues to S-wave coda. Particle motions of a 12-Hz component in main portion of the S-wave show that the vibration is almost horizontal, and that its predominant direction nearly matches the landslide axis, but gradually changes with time according to the direction of stress free. From the survey of seismic activity in Aranayake landslide area, it is determined that microearthquakes with $Ts\text{-}p < 1.0$ s and the velocity magnitude $2 < M < 3$ occur several ten times a month. The landslide slope is frequently attacked by such microearthquakes, and is shaken by the 12-Hz resonant vibration.

Keywords

Site amplification effect · Landslide · Resonant vibration · Seismic activity

1 Introduction

Earthquakes are commonly associated with other geological phenomena such as landslides or liquefaction, which can give rise to equally destructive infrastructure damage and loss of life. On October 9, 1963, the most tragic dam disaster at Vajont Dam in Italy was caused by an enormous landslide. This disastrous landslide was preceded by an interval of maximum seismic activity in September 1963. The landslide is thought to have been affected by the seismic activity that occurred about a month earlier. On the other hand, the June 2008 Aratozawa Dam Landslide in Japan was triggered simultaneously by the 2008 *M*7.2 Iwate Miyagi Nairiku Earthquake. This large earthquake also induced a large number of landslides in the epicentral area.

In Sri Lanka, landslides have been frequently observed in the Aranayake, Kandy, Athwelthota, Kalutara and Badura areas. However, in slope stability research, the influence of seismic activity on landslides has been neglected (Vithanage 1994), because Sri Lanka was traditionally believed to be tectonically stable and free from damaging earthquakes. However, in September and December 1993, two earthquakes shook the entire island of Sri Lanka. Shortly afterwards, it was announced that the first damaging earthquake in Sri Lanka occurred on April 14, 1615 (Dr. Wimalaratne, Director, National Archives, Daily News, Dec. 23, 1993).

K. Matsunami (✉) · K. Sassa
International Consortium on Landslides, Kyoto, Japan

R. Weerasinghe
National Building Research Organization, Colombo, Sri Lanka

T. Munasinghe
ICL SATREPS Office in Colombo, Colombo, Sri Lanka

University of Colombo, Colombo, Sri Lanka

L. Doan
International Consortium on Landslides, Kyoto, Japan

Institute of Transport Science and Technology, Hanoi, Vietnam

© The Author(s) 2025

B. Abolmasov et al. (eds.), *Progress in Landslide Research and Technology, Volume 3 Issue 2, 2024*, Progress in Landslide Research and Technology, https://doi.org/10.1007/978-3-031-72736-8_6

According to records preserved in the National Archives, 200 houses fell to the ground and the death toll was over 2000 (Wimalaratne 1993). Furthermore, according to this reliable historical record, the seismic event could have reached *M*6.5 on Richter Scale, and was the most intensive earthquake, with an epicentre either on land in Colombo or very close offshore. The two felt earthquakes in 1993 and the 1615 damaging earthquake proved that" We can expect 6.5 magnitude earthquakes anywhere in Sri Lanka" and further destroyed the traditional belief that" Damaging earthquakes do not occur in Sri Lanka".

In Sri Lanka, three large dams have been constructed in Kotmale (1982), Victoria (1984), and Randenigale (1986) areas. Because of the relatively large size of the reservoirs and the height of their dams (90 m to over 100 m), and the presence of well-developed major lineaments in and around these dam areas, microseismical monitoring was initiated in 1982 by the Department of Earthquake Engineering, University of Roorkee, India (Agrawal 1983). The objective of the monitoring was to determine whether any of the pre-existing lineaments were active and may give rise to a reservoir induced earthquake. In 1990, the microseismical monitoring with the eight seismographs concluded with no significant seismic activity recorded, As such, there was no single seismograph available in Sri Lanka to record the large earthquake that rocked the whole Island in December in 1993.

In and around the Victoria Dam, small-scale earthquake swarms occurred in 2020. These were reservoir-induced earthquakes. This dam lake was filled with water in 1985, so 15 years have passed before the reservoir-induced earthquake occurred. With no induced earthquakes between 1990 and 2020, the time lag between the initial filling and occurrence of triggered earthquakes was 15 years. Kotmale Dam may also experience reservoir-induced earthquake swarms in the future.

Despite the collapse of the traditional belief that" damaging earthquakes do not occur in Sri Lanka", there is no research on the behavior of landslides during earthquakes based on seismic motion observations. For example, no empirical data has been obtained regarding the vibration characteristics of landslide slopes due to earthquakes. The basic question of which parts of landslide slopes shake and how during an earthquake remains to be addressed.

To investigate the behavior of landslide slope during earthquakes, we are carrying out continuous observations of wide dynamic-range earthquake motions, microtremors, ground tilts and rainfall in Aranayake, Kalugala, Kandy and Athwelthota landslide areas of Sri Lanka. Furthermore, similar continuous observations have begun in the Kotmale area to monitor reservoir-induced earthquakes.

In this paper, first, we investigate the assumption that a nearby rock site represents the reference motion for a soil site. To do this, we use two rock sites with topographically different locations. One is located at the foot of the mountain, while the other is on the mountain ridge.

Next, we investigate resonant vibration characteristics of an unstable slope through the comparison of S-wave forms observed at unstable sites in the landslide area, and at stable rock sites outside the landslide area. Furthermore, we investigate the dominant vibration direction of resonance on the landslide slope from the particle motion diagram of the S-wave components.

From the continuous observations of wide dynamic-range earthquake motions, we construct a very valuable seismic waveform database. Microearthquake observation data obtained by using high-sensitivity seismometers is useful for investigating seismic activity. We investigate seismic activity directly beneath the landslide area by using the database. This type of challenging investigation is the first of its kind in Sri Lanka and elsewhere. The findings of this study are discussed at the end of the paper.

2 Observations

As part of the SATREPS project on Developing Early Warning Technology for Rain-Induced Rapid and Long-Travelling Landslides (RRLL), we installed a wide dynamic-range earthquake motion array on geomorphologically distinctive landslide blocks in the Alanayake, Kandy, Athwelthota, and Kotmale areas of Sri Lanka (Fig. 1). A 3-axis MEMS (Micro Electromechanical Systems) accelerometer was used to measure small to large earthquake ground motions (measuring range:22μG to 2G, sensitivity:0.4 volt/G, G: gravitational acc.) at the landslide site, and a high-sensitivity 3-axis velocity-type seismometer (natural frequency:2 Hz, Sensitivity:0.9 volt / cm/s) used to measure micro-earthquake motions and microtremors. The MEMS accelerometer was also used to monitor the tilt of the landslide ground (resolution: 0.001 degree) as an important indicator for predicting landslide occurrence and estimating landslide ground movement.

The observation points were selected on an unstable slope with a high possibility of ground sliding and on a stable exposed bed rock outside the landslide block (Table 1). Observation data were transmitted from each site to the data server via a mobile network and recorded on an SD card. The power supply at the observation sites was a deep-cycle storage battery with solar panel. Array observations using microtremors were undertaken to investigate the ground structure up to the basement rock directly below the unstable ground site.

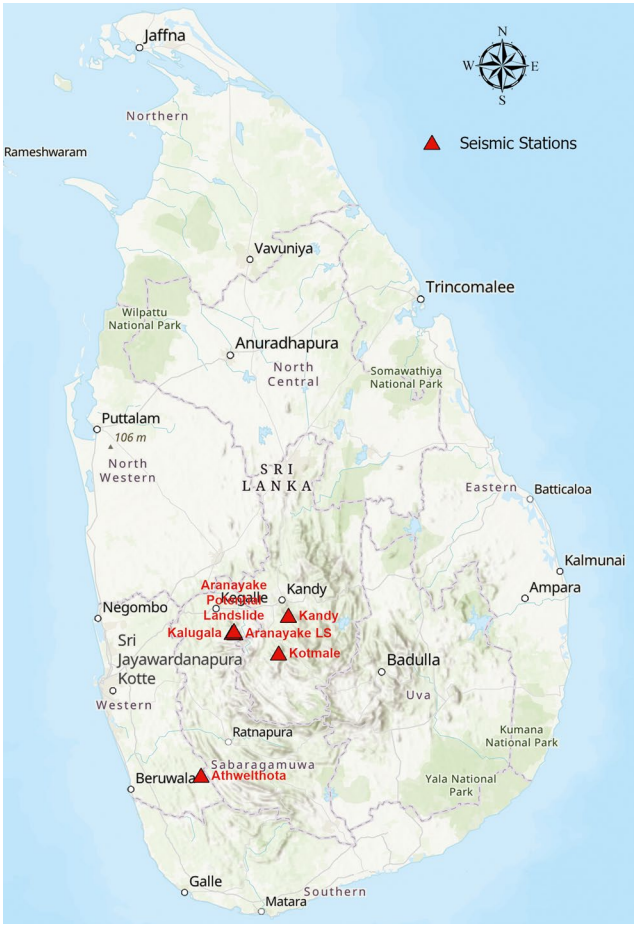


Fig. 1 Location map of seismic stations installed in Sri Lanka

Table 1 Stations and site condition

	Station list	
Name	Area	Site condition
St01	Aranayake landslide	Bedrock outcrop (mountain top)
St02	Aranayake landslide	Debris (landslide body)
St03	Aranayake landslide	Potential unstable mass (over the main scarp)
St04	Kalugala Primary School	Unstable soil (cut slope)
St05	Kalugala Primary School	Bedrock outcrop
St06	Kandy	Bedrock outcrop
St07	Kandy	Soil (colluvium)
St08	Athwelthota landslide	Bedrock outcrop
St09	Athwelthota landslide	Unstable soil

Figure 2 shows distributions of events that occurred in 2023 and the monitoring stations. The detailed station locations in Aranayake Landslide area and Kalugala area are shown in Fig. 3. These two areas were located on the same mountain, but on opposite sides of the ridge. In Aranayake LS area, there were three stations: one station (St01) on rock site near the mountain ridge; and two stations (ST02 and St03) on the landslide slope. Specifically, St03 was located on unstable mass over the main scarp, while St02 was positioned on colluvial debris (landslide body). In the Kalugala area, there were two stations at the mountain foot, one on rock site (St05), and the other (St04) near the foot of the landslide slope.

In this study, we investigate characteristics of high frequency vibrations exited by earthquakes from comparisons of wave motions observed at an unstable soil site station on the landslide slope and those at a rock site station as a reference outside the landslide area.

Figure 4 shows seismograms observed at St03 and St05 during the 1-7-2023 *M*5.8 earthquake shown in Fig. 2. St03 was located on an unstable mass over the main scarp in Aranayake landslide area, and St05 was positioned on stable rock at the mountain foot. From a comparison of the seismograms observed at the two stations, an excitation of high-frequency vibrations was clearly detected on the seismogram of the unstable St03.

As discussed later, microseismicity was active directly beneath Aranayake landslide area. Therefore, we examined whether high-frequency vibrations were excited using microseismic waveforms observed at St01 and St03. Figure 5 shows waveforms of a microearthquake observed simultaneously at the two stations. It confirms the occurrence of high-frequency vibrations at St03. Looked at in detail, this vibration occurs not only in S-wave portion, but also immediately after P-wave arrival to S-wave coda.

Although the earthquake observed is a local microearthquake, the waveform is distorted. This is because when the amplitude of the seismic waves input to a seismograph reaches a certain magnitude, the recorded seismic waves can no longer increase in proportion to the input.

Furthermore, it appears from Fig. 5 that two different earthquakes occurred at the same time. Figure 5 shows that simultaneous earthquakes have often occurred directly beneath this area.

The excitation of high-frequency vibration is also seen in other landslide areas. Figure 6 shows seismograms observed at St09 and St08 during the M5.8 event shown in Fig. 2. St09 is located on unstable soil in Athwelthota landslide area and St08 on stable rock outside the area, respectively. The vibrations at the soil site St09 are clearly higher frequency compared to those at the rock site St08.

Figures 4, 5, 6 confirm the occurrence of high-frequency vibrations at the unstable soil sites as St03 and St09.

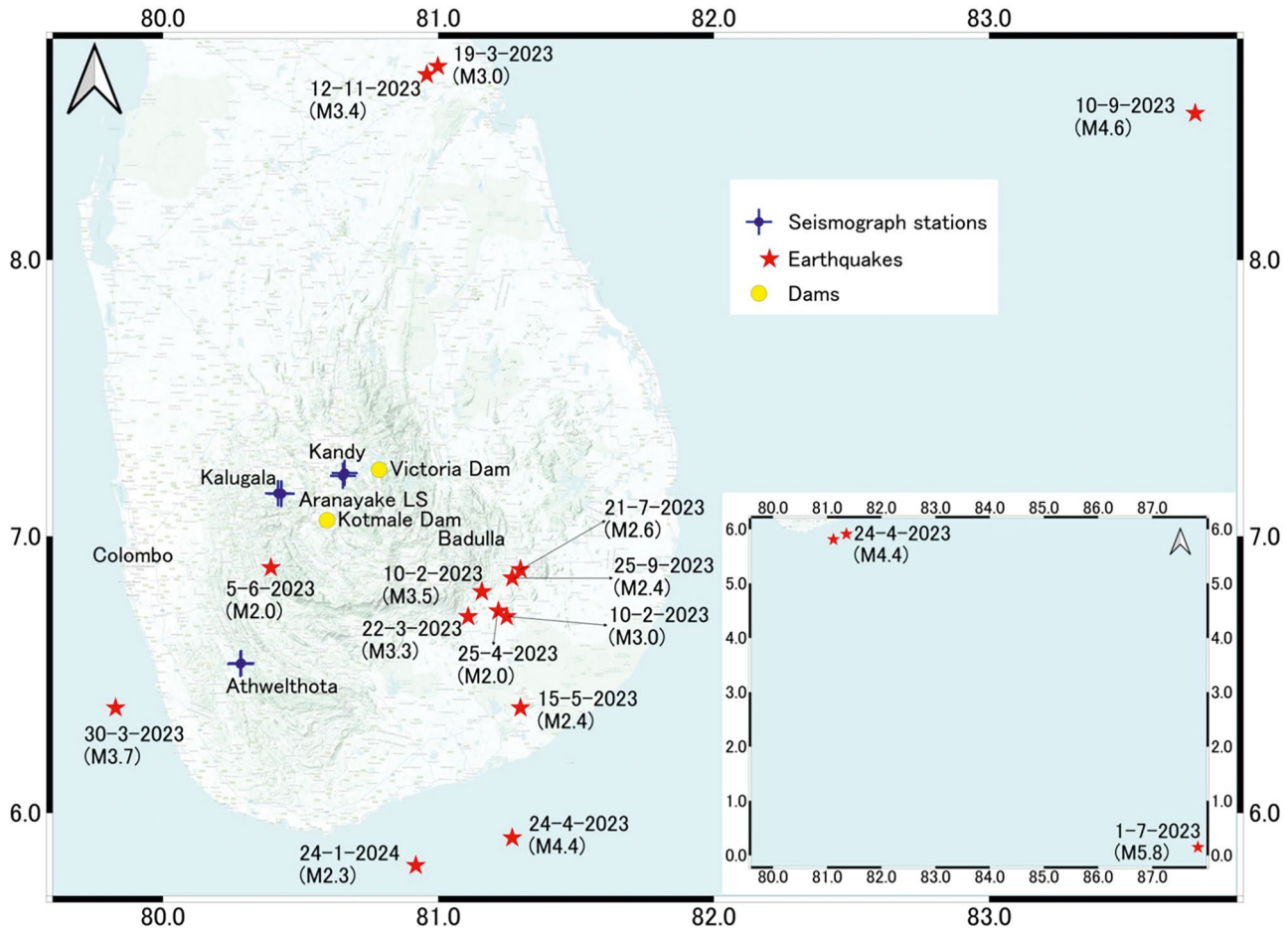


Fig. 2 Distribution of earthquake events, dams, and seismic stations

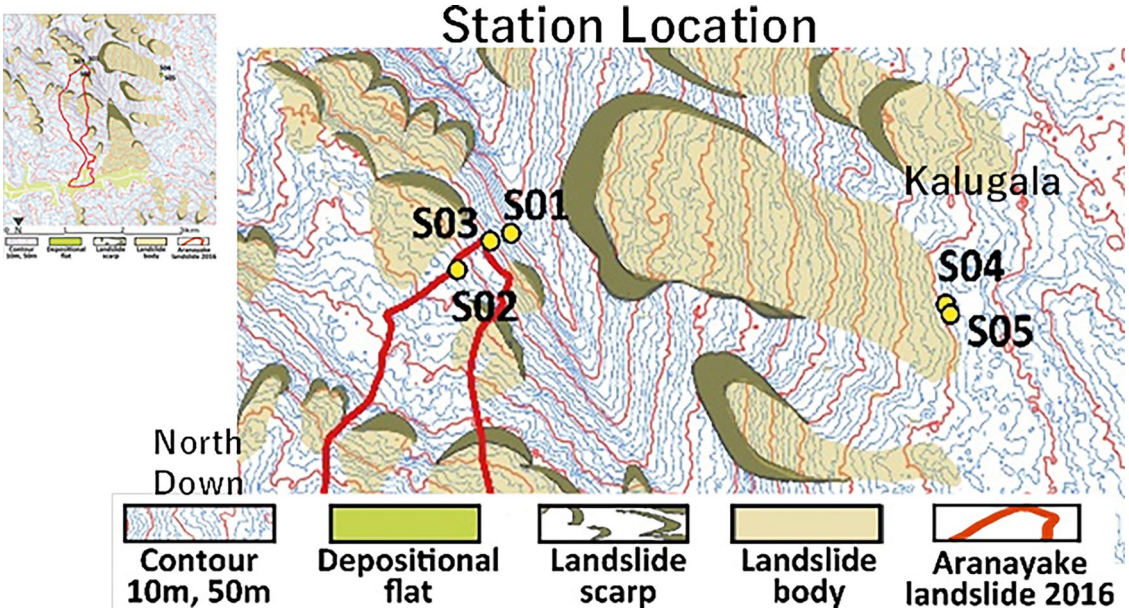


Fig. 3 Detailed station location in Aranayake Landslide area and Kalugala area. S01, S02, S03, S04, and S05 are St01, St02, St03, St04, and St05, respectively

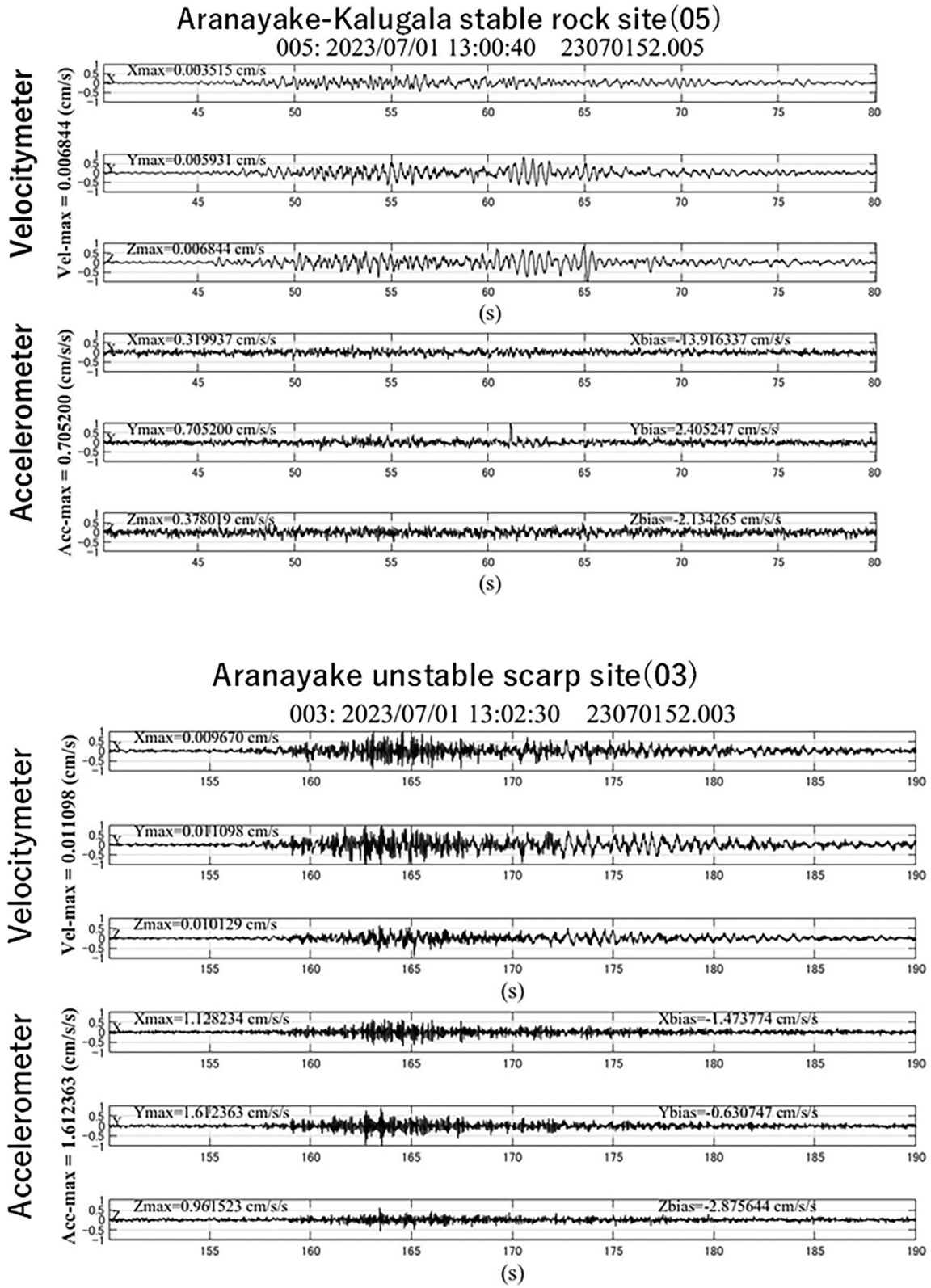


Fig. 4 Waveforms of S-wave portion in enlarged time axis. Those are observed simultaneously at St05 on the rock site in the foot of the mountain and St03 on the unstable mass in Aranayake landslide area during the 1-7-2023 *M*5.8 event. Clear excitation of high-frequency vibrations can be seen at St03. Xbias, Ybias and Zbias are the DC components of the accelerometer output. These are used to monitor the tilt angle of the landslide slope

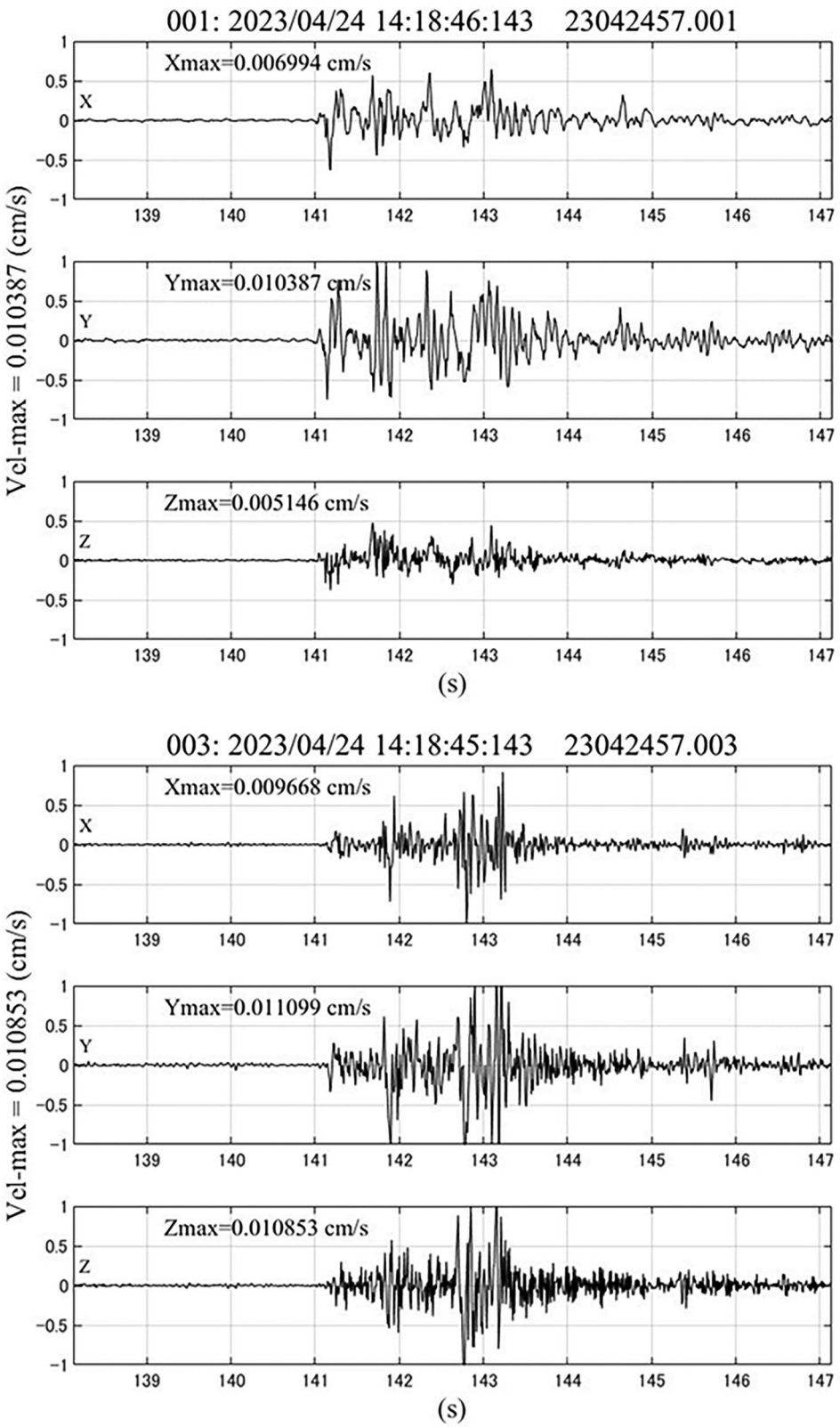


Fig. 5 Seismic waveforms observed simultaneously at St01 on the rock site in Aranayake landslide area and St03 on the unstable mass. Clear excitation of high-frequency vibrations can be seen at St03 from immediately after P-wave arrival to S-wave coda. It can be seen that two microearthquakes occurred at almost the same time

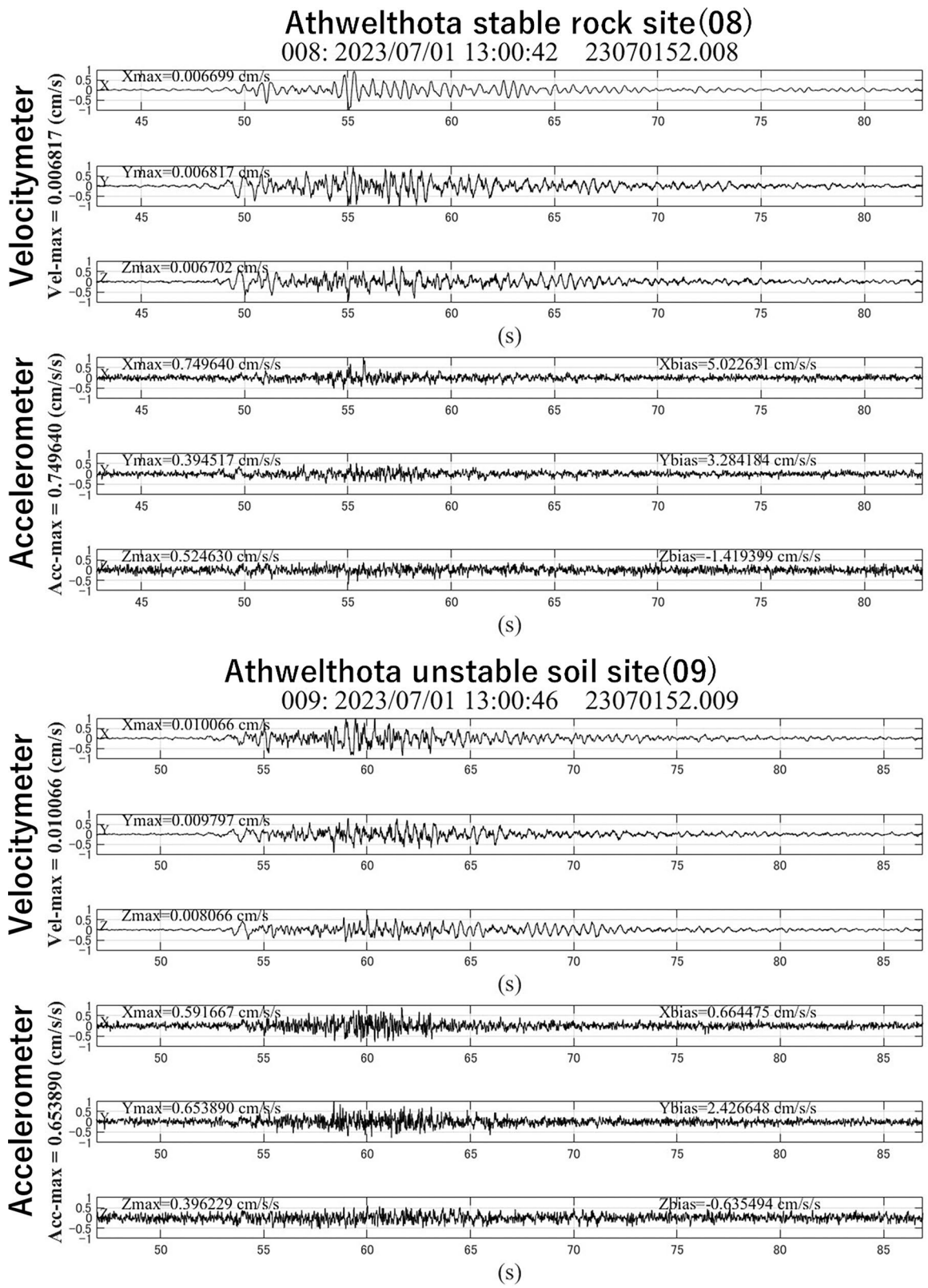


Fig. 6 Waveforms of S-wave portion in enlarged time axis. Those were observed simultaneously at St08 on the rock site in Athwelthota area and St09 on the unstable soil during the 1-7-2023 *M*5.8 event. Clear excitation of high-frequency vibrations can be seen at St09. Xbias, Ybias and Zbias are the DC components of the accelerometer output. These are used to monitor the tilt angle of the landslide slope

3 Methods

S-wave horizontal and vertical components are analyzed in this study. The amplitude spectrum of the horizontal component *Hr*(*f*) can be calculated by:

$$H_r(f) = \sqrt{Ns^2(f) + Ew^2(f)}, \quad (1)$$

where *f* is the frequency, *Ns* and *Ew* represent the north-south and east-west components of the accelerogram. For all spectra, smoothing was performed using a Hanning window with a bandwidth of 0.5 Hz.

In this analysis, we use the 24-4-2023 *M*4.4 Hambantota-offshore earthquake shown in Fig. 2, This is the only event observed at all the stations in the Aranayake and Kalugala landslide areas. Assuming that S waves are radiated spherically from the earthquake source, the Fourier amplitude spectrum of the observed S wave can be expressed as follows:

$$O_j(f) = S(f)G_j(f)\frac{1}{R_j}exp^{\left(-\frac{\pi f R_j}{Q_s(f)V_s}\right)}, \quad (2)$$

where $O_j(f)$ is the S-wave Fourier amplitude spectrum of the event recorded at the *j*th station, $S(f)$ is the source term for the event, $G_j(f)$ and R_j are the site effect term and the hypocentral distance for the event and the *j*th station, respectively, and $Q_s(f)$ and V_s denote the average quality factor and the average velocity of the S waves in the medium, respectively. When the reference station is the *r*th station, the S-wave Fourier amplitude spectrum of the event recorded at the *r*th station can be expressed as follows:

$$O_r(f) = S(f)G_r(f)\frac{1}{R_r}exp^{\left(-\frac{\pi f R_r}{Q_s(f)V_s}\right)}, \quad (3)$$

The spectral ratio between the *j*th station and the *r*th station is obtained by

$$\frac{O_j(f)}{O_r(f)} = \frac{G_j(f)}{G_r(f)}\frac{R_r}{R_j}exp^{\left\{-\frac{\pi f(R_j-R_r)}{Q_s(f)V_s}\right\}}, \quad (4)$$

All stations in the Aranayake and Kalugala landslide areas were installed in the same mountain. The epicenter of the 24-4-2023 earthquake is approximately 150 km away from the mountain, so S-wave incident azimuth to each station and S-wave incident angle to each station are nearly the same for all stations in the two landslide areas. Furthermore, S-wave travelling distance to each station in the two landslide areas is approximately the same. In Eq. (4), therefore, $R_j \cong R_r$, and Eq. (4) can be rewritten as follows:

$$O_j(f)/O_r(f) \cong G_j(f)/G_r(f) \quad (5)$$

In this way, we can evaluate the site amplification effect relative to a rock site as a reference in the case of the 24-4-2023 earthquake. We use St05 as a reference in this study, because it is located at the foot of the mountain where all the other stations are located.

In the frequency analysis, a 10-s time window is used to extract S waves, and a 5% Hanning taper is applied to the time window. A 10-s time window before the P-wave arrival is used to examine the noise level. As a result, the S/N-ratio is 2 or less at 1.6 Hz, or less at some stations. The site amplification effect above 2 Hz is investigated for all stations in the following section.

4 Analysis and Discussion of Results: Relative Site Amplification in Aranayake Area

Figure 7 shows the amplitude spectra of the horizontal component (Hr) and the vertical component (Ud) for all stations in the Aranayake and Kalugala areas during the 24-4-2023 *M*4.4 earthquake. From this figure, we first notice that although all stations have nearly the same amplitudes at frequencies lower than 6 Hz, the amplitude of each station differ depending on site condition at frequencies higher than 6 Hz. If we look more closely, we find the following two characteristics. (1) Although both St01 and St05 stations are located on rock sites, the decreasing rate of the amplitude with the increase of frequency is clearly different at frequencies higher than 8 Hz for both. The rate of St01 located in the mountain ridge is larger than that of St05 located at the mountain foot. (2) The amplitude of St03, located on unstable soil site in Aranayake landslide area, exhibits a clear peak at 10 to 14 Hz, then decreases with frequency. Similarly, the amplitude of St04 located on a soil site in Kalugala landslide slope also has a small peak at 24 to 26 Hz. Characteristics (1) and (2) are investigated in detail using the Hr-component of the amplification spectrum, with St05 as the reference.

First, based on (1) above, we investigate site effect of the two rock site stations, St01 and St05, with topographically different locations. St05 is located at the foot of the mountain and St01 on the mountain ridge, respectively. Figure 8 shows the amplitude spectra for the two stations and the amplification spectra (St01/St05). The amplification spectra are nearly 1.0 at frequencies lower than 6 Hz, having a gentle peak of 2 or more at 6 to 8 Hz, gradually decreasing with increasing frequency, and becoming less than 1 above 10 Hz. This behavior reveals that the rock site St01 does not show the same response as the rock site St05, having a characteristic frequency-dependent site effect. Especially, the rock site St01 exhibits amplification of 2–3 at 6 to 8 Hz. When St01 is used as a reference, this bias will lead to underestimations of wave amplification in a surface layer lying on the basement

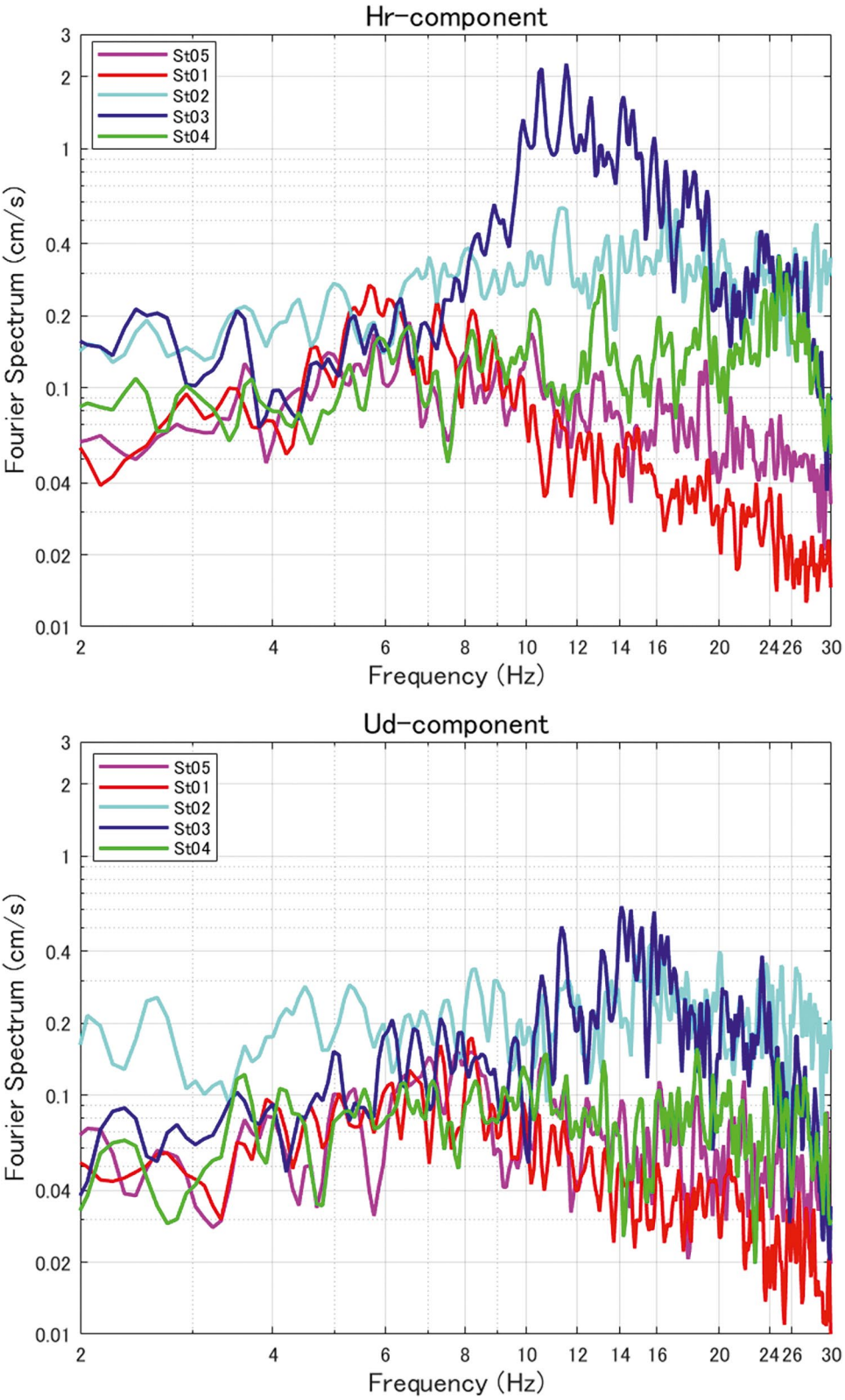


Fig. 7 **Top:** amplitude spectra of horizontal component (Hr) for all stations in Aranayake Landslide area and Kalugala area. **Bottom:** amplitude spectra of vertical component (Ud)

rock, compared to when St05 is used as a reference. Furthermore, the amplification spectra decrease with frequency and becomes less than 1 above 10 Hz. This will lead to overestimations of wave amplification in a surface layer. Thus, the assumption that the ground motion of a nearby rock site (St01) represents the reference motion for soil sites (St02 and St03) does not hold for frequencies higher than about 6 Hz, at least in the present case. This supports other

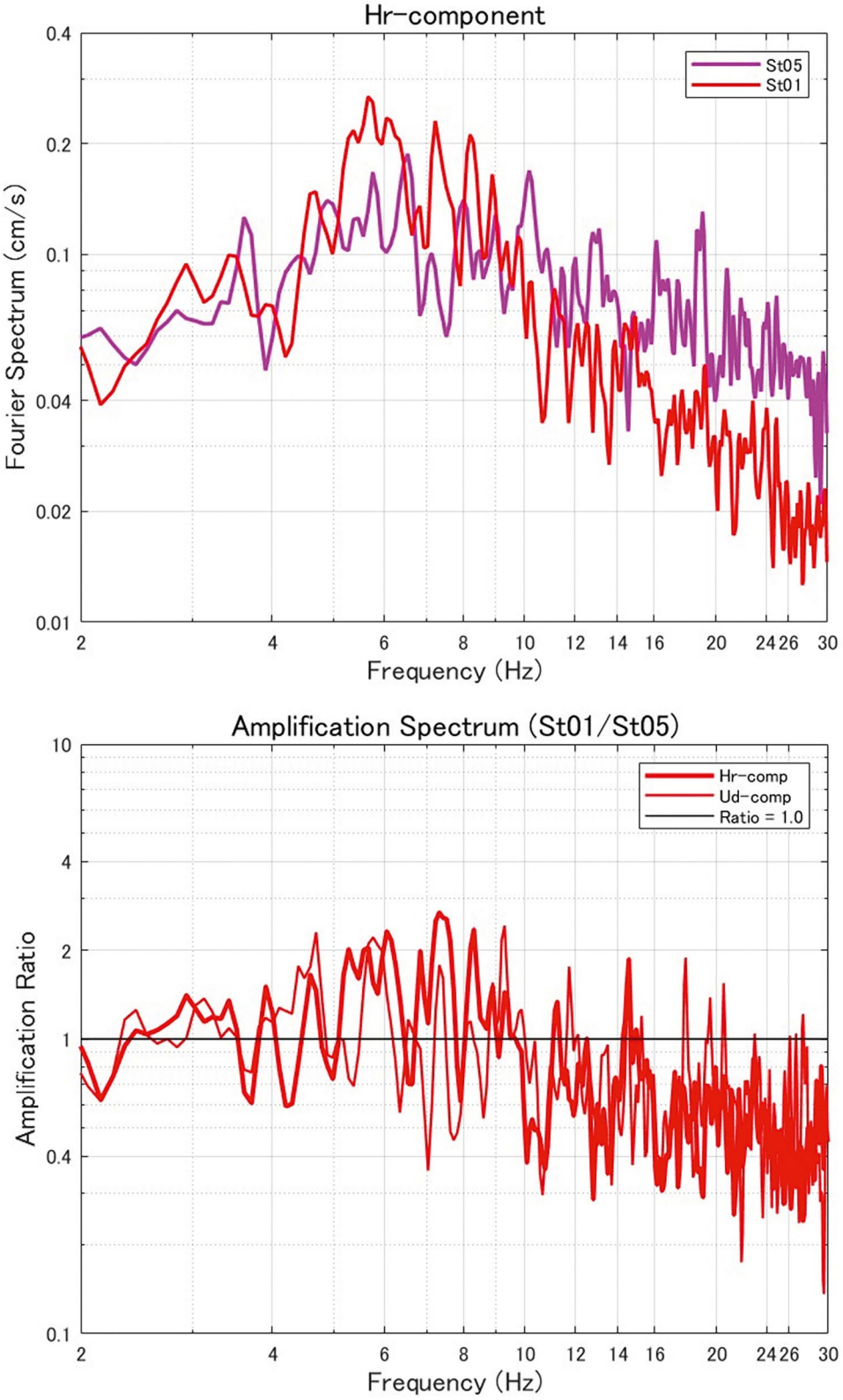


Fig. 8 **Top:** amplitude spectra of Hr-component for St01 and St05. **Bottom:** amplification spectra (St01/St05) of Hr- and Ud-components in the case of St05 as the reference. St01 is located on the rock site in the mountain ridge and St05 also does on the rock site in the mountain foot, respectively. Hr.-component and Ud-component are horizontal and vertical components, respectively

reports (Steidle et al. 1996; Boore and Joyner 1997; Matsunami et al. 2003). Thus, the amplification ratio obtained by using the nearby rock site St01 as a reference is a relative site amplification depending on the reference rock site St01. Similarly, when the rock site St05 at the mountain foot is used as a reference, the amplification ratio obtained is also a relative site amplification depending on the St05. Matsunami et al. (2003) showed that an underground rock

site station or a borehole rock site station represents a very accurate reference for seismic hazard analysis when the destructive interference of waves reflected from the surface is taken into account.

Usually, the seismic behavior of a surface rock site is affected by the weathered and fractured nature of basement rock, and by topography of the rock site. For the rock site St01, the weathering and fracturing effects correspond to the decrease of the amplification spectra (St01/St05) at frequencies higher than 6 to 8 Hz. Although an amplification peak due to a topographical effect such as mountain vibration is not clear in the frequency range of 2 to 30 Hz, the peak (Ratio = 2 or high) at 6 to 8 Hz may correspond to this phenomenon. The resonant frequency of mountain vibration depends on the volume and mass of mountains. Therefore, it is also necessary to search the amplification peak in frequencies lower than 2 Hz. In the present case, however, we cannot reveal and discuss the mountain vibration in the lower frequencies because the S/N-ratio of observed seismic data is poor at frequencies lower than 1.6 Hz.

Next, based on (2) above, we first investigate the site amplification of the two soil site stations (St02 and St03) in Aranayake landslide areas. St02 and St03 are located on colluvial debris in landslide body and on the unstable mass over the main scarp, respectively. Figure 9 shows the amplitude spectra (Hr-component) and the amplification spectra (St03/St05 and St02/St05) for the two stations. From the amplification spectra, St03 exhibits a clear amplification at 10 to 14 Hz. The amplification ratio at the dominant frequency of about 12 to 14 Hz is about 20 to 30. If the amplification at the dominant frequency is due to resonant vibration in a surface layer with a thickness of H resting on the basement rock (St05), then the observed amplification ratio is equal to the inverse of the impedance ratio between the surface layer and the basement rock. When the amplification ratio is 20 to 30, the impedance ratio becomes to 1/20 to 1/30. Furthermore, when the density ratio between the surface layer and the basement rock is 1.0, the S-wave velocity ratio becomes to 1/20 to 1/30. If S-wave velocity of the basement rock is 2000 to 3000 m/s, the S-wave velocity of the surface layer is about 66 to 150 m/s. When the S-wave velocity of the surface layer is 66 to 150 m/s and the dominant frequency is 12 to 13 Hz, the layer thickness H becomes to roughly 1.2 to 3.1 m. From an overview at the landslide slope, the thickness of the landslide layer is thought to be around 3 to 5 m, and this calculation seems reasonable.

We next investigate the site amplification of the soil site station (St04) in the Kalugala landslide area. St04 is located on unstable soil on the cut slope. Figure 10 shows the amplitude spectra (Hr-component) and the amplification spectra (St04/St05) for St04. As shown in Fig. 3, St04 is located at the foot of the landslide slope, and St05 on a nearby rock. The distance between St04 and St05 is several tens of meters. Comparing the amplitude spectra of St05 and St04 (in the top of Fig. 10), we notice that the two stations have clear peaks at 13, 19, and 25 Hz, and St04 is amplified by several times at those frequencies. We suggest these vibrations are generated in the basement rock by some mechanism. Furthermore, the rock site St01 on the mountain ridge does not exhibit this form of vibration. Therefore, it is questionable that the peak of the amplification spectra of St04/St05 at 25 Hz is due to resonant vibration in the surface layer resting on the basement rock. If the peak of 5.0 at the frequency of about 25 Hz in the bottom of Fig. 10 is due to resonant vibration in the surface layer resting on the basement rock with S-wave velocity of 2000 m/s, the S-wave velocity of the surface layer is about 400 m/s, and the layer thickness (H) is 4 m. We suggest that the underground structure calculated by using the resonant vibration model in the surface layer deviates significantly from the real structure.

Unstable soil site St03 is shaken by clear resonant vibration at frequencies 10 to 14 Hz. Theoretical wave characteristics of this vibration are examined by drawing particle motions in the main part of S-wave ground motions observed during the 24-4-2023 Hambantota-offshore *M*4.4 earthquake. Figure 11(top) shows the record of seismic ground motions used in the analysis. The 8- to 16-Hz band-pass filtered records are used to draw particle motions since the dominant frequency of the excited vibrations is 10 to 14 Hz. Main part of S-wave ground motions is divided into four windows for time, and particle motion is drawn in each time window. Figure 11 (middle) shows S-wave forms and particle motions (bottom) in each time window. From the particle motion diagram, the following can be extracted. Except for the time of S-wave arrival (S1-window), S-wave parts vibrate almost horizontally. The horizontal vibration in each time window exhibits each dominant direction, but the dominant direction gradually changes as time progresses (from S2-window to S4-window). The dominant direction in S2-window is *N*50 ° *E*; in S3-window the ENE-WSW direction dominates; while in the S4-window, the E-W direction is dominant. Figure 12 shows the location of St03 in the landslide area. According to the photograph, the landslide axis (valley direction) is *N*40 ° *E* and the landslide scarp direction is *N*35 ° *W*,respectively. The landslide axis is almost perpendicular to landslide scarp direction. The dominant direction in S2-window nearly matches the landslide axis. However, the dominant directions in S3-window and S4-window differ from the landslide axis, and gradually approaching the EW orientation. Generally, the direction of resonant vibration is perpendicular to the landslide scarp direction because the scarp is free from stress in the direction of the valley line. As shown in Fig. 12, St03 is not located in a part where the scarp linearly extends, but at the corner where the scarp is curved. This implies that the direction of vibration gradually changes according to the direction of stress-free slope conditions. This is suggestive for predicting the direction of future scarp collapses.

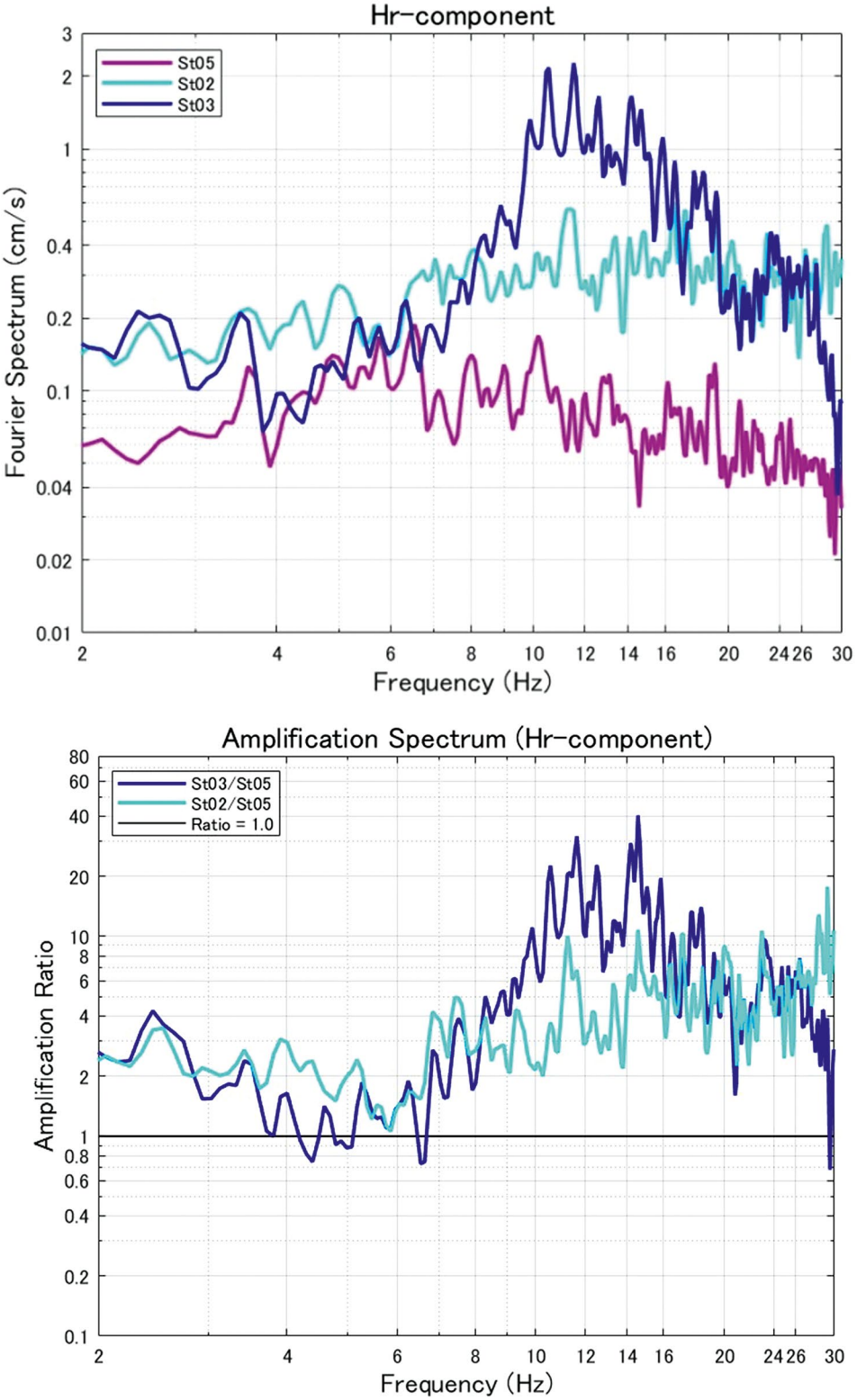


Fig. 9 **Top:** amplitude spectra of Hr-component for St02, St03 and St05. **Bottom:** amplification spectra (St03/St05 and St02/St05) for Hr-component. St02 is located on the debris in landslide body in Aranayake LS area and St03 on the unstable mass over the main scarp in the area, respectively. St05 on the rock site in the mountain foot and is used as the reference station. Hr-component is horizontal component

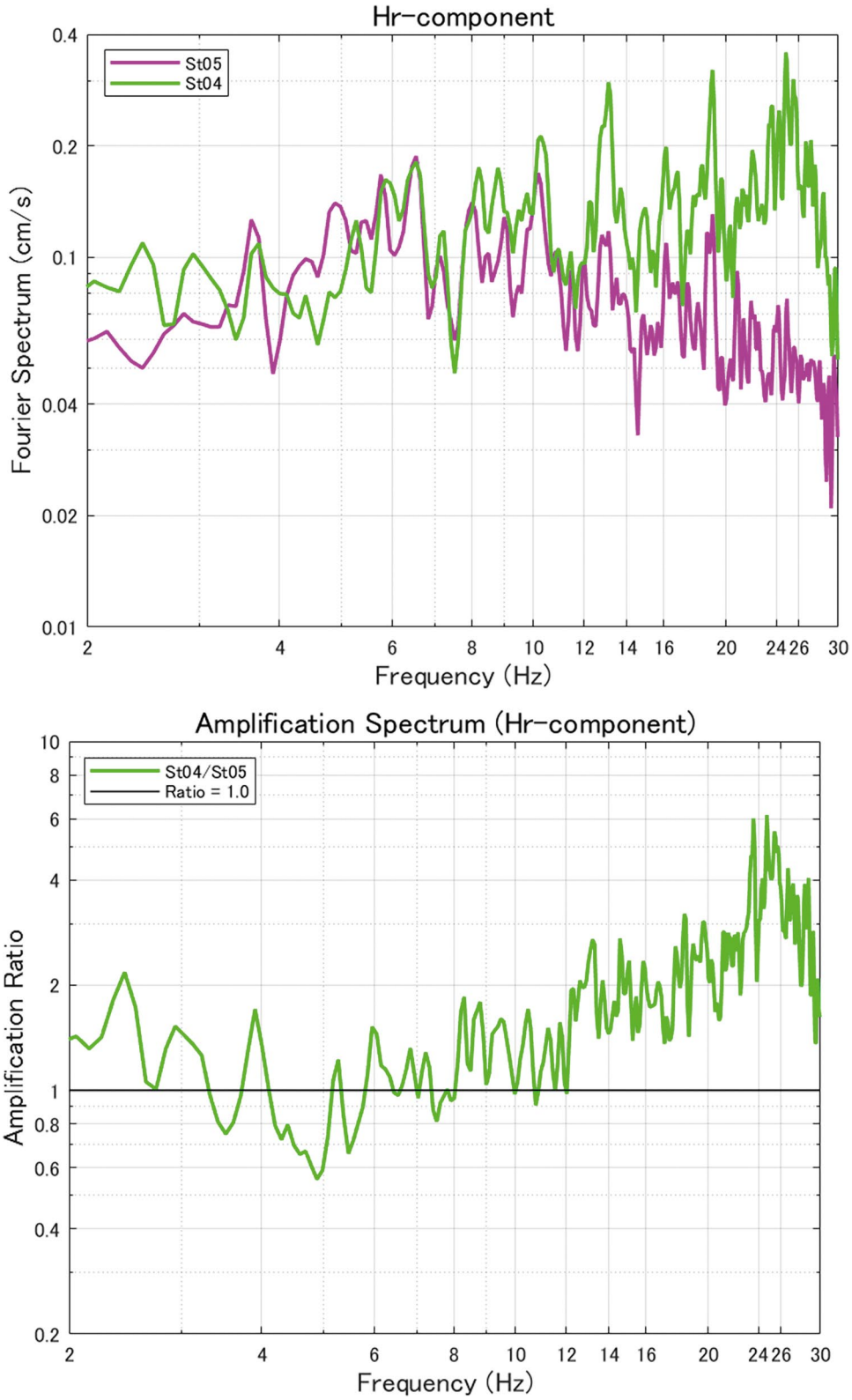


Fig. 10 **Top:** amplitude spectra (Hr-component) for St04 and St05. **Bottom:** amplification spectra (St04/St05). Hr-component is horizontal component

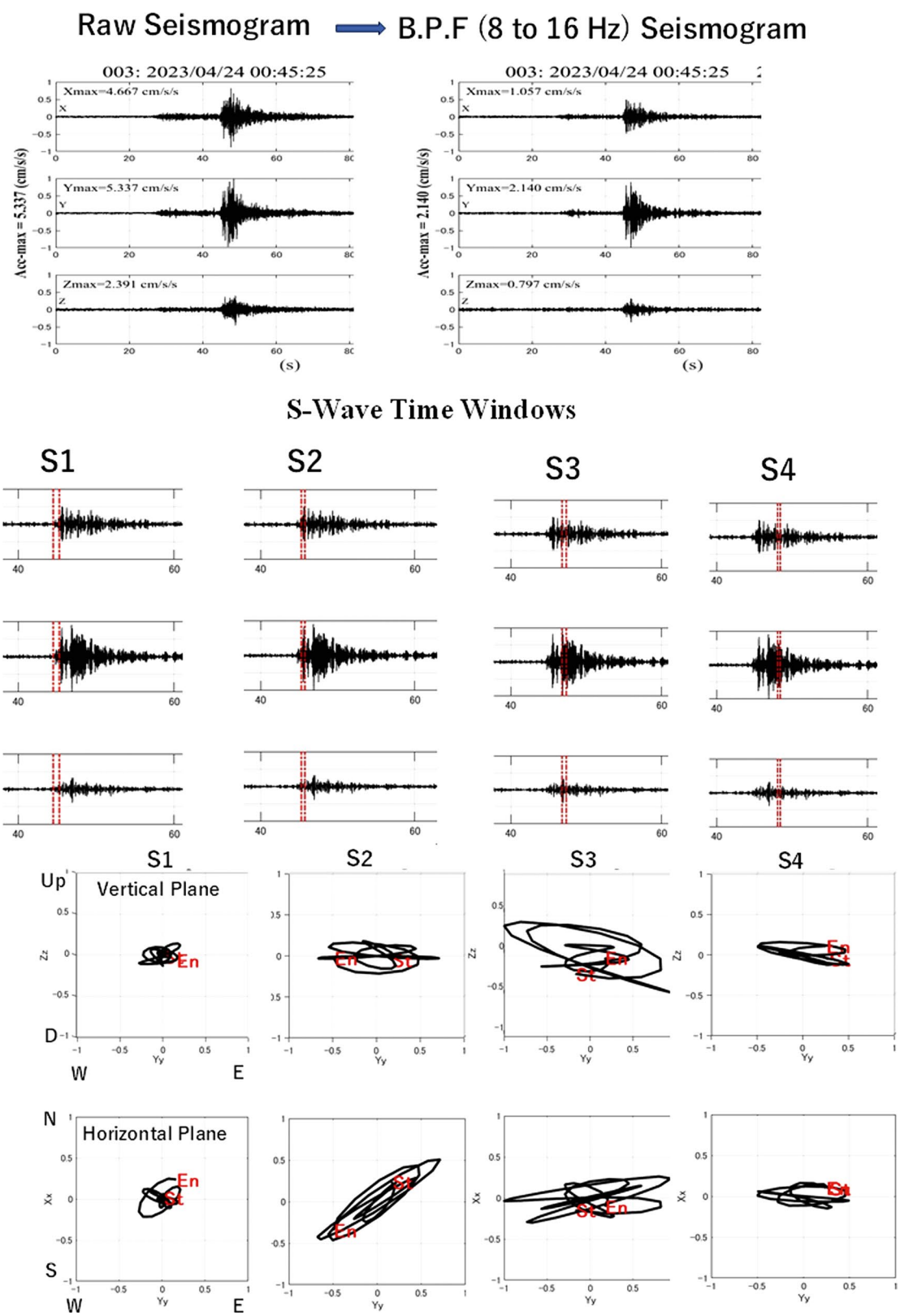


Fig. 11 **Top:** raw and band-path (8 to 16 Hz) filtered seismograms used. Raw seismograms during the 24-4-2023 *M*4.4 event. Middle: S-wave forms in each S-wave time window. **Bottom:** particle motion diagrams in each time window. St in red shows starting point of the particle motion diagram, and En in red does end point of the particle motion diagram

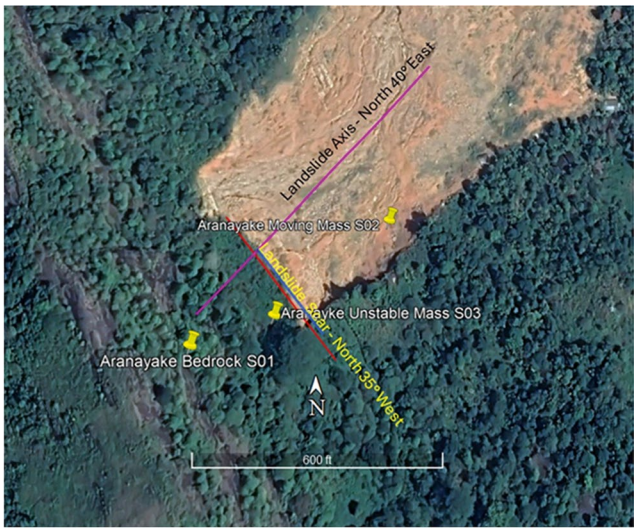


Fig. 12 Detailed location of St03 on the landslide scarp in the Aranayake landslide area

4.1 Earthquake Activity in Aranayake Landslide Area

Seismic waveform records (image-file) observed by the wide dynamic-range earthquake motion array are compiled into database and stored on the NBRO (National Building Research Organization, Colombo, Sri Lanka) server. We use this freely downloaded database to investigate seismic activity in Aranayake landslide area. Since most of the earthquakes observed at St03 are earthquakes with $Ts\text{-}p < 5$ s, we first examine the monthly number (N (*Month*, $Ts\text{-}p < 5$)) of earthquakes with $Ts\text{-}p < 5$ s, where $Ts\text{-}p = Ts—Tp$, Tp is P-wave arrival time, and Ts is S-wave arrival time. Here, we define as follows. Let the month name be *Month*, and let N (*Month*, $Ts\text{-}p < 5$) be the number of earthquakes with $Ts\text{-}p < 5$ s observed in that month. Here, Month is from *Apr* to *Nov*.

The top of Fig. 13 shows the monthly graph for N (*Month*, $Ts\text{-}p < 5$) observed at St03 from April to November 2023. From this graph, the average of N (*Month*, $Ts\text{-}p < 5$) for 6 months from *April* to *November* is an estimated 33. Furthermore, since earthquakes with $Ts\text{-}p < 1.0$ s are frequently observed, we investigate the ratio (*Ratio*(*Month*) = N(*Month*, $Ts\text{-}p < 1.0$) / N(*Month*, $Ts\text{-}p < 5.0$)) of the earthquake number with $Ts\text{-}p < 1.0$ s to that with $Ts\text{-}p < 5$ s by *Month*. The bottom of Fig. 13 shows *Ratio* (*Month*). From this figure, we find that about 70% of the observed events are earthquakes with $Ts\text{-}p < 1.0$; that is, they occur within approximately 8 km of observation point St03 (Omori 1899; Lay and Wallace 1995). Even if the magnitude of an earthquake is small, if it occurs close to the observation point, the observed seismic motion will be larger than expected. To examine this effect, the number (N) of earthquakes counted for each S-wave maximum amplitude (*Amp*), that is N (*Amp*, $Ts\text{-}p$), is examined in the case of $Ts\text{-}p < 1.0$ and $Ts\text{-}p < 5.0$.

The top of Fig. 14 shows N (*Amp*, $Ts\text{-}p < 5$). It decreases with the increase of *Amp*. When *Amp* is 0.010 to 0.011 cm/s, it becomes very large (close to 70). These levels of *Amp* exceed the linearity range of the microseismometer used, so the recorded seismic waveforms are largely distorted as shown in the bottom of Fig. 15. To examine why earthquakes with large amplitudes are so many, the percentage of earthquake number with $Ts\text{-}p < 1.0$ s to that with $Ts\text{-}p < 5$ s was calculated from *Ratio* (*Amp*) = N (*Amp*, $Ts\text{-}p < 1$) / N (*Amp*, $Ts\text{-}p < 5$) by *Amp* and plotted in the bottom of Fig. 14. We find that *Ratio* (*Amp*) for *Amp* = 0.008 to 0.010 is very large, becomes 62 to 100%. Thus, the large increase of N (*Amp*, $Ts\text{-}p < 5$) for *Amp* = 0.010 to 0.011 is due to large value (62%) of N (*Amp*, $Ts\text{-}p < 1.0$). This shows that microearthquakes with $Ts\text{-}p < 1.0$ s and *Amp* > 0.008 cm/s frequently occur in the vicinity of St03.

Watanabe (1971) obtained an empirical equation for determining microearthquake magnitude M from maximum amplitude Av of vertical component of velocity-type seismometer. The equation is as follows:

$$0.85\,M = \log Av + 1.73 \log R + 2.50, \qquad (6)$$

where R is the hypocentral distance of a microearthquake.

When we calculate the magnitude M of a microearthquake using R = 8 km (Ts-p < 1.0 s) and Av = 0.01 cm/s which are characteristic to Aranayake landslide area, M is 2.4. Accordingly, the magnitude M of microearthquakes with $Av > 0.01$ cm/s is roughly estimated to 2 to 3.

The survey of seismic activity in Aranayake land slide area revealed the following. On average, about 33 microearthquakes occur every month in the vicinity of St03, and about 70% of them have $Ts\text{-}p < 1.0$ s. Especially for microearthquakes with $Av > 0.01$ cm/s, the velocity magnitude M is 2 to 3. The maximum amplitude of microearthquakes with $M > 2$ exceeds the linearity range of the velocity-type microseismometer, so the observed seismic waveforms are largely distorted

Figure 15 shows examples of seismic waveforms observed at St03. The top of Fig. 15 shows waveforms for $Ts\text{-}p$ = 18.3 and 7.2 s, the middle does for $Ts\text{-}p$ = 2.0 and 0.2 s, and the bottom does for $Ts\text{-}p = 0.1$ and $Ts\text{-}p < 0.1$. What is particularly characteristic is that when $Ts\text{-}p < 1.0$, the amplitude of the input seismic wave is too large, causing "saturation" of the waveform, which strongly distorts the waveform. Such earthquakes occur frequently beneath the Aranayake landslide area. St03, which is on the unstable soil over the main scarp, is frequently shaken by such earthquakes, so special attention is required especially during times of heavy rainfall.

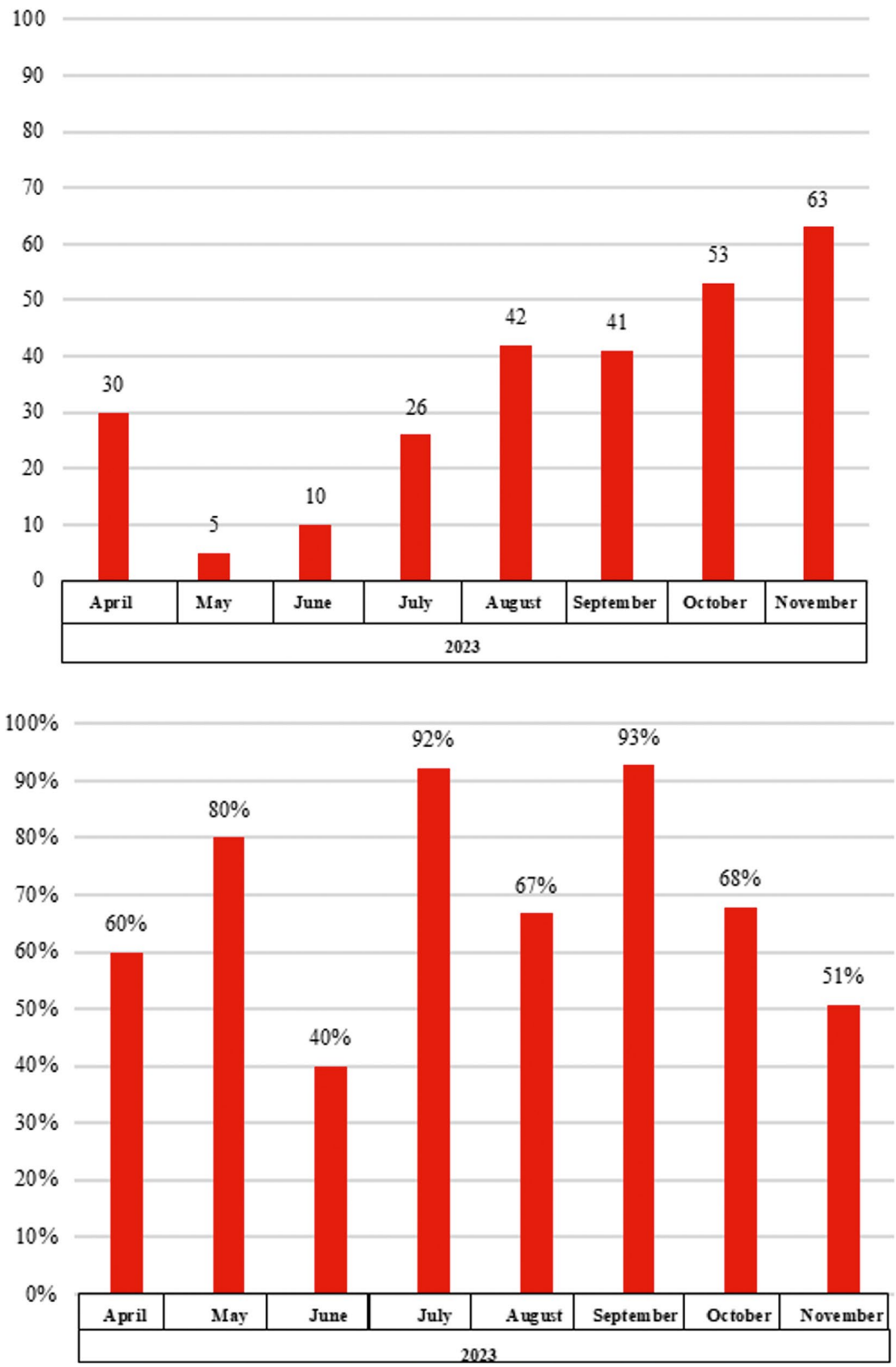


Fig. 13 **Top:** *N* (*Month*, *Ts-p* < 5), numbers of earthquakes with *Ts-p* < 5 s by *Month*. **Bottom:** *Ratio* (*Month*) = *N* (*Month*, *Ts-p* < 1) / *N* (*Month*, *Ts-p* < 5), percentage of the earthquake number with *Ts-p* < 1.0 s to that with *Ts-p* < 5 s by *Month*

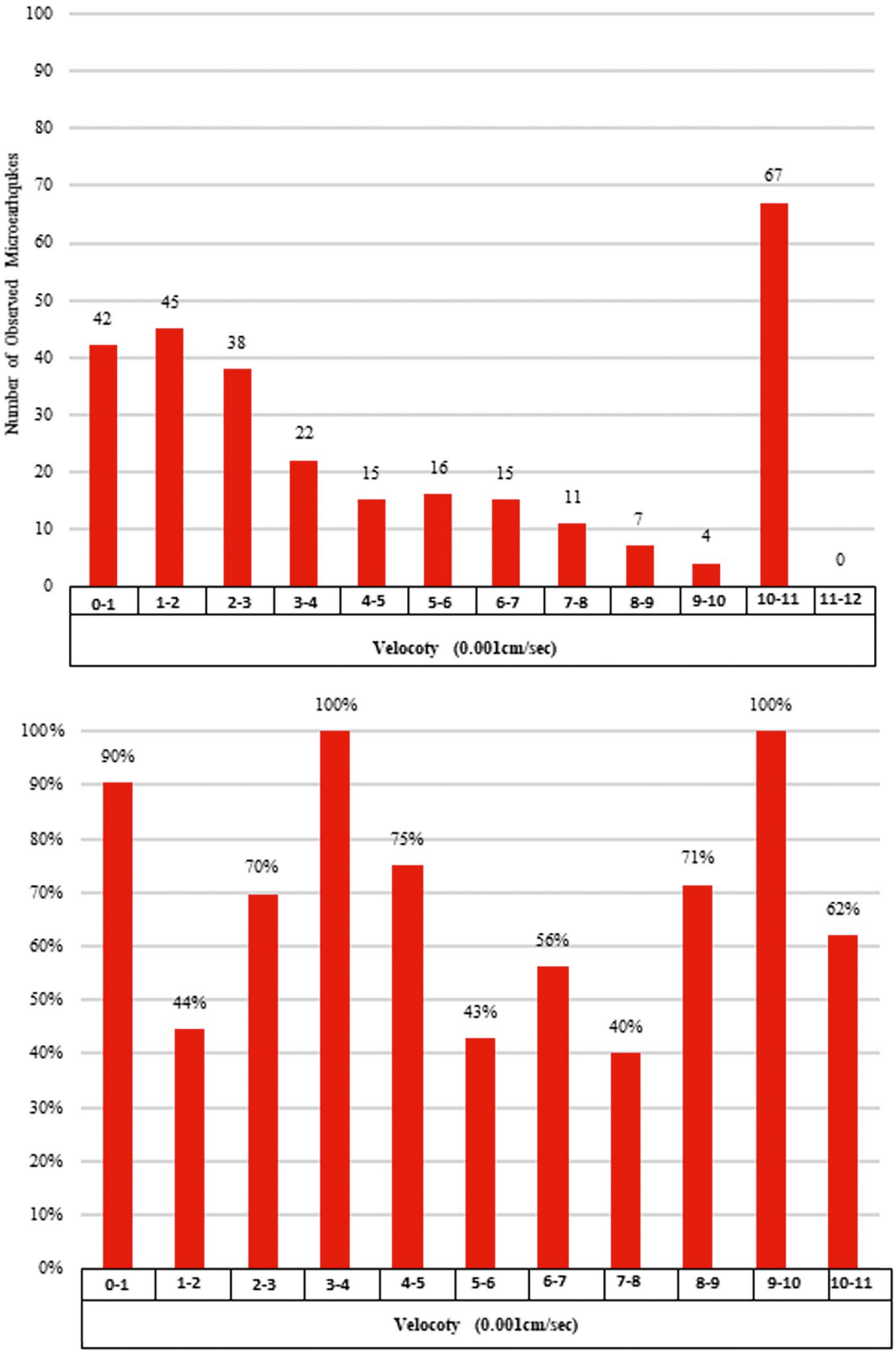


Fig. 14 **Top:** *N* (*Amp*, *Ts-p* < 5), numbers of earthquakes with *Ts-p* < 5 s by maximum amplitude (*Amp*). **Bottom:** *Ratio* (*Amp*) = *N* (*Amp*, *Ts-p* < 1) / *N* (*Amp*, *Ts-p* < 5), percentage of earthquake number with *Ts-p* < 1.0 s to that with *Ts-p* < 5 s by maximum amplitude (*Amp*)

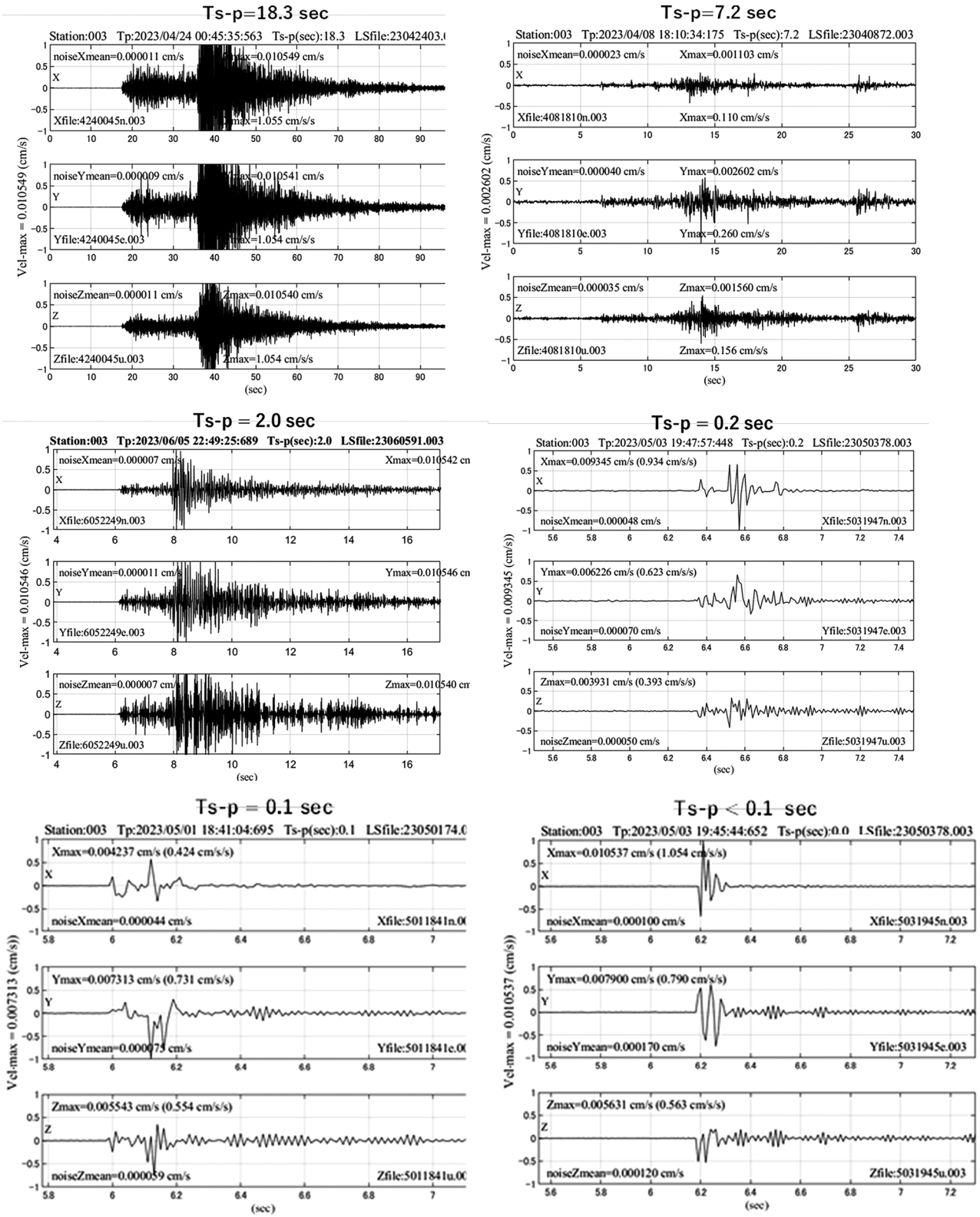


Fig. 15 **Top:** waveforms of earthquakes with *Ts-p* = 18.3 and 7.2 s. **Middle:** those with *Ts-p* = 2.0 and 0.2 s. **Bottom:** those with *Ts-p* = 0.1 and *Ts-p* < 0.1 s. For *Ts-p* < 1.0, it is found that strong distortions of waveforms occur by saturation of seismic waves input to seismographs

5 Conclusions

This study analyzes the site amplification effect of landslide areas in Sri Lanka using records observed by the wide dynamic-range earthquake motion array with unstable soil-site and stable rock-site stations. The Aranayake Landslide area and the Kalugala area are located on the same mountain, but on opposite sides of the ridge. In the Aranayake Landslide area, St01 is located on a rock site near the mountain ridge and St03 is on an unstable mass overlying the main scarp. In the Kalugala area, St05 is located on a rock site at the mountain foot and St04 is near the foot of the landslide slope.

Seismic waveform records observed by the wide dynamic-range earthquake motion array are compiled into database and stored on the NBRO (National Building Research Organization, Colombo, Sri Lanka) server. These data can be freely downloaded: seismic raw data—http://124.43.69.113:60080/Data/Seismic/.

Using the data base, we investigated seismic activity in Aranayake landslide area.

The principal conclusions of this study can be summarized as follows.

1. Rock site St01 does not have the same response as the rock site St05. Rock sites display a characteristic frequency-dependent site effect; that is, a relative site effect depending on a reference rock site. The relative site effect of Ratio (St01/St05) is nearly 1.0 at frequencies lower than 6 Hz, having a peak of 2 or more at 6 to 8 Hz (1-a), gradually decreasing with increasing frequency, and becoming less than 1 above 10 Hz (1-b).
2. When St01 is selected as a reference site, (1-a) leads to underestimations of wave amplification in a landslide layer resting on basement rock, while (1-b) leads to overestimations of wave amplification in a landslide layer resting on basement rock.
3. St03 exhibits a clear amplification at 10 to 14 Hz. The amplification ratio (St03/St05) at the dominant frequency of 10 to 14 Hz is about 20 to 30.
4. Particle motion analysis of S-wave main parts reveals that except at the time of arrival, S-wave components vibrate almost horizontally. The dominant direction of the horizontal vibration in the early part of main wave motion nearly matches the landslide axis of $N40\ ^\circ\ E$, but gradually changes to an EW orientation with the progress of time. This suggests the gradual change of orientation is toward a direction free from stress, dependent on the location of St03 at the corner, rather than on the central part of the landslide scarp.
5. Assuming (3) and (4) are due to resonant vibration in a surface layer with a thickness of H m resting on the basement rock with S-wave velocity of 2000 to 3000 m/s, S-wave velocity of the surface layer is estimated as 66 to 150 m/s and the layer thickness H, 1.2 to 3.1 m. From an overview at the landslide slope, the thickness of the landslide layer is thought to be around 2 to 3 m, and this calculation seems reasonable.
6. A survey of seismic activity reveals the following: on average, about 33 microearthquakes occur every month in the vicinity of St03, and about 70% of them have $Ts\text{-}p < 1.0$ s. Especially for microearthquakes with the maximum amplitude $Av > 0.01$ cm/s, the velocity magnitude M is 2 to 3. The maximum amplitude Av of microearthquakes with $M > 2$ exceeds the linearity range of the velocity-type microseismometer used, so the observed seismic waveforms are largely distorted.
7. Such earthquakes occur frequently beneath the Aranayake landslide area. St03, which is on unstable mass over the main scarp, is frequently shaken by such earthquakes, so special attention is required to reduce the risk of landslide disasters in this region of Sri Lanka.

References

Agrawal PN (1983) Progress report on microearthquake studies for Kotmale Project, Sri Lanka. Dept. of Earthquake Eng. Univ., Roorkee, India, pp 1–27

Boore DM, Joyner WB (1997) Site amplification for genetic rock sites, Bull Seism Soc Am 87:327–341

Lay T, Wallace TC (1995) Modern global seismology. Academic Press, San Diego

Matsunami K, Zhang W, Irikura K, Xie L-L (2003) Estimation of seismic response in the Tangshan area, China, using deep underground records. Bull Seism Soc Am 93(3):1065–1078

Omori F (1899) Note on the preliminary tremor of earthquake motion. J Coll Sci, Imp Univ Tokyo, Japan 11:147–159

Steidle JH, Tumarkin AG, Archuleta RJ, (1996) What is a reference site? Bull Seism Soc Am 86:1733–1748

Vithanage PW (1994) Seismicity—neglected aspects of Sri Lankan landslide studies. National Symposium on Landslide in Sri Lanka, Colombo, Sri Lanka

Watanabe H (1971) Determination of earthquake magnitude at regional distance in and near Japan, "Zisin". J Seism Soc Japan 24:189–201

Wimalaratne KD (1993) The first earthquake recorded in Sri Lanka, Daily News, Thursday, Dec. 23: 8

Open Access This chapter is licensed under the terms of the Creative Commons Attribution 4.0 International License (http://creativecommons.org/licenses/by/4.0/), which permits use, sharing, adaptation, distribution and reproduction in any medium or format, as long as you give appropriate credit to the original author(s) and the source, provide a link to the Creative Commons license and indicate if changes were made.

The images or other third party material in this chapter are included in the chapter's Creative Commons license, unless indicated otherwise in a credit line to the material. If material is not included in the chapter's Creative Commons license and your intended use is not permitted by statutory regulation or exceeds the permitted use, you will need to obtain permission directly from the copyright holder.



Experiments of Modelling Subaqueous Landslide Susceptibility in Lake Albano of Castel Gandolfo

Antonio Patera and Andrea G. Fabbri

Abstract

Our modelling experiments aim at generating and interpreting the *prediction patterns* of subaqueous landslides within the Lake Albano maar, a complex volcanic depression located southeast of Rome. These patterns, which assess the possibility of future events, are based on the spatial distribution of historical landslide forms within the lake, analyzed in conjunction with continuous field values derived from high-resolution digital elevation models. To establish the mathematical framework for modelling these spatial patterns, we employed empirical likelihood ratios and utilized a fuzzy set function to integrate the spatial relationships, both in the presence and absence of landslide forms in the study area. In constructing our analysis, we deployed a high-resolution raster database to pinpoint the locations of 42 linear and 23 polygonal subaqueous landslide forms generating a digital elevation raster and deriving six topographic-surface continuous fields: aspect, digital elevation model, slope, curvature, planform, and profile. No additional information was available besides the six conditionally dependent continuous fields. Our modelling approach involved evaluating *prediction patterns* through sequential exclusions of individual landslide occurrences or groups, generating cross-validations with partial *prediction patterns*. Following comparisons of relative ranks within the *prediction patterns*, we conducted uncertainty analyses and geological interpretations to identify critically susceptible areas, particularly the topple scarps and landslide scarps surrounding the lower escarpment of Lake Albano. These features are situated within the context of past lahar deposits and suspected catastrophic floods, such as those documented in 398 BC, which impacted the volcanic crater of Lake Albano during Roman times. It is imperative to recognize the multi-hazard context of this region, which poses serious risks to urbanization, recreational activities, and heritage sites. Despite the reclassification of the volcanic crater from extinct to dormant, the potential for future subaqueous landslides underscores the ongoing need for proactive risk management strategies in the area surrounding Lake Albano.

Keywords

Prediction pattern · Subaqueous landslide susceptibility · Maar · Empirical likelihood ratio · Fuzzy set function · Cross-validation

1 Introduction

Lake Albano is described as a maar, a complex volcanic depression located approximately 20 km southwest of the metropolitan city of Rome. Patera and Fabbri (2023) provided an overview of its geologic-geomorphologic history.

The lake area is a site of several hazardous processes, including slope instability inside the crater, lowering of water level, hydrothermal circulation, seismicity, uplifts, and gas emissions of H_2S and CO_2, with stratification of gas concentrations reaching 200 mg/l of CO_2 at the bottom. Additionally, tsunami waves as secondary effects of subaqueous landslides have been inferred (Carapezza and Tarchini 2007; Chiodini et al. 2012; Barberi et al. 1989).

Lake Albano represents part of the Colli Albani (Albani Hills) Quaternary volcanic system: the final hydromagmatic phase. The crater reaches elevations between 390 m and 585 m a.s.l. with the coastline at 290 m and a maximum depth of 167 m. It covers 6 Km^2 and shows three

A. Patera
Istituto Nazionale di Geofisica e Vulcanologia, Rome, Italy
e-mail: antonio.patera@ingv.it

A. G. Fabbri (✉)
Dipartimento di Scienze dell'Ambiente e della Terra, Università di Milano-Bicocca, Milan, Italy
e-mail: andrea.fabbri@unimib.it

© The Author(s) 2025

B. Abolmasov et al. (eds.), *Progress in Landslide Research and Technology, Volume 3 Issue 2, 2024*, Progress in Landslide Research and Technology, https://doi.org/10.1007/978-3-031-72736-8_7

sub-lake platforms. The first one is located 10 m to 12 m below the water surface, next to an 80 m escarpment. It is followed by a ring-shaped second platform positioned at the center, next to a 35 to 50 m escarpment. The third platform is at the bottom of the lake at 126–133 m a.s.l., filled by sediments 14 m in thickness (Bozzano et al. 2009; Anzidei et al. 2006).

Since historical times, there is knowledge of episodes of leakage of lake water from the topographically lowest point of the northwestern edge of the crater. Volcanologists indicate that they were probably a consequence of emission from the bottom of the lake of fluids of magmatic origin rich in CO_2, which have generated a succession of lahar deposits along the outer slope, towards the Ciampino plain to the North. More recently, lahar deposits were mapped also at the lowest point of the maar rim (Funiciello et al. 2002, 2003). The last of these catastrophic events, described by Plutarch in the Histories of Themistocles and Camillus and Titus Livius in his Natural History, is dated 398 BC, following which the Romans in 394 BC built a drainage tunnel that has since kept the lake level at 70 m below the lowest threshold of the crater (Galeazzi et al. 2015).

The assessment of the risk due to the instability of the inner slopes of the crater must also take into account the secondary effects of tsunami waves, possibly generated as a result of the impact of landslide subaerial landmasses on the surface of the lake or due to underwater mass movements. The extinct volcano has been reclassified as quiescent (Funiciello et al. 2003; Marra et al. 2016).

Patera and Fabbri (2022) made a preliminary assessment of subaerial landslide susceptibility. The assessment considered a multitude of subaerial landslides and a few submerged prosecutions of subaerial accumulations. The results of their work encouraged the present experiments as a follow-up focused on the remaining subaqueous landslides.

It has to be emphasized that the lake is a valuable heritage and economic asset: it has been for historical times a center of tourism, sports, science, and the arts, including poetry, novels, and paintings. These include the Pope's summer residence of Castel Gandolfo, a Roman outlet, and castles and mansions attracting visitors. All of these are located in the densely urbanized immediate surroundings of the lake. Web queries such as "poetry or literature or novels or heritage on Lake Albano" provide a multitude of websites covering all kinds of attractions. Novels worth of mention are Stendhal's "The Abbess of Castro," George Gordon Lord Byron's "Child Harold" or Mary W. Shelley's "The Sisters of Lake Albano" (see also "Alban Hills" on https://en.wikipedia.org/wiki/Alban_Hills).

The problem of assessing landslide susceptibility with the remaining subaqueous landslides, however, is somewhat different due to the unavailability of land use and lithology maps that were available for subaerial landslides: only high-resolution digital elevation data are available. What can we do with such limited information of heavily conditionally dependent continuous fields to complement the previous studies? We have addressed this question.

The next section describes the database followed by a section on the modelling. The experiments on susceptibility prediction are next with analytical steps, strategy of processing, examples, and discussion of the resulting prediction patterns. Concluding remarks on the significance of the modelling process, its advantages and limitations complete the study.

2 The Lake Albano Study Area and Database

The preliminary work of Patera and Fabbri (2022) used a raster database at 5 m resolution. Besides the distribution images of 150 linear and polygonal subaerial landslide forms, the database consisted of eight additional digitized maps. Land use and lithology maps, categorical, cover the part of the study area above water. Six continuous fields, derived from dense topographic elevation values, aspect, digital elevation model or DEM, slope, curvature, planform, and profile, include the part below water.

We used the same database and the distribution images of 65 subaqueous landslides. In addition, we produced a new database using 1 m resolution elevation values and redigitized the linear subaqueous landslide forms. In our analyses, the 5 m and the 1 m study areas were limited to the ground below the water surface of the lake. Figures 1 and 2



Fig. 1 Position of Lake Albano in central Italy (source: Earthstar Geographics LLC)



Fig. 2 Lake Albano with the surrounding urbanization (source: Earthstar Geographics LLC)

show the location of Lake Albano, Southeast of the City of Rome, and its densely urbanized surroundings.

The Lake Albano database consists of raster digital images of 5 m resolution. All images of dimension 1002 × 1202 picture elements or pixels are in a one-to-one correspondence. Figure 3 shows the distribution of all landslide forms and the corresponding digital maps for the study. An additional database at 1 m resolution had images of size 3000 × 3000 pixels.

The study areas are limited by the shoreline of the lake. The 5 m study area covers 229,311 pixels while the 1 m database covers 5,723,475 pixels.

Tables 1 and 2 provide names, short names, and value ranges of the images in the Lake Albano database. The short names are to simplify the description of the experiments and the results. We have proposed the term "*pattern*" to indicate the spatial configuration of the transformation of the initial image values or numerical labels (continuous fields or categorical labels), which are converted into quantitative support of the modelling.

For support, we imply the presence of landslides in the context of their environmental setting represented by the continuous field values at their location.

We used the terms direct supporting patterns, DSP, to indicate the images of distribution of subaqueous landslide forms and indirect supporting patterns, ISP, to refer to the images of continuous fields.

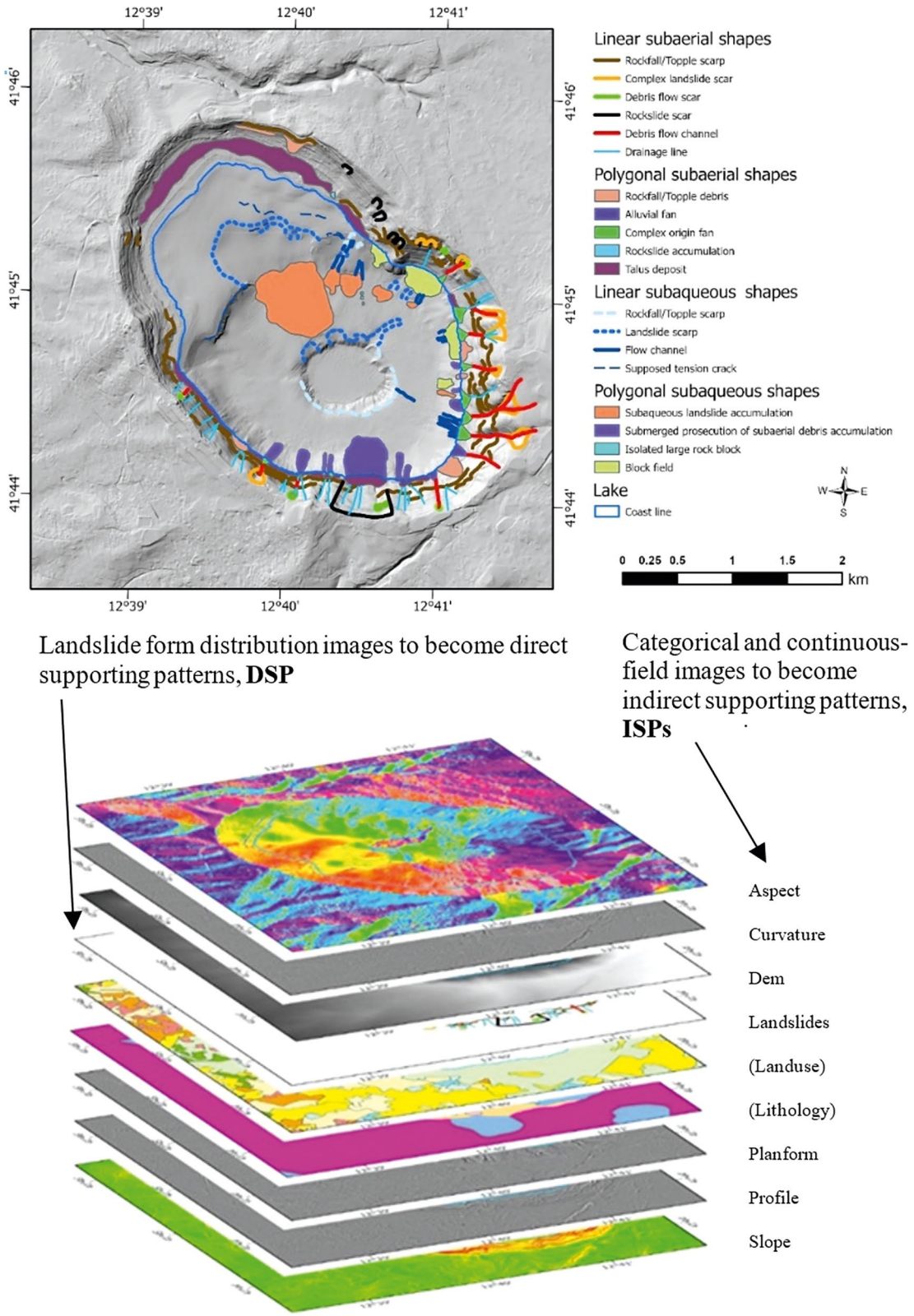


Fig. 3 The Lake Albano database of digital images (modified after Patera and Fabbri (2023). **Top:** the distribution of subaerial and subaqueous landslide forms over the internal slopes of the lake. The subaqueous study area is within the coastline. **Bottom:** the 5 m-resolution digital images of categorical and continuous field maps used for landslide maps used for landslide susceptibility modelling. Landuse and lithology (names within brackets) are not available for the subaqueous study area

Table 1 Subaqueous linear and polygonal landslide forms of Lake Albano and corresponding short names. Their distribution images were converted to direct supporting patterns, DSP (modified after Patera and Fabbri 2022)

Subaqueous linear form	Short name	Subaqueous polygonal form	Short name
Flow channel	**LA1**	Block field	**PA1**
Landslide scarp	**LA2**	Isolated large rock block	**PA2**
Rockfall/topple scarp	**LA3**	Subaqueous landslide accumulation	**PA3**
Supposed tension crack	**LA4**	Submerged prosecution of subaerial accumulation	**PA4**

Table 2 Continuous field value ranges from 5 m-resolution, digital elevation surveys converted into indirect supporting patterns, ISP (modified after Patera and Fabbri 2022)

Continuous field	Short name	Minimum value	Maximum value	Description
Aspect	**a**	0°	359°	In degrees from the north direction
Dem, elevation	**d**	121.95 m	636.15 m	In m a. s. l.
Slope	**s**	0°	76.04°	In degrees
Curvature	**c**	−236.58	241.66	Planform + profile
Planform	**f**	−151.60	149.05	Divergence and convergence of the water flow (+ convex surface; − concave surface in direction of maximum slope).
Profile	**p**	−135.87	117.87	Acceleration and deceleration of the water flow (+ concave surface, − convex surface perpendicularly to direction of maximum slope).

3 Favourability Function Modelling

Patera and Fabbri (2022) obtained *prediction patterns* of future linear and polygonal subaerial landslides by estimating spatial relationships through empirical likelihood ratios and integrating the ratios using mathematical models based on fuzzy set membership functions and logistic discriminant functions. Within a constrained environment with a high density of occurrences, those patterns identify areas considered more likely to be affected by future subaerial landslide occurrences. Given the high density of landslides, overlaps exist between *prediction patterns* of subaerial linear and polygonal forms. The results appeared as reliable representations of the future with low variability and uncertainty of classification. In conclusion, they provide a feasible assessment of subaerial landslide susceptibility in the lake.

In Sect. 2, we described the Lake Albano database consisting of raster digital images with a resolution of 5 m, sized 1002 × 1202 pixels. An additional database at 1 m resolution had images sized 3000 × 3000 pixels. Our purpose in constructing the databases was to represent the past occurrence distribution of separate forms of subaqueous landslides (converted to DSPs) and spatially relate them with the distribution of continuous values (converted to ISPs), which partially portray the physical conditions or settings of occurrence.

The past landslide occurrence locations provide binary images of presence and absence over the subaqueous study area. The area can then be divided into two unequal parts: a smaller area corresponding to the presence of the occurrences and a much larger one corresponding to their presumed absence (there might be a few missed or unmapped occurrences but we do not know them). For each presence of a set of landslide occurrences, we compare the frequency of continuous values with that in their absence in the study area. This is to obtain a measure of contrast with a spatial relationship, hopefully separating the characteristics of presence from those of assumed absence. Before modelling, we make assumptions on the quality of the database, significance of occurrence distribution, and of the continuous fields to be converted to DSPs and ISPs, respectively, sufficiently representing the past, present, and future settings of the landslides.

Various interpretations exist of the spatial relationships and their integrations: sureness, likelihood, probability, certainty, belief, plausibility, or possibility that a proposition (a mathematical statement) like the following is true:

$$\mathbf{P}_i \text{ that a point } \boldsymbol{i} \text{ in the study area is affected by a type of subaqueous landslide (a DSP), given, "|" the presence of spatial evidence (ISPs)} \quad (1)$$

In our application, we have chosen the possibility interpretation, i.e., applying a fuzzy set membership function and its implicit assumptions (Chung and Fabbri 2001; Fabbri and Chung 2018; Patera and Fabbri 2022), and selected the Favourability Function Modelling framework (Chung and Fabbri 1993, 2003; Fabbri and Patera 2021). We have proposed the term "*pattern*" to indicate the spatial configuration of the transformation of the initial image values or numerical labels (continuous fields or categorical labels), which are converted into quantitative support of the proposition in (1) for the modelling. In our case, a continuous field image becomes an ISP by establishing its spatial relationship with an image of presence/absence of one type of subaqueous landslides forms, DSP, in the study area. This is an image with a numerical label for each occurrence. The term "*prediction*" assumes that the conditions of occurrences represented by the database are similar to the ones to be experienced in the future.

The following steps encapsulate the modelling framework:

E**stablish:** spatial relationships.
Integrate: prediction image.

Rank: *prediction pattern.*
Validate: prediction-rate curve.
Quantify Uncertainty: *Uncertainty Pattern.*

For all the steps, we require satisfying assumptions and selecting patterns, models, and computational strategies to obtain relative measures or estimates in line with our physical interpretation of the study area. These selections often are arbitrary and require trial and error procedures.

The experiments in the next section follow and explain the Favourability Function Modelling approach. The purpose is to compute *prediction patterns* of sets of subaqueous landslides showing areas more likely to be affected by future landslide occurrences.

4 Experiments of Predicting Susceptibility of Subaqueous Landslides in Lake Albano

The subaqueous landslide forms of Lake Albano consist of two groups, linear and polygonal, listed in Table 1. The polygonal forms are accumulations distributed over shallow slopes while the linear forms are located at the edges of escarpments. We will be modelling the linear forms and observing their distribution with respect to the accumulations.

The experiments that follow describe the five-step strategy applied to arrive at the parts of *prediction patterns* considered having the highest possibility to affect the bottom area of the lake and to contribute to a damaging tsunamis effect.

4.1 Establish

We have used the Empirical Likelihood Ratio, ELR, as a general measure of spatial relationships. For instance, in the subaqueous study area for 10 landslide scarps, **LA2**, Fig. 4 shows the DEM, **d**, and curvature, **c**, density functions and their corresponding ELR functions. In the illustration, on the horizontal axis, the range of DEM values is 122–288 m a.s.l. and the range of curvature values is −64–+72 (DEM values × 10 and curvature values +240, respectively). On the vertical axis in the upper diagrams are the density functions, the relative proportion of occurrence pixels, blue curve, and of the outside pixels, red curve (Fig. 4). In the corresponding lower diagrams are the ELR functions, i.e. the ratios of the two density functions, occurrences/outside.

For instance, a rule of thumb is that ELR values ≥2 indicate frequencies in the presence of the landslide occurrences twice or more than the ones in their absence, thus characterizing the presence. Values close to 1 indicate frequencies with no separation power between presence and absence in the study area. ELR values range from zero to infinity. The two picks in Fig. 4a, at about 165 m and 250 m, with ELR values of 4.5 and 4.2 respectively, correspond to the two elevation ranges of the landslide scarps shown in Fig. 6b, as white lines. The two curvature density functions in Fig. 4b overlap almost entirely and provide marginal or minimal support to the separation of presence from absence of landslides. In order to assess their support as ISPs, we obtained ELR values and diagrams for the four subaqueous linear forms using all six continuous fields.

Table 3 lists the ELR values for the subaqueous landslide forms in Lake Albano. Names and short names of the DSP are in column 1, the numbers of landslides and of the corresponding pixels are in columns 2 and 3. In column 4 are the ELR values for the continuous fields, the ISPs: the values with ratio above a threshold of ≥2 (sometime ≥1) are in italics font and within brackets is the maximum ratio reached and its corresponding value. All ratios ≥2 are in bold. The table summarizes the histograms like those in Fig. 4, for all continuous fields of the linear forms.

For instance, in Table 3, the first form, **LA1** with 21 flow channels, affects 578 pixels. It has ratios ≥2 for aspect, **a**, in range *242–313* degrees, reaching a maximum ratio of **5.03** at value *285* degrees; for DEM, **d**, in range *205–234* m with maximum ratio **2.39** at value *217* m; and for slope, **s**, in range *0–76* degrees with maximum ratio **4.04** at value *20* degrees of slope. Clearly for **LA1**, ISPs **a**, **d** and **s** provide acceptable support to the proposition in (1).

4.2 Integrate

We generated images of ELR values for the six ISPs, for each linear form of landslide, DSP. We have six such images for each DSP. Each image tells us how much it is able to discriminate or classify the presence over the absence of landslide occurrences. We now need to integrate the six ELR images into an index providing an estimate of likelihood or probability or possibility of future occurrence.

To integrate (combine) the ELR values we need a mathematical framework with a model that enable balancing the discriminating power of the ratio values between ISPs given a DSP. The ELR values (0–∞) have to be transformed into fuzzy set, FZ, membership function values (0–1). Then, integration has to follow one of various combination rules or operators (Chung and Fabbri 2001). We have selected the gamma function operator with $\gamma = 0.5$, i.e. a combination of an algebraic product and an algebraic sum. The result of the integration produces values, the prediction rates, also ranging between 0 and 1 with appropriate numerical precision. We termed them "prediction images."

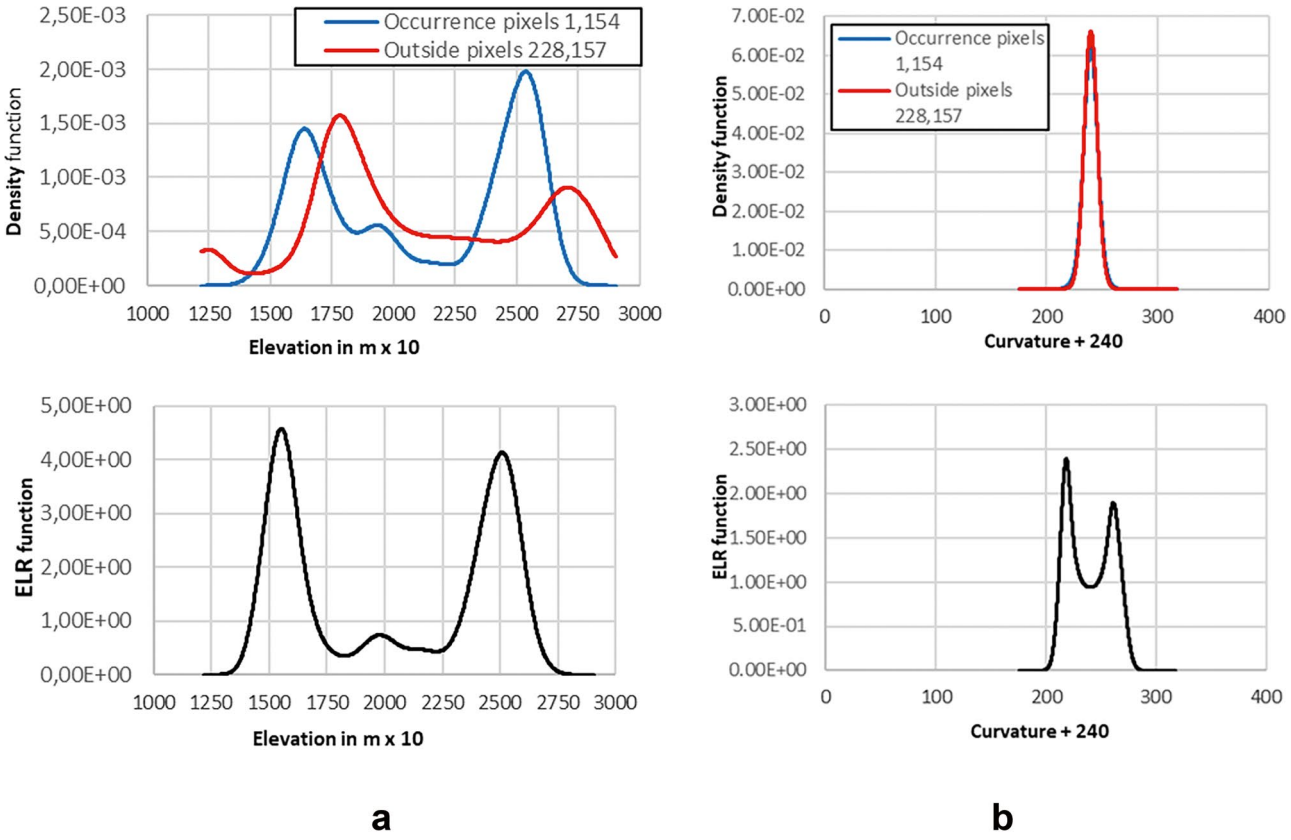


Fig. 4 Two examples of empirical likelihood ratios, ELR, to extract the spatial relationships for the 10 subaqueous landslide scarps, **LA2**, with elevation, **d**, in (**a**), and with curvature, **c**, in (**b**). The upper diagrams show the continuous ISP density functions while the lower diagrams the corresponding ELR functions. ELR values of 2 correspond to frequencies in correspondence of the landslide scarps twice those in their absence within the study area. See the ratios in Table 3 for **a** and **c** in in column 4 and the distribution of the forms as white lines in Fig. 6b. Here, at 5 m resolution, the study area covers 229,311 pixels of which 1154 with the presence of landslide scarps and 228,157 with their assumed absence in the remainder of the study area

4.3 Rank

As such, however, the prediction images are hard to visualize and interpret. It becomes convenient converting the prediction rates into equal-area ranks. We have selected 200 relative ranks, covering the actual of 0–1 range of values, each corresponding to the 0.5% of the study area. For this, we have sequenced in descending order all the pixels in the prediction image and then selected the 200 equal-area ranks. The ranking enables to visualize the integrated prediction images as *prediction patterns*, grouping the ranks into classes. For instance, higher ranks, of greater interest, can have narrow classes while lower ranks can have wider classes. Assigning the colors from a pseudo-color lookup table, we can easily display the *prediction patterns* (see Figs. 5, 6, 8 and 10) over an enhanced DEM.

To visualize the contribution of the ISPs to the generation of different *prediction patterns* we compare them maintaining the same legend of identical groups of equal-area ranks. All *prediction patterns* to follow use the same legend, thus facilitating recognition and comparison.

Fourteen colors of a pseudo-color lookup table identify the groups, as done in the legend of Fig. 5 for the FZ pattern of 21 Flow channels, **LA1**, displayed as white lines over the classes of ranks. Figure 5 shows the patterns that used only some or all of the ISPs: **ad** in (**a**), **as** in (**b**), **ds** in (**c**) and **ads_cfp** in (**d**). As can be seen, the use of just **as** already defines a pattern with strong similarity with that using all six, **ads_cfp**. It means that **cfp** are redundant or ineffective support of the proposition in (1). This we suspected from the ELR diagrams like the one in Fig. 4b. If we compare Fig. 5d, using **ads_cfp** with Fig. 6a, using only **ads**, the pattern difference is hardly detectable with the ranking color legend applied. To memorize the patterns we short named them using the abbreviation sequence, model name, DSP, number of landslides, and list of ISPs, e.g. **FZ_LA1_21_ad** in Fig. 5a.

The *prediction patterns* in Fig. 6 show the support of **ads** for linear forms **LA1** to **LA4**. A comparison of the *prediction patterns* of the four landslide forms in the illustration reveals the areas likely to have similar **ads** settings for each type of form. E-NE in (**a**), N-NW, and center in (**b**), deep center and

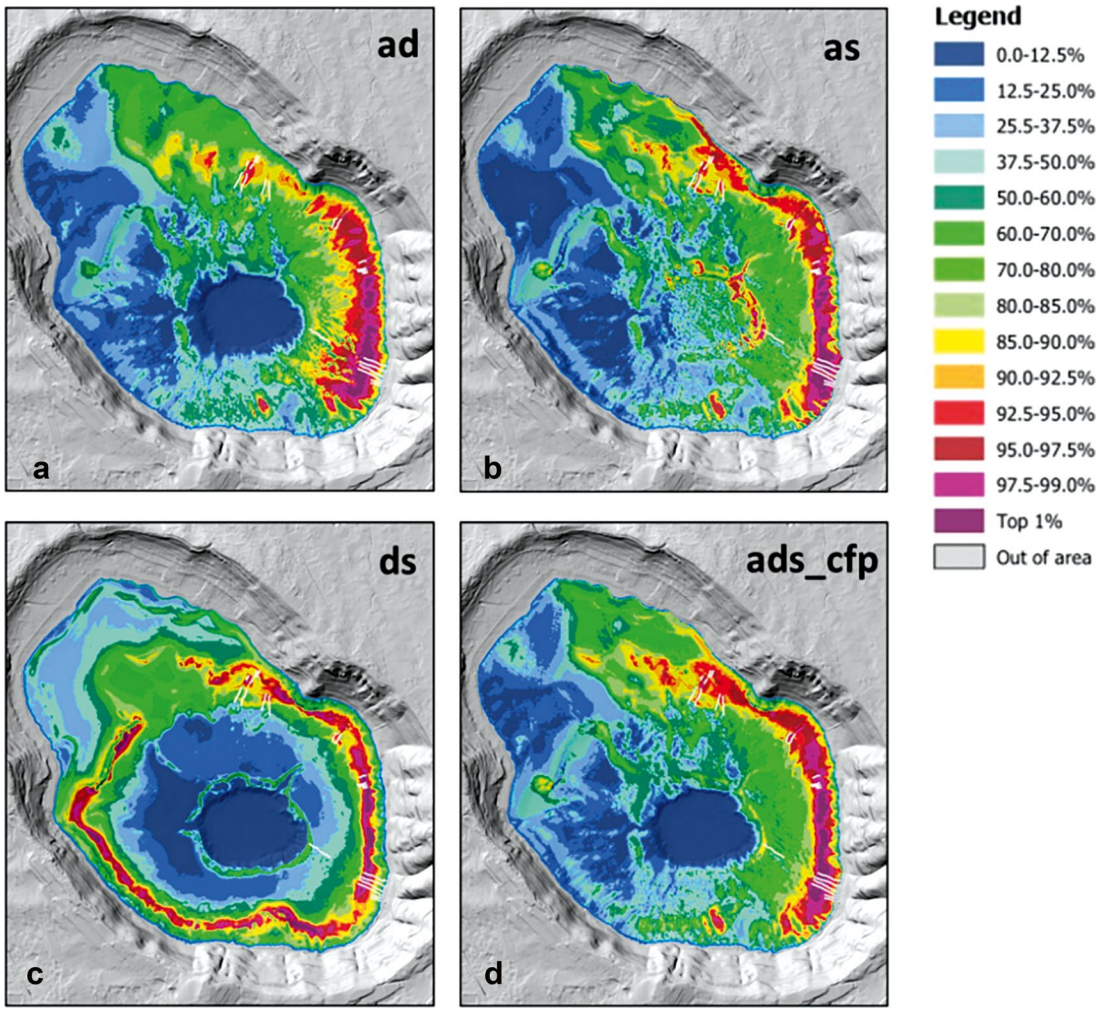


Fig. 5 **FZ** *prediction patterns* of 21 Flow channels as DSP, **LA1_21**, generated using different ISPs. In (**a**), (**b**), (**c**) and (**d**), we used **ad**, **as**, **ds** and **ads_cfp**, respectively. We have short named the patterns as follows: **FZ_LA1_21_ad**, **FZ_LA1_21_as**, **FZ_LA1_21_ds**, **FZ_LA1_21_ads_cfp** (listing model, DSP, number of landsides, ISPs). The Top 1% class in the legend contains the highest 1% ranks of the study area

Table 3 ELR values for Linear, **LA1–LA4**, Subaqueous Forms, DSP, using as ISPs the continuous fields derived from the 5 m resolution elevation, **a**, **d**, **s**, **c**, **f** and **p**. Abbreviations are as in Table 1. Ratios are bold if ELR ≥ 2.00. The corresponding ranges of classes is in *italics* with the maximum class and ratio in brackets (modified after Patera and Fabbri 2022)

Forms	No.	Pixels	Continuous ISP
LA1 flow channel	21	578	**a** ≥ 2, *242–313* (max **5.03** at *285*d); c ≥ 1, *−43 –-3* (max 1.14 at *−34*); **d** ≥ 2, *205–234* (max **2.39** at *217* m); f ≥ 1, *−26 –-2* (max 1.15 at *−20*); p ≥ 1, *2–34* (max 1.48 at 28); **s** ≥ 2, *0–76* (max **4.04** at *20*d)
LA2 landslide scarp	10	1154	**a** ≥ 2, *154–183* (max **2.10** at *162*d); **c** ≥ 2, *215–222* (max **2.40** at 218); **d** ≥ 2, *146–166* (max **4.58** at *155* m); *238–261* (max **4.14** at *251* m); f ≥ 1, *139–150* (max 1.99 at *142*), *156–168* (max 1.50 at *162*); **p** ≥ 2, *148–153* (max **2.43** at *151*); s ≥ 1, *6–26* (max 1.92 at *10*)
LA3 rockfall /topple scarp	5	444	**a** ≥ 2, *0–90* (max **2.23** at *0*d); **c** ≥ 2, *218–220* (max **2.03** at *219*); *254–274* (max **6.86** at *265*); **d** ≥ 2, *144–173* (max **10.08** at *155*); **f** ≥ 2, *135–144* (max **4.61** at *138*), *159–166* (max **3.46** at *163*); **p** ≥ 2, *113–128* (max **9.36** at *120*); **s** ≥ 2, *12–20* (max **2.95** at *16*d), *27–36* (max **3.04** at *32*d)
LA4 supposed tension crack	6	456	**a** ≥ 2, *109–116* (max **2.03** at *112*d); *139–197* (max **3.51** at *166*d); **c** ≥ 2, *260–270* (max **2.16** at *266*); **d** ≥ 2, *230–268* (max **7.31** at *245* m); **f** ≥ 2, *164–165*; (max **2.03** at *165*); **p** ≥ 2, *118–125* (max **2.75** at *121*); **s** ≥ 2, *26–39* (max **6.68** at *33*d)

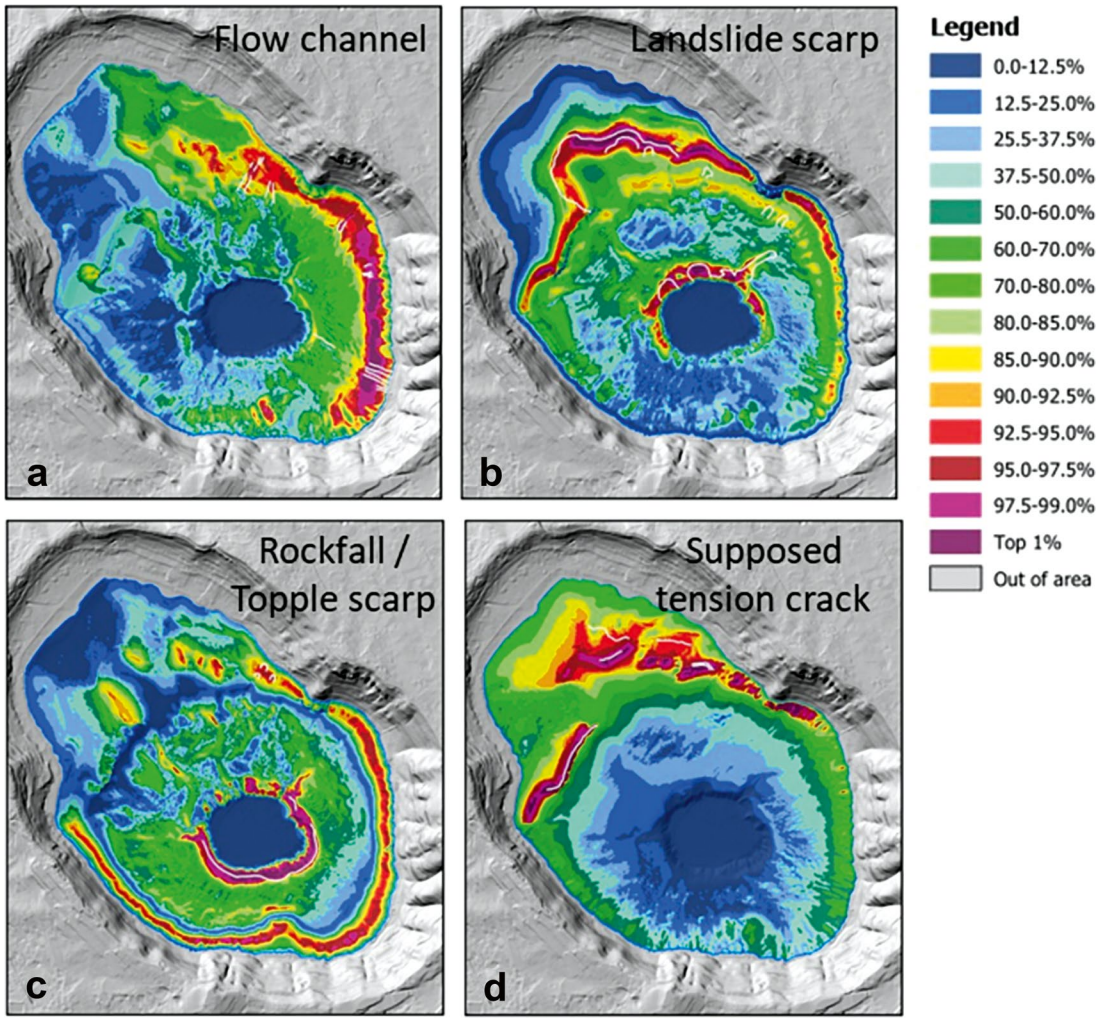


Fig. 6 **FZ** *prediction patterns* of different subaqueous linear landslide forms obtained using only **ads** as ISPs. In (**a**), the Flow channels, **LA1_21**; in (**b**) the Landslide scarps, **LA2_10**: in (**c**) the Rock fall/ Topple scarps, **LA3_5**; and (**d**), the Supposed tension cracks, **LA4_8**. We have termed the patterns as follows: **FZ_LA1_21_ads**, **FZ_LA2_10_ads**, **FZ_LA3_5_ads** and **FZ_LA4_8_ads**. The Top 1% class in the legend contains the highest 1% ranks of the study area

all around shallow margins in (**c**), and N-NW in (**d**). There are similarities of high-rank distribution between the patterns in (**b**) and (**c**), and with (**b**) and (**d**). For this reason, given the constrained settings of the forms within the lake basin, we found it useful to regroup the forms into more cohesive neighborhoods.

Figure 7 shows the redistribution into three groups, **GR1**, **GR2** and **GR3**. The corresponding *prediction patterns* are in Fig. 8. The patterns of the three groups of forms show how the higher ranks, from red to purple, extend beyond the distribution of the forms in white, used for modelling the pattern, with **ads** as ISPs: **GR1** to the N and **GR3** to the E-NE. Of particular concern is the pattern of **GR2** in (**b**) that shows extensions of high ranks from the lower edge of the central escarpment to higher elevations towards other forms. In (**d**) we have added the border of the landslide accumulations, **PA3**, and submerged prosecutions of subaerial accumulations, **PA4**, to show how the higher ranks curl up near the edges of the accumulations where slopes increase. The relationships between polygonal forms and the lower linear forms are evident. We can assume that the edges of the accumulations will eventually provide sediments that will reach the higher ranks of linear prediction patterns at lower elevations. The same can be seen for most polygonal subaqueous forms.

4.4 Validate

To consider the relative strength or classification quality of the ranks we used the procedures of cross-validation and of uncertainty quantification of the *prediction patterns*. We did that under the assumptions of the model, of the quality of the database, and of the computational strategy followed.

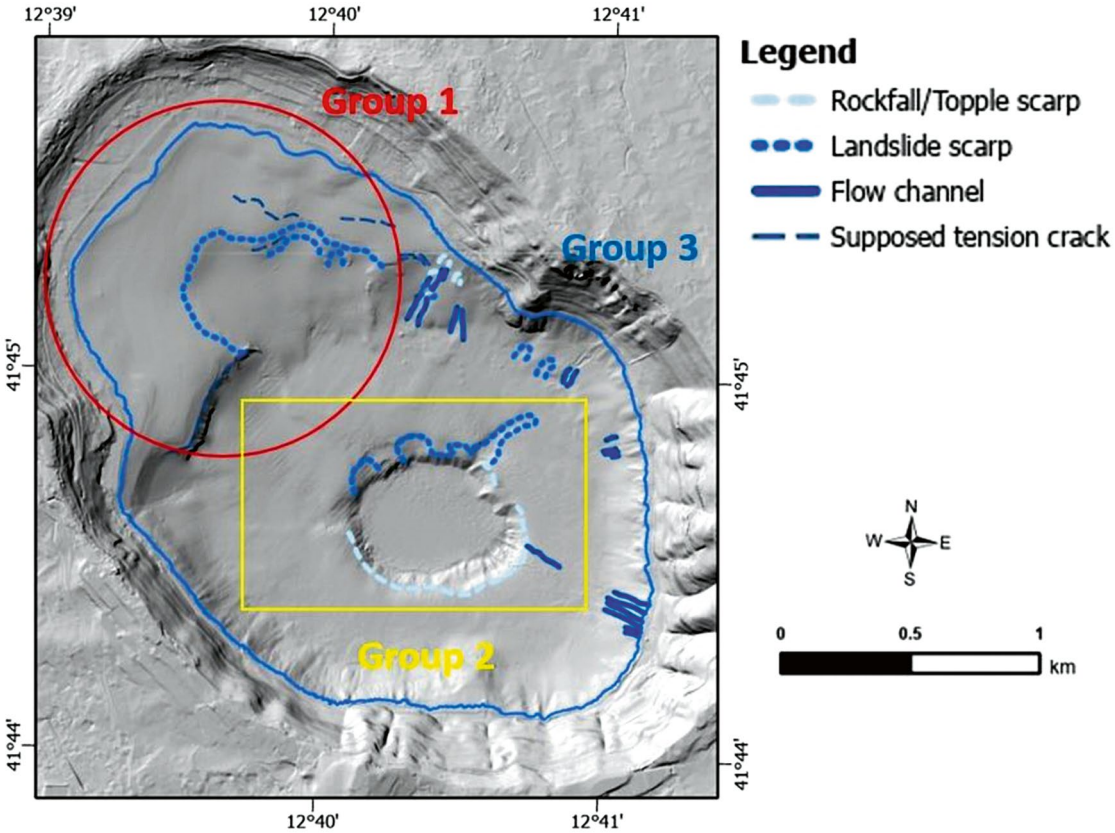


Fig. 7 Distribution of subaqueous forms into three neighborhoods or groups: NW, E, and Central renamed **GR1**, **GR2,** and **GR3**, respectively

We can split the DSP into two or more sets. One set, say the older one, is used as DSP to generate a *prediction pattern,* and the other, the younger one, to verify how well its landslides are distributed in areas with relatively higher ranks. Should we be unable to make a time separation of the landslides that would lead to a pattern validating the younger, "future" occurrences, we can resort to iterative ways of splitting the DSP. Examples are, sequential exclusion of one or more occurrences of the DSP, sequential selection, and random selection, or in some cases, use some arbitrary selections.

The result of iterative cross-validation is a sequence of prediction rates for the landslides not used in the modelling. Ordering the prediction rates, we can generate prediction-rate curves as done in Fig. 9.

The curve represents how well a *prediction pattern* classifies the future landslides in high ranks. On the horizontal axis, we have, from highest to lowest rank, the cumulative proportion of study area classified as susceptible, and on the vertical axis the corresponding cumulative proportion of validation (future) landslides in the class.

The prediction in such cases will be for the "next" one or more landslide occurrences. The steeper the prediction-rate curve the higher the number of highly classified occurrences in the corresponding classes.

For instance, in Fig. 9a, the orange curve for flow channel, **LA1**, indicates that the top 4% ranks contain (predict) about 40% of the landslides, the top 10% contain 75% and the top 20% ranks contain 94%. As to the yellow curve for the 5 rock falls, the corresponding percentages are approximately the top 0.7%, 1.1%, and 2.3%.

Figures 9a and b show the prediction-rate curves from iterative cross-validation processes for the four linear subaqueous forms, **LA1** to **LA4**, and for the three groups, **GR1** to **GR3**, using 5 m resolution data. Figures 9c and d show the corresponding curves for the 1 m resolution data.

We can see how going from the four individual forms to the three groups, the curves acquire greater steepness and that the corresponding curves at 1 m resolution appear even steeper. The gray curve in Fig. 9d, almost vertical, tells us that the top 3.4% ranks classify all the eight landslides in **GR2**.

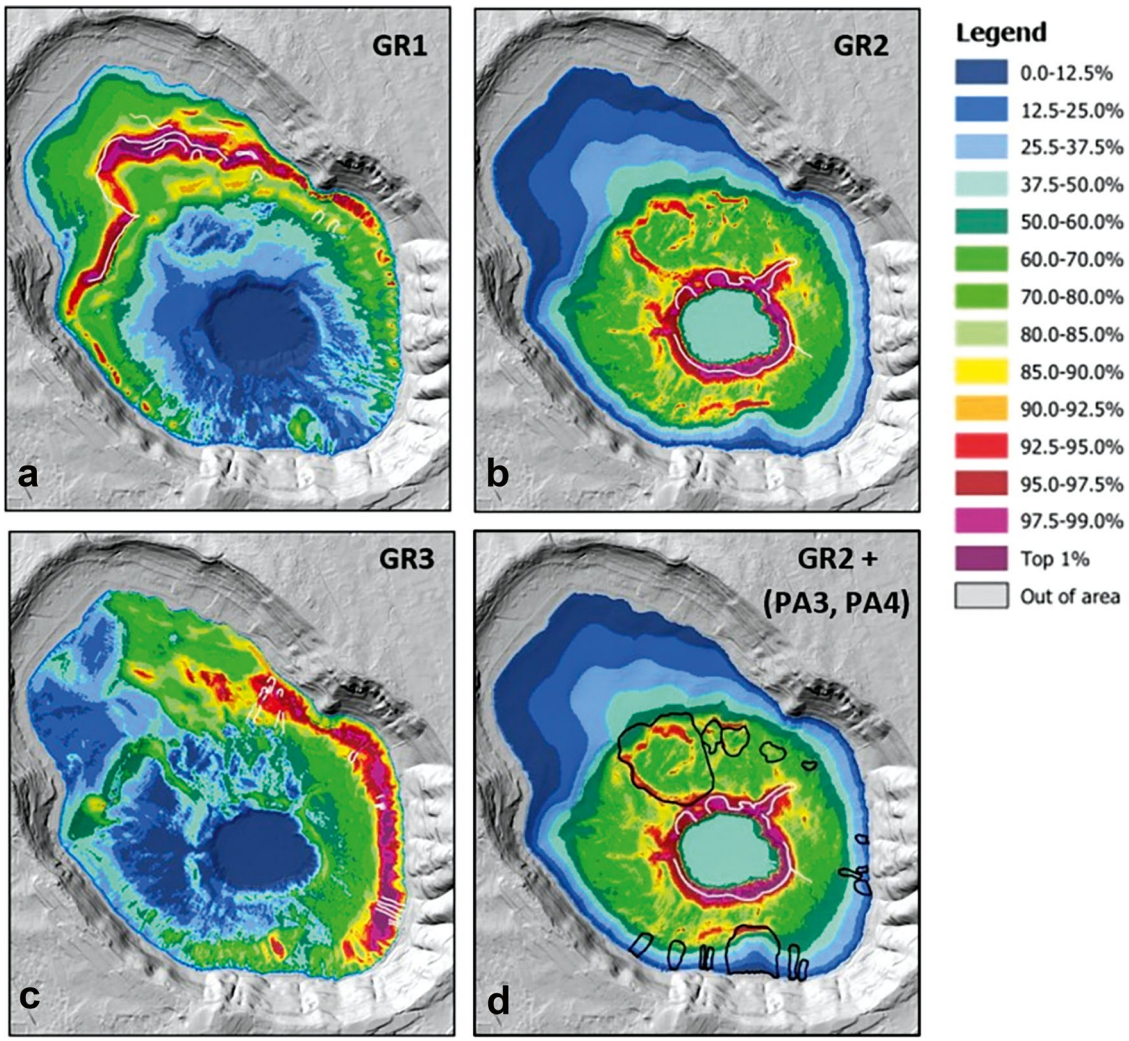


Fig. 8 **FZ** *prediction patterns* using **ads** as ISPs and **GR1** in (**a**), **GR2** in (**b**), and **GR3** in (**c**) as DSP, plotted as white lines. The boundaries of subaqueous landslide accumulations, (**PA3**), and submerged prosecutions of subaerial accumulations, (**PA4**) are added as black contours in (**d**). We have termed the patterns **FZ_GR1_12_ads**, **FZ_GR2_7_ads** and **FZ_GR3_23_ads**. The Top 1% class in the legend contains the highest 1% ranks of the study area

4.5 Quantify Uncertainty

To establish confidence in the *prediction patterns* it becomes important to generate some measure of certainty of classification. The results of cross-validation are not only the prediction rates of the landslides used for cross-validation and the respective prediction-rate curves to assess the quality of the *prediction pattern* as a predictor of "future" or "next" landslide occurrences. Iterative cross-validation can also generate sequences of slightly different *prediction patterns*. Having a sequence of ranked *prediction patterns*, we can use rank-based statistics such as the median rank for each pixel to generate a *Target Pattern*, and the rank of the range around the median as a measure of the *Uncertainty Pattern*. The *Target Pattern* then becomes the "ideal pattern we are looking for" because it offers measures of uncertainty of the *prediction pattern*.

We can display those patterns and their combination, after selecting a threshold of uncertainty to visualize the less uncertain part of the *Target Pattern*. Figure 10 shows those patterns for the group **GR2** of forms from the 1 m-resolution database. We have generated a new 1 m-resolution set of elevation values, computed the six continuous functions, and on it digitized all the detectable shapes of the four types of linear subaqueous forms, **LA1** to **LA4**, and of the three groups **GR1** to **GR3**. We have then repeated all the 5-step analyses. In Fig. 10, we have the *Target Pattern*, the *Uncertainty Pattern,* and the 50% *Combination Pattern* for

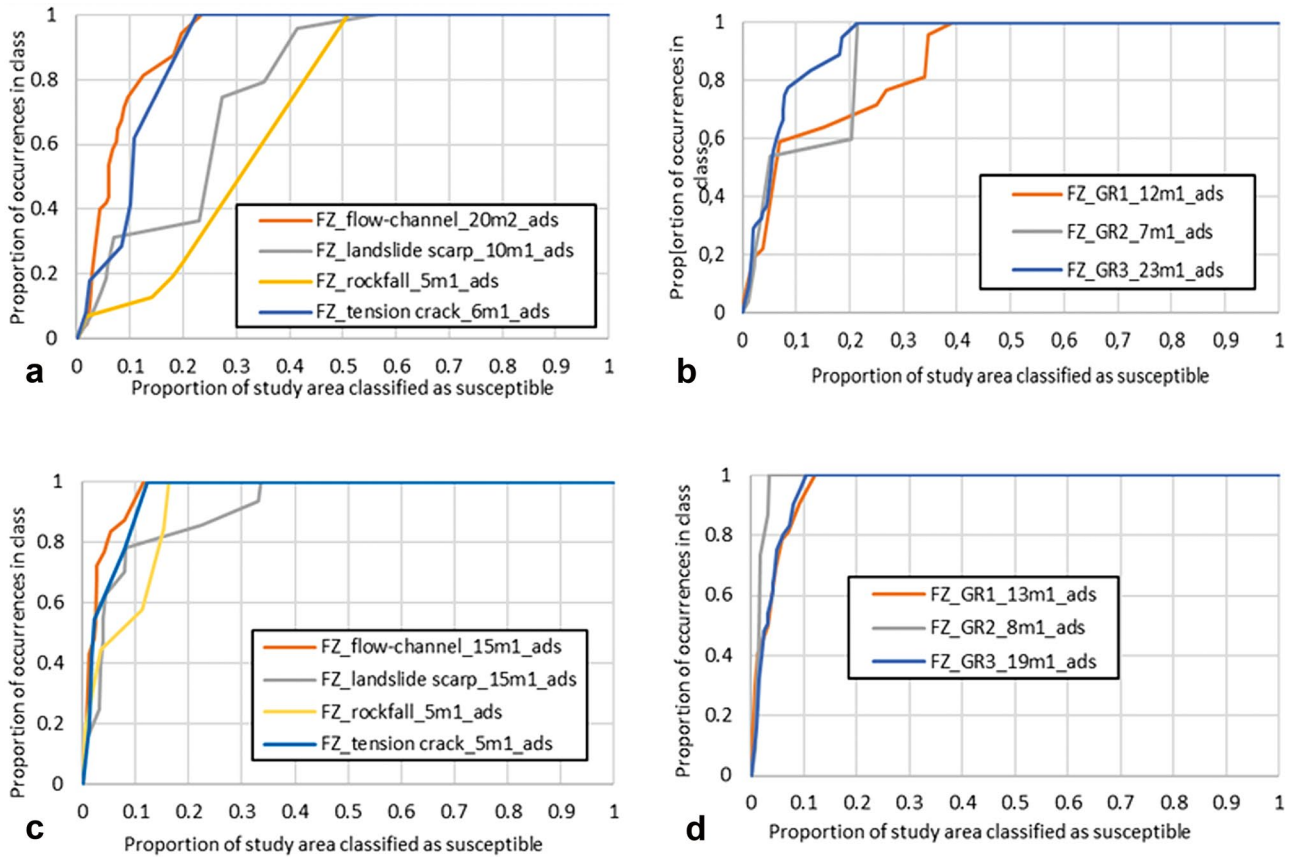


Fig. 9 **FZ** prediction-rate curves for linear subaqueous forms, groups, and resolutions obtained by iterative cross-validation using sequential elimination. In (**a**) for the four linear subaqueous forms, **LA1** to **LA4**; and in (**b**) for the groups **GR1** to **GR3** from the 5 m-resolution database. In (**c**) and (**d**), respectively, the corresponding curves from the 1 m-resolution database of Lake Albano. In the curve names the letter **m** stays for minus

GR2. The latter pattern shows the ranks of the *Target Pattern* only corresponding to the lower 50% of the uncertainty ranks of the *Uncertainty Pattern.*

Figure 10 tells us that the higher ranks of our *prediction pattern* for **GR2** have relatively low uncertainty of classification and the gray prediction-rate curve in Fig. 9d shows very high quality of classification with the eight linear subaqueous forms in **GR2** all classified, i.e. located over, the top 3.4% ranks of the study area. The results provide confidence in the circular *prediction pattern* showing critical hazards towards the bottom of the lake. The *50% Combination Patterns* in (**c**) and (**d**) were obtained using **ads** and **ads_cfp**, respectively, to visualize the minimal differences between them.

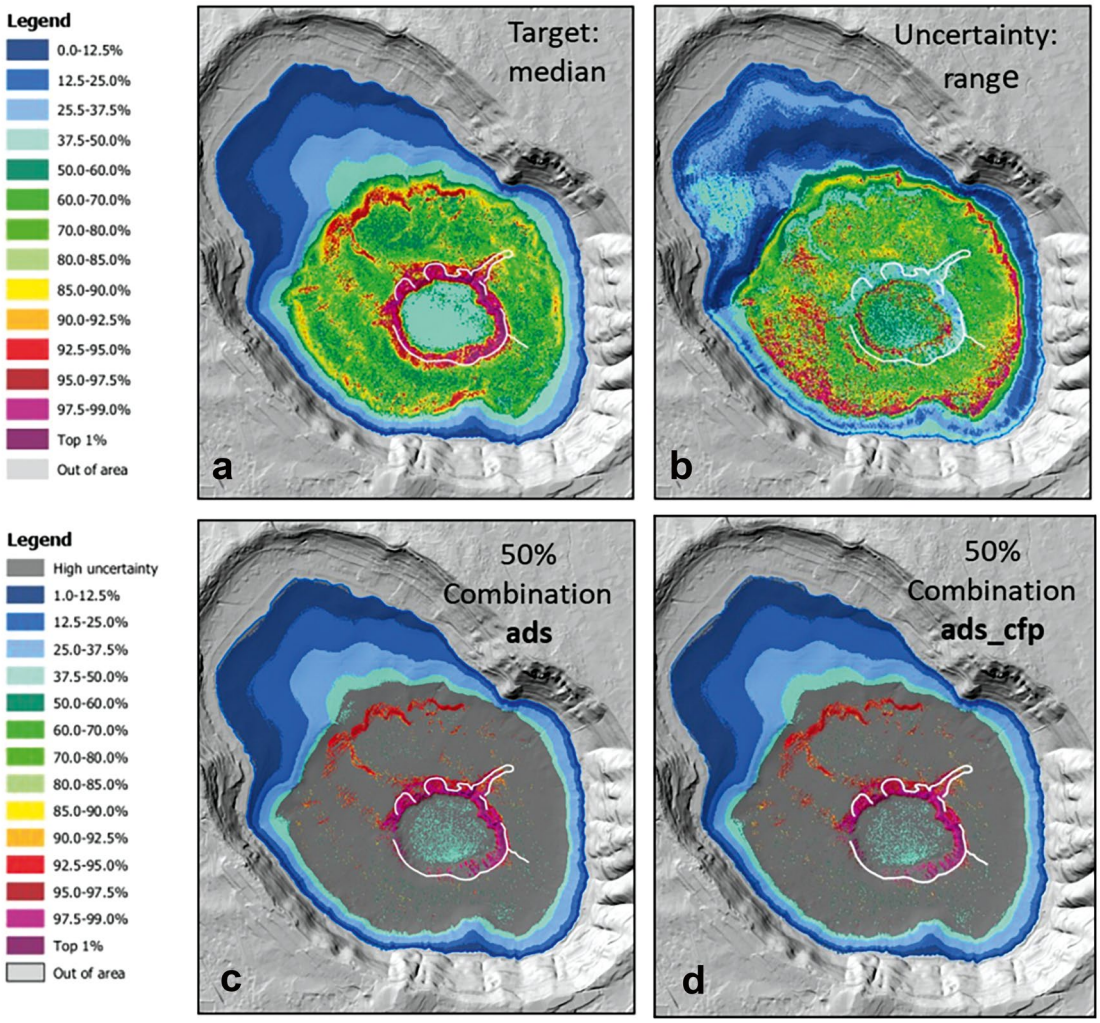


Fig. 10 FZ **Target** in (**a**), **Uncertainty**, in (**b**), and 50% **Combination** patterns in (**c**) and (**d**), for the eight landslides in **GR2** from the 1 m-resolution database. We have termed the patterns as follows: **T_FZ_GR2_8m1_ads**, **U_FZ_GR2_8m1_ads**, **C50_FZ_GR2_8m1_ads**, and **C50_FZ_GR2_8m1_ads_cfp,** respectively. The Top 1% class in the legend contains the highest 1% ranks of the study area. The letter **m** stays for minus

5 Concluding Remarks

This study delved into the prediction of future landslides within the Lake Albano maar, focusing on subaqueous landslide susceptibility. Our analyses centered on identifying areas prone to these events based on historical patterns and spatial data, aiming to enhance proactive risk management strategies for the region.

Through meticulous examination of historical subaqueous landslides and the utilization of a high-resolution digital elevation model, we have modeled *prediction patterns* to assess future landslide likelihoods within the lake. By integrating various spatial relationships and continuous field data, we have generated patterns indicative of potential landslide occurrences.

In the first step of the experiment, we obtained patterns for a single type of form, flow channel, to have informative combinations of ISPs and to visualize their individual support of the proposition. Then we computed the patterns of the four types of linear forms as DSPs using the three ISPs: aspect, digital elevation model, and slope. Later on, by rearranging the four types of forms into three groups, we improved the predictive quality of their patterns.

Subsequently, we focused on the second group of linear forms, combining landslide scarps and topple scarps around the lower escarpment of the lake, and observed their *prediction pattern* in the context of the distribution of the polygonal accumulation forms. A spatial relationship became evident between the edges of the accumulations and the higher ranks of the pattern. Furthermore, the use of 1 m-resolution data provided even better prediction rates and patterns with rela-

tively low uncertainty. In essence, the patterns represent reliable possibilities of future landslide occurrences, and rearrangement into groups at 1 m resolution provides relatively good predictions with low uncertainty. The group of scarps, at the lower center of the lake, shows high landslide susceptibility. Accumulations and flow channels at higher elevations can trigger deeper mass movements.

One significant advantage of our analysis lies in the ability to pinpoint critically susceptible areas within the lake, particularly around the lower escarpment, aiding in targeted risk mitigation efforts. Moreover, our results complement the findings of previous authors and indicate a high susceptibility to mass movements generating outflow, particularly so should hazardous processes cumulate or synchronize towards the bottom of Lake Albano.

However, limitations exist, notably in the availability of comprehensive datasets, the limited number of continuous fields used, all computed from the high-resolution elevation survey, the lack of data on the types and age of the sediments in the lake, and the age of the landslides, which could enhance the accuracy of our predictions. Additionally, the absence of continuous monitoring stations and sensors within the lake, apart from a defunct network of temperature sensors located at the bottom of the lake and the shoreline, presents challenges in real-time hazard assessment. Nevertheless, the prediction patterns obtained, even with relatively poor data, point to convincing and interpretable areas of high susceptibility in Lake Albano.

Therefore, while existing literature provides valuable insights into past landslide occurrences and geological features, there remains a gap regarding ongoing monitoring efforts. Future research could focus on addressing these gaps to refine prediction models further. The findings underscore the multi-hazard nature of the region, posing risks to urbanization, recreational activities, and cultural heritage sites. Despite reclassification from extinct to quiescent, the potential for future subaqueous landslides necessitates ongoing vigilance and proactive risk management measures in the Lake Albano vicinity. This conclusion aims to address the questions posed and provide a clearer summary of the study's contributions, limitations, and implications for future research and risk management efforts.

References

Anzidei M, Esposito A, De Giosa F (2006) The dark side of the Albano crater lake. Ann Geophys 49:1275–1287

Barberi F, Chelini F, Marinelli G, Martini M (1989) The gas cloud of Lake Nyos (Cameroon, 1986): results of the Italian technical mission. J Volcanol Geotherm Res 39:125–134

Bozzano F, Mazzanti P, Anzidei M, Esposito C, Floris M, Bianchi Fasani G, Esposito A (2009) Slope dynamics of Lake Albano (Rome, Italy): insights from high-resolution bathymetry. Earth Surf Process Landf 34:1469–1486

Carapezza ML, Tarchini L (2007) Magmatic degassing of the Alban Hills volcano (Rome, Italy): geochemical evidence from accidental gas emission from shallow pressurized aquifers. J Volcanol Geotherm Res 165:5–16

Chiodini G, Tassi F, Caliro S, Chiarabba C, Vaselli O, Rouwet D (2012) Time-dependent CO_2 variations in Lake Albano associated with seismic activity. Bull Volcanol 74:861–871. https://doi.org/10.1007/s00445-011-0573-x

Chung CJ, Fabbri AG (1993) Representation of geoscience data for information integration. Nat Resour Res 2:122–139

Chung CJ, Fabbri AG (2001) Prediction models for landslide hazard using fuzzy set approach. In: Marchetti M, Rivas V (eds) Geomorphology and environmental impact assessment. Balkema, Rotterdam, pp 31–47

Chung CJ, Fabbri AG (2003) Validation of spatial prediction models for landslide hazard mapping. Nat Hazards 30:451–472

Fabbri AG, Chung CJ (2018) How credible is my hazard map? Dissecting a prediction pattern of landslide susceptibility. WIT Trans Eng Sci 121:3–19. https://doi.org/10.2495/RISK180011

Fabbri AG, Patera A (2021) Spatial uncertainty of target patterns generated by different prediction models of landslide susceptibility. Appl Sci 11(3341):1–20

Funiciello R, Giordano G, De Rita D, Carapezza ML, Barberi F (2002) L'attività recente del cratere del Lago Albano di Castelgandolfo. Rendiconti dell'Accademia dei Lincei (Scienze Fisiche e Naturali) ser 9 13:113–143

Funiciello R, Giordano G, De Rita D (2003) The Albano maar lake (Colli Albani volcano, Italy): recent volcanic activity and evidence of pre-Roman age catastrophic lahar events. J Volcanol Geotherm Res 123:43–61. https://doi.org/10.1016/S0377-0273(03)00027-1

Galeazzi C, Germani C, Casciotti L (2015) The drainage tunnel of Lake Albano (Rome, Italy) and the 3-year study program "project Albanus": a progress report. Hypogea 2015, Proceedings of the international congress of speleology of artificial cavities, Rome, March 11–17, pp. 178–191

Marra F, Gaeta M, Giaccio B, Jicha BR, Palladino DM, Polcari M, Sottili G, Taddeucci J, Florindo F, Stramondo S (2016) Assessing the volcanic hazard for Rome: $^{40}Ar/^{39}Ar$ and in-SAR constraints on the most recent eruptive activity and present-day uplift at Colli Albani Volcanic District. Geophys Res Lett 43:6898–6906. https://doi.org/10.1002/2016GL069518

Patera A, Fabbri AG (2022) Can we assess landslide hazards in the volcanic crater of Lake Albano? In: Hernández S, Garzia F, Lombardi M, Fabbri A (eds) Risk analysis, Hazard mitigation and safety and security engineering, vol XIII, 214. WIT Transactions on THE BUILT Environment, WIT Press, pp 3–25. https://doi.org/10.2495/SSR220011

Patera A, Fabbri AG (2023) Analisi della pericolosità di frana dei versanti interni del Lago Albano. Rapporti Tecnici INGV 461:1–58. https://doi.org/10.13127/rpt/461

Open Access This chapter is licensed under the terms of the Creative Commons Attribution 4.0 International License (http://creativecommons.org/licenses/by/4.0/), which permits use, sharing, adaptation, distribution and reproduction in any medium or format, as long as you give appropriate credit to the original author(s) and the source, provide a link to the Creative Commons license and indicate if changes were made.

The images or other third party material in this chapter are included in the chapter's Creative Commons license, unless indicated otherwise in a credit line to the material. If material is not included in the chapter's Creative Commons license and your intended use is not permitted by statutory regulation or exceeds the permitted use, you will need to obtain permission directly from the copyright holder.



An Approach to Rockfall Hazard Scenarios Based on Earthquake Ground Motion

Antonella Peresan, Massimiliano Alvioli, Elisa Zuccolo, Franco Vaccari, and Hazem Badreldin

Abstract

After an earthquake event, major ground effects include landslides. In Italy, the most common type of earthquake-induced landslides are rockfalls. The assessment of the extent and magnitude of an earthquake-induced landslide event may be of importance for both preparedness and response operations. An earlier work devised a modeling chain including an empirical ground shaking scenario and a three-dimensional model for rockfalls, which can be calibrated and possibly applied in real time after an earthquake event. In this study, we explore the combined use of two physics-based methods for both earthquake and rockfall modeling and their possible contribution towards a better understanding of the triggering mechanisms and characterization of seismically induced rockfalls. Specifically, by modeling a set of ground shaking scenarios, which account for increasingly complex details (including multiple seismic events, as well as point and extended sources) and the related rockfall scenarios, we aim to capture the main spatial patterns of observed rockfalls. Application of the proposed modeling chain suggests an advantage of using multiple sources over a single source, and point sources with respect to approximate extended representations when constrained by limited available data. This follows from the comparison of rockfall trajectory simulations for the Friuli 1976 event in Northern Italy with observed rockfalls induced by the seismic sequence. The obtained results evidence the opportunity of including topographic effects in the ground shaking simulations and highlights the possibility of further investigating the cumulative effect of complex seismic sequences and their influence on modulating landslide susceptibility.

Keywords

Earthquake scenario modeling · Coseismic rockfalls · Seismic ground shaking · Physics-based models · Multi-hazard

1 Introduction

The response of slopes under the action of ground shaking caused by a strong earthquake, can result in ground deformations and failures. Major ground effects include landslides; in Italy, the most common type of earthquake-induced landslides are rockfalls. Numerous studies have demonstrated a strong connection between the spatial distribution pattern of coseismic landslides/rockfalls and ground motion intensities (e.g., Keefer 2000; Luzi and Pergalani 2000; Jibson 2011; Tiwari et al. 2017; Alvioli et al. 2024). Specifically speaking, for the 1997 Mw5.5 Umbria-Marche earthquake in Italy, the landslide density map was quite well correlated with Arias Intensity by Luzi and Pergalani (2000). These studies collectively emphasize the significant contributions of controlling factors in the occurrence and distribution of coseismic landslides. In a previous work (Alvioli et al. 2024), they sug-

A. Peresan (✉) · E. Zuccolo
Seismological Research Center, National Institute of Oceanography and Applied Geophysics - OGS, Udine, Italy
e-mail: aperesan@ogs.it; ezuccolo@ogs.it

M. Alvioli
Istituto di Ricerca per la Protezione Idrogeologica, Consiglio Nazionale delle Ricerche, Perugia, Italy
e-mail: massimiliano.alvioli@irpi.cnr.it

F. Vaccari
Department of Mathematics, Informatics and Geosciences, Trieste, Italy
e-mail: vaccari@units.it

H. Badreldin
Seismological Research Center, National Institute of Oceanography and Applied Geophysics - OGS, Udine, Italy

National Research Institute of Astronomy and Geophysics, Cairo, Egypt
e-mail: hbadreldin@ogs.it

© The Author(s) 2025

B. Abolmasov et al. (eds.), *Progress in Landslide Research and Technology, Volume 3 Issue 2, 2024*, Progress in Landslide Research and Technology, https://doi.org/10.1007/978-3-031-72736-8_8

gested a method for rapid post-earthquake rockfall scenario assessment, adopting ground-shaking estimates from empirical models (i.e. Ground Motion Models, GMMs) and the three-dimensional model STONE for rockfall trajectories. In the proposed method, ground-shaking maps corresponding to the May sixth 1976 Friuli earthquake (FVG, Friuli Venezia Giulia region, North-Eastern Italy) were used to suppress the probability of activation of rockfall sources at locations with low ground shaking, while enhancing that in areas close to the epicenter. Results of the modeling chain compared with an accurate inventory of earthquake-induced rockfalls (Govi 1977), suggested that the framework may be suitable for rapid rockfall impact assessment using ground-shaking estimates, in the immediate aftermath of a seismic event (Tanyaş et al. 2019). Here, we explore the possibility of replacing the adopted GMM with the physical modeling of seismic waves propagation, seeking an improvement of the agreement between the full modeling chain results and the rockfalls observed after the FVG 1976 earthquake sequence (see also Valagussa et al. 2014).

The study area (Fig. 1) is prone to a high seismic hazard, as confirmed by historical seismicity (Rovida et al. 2022) and studies based on morphostructural analysis (Gorshkov et al. 2009). The region is on the Alps-Dinarides junction, with compressional seismotectonic regime, with E-W trending thrust systems, mostly south dipping, with a subordinate strike-slip component to the east. Seismicity, spatial, and kinematic characteristics of main seismogenic sources of the area are summarized in Slejko et al. (1999), Bressan et al. (2018), and Aoudia et al. (2000). Complex seismic sequences are possible in this region (Peresan and Gentili 2018), the most damaging and recent one being the sequence associated with the 1976 FVG earthquake. Accordingly, this study aims at assessing the possible combined use of physics-based methods for both earthquake and rockfall modeling, towards an improved characterization of seismically induced rockfalls.

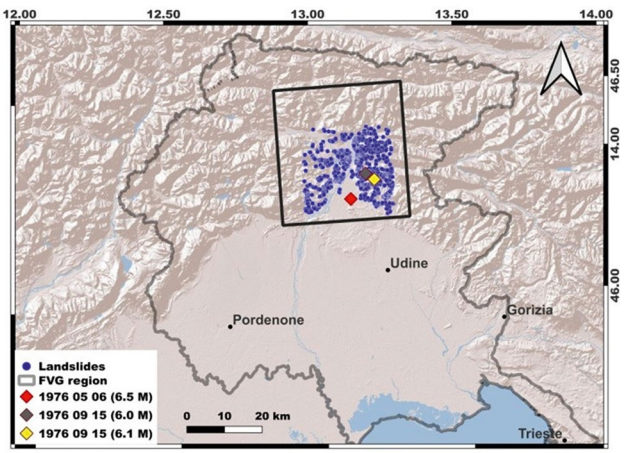


Fig. 1 Location of the study area within the FVG region (delimited in brown), illustrating the ground motion simulation domain (black rectangle). The map includes the earthquake epicentres of the Mw = 6.5 sixth May 1976 main shock (red diamond), and its strongest aftershocks (grey and yellow diamonds for the first and second aftershock, respectively). The rockfalls location points (blue circles) are from Govi inventory (1977)

Specifically, by modeling a suite of ground shaking scenarios, which capture increasingly complex features of earthquakes occurrence (including multiple seismic events, point and extended source representations), we attempt to investigate the cumulative effect of a complex seismic sequence and its possible influence on modulating landslide susceptibility.

In the previous study (Alvioli et al. 2024) they used Peak Ground Acceleration (PGA) to represent ground shaking associated to the May sixth, 1976 mainshock. We obtained a PGA map with the ShakeMap software (Worden et al. 2020), using few ground motion observations available and the ground motion model (GMM) of Akkar and Bommer (2007). Despite being a fast tool for studying the dependence between rockfall occurrences and seismic shaking, shakemaps can be unreliable if based on limited data. In scenarios like the Friuli 1976 seismic sequence, the selected GMM plays a crucial role, highlighting their inherent limitations. In fact, the ergodic assumption required by GMMs is not always fulfilled in seismic scenarios. Moreover, GMMs may contain significant uncertainties and biases due to the limited data used to constrain them. Consequently, GMMs may not capture significant features of earthquake waveforms, such as topographic amplification, shaking duration, and rupture directivity. These characteristics are crucial in understanding phenomena like landslide occurrence (Fan et al. 2019; Dahal et al. 2023).

A better way for accurately estimating ground shaking intensity parameters involves the computation of broadband synthetic seismograms. This approach utilizes physics-based simulations that convolve the contributions of seismic source, and path to the site(s) of interest. Various methods exist to obtain synthetic seismograms (e.g., Panza et al. 2001, 2012; Igel 2016), each offering different levels of accuracy depending on the availability of parameters describing the seismic source (i.e. fault geometry and slip distribution) and subsurface mechanical properties along the propagation path. The calculation of synthetic seismograms requires geological/geophysical and seismological data from the region of interest, ensuring a comprehensive representation of seismic activity specific to that area. However, modeling a specific past event often involves considerable uncertainties, particularly when limited data is available to provide a basis for comparison with full waveform modeling. In the case of the FVG 1976 seismic sequence, significant uncertainty exists not only regarding the source process, but also concerning the epicenter's location (e.g, Aoudia et al. 2000, Rovida et al. 2022).

The main objective of this work is to answer the question: how well do the modeled ground shaking scenarios capture the spatial distribution of observed coseismic rockfalls, and which scenario(s) best fits such distribution? We conducted tests to explore the connection between ground motion acceleration and rockfall distribution patterns. We assessed if PGA maps from physics-based simulations using point and extended source models for the main shock alone can explain landslide distribution. Understanding this connection is crucial for gaining insights in pre-disaster prevention and implementing efficient mitigation strategies.

2 Methods

2.1 Physics-Based Ground Motion Simulations

Simulations of the FVG 1976 seismic sequence, including wave propagation from the source to the area of interest, allowed us to obtain synthetic seismograms in the $0 \leq f \leq 10$ Hz frequency band. Convolution of the source term with the Green function, according to the representation theorem, is a common way to do that. We modeled earthquake scenarios considering both point and extended source models approximation. In the calculation of Green's functions we represented the structural model by a semi-infinite space in plane and parallel inelastic layers, corresponding to laterally homogeneous media, using the discrete wavenumber technique-DWN (Pavlov 2009), which allows the computation of synthetic accelerograms also in the near field.

In the point-source case, we produced the synthetic accelerograms for double-couple point sources, which are scaled for their dimensions using the spectral scaling laws proposed by Gusev (1983), as reported in Aki (1987). This was accomplished by leveraging some modules of the Neo-Deterministic Seismic Hazard Assessment (hereafter referred to as NDSHA, Panza et al., 2001, 2012) package, which relies on defining earthquake ground motion through the calculation of synthetic seismograms for a range of earthquake scenarios. In the extended-source case, the fault surface is represented by a rectangle modeled as a grid of point sub-sources, whose seismic moment is calculated by considering each of them as a component of a realization of a non-stationary random process.

Assuming a realistic kinematic description of the rupture process, the extended seismic source model allows for generating a spectrum (in amplitude and phase) of the temporal function of the source that takes into account both the rupture process and the effects of directivity. We used the algorithm PULSYN06 (Gusev 2011) for the simulation of the space and time evolution of the rupture. For each scenario, different possible realizations of the rupture process can be considered to take into account the stochastic nature of the fault rupture. Each realization is characterized by a different slip distribution on the fault plane, nucleation point, and time evolution. However, in this study, only one realization for each considered seismic source was selected, thus neglecting the uncertainties associated with the rupture process.

From the set of complete synthetic seismograms, various maps of ground shaking describing the maximum ground shaking parameters at the bedrock can be extracted. From the several parameters representative of earthquake ground motion we have focused on the horizontal PGA (i.e., the vector sum of the two horizontal components) computed considering bedrock conditions.

2.2 Three-Dimensional Rockfall Modeling

We adopted the three-dimensional program STONE to simulate block trajectories initiated from user-defined grid cells (Guzzetti et al. 2002). In this work, and following previous work, we adopted a set of "static" rockfall sources singled out on a 10 m × 10 m digital topography with statistical considerations, specific of the area, based on a set of expert-mapped rockfall sources (Alvioli et al. 2021) within a large sample of slope units (Alvioli et al. 2020). Combination with seismic shaking allows selecting a subset of "static" rockfall sources, thus obtaining "dynamic" sources, specific of a particular earthquake. Running STONE with "dynamic" sources provides a probabilistic estimate of potential rockfalls triggered by the earthquake. Results by Alvioli et al. (2024) show that the data available for the FVG 1976 earthquake allows tuning of the parameters involved by the models in the framework outlined above. The same method, with few variations, was applied before either at smaller scale (Alvioli et al. 2022), and at national scale, using maps of maximum expected PGA with different return times (Alvioli et al. 2023).

2.3 Input Data and Results

To analyze the results of the modeling chain for seismically induced rockfalls adopted here, first applied in the same area by Alvioli et al. (2024), we show the main input data and outcome of different steps, leading to the final rockfall simulation maps. First, we show results for the PGA maps, obtained using different modeling approximations to describe the FVG 1976 seismic sequence sources, relating them to the real coseismic rockfall distribution triggered by the seismic sequence. Next, we analyze the different ground motion scenarios considering the landslides/rockfalls observed after the sequence. Finally, we show results of probabilistic simulations of rockfall trajectories by STONE

Table 1 Parameters of the seismic point sources considered in this study. The DISS-ID column also identifies the individual sources of the DISS 3.3.0 database (DISS Working Group 2021) used to retrieve the fault geometry for the extended source approximation. SRC stands for source; time in 24 h notation

No. SRC	Date	Time	Mw CPTI15	Lon. [deg]	Lat. [deg]	Depth [km]	Strike [deg]	Dip [deg]	Rake [deg]	DISS-ID	Mw DISS3.3.1
1	05/06/1976	20:00	6.45	46.24	13.12	5.7	290	30	105	ITIS120	6.5
2	09/15/1976	03:15	5.93	46.28	13.20	6.8	274	35	90	ITIS121	6.0
3	09/15/1976	09:21	5.95	46.30	13.17	11.2	276	35	110	ITIS122	6.1

model, with different ground motion scenarios and two parametrizations of the coupling between maps of PGA and rockfall sources.

We considered three earthquake sources of the FVG 1976 seismic sequence (Fig. 1), with a magnitude close to 6.0 or larger, for the physics-based simulations described in previous section. Table 1 lists the input parameters for the point source approximation (longitude, latitude, and depth), retrieved from the CPTI15 catalog (Rovida et al. 2022), to which the focal mechanisms taken from the Database of Individual Seismogenic Sources (DISS 3.3.0, DISS Working Group 2021) were associated. The DISS3.3.0 was also adopted as a reference database for the magnitude and fault geometry associated with the extended source models (Table 1).

The 1D structural models adopted for the computation of the Green's functions were defined according to the average models associated with the regional polygons previously defined in the framework of GNDT (*Gruppo Nazionale per la Difesa dai Terremoti* of the *Consiglio Nazionale delle Ricerche*, Rome) activities, which were widely adopted for NDSHA purposes (Panza et al. 2001, 2012). Each layer of the 1D structural model has homogeneous values of thickness, P-wave velocity, S-wave velocity, density, and quality factors associated with both P- and S- waves.

2.4 Ground Motion Modeling

The PGA values were estimated at regular grid points with a spacing 2 × 2 km, considering four different earthquake scenarios, namely: one earthquake point source (the main shock), three aggregated earthquake point sources, one earthquake extended source (the main shock) and three aggregated earthquake extended sources. The grid covering the study area is composed by 306 cells, for a total area of 1224 km^2 (Fig. 2). Subsequently, we compared the spatial distribution patterns of landslides/rockfalls and PGAs for the site of interest using the Quantum Geographic Information System (QGIS) tool.

Govi (1977) mapped the landslides collectively triggered by the earthquakes of May 6, 1976 (6.5 Mw), September 15, 1976 (6.0 Mw), and September 15, 1976 (6.1 Mw) altogether, and developed a landslide inventory consisting of 1007 landslide occurrences (Figs. 1 and 2). Moreover, to perform geo-statistical analyses and relate the landslides distribution with PGA values, the PGA computed at the centre of each grid cell is assigned to the entire grid cell; the resulting discrete spatial distribution of PGA accounts for actual density of modelling results and avoids interpolations. On account of seismic ground motion uncertainty and significance (particularly relevant considering that historical information largely relies on macroseismic data), it is important to note that a doubling of the values of shaking roughly corresponds to a variation of one degree in the scale of macroseismic intensities, as formally defined by Cancani (1904) and demonstrated, on solid numerical basis by Panza et al. (1997). Accordingly, six PGA thresholds are used, namely: 20–40; 40–80; 80–150; 150–300; 300–600; and > 600 gal, which roughly correspond to different macroseismic intensity levels of the Mercalli-Cancani-Sieberg Intensity scale (MCS).

In the case the main earthquake (i.e. Mw 6.5 6th May, 1976 earthquake) is modeled as a point source, for the ground shaking threshold PGA ≥ 40 gal an area equal to the 78% of the entire grid is identified, and all of the triggered landslides are located within this area, as shown in Fig. 2a and summarized in Table 2. When selecting the territory affected by the strongest shaking, namely for PGA ≥ 300 gal, we find that only 17% of the area is assigned this PGA value and about 70% of the observed landslides is missed (i.e. 70% of landslides are located outside the area where PGA ≥ 300 gal). While considering three earthquakes (i.e. 6th May, 1976, Mw 6.0 15th September, 1976, and Mw 6.1 15th September, 1976), simulated using the point source approximation, for the same PGA thresholds (i.e. PGA ≥ 40 gal and PGA ≥ 300 gal), 83% and 18% of the grid area is selected and none and 70% landslides are missed, respectively (Fig. 2b and Table 2). On the other hand, the extended source models (Fig. 2c, d) provide slightly different spatial patterns of ground motion and higher values of shaking, for both the May 6, 1976 earthquake scenario and for the three earthquake scenarios computed using point source model (Fig. 2a, b, respectively). When he extended source models are used, practically all the territory (99%) is selected and no landslides are missed in the case of PGA ≥ 40 gal, while for PGA ≥ 300 gal about 34% of the territory is

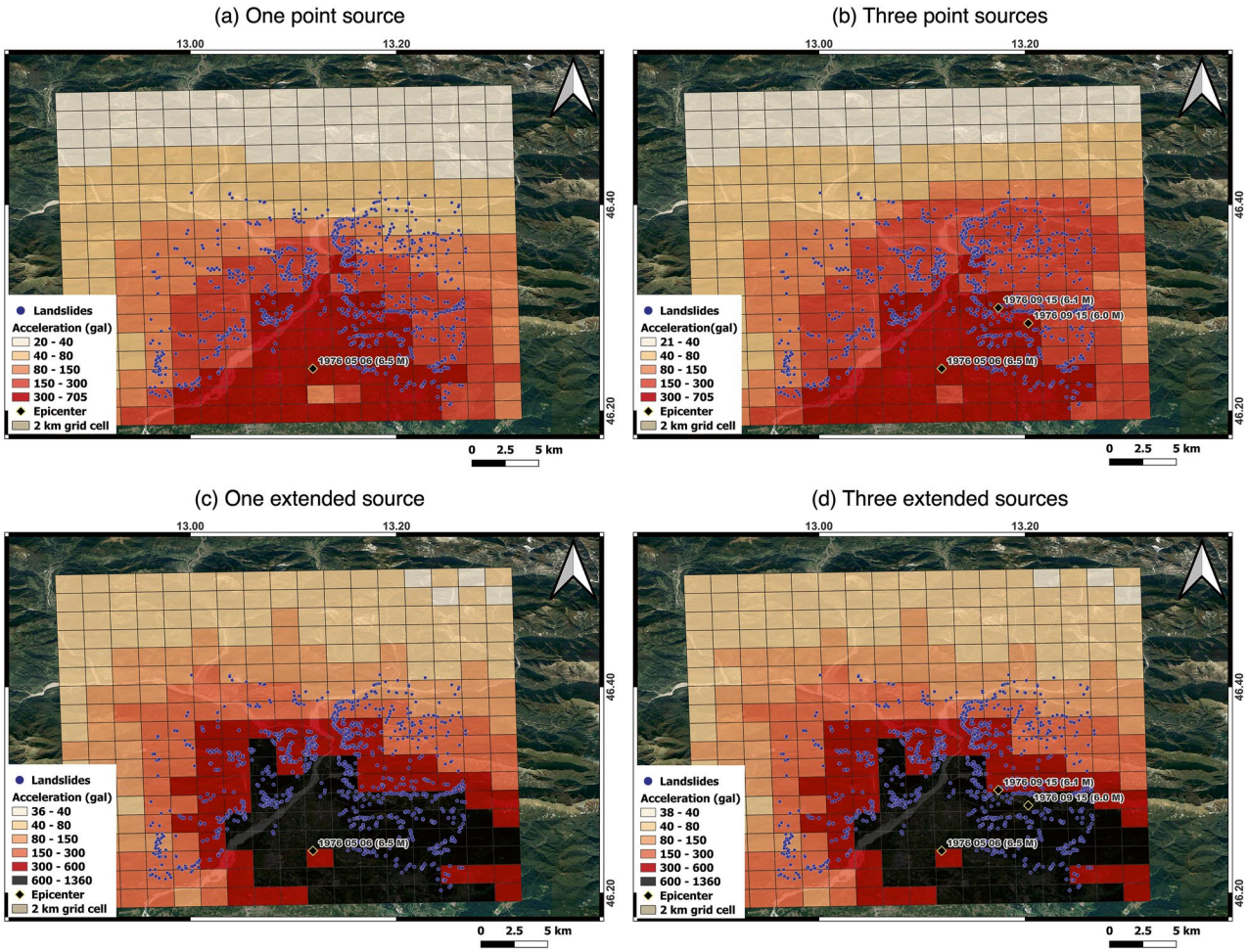


Fig. 2 Spatial distribution of modeled ground shaking (PGA [gal]) for: (**a**) the point-source main shock, (**b**) the three aggregated point sources, (**c**) the extended-source main shock and (**d**) the three aggregated extended sources. The locations of landslide points from Govi (1977) inventory are marked by blue dots. The grid cells are colored according to the PGA values computed at their central points. The black diamonds indicate the epicenters of the earthquakes considered in each panel

Table 2 Forecasting scores for the predictive analysis of rockfalls versus modeled ground shaking. The events to be predicted correspond to the landslide points reported in the inventory by Govi (1977). The errors obtained for each PGA threshold are compared for the four different models. The best prediction result, providing the lowest total error, is highlighted in bold

	One point source			Three point sources			One extended source			Three extended sources		
PGA threshold gal)	Area (α%)	Missed landslides (η%)	Total error (α + η)	Area (α%)	Missed landslides (η%)	Total error (α + η)	Area (α%)	Missed landslides (η %)	Total error (α + η)	Area (α%)	Missed landslides (η %)	Total error (α + η)
40	78.1	0.0	78.1	83.0	0.0	83.0	98.4	0.0	98.4	99.0	0.0	99.0
80	53.3	6.6	59.8	60.8	0.6	61.4	70.9	0.1	71.0	71.2	0.1	71.3
150	34.6	27.3	62.0	44.8	8.3	**53.1**	52.9	6.6	59.5	52.9	6.6	59.5
300	17.3	70.7	88.0	18.0	69.9	87.9	34.6	27.2	61.9	34.6	27.2	61.9
600	=	=	=	=	=	=	19.6	61.7	81.3	19.6	61.7	81.3

selected and about 27% landslides are missed (Table 2). The main information we obtained from the set of the four different simulations, shown in Fig. 2, is that using three earthquake sources either modeled according to a point or extended source approximation is important to reproduce the spatial distribution pattern of ground shaking that corresponds to, or encompass, the whole region affected by landslides.

2.5 Assessing the Correspondence Between Ground Motion and Rockfall Spatial Patterns

To explore the relation between the spatial pattern of ground motion and its possible effects on rockfall occurrences, we adopt a binary "forecasting" approach. Basically, we assess the presence (or absence) of rockfalls within a territory selected according to a specific value of the ground shaking parameter, and then we check whether the number of rockfalls identified based on ground motion is larger than that from a random guess. According to this scheme, by setting a threshold for a ground motion parameter, we identify the area (namely a set of grid cells) where this threshold is exceeded and which is assumed prone to the occurrence of rockfalls/landslides. When a landslide occurs within such *alerted area*, then it is counted as a *successful prediction*, otherwise it is referred as *failure to predict*; if no landslide occurs within a selected cell, then the cell is considered as a *false alarm*.

Following Molchan (1990), the results of this forecasting scheme can be characterized by two types of errors. The first one is the percentage η of failures to predict: $\eta = F/N$, where F is the number of failures to predict (i.e. rockfalls outside the alerted area) and N is the total number of occurred rockfalls. The second one is the percentage α of alarms: $\alpha = A/T$, where A is the extent of the alarmed area (the alerted cells) and T is the extent of the study area (the entire grid). The strength of a prediction is estimated by the analysis of the error diagram, collecting information on both types of errors. In order to characterize the quality of forecasting results in terms of the errors η and α, it is possible to consider any convex function $\Omega = f(\eta,\alpha)$; amongst the several possible functions, the sum of errors is the most straightforward and widely used for the evaluation of forecasting results (Molchan 1990, 1997).

Hence in this study the quality of rockfall predictions is quantified by the sum of errors: $\Omega = \eta + \alpha$, but different possible measures are possible as well (e.g. Dahal et al. 2023). Accordingly, one can roughly estimate the quality of rockfalls prediction by the deviation of Ω from the percentage $\Omega = 100\%$, which corresponds to random prediction results. Low values of Ω characterize accurate predictions, while as Ω increases toward 100% the quality of results decreases. Graphically in the errors diagram, the diagonal line from the upper left corner to the lower right corner corresponds to the points for which it holds $\Omega = \eta + \alpha = 100\%$, namely to the results that can be obtained by random guess. The more the results are distant from the diagonal line (corresponding to a random guess) and close to the origin of the axes (i.e., for low fraction of both alarms and failures), the better the forecast performance.

The forecasting scores, obtained for the four different scenarios and for the selected PGA thresholds, considering the landslide points reported by Govi (1977), are shown in Fig. 3 and listed in Table 2. The forecasting results, obtained only from the spatial distribution of slope angles and with no information about ground shaking, are provided for comparison.

The landslide inventory prepared by Govi (1977) after the seismic sequence includes 272 polygons, corresponding to a subset of the 1007 landslide points, consisting almost entirely by rockfalls. The polygons have area in the range 389 m^2–72,753 m^2. We used this subset of the inventory to measure the performance of rockfall modeling, counting the number of simulated trajectories crossing each landslide body.

Physically based rockfall assessment was performed using the TINITALY digital elevation model, with a 10 m grid cell size (Tarquini et al. 2007), and terrain parameters entering the STONE model were extracted using the 1:100,000 lithological map of Italy by Bucci et al. (2022). The high resolution of elevation data dictates the resolution of the simulated rockfall trajectories. This implies that using point landslide data to assess results would be difficult at this level of detail, thus we opted for the polygonal set of the inventory, in the following.

Figure 4 shows histograms of the distribution of the number of polygonal landslides (a, b; yellow bars) and the total

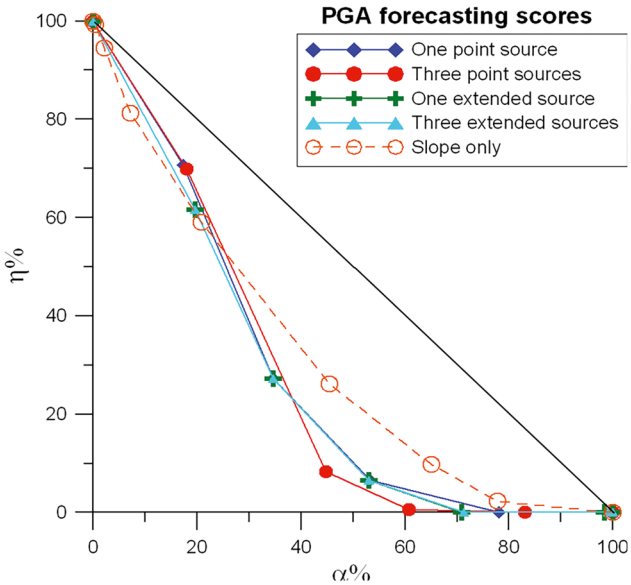


Fig. 3 Errors diagram for the predictive analysis of rockfalls versus modeled ground shaking (PGA [gal]).The percentage of failures to predict is η%, and α% is the percentage of total area selected by a specific PGA threshold. The diagonal line corresponds to the results of a random guess ($\eta + \alpha = 100\%$). The different curves correspond to the results obtained for the four different models and the PGA thresholds listed in Table 2. The prediction results, obtained based only on the spatial distribution of ground slope angles are provided for comparison

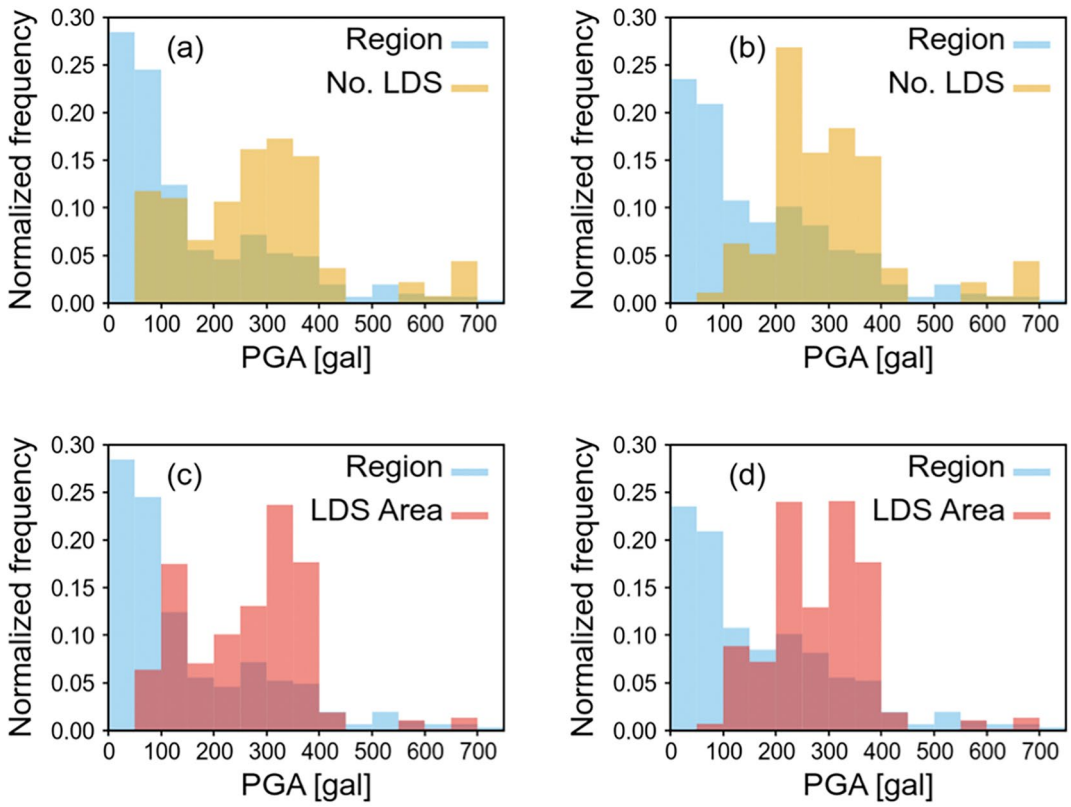


Fig. 4 Distribution of the number of observed landslides (LDS; **a, b**) and of total landslide area (**c, d**) as a function of PGA values, in intervals of 50 gal. In all of the plots, the background blue distribution of the number of PGA grid cells (*cf.* Fig. 1, top row). The distributions in (**a**) and (**c**) correspond to one point source, in (**b**) and (**d**) to three point sources

landslide area (c, d; red bars) as a function of PGA, for the approximations of one and three point sources, respectively, corresponding to panels (a) and (b) in Fig. 2. All of the distributions compare the number/area histograms to the overall distribution of PGA in the study area (blue bars). One can see that simulating three point sources gives an advantage with respect to the case based on one source only, both in terms of number of landslides associated with larger values of PGA, and in terms of the area occupied by the corresponding polygons. This can be considered as a quantitative evidence of the conclusions drawn from visual assessment of the results in Figs. 2 and 3. This analysis compares with that of Dahal et al. (2023).

Eventually, Fig. 5 shows the actual simulations of rockfall trajectories with the three-dimensional model STONE. The four different maps distinguish different approximations both on the modeled earthquake scenarios side and on the rockfall modeling side. Specifically, two different scenarios are considered for the earthquake sources (one point source—left panels, and three point sources—right panels) and two different parametrizations are used for the coupling between shake maps and rockfall initiation points (linear rescaling of PGA—top panels, and non-linear rescaling—bottom panels, see Alvioli et al. (2024) for details on the functional forms).

Visual assessment of the results clearly suggests that the three-source description has an advantage with respect to the one-source case. That could be expected, considering the ground shaking maps alone (Fig. 2a, b), which already suggest better agreement on the three-source case. On the other hand, the approximations for the PGA-rockfall sources coupling seem equally valid, and it is difficult to understand the balance of positive and negative predicted areas with respect to observed landslides. Thus, in Table 3 we reported numerical values describing the agreement between the output of the model STONE and observed landslides. The model calculates rockfall trajectories, and the output is a raster containing the count of the number of trajectories crossing each grid cell.

The table shows the percentage area of rockfall polygons crossed by at least one simulated trajectory, in the four dif-

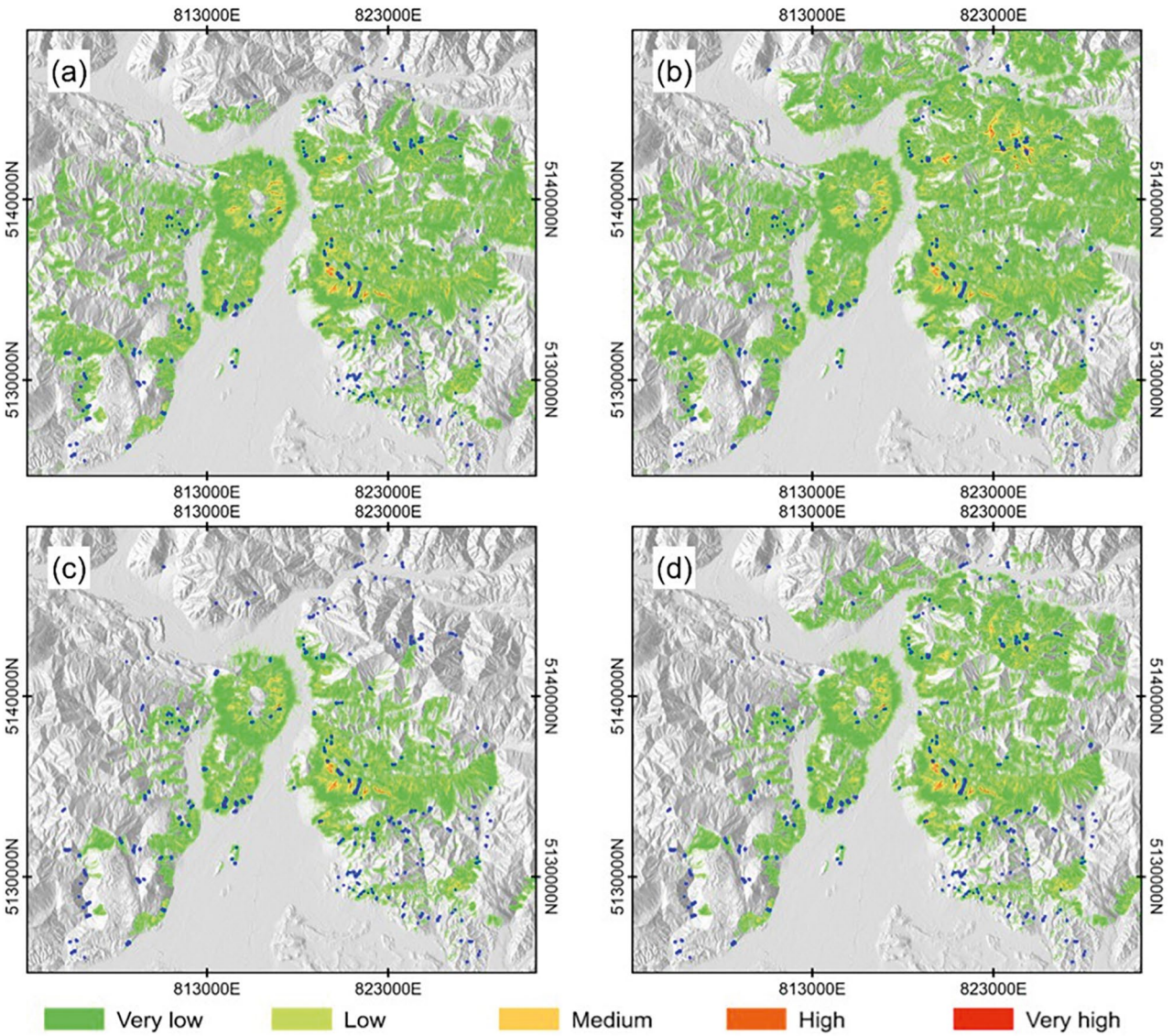


Fig. 5 Maps of cumulative counts of trajectory obtained with STONE. We adopted two different approximations for the seismological simulations (left panels: one point source; right panels: three point sources), and two different approximations for the selection of dynamic rockfall sources from the static rockfall sources (top panels: linear rescaling of PGA; bottom panels: non-linear rescaling of PGA using a normalized tunable sigmoid function, see Alvioli et al. 2023). Blue polygons represent observed rockfalls. The trajectory counts are classified with a head/tail algorithm. See Table 3 for numerical results

Table 3 Agreement between probabilistic, modeled rockfall run out and observed rockfall polygons. The first two rows represent the percentage of rockfall area intersected by at least one rockfall trajectory; the last row represent the percentage gain using the PGA map obtained from three point sources, with respect to using the one corresponding to one point source

	Linear	NTSF 1
One point source	68.5%	52.5%
Three point sources	71.4%	61.3%
Gain	4.2%	16.3%

ferent cases, and the percentage gain using the PGA obtained from three seismic sources with respect to a single source, in both PGA-rockfall initiating points coupling schemes. The gain is larger in the non-linear coupling case, 16.3% *vs.*4.2% for the linear case. That is at the expense of overall lower percentage area correctly predicted as unstable in both one-source and three-sources earthquake simulations.

3 Discussion and Conclusions

The aim of this study is to analyze the spatial distribution pattern of rockfalls triggered by the FVG 1976 seismic sequence, considering various earthquake scenarios. We utilized a physics-based approach to compute the corresponding PGA and landslides density at a regular grid of 2 × 2 km, incorporating both point and extended source models for one earthquake (the main shock), as well as an aggregated scenario of three earthquakes (main shock and the strongest aftershocks with Mw close to 6.0) shown in Table 1 and Fig. 1. Next, we compared the spatial distribution patterns of landslides/rockfalls and PGAs for the site of interest using the Quantum Geographic Information System (QGIS) tool. Overlaying both datasets in a geographic information system enabled us to assess whether ground motion simulation scenarios accurately capture the observed distribution patterns of landslides. Additionally, we investigated which earthquake scenario, if any, effectively captures this pattern.

Associating the spatial distribution pattern of observed landslides, triggered by the Friuli 1976 seismic sequence, with the PGA pattern computed for the main shock using a point source model seems unsatisfactory, as compared to those obtained for the aggregated scenario of the seismic sequence (Fig. 2a, b). Additionally, we tested the extended source model for both the main shock and the three earthquakes aggregated scenario. Though the resulting ground motion simulations slightly improved the spatial pattern, compared to those from the single point source model, the improvement was not as evident as that achieved with the three point sources model (see Fig. 2).

The map depicting the difference between the PGA maps of the three earthquakes aggregated scenario and the main shock (both from point source models), combined with rockfall density, supports this conclusion (Fig. 6). The map shows that the aftershocks of the Mw 6.5 1976 Friuli earthquake significantly influenced the PGA ground shaking pattern, prevailing in the north-eastern parts of the study area, where high rockfall density is observed as well. This conclusion is corroborated by the error diagram analysis, shown in Fig. 3, which shows how well the modeled ground shaking "predicts" the spatial distribution of rockfalls, comparing the percentage of failures η and the percentage of area α selected by a specific PGA threshold, for increasing threshold values. The curves obtained for the four different models and the PGA thresholds listed in Table 2, show that the three point source scenario best capture the spatial pattern of observed landslides. Moreover, all modeled ground shaking scenarios display better prediction results than those obtained considering only the spatial distribution of ground slope angles, which are provided for comparison.

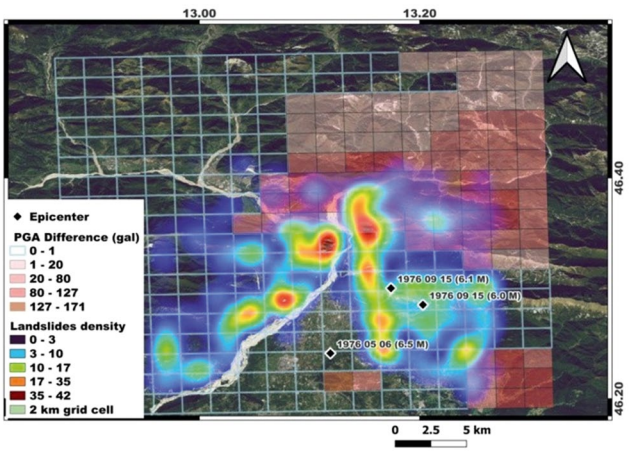


Fig. 6 Map of the difference between PGA computed for three earthquake aggregated scenario and one main earthquake for point source model compared with the density of observed landslides

The complete modeling chain considers physical three-dimensional modeling of rockfall trajectories, coupled with ground-shaking scenarios. High resolution analysis gives the opportunity of considering the polygonal subset of the inventory compiled after the FVG 1976 seismic sequence. We analyzed the distribution of number of landslides and landslide area as a function of PGA from the two-point source scenarios, with the same conclusions of the 2 × 2 km grid analysis (Fig. 4). Moreover, runs of the code STONE for a probabilistic assessment of rockfall trajectories in the two scenarios with point sources at 10 m resolution, suggests a better match with observed landslide polygons and the scenario with three point sources (Fig. 5, Table 3). This study suggests us further exploring the numerous possibilities offered by the combined use of physics-based methods, for both earthquake and rockfall modeling, and their possible contribution towards a better understanding of the triggering mechanisms of Coseismic rockfalls, including the influence of topography on seismic ground shaking.

The results of the current study highlighted an important aspect: the potential of the strongest aftershocks of the 1976 FVG seismic sequence on the final spatial distribution pattern of these rockfalls cannot be overlooked. It is crucial to consider that the susceptibility to landslides might increase in the aftermath of the main shock. In fact, the shaking caused by earthquake can destabilize slopes by loosening the soil or rock material. This increased instability can lead to landslides occurring both during and after the shaking. Moreover, aftershocks can continue to shake the ground and further weaken already compromised slopes, potentially triggering new landslides/rockfalls.

The spatial distribution pattern and density of coseismic landslides induced by the 1976 Friuli sequence well corresponds to the peak ground acceleration obtained modeling the main shock along with the two strongest aftershocks. This is quite evident in the maps showing the difference between the PGA estimated separately for the main shock and the sequence. It is apparent that the PGA values from the sequence display a better correlation with the coseismic landslide density map, compared to those from the main shock alone.

Acknowledgments The authors are grateful to Hany M. Hassan for the insightful discussions and for his contribution to manuscript preparation. The authors are also indebted to Giuliano Panza, Fabio Romanelli, Andrea Magrin and the team who developed the NDSHA modeling package, some modules of which were used in this study. The study is a contribution to the RETURN Extended Partnership (European Union Next-Generation EU—National Recovery and Resilience Plan—NRRP, Mission 4, Component 2, Investment 1.3 –D.D. 1243 2/8/2022, PE0000005).

References

Aki K (1987) Strong motion seismology. In: Erik M, Toksöz M (eds) Strong ground motion seismology, NATO ASI series, series C: mathematical and physical sciences, vol 204. D. Reidel Publishing Company, Dordrecht, pp 3–39. https://doi.org/10.1007/978-94-017-3095-2_1

Akkar S, Bommer JJ (2007) Prediction of elastic displacement response spectra in Europe and the Middle East. Earthq Eng Struct Dyn 36(10):1275–1301. https://doi.org/10.1002/eqe.679

Alvioli M, Guzzetti F, Marchesini I (2020) Parameter-free delineation of slope units and terrain subdivision of Italy. Geomorphology 358:107124. https://doi.org/10.1016/j.geomorph.2020.107124

Alvioli M, Santangelo M, Fiorucci F, Cardinali M, Marchesini I, Reichenbach P, Rossi M, Guzzetti F, Peruccacci S (2021) Rockfall susceptibility and network-ranked susceptibility along the Italian railway. Eng Geol 293:106301. https://doi.org/10.1016/j.enggeo.2021.106301

Alvioli M, De Matteo A, Castaldo R, Tizzani P, Reichenbach P (2022) Three-dimensional simulations of rockfalls in Ischia, southern Italy, and preliminary susceptibility zonation. Geomat Nat Haz Risk 13(1):2712–2736. https://doi.org/10.1080/19475705.2022.2131472

Alvioli M, Falcone G, Mendicelli A, Mori F, Fiorucci F, Ardizzone F, Moscatelli M (2023) Seismically induced rockfall hazard from a physically based model and ground motion scenarios in Italy. Geomorphology 429:108652. https://doi.org/10.1016/j.geomorph.2023.108652

Alvioli M, Poggi V, Peresan A, Scaini C, Tamaro A, Guzzetti F (2024) A scenario-based approach for immediate post-earthquake rockfall impact assessment. Landslides 21:1–16. https://doi.org/10.1007/s10346-023-02127-2

Aoudia A, Saraò A, Bukchin B, Suhadolc P (2000) The 1976 Friuli (NE Italy) thrust faulting earthquake: a reappraisal 23 years later. Geophys Res Lett 27(4):573–576. https://doi.org/10.1029/1999GL011071

Bressan G, Barnaba C, Bragato P, Ponton M, Restivo A (2018) Revised seismotectonic model of NE Italy and W Slovenia based on focal mechanism inversion. J Seismol 22:1563–1578. https://doi.org/10.1007/s10950-018-9785-2

Bucci F, Santangelo M, Fongo L, Alvioli M, Cardinali M, Melelli L, Marchesini I (2022) A new digital lithological map of Italy at 1:100,000 scale for geo-mechanical modeling. Earth Syst Sci Data 14:4129–4151. https://doi.org/10.5194/essd-14-4129-2022

Cancani A (1904) Sur l'emploi d'une double échelle sismique des intensités, empirique et absolue. Gerl Beitrage Geophys 2:281e283

Dahal A, Alejandro Castro-Cruz D, Tanyaş H, Fadel I, Mai PM, van der Meijde M, van Westen C, Huser R, Lombardo L (2023) From ground motion simulations to landslide occurrence prediction. Geomorphology 441:108898. https://doi.org/10.1016/j.geomorph.2023.108898

DISS, Working Group (2021) Database of Individual Seismogenic Sources (DISS), Version 3.3.0: a compilation of potential sources for earthquakes larger than M 5.5 in Italy and surrounding areas. Istituto Nazionale di Geofisica e Vulcanologia (INGV). https://doi.org/10.13127/diss3.3.0

Fan X, Scaringi G, Korup O, West AJ, van Westen CJ, Tanyas H, Hovius N, Hales TC, Jibson RW, Allstadt KE (2019) Earthquake-induced chains of geologic hazards: patterns, mechanisms, and impacts. Rev Geophys 57(2):421–503. https://doi.org/10.1029/2018RG000626

Gorshkov AI, Panza GF, Soloviev AA, Aoudia A, Peresan A (2009) Delineation of the geometry of nodes in the Alps-Dinarides hinge zone and recognition of seismogenic nodes ($M \geq 6$). Terra Nova 21(4):257–264. https://doi.org/10.1111/j.1365-3121.2009.00879.x

Govi M (1977) Photo-interpretation and mapping of the landslides triggered by the Friuli earthquake (1976). Bull Eng Geol Environ 15(1):67–72. https://doi.org/10.1007/BF02592650

Gusev AA (1983) Descriptive statistical model of earthquake source radiation and its application to an estimation of short period strong motion. Geophys J R Astron Soc 74:787–800. https://doi.org/10.1111/j.1365-246X.1983.tb01904.x

Gusev AA (2011) Broadband kinematic stochastic simulation of an earthquake source: a refined procedure for application in seismic hazard studies. Pure ApplGeophys 168(1–2):155–200. https://doi.org/10.1007/s00024-010-0156-3

Guzzetti F, Crosta G, Detti R, Agliardi F (2002) STONE: a computer program for the three-dimensional simulation of rockfalls. Comput Geosci 28:1079–1093. https://doi.org/10.1016/S0098-3004(02)00025-0

Igel H (2016) Computational seismology: a practical introduction. https://doi.org/10.1093/acprof:oso/9780198717409.001.0001

Jibson RW (2011) Methods for assessing the stability of slopes during earthquakes—a retrospective. Eng Geol 122(1–2):43–50. https://doi.org/10.1016/j.enggeo.2010.09.017

Keefer DK (2000) Statistical analysis of an earthquake-induced landslide distribution—the 1989 Loma Prieta, California event. Eng Geol 58(3–4):231–249. https://doi.org/10.1016/S0013-7952(00)00037-5

Luzi L, Pergalani F (2000) A correlation between slope failures and accelerometric parameters: the 26 September 1997 earthquake (Umbria–Marche, Italy). Soil Dyn Earthq Eng 20(5–8):301–313. https://doi.org/10.1016/S0267-7261(00)00063-4

Molchan GM (1990) Strategies in strong earthquake prediction. Phys Earth Planet Inter 61(1–2):84–98

Molchan GM (1997) Earthquake prediction as a decision-making problem. Pure Appl Geophys 149:233–247. https://doi.org/10.1007/BF00945169

Panza GF, Vaccari F, Cazzaro R (1997) Correlation between macroseismic intensities and seismic ground motion parameters. Ann Geophys 15:1371e1382

Panza GF, Romanelli F, Vaccari F (2001) Seismic wave propagation in laterally heterogeneus anelastic media: theory and applications to seismic zonation. Adv Geophys 43:1–95. https://doi.org/10.1016/S0065-2687(01)80002-9

Panza GF, La Mura C, Peresan A, Romanelli F, Vaccari F (2012) Seismic hazard scenarios as preventive tools for a disaster resil-

ient society. Adv Geophys 53:93–165. https://doi.org/10.1016/B978-0-12-380938-4.00003-3

Pavlov VM (2009) Matrix impedance in the problem of the calculation of synthetic seismograms for a layered-homogeneous isotropic elastic medium. Izv Phys Solid Earth 45:850–860. https://doi.org/10.1134/S1069351309100036

Peresan A, Gentili S (2018) Seismic clusters analysis in northeastern Italy by the nearest-neighbor approach. Phys Earth Planet Inter 274:87–104. https://doi.org/10.1016/j.pepi.2017.11.007

Rovida A, Locati M, Camassi R, Lolli B, Gasperini P, Antonucci A (2022) Catalogo Parametrico dei Terremoti Italiani (CPTI15), versione 4.0 [Data set]. Istituto Nazionale di Geofisica e Vulcanologia (INGV). https://doi.org/10.13127/cpti/cpti15.4

Slejko D, Neri G, Orozova I, Renner G, Wyss M (1999) Stress field in Friuli (NE Italy) from fault plane solutions of activity following the 1976 main shock, Bull. Seism Soc Am 89:1037–1052

Tanyaş H, van Westen CJ, Persello C, Alvioli M (2019) Rapid prediction of the magnitude scale of landslide events triggered by an earthquake. Landslides 16:661–676. https://doi.org/10.1007/s10346-019-01136-4

Tarquini S, Isola I, Favalli M et al (2007) TINITALY/01: a new triangular irregular network of Italy. Ann Geophys 50:407–425. https://doi.org/10.4401/ag-4424

Tiwari B, Ajmera B, Dhital S (2017) Characteristics of moderate-to large-scale landslides triggered by the M w 7.8 2015 Gorkha earthquake and its aftershocks. Landslides 14:1297–1318. https://doi.org/10.1007/s10346-016-0789-0

Valagussa A, Frattini P, Crosta GB (2014) Earthquake-induced rockfall hazard zoning. Eng Geol 182:213–225. Special issue on: the long-term geologic hazards in areas struck by large-magnitude earthquakes. https://doi.org/10.1016/j.enggeo.2014.07.009

Worden CB, Thompson EM, Hearne M et al (2020) Shake map manual online: technical manual, user's guide, and software guide. Geological Survey, US. https://doi.org/10.5066/F7D21VPQ

Open Access This chapter is licensed under the terms of the Creative Commons Attribution 4.0 International License (http://creativecommons.org/licenses/by/4.0/), which permits use, sharing, adaptation, distribution and reproduction in any medium or format, as long as you give appropriate credit to the original author(s) and the source, provide a link to the Creative Commons license and indicate if changes were made.

The images or other third party material in this chapter are included in the chapter's Creative Commons license, unless indicated otherwise in a credit line to the material. If material is not included in the chapter's Creative Commons license and your intended use is not permitted by statutory regulation or exceeds the permitted use, you will need to obtain permission directly from the copyright holder.



Landslides of Moscow River Valley (Russia): Types and Features of their Origin in Different Geological Conditions

Pavel V. Novikov, Oleg V. Zerkal, Olga S. Barykina, and Eugene N. Samarin

Abstract

The Moscow River valley is an actively developed area in Russia within the Moscow agglomeration, where landslide processes are widely developed. There are four main types of landslides here. The greatest hazard for economic activity is large rotational slides. Such landslides differ in size, features of displacement zones and sediments involved in displacement. It was found that landslide massifs formed in different geological conditions have significant differences in internal structure and present-day activity. A detailed study of landslide processes in several areas of the Moscow River valley and its tributaries revealed key features of changes in the internal structure and properties of the main deformable horizons during the development of landslide processes.

Keywords

Rotational slides · Moscow river · Dormant landslides · Landslideactivity · Landslide deformations

1 Introduction

The Moscow River valley is located in the European part of Russia, in the central part of the East European Platform.

Among the landslides developed in the area, rotational slides (earth slumps (by O. Hungr (Hungr et al. 2014)), multi-storeyed landslides (by G. Ter-Stepanian (Ter-Stepanian 1977)), stepped landslides, earth flows, complex landslides are currently distinguished (Zerkal et al. 2021). The earth slumps associated with pre-Quaternary sediments are of greatest interest. About 50 such landslide massifs are known within the study area (Fig. 1), the best known sites are "Vorobyovy Gory", "Fili-Kuntsevo", "Kolomenskoye", "Khoroshevo-I".

The Moscow River valley is a relatively well-studied area in terms of landslide development. References to landslide processes are known since 1837. Targeted research on landslides in the valley of the Moscow River began in the beginning of the last century, but up to the middle of the twentieth century it was not systematic. Predominantly, separate parts of landslide massifs were studied for construction purposes. The study of landslide processes became systematic in the 1950s when the Moscow Landslide Station get started. For more than 30 years, studies of landslide processes were carried out in the valleys of the Moscow and Oka rivers within the Moscow, Ryazan and Kaluga regions. The main objectives of the Moscow landslide station were to study the occurrence, dynamics and mechanism of landslide processes.

Opportunities to observe the natural dynamics of landslide processes were severely limited due to active strengthening of landslide areas in the Moscow River valley. The available ideas about the geological structure of pre-Quaternary sediments did not allow detailed dissection of sediments involved in landslide processes, and the observation equipment did not allow to accurately identify the zones of deep deformations. The combination of these factors has led to the fact that many features of the internal structure and dynamics of landslide processes have been given only general information on the basis of indirect features.

In the 2000s, a new stage of studies of landslide massifs in the Moscow River valley began due to the activation of landslide movements in some areas (Khoroshevo-I, Khoroshevo-II, Vorobyovy Gory, Kolomenskoye, Moskvorechye-Saburovo) (Fig. 1). These studies were characterized by the use of high-precision equipment for observing landslide processes (inclinometer points). Due to the fact that the views were largely based on the works of the Moscow

P. V. Novikov · O. V. Zerkal (✉) · O. S. Barykina · E. N. Samarin
Geological Department, Lomonosov Moscow State University, Moscow, Russia
e-mail: zerkalov@geol.msu.ru; barykina@geol.msu.ru

© The Author(s) 2025

B. Abolmasov et al. (eds.), *Progress in Landslide Research and Technology, Volume 3 Issue 2, 2024*, Progress in Landslide Research and Technology, https://doi.org/10.1007/978-3-031-72736-8_9

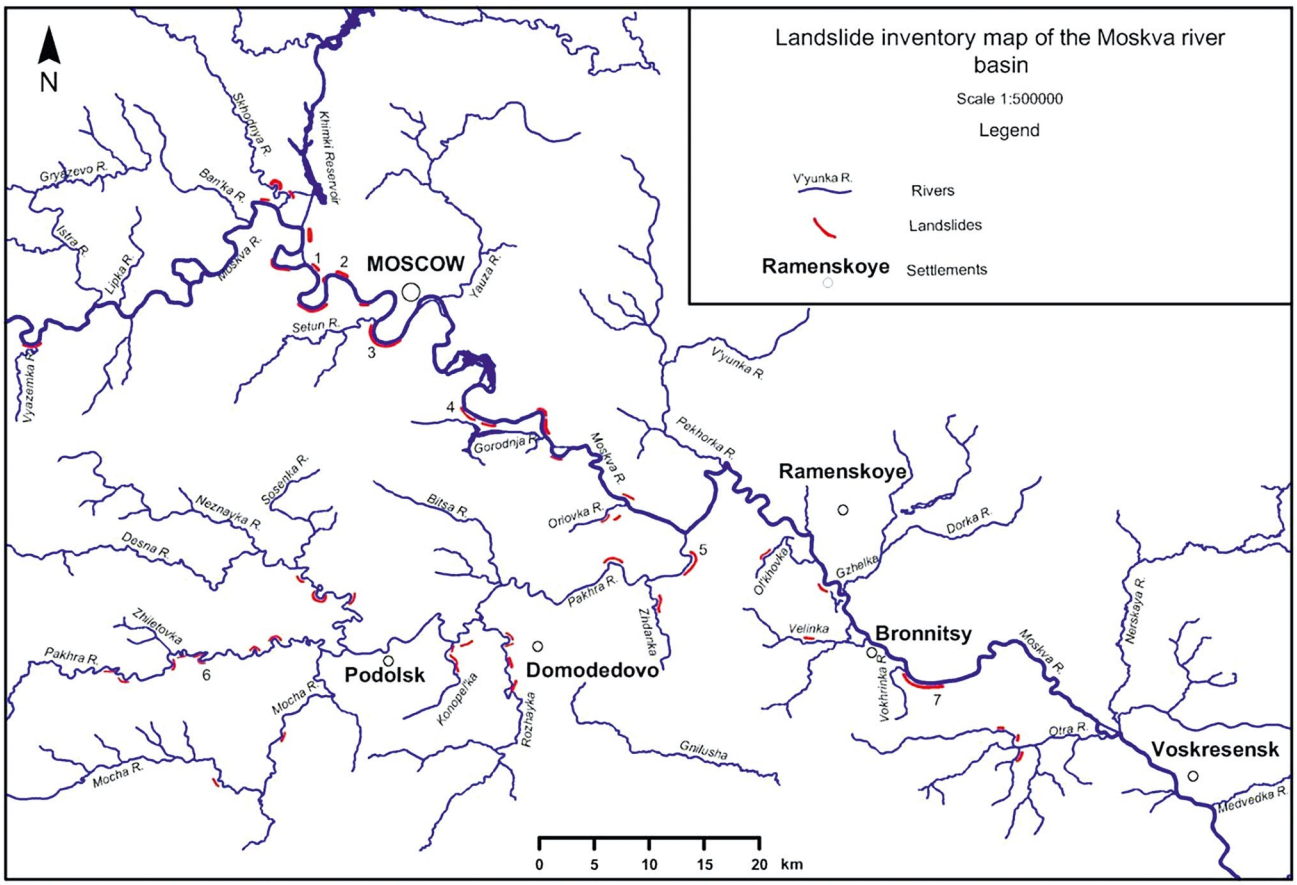


Fig. 1 Landslide inventory map of the Moscow river valley. Numbers indicate landslides: 1—Khoroshevo-I, 2—Khoroshevo-II, 3—Vorobyovy Gory,4—Kolomenskoye, 5—Zelena

Landslide Station, a number of researchers (Kuntsel 1980; Kazeev and Postoev 2012) tried to explain the new data on the basis of direct extrapolation of the views obtained in 1955–1991. This led to a number of contradictions between the actual data and ideas about the mechanism of the process, which were identified, including by the authors of this study earlier (Barykina et al. 2019; Zerkal et al. 2020; Novikov et al. 2023).

For a long time, it was considered that deep landslides associated with Jurassic clayey sediments developed by extrusion mechanism. Currently, most researchers are of the opinion that deep landslides in the Moscow River valley should be considered as sliding landslides. Nevertheless, for large landslide massifs, a number of questions remain regarding their age, number of generations, and deformation peculiarities of strata overlying Jurassic clayey formations (involved in displacement).

The purpose of the article is to clarify data on the age of landslide massifs in the valley of the Moscow River, peculiarities of landslide deformation zones and correlation of landslides with erosion bases.

For this purpose, the authors analyzed the works of the Moscow landslidestation, analyzed the results of inclinometric observations at several landslide sites, carried out route observations, carried out detailed description and documentation of geological boreholes and pits at several landslide sites.

2 Geological Structure

The Moscow River valley is located in the center of the East European platform at the south-western edge of the Moscow syneclise. This area is characterized by subhorizontal sediments; the landslide processes in different areas involve deposits of the upper part of the geological section represented by deposits of the Carboniferous, Jurassic, Cretaceous and Quaternary systems (Fig. 2).

Carboniferous deposits are represented mainly by limestone and clay of the middle and upper sections, up to 160 m thick (Osipov and Medvedev 1997). In the study area, these sediments are not actively involved in landslide processes. Despite this, they significantly limit the spatial and altitudinal distribution of landslide massifs. In areas where the river valley is cut into coal deposits, the displacement surface coincides with their roof. In addition, limestone and dolo-

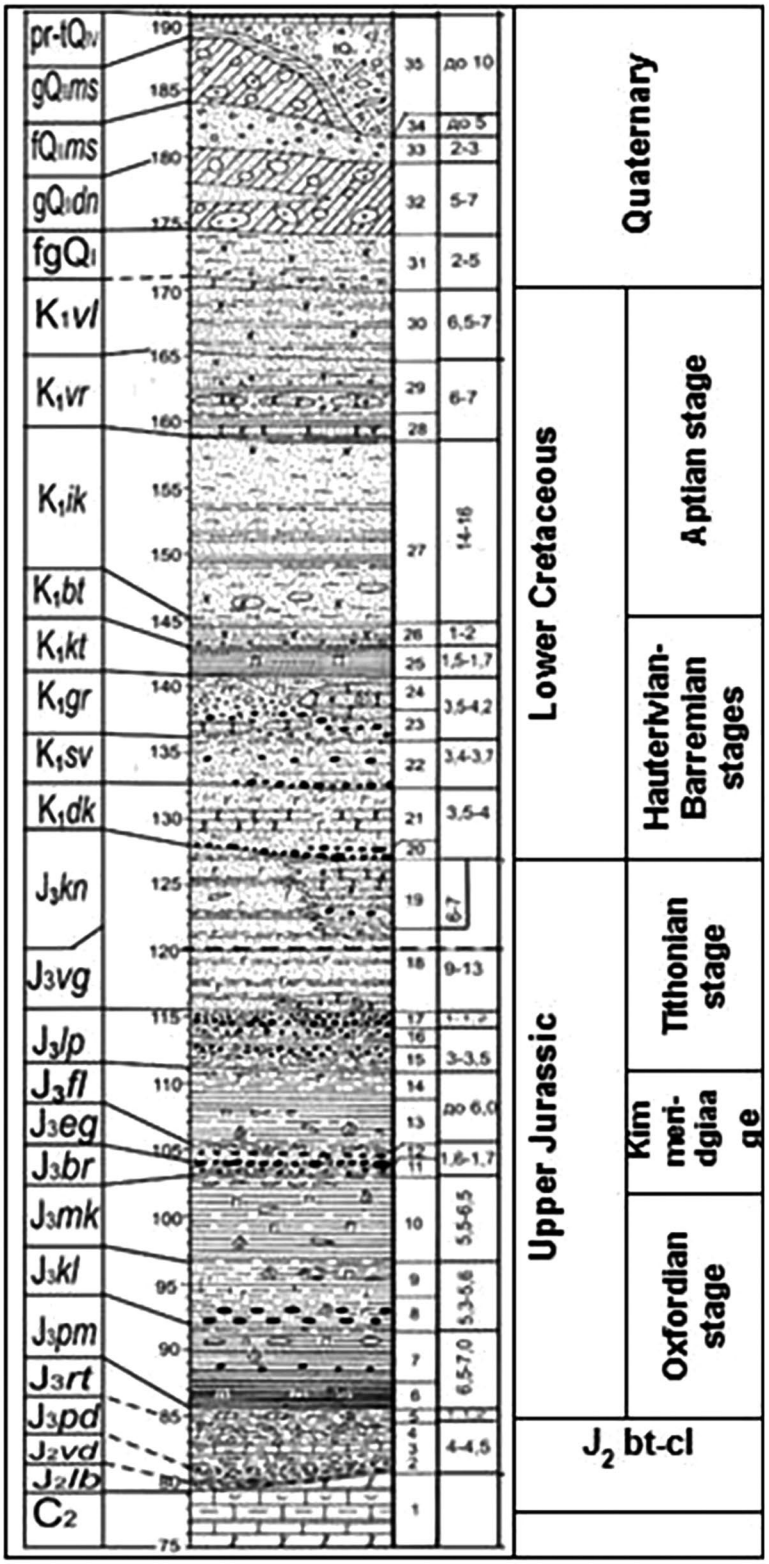


Fig. 2 Fragment of stratigraphic column o of the Moscow River valley (Osipov and Medvedev 1997)

mite of the Carboniferous age contain several pressure aquifers, which may influence the pore pressure in the Jurassic sediments.

The Jurassic sediments are of the greatest importance for development of deep earth slumps. They are represented by the Bayosian and Titonian stages.

The Bayossian, Bathian and lower part of the Kellovianstage are composed of clayey-sand formations of the Kudinovskaya and Moskvoretskaya strata of continental origin and the Alpatievskaya and Kriushskaya formations of marine genesis. They fill ancient erosion cuts. The total thickness within the landslide areas is up to 17 m (Mitta et al. 2012). Deposits of the Kudinovskaya formation and the Kriushskaya formation are predominantly clay, and those of the Moskvoretskaya-Alpatievskaya formation are sandy strata with clay interlayers. These sediments are generally not directly involved in landslide processes, but contain a pressurized aquifer that may have a significant influence on pore pressure in the Jurassic clayey sediments.

Deposits of the middle and upper sections of the Kellovian and Oxfordian-Kimmeridgian stages are represented by the Chulkovskaya and Gorkinskaya formations, up to 23–25 m thick. These stratigraphic units are represented by clays of marine clay genesis, which are the main deformable horizon for deep earth slumps. Their most characteristic features are overconsolidation, anisotropy of strength and deformation properties, relatively high strength characteristics in natural occurrence (φ up to 16–18°, C up to 100–120 kPa) and low in disturbed structure (φ up to 1–5°, C up to 20–70 kPa). These features have a determining influence on the development of deep landslides in the valley of the Moscow River.

Deposits of the middle-upper sections of the Titonian stage are represented by clays and clayey siltstones of the Mnevnikovskaya formation and sands of the Kostromskaya formation. At the areas of landslide processes their total thickness, as a rule, does not exceed 10 m. Large landslides associated with the deposits of the Titonian stage have not been reliably established, as a rule, they play a subordinate role in the development of deformations in the thickness of the Oxfordian and Kimmeridgian undivided stages. These sediments have an increased content of sandy and dusty fraction and, as a consequence, relatively high strength characteristics (φ up to 18–22°, C up to 60–80 kPa). The sandy deposits of the Kostromskaya and lower part of the Mnevnikovskaya formations, which contain an aquifer, deserve special attention. During the development of landslide processes, these waters can get directly into the area of deformation development and lead to additional moistening and softening of landslide masses.

Deposits of the upper part of the Titonian stage and Barremian stage are represented by deposits of the Lopatinskaya and Butovskaya formations, with a total thickness of up to 40–41 meters. They are represented mainly by sandy strata with lenses of clays and siltstones. The deposits of the Diakovskaya, Gremyachevskaya, Kotelnikovskaya and Butovskaya formations are of the greatest importance for landslide processes understanding. They are layered strata with numerous lenses of clay and clayey siltstones. This structure of the strata results in the presence of weakened zones where landslide deformations may develop.

The Aptian stage is a sandy stratum of the Ikshinskaya and Volgushinskaya formations with a thickness of up to 26 m. The Ikshinskaya and Volgushinskaya formations are represented by sands, while the Vorokhobinskaya formation is a thin interlayer of sands, clays and siltstones. Clays and siltstones have reduced strength characteristics compared to the sandy sequence and are natural surfaces on which landslide deformations may develop.

Quaternary sediments are represented mainly by moraine, fluvio-glacial, lake-glacial, alluvial deposits and technogenic formations, with a total thickness up to 35–50 m. As a rule, they play a subordinate role in the development of large landslides associated with Jurassic and Cretaceous sediments (exception—Khoroshevo-II). Nevertheless, most of the small landslides are associated with moraine and fluvio-glacial sediments.

Sandy sediments of the Cretaceous and Quaternary systems contain a Cretaceous-Quaternary aquifer complex that directly influences landslide massifs.

3 Types of Landslides in the Moscow River Valley

In terms of the main deformable horizon, several predominant types of landslides are distinguished:

1. Shallow slides associated with clayey, silty, less often sandy glacial, water-glacial and alluvial sediments of the Quaternary system. Landslide bodies of this type are widespread in the valley of the Moscow River and its tributaries. Such bodies have the most diverse shape: from frontal to circular. The width of landslide bodies as a rule does not exceed 25–30 m, length—no more than 15–20 m, depth of capture up to 2–3 m. In the 50–60 s, a large number of small landslides were recorded within large landslide massifs, being secondary to other types of landslides. Examples of such sites are the "Vorobyovy Gory", "Fili-Kuntsevo", and "Kolomenskoye".
2. Rotational slidesand earth flows associated with clays of the Carboniferous system in the valley of the Moscow River are locally widespread. Single occurrences are known in the upper course of the Moskva River and the Pakhra River. The impact of these landslides on the economic development of territories is insignificant, therefore, detailed studies of this type of landslides have not been carried out. In morphology these landslides are usually of frontal type. According to V.V. Kuntsel, the displacements involve not only coal clays, but also limestones and Meso-Cenozoic sediments overlying them (Kuntsel 1980).



Fig. 3 Stepped relief of the landslide site "Khoroshevo-I"

3. Rotational slides (deep earth slumps) with displacement associated with Jurassic clay deposits. Currently, more than ten cases of activation of this type of landslides are known. In terms of morphology, landslides are usually circular (Khoroshevo-I (Fig. 3), Milkovo, Krasnaya Pakhra, etc.), less often frontal (Vorobyovy Gory, Fili-Kuntsevo). This is the most widespread type of landslides more than 50 such landslide massifs are known.
4. Landslides (earth slumps) associated with clay-sandy strata of Cretaceous sediments. They are common in areas with the Jurassic clayey sediments below the erosion base.

   As a rule, the size of landslide bodies does not exceed several meters. The exception is the Vorobyovy Gory site, where the depth of capture by this type of landslides reaches up to 40 meters.

The main factors in the landslide development of type 1 are: overwatering of near-surface soil layers, suffosion of fine fraction, river and gully erosion. For landslides of the second type the greatest importance is played by river erosion and weathering of clay sediments. Type 3 and 4 landslides are developed mainly due to river erosion and anthropogenic impacts.

From the point of view of landslide science, types 3 and 4 are of the most interest. They are widespread in the actively developed areas of the Moscow River valley: in the areas of tributary slopes and slopes of 2–3 floodplain terraces. Their development determines the economic development of a significant part of the slopes; however, some issues of the development and internal structure of these landslides are still unresolved.

4 Landslides Associated with Jurassic Clay Deposits

Later, Korchebokov and Danshin and other researchers established the existence of landslide deformation zones in Jurassic clayey sediments significantly below the modern erosion base, in connection with which an assumption was made about the antiquity of the landslide massif (Danshin 1937; Korchebokov et al. 1938), Later, the data were supplemented with materials from the Moscow landslide station, on the basis of which V.V. Kuntsel concluded the age of the Vorobyovy Gory landslide massif, which corresponded to the Pleistocene-Holocene boundary (Kuntsel 1980). The deep position (~70–80 m) of the lower displacement surface was explained by the peculiarities of the landslide process mechanism: based on morphological similarity with landslides of the Odessa Black Sea coast (Ukraine), it was accepted that the landslides of the Moscow River valley in general and the Vorobyovy Gory in particular could be characterized as extrusion landslides.

More recent studies have revealed that large landslides are characterized by displacement by the sliding (not extrusion) mechanism (Barykina et al. 2019; Zerkal et al. 2017, 2020). This has led to a contradiction in terms of the correspondence of the moment of landslide massif formation with the existing erosion incision. A number of researchers ignored this fact (Kuntsel 1980; Kropotkin 2016), other researchers (Barykina et al. 2019; Zerkal et al. 2020, etc.) paid special attention to this fact: it was shown that the landslide massif consists not only of modern, but also of ancient landslide bodies. At present it is established that in the valley of the Moscow River the depth of slip surface of modern landslide bodies reaches about 20–70 m, and ancient ones—up to 100 m.

Landslide relief is stepped, landslide bodies are characterized by block structure (Fig. 3). The structure of the landslide body is characterized by several landslide blocks associated with a single subhorizontal displacement surface. At the same time, the thickness and peculiarities of the internal structure are largely determined by the thickness and nature of occurrence of clays of the Makarjevskaya-Podmoskovnaya formation (Oxfordian-Kimmeridgean stages).

In terms of morphology, multi-storeyed and stepped bodies predominate. Most of the largest landslide massifs do not represent a single landslide body, but several generations of bodies shearing each other. This means that inside the landslide blocks of younger generations there are currently inactive zones along which further deformation of the landslide massif and moistening of landslide masses are possible.

The overlying sediments play a much less role in the development of landslide processes, but largely determine the nature of secondary deformations and changes during the periods of preparation and temporary stabilization. In particular, landslide bodies at the "Kolomenskoye", "Khoroshevo-I", "Khoroshevo-II" sites have a similar structure, despite the different composition of sediments overlying clays of the Kimmeridge-Oxfordian stage.

Due to the fact that vertical displacements prevail during the detachment of a new block, the surface of the upper block retains a subhorizontal position. In some cases, this displacement pattern leads to the formation of elevated fractures of shear kinematics (Khoroshevo-I, Krasnaya Pakhra) (Fig. 4).



Fig. 4 Uplifted fracture of shear kinematics at the "Khoroshevo-I" site

The researchers of the Moscow Landslide Station tried to find a dependence between different geometrical characteristics of landslides in order to be able to assess the condition of different landslide massifs with its help, but in this approach the authors did not take into account neither the age of landslide massifs, nor the peculiarities of their development. It is difficult to use these dependencies, the studies carried out in 2005–2023 showed that the number of landslide blocks, generations and age of a significant part of landslides differ from the 1970–1990s views.

Among modern landslides, the Khoroshevo-II massif deserves special attention. Unlike other massifs, the main factor in the development of landslide processes at the site is not lateral erosion of the Moscow river, but loading of the slope with embankment soils. The thickness of the embankment in some areas reaches 12 meters. The development of landslide processes is most characteristic for the area of the backfilled Studenogo gully: after the formation of the erosion cut, clay deposits in the gully watercourse were decompacted, which led to a decrease in physical and mechanical properties. Later, embankment soils were placed on these clays, which led to a change in the stress-strain state and stresses exceeding the shear strength appeared in the thickness of Jurassic clays. Thus, a significant part of the landslide body is composed of embankment soils, with the main deformable horizon being sediments of the Makarievskaya and Kolomenskaya formations of the Oxford-Kimmeridge stage.

5 Landslides Associated with the Lower Cretaceous Clay-Sand Strata

The first views on the structure of large landslide massifs with clay-sandy strata of the Lower Cretaceous are reflected in the work of A.P. Pavlov (1908). He considered landslide processes on the Vorobyovy Gory as related to the modern base of erosion and to the displacement surface confined to the roof of Jurassic sediments. Thus, the existence of landslide processes associated with Cretaceous sediments was assumed. In the report of the "Fundamentproekt" Institute this idea was further developed: it was assumed that Cretaceous-Quaternary sediments were crushed into peculiar folds during landslide processes (Kuntsel 1980).

It is assumed that the youngest generation of landslide bodies on the territory of "Vorobyovy Gory" site is developed in the Cretaceous and, partially, Quaternary formations. For a long time, no significant attention was paid to the deformation features of the Cretaceous strata. Numerous laboratory studies of the Cretaceous strata have established their relatively high strength characteristics. On this basis it was concluded that it is impossible to form independent landslide bodies in the Cretaceous strata. It should be noted that during the study of Cretaceous sediments sandy varieties were mainly tested, while clay interlayers were not given enough attention.

This led to the overestimation of the strength characteristics of the Cretaceous sediments and the conclusion that large block landslides of this type are impossible to develop.

During construction works in the central part of "Vorobyovy Gory" site in the area of the Ski jump, in 2022, the constructors penetrated several excavations that uncovered deposits of the Butovskaya and Volgushinskaya formations. A detailed study revealed a number of peculiarities.

Collapse of the Cretaceous stratum is brittle; in addition to the main displacement surface, many secondary displacement zones are formed with the isolation of a whole series of narrow blocks, ranging from 0.1 to several meters wide (Fig. 5). Most of these zones gravitate towards larger displacement surfaces, but some of them blindly terminate within the sandy strata. The total amplitude of deformation within a single landslide unit can be more than 2 m.

In terms of major displacement, the characteristic feature is the stretching of clay interlayers across the displacement surface. In one of the sides of the excavation, the marking clay horizon in the Butovskaya formation has a thickness of about 15–20 cm and is intersected by 2 displacement zones with displacement amplitudes of 0.9 and 0.7 m, respectively. Thus, the thickness of the clay interbed is about 4 times less than the displacement amplitude, but the zone in the area of the marking clay horizon is completely filled with clayey matter. Not only the deformation zone itself is of interest, but also the ratio of sediments in the immediate vicinity of the zones. It was noticed that in the nearest to the river (northern) block the thickness of the marking horizon gradually decreases to the displacement zone to 5–6 cm, jumping up in the southern block to its normal thickness of 15 cm. This may indicate a peculiar "squeezing" of clayey sediments into the displacement zone (Fig. 6).

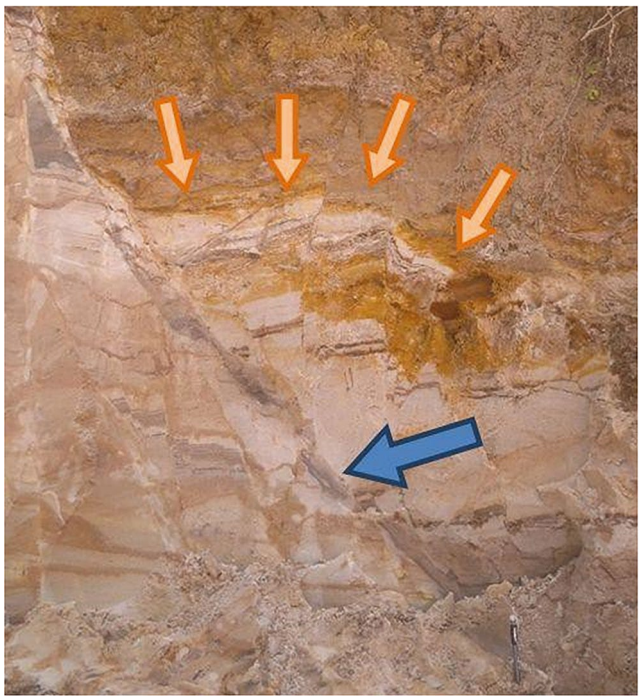


Fig. 5 Numerous small blocks in the thickness of the Butovskaya formation (orange arrows) trending toward a larger displacement surface (blue arrow), central part of the "Vorobyovy Gory" site



Fig. 6 Deformation of clay interlayers of the Butovskaya formation in the landslide deformation zone, central part of the "Vorobyovy Gory" site

A detailed investigation of the neighboring excavation site revealed, presumably, one of the main displacement surfaces in the Cretaceous sediments. Here, a clay interbed was detected in the deposits of the Butovskaya Formation, steeply cutting the natural surfaces of the sandy-clay strata. The layering is oriented parallel to the displacement zone, indicating reorientation of particles within the displacement zone. In the lower part of the outcrop, the landslide deformation zone almost coincides with the marking horizon of clay composition. It can be assumed that in other areas, the displacement zones of landslide bodies in the sandy-clay strata of the Lower Cretaceous sediments have a combined character: partially they are oriented along the clay interlayers, and at others they cut them (Fig. 7).

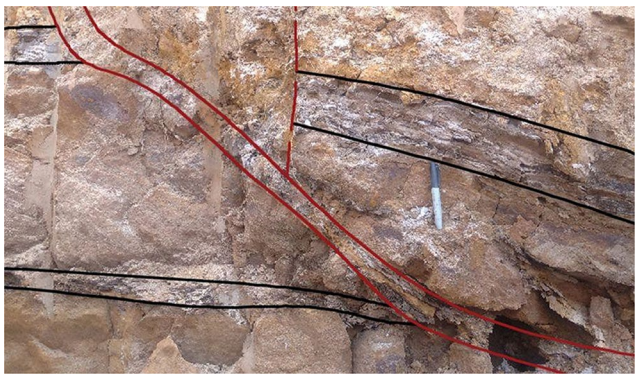


Fig. 7 Displacement zone in the Butovskayaformation. Red colour—boundaries of the displacement zone, black colour—marking clay horizons. Central part of the "Vorobyovy Gory" site

Thus, the role of clay interlayers in the landslide development in the Cretaceous strata of the "Vorobyovy Gory" site is significantly higher than previously assumed. A significant part of deformation zones is associated directly with clays of the Butovskaya and Kotelnikovskaya formations. This means that the morphology of landslides should be subordinated to the spatial position and thickness of these deposits.

Landslides associated directly with Cretaceous sediments are currently known only on the territory of the Vorobyovy Gory. This is due to the fact that sediments containing clay interbeds (Kotelnikovskaya, Butovskaya, Vorokhobinskaya formations) in the area of the Moscow River valley are developed mainly in the areas of the watershed surfaces. Large landslides of type 4 may be developed not only at the "Vorobyovy Gory" site, but also at the "Krylatskie Holmy" site; this issue requires further research.

6 Secondary Changes in Landslide Massifs

Among the secondary changes, several multidirectional processes leading to both increase and decrease of stability were established.

The most characteristic changes in the properties of the sand column were identified at the "Vorobyovy Gory" site. One of the main secondary changes is precipitation of bivalent iron in the form of oxides and hydroxides in areas with increased permeability, i.e. in the immediate vicinity of landslide deformation zones. This resulted in intensive iron galling. In some areas, the degree of gelation was so high that it led to the transformation of silty-sandy strata into sand-

stones. This effect is established both in the upper part of the slope for the Vorokhobinsky formation and in the lower part of the slope for the Butovskaya formation.

Secondary changes in Jurassic clays consist mainly in changes in consistency and structural-textural features. It was found that landslide bodies associated with Jurassic clay deposits are characterized by a narrow zone of changes in structural and textural features of clays. Thus, at Khoroshevo-I and Khoroshevo-II it does not exceed 0.5–0.6 m, at "Vorobyovy Gory" site it ranges from 0.2–0.4 m in the central part of the landslide body, to 3.0 m in the area of the rear seam, while the zone itself is a system of slip mirrors, the consistency of clays is close to natural, but clays acquire shale texture. In some areas in the lingual part of the landslide body the situation differs significantly. Thus, in the central part of "Vorobyovy Gory" site, one of the wells found several deformation zones up to 4 m thick. Clays in this zone are characterized by disturbed texture: wrinkled, sometimes lumpy, consistency of clays is stiff-plastic to soft-plastic. Similar character of changes was observed also on the landslide massif "Krasnaya Pakhra". For a long time, there was very little information about these zones, it was believed that this zone is a shaft of landslide bodies protrusion. It should be noted that such zones occur only in some areas and are not typical for the entire frontal part of the landslide massif, which was confirmed by drilling data in most landslide areas. At the site of Khoroshevo-I, neither the formation of a bulge shaft nor a thick zone of plastic deformation was found during the activation of landslide processes. Thus, the formation of thick zones with disturbed structure can be explained by moistening of clayey soils by infiltration of groundwater and surface water along the already formed slip surfaces. Secondary deformations contributed to the increase in the thickness of this zone, which led to the current state of the landslide massif.

The thick crushed zones should be given special attention in further studies. The occurrence of such zones with disturbed texture can lead to transformation of the landslide mechanism in some areas from sliding landslides to so-called composite extrusion-sliding landslides, i.e., the occurrence of local plastic deformations.

The occurrence of zones of significant thickness by such a mechanism is confirmed by observations at the Borshevo site. Here, the formation of flow landslides was detected on top of block slip landslides during wetting of the landslide deposits of the Jurassic system.

7 Correlation of Erosion Base and Landslide Deformation Zones

The question of correlation between the erosion base and the displacement surface of landslide bodies is one of the most actual questions concerning, mainly, landslides of type 3. For many areas of the East European Platform and its frame, a close correlation between the position of the displacement surface and the modern erosion base is known, but for landslides in the Moscow River valley such a correlation has not been established before.

There was identified several types of slope massifs according to the correlation between the modern river level and the position of Jurassic clay deposits (Fig. 8). Large differences in the identified geologic conditions served as a basis for the hypothesis about the possibility of the existence of landslides of Pleistocene age within the Moscow River valley, but this idea was not further developed.

In recent years, a large amount of data on displacement surfaces of landslide bodies of type 3 has been collected, which allows us to clarify the ideas about the correlation of landslide deformation zones with the base of erosion.

From the point of view of analyzing deep deformations, of particular interest are landslide massifs on which inclinometer boreholes were installed, namely: Vorobyovy Gory, Kolomenskoye, Khoroshevo-I, Khoroshevo-II.

On the landslide massif Kolomenskoye, on the basis of inclinometric observations were established absolute marks of the zone of landslide deformations in the thickness of clays of the Oxford tier of the order of 102–103 meters. This is considerably deeper than the river day surface (absolute mark of about 110 m). A more detailed analysis of the boreholes drilled on the opposite bank of the river made it possible to establish the position of the bottom of modern alluvial deposits in the area of Kolomenskoye 105 m. Thus, the absolute marks of the main displacement surface are close to the Holocene erosion incision.

At Khoroshevo-I site, based on the results of monitoring in 2006–2007, it was established that the depth of the modern displacement surface in the clays of the Makaryevskaya-Kolomenskaya formations (Oxfordian stage) corresponds to

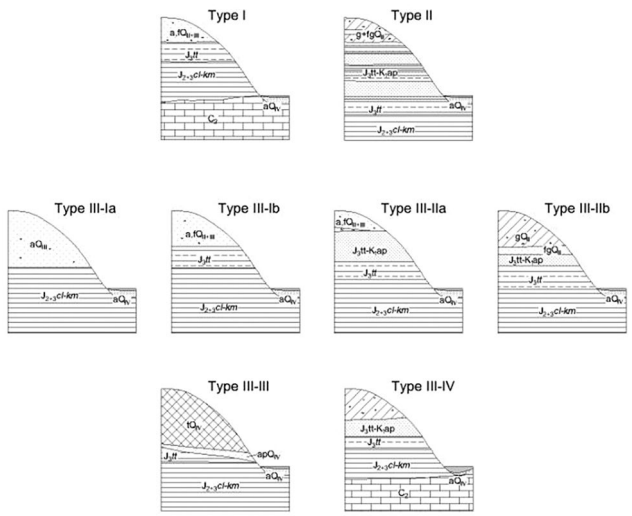


Fig. 8 Types of slope massifs

absolute marks of 118–119 m, which agrees well with the marks of the local erosion base (about 114–115 m). On the landslide massif Khoroshevo-II inclinometric observations conducted by the authors (P.V. Novikov) in 2022–2023 allowed to establish the position of the landslide deformation zone at the marks 116–120 m at the modern erosion base of about 114 m.

The results obtained allowed to establish that the displacement surface of modern landslides is close to the modern erosion base.

The "Vorobyovy Gory" site is an exception. Long-term inclinometric observations conducted in the area of the metro bridge allowed to establish one of the displacement surfaces of the landslide massif at absolute elevations of about 90 m (Zerkal et al. 2021). This is 20 m below the local base of erosion of the Moskva River. It should be noted that the modern erosion incision does not reach the roof of the main deformable horizon. This excludes a significant change in the properties of clayey sediments due to the impact of surface water. Most likely, the formation of the landslide massif took place in conditions different from the modern ones. This is confirmed by palynological analysis of the well drilled in the rear seam depression (Kropotkin 2016). It was found that the lower part of the landslide hollow was filled with a stratum dating to the late Pleistocene. Thus, it can be concluded that the observed deep deformations on the Vorobyovy Gory territory are associated with ancient surfaces of rupture formed at an erosion base different from the modern one.

The analysis of the correlation of the position of displacement surfaces relative to erosion incisions allowed to establish that "Vorobyovy Gory" is not the only ancient landslide massif. Among the known landslide sites a number of massifs with the position of the base of the clayey main deformable horizon above the modern base of erosion stands out. The most characteristic are "Poklonnaya Gora" and "Zelenaya Sloboda" sites. These areas are characterized by the raised relief, without expressed signs of landslide processes. Due to the position of the base of Jurassic clay deposits above the riverbed—limestones of the middle-upper parts of the Carboniferous sediments are exposed to erosion. This excludes active erosion of landslide formations of the Moscow river and the Pakhra river at present. The altitudinal position of the displacement surface of these landslide massifs suggests that the formation of the massifs in time corresponded to the period of accumulation of sediments of the I upper floodplain terrace, which corresponds to the late Pleistocene.

The Khoroshevo-I landslide massif was formed in the early Holocene. The existence of 2 generations of landslides was established. In addition to the generation corresponding to the modern erosion base, a deformation zone with absolute displacement surface elevations of about 110–112 m was found, which corresponds to the depth of erosion incision during the active deepening of river valleys at the Pleistocene-Holocene boundary.

8 Conclusion

There are four types of landslides in the valley of the Moscowriver. Rotation slides in the deposits of the Cretaceous and Jurassic systems are the most important for the impact on the planning of economic activities. Landslides associated with Jurassic clays are most characterized by displacement along surfaces close to circular. On the contrary, landslide bodies associated with the sandy-clay strata of the Lower Cretaceous are characterized by a complex shape of the displacement surface: partly the surface of rupture is confined to clay interlayers, and partly crosses the layering at a steep angle. Both modern and ancient landslide bodies with similar internal structure and displacement mechanism are developed in the valley of the Moscow river. An important role in the development of landslide processes is played not only by the main factors of formation of landslide bodies, but also by secondary changes that can lead not only to changes in stability, but also in the mechanism of landslide processes, as well as contribute to the development of smaller landslides.

Further study of slope processes in the Moscow river valley is of great importance for economic activity. This will help to better understand the landslide massif evolution in the Moscow river valley areas, and will allow more competent and rational planning of engineering protection of the territory.

References

Barykina OS, Zerkal OV, Samarin EN, Gvozdeva IP (2019) The history of slope evolution – primary cause of its modern instability (by example of the "Vorobyovy gory" landslide, Moscow). In: Natural hazards and risk research in Russia: innovation and discovery in russian science and engineering. Springer, pp 345–361. https://doi.org/10.1007/978-3-319-91833-4_24

Danshin BM (1937) The geological structure of the Leninskie Hills in connection with some issues of the stratigraphy of deposits of the cretaceous system and landslide phenomena along the banks of the Moskva river. Izvestiya Moskovskogo geologicheskogo tresta [News of the Moscow Geological Trust] 4:3–23. (in Russian)

Hungr O, Leroueil S, Picarelli L (2014) The Varnes classification of landslide types, an up-date. Landslides 11(2):167–194. https://doi.org/10.1007/s10346-013-0436-y

Kazeev AI, Postoev GP (2012) Estimation of the possibility and scale of the phenomenon of the catastrophic phase of the development of the landslide process in the landslide areas in the valley of the Moscowriver. Problems of reducing natural hazards and risks. Proc. Internat. Conf. "Georisk-2012".RUDN press, Moscow. v. 1: 98–103. (in Russian)

Korchebokov NA, Romanov AV, Yakovlev S (1938) Landslides of the Lenin mountains. Geologija v reconstruktsiy Moskvy [Geology in the reconstruction of Moscow]. ANS SSSR. Moscow-Leningrad, pp 377–390 (in Russian)

Kropotkin MP (2016) Landslide threat assessment for the Vorobyovy gory metro bridge in Moscow. Eng Geol World 3:6–15. (in Russian)

Kuntsel VV (1980) Regularities of the landslide process in the European part of the USSR and its regional forecast. Nedra Moscow:213. (in Russian)

Mitta VV, Alekseev AS, Shik SM (eds) (2012) Unified regional stratigraphic scheme of the Jurassic of East European platform. Explanatory note. Moscow, PIN RAS-VNIGNI. 64. (in Russian)

Novikov PV, Averin IV, Zerkal OV, Samarin EN (2023) New data on the structure of the landslide massif on the territory of Karamyshevskaya embankment. In: Sergeev readings (conf.): fundamental and applied issues of engineering geodynamics (Issue 24). Geoinfo, Moscow, pp 109–112. (in Russian)

Osipov VI, Medvedev OP (eds) (1997) Moscow: geology and city. In: Moscow textbooks and Cartolithography, Moscow, p 400. (in Russian)

Ter-Stepanian G (1977) Types of compound and complex landslides. Bull IAEG 17:72–74

Zerkal OV, Barykina OS, Samarin EN, Gvozdeva IP (2017) The influence of paleo-landslide activity on the modern slope stability. Proc. of ICL-IPL Conference at UNESCO, Paris, pp 89–92

Zerkal OV, Barykina OS, Fomenko IK (2020) Problems and modern development of ideas about large landslides of Moscow (comments on the paper by M.P. Kropotkin, N.A. Orlova “Large landslides of Moscow – new views or new misconceptions?”). Eng Geol World XV(4):30–41. (in Russian)

Zerkal OV, Averin IV, Barykina OS, Malenkina SY, Samarin EN, Fomenko IK, Gvozdeva IP (2021) Landslide processes at the Vorobyovy gory site (Moscow): history of the development of ideas and modern views. In: Proc. “Lomonosov Chteniya (Conf.) 2021”. Section “geology”. MSU Press, Moscow, pp 36–40. (in Russian)

Open Access This chapter is licensed under the terms of the Creative Commons Attribution 4.0 International License (http://creativecommons.org/licenses/by/4.0/), which permits use, sharing, adaptation, distribution and reproduction in any medium or format, as long as you give appropriate credit to the original author(s) and the source, provide a link to the Creative Commons license and indicate if changes were made.

The images or other third party material in this chapter are included in the chapter's Creative Commons license, unless indicated otherwise in a credit line to the material. If material is not included in the chapter's Creative Commons license and your intended use is not permitted by statutory regulation or exceeds the permitted use, you will need to obtain permission directly from the copyright holder.



High-Resolution Rainfall Simulations for Early Warning of Rain-Induced Rapid Long-Traveling Landslides in Sri Lanka

Ryo Onishi, H. A. A. I. S. Bandara, and Koki Matsumoto

Abstract

Reliable rainfall prediction is a key for successful early warning of rain-induced long-traveling landslides. This study assesses the rainfall prediction skill of a high-resolution weather prediction model named the Multi-Scale Simulator for the Geoenvironment (MSSG). The rainfall accumulation is more crucial rather than hour-to-hour rainfall intensity for long-traveling landslide. Three heavy rain events, which caused devastating landslide events in Sri Lanka, are chosen for the assessment: (i) Aranayaka in 2016, (ii) Rilpola in 2017 and (iii) Kiribathgala in 2014. The raingaunge observatory data are compared with the 2 km-resolution MSSG simulation and the Global Satellite Precipitation Map (GSMaP) data with approximately 10 km resolution. Comparison results show that the high-resolution MSSG simulation can represent the 3 day and 24 h rainfall accumulations and also the maximum rainfall intensities better than the GSMaP data. In addition to the assessment for rather short-term prediction, we investigate the exceedance probabilities (EPs) of daily maximum of hourly rainfall intensities at two adjacent raingauge points. The EPs show large difference between the mountainous point and plain point even though their separation is just 4.6 km. The 2 km-resolution MSSG simulation can capture the difference in the two EPs. This confirms the MSSG's reliability in capturing the topographic enhancement of rainfall intensities.

R. Onishi (✉)
Supercomputing Research Center, Institute of Integrated Research, Institute of Science Tokyo, Tokyo, Japan
e-mail: onishi.ryo@gsic.titech.ac.jp

H. A. A. I. S. Bandara · K. Matsumoto
School of Engineering, Department of Mechanical Engineering, Institute of Science Tokyo, Tokyo, Japan
e-mail: bandara.a.aa@m.titech.ac.jp; matsumoto.k.bj@m.titech.ac.jp

Keywords

Rainfall prediction · Numerical weather simulation · Long-traveling landslide · Early warning · Exceedance probability

1 Introduction

In tropical regions including Sri Lanka, rainfall is one of the main triggering factors of landslides. For example, Aranayaka region received high-intensity rainfall and resulting devastating long-travelling landslide in May 17, 2016, causing severe human and economic loss.

The rainfall monitoring is of course crucial for landslide warning. However, we need prediction information for early waning for securing enough time for evacuation. The numerical weather simulation is a promising tool for providing rainfall predictions.

Sri Lanka, as a tropical island, receives intense rainfall during two major monsoons each year: the first monsoon (South and Southwestern region) in May to September and the second (North and Northeastern region) in December to February. During these seasons, catastrophic landslides have occurred periodically, and records show an increasing tendency of events and losses. Particularly, long-traveling debris flows due to landslides tend to cause severe damages as they destruct widely. Those landslides seem to be caused by large amount of rainfall accumulations. Examples include 240 mm of 3-day rainfall accumulation triggered a long-travelling landslides in Rilpola, Sri Lanka, on 26 December, 2014; 418 mm one in Aranayake on May 17, 2016; 326 mm one in Athweltota on May 25, 2017; 500 mm one in Morawakkanda on May 25, 2017 and 420 mm one in Kiribathgala on May 26, 2017. This study thus focuses the rainfall accumulation predictions as well as the hourly rainfall intensities.

Figure 1 explains the Multi-Scale Simulator for the Geoenvironment (MSSG) (Takahashi et al. 2006; Onishi

© The Author(s) 2025

B. Abolmasov et al. (eds.), *Progress in Landslide Research and Technology, Volume 3 Issue 2, 2024*, Progress in Landslide Research and Technology, https://doi.org/10.1007/978-3-031-72736-8_10

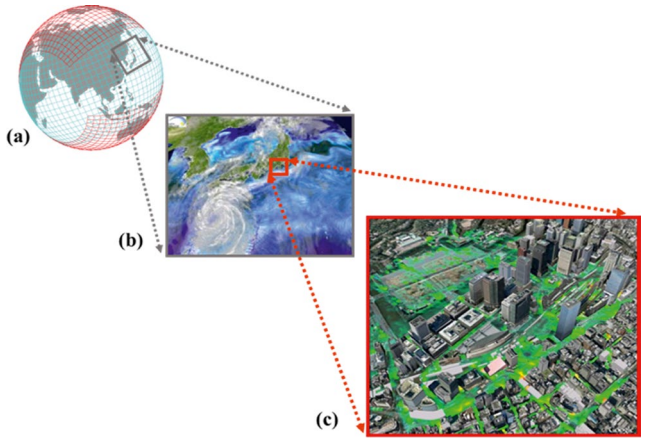


Fig. 1 MSSG is designed to be applicable to (**a**) global scale, (**b**) meso scales and up to (**c**) urban scales. The Yin-Yang grid system, which consists of two overlapping latitude-longitude grids indicated in blue and red, is adopted for global simulations

and Takahashi 2012; Takahashi et al. 2013) developed by Tokyo Institute of Technology, Japan Agency for Marine-Earth Science and Technology and Waseda University, which is one of the numerical weather models. MSSG is a coupled non-hydrostatic atmosphere-ocean-land global circulation model that permits seamless simulations among climate (global), weather (regional) and up to urban (local) scales. This MSSG can provide local rainfall predictions that can meet the need of the landslide early warning system in Sri Lanka. In the regional scale simulations, MSSG adopts a conventional latitude-longitude system to allow using robust high-order differential schemes.

In this study, we assess the reliability of MSSG high-resolutions simulations in comparison with the local rain-gauge observation data in Sri Lanka.

2 MSSG Simulations for Heavy Rainfall Events in Sri Lanka

2.1 Heavy Rain Events in Sri Lanka

Sri Lanka often suffers from devastating landslides caused by heavy rainfall. This study focuses on long-traveling landslides, which are usually caused by large rainfall accumulations rather than time-to-time rainfall intensities. Table 1 shows recent three major landslide events that are selected for the present rainfall simulation assessment. Those selected events were thought to be caused by 3-day continuous rainfall with last 24 h accumulation exceeding 100 mm. Figure 2 shows the locations of three selected landslides. All the three landslides happened in the mountain region in the south of Sri Lanka.

Table 1 Three recent devastating landslide events in mountainous regions in Sri Lanka

	Area name	Location (lon, lat)	Altitude	Incident time
Event-1	Aranayaka	(80.43E, 7.15 N)	905 m	11:00UTC 2016/5/17
Event-2	Rilpola	(81.06E, 6.94 N)	908 m	1:20UTC 2014/12/26
Event-3	Kiribathgala	(80.51E, 6.61 N)	384 m	2:30UTC 2017/5/26

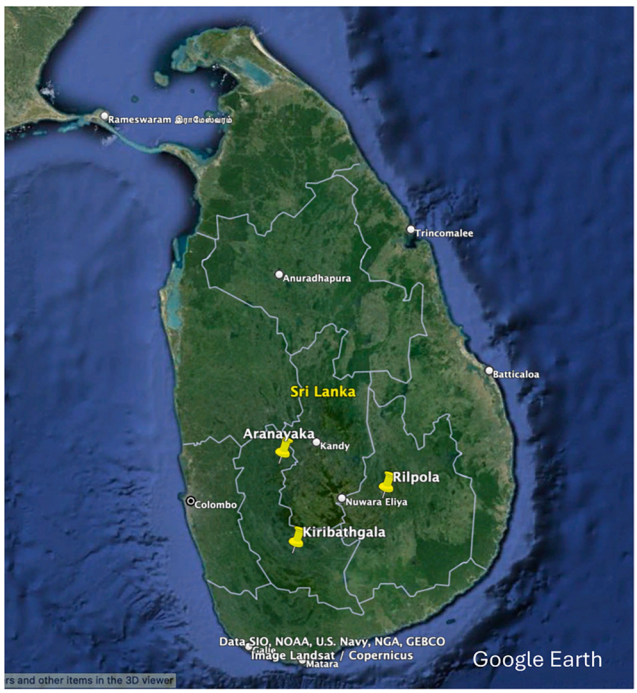


Fig. 2 Recent three major long-traveling landslide locations in Sri Lanka

Table 2 Specification of rainfall that caused the landslide events in

	Simulation period (3 days)
Event-1	00UTC May15 - 00UTC May 18, 2016
Event-2	00UTC Dec 23 - 00UTC Dec 26, 2014
Event-3	00UTC May 23 - 00UTC May 26, 2017

2.2 Computational Setting

We performed MSSG rainfall simulations for three heavy rainfall events shown in Table 1 to evaluate the MSSG simulations. Table 2 shows the simulation periods, which target the landslide incident times. The MSSG simulations computed the meso-scale weather in three two-way-coupled nest domains. Figure 3 shows the computational domains for Event-1, centering the Aranayaka landslide area. Three two-way-coupled nest-

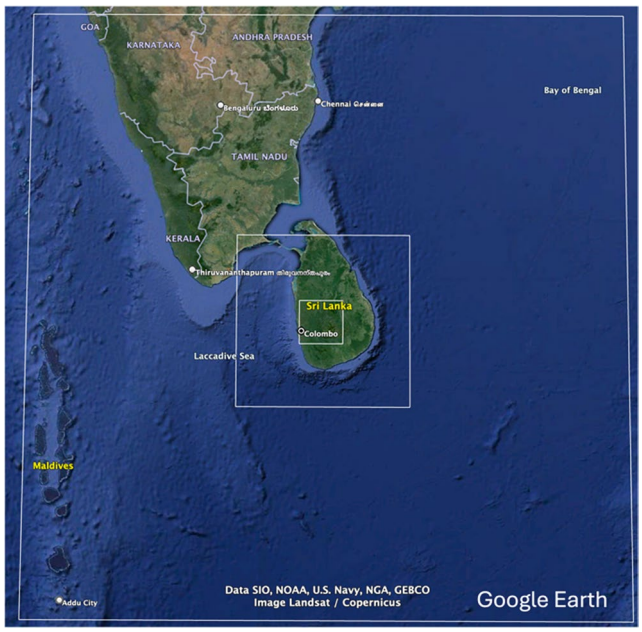


Fig. 3 Computational domain for Event-1. Three two-way-coupled nesting domains center the landslide area

ing domains re used. Table 3 shows the grid and resolution settings for the domains. For the other two events, the domains centered the corresponding landslide areas, shown in Table 1.

The global-scale model (GSM) data of Japan Meteorological Agency (JMA) was used for the initial and boundary conditions for the MSSG simulations. Each MSSG simulations were performed for 6 h and restarted every 6 h for the present validation experiment. That is, 12 simulations were successively performed for each 3-day simulations. The JMA-GSM data were assimilated into the MSSG restart files with the optimal interpolation method. This data assimilation method can be used for operations. The detail explanation on methodology can be seen in our previous study (Bandara and Onishi 2023).

2.3 Raingauge Data

The National Building Research Organization (NBRO), Sri Lanka, establishes a rainfall monitoring network to landslide prone region (South-West part) in Sri Lanka. The realtime monitoring data can be seen in the internet (http://www.rainfall.nbro.gov.lk:8080/mapforweb/all/mapview.aspx). The authors calculated the monitoring cover area using google map and the estimate was roughly 13,000 km^2. 331 raingauges are installed and in operation. That is, the raingauges are installed roughly every 6 km.

This study uses the data obtained by the raingauges located nearby the landslide incident locations. For Event-1, the data at (80.459E, 7.159N) (R27-Aranayake point) was used. The distance between the landslide incident location and the raingauge location is 3.5 km. For Event-2 and -3, the distances are 4.0 km and 3.5 km, respectively.

Table 3 Grid and domain settings for each nest domain

	Number of horizontal grids	Horizontal grid spacing
Level-0 domain	64 × 64	20 km
Level-1 domain	64 × 64	8 km
Level-2 domain	64 × 64	2 km

2.4 GSMaP Data

The Global Satellite Precipitation Map (GSMaP) is a global rainfall map developed under the Global Precipitation Measurement (GPM) project by combining the dual-frequency precipitation radar onboard the GPM satellite, multiple rainfall monitoring satellites and geostationary meteorological satellites (Kubota et al. 2020). The data is available in the internet (https://sharaku.eorc.jaxa.jp/GSMaP/index.htm). The spatial resolution of the GSMaP rainfall data is 0.1 degrees (i.e., about 11 km resolution near the equator) and the temporal resolution is 1 h. The data can be categorized as an observation, not simulation data.

The difference between the GSMaP and raingauge data is in the spatial resolution: The raingauge data is obtained at a point, while the GSMaP data shows the rainfall averaged over approximately 10 km × 10 km area. It should be noted that the weather numerical simulations, which compute meteorological variables on finite-sized grids, cannot obtain point data but spatially-averaged data, specifically data averaged over grid volume. It is, therefore, not very correct to directly compare the raingauge data and simulation results. The GSMaP data, which provides spatially-averaged observation data, can fill the gap between the raingauge data and simulation results.

2.5 Results and Discussion

Figure 4 shows hourly-rainfall intensities obtained from the raingauge observation, GSMaP analysis and the MSSG simulation. The MSSG plots show the rainfall intensities at a grid point (with 2 km size) near the raingauge location. For Event-1, the MSSG data location was (80.455E, 7.166N) and the location distance between the MSSG grid point and raingauge location was 1.1 km. For Event-2 and -3, the distances were 0 km and 1.1 km, respectively. There are significant mis-

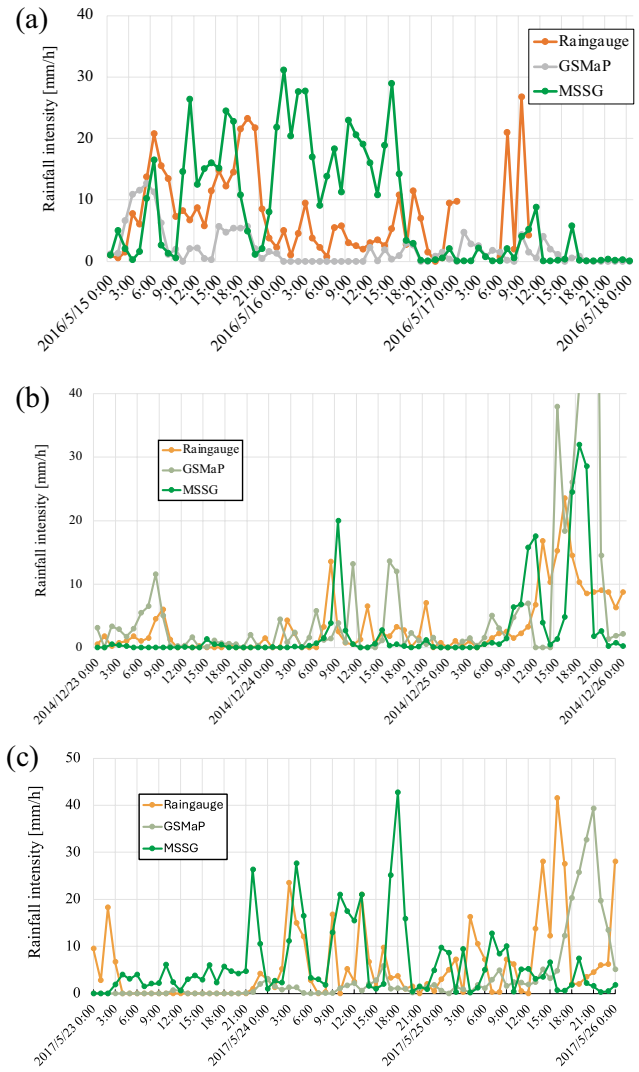


Fig. 4 Hourly rainfall intensities for (**a**) Event-1, (**b**) Event-2 and (**c**) Event-3

Table 4 Rainfall statistics for Event-1. The last column shows the 24 h rainfall accumulation preceding to the landslide incident, i.e., accumulation from 11UTC May 16 to 11UTC May 17

	3 day rainfall accumulation	Max hourly-rainfall intensity	24 hour rainfall accumulation
Raingauge	418.8 mm	26.8 mm/h	124.3 mm
GSMaP	144.6 mm	12.7 mm/h	34.2 mm
MSSG	604.3 mm	31.1 mm/h	141.0 mm

matches in hour-to-hour timings between the raingauge observations and MSSG results. Nevertheless, the MSSG simulations reproduce the level of rainfall intensities well. That is, even though the MSSG cannot predict the heavy rains in short timescales, it can do accumulations for long terms.

Tables 4, 5 and 6 show the rainfall statistics for Event-1, -2 and -3, respectively. The agreement between rain-

Table 5 Rainfall statistics for Event-2. The last column shows the 24 h rainfall accumulation preceding to the landslide incident, i.e., accumulation from 00UTC Dec 25 to 00UTC Dec 26

	3 day rainfall accumulation	Max hourly-rainfall intensity	24 hour rainfall accumulation
Raingauge	240.9 mm	23.5 mm/h	172.5 mm
GSMaP	467.0 mm	120 mm/h	349.2 mm
MSSG	189.2 mm	31.9 mm/h	150.6 mm

Table 6 Rainfall statistics for Event-3. The last column shows the 24 h rainfall accumulation preceding to the landslide incident, i.e., accumulation from 00UTC May 25 to 00UTC May 26

	3 day rainfall accumulation	Max hourly-rainfall intensity	24 hour rainfall accumulation
Raingauge	420.0 mm	41.5 mm/h	239.3 mm
GSMaP	241.4 mm	39.3 mm/h	205.8 mm
MSSG	461.4 mm	42.7 mm/h	106.3 mm

gauge data and MSSG results is overall better than that between raingauge data and GSMaP data. One exception is the 24 h rainfall accumulation for Event-3, for which the MSSG result shows significant underestimation. The MSSG, however, succeeded in reproducing the large accumulation over 100 mm. As for the 3 day rainfall accumulation and the maximum of hourly-rainfall intensities, the MSSG results match the raingauge data better than GSMaP data. This means that the high-resolution (2 km horizontal resolution in this study) of MSSG simulations contributes to the better representations of rainfall statistics.

3 Exceedance Probability of Daily-Maximum Rainfall Intensity in Aranayaka Region

3.1 Exceedance Probability

The probability density distribution (PDF) is usually investigated in order to examine the occurrence probability of severe phenomena. However, obtaining a sufficiently reliable PDF requires a large amount of data. When discussing occurrence probabilities with limited data, the exceedance probability (EP) can be another option. An EP refers to the probability of an event occurring above (or below) a certain value. It is used widely in the quantitative assessment of risks such as earthquakes and floods.

The EP (p_{exd}) of value X shows the probability that the value of a target variable exceeds X. The EP is derived as

$$p_{exd} = \frac{m(X)}{N+1} \times 100, \quad (1)$$



Fig. 5 Raingauge locations. Aranayaka raingauge (ARA) locates in steep mountain area, while Hemmatagama one (HEM) in relatively flat area. The distance between the two raingauges is 4.6 km

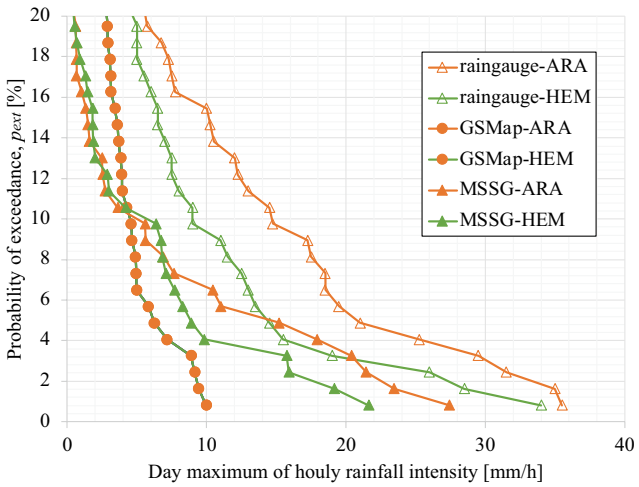


Fig. 6 Exceedance probability of daily maximum of hourly rainfall intensities for 4 months of April–July 2023

Table 7 Grid and domain settings for each nest domain

	Number of horizontal grids	Horizontal grid spacing
Level 0 (parent domain)	64 × 64	8 km
Level 1 (child domain)	64 × 64	2 km

where N shows the total number of events or data points on record and m ($1 \leq m \leq N$) represents the rank (order) of the data with the value of X out of the whole record.

In this study, we focus on the daily maximum of hourly rainfall intensities for the 4 months (122 days) of April–July in 2023, a south-west monsoon season in Sri Lanka.

3.2 Observation Data and MSSG Simulations

We collected raingauge data in Aranayaka region. Figure 5 shows the 2 raingauges selected; R27-Aranayake point (ARA) at (80.459E, 7.159 N) and L83-Hemmentagamma point (HEM) at (80.498E, 7.173 N) locating next to each other. The distance between the two points is 4.6 km.

MSSG simulation was performed to the same period with the obtained raingauge data, i.e., for the 4 months of April-July in 2023. The two two-way-coupled nesting domains were used as in Table 7, centering the Aranayaka area. Each simulation was for 6 h and it was restarted every 6 h to cover the 4 months. The JMA-GSM data were used for the initial (00:00UTC, 2023/4/1) and boundary conditions.

3.3 Comparison Results

Figure 6 shows the EPs of daily maximum of hourly-rainfall intensities at the 2 raingauge locations (ARA and HEM). The ARA raingauge data show significantly larger EP for large rainfall intensities than the HEM. As shown in Fig. 5, ARA locates in mountainous area, while HEM in rather flat area. Thus, the difference in EPs can be attributed to the topographic rainfall; steep topographies intensify the rainfall due to updrafts along slopes and consequent adiabatic expansion, which enhance cloud formation and rainfall.

The MSSG results underestimate EPs, while show the same tendency that the EPs for ARA are larger than those for HEM with that observed in raingauge data. For comparison purpose, GSMaP data are also drawn in the figure. GSMaP data also significantly underestimate the EPs. Furthermore, GSMaP data for ARA are exactly the same with that for HEM. This happens because GSMaP resolution is approximately 10 km, which is larger than the separation between ARA and HEM locations. MSSG EPs are more closer to the raingauge EPs for large rainfall intensities over 10 mm/h. These results confirm that the MSSG simulation, owing to its high resolution, can capture the topographic influence that enlarges rainfall intensities.

4 Future Directions

4.1 Higher Resolution Simulations

Our previous study (Bandara and Onishi 2023) showed that 500 m horizontal resolutions are required to capture the steep orography in mountainous regions in Sri Lanka. This study performed up to 2 km resolutions as the computational cost is intense for long time integrations such as the integration for 4 months of April–July in 2023. We have developed a deep neural-network (DNN) super-resolution (SR) method (Onishi et al. 2019; Yasuda et al. 2022) to downscale 2 km resolution rainfall maps into 500 m resolution ones. The inte-

gration of 2 km resolution simulations and the DNN-SR method can offer feasible computational cost even on a workstation, rather than a supercomputer.

4.2 Turbulence Impact on Topographic Rainfall

Recent research has proven that the turbulence enhancement of collision growth can impact on cloud development (Falkovich and Pumir 2007; Grabowski and Wang 2013). Our previous study (Bandara and Onishi 2023) implemented the turbulence-aware cloud microphysics (Seifert and Onishi 2016) into MSSG and showed that the turbulence enhancement of droplet collisional growth can impact on topographic rainfall significantly. The impact was investigated for idealized topography, i.e., two-dimensional bell-shaped mountains. The impact for real topography has not been clarified yet. This should be assessed, and the present study can be a basis for the assessment of the impact.

5 Conclusions

The rainfall prediction map from numerical weather simulations is one of the relevant keys for the successful early warnings of long-travelling landslides. The high-resolution Multi-Scale Simulator for the Geoenvironment (MSSG) that can capture the topographic impact on the rainfall intensities is one of the promising weather simulation model. This study selected recent three heavy rain events, that caused devastating long-traveling landslides in Sri Lanka: (i) Aranayaka in 2016, (ii) Riplola in 2014 and (iii) Kiribathgala in 2017. The raingauge data are compared with the 2 km-resolution MSSG simulation results and GSMaP data that has approximately 10 km resolution. Comparison results show that the high-resolution MSSG simulation can represent the 3 day and 24 h rainfall accumulations and also the maximum rainfall intensities better than the GSMaP data.

In addition, we have investigated the exceedance probabilities (EPs) of daily maximum of hourly rainfall intensity for 2 different adjacent raingauge points, whose distance is 4.6 km, in Aranayaka region in Sri Lanka. The observatory EPs show large difference between the mountainous point and plain point even though their separation is a walking distance. The difference can be attributed to the topographic impact on rainfall intensities. That is, steep slope can enlarge rainfall intensities. The 2 km-resolution MSSG simulation can capture the difference in the two EPs. This confirms the MSSG's reliability in capturing the topographic enhancement of rainfall intensities.

Acknowledgments This research was supported by the Science and Technology Research Partnership for Sustainable Development (SATREPS). The authors thank the National Building Research Organization (NBRO), Sri Lanka, for providing the raingauge observatory data. Part of the MSSG simulations were performed on the supercomputer system, Tsubame3.0, in Tokyo Institute of Technology.

References

Bandara HAAIS, Onishi R (2023) High resolution numerical weather simulation for orographic precipitation as an accurate early warning tool for landslide vulnerable terrains. Prog Landslide Res Technol 2(2):239–246

Falkovich G, Pumir A (2007) Sling effect in collisions of water droplets in turbulent clouds. J Atmos Sci 64:4497–4505

Grabowski WW, Wang L-P (2013) Growth of cloud droplets in a turbulent environment. Annu Rev Fluid Mech 45:293–324

Kubota T, Aonashi K, Ushio T, Shige S, Takayabu YN, Kachi M, Arai Y, Tashima T, Masaki T, Kawamoto N, Mega T, Yamamoto MK, Hamada A, Yamaji M, Liu G, Oki R (2020) Global satellite mapping of precipitation (GSMaP) products in the GPM era. In: Satellite precipitation measurement. Springer. https://doi.org/10.1007/978-3-030-24568-9_20

Onishi R, Takahashi K (2012) A warm-bin-cold-bulk hybrid cloud microphysical model. J Atmos Sci 69:1474–1497

Onishi R, Sugiyama D, Matsuda K (2019) Super-resolution simulation for real-time prediction of urban micrometeorology. SOLA 15:178–182

Seifert A, Onishi R (2016) Turbulence effects on warm-rain formation in precipitating shallow convection revisited. Atmos Chem Phys 16:12127–12141

Takahashi K, Peng X, Onishi R, Ohdaira M, Goto K, Fuchigami H, Sugimura T (2006) Multi-scale weather/climate simulations with Multi-Scale Simulator for the Geoenvironment (MSSG) on the Earth Simulator, Annual Report of the Earth Simulator Center, April 2005–March 2006, pp. 31–39

Takahashi K, Onishi R, Baba Y, Kida S, Matsuda K, Goto K, Fuchigami H (2013) Challenge toward the prediction of typhoon behaviour and down pour. J Phys Conf Ser 454(012):072

Yasuda Y, Onishi R, Hirokawa Y, Kolomenskiy D, Sugiyama D (2022) Super-resolution of near-surface temperature utilizing physical quantities for real-time prediction of urban micrometeorology. Build Environ 209:108597

Open Access This chapter is licensed under the terms of the Creative Commons Attribution 4.0 International License (http://creativecommons.org/licenses/by/4.0/), which permits use, sharing, adaptation, distribution and reproduction in any medium or format, as long as you give appropriate credit to the original author(s) and the source, provide a link to the Creative Commons license and indicate if changes were made.

The images or other third party material in this chapter are included in the chapter's Creative Commons license, unless indicated otherwise in a credit line to the material. If material is not included in the chapter's Creative Commons license and your intended use is not permitted by statutory regulation or exceeds the permitted use, you will need to obtain permission directly from the copyright holder.



Application of Subsurface Drainage for Cost-Effective Mitigation Strategies: A Case Study of Hakgala Landslide, Sri Lanka

S. H. S. Jayakody, Buddhika Kumarage, and Asiri Karunawardena

Abstract

Subsurface drainage is a common technique used to stabilize slopes and maintain sustainable water levels. This paper discusses the use of subsurface drainage to stabilize a backslope of a retaining wall located at an arterial highway in Sri Lanka that had undergone failure due to excess water pressure. The sustained loading from the failed debris on the structurally conceded wall made the rectification work more challenging. Therefore, it was necessary to adopt a cost-effective solution as a temporary measure to hold the failed debris until permanent measures were implemented. The study used field measurements and numerical modelling to analyze the effects of infiltration and groundwater flow on the slope before and after subsurface drains were employed. Introducing subsurface drains and controlled infiltration improved the slope's stability and significantly avoided forming a perched water table. With the successful completion of this project, using non-structural measures accompanied by an accurate seepage analysis, design, and a monitoring plan proved to be a cost-effective solution for stabilizing highly saturated unstable slopes.

Keywords

Subsurface drainage · Slope stability · Seepage analysis · Road cut failures

S. H. S. Jayakody (✉)
Disaster Prevention Research Institute, Kyoto University, Kyoto, Japan
e-mail: jayakody.sanchitha.8d@kyoto-u.ac.jp

B. Kumarage · A. Karunawardena
National Building Research Organisation, Colombo, Sri Lanka

1 Introduction

Sri Lanka, a country with tropical weather, is now experiencing climate change, resulting in high-intensity and prolonged rainfall. Similar to many parts of the globes, these are significant factors in triggering slope failures in Sri Lanka (Nawagamuwa and Perera 2017). Apart from rapid and long traveling landslides akin the Aranayaka landslide in 2016 (Dang et al. 2019), road cut failures are indeed found to be a major and recurring threat to the national highway and requires special attention almost every year. This threat causes us to spend millions of dollars on direct costs associated with repairing and implementing structural measures and indirect costs such as increased travel distance.

Given slope properties and geometry are vital conditions for assessing slope stability, rainfall infiltration is one such process that can generate excess pore water pressure within the slope when combined with groundwater flow. It is a well-accepted fact that the excess porewater pressure produced by the hydrological process can reduce the effective stresses on the soil, increasing the likelihood of slope instability. Accordingly, drainage trenches, vertical drainage systems, and horizontal drains often stabilize road-cut slopes and prevent excess porewater pressures. The utilization of horizontal drainage (HD) systems has been frequently demonstrated to be an effective and economically viable dewatering technique for maintaining slope stability not only in road-cut slopes (Rahardjo et al. 2011) but also in slow-moving landslides (Kankanamge 2020).

For a given slope, the effectiveness of an HD system is contingent upon a range of factors, including the position of the drain on the slope, the inclination, and the length, as found out by many researchers over the past few decades in addition to the inherent properties of soil in the region. Additionally, Lakruwan et al. (2021) examined different types of perforations, and longitudinal perforations provided

© The Author(s) 2025

B. Abolmasov et al. (eds.), *Progress in Landslide Research and Technology, Volume 3 Issue 2, 2024*, Progress in Landslide Research and Technology, https://doi.org/10.1007/978-3-031-72736-8_11

the best performance. Numerical simulation of HD and its performance were elaborated, taking simple examples as well as considering case studies (Cai et al. 1998, Rahardjo et al. 2003). These works provided valuable insight into determining optimum conditions for the proper functioning of HD to minimize the development of excess porewater pressure, thus reducing the probability of slope failures.

In essence, this study details the process of backslope stabilization during the replacement of the damaged retaining wall adjacent to the Peradeniya-Badulla National Highway at Hakgala in the Nuwara Eliya district of Sri Lanka. This paper aims to present a case study incorporating theories of unsaturated soil mechanics to enhance the effective stress of soil by removing excess porewater pressure, thus formulating a cost-effective non-structural solution for stabilizing a highly vulnerable slope under rainfall infiltration and groundwater flow.

The failure mechanism was studied in terms of rainfall intensity, hydraulic properties of the slope, geomorphology, geological setting, and soil parameters. A pre-construction study was conducted to examine the utilization of efficient subsurface drainage control to stabilize the backslope. The effectiveness of the proposed measures was evaluated using a numerical simulation, which utilized data from field instruments and test data obtained from soil samples at different depths. The influence of infiltration and groundwater flow in correspondence with predefined precipitation events was investigated through seepage analysis. Additionally, the stability of the slope corresponding to each seepage condition was evaluated using limit-equilibrium analysis. This paper presents the outcomes and discoveries of the pre-construction study herein. The design and analysis of the new gravity wall proposed to retain the failed slope were also carried out as a part of this project. However, the authors do not discuss this process in this paper.

2 Distinguishing Problems of the Project

This project distinguishes itself from conventional slope stabilization methods due to a combination of distinctive design and application complexities:

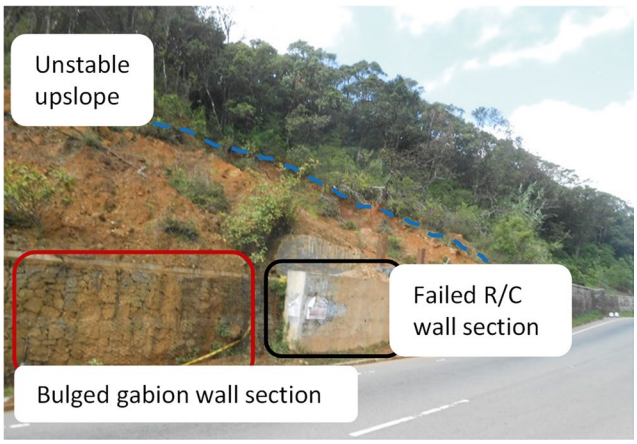


Fig. 1 Condition of the slope at the investigation stage

1. The existing reinforced concrete retaining wall had undergone stem base failure due to unsustainable destabilizing moments (Fig. 1).
2. The relatively steep slope behind the failed wall, combined with the presence of slurry-like debris, continued to apply destabilizing forces to the already failed wall.
3. The geological characteristics of the slope facilitated the development of a shallow perched water table aided by the large catchment feeding the study area (Fig. 2).
4. The conditions outlined in points 2 and 3, along with the slope extending a considerable distance from the top of the wall without any breaks or steps, introduced a high degree of unreliability to any steep excavation.
5. The existence of dense residual layers rendered the installation of temporary retaining solutions, such as sheet piles, unfeasible.
6. Due to the nearby creek, there was limited space available for rerouting the current highway, and there needed to be more room to build an extra gravity wall to stabilize the slope without dismantling the existing wall.

Hence, the standard stabilization methods commonly used, including soil nailing, anchoring, sheet piling, and secondary gravity walls, were deemed unsuitable at the initial project proposals. The most favorable approach was to install a replacement gravity wall section.

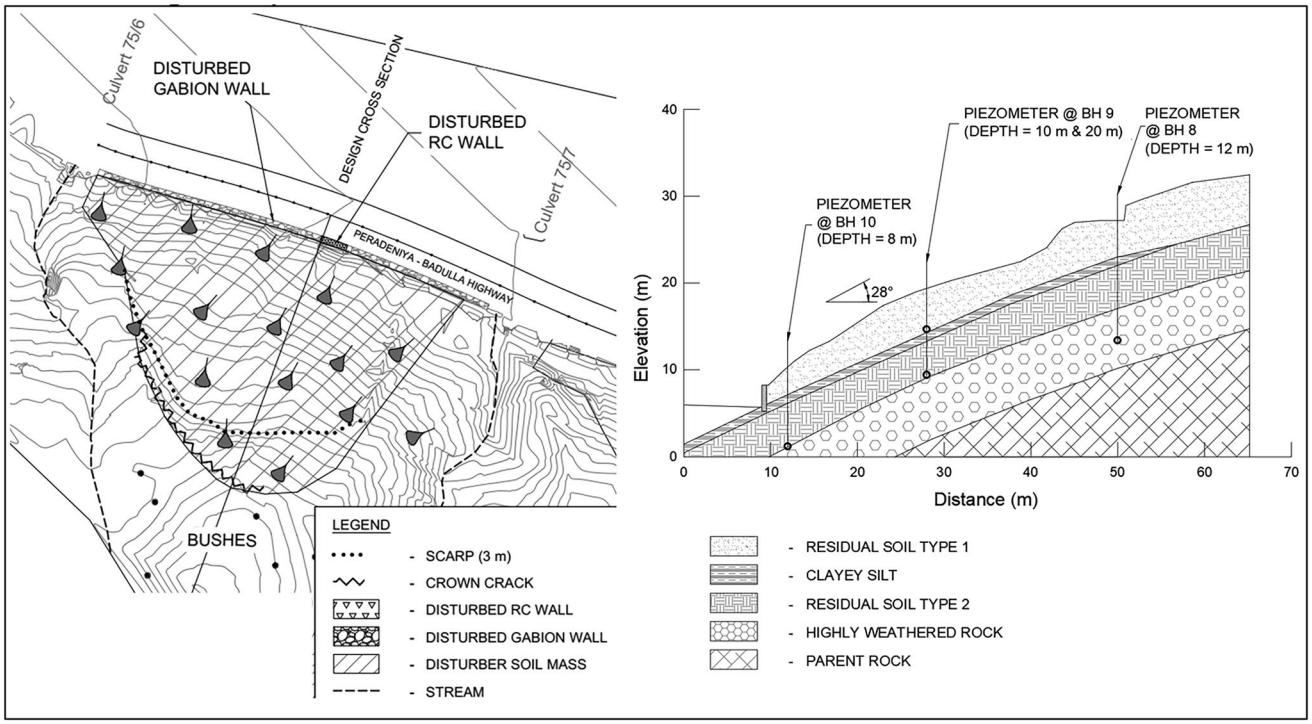


Fig. 2 (**a**) Plan view of the study area (**b**) Cross section of the geotechnical model and the details of piezometers

3 Geological Condition and the History of the Study Area

The slope under consideration is adjacent to the Peradeniya-Badulla National Highway between culvert 75/6 to 75/7 at Hakgala in the Nuwara Eliya district of the Central Highlands of Sri Lanka. The slope rectification of this area was conducted as a part of a large slope rectification project named "Climate Resilience Improvement Project (CRiP)," funded by the World Bank and implemented from 2017 to 2019.

Previously, the slope had been retained by a reinforced concrete retaining wall flanked by two Gabion wall sections, consequent to the road widening. With inclement rainfall, the wall's backslope underwent failure, resulting in a wall stem failure. From time to time, starting in 2010, progressive collapses have despite the attempts made by authorities to strengthen the walls. The overall slope angle was 25–30 degrees, and the wall stem was 2.5 m in height and 550 mm thick. The 2.5 to 3 m high adjacent Gabions had also been bulged and tilted due to the backslope failures (Fig. 1). The slope ascends towards the Hakgala mountain range beginning from the crest of the wall without any slope breaks. This continuation of slope indicates that the wall is located at the toe of a large catchment, which receives a relatively high level of precipitation.

The site is located in between the Gurutalawa synform and Nuwara Eliya antiform overlying a Garnet-Sillimanite-Biotite Gneiss parent rock as per the geology maps of Sri Lanka. The area's subsoil consisted of residual formations of brownish sandy/silt clay. Outcrops of fractured rock are also present at adjacent slopes but in the study area. Shallow transitional slides at the backslope and a 3.0 m scarp at the crown of the failure were visible during the investigation phase. Loose colluvial soils originating from the initial slide were seen at the toe region of the slope near the crest of the tilted wall. Slump blocks formed during the initial slope failure were also visible below the top scarp (Fig. 2). A comprehensive analysis of the weathering profile of the slope verified that the subsurface of the slope mass had formed through the disintegration of Precambrian-aged Garnet-Sillimanite-Biotite Gneiss parent rock. A weak soil stratum underlying relict geological structures inherited from the parent bed rocks plays a significant role in slope failures in Sri Lanka, particularly in the Central Highlands. Studies of landslides in these regions provide clear evidence to suggest that the slips occur due to the breakdown of Precambrian-age quartzite, pegmatite, and marble-metasedimentary/meta igneous parent rocks (Amarasinghe et al. 2002).

Similarly, the slip surface in the study area had developed underlying a soft clay stratum of kaolin composition, which is of whitish appearance. Kaolin clay is one of the fully weathered derivatives of the parent Garnet-Sillimanite-Biotite Gneiss rock, which is feldspar-dominant. Soils of quartzite origin, characterized by a high degree of permea-

bility, overlie the slip surface material, facilitating substantial surface water infiltration and forming a shallow perched water table above the slip surface area. Seepage was identified through the slope at the crest level of the wall and the Gabions, suggesting a stratum with lower permeability underlying the slope mass.

4 Investigations of the Surface and Subsurface

The study began with a simultaneous implementation of a topographical survey and a superficial geological examination of the study area. Concurrent execution of these tasks enabled the production of a comprehensive outcome that encompasses all topographical elements crucial for informed decision-making during the problem-resolution process. Based on the output of these initial investigations, a borehole investigation was conducted. Three borehole investigations were conducted along the problem area's most critical cross-section to identify the slip surface's depth and formation. The substratum was determined with the aid of investigations, as shown in Fig. 2b.

Moreover, two 2.0 m deep test pits were used to identify the underlying weak stratum, which may not be detected from the borehole investigation results due to the layer's thinness (Fig. 3). Observing the sides of the test pits, we easily identified the underlying soft clay stratum of kaolin composition from the whitish appearance. Additionally, from the bands of pink to red in this layer, it was further determined that this stratum is the completely weathered Garnet-Sillimanite-Biotite Gneiss parent rock.

Additionally, the exposures at the scarp were also taken into consideration when developing the subsurface profile.

Figure 2b depicts piezometer depths and elevations for clarity. Recorded rainfall data for the site was retrieved from the rain gauges operated by the Department of Meteorology close to the study area to derive the design of critical rainfall events. Moreover, the seepages observed through the Gabions and the slope face during the field investigation were documented for consideration in the seepage analysis.



Fig. 3 Mid-slope test pit confirming underlying soft clay stratum of kaolin composition and the perched water table

5 Seepage Analysis

5.1 Seepage Model

The seepage evaluation was conducted utilizing the SEEP/W (GEO-SLOPE International Ltd. 2012b) module of GEO STUDIO 2012 software. SEEP/W module was used to generate the pore water pressures for each type of stability analysis discussed in the following sections. "Transient" seepage analysis was used to assess the variations of infiltration and pore water pressure with time. The initial head was defined using a piezometric line based on the piezometer readings at steady-state groundwater conditions. The hydraulic parameters derived based on the data acquired during the site investigation presented in Table 1 were assigned to each material in the seepage model. The seepage model for the initial analysis is presented in Fig. 4. The geometry of the model, however, was changed in each analysis situation, as described in later sections. The boundary conditions used in the model are presented in Table 2.

Table 1 Material properties used in SLOPE/W and SEEP/W modules

Soil type (from top to bottom)	legend	Cohesion (kPa)	Friction angle (Deg)	Unit weight (kN/m3)	Saturated permeability (m/s)	SWCC	Permeability function
Residual soil—Type 01		8	28	17	4e-06	Silty sand [a]	Estimation based On VG [b]
Clayey silt		6	20	17.5	2e-08	Silty clay [a]	
Residual soil—Type 02		12	32	18	2e-07	Silty sand [a]	
Highly weathered rock		50	45	20	5e-09	Saturated only material model	
Parent rock/ RC Wall		High strength material model		22		NA	

[a] Built-in function available in the SEEP/W module
[b] Based on the estimation method by Van Genuchten (VG) (1980) available in the SEEP/W module

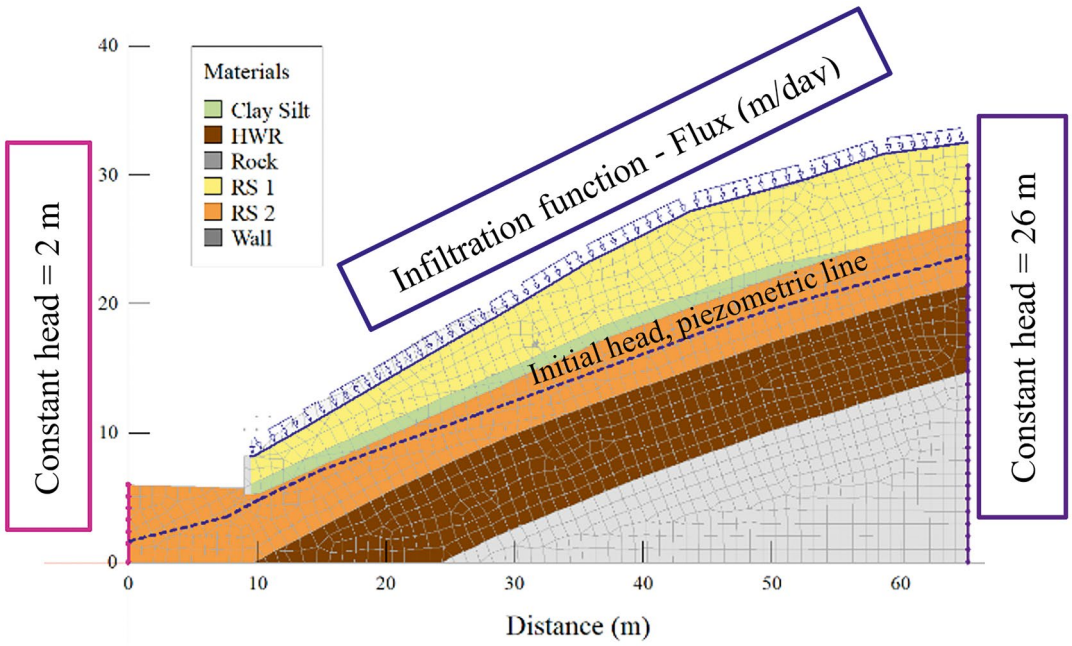


Fig. 4 Seepage model for the slope before failure and boundary conditions used

Table 2 Boundary conditions used in the seepage model

Name	Color	Kind	Constant/ Function
Rainfall		Water flux	Function (Fig. 5)
Head—RHS		Water total head	Constant = 26 m
Head—LHS		Water total head	Constant = 2 m

A function of rainfall flux vs time was used as the "Rainfall" boundary condition input, and the data used in this function is presented in Fig. 5 as a graph. This function would, however, also be varied in each analysis situation. In particular, rainfall data during the time of failure were incorporated into this function in the back analysis situations. Moreover, the constant total head functions were based on the data from the installed piezometers.

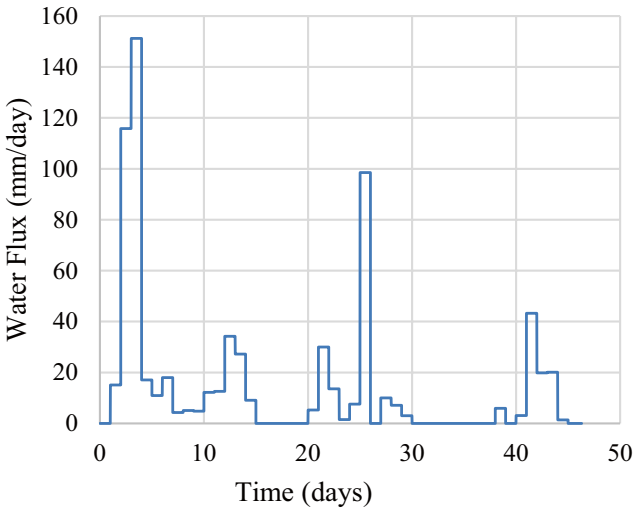


Fig. 5 Rainfall hydraulic boundary function (Used for the initial back analysis of failure)

5.2 Seepage Model Calibration

Calibration of the seepage model in terms of geometry and the seepage parameters of the materials was done using piezometer readings as well as the observed seepages through the slope face corresponding to rainfall events. Piezometer readings were taken for a period of 45 days during the periods of relatively high rainfall in April—May 2018. The recorded data from Piezometers were compared side by side with the pore water pressure head values obtained in the seepage analysis conducted on the model. The correlation between the readings from piezometers, pressure head values obtained from the seepage model, and the daily recorded rainfall values is depicted in Fig. 6.

The following could be identified by observing the piezometer data. At a depth of 5 m, where a clay layer was identified as the underlying stratum, a rapid increase in porewater pressure was observed following precipitation events. Furthermore, the porewater pressure at a depth of 10 m, where a residual soil layer was identified as the overlying stratum, appeared to decrease slower than the pressure observed at the 5 m depth. These findings suggest that the presence of a clay layer has a detrimental effect on the porewater pressure conditions of the slope, which in turn leads to a decrease in the effective strength of the soil and the elimination of the matric suction effect. Additionally, it was discovered that the pressure head variation obtained from the piezometer is substantially consistent with the results obtained from the seepage analysis. This observation supports the conclusion that the geotechnical model employed is reasonably accurate.

6 Slope Stability Assessment

6.1 Geotechnical Model

A geotechnical slope model was generated based on the data acquired during the site investigation as well as the instrumentation. The surface soil layer was determined to be a silty

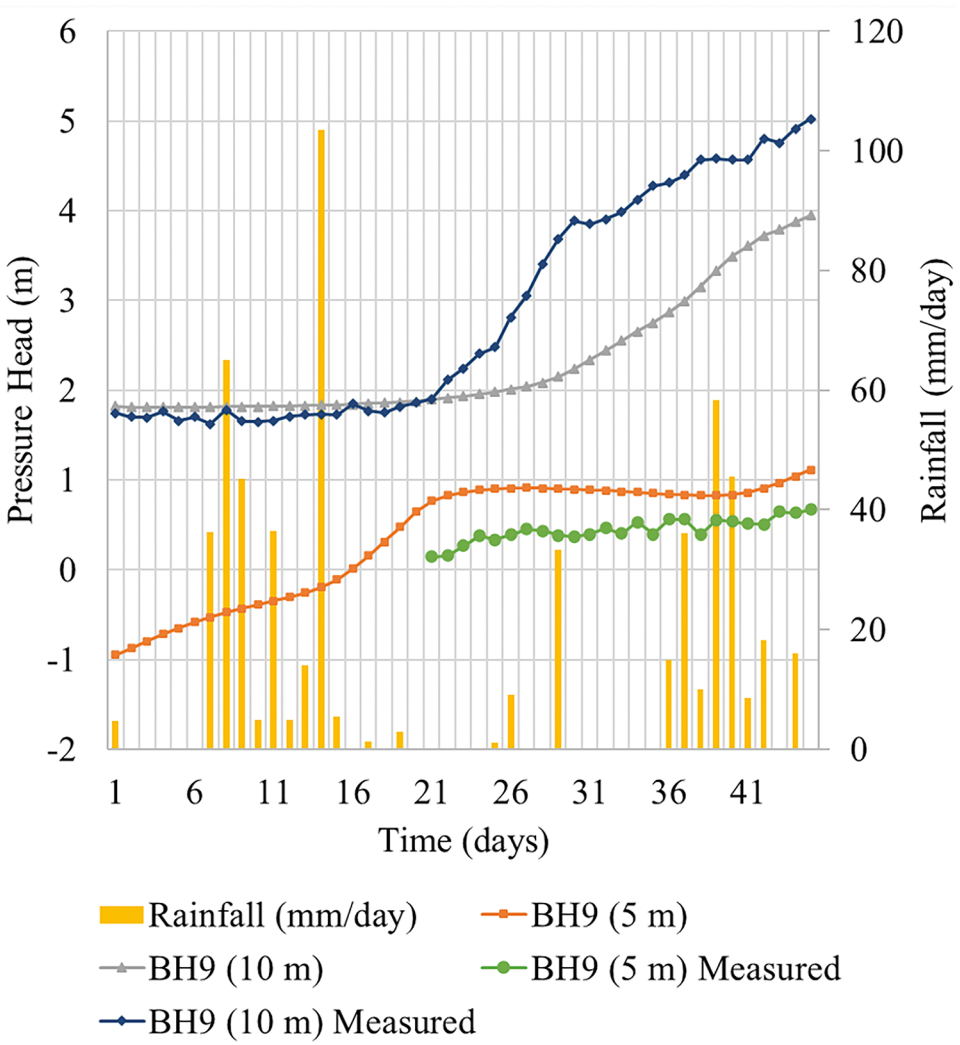


Fig. 6 Pressure head values obtained from the installed piezometer at BH9, and pressure head values obtained from the seepage model against the recorded rainfall during April—May 2018

sand residual soil of relatively high permeability. The clay layer underlying the topsoil layer was identified from the test pits and modeled with a lower permeability characteristic, as confirmed via the piezometer readings. This layer was considered relatively lower in shear strength, as suggested by the outcome of SPT value at these depths. Similarly, the third soil layer from the surface was modeled as a silty sand layer of completely weathered rock with relatively high shear strength values. The parameters used for the geotechnical model are given in.

Table 1 The Mohr-Coulomb material model was used for all materials except for the parent rock layer was modelled as a high-strength material in the limit equilibrium analysis. The data from field instruments and test data obtained from non-disturbed soil samples at different depths were used to calibrate the numerical model further.

6.2 Back Analysis of the Initial Slope Failure

A back analysis simulating the initial slope failure was carried out to verify the numerical model before the effect of the planned mitigation was evaluated through a limit equilibrium analysis. The stability analysis was conducted utilizing the SLOPE/W (Geo-Slope International Ltd. 2012a) and SEEP/W (GEO-SLOPE International Ltd. 2012b) modules of GEO STUDIO 2012 software. The slope geometry before the failure was derived based on the curvature of the contours as well as past satellite images. The geotechnical model described herein was incorporated into the assumed initial slope geometry.

Stability analysis was carried out using the Spencer limit equilibrium approach incorporating the pore water pressure conditions generated from the SEEP/W module seepage analysis. A slip surface search was conducted using several approaches; however, the Grid and Radius method derived the most critical slip surfaces. At the initiation of the design rainfall, the stability of the slope was 1.11, and the matric suction effect could be observed from the result of the seepage analysis (Fig. 7a). Then, the factor of safety (FOS) decreased as the rainfall progressed (Fig. 7b) and the loss of matric suction could be observed from the seepage model (Fig. 8). Eventually, a FOS of less than 1 was obtained, and the geometry of the critical slip surface turned out to be more or less similar to that of the actual failure (Fig. 9). This was achieved approximately on the 25th day of the rainfall sequence. As such, it could be verified that the implemented geotechnical model was reasonably accurate, and we decided to continue with this model in analyzing mitigation measures.

6.3 Analysis of the Existing Slope after Failure

It was deemed necessary to evaluate the slope's stability post-failure in order to make informed decisions regarding its future condition. A seepage analysis was conducted to the slope post-failure, utilizing the design precipitation pattern as in the back analysis. Accordingly, the FoS of the slope before the occurrence of rainfall was calculated to be 1.23 and decreased to 1.03 as the design rainfall progressed. (Fig. 10). The analysis indicated that the post-failure geometry of the slope had become more favorable and stable. Nevertheless, at this stage, the wall at the toe of the slope had sustained structural failure. Consequently, it was determined that, despite the slope having a FoS above 1, the risk of slope failure was imminent due to the compromised condition of the toe wall.

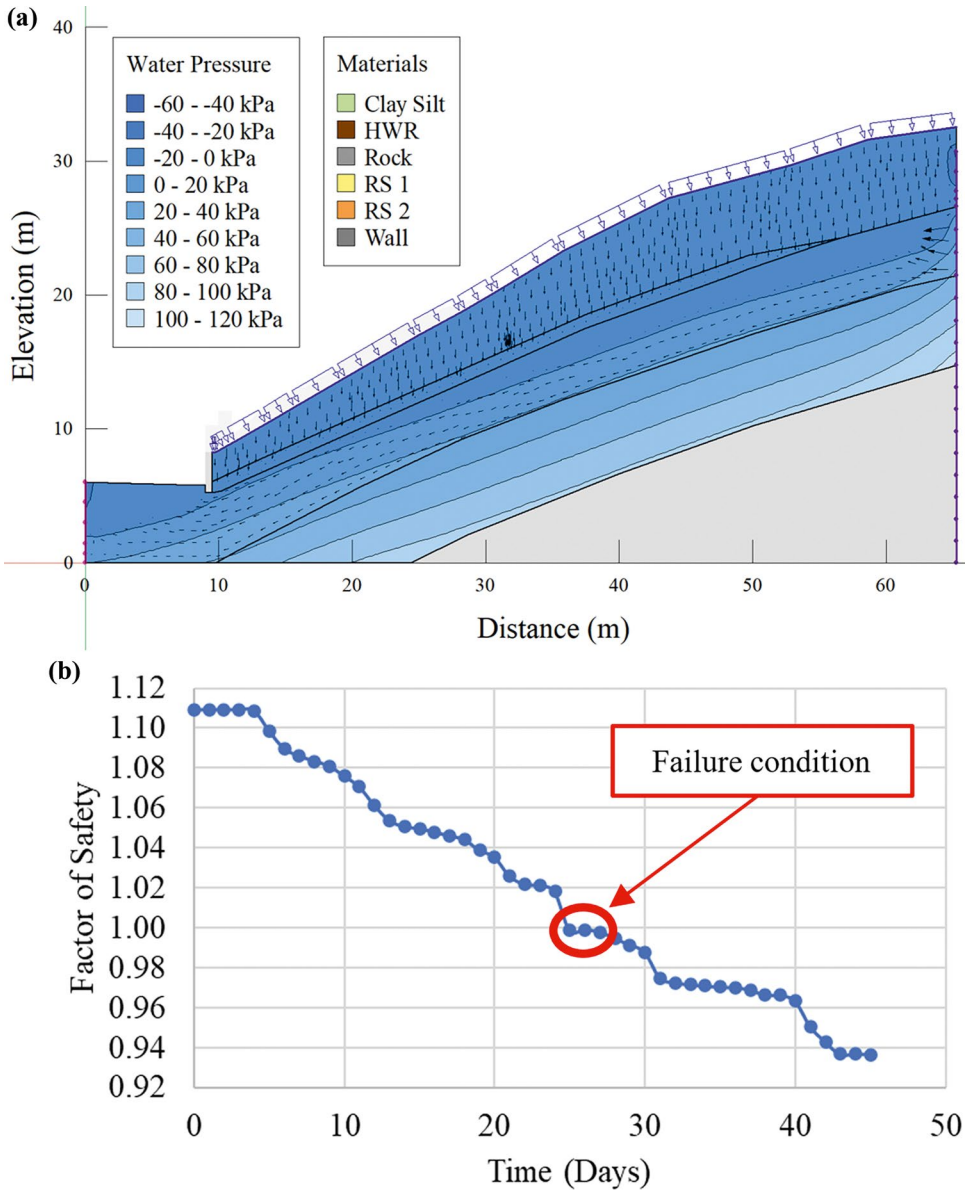


Fig. 7 (**a**) Pore water pressure condition at the initiation of rainfall. (**b**) The gradual decrease of FoS with design rainfall

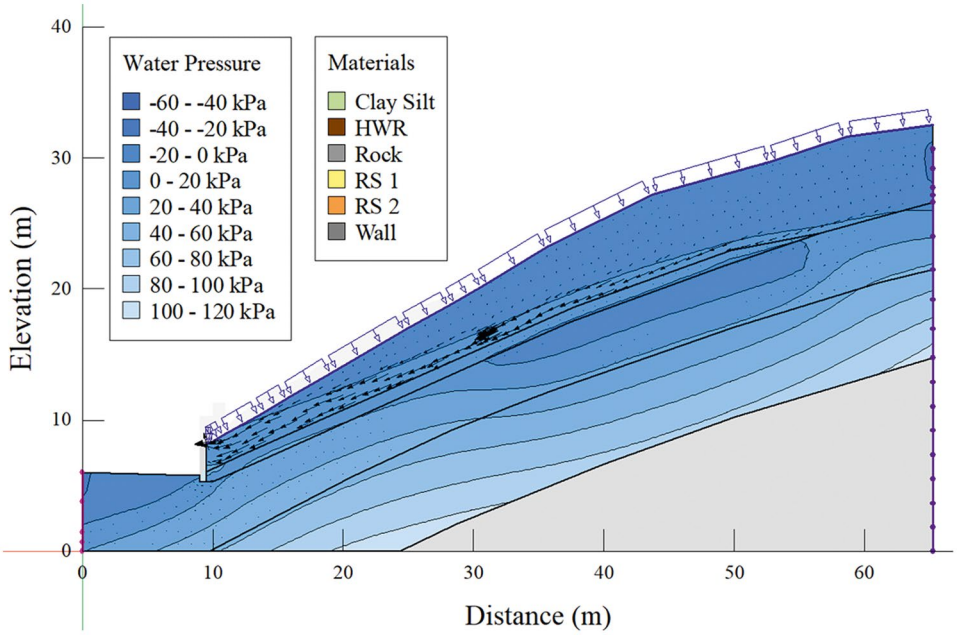


Fig. 8 PWP conditions at the critical stage of the back analysis (FoS < 1 at 25th day of rainfall sequence)

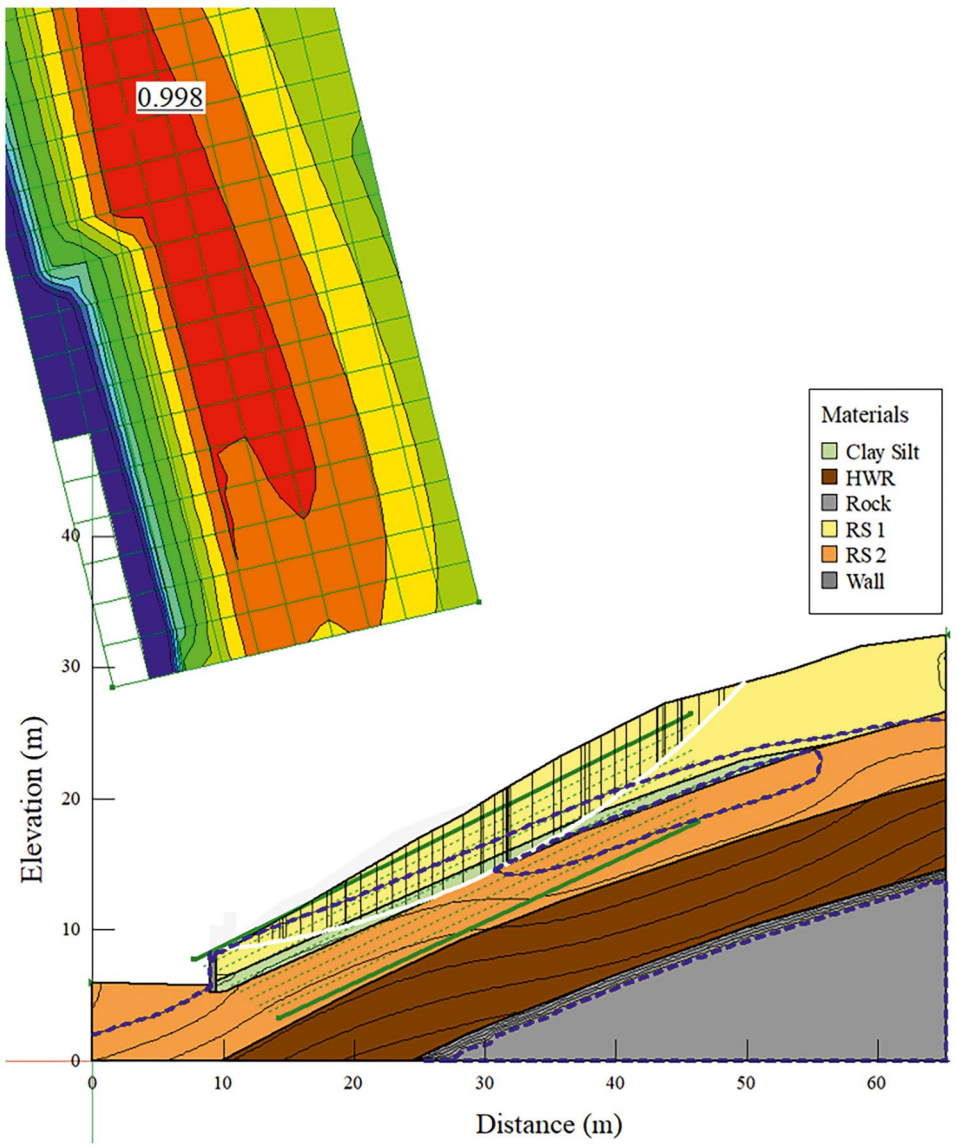


Fig. 9 Failure surface of the back analysis at the critical stage (FoS = 0.998)

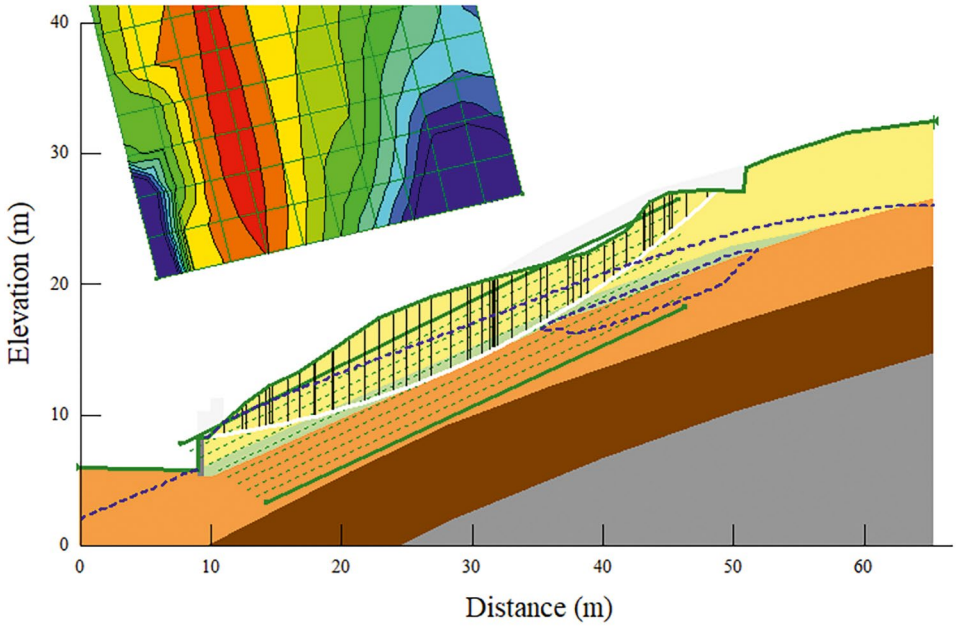


Fig. 10 Post-failure stability analysis during design rainfall (FoS = 1.03)

7 Mitigation Design

The primary objective of the mitigation was to rectify the damaged retaining wall at the toe of the slope. However, due to the insufficient strength of the overburden above the retaining walls, dismantling the walls was not feasible. Therefore, a methodology was devised consisting of the following sequential procedures for the rectification process.

1. Reshaping the slope to remove failed soil mass, forming a berm mid-slope to reduce overburden.
2. Installing lateral gravity drains (Horizontal drains) and constructing subsurface aggregate drains to temporarily stabilize the backslope.
3. Excavating and dismantling the damaged walls
4. Erecting new wall section and backfill with granular material.

During the analysis of rectification measures, a minimum Factor of Safety (FoS) of 1.1 was established. Although the targeted FoS may appear lower, it is pertinent to a short construction phase, namely, the period commencing from the excavation and dismantling of the current wall until the completion of the new retaining wall's erection.

7.1 Analysis of the Reshaped Slope

The effectiveness of reshaping was evaluated, and the reshaped slope maintained a FoS above 1.1 during and after the critical design-rainfall event (Fig. 11). The analysis determined that no additional remediation measures were necessary. However, it is important to note that this stability assessment assumed that the retaining wall at the toe is functioning at optimal capacity. As such, it was necessary to evaluate the next step of the planned rectification; dismantling the retaining wall.

7.2 Stability After Dismantling the Retaining Wall Without Improving Drainage Conditions

Consequently, a seepage and a stability analysis were performed to examine the stability of the proposed slope geometry following excavation and removal of the toe wall (Fig. 12). Despite reshaping and eliminating the surplus overburden, the factor of safety was found to decrease to 0.952 as a result of the excavation undertaken to remove the existing wall, combined with critical seepage conditions associated with the design rainfall. Given the observed conditions, slope toe failure was imminent. As such, it was deemed necessary to undertake a stability evaluation after the implementation of subsurface drainage measures.

7.3 Stability After Dismantling the Retaining Wall After Improving Drainage Conditions

Consequently, a seepage analysis was conducted to evaluate the pore water pressure conditions after the subsurface drainage improvement measures were introduced.

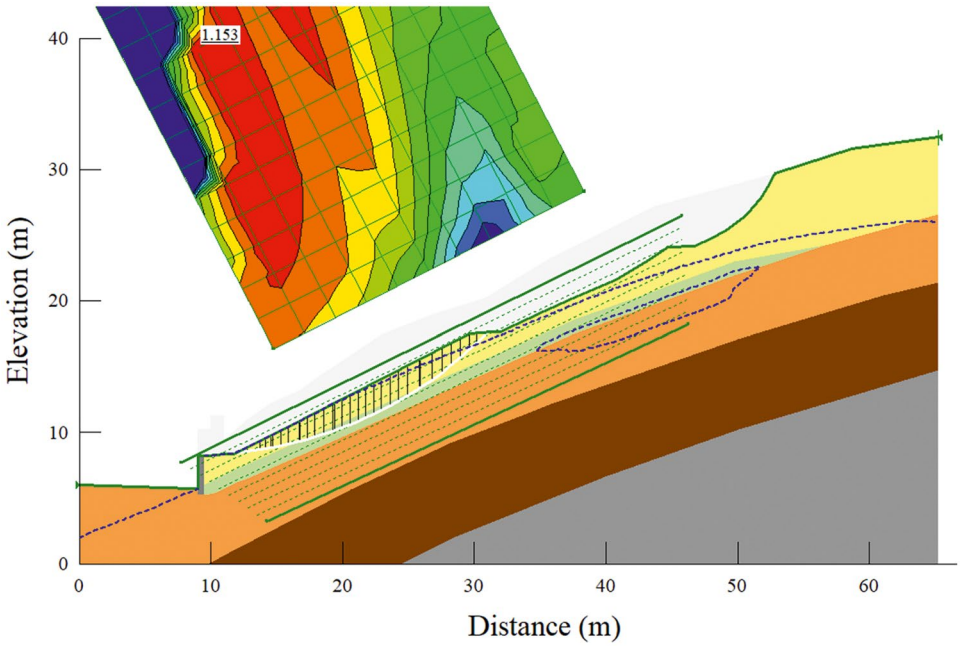


Fig. 11 Result of the stability analysis of the reshaped slope during design rainfall (FoS = 1.153)

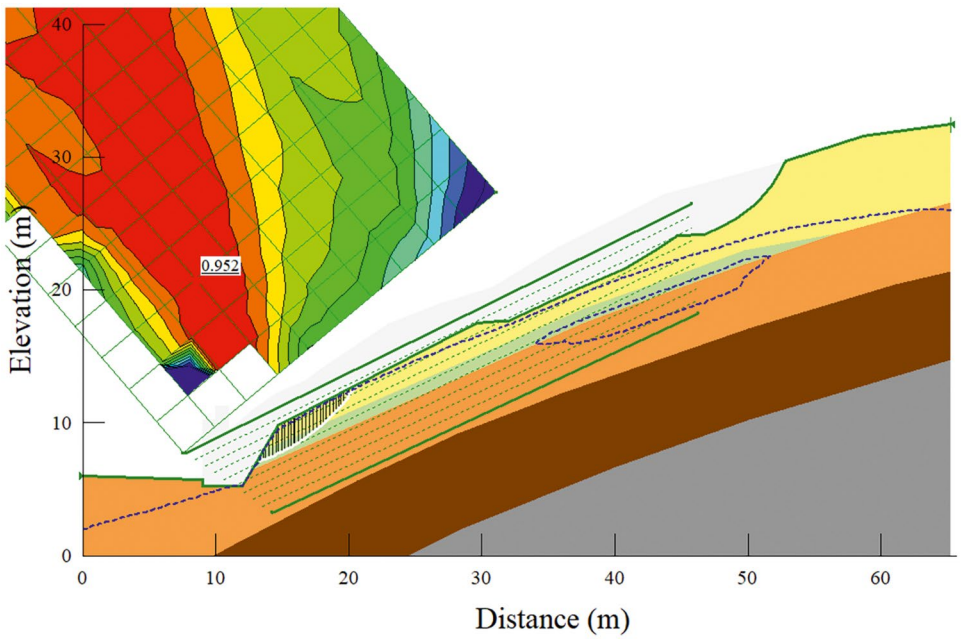


Fig. 12 Result of the stability analysis after dismantling the retaining wall without improving drainage conditions (FoS = 0.952)

Proposed drainage measures were of the following configuration, and as illustrated in Fig. 13b.

1. Horizontal drains
   - Location: 2 nos at the toe of the slope, and another at the level of the berm formed during reshaping
   - Length: 20 m
   - Inclination: 10 degrees
2. Aggregate-filled subsurface drains configured as presented in Fig. 13a along the berm of the slope.

Horizontal drains were modelled as a "Water Rate" boundary with a 0 m^3/s constant flow rate and then enabling the "potential seepage review option". Using this hydrological boundary condition would make the program mimic the function of a subsoil drain, evacuating all inflow towards it.

As indicated by the seepage analysis results, it is apparent that the implementation of the proposed measures led to the creation of negative porewater pressures near the surface of the slope Fig. 13b, thus improving the stability of the slope. Subsequently, a stability analysis was conducted to assess the

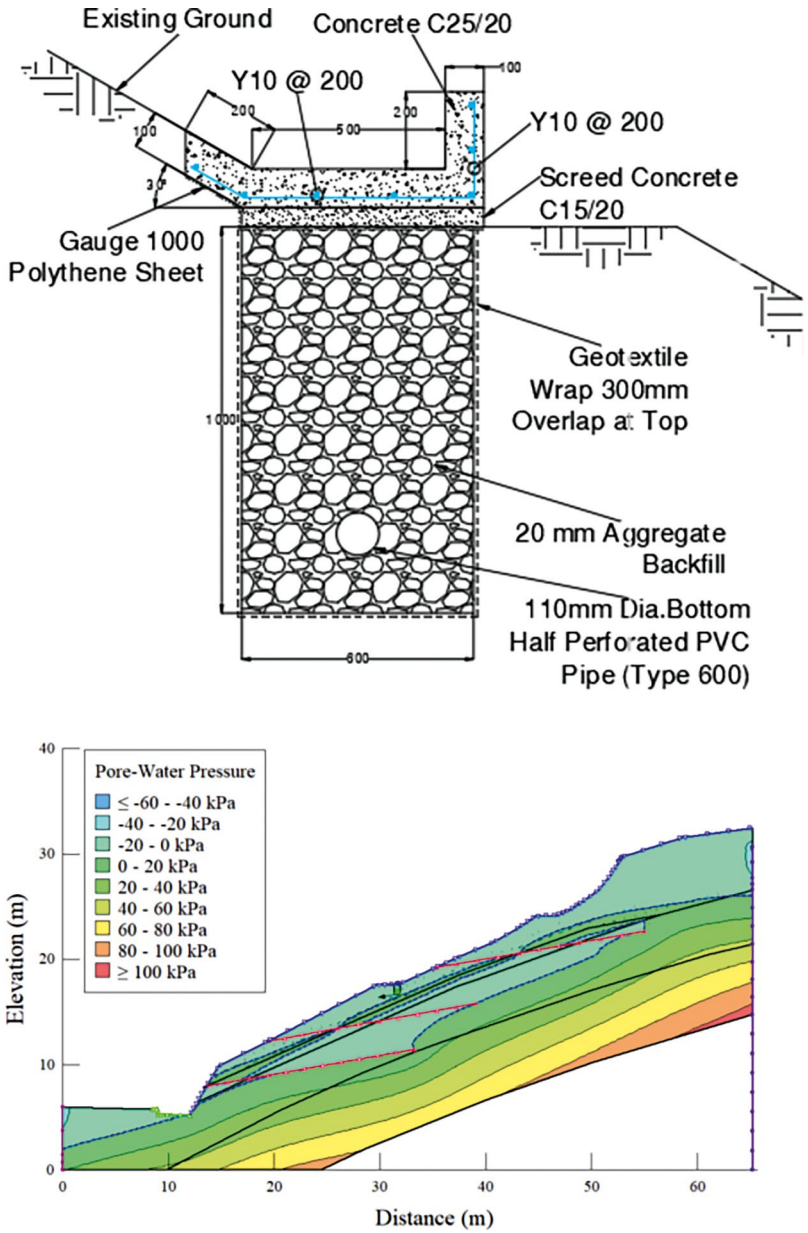


Fig. 13 (**a**) Detail of the proposed subsurface drain (**b**) Pore water pressure condition of the slope at the design rainfall event after subsurface drainage improvement

integrity of the proposed slope geometry after excavation and removal of the toe wall, considering the obtained pore water pressure conditions. By implementing improved drainage measures, the overall stability of the slope was determined to have improved to 1.16. This factor of safety margin was considered acceptable given the corresponding construction phase will be carried out in a relatively short timeframe.

8 Limitations

The seepage and geotechnical models have been developed based on limited investigation data. The steeper morphology of the slope and the slurry-like surface conditions prevented accurate deep investigations from being carried out. The failure of the cantilevered retaining wall at the bottom of the slope cannot be accurately simulated using a limit equilibrium type analysis due to its' limits in calculating structural load development. However, the form of the slip surfaces generated has given an approximate confirmation of the overloading of the wall.

The horizontal drains modeled in the 2D space of the SEEP/W model overestimate their actual effect because the boundary used in the model is not discrete along the slope, unlike the actual drains, which would be installed 2 m apart.

9 Discussion and Conclusion

This study investigated the feasibility of utilizing subsurface drainage to prevent a catastrophic slope failure when removing critical toe-supporting wall. The horizontal drains com-



Fig. 14 Successfully functioning subsurface drain and horizontal drains in the study area

bined with subsurface drains could relieve perched water tables arising due to an impermeable stratum at a shallower depth of the slope. Numerical analysis was conducted to evaluate the effectiveness of the subsurface drainage measures in lowering water tables during the excavation phase and critical design rainfall events. Additionally, the study conducted a post-rainfall analysis to evaluate the effectiveness of the dewatering measures in maintaining stability. The results of this analysis indicate that subsurface drainage measures not only led to an increase in the Factor of Safety (FoS) before rainfall events but also resulted in a more rapid increase in FoS following these events. The functionality of the subsurface drains and horizontal drains was continuously observed at the site after construction (Fig. 14).

In addition to the subsurface drainage measures, surface drainage arrangements were also established in the study area when the actual excavation works were conducted. Moreover, the reshaped slopes were covered with impermeable membranes to prevent rainwater infiltration. This study emphasizes the utility of subsurface drainage improvement measures as a cost-effective technique for ensuring adequate safety margins in slopes during high-risk excavation activities and prolonged high-intensity rainfall events.

Acknowledgments The authors would like to acknowledge The World Bank and Road Development Authority, Sri Lanka, for funding the Climate Resilience Improvement Project (CRiP). and National Building Research Organisation, Sri Lanka, for providing necessary guidance throughout the project.

References

Amarasinghe UB, Dahanayake K, Seneviratne N (2002) Role of weak soils and relict geological discontinuities in creeping slope failure at pooliyadda, Sri Lanka. Ceylon J Sci Phys Sci 9:23–36

Cai F, Ugai K, Wakai A, Li Q (1998) Effects of horizontal drains on slope stability under rainfall by three-dimensional finite element analysis. Comput Geotech 23:255–275. https://doi.org/10.1016/S0266-352X(98)00021-4

Dang K, Sassa K, Konagai K et al (2019) Recent rainfall-induced rapid and long-traveling landslide on 17 May 2016 in Aranayaka, Kagelle District, Sri Lanka. Landslides 16:155–164. https://doi.org/10.1007/s10346-018-1089-7

Geo-Slope International Ltd. (2012a) Stability modeling with SLOPE/W, 2012th edn

GEO-SLOPE International Ltd. (2012b) Seepage modeling with SEEP/W, July 2012

Kankanamge LUM (2020) Effectiveness of subsurface drainage and vegetation in enhancing the slope stability, (Masters' thesis) University of Moratuwa. http://dl.lib.mrt.ac.lk/handle/123/16209

Lakruwan M, Oikawa H, Kamura A et al (2021) Experimental evaluation of effect of perforation arrangement on performance of horizontal drains in landslide mitigation. Landslides 18:3707–3714. https://doi.org/10.1007/s10346-021-01724-3

Nawagamuwa UP, Perera LP (2017) Recommending rainfall thresholds for landslides in Sri Lanka. In: Advancing culture of living with landslides, pp 267–272. https://doi.org/10.1007/978-3-319-53483-1_31

Rahardjo H, Hritzuk KJ, Leong EC, Rezaur RB (2003) Effectiveness of horizontal drains for slope stability. Eng Geol 69(3–4):295–308. https://doi.org/10.1016/S0013-7952(02)00288-0

Rahardjo H, Santoso VA, Leong EC, Ng YS, Hua CJ (2011) Performance of horizontal drains in residual soil slopes. Soils Found 51(3):437–447. https://doi.org/10.3208/sandf.51.437

Open Access This chapter is licensed under the terms of the Creative Commons Attribution 4.0 International License (http://creativecommons.org/licenses/by/4.0/), which permits use, sharing, adaptation, distribution and reproduction in any medium or format, as long as you give appropriate credit to the original author(s) and the source, provide a link to the Creative Commons license and indicate if changes were made.

The images or other third party material in this chapter are included in the chapter's Creative Commons license, unless indicated otherwise in a credit line to the material. If material is not included in the chapter's Creative Commons license and your intended use is not permitted by statutory regulation or exceeds the permitted use, you will need to obtain permission directly from the copyright holder.



Assessing and Contextualizing Site-Specific Landslide Risk in the Philippines

Cathleen Joyce Cordero, Kenneth Gesmundo, and Arturo Daag

Abstract

As an attempt to understand and reflect on the unique circumstances of communities in assessing landslide risk, the Dynaslope Project, under the Department of Science and Technology-Philippine Institute of Volcanology and Seismology (DOST-PHIVOLCS), conducts community landslide risk assessment (CLRA). It is a participatory process of assessing landslide hazards, exposure, vulnerabilities, and capacities of at-risk communities. CLRA includes hazard assessment, participatory community workshops, focus group discussions, and surveys. Risk components are assessed, and results are integrated through a semi-quantitative method that utilizes a scoring system with equivalent categorical labels, i.e., low, moderate, and high, to classify each risk component and the overall landslide risk. It was first conducted in four project sites. Priorities of the communities are taken into account in the assessment by letting them identify and validate the elements-at-risk, vulnerability, and capacity indicators, and the corresponding weights used in the scoring system. The results are presented in household-level risk maps and landslide risk assessment reports. Participatory identification of risk indicators helps in drawing out different community contexts which is useful in developing site-specific risk management strategies and actions.

Keywords

Community landslide risk assessment · Participatory method · Risk indicators · Landslide risk · Philippines

C. J. Cordero · K. Gesmundo (✉) · A. Daag
Department of Science and Technology-Philippine Institute of Volcanology and Seismology-Dynaslope Project, Quezon City, Philippines
e-mail: dynaslope@phivolcs.dost.gov.ph; arturo.daag@phivolcs.dost.gov.ph

1 Participatory Approach in Disaster Risk Reduction and Management

In disaster risk management, participatory approaches are valuable because people are empowered by strengthening individual capabilities and community ties, which can help them face challenges independently or collectively (Twigg 2009). Communities are able to gain disaster risk management knowledge that enhances their understanding of their own risk, which ushers them to maximize their capacities to unravel challenges (Nkombi and Wentink 2022).

A participatory approach is a process through which stakeholders are able to actively and collaboratively participate in different initiatives (The World Bank Participation Sourcebook 1996; Duraiappah et al. 2005; Titz et al. 2018). Stakeholders are able to influence decisions and share control over resources that have an impact on them. The approach intends to collect information grounded to the communities "to foster their active participation in the process, and provide the basis for them to discover their own means of solving their difficulties" (van Aalst et al. 2008, p. 167). A good participatory approach seeks to empower by mobilizing the community while refraining from giving in to the dominance of select groups or excluding other groups (Twigg 2009). It reiterates that efforts must be made to sustain communication between stakeholders to better understand, relate, and help one another (Participatory Development Models 2013).

In terms of landslide risk, there is no lack of effort in applying the participatory approach in the assessment process. Communities are tapped in hazard assessment, usually through landslide mapping or landslide inventory (e.g., Perera et al. 2022; Project LIGTAS n.d.; Anshori et al. 2022), in vulnerability and capacities assessments (e.g., Gumiran et al. 2019), to brainstorming and involvement in the execution of measures (e.g., Preuner et al. 2017; Anderson and Holcombe 2013). However, the participation of communities is mostly limited to providing source data for risk assessment. This study aims to further expand the community par-

© The Author(s) 2025

B. Abolmasov et al. (eds.), *Progress in Landslide Research and Technology, Volume 3 Issue 2, 2024*, Progress in Landslide Research and Technology, https://doi.org/10.1007/978-3-031-72736-8_12

ticipation in landslide risk assessment; from data gathering, to analysis, and to the determination of classification of their landslide risk. This was done by translating community priorities to weights of landslide exposure, vulnerabilities, and capacities.

In the Philippines, steps are being taken to institutionalize the provision of an enabling environment that allows maximum public participation in disaster risk reduction and management (DRRM). One is through the enactment of Republic Act 10121 or the "Philippine Disaster Risk Reduction and Management Act of 2010". The Act emphasizes that the people are at the center of the decisions and implementation of the DRRM activities. It states that a community-based disaster risk reduction and management (CBDRRM) actively engages at-risk communities in the identification, analysis, monitoring, and evaluation of disaster risks to address vulnerabilities and enhance their capacities (Bawagan 2011). CBDRRM hopes to increase people's involvement in all aspects of the DRRM process which is expected to result in more sustainable and effective measures. It emphasizes the significance of using participatory processes to examine the vulnerabilities of at-risk populations (Pandey and Okazaki 2005).

2 Vulnerability-Focused and Participatory Approaches to Risk Assessments

In the literature, numerous studies on landslide risk assessments focus primarily on examining the threat of landslide hazards. These include emphasizing assessment of the geology, material, intensity, or stability of land mass, among others (e.g., Varnes DJ, the International Association of Engineering Geology Commission on Landslides and Other Mass Movements on Slopes 1984). Other literature, however, expanded the risk assessments made by also analyzing the exposure and vulnerabilities present in the hazard areas (e.g., Fell et al. 2005; Althuwaynee and Pradhan 2017). This development takes root in the paradigm shift from a hazard-centric approach into a development-oriented approach in dealing with risk (Birkmann 2006; Faas 2016). The United Nations Office for Disaster Risk Reduction (UNDRR 2009) primarily promotes a vulnerability approach for disaster risk reduction, which was also the framework used by other proponents of disaster risk research (e.g., Wisner et al. 2004; Cardona et al. 2012; Safeland 2011). Participatory approaches to risk assessment entail that the at-risk communities are the center of identifying the vulnerabilities, and other defining characteristics, as well as the impacts that these factors have on their risk.

Participatory risk assessment is conducted through the utilization of interviews, focus group discussions, and workshops. Organizations gather qualitative information on the characteristics of communities by employing tools such as historical timelines, seasonal calendars, vulnerability and capacity matrices, and others (Liu et al. 2018; Mcleod et al. 2015). Overall, the risk of communities is assessed based on these components—which vary between different literature—hazard, exposure, vulnerability, and capacity.

While indicator-based assessments are commonly used to analyze landslide risk (e.g., Bera et al. 2020; Agliata et al. 2022), only a limited number of studies place emphasis on the role of vulnerabilities or capacities in their examination of landslides. For example, Cutter et al. (2012) underscored the significance of social vulnerability by heavily basing their assessment on social vulnerability indicators. Vulnerability-focused and participatory approaches can surface urgent issues and inform priority actions (Antronico et al. 2020). The Pressure and Release (PAR) model serves as an effective framework for systematically analyzing the underlying drivers that influence vulnerability and resilience (Wisner et al. 2004). By working with at-risk communities to identify historical pressures and current vulnerabilities through a participatory process, a more holistic understanding of risk can be achieved.

Knowledge products like hazard and risk maps are important outputs that spatially represent vulnerabilities alongside physical risks when decision-makers aim to plan and build resilience. In the case study by Perera et al. (2019), vulnerability indicators were incorporated with physical indicators primarily to map vulnerabilities and utilize spatial data for planning and decision-making.

3 Framework on Community Landslide Risk Assessment

The community landslide risk assessment (CLRA) employed in this study anchors on the UNDRR (2009) definition of risk and the Pressure and Release (PAR) model as guides in assessing landslide risk and understanding the context of the community.

The UNDRR (2009) looks at risk as a function of hazard, exposure, vulnerabilities, and capacities. It should be emphasized that understanding the risk components and their interaction with each other is important in discerning landslide risk. Gender, governance, and climate change should also be recognized as inevitably intertwined in the discussion of landslide risk.

Progression of Vulnerability and Progression of Safety concepts of the PAR model (Wisner et al. 2004) are used in articulating the subtexts of the vulnerabilities and capacities of the community. The PAR models disaster as "the intersection of two opposing forces: those processes generating vulnerability on one side, and the natural hazard event (or

sometimes a slowly unfolding natural process) on the other" (Wisner et al. 2004, p. 50). The Progression of Vulnerability aims to contextualize risk through a thorough understanding of the unsafe conditions, the underlying causes of these unsafe conditions, and the root causes of the underlying conditions. Progression of Safety supposes that disaster can be reduced if pressure is relieved. One way of lowering pressure is to reduce vulnerabilities by increasing capacities.

4 CLRA and the Roles of Community Stakeholders

In CLRA, the community is at the forefront of assessing their landslide risk. The community's local knowledge of landslide hazards is complemented with scientific knowledge. Most importantly, the community is given the lead role in appraising their exposure, vulnerabilities, and capacities. To capture diversity, representatives from different sectors of the at-risk communities, such as vulnerable groups, members of community-based or people's organizations, and barangay local government units (BLGU), are involved in the assessment. However, actual participation is still dependent on the availability of the stakeholders.

Throughout the CLRA process, the community provided valuable information and insights. To ensure that the rights of the community are respected throughout the process, the researchers put in the utmost effort to follow ethical principles and standards during the CLRA and this research. Informed consent was gathered from participants during the stages of the risk assessment. Anonymity and confidentiality are ensured during the research to adhere to the Republic Act 10173 or the Data Privacy Act of 2012. The sites and participants' names in this research are redacted to ensure anonymity. Lastly, to establish transparency and integrity, the results are presented and validated with the community after the initial results consolidation process made by the researchers.

4.1 Community Participation in Landslide Hazard Assessment

Landslide hazard assessment aims to determine the probability of occurrence of a landslide and its most probable extent. It is conducted through on-site investigations and desktop analysis.

The community is primarily involved in landslide hazard assessment by providing eyewitness accounts and observations that are crucial in the conduct of on-site investigations. They are able to physically guide the survey team on specific locations of features and changes that may not be easily distinguishable for non-locals and through desktop analysis. Their knowledge of the history of site ground movement and events concurrent with these movements provides the survey team with crucial details on the possible site conditions that may have caused and events that may have triggered the movement.

During the CLRA validation process, the results of the hazard assessment are presented to the community in the form of landslide hazard map and historical timeline. The presentation primarily aims to verify information gathered regarding the landslide. The map also serves as a tool for the community to help them visualize the hazard that they are facing. On top of this, it also shows the community a tangible translation of their contributions to the assessment. This process provides the community with proper knowledge that would help them understand the landslide hazard. Without proper knowledge, they may think that they are powerless against natural hazards (Kulatunga et al. 2010). However, once their local knowledge is complemented with scientific knowledge and vice versa, they will have a proper understanding of the landslide hazard and they can strategically identify or devise measures to prevent or mitigate the damages it may cause.

4.2 Community Exposure Assessment

Exposure assessment aims to identify the elements at risk of landslide hazard. Additionally, it intends to categorize the elements-at-risk and subsequently assess the level of exposure.

Tools such as participatory 3D mapping, surveys, and focus group discussions are conducted to identify and map out the exposed people, structures, and critical areas, among others. Table 1 categorizes the elements that may be located in the landslide hazard zone. The community identifies which exposure categories are applicable in their context. Participatory workshops are conducted for the community to decide on the importance of each category and translate these into weights. This is done based on Saaty's (1987) concept of pairwise comparison, wherein participants rank the categories according to importance and assign scores using numbers or text descriptors of relative importance (Fig. 1).

4.3 Community Vulnerability and Capacity Assessment

Vulnerability and capacity assessments primarily identify the characteristics of the community that aggravate and reduce the landslide risk. Both qualitative and semi-quantitative tools are utilized in the assessment. Vulnerabilities and capacities are qualitatively identified using tools such as problem and solution trees, vulnerabil-

Table 1 Summary of exposure categories

Category	Definition	Dimension
Residential	Buildings intended for private occupancy, e.g., houses, boarding houses.	Social
Institutional	Structures and areas that are meant to provide service to the community. Structures are grouped according to function, such as: • Educational/recreational: e.g., schools, parks, gyms, courts, day care centers • Religious: e.g., churches, temples • Government service: e.g., barangay hall, other government offices • Health and emergency: e.g., clinics, hospitals, evacuation center, community bathrooms, septic tanks, and sewage facility	Social
Commercial	Structures and areas mainly used for trade or business. Commercial structures are grouped according to service provided, such as: • Food: e.g., wet/dry market, restaurants • Retail: e.g., sari-sari-store, grocery • Industrial: Medium- to large-scale processing or manufacturing plants • Tourism: e.g., museums, view deck • Other services: e.g., vulcanizing shops, car wash, laundry, accommodations	Economic
Transportation	Infrastructures developed primarily for transportation, such as: • Roads: e.g., access road, barangay, municipal, provincial, and national roads • Bridges • Waiting sheds, terminals, and motorpool	Social
Utilities	Infrastructures that provide basic amenities to the community, such as: • Power: e.g., electrical towers, solar power storage • Water: e.g., well, water tanks • Communication: e.g., communication towers	Social
Cultural landmarks	Structures and sites that have cultural significance to the community such as monuments, burial grounds, and others. This also includes areas or structures that the community deems important for congregation, assembly, or social gathering.	Social
Agricultural	Structures and areas used for agricultural activities, such as for: • Crops: e.g., garden, plantation, orchard • Livestock/poultry: e.g., piggery, poultry, pasture land • Others: processing/storage	Economic
Natural resources	Existing natural environment with tapped and untapped resources, such as: • Natural cover/vegetation: e.g., forest, grassland, wetland, etc. • Water bodies: e.g., sea, river, lake, pond, falls, etc. • Areas with mineral resources and other raw materials	Environmental
Population	People that may be harmed in case of a landslide. Parameters for this category are: • Occupant count: number of occupants per building or area • Traffic count: vehicular and pedestrian count passing through transportation networks Count may vary at different times, e.g., daytime, nighttime, seasonal.	Human

ity and capacity matrices, seasonal calendar, and stakeholder analysis, among others. Data gathered through these tools are then analyzed following the PAR framework to uncover the root causes of the community's vulnerability.

Semi-quantitative methods involve the use of indicators to identify vulnerabilities and capacities. The community's role is to identify the vulnerability and capacity indicators based on their experiences and contexts. The community also contributes to the assignment of weights of the identified indicators depending on what they perceive to contribute more to their landslide risk (Fig. 2). The weights are based on the ranking and relative comparison of the indicators for vulnerability and capacities. Household data are gathered per indicator which are used as inputs to compute their landslide risk (Fig. 3).

4.4 Integrating Risk Components in Producing Risk Knowledge

Results of the hazard, exposure, vulnerability, and capacities assessments are integrated through a semi-quantitative method that utilizes a scoring system with equivalent categorical labels, i.e., low, moderate, and high, to classify each risk component and the overall landslide risk. Scoring for the components is similar to the Bollin and Hidajat (2006) community-based disaster risk index.

Landslide hazard is classified as high or moderate based on the zone. High for the landslide source and the runout area, and moderate for the buffer zone. Exposure is classified as low, moderate, or high depending on the exposure score of the at-risk element. The exposure score is based on the functions of the at-risk element and the weights assigned by



Fig. 1 Exposure ranking activity where community members rank and discuss the prioritization and impacts of different exposure categories

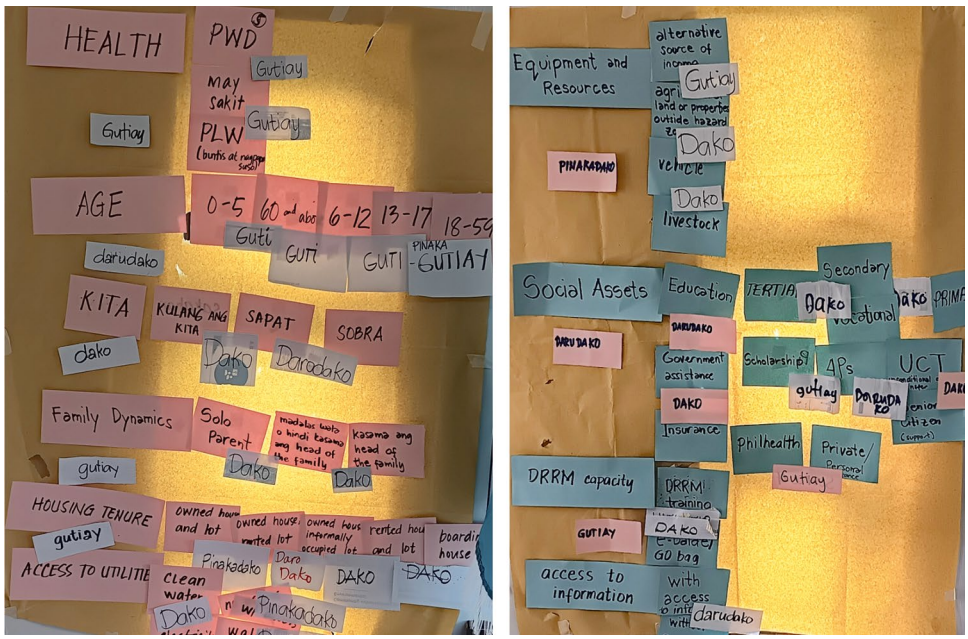


Fig. 2 Workshop outputs on vulnerability (left) and capacity (right) weights. Local language is used to represent the intensity of importance of indicators

the community to the exposure categories. Capacities and vulnerabilities of the households are classified based on the vulnerability and capacity scores, which are computed from the community-identified indicators and weights. For this study, only the households have identified indicators. Further study is needed to identify vulnerabilities and capacities of other elements-at-risk. The component assessment results are combined through a risk matrix to determine the landslide risk classification of a household (Fig. 4), cognate to Jhong et al. (2019) risk assessment matrix.

The landslide risk classifications are then visually presented through a risk map. The map, which is one of the three major tangible outputs of the CLRA, spatially presents the household-level landslide risk. Another output produced is the landslide risk database, which contains details of the elements-at-risk and their corresponding component and risk

		Household count			Sex				Age group										
label	Age as of September 28, 2022	total members	daytime	nighttime	Female	total female	Male	total male	0-5 (- - no 1 - yes)	0-5	6-12 (- - no 1 - yes)	6-12	13-17 (- - no 1 - yes)	13-17	18-59 (- - no 1 - yes)	18-59	60 abv (- - no 1 - yes)	60 abv	PWD (checked-yes unchecked - no)
H1	27	1	0	1	☐	0	☑	1	-	0	-	0	-	0	1	1	-	0	☐
H2	26	3	2	3	☐	2	☑	1	-	1	-	0	-	0	1	2	-	0	☐
	27				☑		☐		-		-		-		1		-		☐
	0				☑		☐		1		-		-		-		-		☐
H3a	54	2	1	2	☑	1	☐	1	-	1	-	0	-	0	1	3	-	0	☐
	24				☐		☐		-		-		-		1		-		☐
	5				☐		☐		1		-		-		-		-		☐
	31				☐		☑		-		-		-		1		-		☐
H3b	28	2	1	5	☐	1	☑	1	-	0	-	0	-	0	1	2	-	0	☐
	26				☑		☐		-		-		-		1		-		☐

	Health									Access to utlities		
label	Sickly (checked-yes unchecked - no)	remark	Sickly	PLW (checked-yes unchecked - no)	remark	PLW	Income classification	housing tenure	Family Dynamics	access to clean water	access to electricity	education (individual)
H1	☐		0	☐		0	sapat	own house, informal lot	solo parent/household	yes	yes	secondary
H2	☐		0	☑	breast-feeding	1	kulang	own house, rented lot	head of household present	yes	none	tertiary
	☐			☐								tertiary
	☐			☐								none
H3a	☐		0	☐		0	kulang	own house, rented lot	solo parent/household	yes	yes	tertiary
	☐			☐								tertiary
	☐			☐								none
	☐			☐								tertiary
H3b	☐	-	0	☐		0	sapat	own house, rented lot	head of household present	yes	yes	tertiary
	☐	-		☐								tertiary

Fig. 3 Database with the indicators identified by the community and the data gathered during the CLRA

classifications. Lastly, a landslide risk assessment report is also produced. The report details the information gathered and analysis made from the hazard, exposure, vulnerability, and capacity assessment.

4.5 Validation

Validation of data and results is an indispensable part of the CLRA process. The validation underscores the role of the community, not only as a source of data but also as frontrunners in the analysis of their landslide risk. Through validation, the community is given an avenue to decide which relevant data should be included in the assessment of their landslide risk. Community priorities are taken into account in the assessment by letting the stakeholders identify and validate the elements-at-risk, vulnerability, and capacity indicators, and the corresponding weights that were used in the scoring system.

The participation of the community from data gathering to analysis and validation increases their understanding and ownership of the result of the assessment. This in turn contributes to the creation of plans that are conformable to and sustainable for the community.

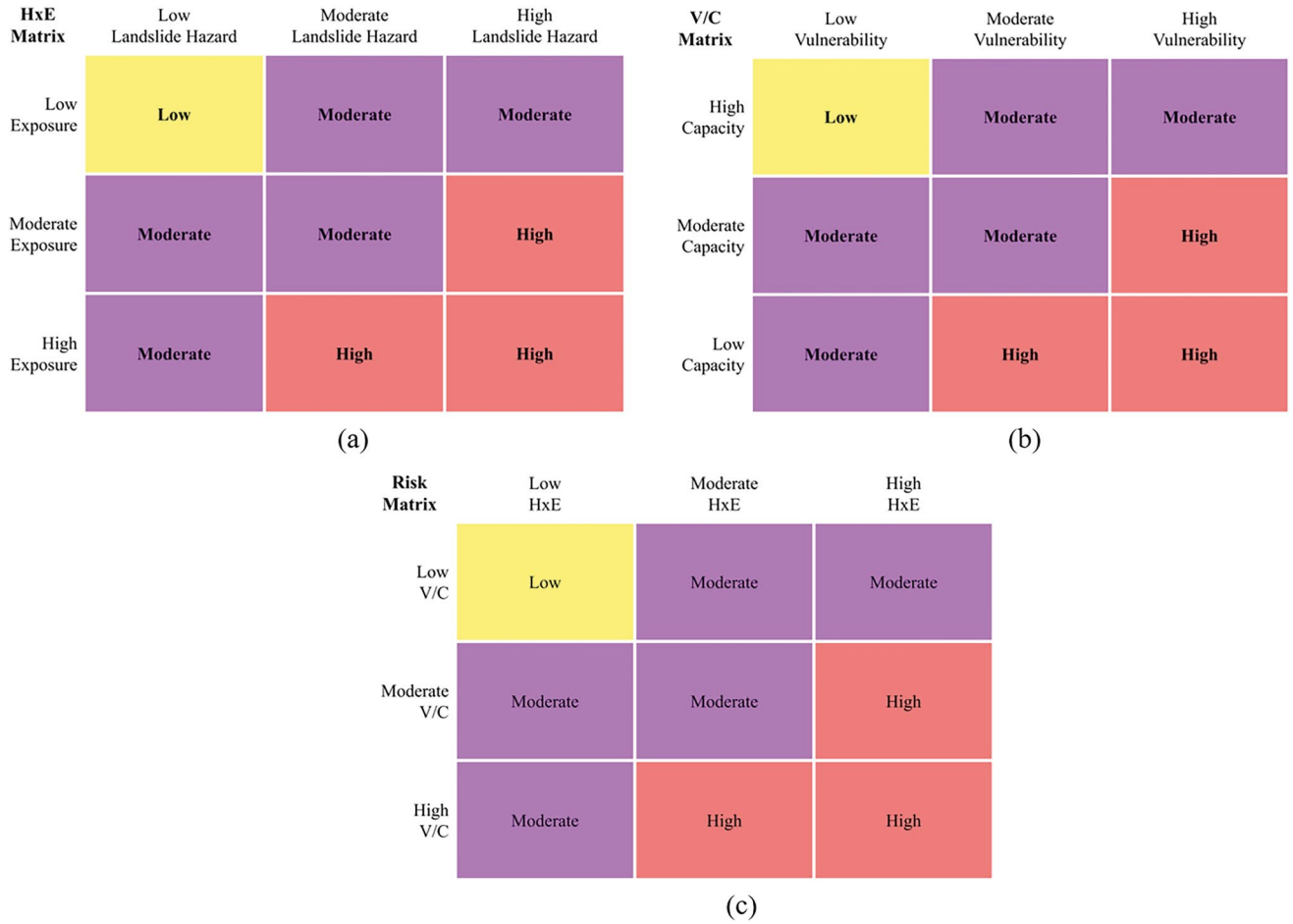


Fig. 4 Matrices of risk component integration for the classification of landslide risk. Two matrices, (**a**) hazard-exposure matrix and (**b**) vulnerability-capacity matrix, are integrated to generate the (**c**) landslide risk matrix, which determines the overall landslide risk of the household

5 Implementation of CLRA

The CLRA is done in accordance with one of the Dynaslope Project's main objectives of comprehensively assessing landslide risk for the implementation of a people-centered early warning system. Dynaslope Project, under the Department of Science and Technology-Philippine Institute of Volcanology and Seismology (DOST-PHIVOLCS), implements landslide early warning systems (EWS) in 52 sites across the country. The landslide EWS provides early warning information (EWI) and services to partner communities and local government units (LGUs) to help them make proper preparations and responses to impending landslide events (Dynaslope Project 2022a, b, c). Dynaslope employs a four-level alert system in the provision of warning information. EWI, which contains the alert level, validity, and recommended response, are disseminated in the form of SMS or bulletin. Alert levels are based on the analysis of data sourced from the installed sensors (i.e., subsurface sensors and rain gauges) and from community on-site measurements and observations (Dynaslope Project 2022b). Each level has corresponding recommended response for the community and LGUs, such as to continue with daily routine for Alert 0, prepare to respond to higher alerts for Alert 1, prepare to evacuate for Alert 2, and evacuate for Alert 3.

The PHIVOLCS-Dynaslope Project conducted CLRA in four sites from 2020 up to the first quarter of 2023. A site is an area within the bounds of the projected landslide hazard zone. These sites have an in-place early warning system, which was established by the Project together with the community. The sites are within the jurisdiction of a *barangay*, the smallest government unit in the Philippines. A brief overview of the sites is discussed in the next section.

5.1 Site A

Site A is in a generally mountainous and hilly barangay. The monitored area is near the ridge of a 160-m high, moderately

steep slope. The slope is composed of 10–30 m of thick soil underlain by intensely fractured rocks. Landslide debris is expected to flow along a channel towards the concentration of houses located less than a kilometer from the foot of the slope.

The most notable ground movement occurred in 2011 when debris reached some of the households. Only small localized failures or changes in the ground were reported and detected from 2015 to 2022. Movements were attributed to the occurrence of rain. A landslide EWS has been in place in the site since 2015. No ground movement alert level warranting an evacuation has been raised on site, but preemptive and mandatory evacuations are conducted with heavy or intense rainfall warnings issued by authorities.

The whole barangay is predominantly a forest area, but the site consists mostly of agricultural and residential areas. The site is along the national highway and is also near the evacuation facility. Elements-at-risk include mostly houses (around 70 households), a few agricultural lands, microscale businesses, and an elementary school. At-risk households are located at the projected runout area and are around 20 min hike away from the landslide source.

Most of the households are dependent on agricultural livelihoods such as planting crops, e.g. rice, coconuts, root crops, bananas, vegetables, and livestock and poultry farming. The participants recognize the importance of the natural resources accessible to the community.

The locals recognize the functions of the barangay local government unit (BLGU) in DRRM. Local organizations are also present.

5.2 Site B

Site B is in a barangay surrounded by slopes. The monitored landslide area is near the ridge of a 110-m-high slope that is moderately steep from upslope to midslope and becomes steeper from midslope towards the foot. Slope is composed of 1.5–6 m-thick soil underlain by marl. Landslide debris is expected to cross the approximately 20-m-wide river at the foot of the slope and reach the cluster of houses.

Residents reported that rainfall-induced landslides occurred on the slope in 1970 and 2012. In 2019, a series of strong shallow earthquakes with magnitudes ranging from 6.1 to 6.6 (DOST-PHIVOLCS 2019) triggered numerous localized failures in the site and its vicinity. The next ground movement observed was the erosion of the steep part of the slope in 2020 due to heavy rainfall. In all these cases, debris only reached the river at the foot of the slope. However, residents said that the 2012 landslide blocked the river, causing it to overflow and flood the nearby houses. The flooding resulted in one casualty. Since the installation of the landslide EWS in 2022, no significant or critical movements have been observed warranting an evacuation.

The site is predominantly covered with agricultural lands and grasslands. The site is accessed from the main road, which is 5–6 km away, through a tertiary road. At-risk households, which is 96 in total, are located at the projected runout area across a river, none are located within the landslide source. Agricultural lands, school, churches, barangay hall, barangay health center, and a multipurpose hall are the other elements at risk of landslides.

Most of the community in site B are dependent on agricultural livelihoods. Crops are mostly, banana, abaca, rubber, root crops, coconuts, vegetables, and rice. Some also raise livestock and poultry. Some do basket and *bilao*- or winnowing basket-making as an alternative livelihood. Some members of the community received livelihood training and capital support from NGOs and government programs. However, participants noted that livelihood improvement is still one of their main concerns.

The locals recognize the functions of BLGU in DRRM. Active sectoral organizations are also present. The community consists of almost 100% indigenous people, which is associated with the culture of sharing, *bayanihan*, and volunteerism. The community acknowledges that there is still a lack of awareness and knowledge on landslides.

5.3 Site C

The barangay where site C is located is characterized by rugged terrain and has dense forest cover. The site is at the foothills of a potentially active volcano and is traversed by an active fault. The monitored landslide area is on a 70-m high and generally steep slope. The slope is composed of 4.5–10.5 m of soil underlain by volcanic bedrock. Landslide debris is expected to flow through a channel towards the barangay road.

The 2019 series of strong shallow earthquakes with magnitudes ranging from 6.1 to 6.6 (DOST-PHIVOLCS 2019) triggered localized failures and the development of cracks on the slope. The 2019 event is the first notable slope movement in the area. No alert level warranting an evacuation has been raised on site since the installation of the landslide EWS in 2022.

The site also has agricultural areas. It is 17 km away from the municipal center and is connected through a tertiary road. The 16 at-risk households are located at the projected runout area. Agricultural lands and infrastructure for water supply are amongst the important elements identified by the participants that may be affected should a landslide occur.

The community is dependent on agricultural livelihoods such as planting crops, e.g. banana, rubber, fruits, coffee, and tiger grass, and raising livestock and poultry. They also have alternative livelihoods, such as basket and *bilao*- or winnowing basket-making, whisk broom-making, and backyard gardening.

BLGU functions in DRRM are recognized by the community. Sectoral organizations are also present. The site is predominantly an IP community that strongly believes in working together, *bayanihan*, and volunteerism. The community recognizes that there is a lack of awareness and participation in DRRM activities related to landslides.

5.4 Site D

Site D generally comprises agricultural and residential areas. The monitored area sits on an approximately 50-m-high, steep slope. Slope is composed of 1.5–12 m thick soil underlain by siltstone. Signs of ground movement, i.e., cracks, seepages, and bulging, were first observed in 2011 after a two-week period of continuous rainfall. The barangay road and at least seven houses were damaged. A landslide early warning system has been in place since 2015 and began transitioning to a community-based early warning system for landslides (CBEWS-L) in 2022. Since the installation of the landslide EWS, no alert level warranting an evacuation response was raised on site.

The site is located less than 500 m from the national road. The 70 at-risk houses, some agricultural land, and microscale businesses are clustered at the footslope and within the run-out zone.

Most barangay residents are dependent on agricultural livelihoods such as planting crops, e.g. rice, corn, banana, vegetables, root crops, and coconuts, and raising livestock and poultry. A communal garden is also present.

Apart from landslides, the community has ongoing concerns about secure land tenure and access to potable water sources. Within the area, few households hold legal ownership over the plots where their homes are situated. Additionally, most dwellings lack connections to formal water infrastructure. While drinking water is delivered commercially, domestic supplies, such as water for cleaning, must be fetched manually from deep wells or from the stream traversing the barangay.

The community has close ties. The BLGU and the Landslide Early Warning Committee, a local community organization spearheading the CBEWS-L, are recognized for their contributions to DRRM.

6 Discussion

6.1 Risk Priorities

By providing a venue to discuss amongst themselves and adapting the concept of relative comparison, participants were able to systematically determine their priorities. Across sites, population was unanimously ranked highest, followed by residential structures. The utilities category is either ranked third or fourth followed by transportation, which is either ranked fourth or fifth. The importance of natural resources varies. Sites A and B put natural resources as the third priority while it is the sixth priority for Site C and the bottom priority for Site D. Institutional categories ranked third, fourth, or seventh, while commercial is consistently placed at the bottom half of the ranking. Cultural landmarks are either placed at the bottom or not considered at all. The most surprising result is the placement of agriculture in the community priorities. A large portion of the community in all the sites depend on agriculture for livelihood, however, only sites A and B ranked agriculture in the top three or four in terms of priorities. Sites C and D ranked agriculture sixth and seventh.

All four sites, identified age, health, income, housing, and lack of access to utilities as indicators of vulnerability, while DRR capacities, social assets, and physical assets as indicators of capacity.

These prioritizations are reflected in the recommendations of the participants. Site A highlighted the importance of natural resources. With natural resources as one of their top priorities, they provided recommendations focused on environmental protection, such as strict enforcement of rules on illegal logging and prevention of backyard burning. Site B, on the other hand, associated vulnerability mainly with human knowledge, skills, and attitude. These are reflected in their recommendation for strengthening DRR awareness and conducting activities for the vulnerable sectors. Site C gave importance to disaster risk reduction (DRR) knowledge and awareness as an aspect of vulnerability. Site D strongly recommended the development of infrastructures for stable water supply, as this was underscored as the main challenge to the community. Site D also put emphasis on the effect of family dynamics on vulnerability. They highlighted the importance of family as the primary unit that gives support to a person.

6.2 Results of Risk Assessment

The integration of the landslide risk components into risk maps (Fig. 5a–d) reveals that most of the households in the sites are at high risk of landslides. Their location in a deep-seated landslide hazard zone greatly puts them at risk. In addition, different vulnerabilities—not limited to social, environmental, and human—intensify their vulnerability, which puts them at higher risk. Figure 5 shows the household-level risk maps of the four sites.

In-depth information and multi-dimensional issues and concerns surfaced during the community workshops and through multi-stakeholder participation. The following are the highlights of the vulnerabilities faced by landslide communities:

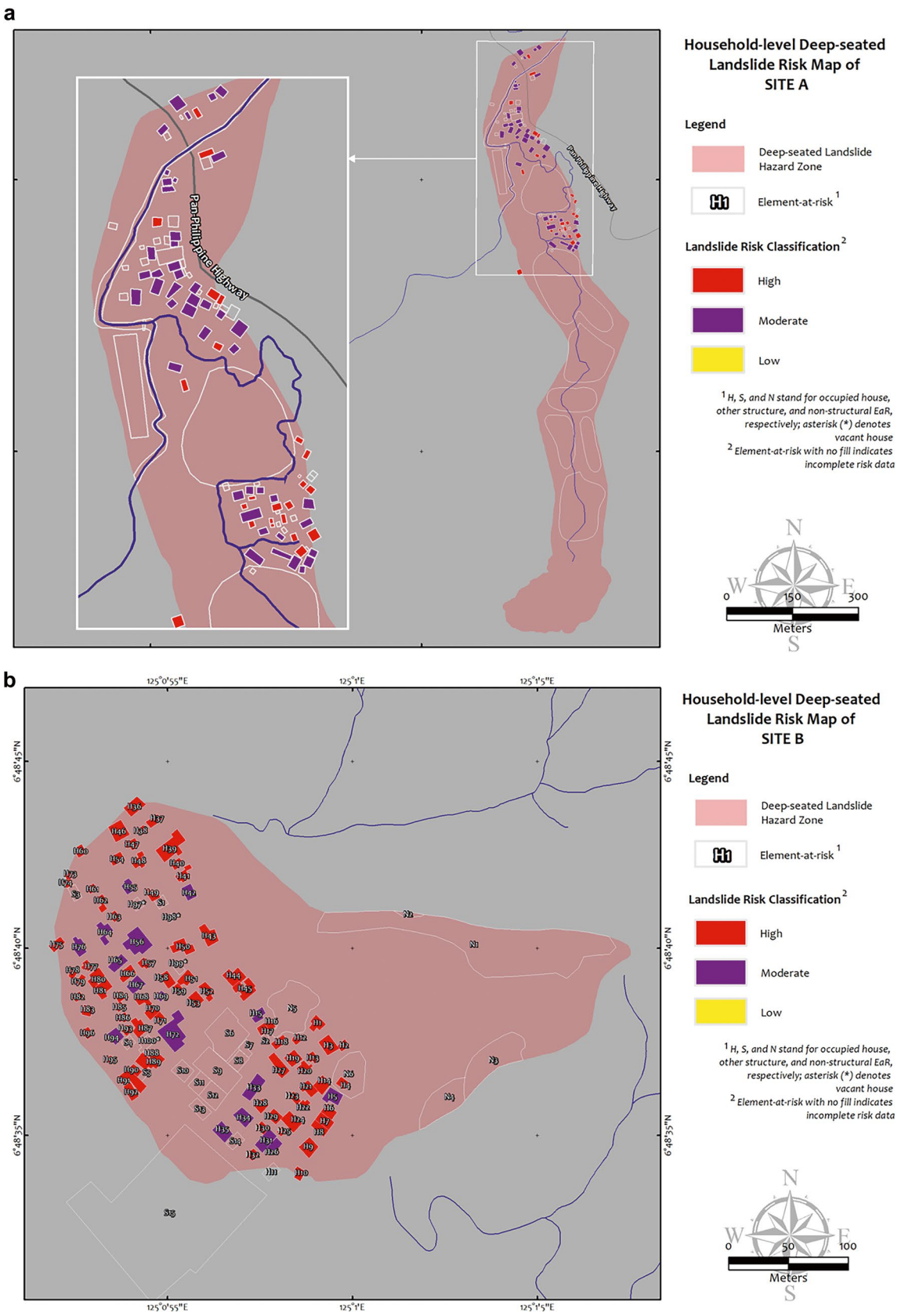


Fig. 5 (**a**) Household-level landslide risk map of Site A. (**b**) Household-level landslide risk map of Site B. (**c**) Household-level landslide risk map of Site C. (**d**) Household-level landslide risk map of Site D

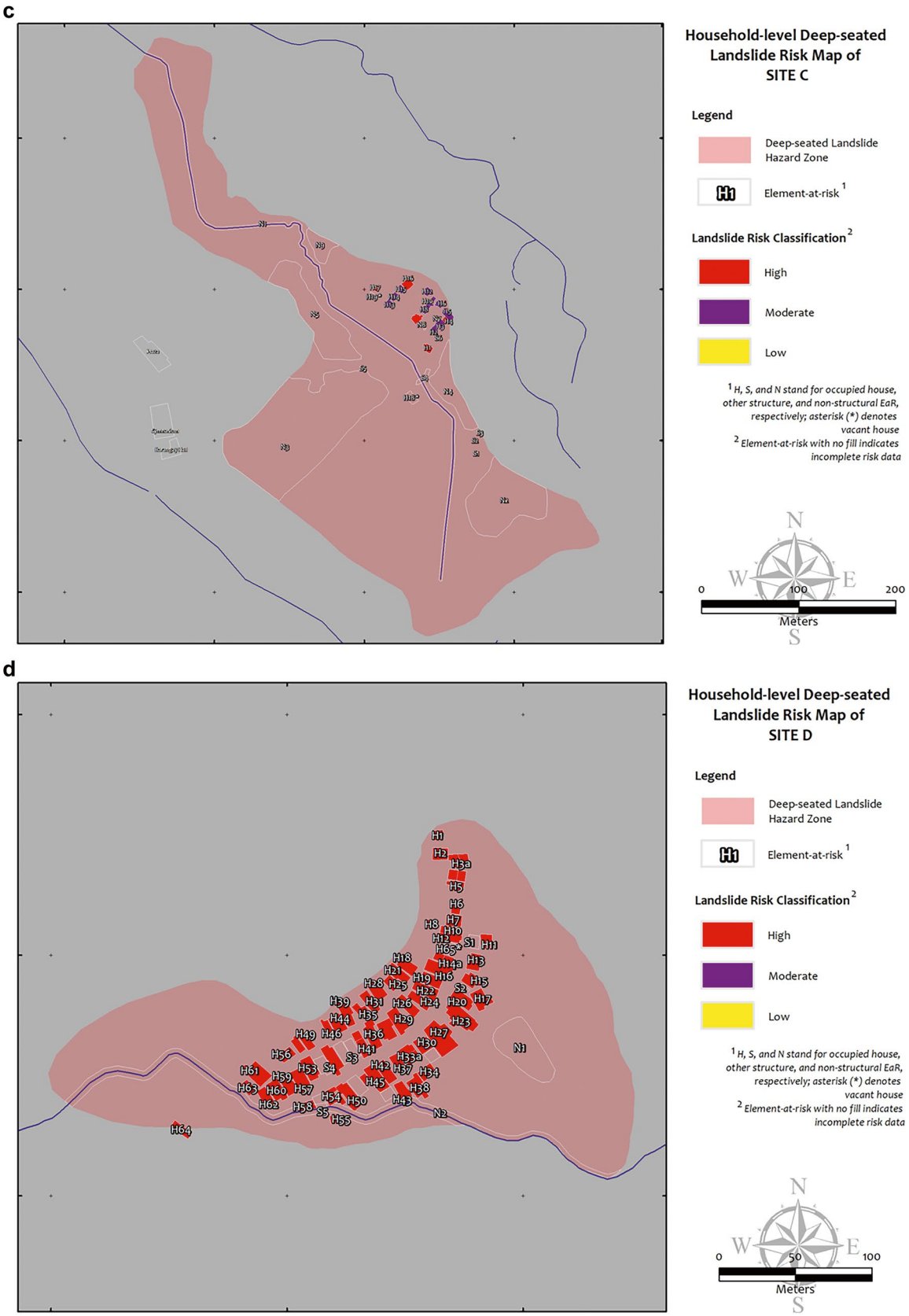


Fig. 5 (continued)

Low income status and lack of financial resources are mainly attributed to their dependence on agricultural-based livelihoods within the hazard area. In all four study sites, agriculture and farming are the major livelihoods identified. The lack of access to alternative livelihood is one of the dynamic pressures of their vulnerability. For landslide communities, there is a heavy reliance on their land. The problem is, that their farmlands are exposed to landslide hazards. Most residents cannot leave their home or their land due to a lack of other opportunities. However, they are willing to relocate to safer locations as long as they have access to their farmlands or if other livelihood activities are present.

Lack of risk knowledge is another major pressure for the vulnerability of the community. Although some residents have attended drills and training, there are still a recognizable number of people in the community who do not have an understanding of the risk present in the village. This is one of the reasons why they are not prepared enough to respond to landslides despite the early warning systems in place.

Ancestral land entitlements and attachments forced some communities to stay on hazard areas. For the study sites living on ancestral domains, i.e., sites B and C, the culture and ancestral land entitlements and attachments keep them from looking for safer areas outside their barangay. According to some residents, they have been living in their lands for 30–40 years or longer and do not consider leaving their ancestral lands behind. This is despite the knowledge that they are exposed to landslide hazards.

Climate change contributes to the vulnerabilities of landslide communities. The communities also recognized that there are more frequent strong typhoon events which worsens the struggle of the farming population for productivity and livelihood. Also, noticeable unpredictable weather conditions destroy non-climate resilient crops which leads to greater loss.

The highlights of community capacities are the following:

Risk management strategies such as the presence of established local plans are present and are required by the local government to provide an enabling environment for the implementation of DRR measures. In the Philippines, every *barangay* is mandated to produce DRRM plans and identify strategies for the community. These include contingency plans and activities for the implementation of a community-based DRRM.

EWS practices such as information dissemination and landslide monitoring are regularly conducted. For the study sites, there is an established people-centered EWS system in place. The community takes part in the monitoring of the landslide site, as well as in disseminating warning information. The residents also take part in capacity-building activities to enhance their knowledge of the risks present at the site. However, participation can still be improved by providing insurance and incentives.

Social capacities such as strong community ties and the recognition of the role of women and the youth contribute to risk management strategies. The local term *bayanihan* or the collective action of the people to achieve a task or reach a common goal is strong in the community. Also, another common capacity is the recognition of the different roles of community members in reducing landslide risk. The women and the youth sector also take part in DRRM and EWS activities such as information dissemination, monitoring, and capacity-building activities.

7 Conclusion

This study corroborates the value of shifting from a hazard-centric to a vulnerability-focused, participatory risk assessment approach through its examination of four landslide-prone communities in the Philippines. By emphasizing social vulnerability and community participation, the intricacies faced by at-risk populations were revealed in richer detail. The paradigm positioned disaster risk not just as a physical phenomenon but as a developmental issue shaped by underlying social, economic, and political determinants.

During the CLRA, in-depth information on vulnerabilities surfaced during the community workshops and through multi-stakeholder participation. Site-specific concerns arise from different community contexts which will be useful in developing site-specific risk management strategies and actions.

The integrated, participatory methodology highlighted the importance of meaningful community participation in all activities. It also showed how the complexity in quantifying exposure, vulnerabilities, and capacities based on extensive data can be simplified by providing the community a venue to discuss and identify their priorities based on the concept of relative comparison. This paper highlighted that integrating different risk components with participatory identification of risk indicators and corresponding weights shows promising results in drawing out different community contexts that may not be captured solely on a definite set of criteria.

From this, utilization and continuous exploration and improvement of participatory tools and methods of landslide risk assessment are recommended to ensure that at-risk communities can realize and articulate factors that aggravate their risk of landslide.

Acknowledgments The authors would like to thank the communities for their generosity in time, energy, and insights. The communities are the core of this study. To Roy Albert Kaimo (colleague), Melody Teodoro (colleague), Mabelline Cahulogan (PHIVOLCS GGRDD-OIC), and Dr. Teresito Bacolcol (PHIVOCS Director), thank you for taking the time, amidst your hectic schedules, to comment on the manuscript. Also, the authors would like to show appreciation to their colleagues who closely worked with them during the workshops.

References

Agliata R, Bortone A, Mollo L (2022) The impact of the aggregation formula on indicator-based method for the assessment of building susceptibility to hydro-meteorological hazards. Int J Disaster Risk Reduct 72:102850

Althuwaynee OF, Pradhan B (2017) Semi-quantitative landslide risk assessment using GIS-based exposure analysis in Kuala Lumpur City. Geomat Nat Haz Risk 8(2):706–732

Anderson MG, Holcombe E (2013) Community-based landslide risk reduction: managing disasters in small steps. World Bank, Washington, DC. https://doi.org/10.1596/978-0-8213-9456-4

Antronico, L., De Pascale, F., Coscarelli, R., & Gullà, G. (2020). Landslide risk perception, social vulnerability and community resilience: The case study of Maierato (Calabria, southern Italy). Int J Disaster Risk Reduct, 46, 101529

Anshori RM, Samodra G, Mardiatno D, Sartohadi J (2022) Volunteered geographic information mobile application for participatory landslide inventory mapping. Comput Geosci 161:105073. https://doi.org/10.1016/j.cageo.2022.105073

Bawagan AB (2011) Community-based disaster-risk reduction and management framework lessons from implementation. Philipp J Soc Dev 3:45–64

Bera S, Guru B, Chatterjee R, Shaw R (2020) Geographic variation of resilience to landslide hazard: a household-based comparative studies in Kalimpong hilly region, India. Int J Disaster Risk Reduct 46:101456

Birkmann J (2006) Measuring vulnerability to promote disaster-resilient societies: conceptual frameworks and definitions. In: Measuring vulnerability to natural hazards: towards disaster resilient societies, vol 1. United Nations University Press, New York, pp 3–7

Bollin C, Hidajat R (2006) Community-based risk index conceptual framework. In: Birkmann J (ed) Measuring vulnerability to natural hazards—towards disaster resilient societies. United Nations University, New York, p 257

Cardona OD, Van Aalst MK, Birkmann J, Fordham M, Mc Gregor G, Rosa P et al (2012) Determinants of risk: exposure and vulnerability. In: Managing the risks of extreme events and disasters to advance climate change adaptation: special report of the intergovernmental panel on climate change. Cambridge University Press, pp 65–108

Cutter SL, Boruff BJ, Shirley WL (2012) Social vulnerability to environmental hazards. In: Hazards vulnerability and environmental justice. Routledge, pp 143–160

DOST-PHIVOLCS (2019) Poster of the October 2019 series of earthquakes in Cotabato and vicinity. www.phivolcs.dost.gov.ph. https://rb.gy/6psp2l. Retrieved 14 April 2024

Duraiappah AK, Roddy P, Parry JE (2005) Have participatory approaches increased capabilities? International Institute for Sustainable Development, Winnipeg

Dynaslope Project (2022a, May 26) Dynaslope Project [video]. YouTube. https://www.youtube.com/watch?v=op4AkscKKsA

Dynaslope Project (2022b, May 27) Dynaslope Project (community) [video]. YouTube. https://www.youtube.com/watch?v=2w56LR1gHGk

Dynaslope Project (2022c, May 27) Dynaslope Project (technology) [video]. YouTube. https://www.youtube.com/watch?v=8eZxLxsAEBM

Faas AJ (2016) Disaster vulnerability in anthropological perspective. Ann Anthropol Pract 40(1):14–27

Fell R, Ho K, Lacasse S, Leroi E (2005) A framework for landslide risk assessment and management. CRC Press

Gumiran BAL, Moncada FM, Gasmen HJ, Boyles-Panting NR, Solidum RU (2019) Participatory capacities and vulnerabilities assessment: towards the realisation of community-based early warning system for deep-seated landslides. Jàmbá 11(1):11. https://jamba.org.za/index.php/jamba/article/view/555/1104

Jhong BC, Huang J, Tung CP (2019) Spatial assessment of climate risk for investigating climate adaptation strategies by evaluating spatial-temporal variability of extreme precipitation. Water Resour Manag 33:3377–3400

Kulatunga U, Amaratunga PD, Zaman AKMM, Parvez A (2010) Community risk assessment for disaster risk reduction: challenges and future. ResearchGate. https://www.researchgate.net/publication/46212904_Community_risk_assessment_for_disaster_risk_reduction_challenges_and_future

Liu W, Dugar S, McCallum I, Thapa G, See L, Khadka P et al (2018) Integrated participatory and collaborative risk mapping for enhancing disaster resilience. ISPRS Int J Geo Inf 7(2):68

Mcleod E, Margles S, Wongbusarakum S, Gombos M, Daze A, Otzelberger A et al (2015) Community-based climate vulnerability and adaptation tools: a review of tools and their applications. Coast Manag 43(4):439–458

Nkombi Z, Wentink GJ (2022) The role of public participation in disaster risk reduction initiatives: the case of Katlehong township. Jamba 14(1). https://doi.org/10.4102/jamba.v14i1.1203

Pandey BH, Okazaki K (2005) Community-based disaster management: empowering communities to cope with disaster risks. Reg Dev Dialogue 26(2):52

Participatory Development Models (2013) Future together. https://www.undp.org/cyprus/publications/participatory-development-models

Perera ENC, Jayawardana DT, Jayasinghe P, Ranagalage M (2019) Landslide vulnerability assessment based on entropy method: a case study from Kegalle district, Sri Lanka. Model Earth Syst Environ 5:1635–1649

Perera ENC, Gunaratne C, Samarasinghe SBD (2022) Participatory landslide inventory (PLI): an online tool for the development of a landslide inventory. Complexity 2022:1–10. https://doi.org/10.1155/2022/2659203

Preuner P, Scolobig A, Linnerooth Bayer J, Ottowitz D, Hoyer S, Jochum B (2017) A participatory process to develop a landslide warning system: paradoxes of responsibility sharing in a case study in Upper Austria. Resources 6(4):54. https://doi.org/10.3390/resources6040054

Project LIGTAS (n.d.) Project LIGTAS. https://ligtasuplb.wordpress.com/

Saaty RW (1987) The analytic hierarchy process—what it is and how it is used. Math Model 9(3–5):161–176. https://doi.org/10.1016/0270-0255(87)90473-8

Safeland (2011) Deliverable D2.4 Guidelines for landslide susceptibility, hazard and risk assessment and zoning. Living with landslide risk in europe: assessment, effects of global change and risk management strategies. https://www.ngi.no/eng/Projects/SafeLand/#Reports-and-publications

The World Bank Participation Sourcebook (1996) The World Bank. https://doi.org/10.1596/0-8213-3558-8

Titz A, Cannon T, Krüger F (2018) Uncovering 'community': challenging an elusive concept in development and disaster related work. Societies 8(3):71

Twigg J (2009, February 19) Disaster risk reduction: mitigation and preparedness in development and emergency programming. PreventionWeb. https://www.preventionweb.net/publication/disaster-risk-reduction-mitigation-and-preparedness-development-and-emergency

UNDRR (2009, January 23) Disaster risk. https://www.undrr.org/terminology/disaster-risk

van Aalst MK, Cannon T, Burton I (2008) Community level adaptation to climate change: the potential role of participatory community risk assessment. Glob Environ Chang 18(1):165–179. https://doi.org/10.1016/j.gloenvcha.2007.06.002

Varnes DJ, the International Association of Engineering Geology Commission on Landslides and Other Mass Movements on Slopes (1984) Landslide hazard zonation: a review of principles and practice. Unesco. https://unesdoc.unesco.org/ark:/48223/pf0000063038

Wisner B, Blaikie P, Cannon T, Davis I (2004) At risk: natural hazards, people's vulnerability and disasters. Routledge

Open Access This chapter is licensed under the terms of the Creative Commons Attribution 4.0 International License (http://creativecommons.org/licenses/by/4.0/), which permits use, sharing, adaptation, distribution and reproduction in any medium or format, as long as you give appropriate credit to the original author(s) and the source, provide a link to the Creative Commons license and indicate if changes were made.

The images or other third party material in this chapter are included in the chapter's Creative Commons license, unless indicated otherwise in a credit line to the material. If material is not included in the chapter's Creative Commons license and your intended use is not permitted by statutory regulation or exceeds the permitted use, you will need to obtain permission directly from the copyright holder.



The Accuracy of Landslide Susceptibility Mapping in Young Glacial River Valleys

Anna Małka, Izabela Laskowicz, and Dariusz Grabowski

Abstract

Many aspects affect the accuracy of the geographical information system- and statistically-based susceptibility maps. These aspects can be divided into four categories related to: (α) study area, (β) scale, (γ) input data, and (δ) methods, used for susceptibility calculation, landslide representation and map visualisation. Most of these aspects have an impact on the others and each of them is very complex. Due to the complexity of this issue, the article is limited to two aspects, i.e. scale and one of the crucial causal factors, namely geology. The selection of the research area is a key aspect in susceptibility mapping. The research area can influence the choice of scale (pixel size), input data, and methods. In the case of the young glacial Lower Vistula and Central Radunia Valleys, small-scale susceptibility maps give an inaccurate conclusion: on the continental scale, the susceptibility of these areas is underpredicted; on the national scale, the susceptibility is usually overpredicted. The geological structure of young glacial river valleys is complex due to the presence of alternating permeable (sands, gravels) and non-permeable (clays, silts) sediments in the profile, which affects water circulation on the slope and landslide activation. According to the prediction rate method for the Lower Vistula Valley and the classification and regression trees method for the Central Radunia Valley, the maps of surface deposits were of little relevance to landslide susceptibility prediction. However, the inclusion of a quasi-three-dimensional geological model—a typical lithologic sequence layer in the susceptibility mapping of the Vistula Valley, shows that it is one of the most important factors.

Keywords

Landslide susceptibility · Scale · Quasi-three-dimensional geological model · River valley

1 Introduction

Various aspects affect the accuracy of the geographical information system (GIS)- and statistically-based models of landslide susceptibility (e.g. Galli et al. 2008; Rossi et al. 2010; Liu and Duan 2018; Fleuchaus et al. 2021).

In landslide susceptibility, the input data are represented by a causal factor and an inventory map (landslide inventory). According to Rossi et al. (2010), Liu and Duan (2018), Fleuchaus et al. (2021) the accuracy of causal factor maps consists of quality, adequacy, abundance, and completeness. Comprehensive topographic and environmental databases are essential for GIS analysis. The selection of geospatial data should be determined by relevance, reliability, and compatibility of scales (Günther et al. 2014). The accuracy of thematic layers is important for susceptibility mapping. Nevertheless, the process of choosing conditioning (causal) parameters is not standardized (Ayalew et al. 2005; Yalcin 2008). Ayalew et al. (2005) attempted to solve this problem by drawing attention to five important criteria. They postulated that in GIS-based studies, the selected factor should be operational, complete, non-uniform, measurable, and non-redundant (Ayalew et al. 2005; Yalcin 2008; Magliulo et al.

A. Małka (✉)
Marine Geology Branch, Polish Geological Institute—National Research Institute, Gdańsk, Poland

Institute of Geosciences, Johannes Gutenberg-University, Mainz, Germany
e-mail: anna.malka@pgi.gov.pl

I. Laskowicz
Carpathian Branch, Polish Geological Institute—National Research Institute, Kraków, Poland
e-mail: izabela.laskowicz@pgi.gov.pl

D. Grabowski
Polish Geological Institute—National Research Institute, Warsaw, Poland
e-mail: dariusz.grabowski@pgi.gov.pl

© The Author(s) 2025

B. Abolmasov et al. (eds.), *Progress in Landslide Research and Technology, Volume 3 Issue 2, 2024*, Progress in Landslide Research and Technology, https://doi.org/10.1007/978-3-031-72736-8_13

2008). Some authors point out that the use of independent factors benefits landslide susceptibility mapping (LSM) accuracy (Chung and Fabbri 2003; Remondo et al. 2003; Ayalew et al. 2005; Magliulo 2012). Other authors claim that using only independent factors in LSM is determined by the choice of the susceptibility calculating method (Grabowski et al. 2022; Małka et al. 2023). However, identification of causal factors that directly influence the landslide is crucial, as including irrelevant factors will reduce the performance of models (Ado et al. 2022).

In addition, landslide susceptibility calculation requires the preparation of a landslide inventory. The use of the most accurate and up-to-date information on landslides enables the implementation of effective susceptibility models (Galli et al. 2008). Landslide inventory should also be characterised by high quality, accuracy, and completeness (Galli et al. 2008; Rossi et al. 2010; Liu and Duan 2018). However, due to a scarcity of historical data, mass movement databases are often incomplete (Van Westen et al. 2008). Furthermore, many researchers show that the selection of data representing landslides has a significant impact on the results of the analysis (e.g. Godt et al. 2012; Magliulo et al. 2008; Süzen and Doyuran 2004). The way of presenting mass movements hampers the accuracy of susceptibility models. As argued by Godt et al. (2012), sizable slope failure representations benefit from being shown in the form of whole landslide polygons or their detachment zones rather than points. According to Magliulo et al. (2008), the difference between a landslide and a landslide detachment zone must occur in geo-environmental classes prone to failure. Moreover, better results are produced when weight values are calculated taking into account the detachment zones (Magliulo et al. 2008). Applying seed cells (i.e. buffer zones to the landslide crown) that show the conditions before a slope failure occurs is advised by some scientists (Süzen and Doyuran 2004; Conoscenti et al. 2008). Furthermore, different types of mass movements may exist in the same study area, and different types of slope failures are influenced by different factors and their representation on a map requires different LSM models (Ruff 2005).

Another aspect is the location and nature of the study area. The presence of slope movements depends on the local geomorphological (Rossi et al. 2010) and geological (Van Westen et al. 2008) setting. Selecting causal factor layers is determined by the nature of the investigated area (Ayalew et al. 2005; Magliulo et al. 2008).

A large number of statistical methods are used in susceptibility calculations (e.g. Pourghasemi et al. 2013; Pourghasemi and Rahmati 2018). So far, different methods have produced different accuracies for LSM (e.g. Mrozek et al. 2004; Vakhshoori and Zare 2016; Pourghasemi and Rahmati 2018). However, the best method has not been identified, as different methods may work better for different areas (Huang and Zhao 2018; Chowdhury 2023). The accuracy of LSM is influenced by the selection of statistical methods, implementation in statistical programs, and also our ability and experience with different statistical methods (Rossi et al. 2010; Althuwaynee et al. 2014). Nowadays, many various statistically-based LSM modelling methods are used, i.e. weight of evidence (e.g. Mrozek et al. 2004; Regmi et al. 2010), landslide susceptibility index (e.g. Pourghasemi et al. 2013), frequency ratio (e.g. Lee and Pradhan 2007; Vakhshoori and Zare 2016, 2018; Akinci and Yavuz Ozalp 2021) and advanced machine learning techniques (MLTs) including conventional, hybrid, ensemble and deep learning techniques (e.g. Lee and Pradhan 2007; Bai et al. 2010; Pourghasemi et al. 2013; Youssef et al. 2016; Kim et al. 2018; Pourghasemi and Rahmati 2018; Akinci and Zeybek 2021; Azarafza et al. 2021; Gaidzik and Ramírez-Herrera 2021; Ado et al. 2022). Another important aspect, albeit difficult to assess and evaluate, is expert knowledge (Fleuchaus et al. 2021).

Although many problems have been identified in regards to the accuracy of susceptibility maps, so far there has been a limited attempt to prioritise these problems and identify what is most important in developing reliable and exact susceptibility maps. This study focused on the problems with accuracy that have not been widely discussed in scientific literature so far, i.e. the scale and one of the crucial causal factors, namely geology. By using the example of young morainic regions, the authors of the article show that the typical flat (2D geological model) way of presenting geological data is insufficient. The use of a quasi-3-D geological model allows for improving the accuracy of LSM predictions. The problem of a scarcity of relevant geological data (drilling) was also discussed. Additionally, an attempt has been made to sort out the factors related to the accuracy of the LSM and their interdependence.

2 Location and General Features of the Study Areas

This study investigates landslide susceptibility assessment using geographic information system (GIS)-based statistical models in river valleys. Two similar areas in Northern Poland were considered, namely the Lower Vistula and the Central Radunia Valleys (Fig. 1).

The Lower Vistula and the Central Radunia Valleys are located in the northern part of the European Lowlands, within Vistulian (Weichselian) Glaciation range (Marks 2012; Fig. 1). In terms of geomorphology, both study areas are located in young morainic areas; the Lower Vistula Valley (LVV) primarily within postglacial plateau, and the Central Radunia Valley (CRV) within an outwash plain. Both the areas are oriented in the SW–NE direction. Both the river valleys form flat-bottomed valleys cut into the plateau. The slopes of the valleys are systematically transformed by mass

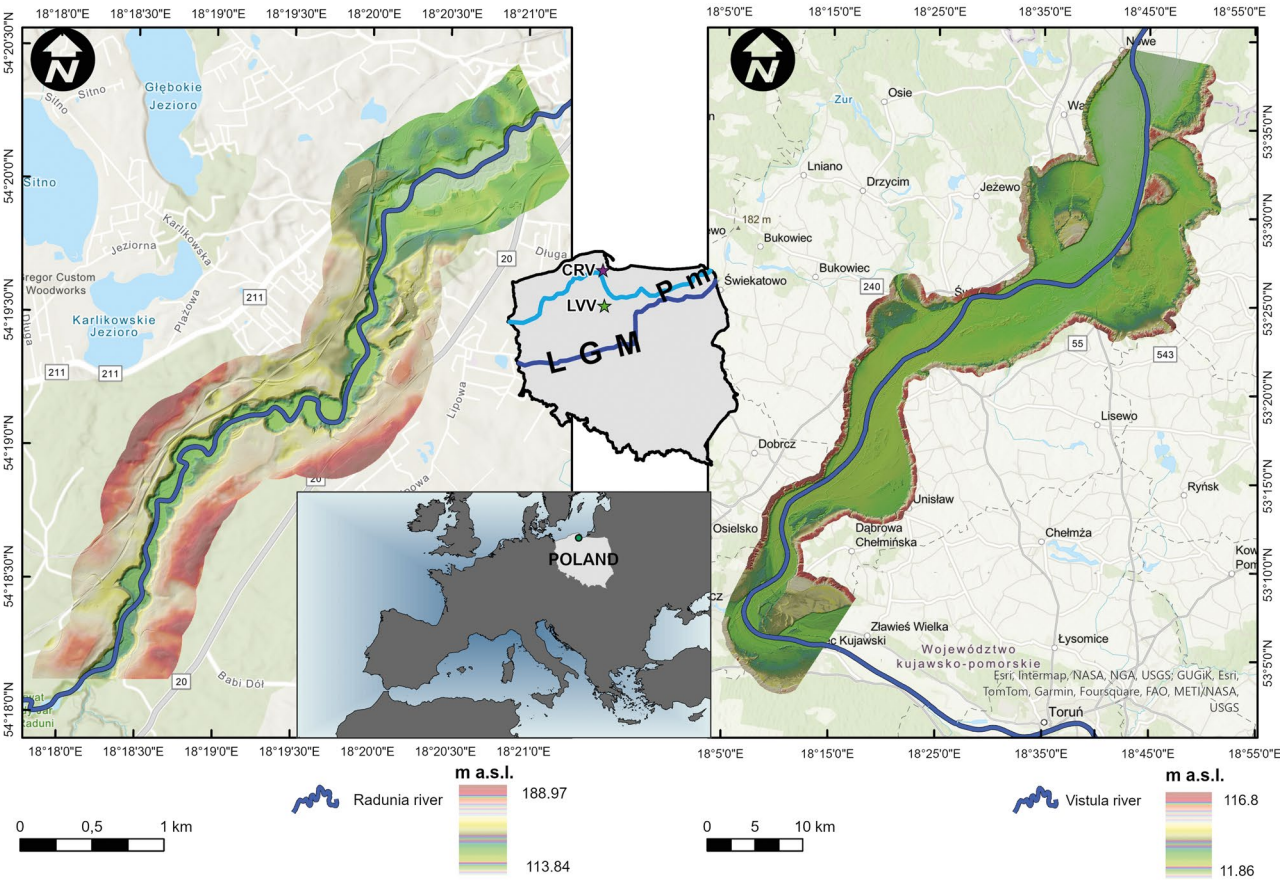


Fig. 1 The study areas—the Central Radunia Valley (CRV) (on the left), the Lower Vistula Valley (LVV) (on the right). Abbreviations: LGM—the Last Glacial Maximum ice sheet extent, and Pm—the Scandinavian Ice Sheet limits during the Pomeranian Phase (the glaciation extent according to Marks 2012). Maps were generated using ArcGIS Pro software, copyright and licensed by ESRI (https://www.esri.com/en-us/arcgis/products/arcgis-pro/overview)

movements. What distinguishes the two rivers is their size (the Vistula, with a total length of 1022 km and the Radunia 103 km).

The LVV occupies 917 km^2 and is 76.5 km long and 5–20 km wide. However, the CRV occupies 4.75 km^2 and is approximately 4.5 km long and up to 0.5 km wide. The terrain relief in both the areas is similar 75 m in the CRV and 104 m in the LVV (Fig. 1). The average annual precipitation is about 530 mm in the LVV and 630 mm in the CRV, with most (350–400 mm) rainfall occurring in summer (Woś 1999; Licbarski 1989; Jereczek-Korzeniewska 2005).

Although most of the study areas are covered by Quaternary sediments, the geological formations in the LVV include Neogene soft rock. In both the areas of interest, Holocene and Pleistocene formations related mainly to the upper stage of the Vistulian Glaciation are exposed on the surface. The geological structure in the LVV is dominated by Pleistocene deposits of glacial origin (tills, boulders, gravels, and sands), fluvioglacial origin (sands, gravels) and local limnoglacial sediments (silty sands, silts, and varved clays). The geological structure in the CRV is dominated by Pleistocene deposits of fluvioglacial origin (sands, gravels) and local glacial origin (tills).

Considering the material type in both investigated regions, only soil landslides occur (Hungr et al. 2014; Grabowski et al. 2022; Małka et al. 2023). However, due to the type of movement, rotational slides or combined complex (slide and flow) dominate (Varnes 1978; Cruden and Varnes 1996; Hungr et al. 2014; Grabowski et al. 2022; Małka et al. 2023). The vast majority of landslides cover the entire slope from their upper rim to the bottom of the valley. Some of the landslides can be considered retrogressive (Cruden and Varnes 1996).

3 Input Data and Research Methodology

This article uses data from previous work for two geomorphological and hydrogeological analogous areas (Günther et al. 2014; Wilde et al. 2018; Wojciechowski 2019; Grabowski et al. 2022; Małka et al. 2023). The authors of the

article aimed to analyse and compare the two river valleys lying in young morainic areas of lowland Poland.

The first stage of work was confining the study areas to homogeneous geomorphological elements, i.e. a steep section of the river valleys entrenched in lowlands. To determine landslide-causing factors and to delineate mass movement digital elevation model (DEM) derived up to a centimetre-scale LIDAR (light detection and ranging) was used. For modelling the LSMs, the data were prepared in the form of raster maps (for the LVV 10 × 10 m and for the CRV 1 × 1 m resolution respectively) and the set of all landslides was randomly divided into training and validation sub-datasets covering 70% and 30% of landslides. Various instability factors (geomorphological, geological, hydro-logical, and environmental) were used in the modelling of LSMs, i.e. for the Lower Vistula Valley 22 and for the Central Radunia Valley 25 factors.

The following methods for LSMs were used: the frequency ratio and predictor rate method (FR & PR) for the LVV and logistic regression (LR) for the CRV (Lee and Pradhan 2007; Bai et al. 2010). The FR and LR values were calculated for the entire area of landslides and for a wide set of factors with several topographic layers derived from DEM, which reflects the specific morphology of the study areas. To measure the weight of a factor in the set of all factors the prediction rate (PR) method for the LVV and the classification and regression trees (C&RT) method for the CRV were used (Althuwaynee et al. 2014; Breiman et al. 1984). The susceptibility assessment for the LVV and the CRV was carried out with a scale of 1: 25,000 and 1: 10,000 respectively.

The performance of the susceptibility model was evaluated using the success and prediction rate curves (SRC & PRC), and area under the curve (AUC) values (Chung and Fabbri 1999). For the PRC evaluation the 30% of the landslides were used. Data input data and methodology was described in detail by Grabowski et al. (2022) and Małka et al. (2023).

For validation of the accuracy of the susceptibility maps the following were used: field surveys and analysis of archival materials. In comparing susceptibility maps with different scales, the authors used their own data (Grabowski et al. 2022; Małka et al. 2023), other research materials (Wojciechowski 2019), and European Landslide Susceptibility Map version 2 (ELSUS v2) available on the European Soil Data Centre (ESDAC) Internet site (Günther et al. 2014; Wilde et al. 2018).

4 Results

Both the study areas are river valleys entrenched in a lowland plateau. Landslide susceptibility studies do not usually focus on these types of areas of interest. However, these river valleys are considered for landslide susceptibility mapping when analyses are done for large regions of national or continental extent. Scale is an important aspect and has a crucial impact on the accuracy of LSMs. A generalised approach to susceptibility is sufficient to identify priority areas on a continental or national scale (Eckelmann et al. 2006). In contrast, detailed susceptibility analyses should be conducted in more homogeneous regions, where specific landslide types and similar environmental conditions are dealt with (Günther et al. 2013).

In both the areas of interest, landslides develop exclusively on the valley slopes on either side of the river. The average size of a landslide for the Lower Vistula Valley is 20,000 m^2 and 3900 m^2 for the Central Radunia Valley. The width of the slopes where landslides can develop does not exceed 800 m in the LVV and 45 m in the CRV. As a result, for the LVV and the CRV zones with a gentle slope (<6°) cover an area of: 89.49% and 51.57% respectively.

The nature of the study areas, the size of the landslides, and the width of the slopes were important factors in the selection of the pixel size. A pixel size of 10 × 10 m and 1 × 1 m was adopted, which made it possible to obtain very good results of the susceptibility models for the LVV and the CRV (Table 1). In general, models with an AUC value between 90 to 100% are considered to have excellent accuracy (Akinci and Zeybek 2021).

For the European Landslide Susceptibility Map (ELSUS v2), a pixel size of 200 × 200 m was assumed (Günther et al. 2014; Wilde et al. 2018). On this map, the area of the LVV was mostly classified as very low, low, and medium susceptibility. The ELSUS v2 susceptibility map was compared with existing landslides in the areas. As a result, it was found that for the LVV, 60% of the landslide areas are classified on ELSUS v2 map as very low and low susceptibility, 36% as medium, and only 4% as high susceptibility. In contrast, for the CRV, 95% of the landslides are located in the zones of very low susceptibility and 5% in the zones of low susceptibility. In the CRV the zones with very low susceptibility include landslides that have become active in recent years, such as the Rutki landslide.

In the case of the susceptibility map of Poland (SMP), the area along the rivers entrenched in a lowland plateau fall within zones of high susceptibility. The map was made with a resolution of 50 × 50 m, and the determining factor for susceptibility was slopes between 9° and 30° (Wojciechowski 2019). Comparing the susceptibility map of Poland with the

Table 1 Ranking of the model configurations according to their effectiveness

Model	AUC for SRC (%)	AUC for PRC (%)
The Lower Vistula Valley	95.90	97.35
The Central Radunia Valley	94.52	93.65

susceptibility maps of the areas investigated in this article (detailed maps), it was found that the widths of the susceptible areas on the SMP are twice as large as on the detailed maps, and sometimes the high susceptibility also includes the flat bottom of the river valleys. The effect of scale on landslide susceptibility results for river valleys entrenched in lowlands is therefore significant.

The next important aspect that affects the accuracy of GIS-based statistical analysis of landslide susceptibility is a scarcity of relevant data, which are difficult to obtain for large areas. Not all relationships between the conditioning factors and landslides observed during field work can be modelled through statistical methods. Causal factors that are undetectable by statistical methods become apparent through field surveys and analysis of archival materials. The use of statistical methods allowed assessing the influence of visualisable factors on the formation and development of landslides, as well as on their distribution. In the case of the LVV and the CRV the validity of each causal factor for the entire area of landslides based on the PR and the C&RT methods was presented in Table 2. LSM modelling for regions of geomorphological similarity shows comparable relationships between the importance of basic passive factors. The most significant geo-environmental variable was the topography (slope inclination, TRI, LS), the NDVI factor and aspect were of secondary and minor importance respectively. However, it is interesting to compare the importance of geology for both areas. Geological structure is of key importance for susceptibility, but standard geological maps are surface deposits maps.

There is a lack of information on the thickness of successive lithological strata; in the case of deep landslides, their slip surfaces usually extend below the first stratum shown on the map.

Then, assigning a certain susceptibility to specific formations does not reflect reality, because in a deep landslide the sediments lying below are involved. In the process of developing a slip surface, deeper strata may in fact be more important than surface ones. In the case of the Vistula Valley, the authors of the article analysed geological cross-section (Fig. 2) and made typical lithologic sequence (TLS) layer to reduce inaccuracies.

In the Vistula Valley, the majority of large and deep landslides have the main slip surfaces developed in silts, clays (Neogene) or at the boundary between silts, clays and the higher lying Quaternary strata. These clays play a crucial role in the formation of deep landslides and are generally covered by two, three, and sometimes four younger geological layers (Fig. 2). They are, therefore, not marked on maps of surface deposits. Ignoring this aspect may give the false result of low influence of the lithological factor on landslide

Table 2 The impact of all the analysed conditioning factors on mass movements for the LVV and CRV

	Lower Vistula Valley		Central Radunia Valley	
No	Causal factor	PR	Causal factor	C&RT
1	Terrain ruggedness index	2.97	Slope inclination	1.00
2	Density of erosional incisions	2.78	Terrain ruggedness index	0.98
3	Topographic wetness index	2.61	SAGA catchment slop	0.88
4	Slope inclination	2.52	Slope mean of upslope area	0.82
5	Landforms	2.47	Length slope factor	0.79
6	Typical lithologic sequence (TLS)	2.18	Topographic wetness index	0.60
7	Profile curvature	2.11	Slope height	0.53
8	Plan curvature	2.11	Valley depth	0.52
9	Length slope factor	2.10	Flow path length	0.42
10	General curvature	2.08	Geomorphons	0.41
11	Distance to Vistula River channel	2.07	SAGA catchment area	0.40
12	Elevation	2.02	Land use and land cover	0.36
13	Surface deposits	2.00	Normalized difference vegetation index	0.31
14	Topographic position index	1.89	MDEM insolation	0.23
15	Normalized difference vegetation index	1.86	Channel network base level	0.23
16	Texture	1.60	DSM insolation	0.23
17	Aspect	1.58	Modified digital elevation model (MDEM)	0.20
18	First aquifer	1.43	Plan curvature	0.20
19	Flow accumulation	1.35	Stream power index	0.19
20	Standardized height	1.20	Profil curvature	0.16
21	Relative slope height	1.13	Surface deposits	0.14
22	Stream power index	1.00	Digital surface model (DSM)	0.12
23			Convergence index	0.11
24			Topographic position index	0.07
25			Aspect	0.06

formation. In fact, the lithological factor plays a very important role (sixth position in Table 2), but only if it is considered as a quasi-3-D model, i.e. a sequence of different slope building lithological strata (TLS) and not just as a surface deposits layer (13th position in Table 2).

Deep-lying geological structures have also an impact on hydrological conditions. The presence of strata influencing water circulation in the slope deposits is of particular importance, e.g. the presence of a sandy layer isolated from below and above by till or clays influences the presence of water on the slope and significantly influences the formation of landslides. In the fluvioglacial sands and gravels (8 and 5 in Fig. 2) there are springs which can activate landslides. The TLS layer was much more significant in susceptibility than the layer of surface deposits.

On the other hand, due to the lack of drilling data, the authors of the article could not make the same layer TLS for the Radunia Valley, where a homogeneous area was also selected for analysis. As a result, the surface deposits map has little significance in susceptibility assessment (21st position in Table 2) and the results of the susceptibility maps validation of the Radunia Valley are worse than in the Vistula Valley. The TLS significance in the Radunia Valley is clearly indicated by the analysis of the Rutki landslide. In the case of the Rutki landslide, the surface is composed of glacial sands and gravels, and humic sand, while the slip surface is developed in lower lying silts and peat (Fig. 3)..

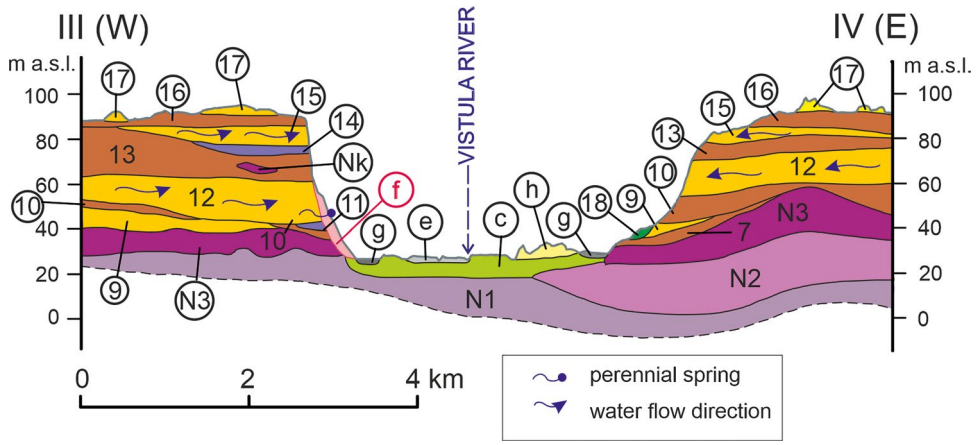


Fig. 2 Geological cross-sections across the Vistula Valley. Neogene: N1—sands, silts, clays, and brown coals, N2—sands, silts, clays, and brown coals, N3—lacustrine clays and silts, Nk—glacitectonic rafts. Pleistocene—Saalian Glaciation: upper layer of glacial tills (1), Vistulian Glaciation: fluvioglacial sands and gravels (2), lower layer of glacial tills (3), limnoglacial silts, clays, and sands (4), fluvial, locally fluvioglacial sands (5), middle layer of glacial tills (6), limnoglacial silts and clays (7), fluvioglacial sands and gravels (8), upper layer of glacial tills (9), fluvioglacial sands (10); Holocene: a—fluvial sands and gravels, b—fluvial silts, loams, and sands, c—colluvial deposit

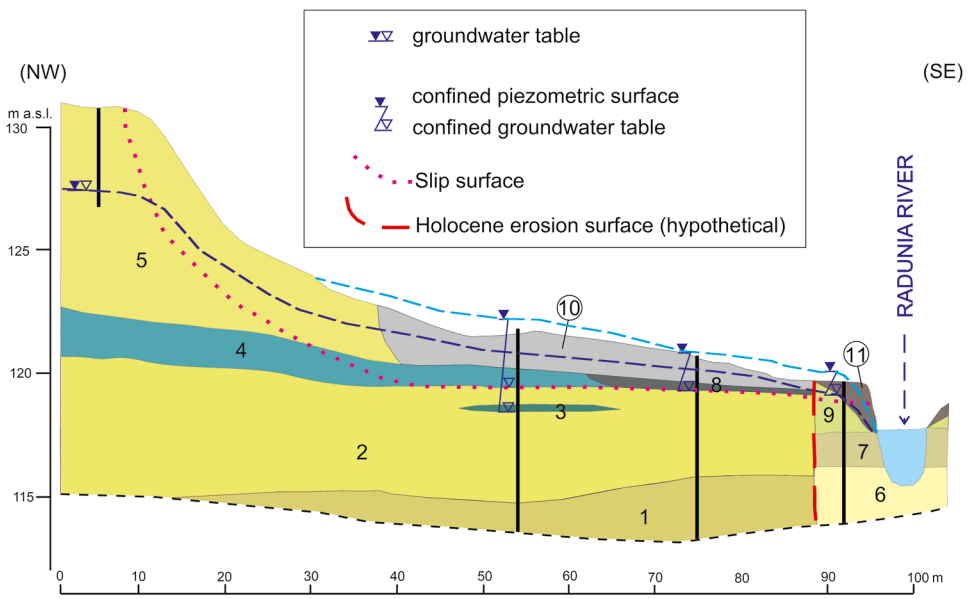


Fig. 3 Geological cross-sections across the Radunia Valley. Stratigraphy: Pleistocene strata (Vistulian Glaciation): fluvioglacial gravel and sand (1), fluvioglacial sands (2), silt (3 and 4), fluvioglacial sands and gravels (5). Holocene: medium- and fine-grained sand (6), gravel (7), peat (8), sand (9), humic sand (10), river embankment (11)

5 Conclusions and Discussion

Various aspects affect the accuracy of GIS- and statistically-based analysis of landslide susceptibility mapping (LSM): (α) study area, (β) scale, (δ) input data, and (γ) methods (Fig. 1). However, the issue is very complicated because almost each of these aspects has an impact on the others and each of these aspects is very complex (Fig. 4). This research makes it possible to assume that a key aspect in a susceptibility study is the selection of the research area. The research area can influence the choice of scale, input data, and methods. Nevertheless, the scale can influence the input data and the input data effects the methods.

Three of these aspects can be compared with each other, for example: different scale (β) (e.g. Guzzetti et al. 1999; Gaidzik and Ramírez-Herrera 2021), different input data (γ) (e.g. Gaidzik and Ramírez-Herrera 2021), different LSMs calculation methods (δ) (e.g. Pourghasemi and Rahmati 2018), different landslide representation (δ) (Magliulo et al. 2008; Süzen and Doyuran 2004; Conoscenti et al. 2008), and different LSMs visualisation (δ) (Grabowski et al. 2022). On the other hand, it is very difficult to compare different study areas (α) with each other. Closely related to the choice of the study area is the scale, which has a crucial influence on the accuracy (Eckelmann et al. 2006).

In the case of young glacial river valleys (the LVV and the CRV), small-scale susceptibility models give an inaccurate conclusion: on the continental scale, the susceptibility of these areas is underestimated and on the national scale, the susceptibility is overestimated. Susceptibility models for both areas based on 10 m and 1 m resolution DEM show excellent prediction accuracy, i.e. AUC values range from 93.65 to 97.35% (Table 1). These results confirm the conclusions of Gaidzik and Ramírez-Herrera (2021) that finer resolution of topographic data leads to more accurate and precise susceptibility models. The high accuracy was not determined by the choice of a susceptibility calculation method. Recently, machine learning techniques have been increasingly applied for landslide susceptibility mapping to improve accuracy (Azarafza et al. 2021). These methods have improved capabilities concerning process adaptability and precision (Sameen et al. 2020). Ado et al. (2022) studied 119 articles and analysed 171 models made by means of machine learning techniques. They proved that only 40% of the models had AUC values over 90% (32% of the conventional MLTs, 47% of hybrid, 33.3% of the ensemble, and 50% of deep learning) (Ado et al. 2022) Nevertheless, using the frequency ratio method, the authors of the article achieved better results for the Lower Vistula Valley (98% > AUC > 95%) than using one of the machine learning techniques for the Central Radunia Valley (95% > AUC > 93%). It indicates that the choice of a susceptibility calculation method is not the most fundamental factor in ensuring high accuracy. In this regard, the selection of a scale as well as accuracy of input data is more significant.

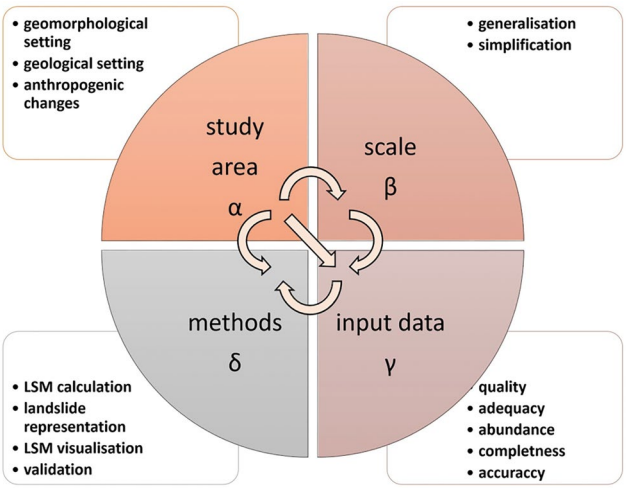


Fig. 4 Aspects affect the accuracy of the GIS-based statistical analysis of landslide susceptibility mapping and their relation

The results of the research described in this article suggest that the range of scale and resolution should depend on the morphological character of the study area. When assessing the susceptibility of the slopes of young glacial river valleys, which form narrow, long bands, the size of pixel should be matched to the width of the bands rather than the size of the study area.

For the two river valleys located in young glacial areas, the significance of the individual factors is similar (Table 2). However, density of erosional incision (DEI), a very important factor in the LVV (second place in Table 2), was not taken into account in the case of the CRV due to the small number of gullies in the area. In addition, in the CRV, gullies are short and their presence increases landslides, while in the LVV, landslides are rare on slopes where gullies are present. Well-developed erosional incisions occur mainly in areas where the aquifer is underlain by glacial till (Bujwid and Muchowski 1973). Therefore, the DEI factor is not valuable for assessing landslide susceptibility of all sections of river valleys entrenched in lowland areas, because these areas can have a different geological structure.

The geological structure of young glacial river valleys is complex due to the presence of permeable (sands, gravels) and impermeable (clays, silts) sediments in the profile, which affects water circulation on the slope. Therefore, the maps of surface deposits used in the calculation of the surface layer susceptibility were of little relevance. The simple way of presenting geology (2D) hampers the accuracy of susceptibility models. Geological maps of lowlands are mainly the result of geological reconnaissance by hand drilling to a depth of 2 m, and most of the landslides in the study area have deeper (>3 m) slip surfaces (Laskowicz et al. 2018a, b). However,

the inclusion of a quasi-3-D geological model—a typical lithologic sequence strata (TLS) in the susceptibility mapping, shows that it is one of the most important factors (in the case of the LVV, sixth position in Table 2). In the LVV and the CRV on slopes with the lithological variability of their vertical profile springs often occur, which was observed during the fieldwork done by the authors of the article. The results suggest that for higher accuracy of LSMs in young glacial river valleys, the use of quasi-three-dimensional geological maps of Quaternary and Neogene sediments will be more beneficial than surface deposits maps.

Acknowledgments The authors would like to thank Adam Trubłajewicz for proofreading. This article was financed by the Ministry of Science and Higher Education, Poland. The task was carried out at the Polish Geological Institute under the number 62.9012.2335.00.0 and 61.2706.2400.00.0.

References

Ado M, Amitab K, Maji AK, Jasińska E, Gono R, Leonowicz Z, Jasiński M (2022) Landslide susceptibility mapping using machine learning: a literature survey. Remote Sens 14(13):3029. https://doi.org/10.3390/rs14133029

Akinci H, Yavuz Ozalp A (2021) Landslide susceptibility mapping and hazard assessment in Artvin (Turkey) using frequency ratio and modified information value model. Acta Geophys 69:725–745. https://doi.org/10.1007/s11600-021-00577-7

Akinci H, Zeybek M (2021) Comparing classical statistic and machine learning models in landslide susceptibility mapping in Ardanuc (Artvin), Turkey. Nat Hazards 108:1515–1543

Althuwaynee OF, Pradhan B, Park HJ, Lee JH (2014) A novel ensemble bivariate statistical evidential belief function with knowledge-based analytical hierarchy process and multivariate statistical logistic regression for landslide susceptibility mapping. Catena 114(2014):21–36. https://doi.org/10.1016/j.catena.2013.10.011

Ayalew L, Yamagishi H, Marui H, Kanno T (2005) Landslides in Sado Island of Japan: Part II. GIS-based susceptibility mapping with comparisons of results from two methods and verifications. Eng Geol 2005(81):432–445

Azarafza M, Azarafza M, Akgün H, Atkinson P, Derakhshani R (2021) Deep learning-based landslide susceptibility mapping. Sci Rep 11:24112. https://doi.org/10.1038/s41598-021-03585-1

Bai S, Wang J, Lu G, Zhou P, Hou S, Xu S (2010) GIS-based logistic regression for landslide susceptibility mapping of the Zhongxian segment in the three Gorges area, China. Geomorphology 115(2010):23–31. https://doi.org/10.1016/j.geomorph.2009.09.025

Breiman L, Friedman J, Olshen R, Stone C (1984) Classification and regression trees. Chapman & Hall, New York

Bujwid H, Muchowski J (1973) Rola naturalnego drenażu wód podziemnych w rozwoju morfologicznym krawędzi dolin rzecznych na przykładzie wybranych odcinków dolin: Wisły i dolnej Bugo-Narwi. Prz Geol 21(1973):396–400

Chowdhury MS (2023) A review on landslide susceptibility mapping research in Bangladesh. Heliyon 9(7). https://doi.org/10.1016/j.heliyon.2023.e17972

Chung CJ, Fabbri AG (1999) Probabilistic prediction models for landslide hazard mapping. Photogramm Eng Remote Sens 65(1999):1389–1399

Chung CJ, Fabbri AG (2003) Validation of spatial prediction models for landslide hazard mapping. Nat Hazards 30(2003):451–472. https://doi.org/10.1023/B:NHAZ.0000007172.62651.2b

Conoscenti C, Di Maggio C, Rotigliano E (2008) GIS analysis to assess landslide susceptibility in a fluvial basin of NW Sicily (Italy). Geomorphology 94(3–4):325–339. https://doi.org/10.1016/j.geomorph.2006.10.039

Cruden D M, Varnes D J (1996) Landslide type and process A.K. Turner, R.L. Schuster (Eds.), Landslides: investigations and mitigation. TRB Special Report, 247 (1996), pp. 36–75

Eckelmann W, Baritz R, Bialousz S, Bielek P, Carre F, Houšková B, Jones RJA, Kibblewhite MG, Kozak J, Le Bas C, Tóth G, Tóth T, Várallyay G, Yli Halla M, Zupan M (2006) Common criteria for risk area identification according to soil threats. European Soil Bureau Research Report No. 20, EUR 22185 EN, Office for Official Publications of the European Communities, Luxembourg

Fleuchaus P, Blum P, Wilde M et al (2021) Retrospective evaluation of landslide susceptibility maps and review of validation practice. Environ Earth Sci 80:485. https://doi.org/10.1007/s12665-021-09770-9

Gaidzik K, Ramírez-Herrera MT (2021) The importance of input data on landslide susceptibility mapping. Sci Rep 11:19334. https://doi.org/10.1038/s41598-021-98830-y

Galli M, Ardizzone F, Cardinali M, Guzzetti F, Reichenbach P (2008) Comparing landslide inventory maps. Geomorphology 94:268–289. https://doi.org/10.1016/j.geomorph.2006.09.023

Godt JW, Coe JA, Baum RL, Highland LM, Keaton JR, Roth JR Jr (2012) Prototype landslide hazard map of the conterminous United states. In: Eberhardt E, Froese C, Turner K, Leroueil S (eds) Landslides and engineered slopes, protecting society through improved understanding. CRC Press, pp 245–250

Grabowski D, Laskowicz I, Małka A, Rubinkiewicz J (2022) Geoenvironmental conditioning of landsliding in river valleys of lowland regions and its significance in landslide susceptibility assessment: a case study in the Lower Vistula Valley, Northern Poland. Geomorphology 419:108490. https://doi.org/10.1016/j.geomorph.2022.108490

Günther A, Reichenbach P, Malet JP et al (2013) Tier-based approaches for landslide susceptibility assessment in Europe. Landslides 10:529–546. https://doi.org/10.1007/s10346-012-0349-1

Günther A, Van Den Eeckhaut M, Malet J, Reichenbach P, Hervas J (2014) Climate-physiographically differentiated Pan-European landslide susceptibility assessment using spatial multi-criteria evaluation and transnational landslide information. Geomorphology 224:69–85

Guzzetti F, Carrara A, Cardinali M, Reichenbach P (1999) Landslide hazard evaluation: a review of current techniques and their application in a multi-scale study, Central Italy. Geomorphology 31(1–4). https://doi.org/10.1016/S0169-555X(99)00078-1

Huang Y, Zhao L (2018) Review on landslide susceptibility mapping using support vector machines. Catena 165:520–529. https://doi.org/10.1016/j.catena.2018.03.003

Hungr O, Leroueil S, Picarelli L (2014) The Varnes classification of landslide types, an update. Landslides 11(2014):167–194. https://doi.org/10.1007/s10346-013-0436-y

Jereczek-Korzeniewska K (2005) Komentarz do Mapy Hydrograficznej Polski w Skali 1:50,000, Arkusz N-34-49-D Gdańsk-Osowa. GUGiK, Warsaw, Poland

Kim JC, Lee S, Jung HS, Lee S (2018) Landslide susceptibility mapping using random forest and boosted tree models in Pyeong-Chang, Korea. Geocarto Int 33:1000–1015

Laskowicz I, Małka A, Mrozek T (2018a) Mapa osuwisk i terenów zagrożonych ruchami masowymi w skali 1:10 000 dla Bydgoszczy Miasta. NAG PIG Warszawa, Warsaw

Laskowicz I, Grabowski D, Rubinkiewicz J, Małka A, Mrozek T (2018b) Mapa osuwisk i terenów zagrożonych ruchami masowymi

w skali 1:10 000 dla powiatu bydgoskiego. NAG PIG Warszawa, Warsaw

Lee S, Pradhan B (2007) Landslide hazard mapping at Selangor, Malaysia using frequency ratio and logistic regression models. Landslides 4(2007):33–41. https://doi.org/10.1007/s10346-006-0047-y

Licbarski P (1989) Komentarz do Mapy Hydrograficznej Polski w Skali 1:50,000, Arkusz 325.1 Pruszcz Gdański. GUGiK, Warszawa, Poland

Liu J, Duan Z (2018) Quantitative assessment of landslide susceptibility comparing statistical index, index of entropy, and weights of evidence in the Shangnan Area. China Entropy 20:868. https://doi.org/10.3390/e201910868

Magliulo P (2012) Assessing the susceptibility to water-induced soil erosion using a geomorphological, bivariate statistics-based approach. Environ Earth Sci 67:1801–1820. https://doi.org/10.1007/s12665-012-1634-y

Magliulo P, Di Lisio A, Russo F, Zelando A (2008) Geomorphology and landslide susceptibility assessment using GIS and bivariate statistics: a case study in southern Italy. Nat Hazards 47:411–435. https://doi.org/10.1007/s11069-008-9230-x

Małka A, Zabuski L, Enzmann F, Krawiec A (2023) Mass-movement causes and landslide susceptibility in river valleys of lowland areas: a case study in the Central Radunia Valley, Northern Poland. Geosciences 13(9):277. https://doi.org/10.3390/geosciences13090277

Marks L (2012) Timing of the late Vistulian (Weichselian) glacial phases in Poland. Quat Sci Rev 44:81–88

Mrozek T, Poli S, Sterlacchini S, Zabuski Z (2004) Landslide susceptibility assessment. A case study from the Beskid Niski Mts., Carpathians, Poland. Pol Geol Inst Sp Pap 15:13–18

Pourghasemi HR, Rahmati O (2018) Prediction of the landslide susceptibility: which algorithm, which precision? Catena 162:177–192

Pourghasemi HR, Moradi HR, Fatemi Aghda SM (2013) Landslide susceptibility mapping by binary logistic regression, analytical hierarchy process, and statistical index models and assessment of their performances. Nat Hazard 69. https://doi.org/10.1007/s11069-013-0728-5

Regmi NR, Giardino JR, Vitek JD (2010) Modeling susceptibility to landslides using the weight of evidence approach: Western Colorado, USA. Geomorphology 115:172–187. https://doi.org/10.1016/j.geomorph.2009.10.002

Remondo J, González A, De Terán JRD, Cendrero A, Fabbri A, Chung F (2003) Validation of landslide susceptibility maps; examples and applications from a case study in Northern Spain. Nat Hazards 30:437–449. https://doi.org/10.1023/B:NHAZ.0000007201.80743.fc

Rossi M, Guzzetti F, Reichenbach P, Mondini AC, Peruccacci S (2010) Optimal landslide susceptibility zonation based on multiple forecasts. Geomorphology 114(3):129–142. https://doi.org/10.1016/j.geomorph.2009.06.020

Ruff M (2005) GIS-gestützte Risikoanalyse für Rutschungen und Felsstürze in den Ostalpen (Vorarlberg, Österreich). PhD thesis, Universitätsverlag Karlsruhe. Karlsruhe, p 132

Sameen MI, Pradhan B, Lee S (2020) Application of convolutional neural networks featuring Bayesian optimisation for landslide susceptibility assessment. Catena 186:104249. https://doi.org/10.1016/j.catena.2019.104249

Süzen M, Doyuran V (2004) Data driven bivariate landslide susceptibility assessment using geographical information systems: a method and application to Asarsuyu catchment, Turkey. Eng Geol 71:303–321. https://doi.org/10.1016/S0013-7952(03)00143-1

Vakhshoori V, Zare M (2016) Landslide susceptibility mapping by comparing weight of evidence, fuzzy logic, and frequency ratio methods. Geomat Nat Haz Risk 7:1731–1752. https://doi.org/10.1080/19475705.2016.1144655

Vakhshoori V, Zare M (2018) Is the ROC curve reliable tool to compare the validity of landslide susceptibility maps? Geomat Nat Hazard Risk 9(1):249–266

Van Westen CJ, Castellanos E, Kuriakose SL (2008) Spatial data for landslide susceptibility, hazard, and vulnerability assessment: an overview. Eng Geol 102(2008):112–131. https://doi.org/10.1016/j.enggeo.2008.03.010

Varnes DJ (1978) Slope movement types and processes. In: Schuster RL, Krizek RJ (eds) Landslides, analysis and control, Special report 176: Transportation research board. National Academy of Sciences, Washington, DC, pp 11–33

Wilde M, Günther A, Reichenbach P, Malet J-P, Hervás J (2018) Pan-European landslide susceptibility mapping: ELSUS Version 2. J Maps 14(2):97–104

Wojciechowski T (2019) Podatność osuwiskowa Polski (in Polish). Prz Geol 67:320–325. https://doi.org/10.7306/2019.25

Woś A (1999) Klimat Polski. Wydawnictwo Naukowe PWN, Warsaw, Poland. ISBN 83-01-12780-5

Yalcin A (2008) GIS-based landslide susceptibility mapping using analytical hierarchy process and bivariate statistics in Ardesen (Turkey): comparisons of results and confirmations. Catena 72(1):1–12. https://doi.org/10.1016/j.catena.2007.01.003

Youssef AM, Pourghasemi HR, Pourtaghi ZS, Al-Katheeri MM (2016) Landslide susceptibility mapping using random forest, boosted regression tree, classification and regression tree, and general linear models and comparison of their performance at Wadi Tayyah Basin, Asir region, Saudi Arabia. Landslides 13:839

Open Access This chapter is licensed under the terms of the Creative Commons Attribution 4.0 International License (http://creativecommons.org/licenses/by/4.0/), which permits use, sharing, adaptation, distribution and reproduction in any medium or format, as long as you give appropriate credit to the original author(s) and the source, provide a link to the Creative Commons license and indicate if changes were made.

The images or other third party material in this chapter are included in the chapter's Creative Commons license, unless indicated otherwise in a credit line to the material. If material is not included in the chapter's Creative Commons license and your intended use is not permitted by statutory regulation or exceeds the permitted use, you will need to obtain permission directly from the copyright holder.



Experimental Research on Rain-Induced Landslide Mechanism Using Large-Scale Rainfall Experimental Facility: Findings and Challenges

Naoki Sakai, Tomohiro Ishizawa, and Toru Danjo

Abstract

This paper presents the novel large-scale rainfall experimental facility, a pioneering development by the National Research Institute for Earth Science and Disaster Resilience (NIED). It delves into the intricacies of various large-scale slope failure experiments at this facility. These model experiments are unique in their approach, involving the attachment of multiple measuring instruments to a simple slope model. The standout feature of these experiments is the use of large-scale models, which facilitate easy handling of slope shaping, sensor placement, and application of realistic rainfalls, all tailored to the study's objectives.

The facility's unparalleled ability to control all experimental parameters is a crucial advantage, enabling the realization of more realistic natural rainfall conditions and external forces. This unique feature makes the experiments invaluable, setting our research apart. However, establishing diverse simulation methods is essential to exploit this advantage fully. The methods will allow us to explore a broader range of scenarios and further benefit from these experiments. While this study primarily discusses slope failure during rainfall, simulating post-collapse flow and transformation into debris flow is also necessary.

The experiments' findings shed light on the intimate relationship between groundwater levels and deformation, offering valuable insights into the collapse mechanism and its prediction. They also pinpoint the crucial points in preparing slope models, underscoring the practical implications of the research in controlling and mitigating slope failures.

N. Sakai (✉) · T. Ishizawa · T. Danjo
National Research Institute for Earth Science and Disaster Resilience (NIED), Storm, Flood and Landslide Research Division, Tsukuba, Ibaraki, Japan
e-mail: sakai@bosai.go.jp

Keywords

Large-scale model test · Heavy rainfall · Slope deformation · Experimental design

1 Introduction

Landslides and mudslides caused by typhoons, long spells of rain in June and September, and torrential rains brought on by training "linear precipitation zones" frequently occur in Japan, resulting in the yearly loss of precious human lives. It is reported that landslides account for about half of the total number of fatalities and missing persons in natural disasters. Landslide disasters remain among the most important natural disasters for which appropriate prevention measures should be taken.

In recent years, the Japan Meteorological Agency and prefectural and municipal governments have been issuing "landslide disaster warning information" and operating a system to support residents' evacuation and thus reduce landslide disasters. Precipitation is mainly used as an indicator, and information to provide warning guidelines is released in units of several-kilometer meshes or units of municipalities. On the other hand, the prediction of whether a particular slope is in danger of collapse is made using extensometers (e.g., Fukuzono 1985).

However, it is difficult to use this method as a warning that allows sufficient time for evacuation because surface failures occur very quickly after deformation begins. In the future, improving "landslide warning information" and establishing a field measurement method to evaluate the safety of specific slopes for the early prediction that goes one step beyond last-minute prediction will be necessary.

Figure 1 illustrates a shallow (1–2 m) slope failure in 2016 in Aso, Kumamoto Prefecture, Japan. The collapse directly above a structure and its impact on a building

© The Author(s) 2025

B. Abolmasov et al. (eds.), *Progress in Landslide Research and Technology, Volume 3 Issue 2, 2024*, Progress in Landslide Research and Technology, https://doi.org/10.1007/978-3-031-72736-8_14



Fig. 1 Traces and residual soils left behind a debris flow (Aso, Kumamoto in 2016)

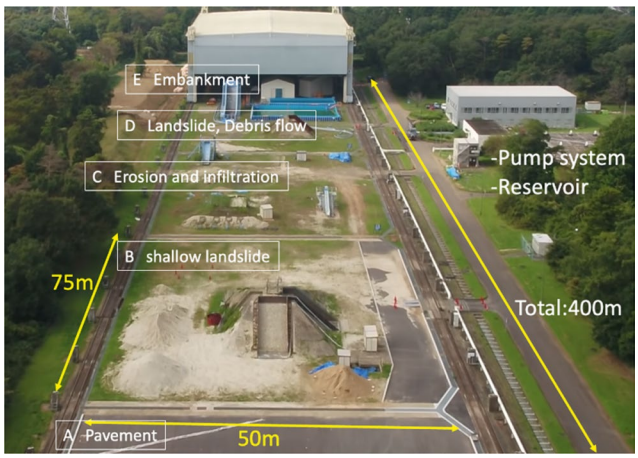


Fig. 2 Panoramic view of the large-scale rainfall experimental facility. Each of the five compartments has its own environment and facilities, and various experiments could be arranged based on the needs of the experiment

below was the result of a surface failure, believed to be a combination of factors including increased pore water pressure due to rainfall infiltration, decreased strength (apparent cohesion), and increased self-weight in the loose weathered layer above its bedrock. For a comprehensive understanding of these phenomena, it is crucial to comprehend the relationships among rainfall infiltration on unsaturated slopes, slope deformation associated with changes in saturation (Sasahara and Sakai 2014, 2017; Ishizawa et al. 2017), and slope deformation associated with the increase in the groundwater table. The authors have conducted field observations, developed analytical methods (Sasahara et al. 2007), and conducted experiments (Sakai and Sakajo 2008) on small slopes to develop a collapse prediction method considering the collapse mechanism. However, small model experiments have limitations in realizing the similarity law and are always different from the real ones (Moriwaki 1988). From this aspect, geotechnical centrifuge tests (e.g., Take et al. 2004) can be helpful for scale modeling of any large-scale nonlinear problem for which gravity is a primary driving force. However, even in centrifugal tests, shear-band development is geometrically determined by the representative soil grain size, which cannot be changed if we use natural sands as model materials. Therefore, large-scale model experiments utilizing the largest rainfall simulator are indispensable to minimize the problems associated with small model experiments and to gain a deeper understanding of slope failures (e.g., Moriwaki et al. 2004).

This paper illuminates the intimate relationship between groundwater levels and deformation, offering valuable insights into the collapse mechanism and its prediction. It also identifies the crucial points in preparing slope models, underscoring the research's practical implications for controlling and mitigating slope failures.

2 Large-Scale Rainfall Simulator

The National Research Institute for Earth Science and Disaster Resilience (NIED) developed a novel large-scale rainfall experimental facility in 1974 in Tsukuba, Ibaraki Prefecture, Japan. Figures 2 and 3 show the panoramic and indoor views of the Large-Scale Rainfall Experiment Facility. The compound (Fig. 3) comprises five experimental zones: a building with a mobile rainfall apparatus, a rainfall pump control building, and a water storage tank. Table 1 presents the rainfall performance of the facility. Among its various functions, the following three features are particularly noteworthy:

1. World's Largest Sprinkling Area:
   The facility can sprinkle water over a maximum indoor area of approximately 3000 m^2 ($\approx 44 \times 72$ m) using 2176 nozzles of four different types with varying spray diameters. Figure 3 shows the area is being sprinkled. This sizeable indoor area allows rainfall experiments using large-scale models close to the actual size. The sprinkling area can also be divided into four smaller sections, enabling multiple simultaneous rainfall experiments.
2. Mobile Rainfall Apparatus:
   The rainfall apparatus can move across five experimental zones on rails (shown in Fig. 2). The building can travel the most extended experimental zone (375 m) at a 1 m/min speed. This movable apparatus allows for the simultaneous execution of sprinkling experiments and model construction. Furthermore, comparative experiments can be conducted between natural and artificial rainfall conditions by moving the rainfall facility to expose the slope models to natural rainfall.

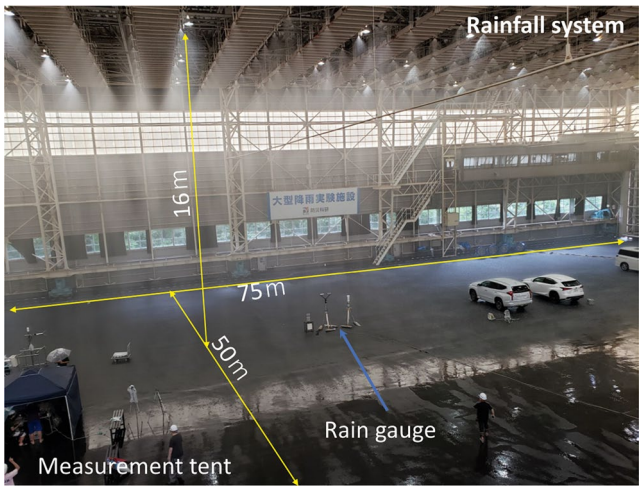


Fig. 3 Indoor view of the large-scale rainfall experimental facility

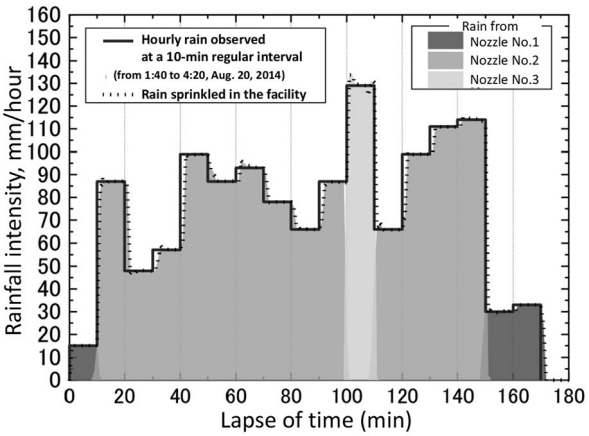


Fig. 4 Rain gauge record in Hiroshima, 2014 and the realized rain sprinkled in the facility

Table 1 Performance of the large-scale rainfall experimental facility

Large-scale mobile rainfall facility	
Structure (area)	Steel-pipe-trussed ferroconcrete (3492 m^2)
Observation room	Floor 7.5 m above the ground
	2 rooms of 65.4 m^2 each
Sprinkling area	50 × 75 m, 5 divisions
Sprinkling facility	
Raindrop size	0.1–8 mm diameter (4 type nozzles)
Rainfall intensity	15–300 mm/h
Rainfall area	50 × 75 m (dividable into quarters)
Nozzles	System 1:15–45 mm/h 544 pcs.
	System 2:40–200 mm/h 544 pcs.
	System 3:120–220 mm/h 544 pcs.
	System 4:200–300 mm/h 544 pcs.
Nozzle height	16 m above the ground
Control	Remote control: flow rate/stress control
Circulating pump	200 kW, 9.4 kg/cm^2, 8.0 kl/min, 2 pumps
Reservoir	
Water storage capacity	2500 m^3
Supply well	80 m^3/h

3. The facility's ability to replicate heavy and sudden downpours is a significant feature that adds a sense of realism and practicality to the research:

The facility can simulate rainfall intensities from a minimum of 15 mm/h to 300 mm/h, with raindrop sizes up to about 8 mm. Experiments can replicate the maximum hourly rainfall recorded in Japan, such as 187.0 mm/h observed in Nagayo Town, Nagasaki in July 1982, and 50.0 mm in 10 min in Murakami, Aga Town, Niigata Prefecture, on July 26, 2011.

Following overhauling the sprinkling system in 2014, the facility enhanced its capability to simulate rainfall intensities up to 300 mm/h, like sudden downpours. It can replicate continuous rainfall conditions with varying intensities, similar to actual rainfall. To verify the sprinkling performance, we reproduced the localized short-duration heavy rain that caused significant damage, such as landslides and floods in Hiroshima during the heavy rain event in August 2014. Figure 4 shows the results of this reproduction. The solid line in the Figure represents the record retrieved from the Automated Meteorological Data Acquisition System (AMeDAS) observation point in Miiro, Hiroshima Prefecture. The broken line shows the 10-min interval sprinkling results reproduced by the facility. The experiment used different nozzles to change the rain intensity every 10 min and accurately reproduce the observed short-duration rainfall. The excellent agreement between the observed and realized rains showed the satisfactory performance of the sprinkling system.

3 Large-Scale Model Slope Experiments in Artificial Rainfalls

In a large-scale model test, it is essential to record the slope failure process to foresee the risk of failure, which is almost impossible on natural slopes. We measured the following processes in the experiments to see how they would develop until the slope started sliding:

1. the saturation process due to rainfall infiltration
2. the change in the groundwater level
3. the ground surface displacements

3.1 Preparations

Each model was prepared in a composite steel soil bin (Figs. 5 and 6) for a total slope length of 23 m (including a 10 m and

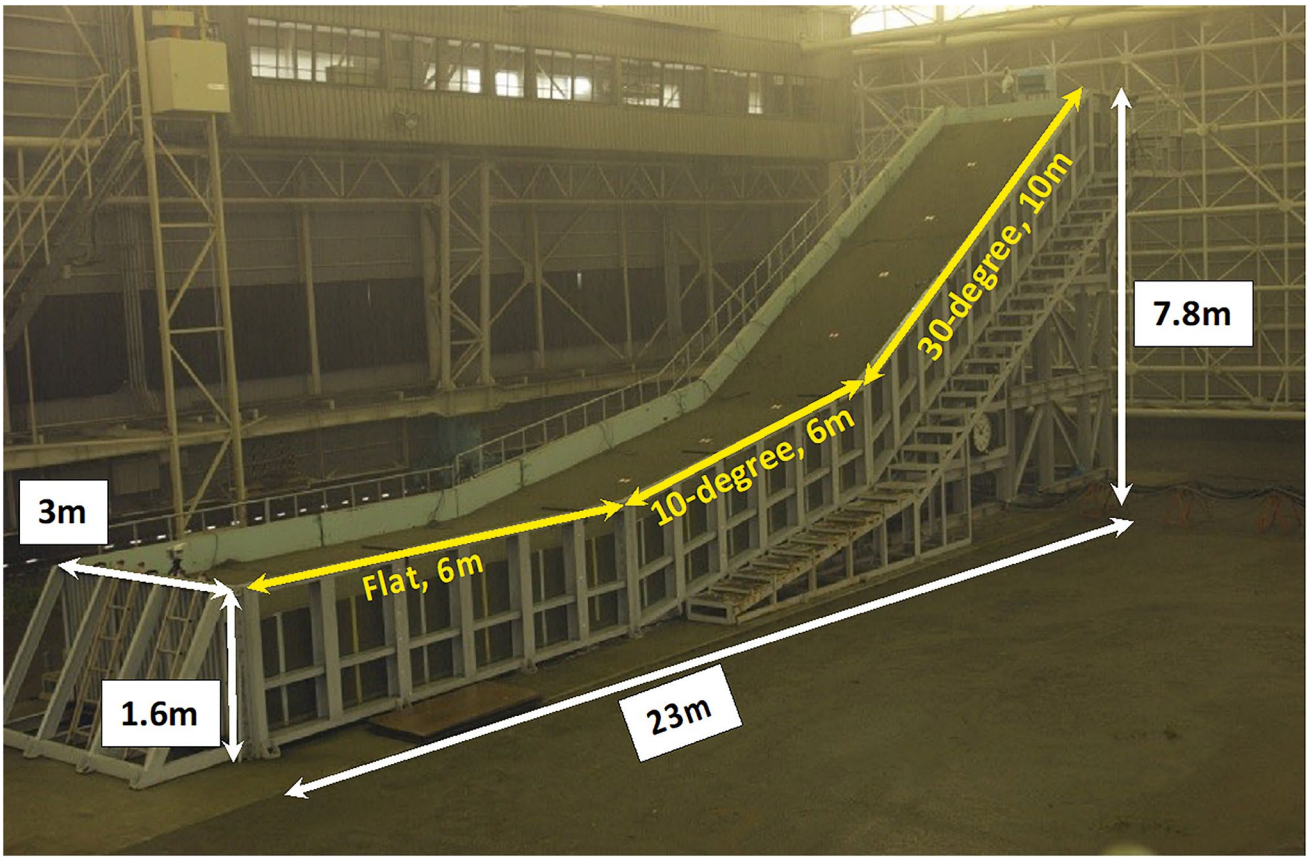


Fig. 5 Composite steel soil bin

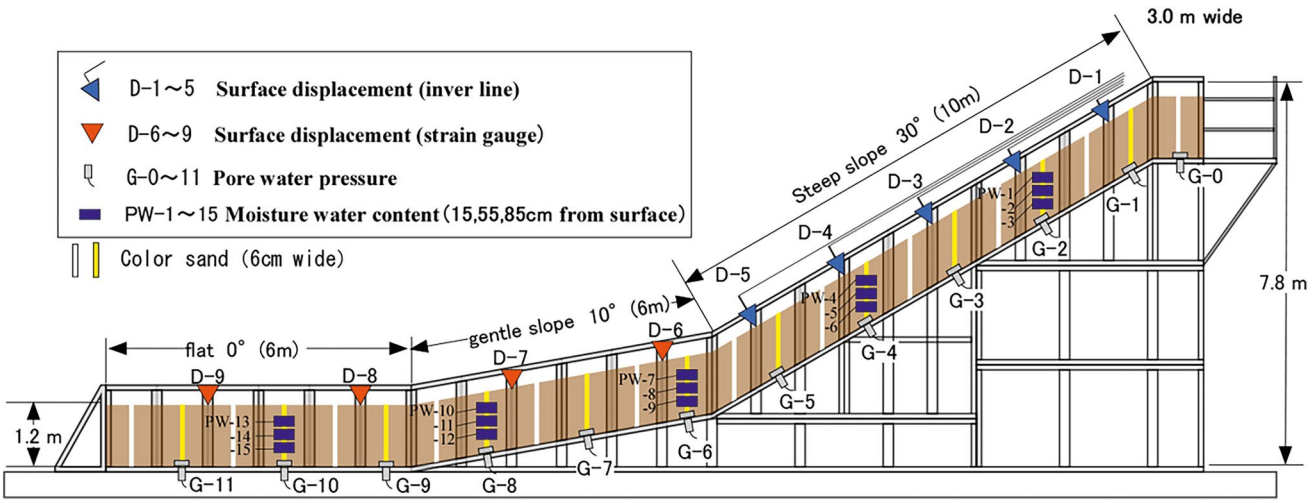


Fig. 6 Arrangement of sensors

30° slope section), 3 m wide, 1.6 m deep (soil layer depth: 1.2 m), and 7.8 m high at the upper end. The lower end of the soil bin is a slit-type retaining wall sealed with a wire mesh, allowing the water in the model to drain through the slits while retaining the soil within the soil bin (Fig. 7). The other sides of the soil bin are entirely impermeable. Cleats are arranged horizontally on the bottom of the slope at regular intervals to stop the soil from sliding. The light walls from the face of the soil bin are glass-paned so that the deforming process of the soil layer can be observed from the outside. The slope model of sand with an initial moisture content of about 8% was compacted manually at every 20 cm thickness (Fig. 8). The prepared slope model's average dry density and pore ratios were 1.37 g/cm^3 and 0.964, respectively.



Fig. 7 Lower end of the soil bin (Slit-type retaining wall sealed with a wire mesh)



Fig. 8 Compacting the slope soil (image)

Surface displacement gauges (D1–D9), soil moisture gauges (PW1–PW15), and pore pressure gauges (G0-11) were installed, as shown in Fig. 6. The surface displacement gauges from D1 to D5 are wire extensometers with their wires' lower ends fixed on the predetermined locations of the slope model's surface with four-legged weights. The other end of each wire with a counterweight hangs down over a pulley of its potentiometer above the top end of the steel soil bin (Fig. 9). The counterweight ensures tension on the wire. D6 to D9 are vertical displacement sensors (Figs. 10 and 11). Each sensor is a cantilever of phosphor bronze with strain gauges pasted; the cantilever is placed immediately above the slope surface. A rigid probe tip attached at the free end of the cantilever is pressed down to a target steel plate placed on the surface of the slope model in such a way that the cantilever is bent upward as its initial condition, thus allowing the vertical displacement of the target plate to be measured until the stress induced in the cantilever is ultimately released.

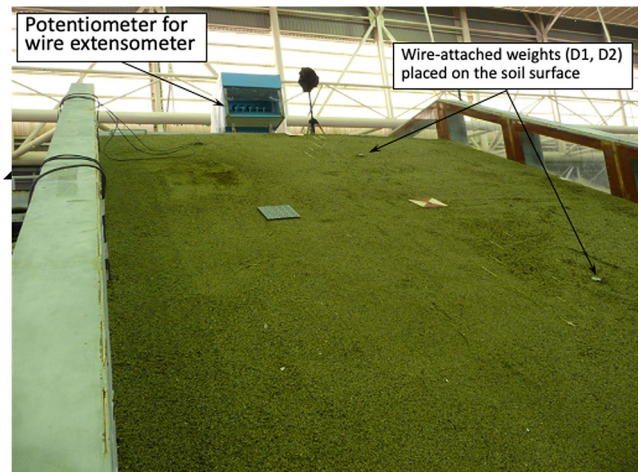


Fig. 9 Potentiometers for wire extensometers (D1–D5) at the top end of the slope model

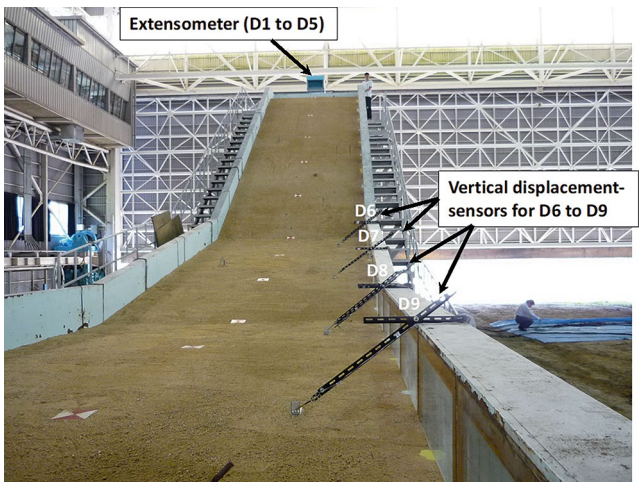


Fig. 10 Extensometer for D1 to D5 and vertical displacement sensors for D6 to D9



Fig. 11 Cantilevers of phosphor bronze with strain gauges pasted: Each cantilever with a rigid probe tip is attached at one end of a steel support. The rigid tip is pressed down to a target plate placed on the surface of the slope model

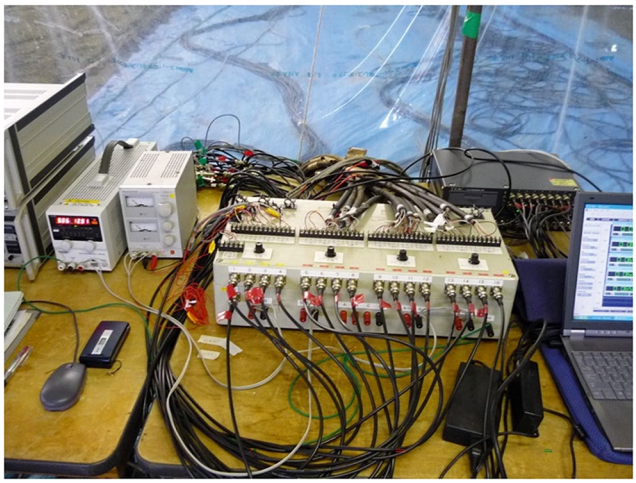


Fig. 12 A signal processing system with dozens of channels



Fig. 13 Data acquisition in a tent

Amplitude Domain Reflectometry (ADR) soil moisture sensors were placed at 15 cm, 55 cm, and 85 cm from the slope surface to measure volumetric moisture contents. Groundwater distribution in the soil layer was calculated from pore water pressures measured at the bottom of the soil bin. The analog signals from the sensors were transferred to a data logger and converted to digital signals every 10 s to be stored in it. The digital signals can be transferred to a computer for further signal processing (Fig. 12).

Though the experiment was conducted indoors, the area was vast and wet, with simulated rains. Therefore, the experiments required a measurement tent (Fig. 13) on the right side of Fig. 5.

Commercially available Sawara sand, classified as gravelly sand, was used to make slope models in all experiments. The uniformity coefficient (Uc) and the diameter corresponding to 20% finer in the particle-size distribution (D20) of the Sawara sand are 3.689 and 0.2284, respectively. Figure 14 shows the cumulative grain-size distribution curve of the Sawara sand. The soil's particle density and saturated permeability are 2.690 g/cm^3 and 2.71 × 10^{-2} (cm/s), respectively.

In addition, a water retention test (multi-step test apparatus) was conducted to determine the ability of the Sawara sand to retain water under suction (Fig. 15). The obtained results show the relationship between suction and saturation degree. The soil specimen was cylindrical, 5 cm in diameter, and 5 cm high. Its dry density was measured in the soil tank. The test methods used were the hydraulic head difference and pressurization methods. The first step of drying was then followed by wetting. The observed hysteresis was weak. This sample's AEV (Air Entry Value) pressure was about several kPa, similar to that of ordinary sand.

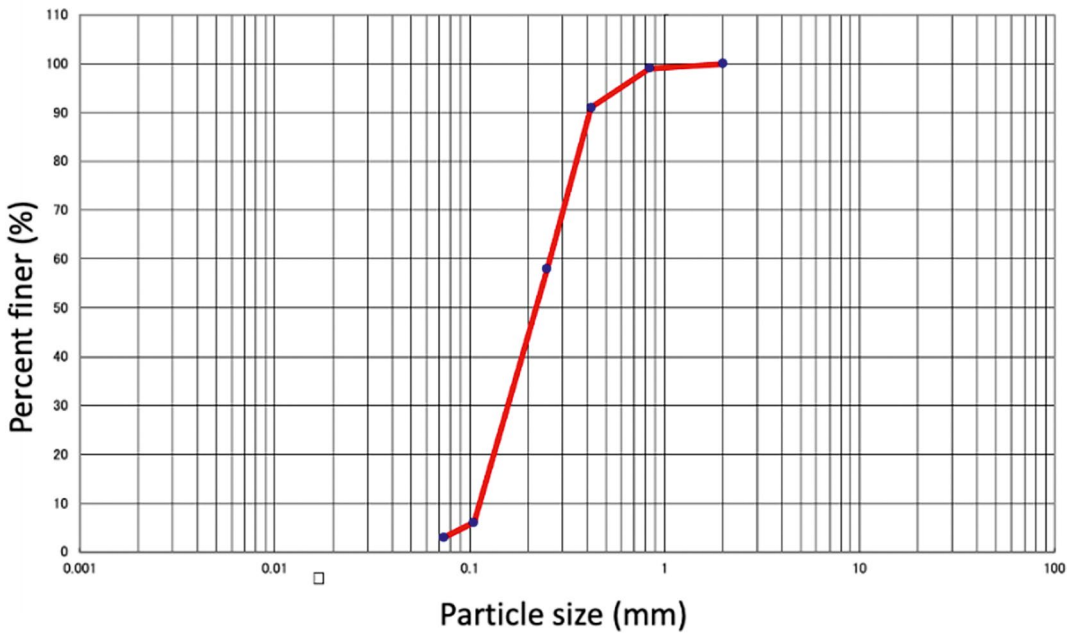


Fig. 14 The cumulative grain-size distribution curve of the Sawara sand

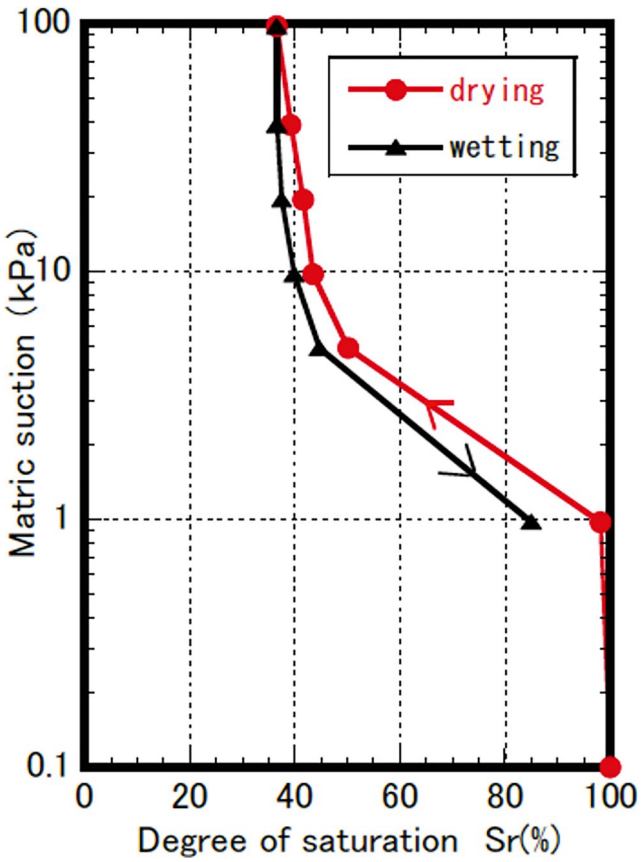


Fig. 15 Water retention curve for Sawara sand

4 Groundwater Formation Processes in the Slopes due to Rainfall

4.1 Case 1 with No Prior Rainfall to the Main Rainfall Event

Under these initial conditions, a steady 100 mm/h rain was continuously given to the model's surface until it collapsed (t = 8515 s, i.e., 2 h and 23 min, Table 2). The soil moisture meters (PW-4, 5, and 6) installed along the bottom of the slope in Fig. 16 showed that the saturation degrees continued to rise from the upper part to the lower parts of the slope (PW-4, PW-5, and PW-6 at around 900 s, 2200 s, and 4500 s, respectively) from their initial values below 40%. These values then converged at their steady state of about 70–80%. This steady state is the pseudo-saturation that appears when a wetting front passes through the location. Later, the complete saturation levels (100%) were reached at PW-6 and then at PW-5 immediately before the collapse time.

Figure 17 shows the chronological changes (t = 3000 to 9000 s) in the groundwater levels measured at five pore pressure gauges from G1 through G5 placed on the bottom of the 30-degree section of the soil bin. At t = 6400 s, G1 and G5 started rising, followed by increases in G2 and G3 (at t = 6800 s) and finally G4 (at t = 7100 s). G1 through G4 increase to conform with each other, while G5 near the lower end of the 30-degree slope shows slightly more significant values. This tendency suggests that the groundwater level was increasing almost parallel to the bottom of the soil bin. Upright broken lines (1), (2), (3), and (4) in Fig. 16, 17, and 18 show 10, 20, and 30 min before the slope collapse time. These times cover the later phase of the experiment, where the groundwater level started to increase. Figure 18 shows that even before 40 min of the collapse, the soil mass on the 30-degree section started to move downslope coherently. At 40 min and later before the collapse, D5, placed at the lower end of the 30-degree section, moved further away from the others. Connecting the estimated groundwater levels (G0 through G11), we obtained the spatial variations of the groundwater levels over the entire model stretch at different times, as shown in Fig. 19. Until 30 min before the entire collapse, the groundwater level (Line (4)) increased remarkably only in the flat toe part and the gentle slope part; this process did not seem to have initiated the downslope movement of the upper 30-degree slope section. After this time, the groundwater level within the 30-degree slope section started to rise, accelerating the downslope creeping mass movement, which developed as shown in Fig. 18. It is noteworthy that this process resembles the final stage of a natural landslide mass movement comprising the initial transient, intermediate steady, and the final accelerating creep processes.

4.2 Case 2 with Prior Rainfalls to the Main Rainfall Event

The slope model in Case 2 was prepared in the same soil bin in the same manner as in Case 1. Then, four intermittent rains were sprinkled before the main torrential 100 mm/h rain, which continued until the entire slope collapsed, as in Case 1 (Table 3). The intention was to see the effect of the preceding four rains on the soil deformation process, which is associated with the water infiltration into the soil model.

Figures 20 and 21 show the chronological changes in saturation and groundwater level, respectively. Both Figures have secondary axes going downward, showing the rainfall intensities of the preceding four rainfalls (30 mm/h) and the actual rainfall (100 mm/h) shown as blue downward bars.

Immediately after the first preceding 4-h rain of 30 mm/h, the groundwater levels at G-3, G-4, and G-5 showed steady increases, surpassing the others at G-1 and G-2. G-3 reached its peak of about 10 cm, and then G-4 and G-5 followed it, reaching slightly higher values (15 cm and 18 cm) one by one. The G-3 peak value appeared about 2 h after the first rain stopped. These groundwater levels then gradually decreased exponentially.

Table 2 Case 1 test condition for rainfall

Rain event	Time before start	Rainfall intensity (mm/h)	Duration (h)	Total rainfall (mm)
Main event	0 day and 0 h	100	2.37 (8515 s)	237 mm

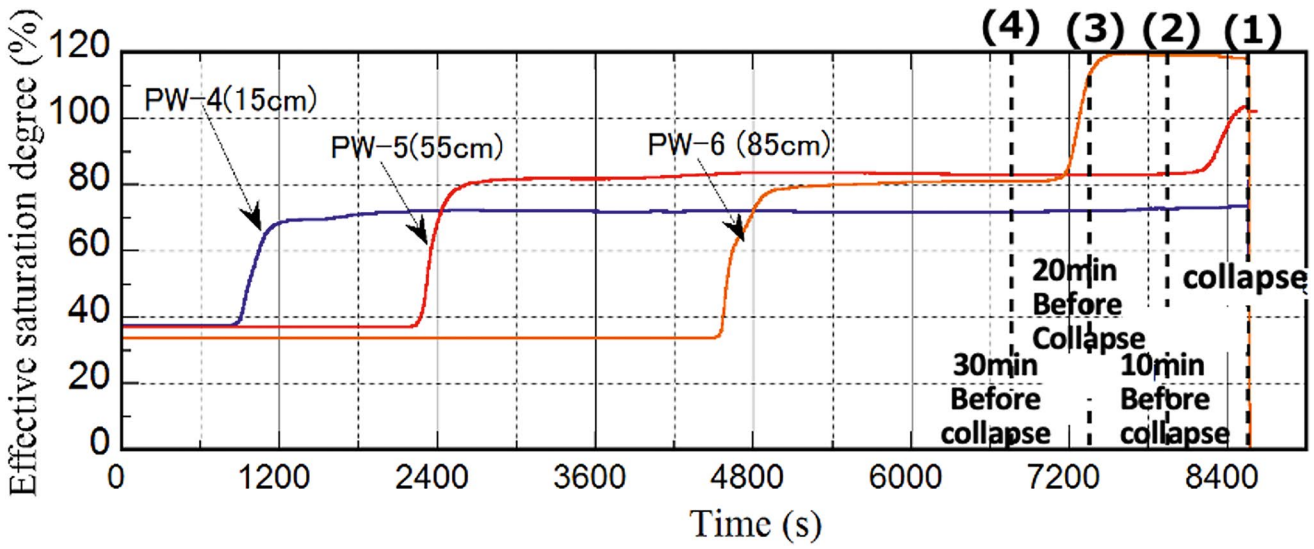


Fig. 16 Chronological changes in saturation degrees (PW-4 to PW-6)

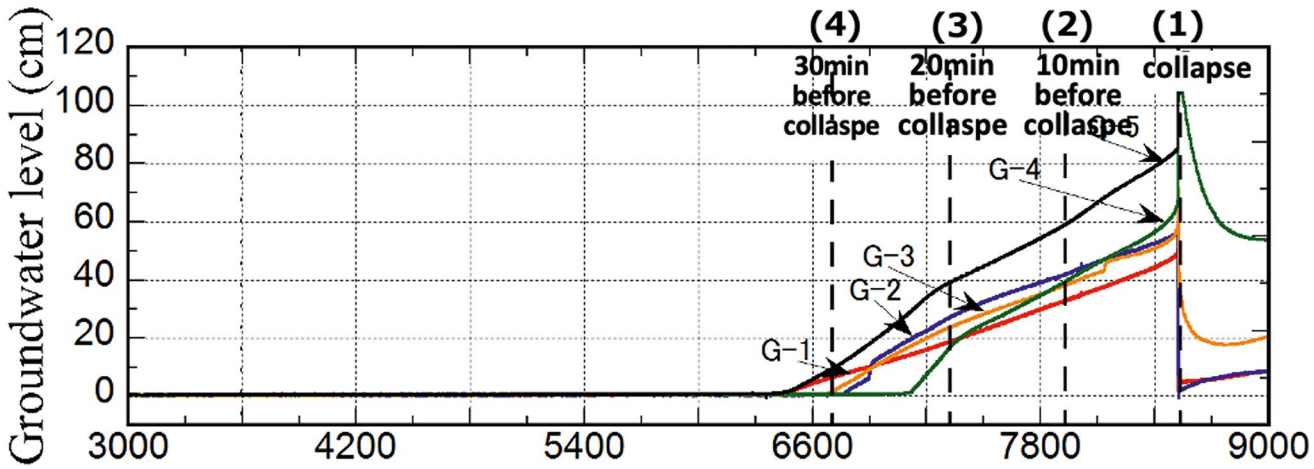


Fig. 17 Chronological changes in groundwater levels (G-1 to G-5)

The second preceding rain of 30 mm/h lasted 3 h. Though the time was shorter than that of the first rain, the peak values reached by G-3, G-4, and G-5 were more significant than 20 mm, suggesting the impact of the first rain.

All moisture gauges show a common trend: the saturation degrees exhibited exponential decaying responses to rainfall. On the other hand, the groundwater levels peaked a few hours after the end of each rainfall event. In all cases, the increase in the water level was faster and predominant in the middle to lower part of the slope (G-3, 4, 5), while they were less significant in the upper part (G-2, 1). This feature suggests groundwater flows from the top to the bottom of the slope. Thus, the groundwater level never becomes parallel to the slope surface but gentler than that, making its depth larger as we go upward. The groundwater-level signals from G-3, G-4, and G-5 went below zero as the groundwater drained, as shown in Fig. 21, due to the suction associated with the interparticle surface tension that appears in the drainage process.

The surface displacement gauges, D1 through D5, placed on the surface of the 30-degree slope section, showed simultaneous stepwise increases (less than 1 cm) immediately after the first rainfall event (1) (Fig. 22). The

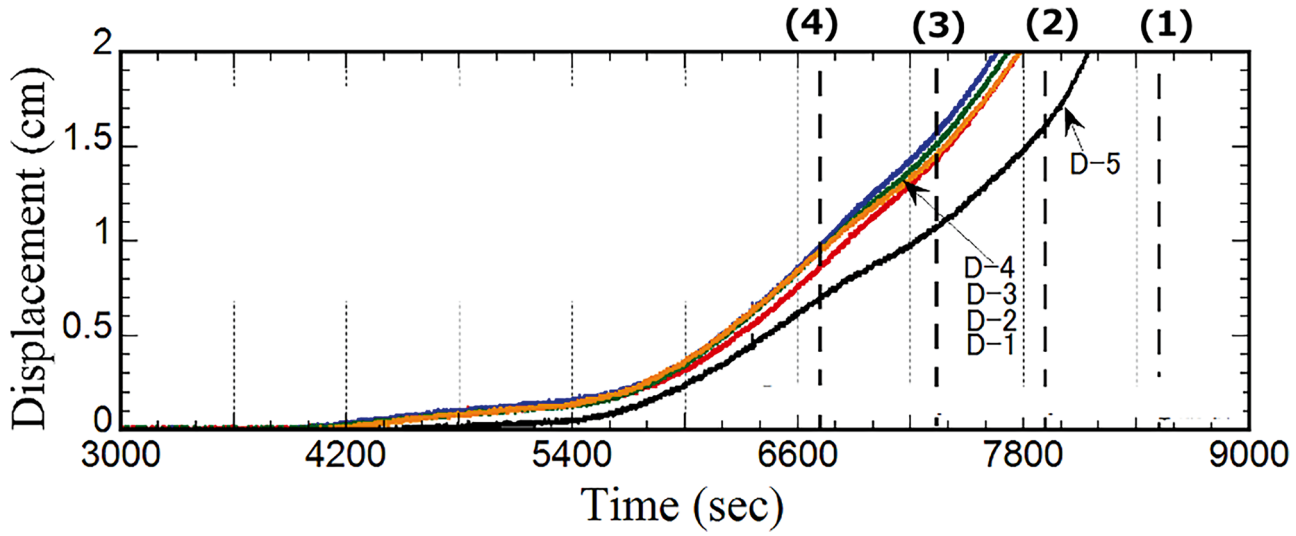


Fig. 18 Downslope movements, D1 to D5, placed over the 30-degree slope section

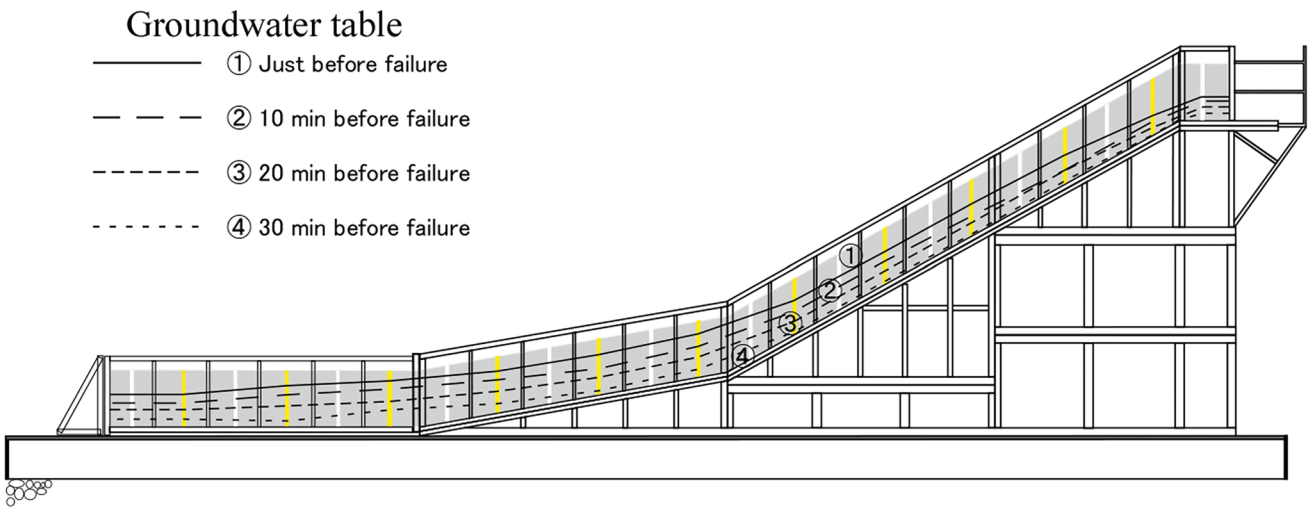


Fig. 19 Chronological change in the groundwater table in Case 1

Table 3 Preceding rains and the main torrential 100 mm/h rain

Rain event	Time before start	Rainfall intensity (mm/h)	Duration (h)	Total rainfall (mm)
Preceding event No. 1	0 day and 0 h	30	4	120
Preceding event No. 2	1 days and 22 h	30	3	90
Preceding event No. 3	3 days and 1 h	30	2	60
Preceding event No. 4	5 days and 22 h	30	3	90
Main event	7 days and 1 h	100	1.69 (6082 s)	168

displacements then gradually increased in small stages on the order of mm. However, no obvious relation was found between the rains that followed the first one and the small changes in the displacements. Though minor, these small deformations of the slope model (particularly in the first rain) can cause transverse cracks to appear, as shown in Fig. 23.

These preceding rains never increased the groundwater level in the 30-degree slope section. Thus, the slope model's main "30-degree" section remained stable. However, the groundwater level increased in the flat toe part and the gentle 10-degree sections from the bottom of the soil bin to the thick broken line in Fig. 24. The rains also increased the average saturation ratio from below 40 % to over 45 %.

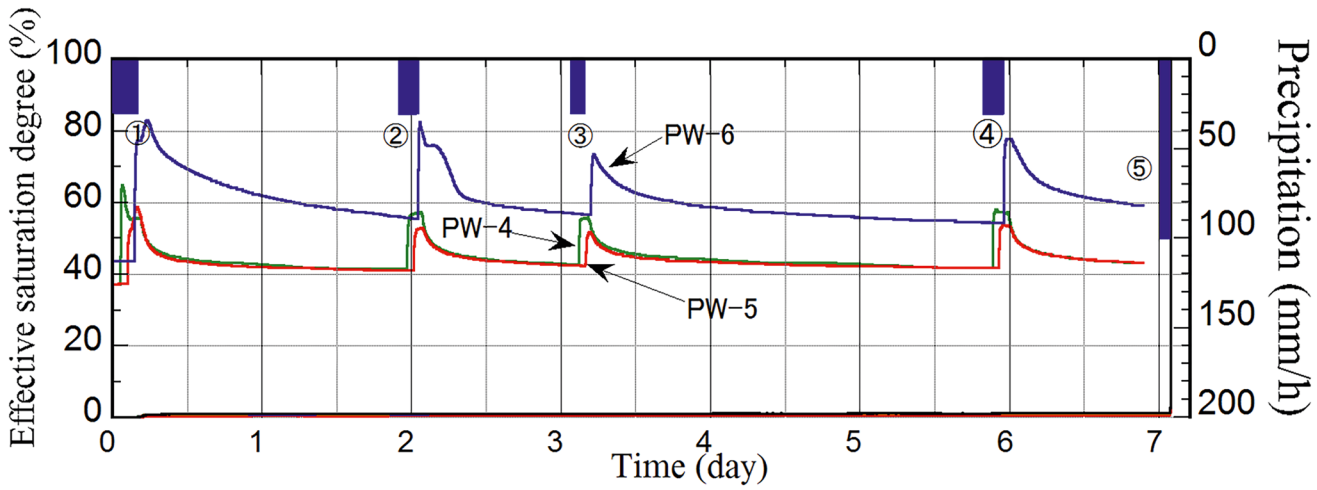


Fig. 20 Chronological changes in saturation degrees and preceding rains

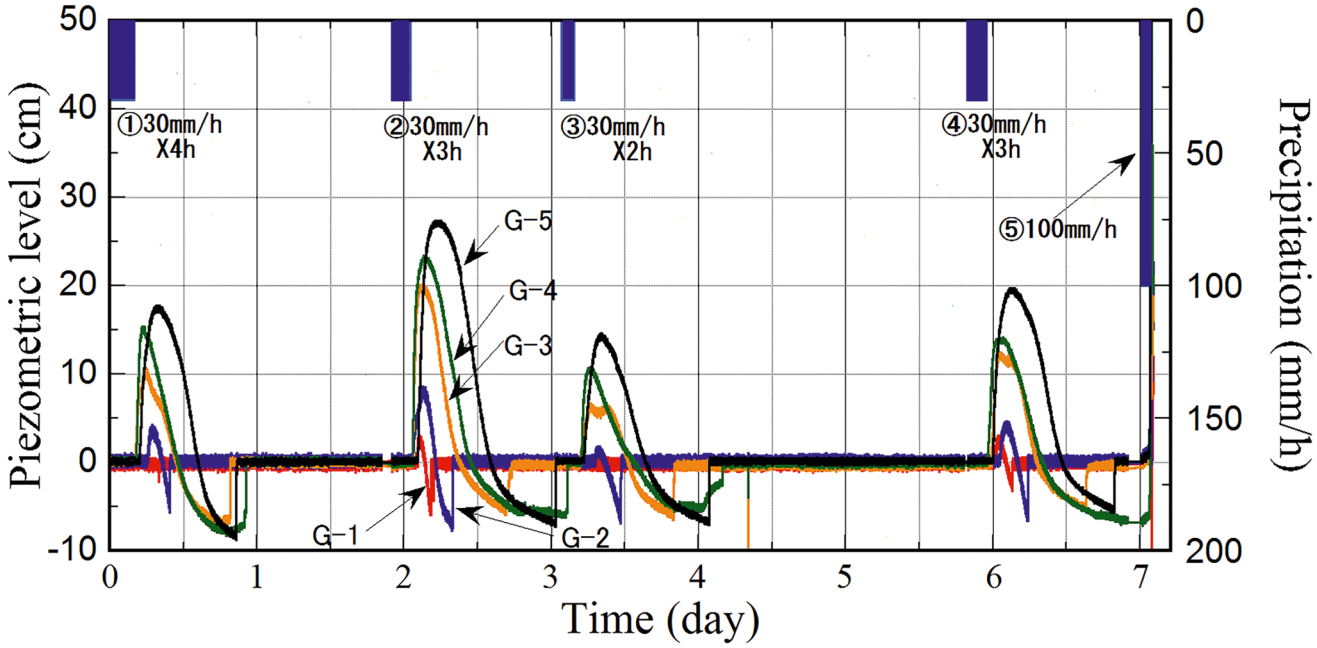


Fig. 21 Chronological changes in groundwater levels and preceding rains

Given the above hydraulic condition as the initial condition, torrential 100 mm/h rain was continuously sprinkled on the slope model's surface, as we did in Case 1.

Figure 25 shows the chronological changes (t = 0 to 6000 s) in the groundwater levels measured at five pore pressure gauges from G1 through G5 placed on the bottom of the 30-degree section of the soil bin. Upright broken lines (1), (2), (3), and (4) in Figs. 25 and 26 show times 10, 20, 30, and 40 min before the slope collapse time. G5 and G4 started to rise at around t = 4200 s (about 40 min before the collapse (4)), which was followed by the increase in G3 at around t = 4500 s, and then G2 and G1 at around t = 4900 s. In short, the groundwater level started to rise sequentially from the lower to the upper parts of the 30-degree section. The upper frontal end of the zone, where the groundwater seeps out from the model's surface, gradually moved up until it reached the lower end of the 30-degree section 10 min before the collapse (1). At this time (1), the groundwater at the top end of the 30-degree section was about 40 cm deep. Then, the whole collapse occurred in 10 min.

Figure 26 shows that the soil mass (D5 to D2) on the 30-degree section started to move coherently downslope at around t = 4900 s. The displacement buildup at D1 (started at t = 5100 s) followed these movements. These displacement buildups were gradually accelerated until the entire slope collapsed. Compared with Fig. 18, the downslope movement

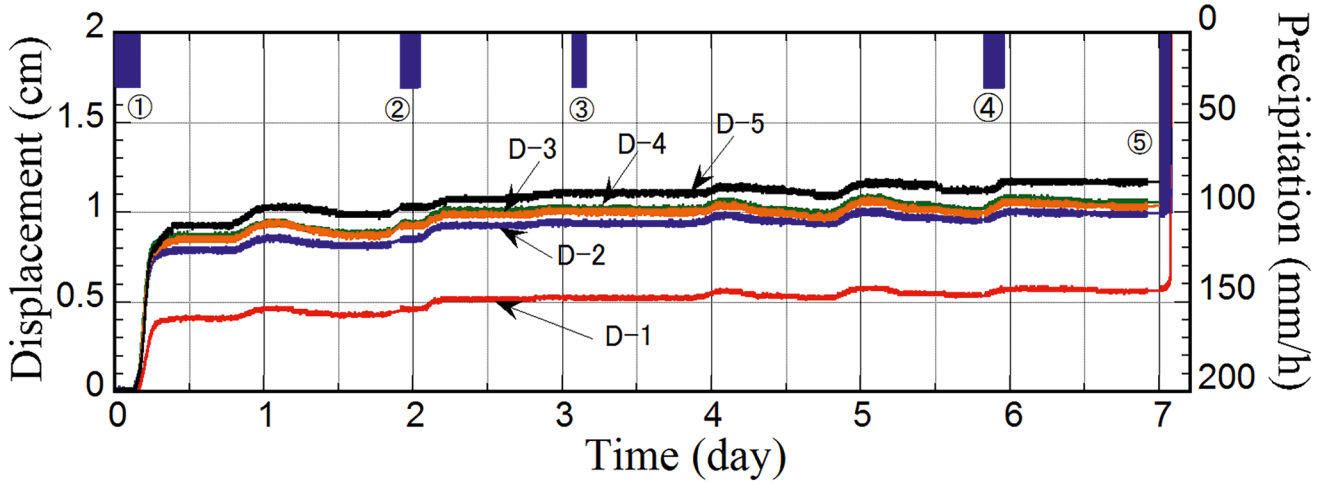


Fig. 22 Chronological changes in downslope displacements (D1 to D5) and preceding rains



Fig. 23 Transverse cracks that appeared near the top end of the 30-degree slope section immediately after the preceding rain No. 1

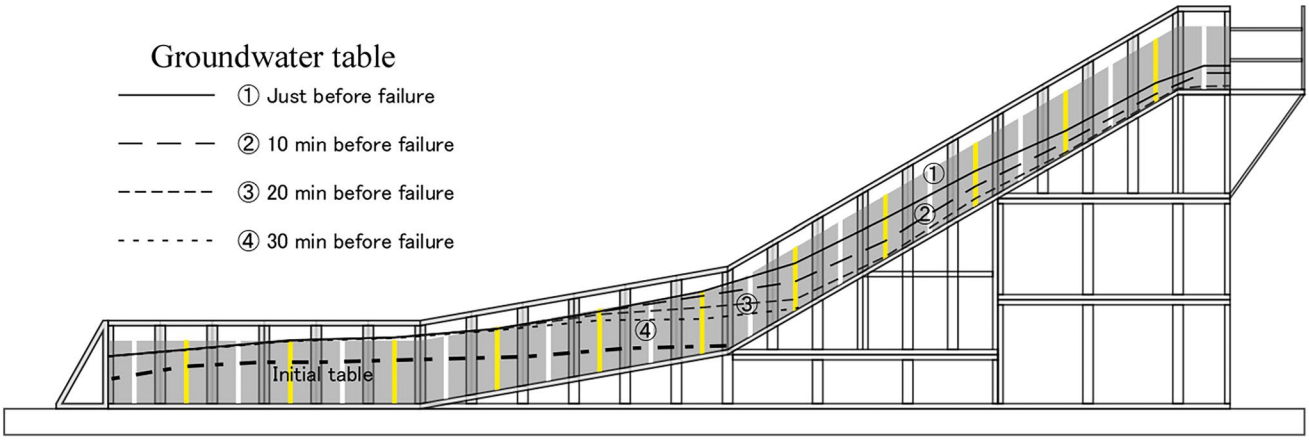


Fig. 24 Chronological change in the groundwater table in Case 2

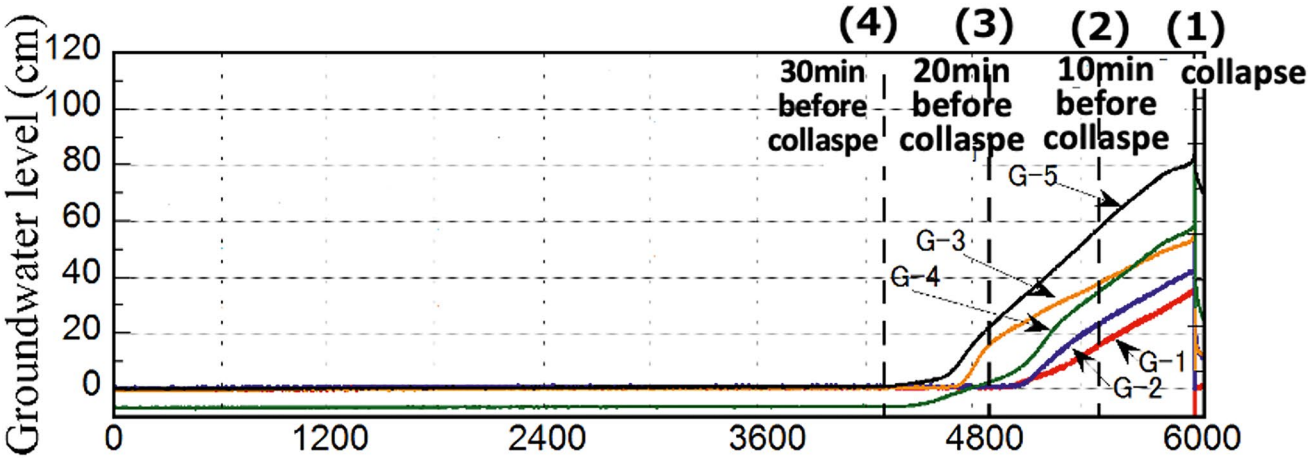


Fig. 25 Chronological changes in groundwater levels (G-1 to G-5, Case 2)

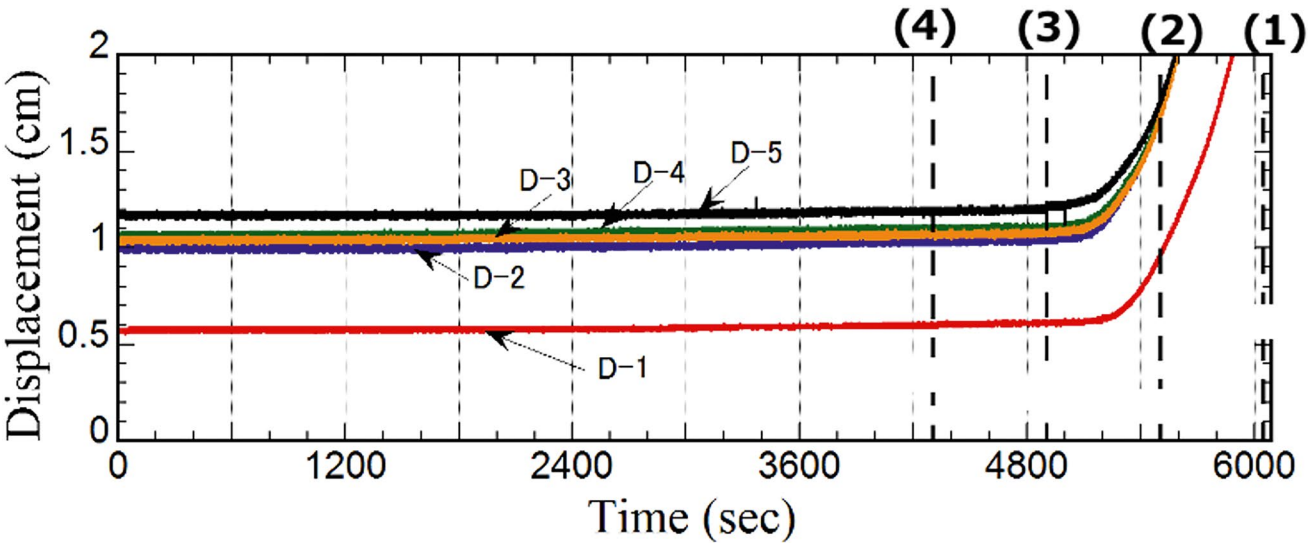


Fig. 26 Downslope movements, D1 to D5, placed over the 30-degree slope section (Case 2)

of the wet soil mass in Case 2 was much faster than in Case 1, reflecting the faster increase in the groundwater level.

5 Slope Deformation Processes due to Heavy Rainfall

The most important feature of this large-scale experiment is that it allows us to directly see the deformation in the slope ground.

In general, it is difficult to clarify the process from deformation to failure in model experiments due to the effects of scale and friction on the circumference.

However, in this large model experiment, the effect mentioned above is minimized because the experiment is conducted on a realistic scale.

The results will be particularly useful for simulation studies of rainfall infiltration and deformation.

This section describes the methodology used to achieve this.

The steel frame for the large model experiment is 23 m in length and is divided into sections.

The top of the slope is 1 m long, the 30-degree slope 10 m long, the 10-degree slope 6 m long, and the flat section 6 m long, each containing a steel frame every 1 m, with reinforced glass in between the frames.

The slope deformation indicator is completed by setting white sand bars between the frames.

Here, numbers (c0–c22) are written on the white sand columns to make it easier to track the changes (see Fig. 27).

As explained earlier, the soil bin's glass-paned side walls allow easy observation of the soil layer's deforming process from the outside (Fig. 27). Though the soil models prepared in Cases 1 and 2 were the same as each other, the slip surfaces that developed in the interiors of these soil models differed, as will be explained herein, reflecting the absence (Case 1) and presence (Case 2) of the pre-wetting processes.

For easy observation of the deforming process, the soil models in Case 1 and Case 2 had white-colored sand columns embedded at regular intervals along the glass-paned wall (Fig. 28). Since each glass-paned side wall has upright stiffeners arranged at regular intervals of 1 m to stiffen the wall against out-of-plane deformations, sand bars were evenly arranged between each pair of the neighboring stiffeners. The following processes made each sand column:

1. filling a plastic half-cylindrical 8 cm-mold with white sand,
2. putting the mold on the glass pane of the soil bin,
3. filling the soil bin with sand to make the slope model, and finally
4. pulling the mold out of the slope model.

5.1 Case 1 with no Prior Rainfall to the Main Rainfall Event

As detailed earlier, the model's collapse occurred precisely 8,515 seconds after the onset of continuous 100 mm/s rainfall. The entire collapse transpired within the final 5 seconds. Fig. 29 presents the last 3-second sequence, providing a frame-by-frame progression (at every 1-second interval) of the slope's ultimate collapse. This process is characterized by the model's surface cracking and bulging at its top and toe parts, as depicted in Fig. 30. The frame-by-frame collapse progression (5 frames at every 1/6-second interval) in Fig. 31 illustrates the development of the slip surface within the 30-degree slope section with meticulous detail.

In (1) of Fig. 29, columns c1 to c9 are tilted forward.

The yellow dotted line drawn in Fig. 29 (2) connects bends and kinks observed in white sand columns c1 through c10, thus showing the deduced slip surface developed over the 30-degree slope section. Sand columns from c3 to c7 faded due to this part's extensive downslope movement. The sand

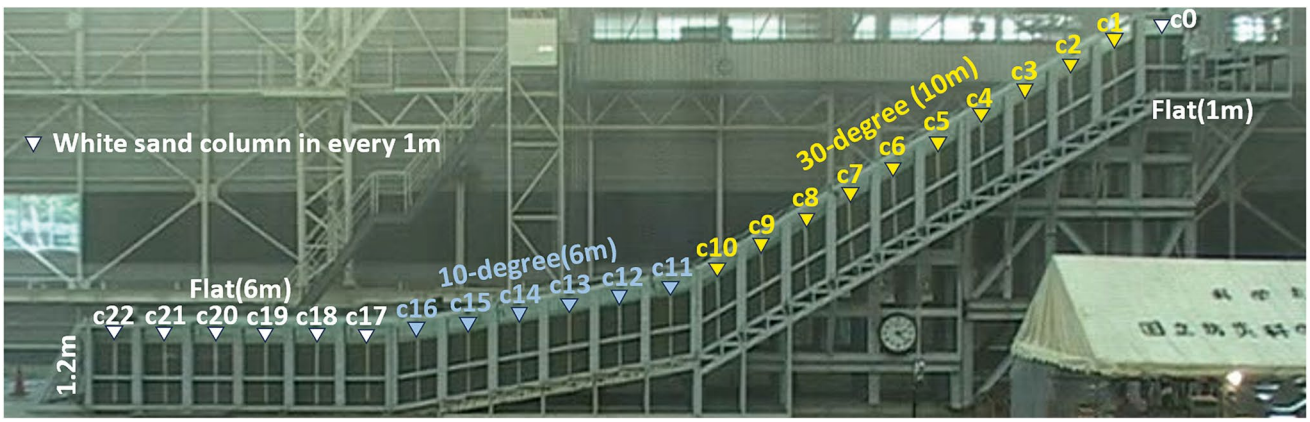


Fig. 27 Side view of the slope model (Case 2): White sand columns can be seen in each glass-paned section (between adjacent stiffeners)

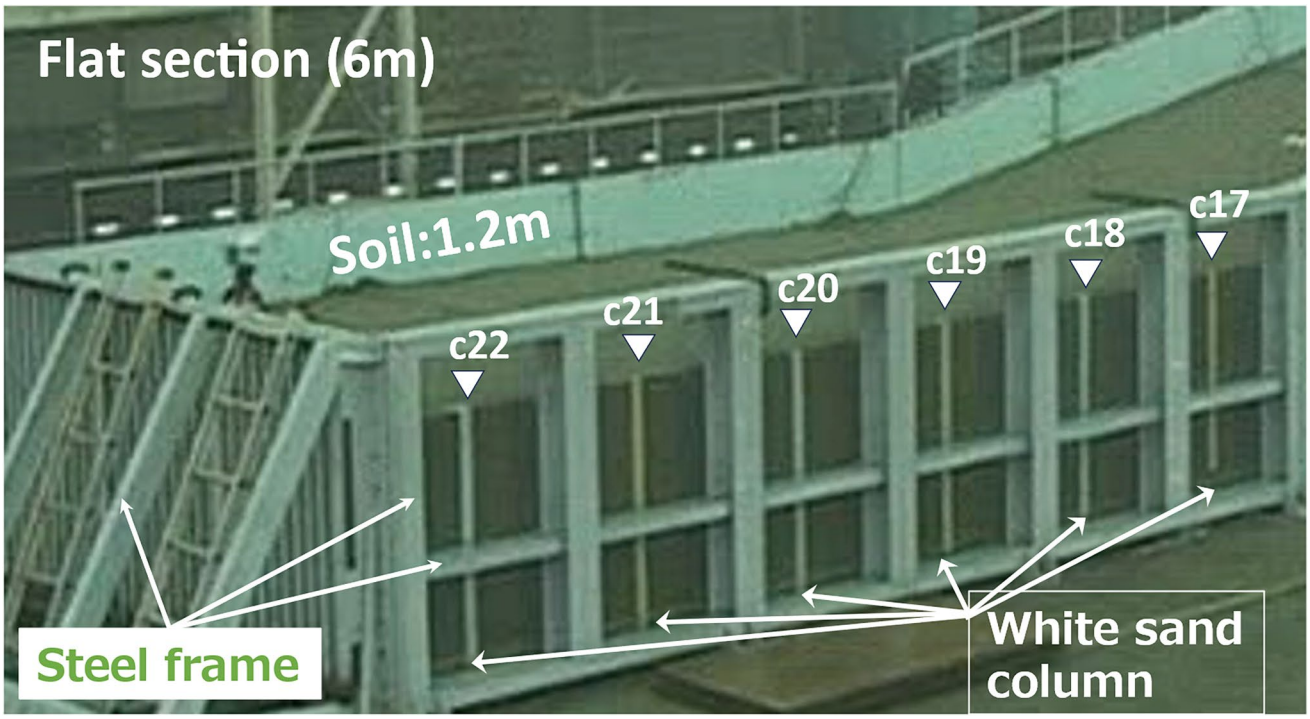


Fig. 28 Close-up of the soil bin's side wall

columns from C11 to C22 remained upright at this stage, showing neither deformation nor tilting. The observations above indicate that the slip surface was exclusively formed in the 30-degree slope area, and the collapse occurred within a one-second window between 8515s and 8516s. In Fig. 29 (3), kinks and bends further developed over the soil columns from c9 to c13, suggesting that a new slip surface was formed. On the other hand, the kinks of white sand columns shown in c6 to c9 show the earlier-developed slip surface, allowing the upper part of the landslide mass to move coherently over the 10-degree slope section. Fig. 29 (3) also shows an early sign of forming another new slip surface near the bottom of the soil bin over sand columns C13 to C15. This early sign developed into a new slip surface in Fig. 29 (4), shown as kinks of the sand columns from C14 to C17. At this stage, the soil mass that spread over the gentle 10-degree slope section has yet to stop moving, perhaps causing the new shear slip surfaces to develop within the undrained 10-degree slope section. Fig. 31 shows the frame-by-frame advance (three consecutive frames at every 1/6 s) of slope collapse taken from a video clip (30 frames/s) showing the whole process of the slip surface formation within the 30-degree slope section. The frame (1) at 8515.17 s in Fig. 31 shows that the sand columns, c1 through c10, developed bends and kinks. These bends and kinks show a slip surface geometry, which is shallower on both ends, including c1 and c2 near the top scar and c8 through c10 near the toe part. Bends and kinks are deep near the bottom of the soil bin at sand columns, c3 to c7, covering the middle part of the landslide mass. The trend is further developed in Fig. 31 (2) at 8515.51 s. The white sand columns c1 through c9 are entirely sheared off, resulting in columns c2 to c8 hiding behind upright steel stiffeners of the soil bin. The slip surface finally developed throughout its stretch in Fig. 31 (3) at 8515.34 s, while the other columns from c11 to c22 showed no remarkable change. Comparing these figures, we can discern that the initial stage of the entire collapse was marked by the appearance of transverse cracks at the top end of the 30-degree slope section (Fig. 29 Frame No. 1). This was associated with slight bends of white sand columns within the 30-degree slope section, as shown in



Fig. 29 Last 3-s swipe for frame-by-frame advance (at every 1-s interval) of the final entire collapse of the slope (Case 1)



Fig. 30 Oblique views of the final stage of slope failure development (Case 1)

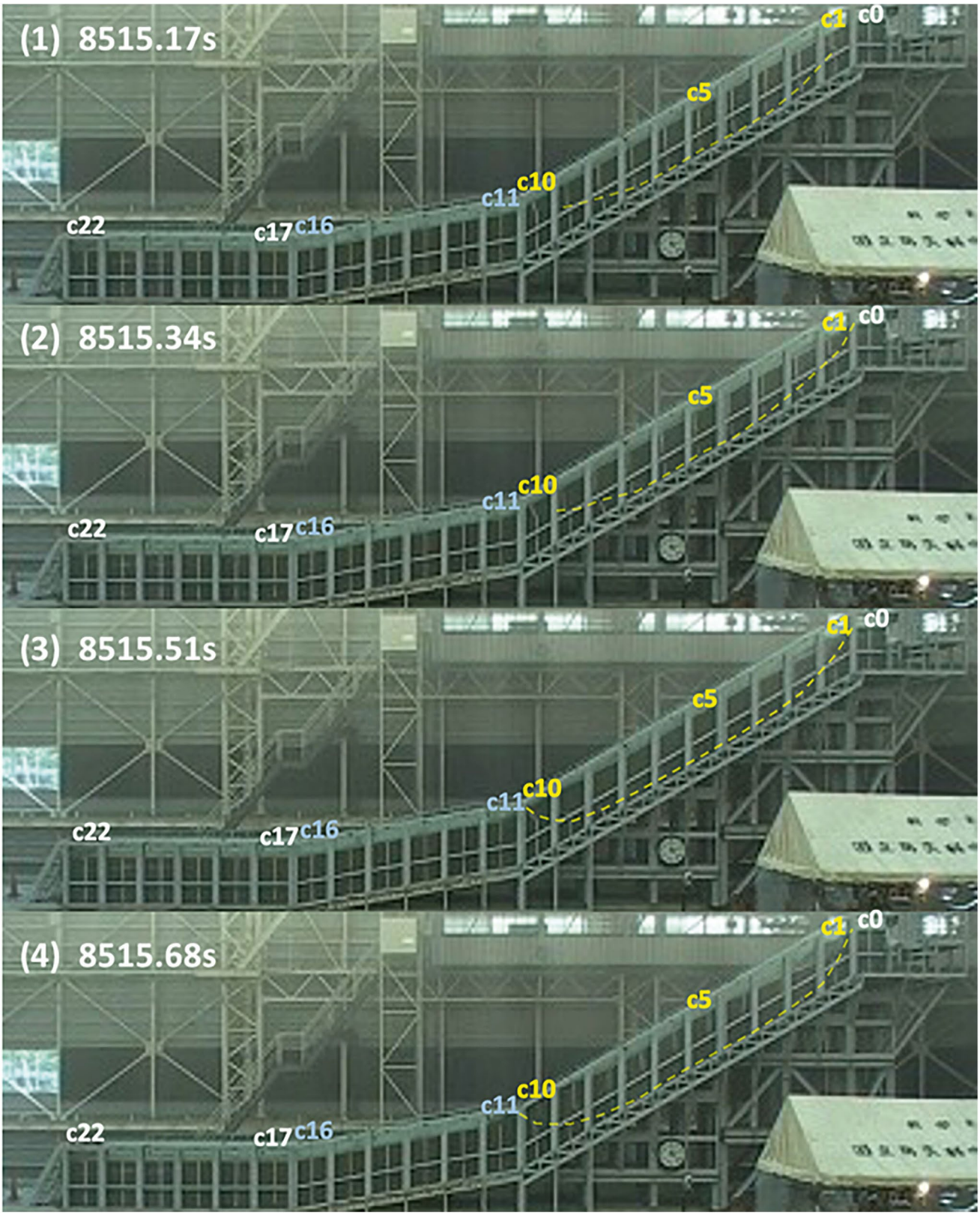


Fig. 31 final frame-by-frame collapse advance (5 frames at every 1/6-s interval, Case 1)

Frame No. 1 in Fig. 28. As time progressed, the appearance of kinks in sand columns indicated the development of a shear slip surface through the sandy soil only within the 30-degree slope section (Frame 2 in Fig. 28). This was associated with the formation of a bulge at the toe part of the 30-degree slope section (Frames 2 in Figs. 28 and 29). Finally, the toe part of the sliding soil mass overrode the gentler 10-degree slope section, entraining the surface part of the 10-degree slope section, thus causing two more shear bands (slip surfaces) to develop within the undrained 10-degree slope section. These findings have significant implications for our understanding of slope collapse dynamics.

5.2 Case 2 with Prior Rainfalls to the Main Rainfall Event

Likewise, as in Case 1, Fig. 32 shows the last 3-s swipe for frame-by-frame advance (at every 1-s interval) of the final entire collapse of the slope. This process is associated with cracking and bulging the model's surface at its top and toe parts, respectively, as shown in Fig. 33. The final frame-by-frame collapse advance (10 frames at every 1/3-s interval) is shown in Fig. 34.

5.3 Summary

Finally, Figs. 35 and 36 compare the developed slip surfaces and groundwater tables in Cases 1 and 2 to visualize better what is explained above.

Significant findings from the above experiments are:

1. The formation of a groundwater table plays a significant role in the soil deformation buildup, contributing to the destabilization and failure of the entire slope.
2. Water retention strongly influences the formation of the groundwater table in the slope's lower part, primarily affected by preceding rains.
3. When the toe part of a slope is soaked up with water, the downslope movement of the soil mass can cause the toe part's liquefaction, leading to faster collapse no matter how steep the slope is. Eventually, the landslide mass becomes more extensive, resulting in severe devastation.
4. Examining underground wet conditions is especially critical because rainfall infiltration and groundwater formation accelerate slope deformation.

6 Concluding Remarks

The large-scale rainfall simulator at the National Research Institute for Earth Science and Disaster Resilience (NIED) has the world's largest indoor rainfall area and sprinkling capacity, producing rainfall intensities between 15 and 300 mm/h. Its unique ability to control all experimental parameters is a crucial advantage, enabling the realization of more realistic natural rainfall conditions and external forces. This unique feature makes the experiments here invaluable, setting our research apart. However, it is crucial to stress the need for diverse simulation methods to exploit this advantage and fully encourage further research.

This article described the (1) outline of the facility, (2) experimental methods unique to large-scale models placed in the vast indoor rainfall area, and (3) experiment examples highlighting the importance of the preceding wetting process for large-scale models.

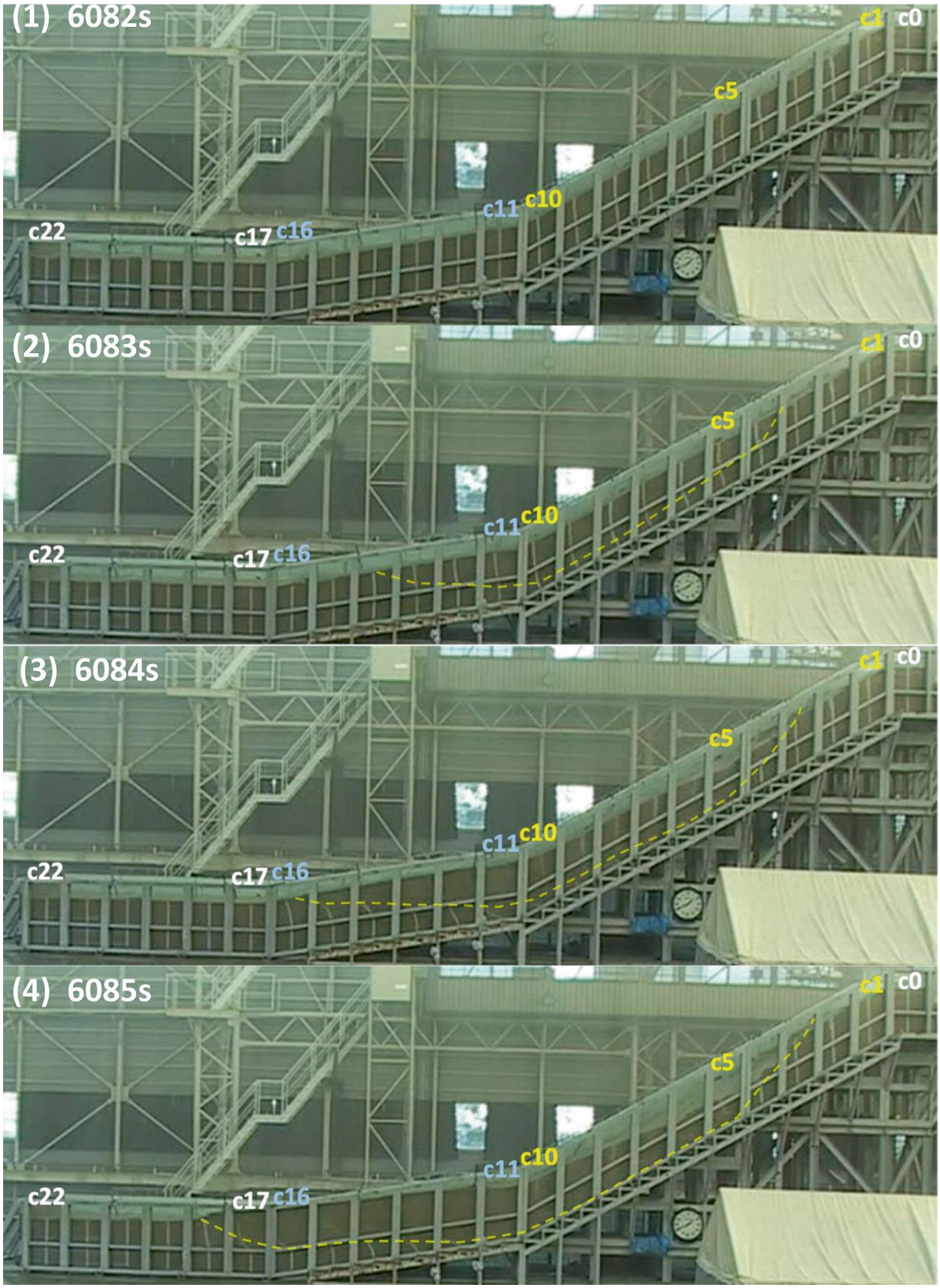


Fig. 32 Last 3-s swipe for frame-by-frame advance (at every 1-s interval) of the final entire collapse of the slope (Case 2)



Fig. 33 Oblique views of the final stage of slope failure development (Case 2)

The two experiment examples (Case 1 and Case 2) in this article are the same regarding the dimensions of the models prepared in a large soil bin, model materials, and compacting methods. The only difference is the pre-wetting process, which was given only in Case 2. The pre-wetting accelerated the model's soaking process remarkably, yielding a faster slope collapse.

The results of the large-scale model experiments showed that the slope ground becomes unstable due to rainfall with a change of a groundwater table. The results may serve as a benchmark test for improving the accuracy of ground deformation simulation due to rainfall infiltration and sediment flow simulation (debris flow) based on large deformation analysis using particle methods, and so on.

We will continue conducting various experiments to gain new insights into how experiments of this large-scale model are to be planned and share this knowledge worldwide.

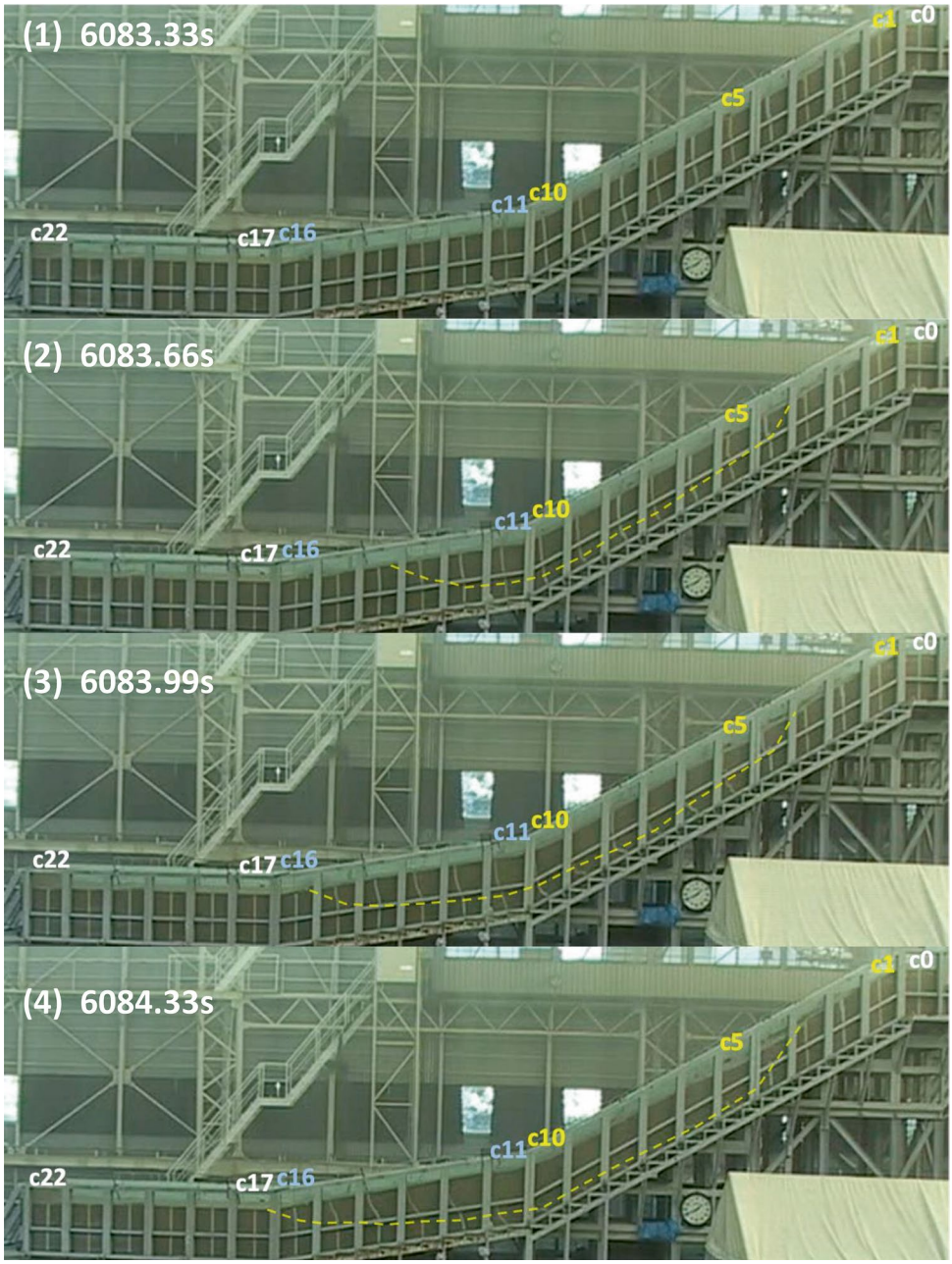


Fig. 34 Final frame-by-frame collapse advance (10 frames at every 1/3-s interval, Case 2)

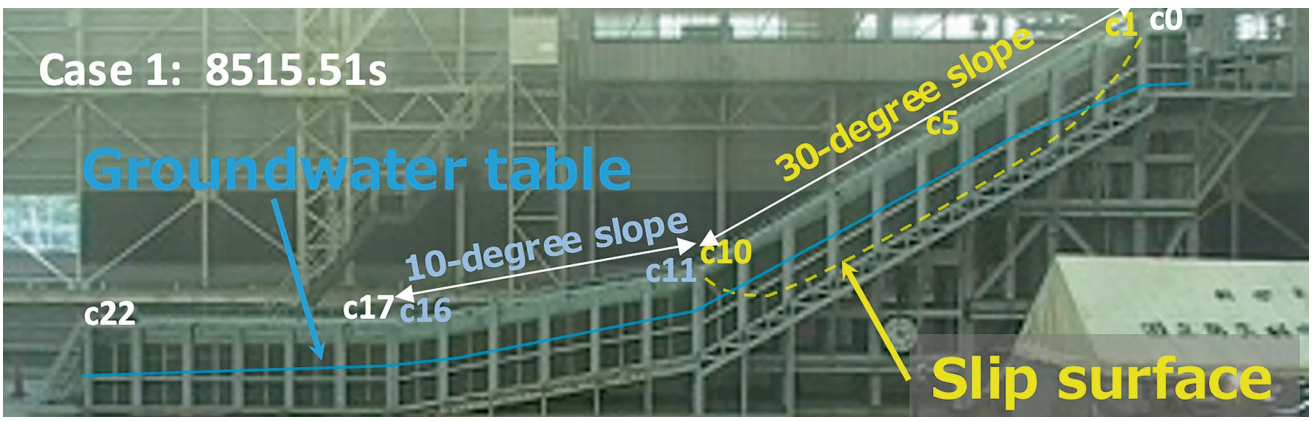


Fig. 35 Developed slip surface and groundwater table in Case 1

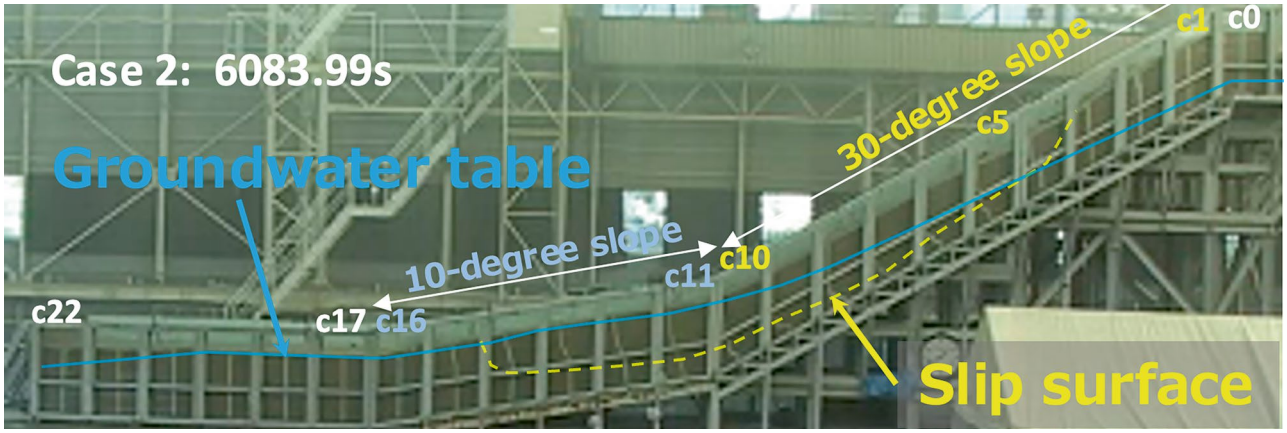


Fig. 36 Developed slip surface and groundwater table in Case 2

References

Fukuzono T (1985) A new method for predicting the failure time of a slope. In: Proceedings of the 4th international conference and field workshop on landslide, Japan landslide society, pp 145–150. Japan Landslide Society

Ishizawa T, Danjo T, Sakai N (2017) Real-time prediction method for slope failure caused by rainfall using slope monitoring records. J Disaster Res 12(5):980–992

Moriwaki H (1988) Current status and problems of slope failure research by model experiments. Geomorphology 9–4:255–268

Moriwaki H, Inokuchi T, Hattanji T, Sassa K, Ochiai H, Wang G (2004) Failure processes in a full-scale landslide experiment using a rainfall simulator. Landslides 1:277–288

Sakai N, Sakajo S (2008) Model tests of collapse of unsaturated slopes in rainfall. In: 10th International Symposium on Landslides and Engineered Slopes (Xi'an), pp 907–912

Sasahara K, Sakai N (2014) Development of shear deformation due to the increase of pore pressure in a sandy model slope during rainfall. Eng Geol 170:43–51

Sasahara K, Sakai N (2017) Shear and compression strain development in sandy model slope under repeated rainfall. Soils Found 57(6):920–934

Sasahara K, Sakai N, Kurihara J, Sun Y, Sakaue S (2007) Application of FEM analysis method to prediction of slope surface displacement and failure time due to rainfall infiltration. In: 42nd JSCE Conference

Take W, Bolton MD, Wong PCP, Yeung FJ (2004) Evaluation of landslide triggering mechanisms in model fill slopes. Landslide 1:173–184

Open Access This chapter is licensed under the terms of the Creative Commons Attribution 4.0 International License (http://creativecommons.org/licenses/by/4.0/), which permits use, sharing, adaptation, distribution and reproduction in any medium or format, as long as you give appropriate credit to the original author(s) and the source, provide a link to the Creative Commons license and indicate if changes were made.

The images or other third party material in this chapter are included in the chapter's Creative Commons license, unless indicated otherwise in a credit line to the material. If material is not included in the chapter's Creative Commons license and your intended use is not permitted by statutory regulation or exceeds the permitted use, you will need to obtain permission directly from the copyright holder.



Part II

Review Articles

Landslide Dam Studies in Uttarakhand, India: Past, Present and Future

Shivani Joshi and Srikrishnan Siva Subramanian

Abstract

A landslide dam is a natural hazard that results from a landslide of any type whose runout and interaction with local topography and relief deposits it to form a barrier or dam that can hold back river water in the upstream region. The water held behind the dam forms a lake upstream and risks breaching at any moment due to the unconsolidated landslide material. When this dammed lake is breached, it increases the risk of flash floods called Landslide Lake Outburst Floods (LLOF) in the downstream region, posing significant risks to infrastructure and livelihood. LLOFs are prevalent hazards in mountainous regions globally, including the seismically active Himalayas. The northwestern Indian Himalayas (Jammu & Kashmir, Ladakh, Himachal Pradesh, and Uttarakhand) are particularly susceptible to landslides and landslide dams due to weak, sheared bedrock and confined river valleys. This review critically evaluates the current knowledge on landslide dams in Uttarakhand, India. While paleo landslide dam and LLOF assessments are common, proactive monitoring and hazard mitigation strategies remain limited. Here, we comprehensively review historical and contemporary landslide dams in Uttarakhand, categorising existing research methodologies into past, present, and future studies. Past studies primarily focus on paleolakes formed after the Last Glacial Maximum (LGM) and employ various dating techniques for reconstruction. The present studies discuss the landslide dams from 1857 to the present and analyse the most affected catchments, districts, months of occurrence, and the dominant landslide types. Future studies review the utilisation of geospatial technology, numerical modelling, and machine learning algorithms to determine the formation and stability of landslide dams. This comprehensive review of historical, ongoing, and future research on landslide dams in Uttarakhand sheds light on these dynamic natural threats. By deepening our understanding, we aim to empower the development of robust mitigation strategies, ultimately contributing to the enhanced disaster preparedness, risk reduction, and effective mitigation measures in the region.

Keywords

Landslide dams · Landslide dam outburst flood (LLOF) · Himalayas

1 Introduction

Uttarakhand is a north-western Himalayan state of India that falls between 28°43″ N–31°27″ N latitude and 77°34″ E–81°02″ E longitude (Khanduri 2021). Internationally, it borders Nepal and Tibet (China) and nationally Uttar Pradesh and Himachal Pradesh. Uttarakhand covers an area of 53,483 sq. km, which is 1.6% of the country's total geographic area. It has a population of 10,086,292, according to the Census of India, 2011 (*Uttarakhand* Population 2022 | *Sex Ratio & Literacy Rate 2024*). The burgeoning urban population in the region, estimated at 12,190,000 in 2023, underscores a trend of accelerating anthropogenic pressures. This urbanisation coincides with a surge in activities like deforestation, agricultural intensification, road networks, hydropower development, and expanding infrastructure. Such land-use modifications within this fragile mountain ecosystem pose a significant threat of environmental degradation, potentially leading to an increased frequency and severity of natural hazards.

Litho-tectonically, Uttarakhand is divided into five zones. The Himalayas override the Indian plate along a decollement fault called the Main Himalayan Thrust (MHT) (Kumar et al. 2016). Its surficial expression in the Himalayas

S. Joshi · S. Siva Subramanian (✉)
Centre of Excellence in Disaster Mitigation and Management, Indian Institute of Technology Roorkee, Roorkee, India
e-mail: shivani_j@dm.iitr.ac.in; srikrishnan@dm.iitr.ac.in

© The Author(s) 2025

B. Abolmasov et al. (eds.), *Progress in Landslide Research and Technology, Volume 3 Issue 2, 2024*, Progress in Landslide Research and Technology, https://doi.org/10.1007/978-3-031-72736-8_15

is determined by the Main Frontal Thrust (MFT), which separates Indo-Gangetic plains in the south to the Siwaliks in the north. Indo-Gangetic plains mainly comprise alluvium, while Siwaliks comprise sedimentary rocks like sandstone, siltstone, and conglomerates in different strata. To the north of MFT lies Main Boundary Thrust (MBT), which separates the Siwaliks and Lesser Himalayas. The Lesser Himalayas comprise meta-sedimentary and sedimentary rocks like quartzite, phyllite, dolomites, limestone, and shales. Above that lies the Main Central Thrust (MCT), which separates the Lesser Himalayas from the Central Himalayas and consists of high-grade metamorphic rocks like schists and gneisses. In the northernmost part of Uttarakhand lies the Trans Himadri Fault (THF), which separates the Central Himalayas from the Trans Himalayas. Trans Himalayas have both meta-sedimentary and igneous lithology. Intense compressional forces associated with major thrust faults and pervasive lineament networks within the Himalayas have subjected the rocks to extensive pulverization. This process of intense deformation generates sheared and brecciated rock formations proximal to the thrust zones. The combination of weakly consolidated lithologies and steep slopes within the Himalayas renders them highly susceptible to mass wasting events. These events are further exacerbated by frequent precipitation events and seismic activity prevalent in the region. The abundance of debris and colluvium, coupled with the pronounced relief and confined valleys, facilitates the formation of landslide dams when mass movements occur in the vicinity of a stream. A landslide dam, therefore, results from a landslide of any form whose runout and interaction with local topography allow its deposits to form a barrier that can hold back water above a 'normal' river level (Fan et al. 2020). According to Costa and Schuster (1988), landslide dams are classified into six types (Type I- VI) based on the valley width and landslide type and size. Based on the commonly occurring landslide type (debris slides) and the presence of narrow river valleys and gorges, types I and II are the most common in the Uttarakhand region.

Mass movement is a natural erosional phenomenon acting on the Himalayan ranges since its formation. Unlike other disasters, landslides cause permanent loss of land that adversely affects the life support strategy of the affected people (Khanduri et al. 2018). Moreover, the availability of productive land in the hills is limited, and landslides cause the loss of this scarce natural resource (Khanduri et al. 2018). When the landslide reach the river and block it entirely or partially, it increase the water level upstream and form a landslide-dammed lake. Breaching this precarious barrier can trigger catastrophic flash floods in the downstream reaches, potentially inundating settlements and causing significant societal disruption. The steep slopes characteristic of the Himalayas affect the downstream propagation of these events, with documented historical floods impacting even distant areas within Uttarakhand. While the formation of landslide dams is comparatively less frequent than landslides themselves, their impact is disproportionately high. Breach-induced inundation can disrupt critical infrastructure networks, including transportation corridors, hydropower facilities, healthcare systems, and educational institutions, even at considerable distances downstream. Most landslide dams have been found in the higher Himalayan ranges due to high relief and narrow valleys. The remoteness of the landslide dam's location has not allowed for much work. Sometimes, the landslide dam breach within hours due to loose debris, which leads to little or no damage or danger to the downstream region. However, as the breaching time increases, the risk of it becoming a disastrous event also increases. This review comprises the landslide dams of the Uttarakhand state (Fig. 1) and reviews the past and present studies along with the future scopes in assessing and evaluating landslide dams.

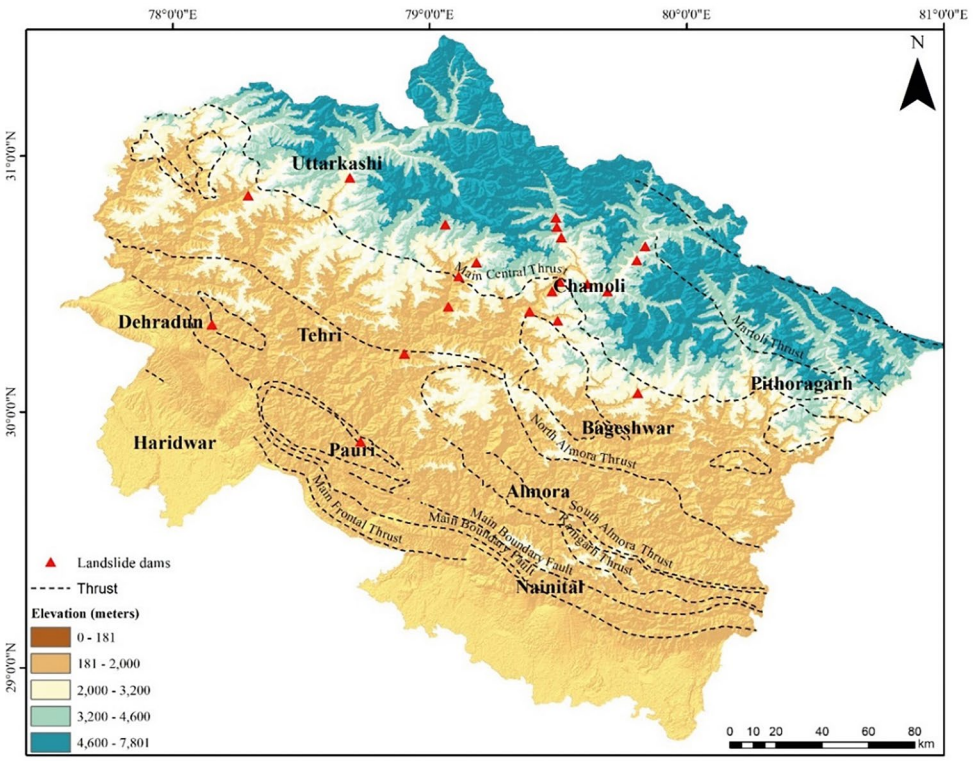


Fig. 1 Map of Uttarakhand, India, showing tectonic thrusts and landslide dam locations

2 Past Scenarios of Landslide Dams in Uttarakhand

The orogenic deformation in the Himalayas is a continuous process, but it intensified in the Last Glacial Maximum (LGM) in the upper Pleistocene epoch. After the LGM, as the glacial receded, they carved out deep valleys and increased mass movement activities due to the changing climatic patterns. After the LGM, there is evidence of numerous landslide dam formations in Uttarakhand. The steep slopes become barren during the cold phase, increasing weathering and erosion. During wetter phases, those loose debris and soil are mobilised down the slope, blocking the streams and creating landslide-dammed lakes (Srivastava et al. 2013). These paleolakes provide an opportunity for sediment deposition and preservation, allowing researchers to study the region's past environmental changes and monsoonal fluctuations by analysing the sedimentary record within the lake sequence. Paleo-landslide dams are usually associated with geomorphic features such as knickpoints, debris aprons and fans, terraces, benches, drainage anomalies, and slackwater deposits. Therefore, these features are helpful indicators and can be used to locate them. Optical Stimulated Luminescence (OSL) dating is generally utilised to study the sediments by determining their luminescence stored in a mineral lattice (mainly quartz) prior to burial in the process of mass movement.

In the lesser Himalayas, tectonics, lithology, and climate play significant roles as preparatory causal factors for slope failures, sometimes leading to the formation of dammed lakes (Sundriyal et al. 2007). Most studies on paleo-landslide dams have been conducted in the Alaknanda Valley (Fig. 2). The investigation of paleolake sequences has been done using geomorphology and geochemistry. The identification of four lake sequences (Lashmoli, Badiyargarh, Dhobighat and Swit Nala) in the Alaknanda valley has been made based on lithofacies determination using a grain-size pattern, a vertical and lateral association of individual depositional units, colour and bioturbation (Sundriyal et al. 2007). For geochemical analysis, samples were collected from fine sand and clayey silt units, where samples for OSL dating were collected from the sandy horizons (Sundriyal et al. 2007). The luminescence chronology suggested that the lakes had formed between 14,000 and 5000 years ago and were terminated due to the large-scale tectonic activity leading to the breaching of lakes and leaving behind a thick deposition of lacustrine sediments.

Another case of paleo-landslide dam study is of the Malari paleo lake (Fig. 3), which was formed in the Late Pleistocene to Early Holocene. It was situated along the Dhauliganga River, a tributary of the Kali River. Tectonically, this lake was situated in the north of the South Tibetan Detachment in the Trans-Himalayan region. The study was conducted to reconstruct past environmental changes and to study the Indian summer monsoon variability using sedimentology,

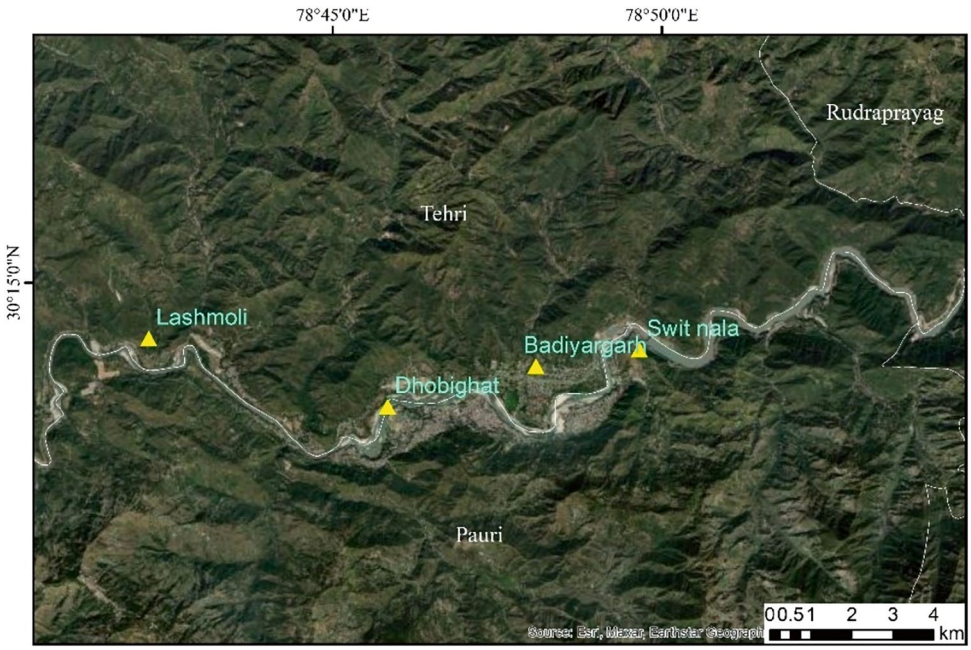


Fig. 2 Map showing paleolakes of Alaknanda Valley, Uttarakhand, India

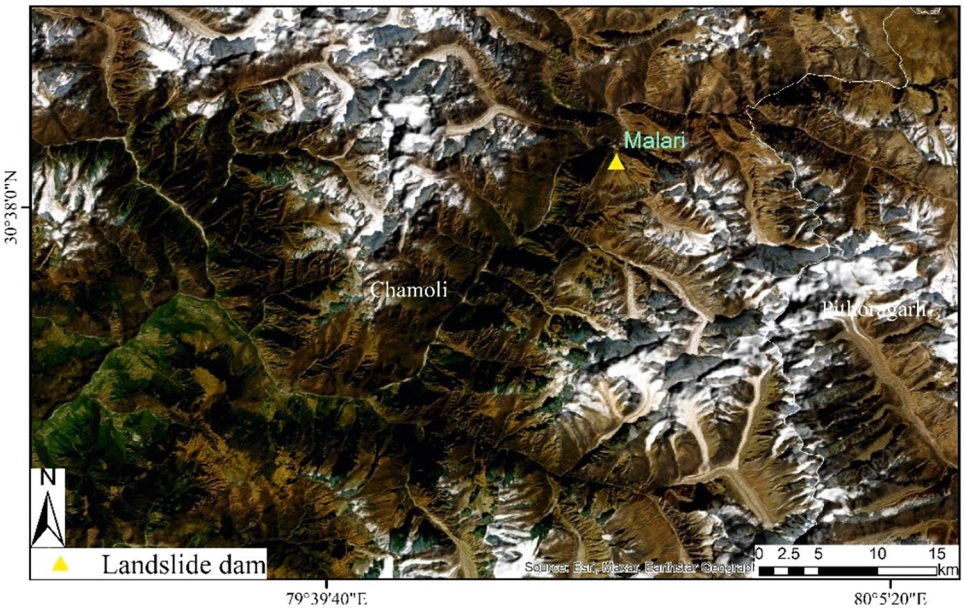


Fig. 3 Map showing spatial distribution of paleolakes of Malari, Uttarakhand, India

pollen taxonomy, environmental magnetism and chemical indices involving major, trace and rare earth elements (Srivastava et al. 2013). The OSL dated the lake as 12,000 years ago. At that time, the southwest monsoons used to be weaker than they are now, followed by some incidents of intensification around 10,000 to 9000 years ago.

3 Present Cases of Landslide Dams in Uttarakhand

The change in climate has been drastically observed in the Himalayan region. Changes in rainfall patterns, monsoonal variations, and rising temperatures have invited frequent disasters in Uttarakhand. With the change in the climatic conditions worldwide, the hills have witnessed abnormally heavy precipitation and associated disasters in recent times (Khanduri et al. 2018).

Uttarakhand has four major river basins: Yamuna, Ganga, Ramganga, and Kaliganga, as well as some sub-basins. In the Central Himalayas, the principal and fast-moving rivers are nurtured by mighty glaciers. Over 900 glaciers contribute their meltwater to nourish rivers like the Yamuna, Ganga, and Kali, along with their numerous tributaries. Among these, the Tons, Bhagirathi, Bhilangana, Dhauliganga (West), Mandakini, Alakananda, Nandakini, Pindar, Dhauliganga (East), and Goriganga carve their paths through the rugged landscape. Descending towards the Lesser Himalayas, the character of the rivers shifts and fluctuates with the season of rain and snowmelt. Rain and spring-fed tributaries like the Saryu, Eastern and Western Ramganga, Kosi, Gaula, and Eastern and Western Nayar take centre stage. Finally, in the foothills of the Siwaliks, the monsoon dictates the flow of the rivers. They become roaring torrents during the rainy season, only to dwindle to mere whispers for the rest of the year. These rivers have varied types of channels based on their river stage. The Central Himalayas consist of narrow valleys and gorges, while in the Siwaliks, broad valleys and floodplains are observed. In the context of landslide dams, narrow valleys are of primary importance. The smaller the valley width, the higher the chance of damming the river by landslides. Another crucial topography for landslide dams is the confluences, which can be seen to be affected by landslides in the higher regions of the state. Uttarakhand has experienced many incidences of Hydro-meteorological disasters since 1816. However, the middle of the nineteenth century up to the present has proved the worst decades as both the magnitude and frequency of these disasters have gone up. The disasters in 1970, 1986, 1991, 1998, 2001, 2002, 2004, 2005, 2008, 2009, 2010, 2012 and 2013 are the major natural calamities in Uttarakhand (Pandey and Mishra 2015).

The present study on landslide dams in Uttarakhand is mainly based on evaluation. There have not been many recent cases, but preparedness measures are crucial to reduce such kinds of disasters in the future. Table 1 mentions the landslide dams in Uttarakhand from 1857 to 2018. No such significant damming has been observed in the state after 2018. Heavy precipitation in the region has triggered a maximum of the landslide dams. The landslide material is usually debris, which is loose and broken rock material. When debris-related mass movement occurs, the river may breach within a few hours or days due to the lack of compaction in

Table 1 List of landslide dams in Uttarakhand, India

Year	Month	River	District	Landslide type	Breach	Triggered by	References
1857		Mandakini	Rudraprayag		3 days		Parkash (2015)
1868		Alaknanda	Chamoli		Temporary		Rautela and Pande (2005)
1893		Alaknanda	Chamoli	Rock fall	Temporary	Rainfall	Pandey and Mishra (2015)
1893	October	Alaknanda	Chamoli	Rock fall/slide	1st in 1894, >75 years		Rana et al. (2013)
1930		Alaknanda	Chamoli	Debris flow	Temporary		Khanduri (2021), Prakesh (2014)
1951	September	Eastern Nayar River	Pauri	Debris flow	Temporary		Khanduri (2021), Prakesh (2014)
1957		Dhauliganga	Chamoli	Avalanche	Filled with debris		Khanduri (2021), Prakesh (2014)
1968	May	Rishiganga	Chamoli	Debris slide	1970		Pandey and Mishra (2015)
1969	September	Alaknanda	Rudraprayag	Rock fall/slide	Temporary	Rainfall	Gulia (2007), Khanduri (2021)
1970	July	Dhak Nala	Chamoli	Debris flow	Temporary		Khanduri (2021)
1970	July	Alaknanda	Chamoli	Debris slide	Temporary		Rautela and Pande (2005)
1970	July	Alaknanda and Dhauliganga	Chamoli	Avalanche	Temporary	Rainfall	Khanduri (2021)
1970	July	Patal Ganga	Chamoli	Debris flow	Temporary		Pandey and Mishra (2015)
1971	August	Kanoldiya Gad, Bhagirathi	Uttarkashi	Debris slide	Temporary		Pandey and Mishra (2015)
1978		Kanoldiya Gad, Bhagirathi	Uttarkashi	Debris slide	Temporary		Pandey and Mishra (2015)
1979	April	Alaknanda	Chamoli	Avalanche	Temporary		Khanduri (2021)
1979	August	Kyunja Gad	Rudraprayag	Debris flow	Temporary		Khanduri (2021)
1998	August	Mandakini	Rudraprayag	Rockslide/fall	12 hours	Rainfall	Khanduri (2021)
1998	August	Kali	Pithoragarh	Rock fall-debris flow	1 day	Rainfall	Paul et al. (2000)
2001	August	Yamuna	Uttarkashi	Debris slide	Temporary	Rainfall	Parkash (2015)
2013	June	Madhyamaheshwar	Rudraprayag	Rock/debris slide	Temporary	Rainfall and flood	Khanduri et al. (2018)
2018	March	Baura Gad, Pindar River tributary	Bageshwar	Debris slide	Still dammed	Reactivated	Khanduri (2018)
2018	August	Song river	Tehri	Rockslide/fall	7 hours		Khanduri (2021)

the material. However, damming the river for even a few hours during heavy rainfall has caused significant damage to life and property. The floods generated by the breaching of landslide-induced dams carry large amounts of sediment that may dominate the sediment yield in the Himalayas (Rana et al. 2013).

As per Fig. 4, Alaknanda River is the most susceptible to landslide damming, followed by Mandakini, Dhauliganga and Bhagirathi. Due to their narrow valleys and gorges, faults, and fractured rocks, the mass movement has easily blocked the rivers, forming lakes upstream. According to Fig. 5, Chamoli district is most affected by landslide dams, followed by Rudraprayag and Uttarkashi. It is evident from Fig. 1 that these districts lie above MBT and MCT, and the sheared rocks contributed to their high susceptibility to landslide dams. Figure 6 depicts the month which is most affected by landslide damming. The month of August being the monsoon month of the state has high percentage of landslide dam events, followed by July and September, which are also the monsoon months of Uttarakhand. Please note that the monsoon period in Uttarakhand lies from July to September. The rainfall, acting as a triggering factor, induced maximum number of landslides during these months. Figure 7 shows percentage of the type of landslides that cause the damming of rivers. As the region is influenced by frequently occurring debris slides, 28% of the damming has occurred due to them, followed by rock falls and debris flow. The Gohna Tal, which was formed by the landslide dam in 1893, has two incidences of breaching: partial breaching in 1894 and complete breaching in 1970 (after 76 years), affecting the downstream region up to Haridwar. The Gohna Lake sustained for about 76 years as it was formed by the rockslide. According to (Wasson et al. 2013), the major floods in the Alaknanda catchments were caused by the landslide dam outburst flood rather than the glacial lake outbursts.

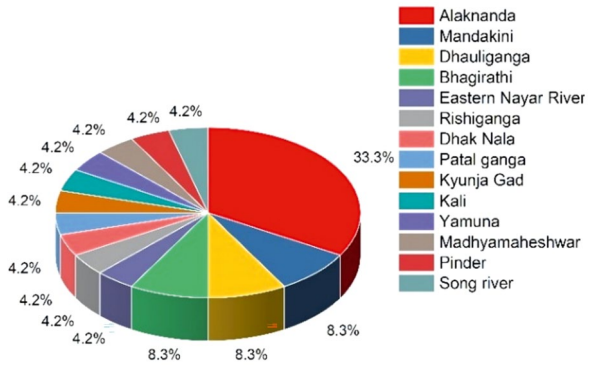


Fig. 4 Graph showing percentage of rivers affected by landslide dams in Uttarakhand, India

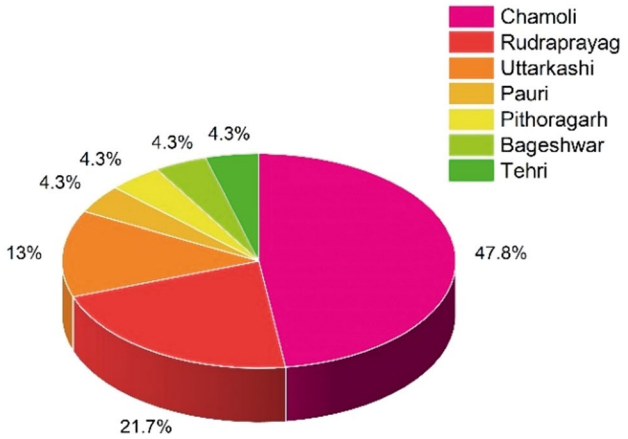


Fig. 6 Graph showing percentage of districts of Uttarakhand, India affected by landslide dams

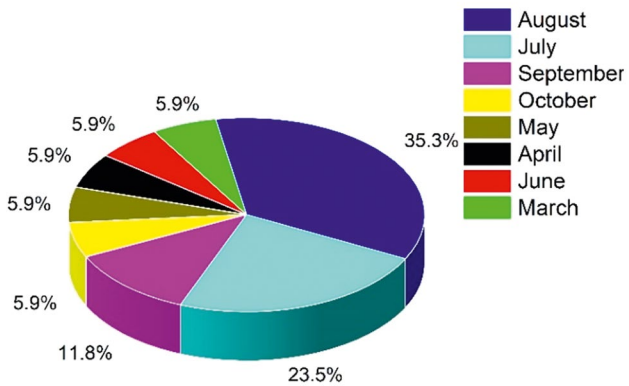


Fig. 5 Graph showing percentage of months affected by landslide dams in Uttarakhand, India

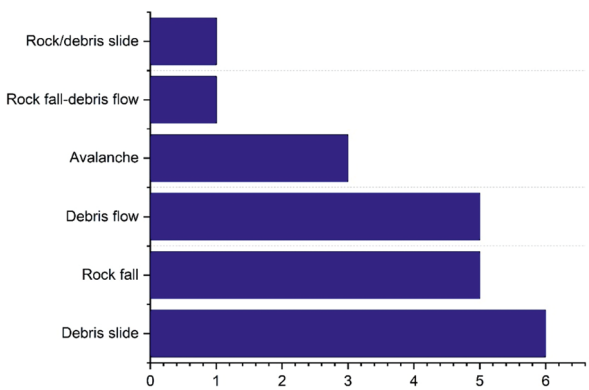


Fig. 7 Graph of landslide types that caused landslide dams in Uttarakhand, India

4 Future Studies in Landslide Dams

The geology of Uttarakhand is ridden with numerous fault lines and thrusts. With the influence of climate change, precipitation intensifies and frequent cloud bursts are observed with high-temperature gradients. Environmental factors have rendered this region susceptible to frequent landslides, flash floods, and Glacial Lake Outburst Floods (GLOFs), resulting in heightened socio-economic vulnerability. The state is also on a path of massive economic and infrastructure growth with various projects, including a large number of hydropower projects, buildings, roads, tourism-related infrastructures, dams, tunnelling, diversion structures, mining, de-siltation of river beds, etc. (Pandey and Mishra 2015). Effective disaster risk reduction strategies, including proper planning and preparedness, are crucial to mitigate the damage caused by these frequent events.

Different geomorphic indices have been developed to assess the probability of landslide damming the river/stream and the stability of dammed lakes to study landslide dams. However, these indices are region-specific but might be utilised in other regions with the same topography. Annual Constriction Ratio, Dimensionless Morpho-Invasion Index, Dimensionless Constriction Index, and Morphological Obstruction Index are some of the few indices used. A few key parameters used are landslide dam height, dam width, dam volume, landslide velocity, density of sliding, landslide grain size, catchment area, water discharge, valley width and lake volume. These parameters can be easily acquired using remote sensing images or field investigation. However, these indices do not include factors such as climatic conditions or seismicity. As per different works by Dufresne et al. (2018), Korup (2004), Tacconi Stefanelli et al. (2016), geomorphic indices may be of help in classifying past landslide dams and tuning parameters, but they are not reliable for making decisions for present cases, especially during an emergency (Fan et al. 2020). Therefore, it is necessary to develop geotechnical indices or stability criteria that consider the internal dam structure and composition for rapid assessment and prioritisation of resources in an event scenario (Fan et al. 2020). Data-driven models such as Logistic regression (LR), support vector machine (SVM), and Fisher's discriminant analysis (FDA) utilise geomorphometric parameters of landslide dams and lakes to assess the stability of landslide dams. These methods are based on training the datasets to train the model and effectively predict the stability of the landslide dam. However, the presence of false positives and true negatives induces errors in the model, and hence, it compromises the accuracy. It also depends on the quality of the inventory dataset provided, making it region-specific.

The advancement of geospatial technology is a boon for disaster management. One can quickly analyse and assess any disaster, even in the remotest areas. However, there are cases of very short-lived landslide dams that got breached within few hours, affected the nearby livelihood, and remain undetectable in the optical satellite image. As the study in landslide assessment is taking a leap towards an early warning system in India, it is necessary to study and monitor landslide dam activities in the Himalayan region. These dams usually form in higher and remote areas, which makes them unnoticeable. However, if these dams transform into landslide dam bursts, they can affect various villages coming in their path, and the damage might be very high. So, to reduce its impact, remote sensing and GIS technology are needed to monitor and assess the damming caused by the landslides. A better understanding of the controlling factors of landslide dams is essential to comprehend their stability and the breaching of the dammed lakes.

5 Conclusion

This review work was an attempt to accumulate all the information on events of landslide dams in Uttarakhand, India and the methods utilised to assess them. There are OSL dating, pollen taxonomy, environmental magnetism, and chemical indices methods to assess the paleo-landslide dams. The paleolake sequence in the Alaknanda catchment and Dhauliganga River is studied to determine the age of landslide dams. Most landslide dams occurred after the Last Glacial Maximum in the Himalayan region, dating from the Upper Pleistocene to the Holocene. Due to the evident climate change, landslide dams in the Higher Himalayas are common. The presence of debris material makes the landslide dam unstable, which may breach within a few hours or days. However, rock fall/slide type landslides form stable landslide dams, which, when breached, cause major floods in the state. The 1970 megaflood of Alaknanda was one such example. In the present scenario, the Alaknanda River and the Chamoli district of Uttarakhand are most susceptible to damming. Analysis reveals debris slides as the most common landslide type, with a notable concentration of landslide dams occurring in August. Globally, landslide dam studies have evolved with time, and different geomorphic indices, geomorphometric parameters, and machine learning algorithms have been utilised to study the stability of landslide dams. The Himalayan region is complex in its own way. Therefore, it is necessary to develop such indices and numerical models specific to the region to assess and monitor the dam's formation and stability to reduce its risk.

Acknowledgements The authors are thankful to the International Consortium on Landslides (ICL) for providing this opportunity to showcase our work in the field of landslides. The first author would also like to express sincere gratitude to the Ministry of Human Resource Development (MHRD) for providing fellowship that supported this research.

References

Costa JE, Schuster RL (1988) Formation and failure of natural dams. Bull Geol Soc Am 100(7):1054–1068. https://doi.org/10.1130/0016-7606(1988)100<1054:TFAFON>2.3.CO;2

Dufresne A, Ostermann M, Preusser F (2018) River-damming, late-quaternary rockslides in the Ötz Valley region (Tyrol, Austria). Geomorphology 310:153–167. https://doi.org/10.1016/j.geomorph.2018.03.012

Fan X, Dufresne A, Siva Subramanian S, Strom A, Hermanns R, Tacconi Stefanelli C, Hewitt K, Yunus AP, Dunning S, Capra L, Geertsema M, Miller B, Casagli N, Jansen JD, Xu Q (2020) The formation and impact of landslide dams – state of the art. Earth Sci Rev 203:103116. https://doi.org/10.1016/j.earscirev.2020.103116

Gulia KS (2007) Discovering Himalaya: tourism of Himalayan region, vol 2. Gyan Publishing House. https://books.google.com/books?hl=en&lr=&id=ugFIz7ph-kEC&oi=fnd&pg=PA9&dq=Gulia,+K.S.,+2007.+Discovering+Himalaya:+Tourism+of+Himalayan+Region.+ISHA+Books,+Delhi.&ots=gPeGKGOBxE&sig=giwJiA1RsoAtSO-OQc7zCQsfXAE

Khanduri S (2018) Landslides over two places of Uttarakhand; an observation. Int J Eng Appl Sci Technol 3(2):52–56

Khanduri S (2021) Formation and failure of natural dams in Uttarakhand Himalaya: an observation from Lwarkha. Chamba Tahsil of Tehri Garhwal District, Chamba, Uttarakhand, India

Khanduri S, Sajwan KS, Rawat A et al (2018) Disaster in Rudraprayag District of Uttarakhand Himalaya: a special emphasis on geomorphic changes and slope instability. J Geogr Nat Disasters 08(01). https://doi.org/10.4172/2167-0587.1000218

Korup O (2004) Geomorphometric characteristics of New Zealand landslide dams. Eng Geol 73(1):13–35. https://doi.org/10.1016/j.enggeo.2003.11.003

Kumar S, Biswal S, Parija MP (2016) S44B-06: active tectonics of Himalayan faults/thrusts system in Northern India on the basis of recent & Paleo earthquake studies. American Geophysical Union

Pandey VK, Mishra A (2015) Causes and disaster risk reduction measures for hydrometerological disaster in Uttarakhand, India: an overview. Int J Curr Res Sci Technol 1(3):61–80

Parkash S (2015) Some socio-economically significant landslides in Uttarakhand Himalaya: events, consequences and lessons learnt. In: Nibanupudi HK, Shaw R (eds) Mountain hazards and disaster risk reduction, Springer Japan, pp 211–232. https://doi.org/10.1007/978-4-431-55242-0_12

Paul SK, Bartarya SK, Rautela P, Mahajan AK (2000) Catastrophic mass movement of 1998 monsoons at Malpa in Kali Valley. Kumaun Himalaya

Prakesh S (2014) Geo-environmental characteristics, natural resources and disasters in Uttarakhand State. In: Retrospect and prospects of natural resource and disaster management in Uttarakhand Himalaya. National Institute of Disaster Management, pp 51–99

Rana N, Singh S, Sundriyal YP, Juyal N (2013) Recent and past floods in the Alaknanda valley: causes and consequences. Curr Sci 105(9)

Rautela P, Pande RK (2005) Traditional inputs in disaster management: the case of Amparav, North India. Int J Environ Stud 62(5):505–515. https://doi.org/10.1080/00207230500034586

Srivastava P, Kumar A, Mishra A, Meena NK, Tripathi JK, Sundriyal YP, Agnihotri R, Gupta AK (2013) Early holocene monsoonal fluctuations in the Garhwal higher Himalaya as inferred from multi-proxy data from the Malari paleolake. Quat Res 80(3):447–458. https://doi.org/10.1016/j.yqres.2013.07.006

Sundriyal YP, Tripathi JK, Sati SP, Rawat GS, Srivastava P (2007) Landslide-dammed lakes in the Alaknanda Basin, lesser Himalaya: causes and implications. Curr Sci 93(4)

Tacconi Stefanelli C, Segoni S, Casagli N, Catani F (2016) Geomorphic indexing of landslide dams evolution. Eng Geol 208:1–10. https://doi.org/10.1016/j.enggeo.2016.04.024

Uttarakhand Population (2022) | Sex Ratio & Literacy rate 2024. https://www.census2011.co.in/census/state/uttarakhand.html. Retrieved 19 February 2024

Wasson RJ, Sundriyal YP, Chaudhary S, Jaiswal MK, Morthekai P, Sati SP, Juyal N (2013) A 1000-year history of large floods in the Upper Ganga catchment, central Himalaya, India. Quat Sci Rev 77:156–166. https://doi.org/10.1016/j.quascirev.2013.07.022

Open Access This chapter is licensed under the terms of the Creative Commons Attribution 4.0 International License (http://creativecommons.org/licenses/by/4.0/), which permits use, sharing, adaptation, distribution and reproduction in any medium or format, as long as you give appropriate credit to the original author(s) and the source, provide a link to the Creative Commons license and indicate if changes were made.

The images or other third party material in this chapter are included in the chapter's Creative Commons license, unless indicated otherwise in a credit line to the material. If material is not included in the chapter's Creative Commons license and your intended use is not permitted by statutory regulation or exceeds the permitted use, you will need to obtain permission directly from the copyright holder.



Risk Identification of Large-Scale Landslides Triggered by Rainfalls and Post-Rainfall Earthquakes in Sri Lanka

Kyoji Sassa, Loi Doan, Koji Matsunami, Toyohiko Miyagi, Ranjan Weerasnghe, Tania Munasinghe, Nilmini Thaldena, Asiri Karunawardena, and Kazuo Konagai

Abstract

Based on the ISDR-ICL Sendai Landslide Partnerships 2015–2025, the ICL and NBRO implemented joint research on the "Development of early warning technology of rain-induced rapid and long-travelling landslides in Sri Lanka" from 2019. This paper reports the achievement of this project from June 2019 to April 2024.

Based on studies of previous large-scale landslides, most large-scale landslides occurred in/around previous large-scale landslides. Then, we identified around 200 previous large-scale landslides in the Aranayake area (20 km × 20 km). Within 50 landslides, we conducted the LS-RAPID analysis, measured the critical pore pressure ratio and identified and recorded the resulted landslide moving area (landslide hazard map). Using MSSG (Multi-Scale Simulator for the Geoenvironment), we obtained the spatial rainfall data and calculated the pore water pressure for each landslide. When the pore water pressure in a potential landslide site exceeds the critical pore water pressure, a landslide moving area (hazard map) is identified. The rainfall and landslide hazard areas are forecasted and presented on an AR (Augmented reality) view for early warning.

The latter part of this paper was devoted to earthquake and microearthquake monitoring in Sri Lanka using the developed ICL type seismographs, which include one velocity type of seismometer and one acceleration type seismometer in one unit. We installed this type of 15 seismographs in Sri Lanka in 2023–2024.

Many nearby earthquakes (P-S time less than 5 s) were monitored throughout the year. The monitoring results are surprising. Nearby earthquakes are small in the magnitude. However, the distance between the landslide and its hypocenters are close. Therefore, the acceleration loading on the landslide is not small. Shaking by the nearby earthquakes in Aranayake and Atwelthota landslides can be the order of 0.01 kine (cm/s), which corresponds to the order of 1 gal (cm/s^2) acceleration. The shaking by the Hambantota earthquake (Mg = 4.4) was 2–5 gal at the Aranayake landslide. The effects of nearby earthquakes after the rainfall were examined in a test slope near the Aranayake.

In February 2024, two seismographs were installed in the Kotmale dam reservoir slope, where a series of past rockslide topography can be identified. Subsequently, many nearby earthquakes were monitored in March and April in 2024. This paper presents and discusses two seismic record examples (P-S time = 3.4 s on 2 March 2024 and P-S time = 0.1 s on 1 April 2024). Distance to the seismic source were 25–30 km and less than 1 km and maximum accelerations were 0.8 and 0.6 gal.

Keywords

Landslides · Post-rainfall earthquakes · Seismographs · Kotmale dam · Sri Lanka

K. Sassa (✉) · K. Matsunami · T. Miyagi · K. Konagai
International Consortium on Landslides, Kyoto, Japan

L. Doan
International Consortium on Landslides, Kyoto, Japan

Institute of Transport Science and Technology, Hanoi, Vietnam

R. Weerasnghe · A. Karunawardena
National Building Research Organisation, Colombo, Sri Lanka

T. Munasinghe
ICL SATREPS Office, Colombo, Sri Lanka

University of Colombo, Colombo, Sri Lanka

N. Thaldena
Geological Survey and Mines Bureau, Colombo, Sri Lanka

© The Author(s) 2025

B. Abolmasov et al. (eds.), *Progress in Landslide Research and Technology, Volume 3 Issue 2, 2024*, Progress in Landslide Research and Technology, https://doi.org/10.1007/978-3-031-72736-8_16

1 Introduction

The ICL and NBRO (National Building Research Organisation, Sri Lanka) joint project was planned as an activity for the ISDR-ICL Sendai Landslide Partnerships 2015–2025 (Sassa 2015 and ICL web <https://www.landslides.org/ipl-info/2015-landslide-sendai-partnership/>).

It was started after the 2016 Aranayake big landslide disaster in 2017 (Dang et al. 2019). This joint project was approved as "IPL-249 Development of early warning technology of rain-induced rapid and long-travelling landslides in Sri Lanka" in 2019.

https://www.landslides.org/projects/ipl-projects/.

This ICL-NBRO joint project was adopted as a 5 years project of the Science and Technology Research Partnership for Sustainable Developments (SATREPS) project which was funded by the Japan Cooperation Agency (JICA) and the Japan Science and Technology Agency (JST) from June 2019 to March 2025 (Konagai et al. 2023). This SATREPS project will be terminated at the end of March 2025.

A catastrophic large-scale landside was triggered by the accumulated rainfalls of 446.5 mm from May 14 to 17 in Kegalle, Sri Lanka. The landslide travelled over an approximately 2 km distance, destroyed 75 houses and killed 127 people. Yellow marks in Fig. 1 are destroyed houses. Farmers working in tea production live in those houses. Tea trees are planted under high-tree forests. High tree leaves reduce strong sunshine and protect the quality of tea leaves. Tea trees are planted around each house. Often, landslide disasters occur in an urban flat area. However, the landslide disaster in the Aranayake landslide occurred in the steep mountain slope covered by forests.

The ISDR-ICL Sendai Landslide Partnerships 2015–2025 is terminated at the end of 2025. However, the global promotion of understanding and reducing landslide disaster risk is a more important task for ICL and ICL-supporting organizations after 2025. Therefore, to continue this initiative, the Kyoto Landslide Commitment 2020 KLC2020) was established in 2020 (Sassa 2021). KLC2020 has been signed by 106 United Nations, Global, International and National organizations.

https://www.landslides.org/ipl-info/the-kyoto-landslide-commitment-2020/

A new project can be initiated under the KLC2020 with target of landslides triggered by earthquakes or post-rainfall earthquakes based on the recent increase of earthquakes in Sri Lanka and the monitoring result of microearthquakes in landslides started from April 2023.

This article reports the progress of the SATREPS project as well as IPL-249 until March 2024 and introduces the initial stage of earthquake monitoring by ICL-type seismograph in/around landslides and potential landslides from April 2023 (Sassa et al. 2023a, b).

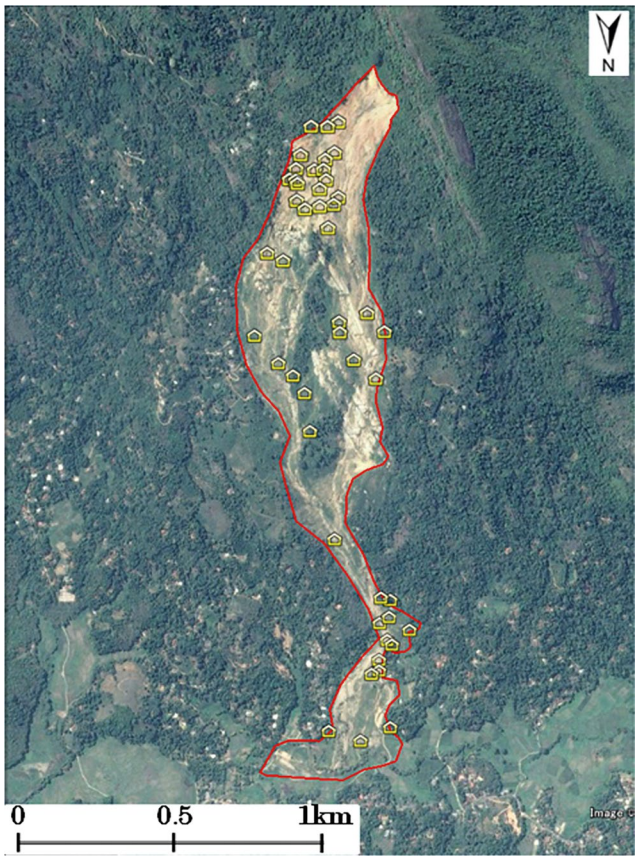


Fig. 1 The 2016 Aranayake landslide in Sri Lanka

2 Forecasting of the Landslide Initiation Time and the Landslide Hazard Area, and AR (Augmented Reality) Presentation for Early Warning of Landslides

As part of the SATREPS Project (Konagai et al. 2023), the landslide dynamics group, together with other groups, has conducted research on forecasting the landslide initiation time, the landslide hazard area and its AR presentation for early warning of landslides.

Figure 2 presents the concept of LS-RAPID: an integrated model simulating the initiation and motion of earthquake and rain-induced rapid landslides (Sassa et al. 2010).

Usual landslide analysis is a stability analysis dealing with the initial stress state until the failure, and a mobility analysis dealing with the motion from the failure to deposit. LS-RAPID is the first integrated model simulating landslide initiation and the post-failure motion. It was possible by the development of the undrained dynamic loading ring shear apparatus and the obtained relationships of shear displacement and mobilized shear stress from the peak stress to the steady state shear strength.

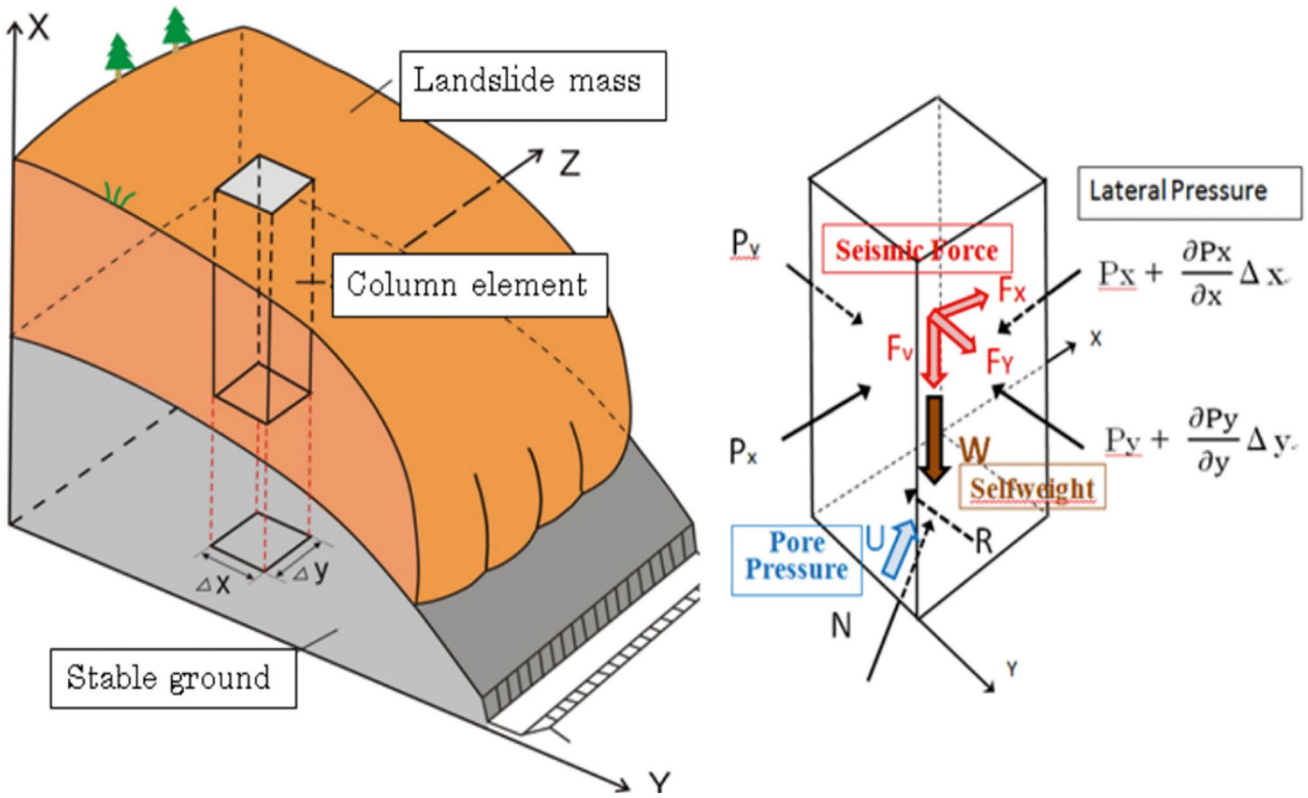


Fig. 2 LS-RAPID concept and the basic equation (Sassa et al. 2010)

The left side figure explains the moving landslide mass (brown color) and the stable ground soil/rock layer (grey color). Stresses loading a vertical column within the landslide mass are shown in the right-side figure. The seismic stress is also included in the loading normal and shear stresses.

All stresses will move the soil mass in the relationship of Eq. (1). The movement of the soil mass is calculated on the projected X–Y horizontal plane. It is effective in the movement on a curved surface between the moving landslide mass and the stable layer.

The landslide mass (m) will be accelerated by acceleration (a) given by the sum of these forces: driving force (Self weight + Seismic forces) + lateral pressure + shear resistance

$$\mathrm{am} = \left(\mathrm{W} + \mathrm{Fv} + \mathrm{Fx} + \mathrm{Fy}\right) + \left(\frac{\partial \mathrm{Px}}{\partial \mathrm{x}}\Delta x + \frac{\partial \mathrm{Py}}{\partial \mathrm{y}}\Delta \mathrm{y}\right) + \mathrm{R} \quad (1)$$

Here, R includes the effects of forces of N and U in Fig. 2 and works in the upward direction of the maximum slope line before motion and in the opposite direction of landslide movement during motion.

The area of LS-RAPID analysis consists of three subareas, as shown in Fig. 3.

Area 1: Source area where the triggering factors of landslides (pore water pressure and seismic force) are loaded in this area.

Area 2: Enlargement area (upper and steeper area) where the displaced landslide mass from the source area moves on this area. Mobilized shear stress is the steady state shear stress which is measured by the ring shear testing of the materials or already known value.

Area 3: Enlargement area (lower and flatter area) where the long-travelling landslide mass reaches the flatter area.

The gentle area is usually more saturated than the other areas. At least three areas are necessary to simulate the motion.

Three areas are initially prepared. However, a landslide mass may stop in Area 2 or even not go out from Area 1. On the other hand, Area 4 becomes necessary at the toe to simulate a fluidized landslide motion.

Figure 4 shows an example of LS-RAPID simulation for the 2016 Aranayake landslides. The left side is an LS-RAPID simulation and the right is a UAV photo taken by NBRO soon after the landslide. In order to make both moving areas very similar, the necessary number of subareas was 8. Material on the ground, its degree of saturation, and surface topography may affect the values of

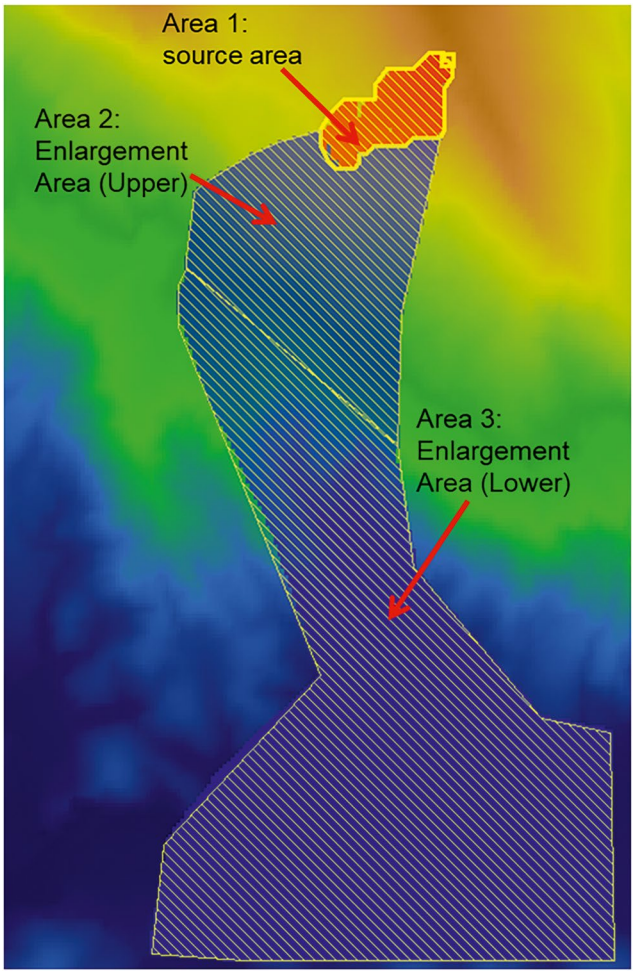


Fig. 3 Three sub-areas (Area 1: Source area, Area 2: Enlargement Area (Upper), Area 3: Enlargement Area (Lower) for parameter decision)

parameters in each area. Namely, the steady stage shear stress (τss), lateral pressure ratio (k) of the moving mass, and the pore pressure generation rate (Bss). Reproduction of past landslide motion is special because the movement is known. In order to create a comprehensive hazard mapping for future potential landslides including many landslides, we cannot decide on so many details. Only three area settings will be practical.

AR (augmented reality) rainfall and landslide hazard map in the Aranayake landslide area were made for early warning of landslides combining the output from the other three groups of the SATREPS project, namely (1) Miyagi et al. (2024) (landslide mapping group), (2) Onishi et al. (2024) (MSSG-rainfall forecasting group), (3) Araki et al. (2024) (AR technology), Doan et al. (2024) (Landslide simulation). Those three articles are published in this issue.

We asked Miyagi and the mapping group to identify previous landslides within 20 km × 20 km in the Aranayake based on AW3D 2.5 m data. Around 200 landslides were identified. The sites are plotted in Google Earth.

The landslide mapping group analysed 50 landslides by LS-RAPID and obtained the critical pore water pressure ratio of each landslide, and the resulting landslide hazard area.

The method to obtain the critical pore pressure ratio and calculate pore water pressure from the MSSG rainfall value of each landslide is explained in Araki et al. (2024) in this issue of P-LRT.

20 km × 20 km is too wide to present it in A4 size printed pages. Then, we chose the 10 km × 10 km area for AR rainfall and hazard mapping. Figure 5 shows the identified landslide topographies (red lines) and 20 landslides which were analysed by LS-RAPID. The critical pore water pressure to initiate landslide motion and also the landslide moving area (hazard area) were recorded for each of 20 landslides. The landslide dynamic group presented two cases: 1. High mobility, 2. Medium mobility. The AR hazard maps in Figs. 6 and 7 show only the high mobility case.

MSSG group provides the simulated rainfall data for the whole area. AR group calculated the pore pressure ratio change within the landslide mass through the rainfalls. If the calculated pore-water pressure exceeds the critical pore-water ratio of a landslide which is decided by LS-RAPID analysis of each potential landslide, the landslide hazards area appears in the AR view.

Figure 6 is an AR view of MSSG rainfalls and LS-RAPID landslide hazard map of the 2016 Aranayake landslide.

AR figure consists of (1) rainfall map (top) with the legend of rainfall intensity (8 colors from 0–80 mm/h).

The rainfall intensity is not easy to be identified. Therefore, we showed the maximum hourly rainfall at each figure.

At the bottom of Fig. 6, we show the monitored rainfall at the NBRO rainfall gauge number IR27 and MSSG simulated rainfalls at around IR27. The real monitored rainfall and MSSG simulated rainfall are not the same, but close. The accumulated rainfalls are 450 mm in the real monitored data and around 550 mm in MSSG simulated rainfall. The maximum hourly rainfall is relatively close, though the timing of rains is somewhat different.

The global-scale model (GSM) data of the Japan Meteorological Agency (JMA) was used for the initial and boundary conditions for the MSSG simulations. Each MSSG simulation was performed for 6 h and restarted every 6 h for the present validation experiment. MSSG simulation rainfall data is obtained in anywhere in Sri Lanka (or other places) without rain gauge monitoring.

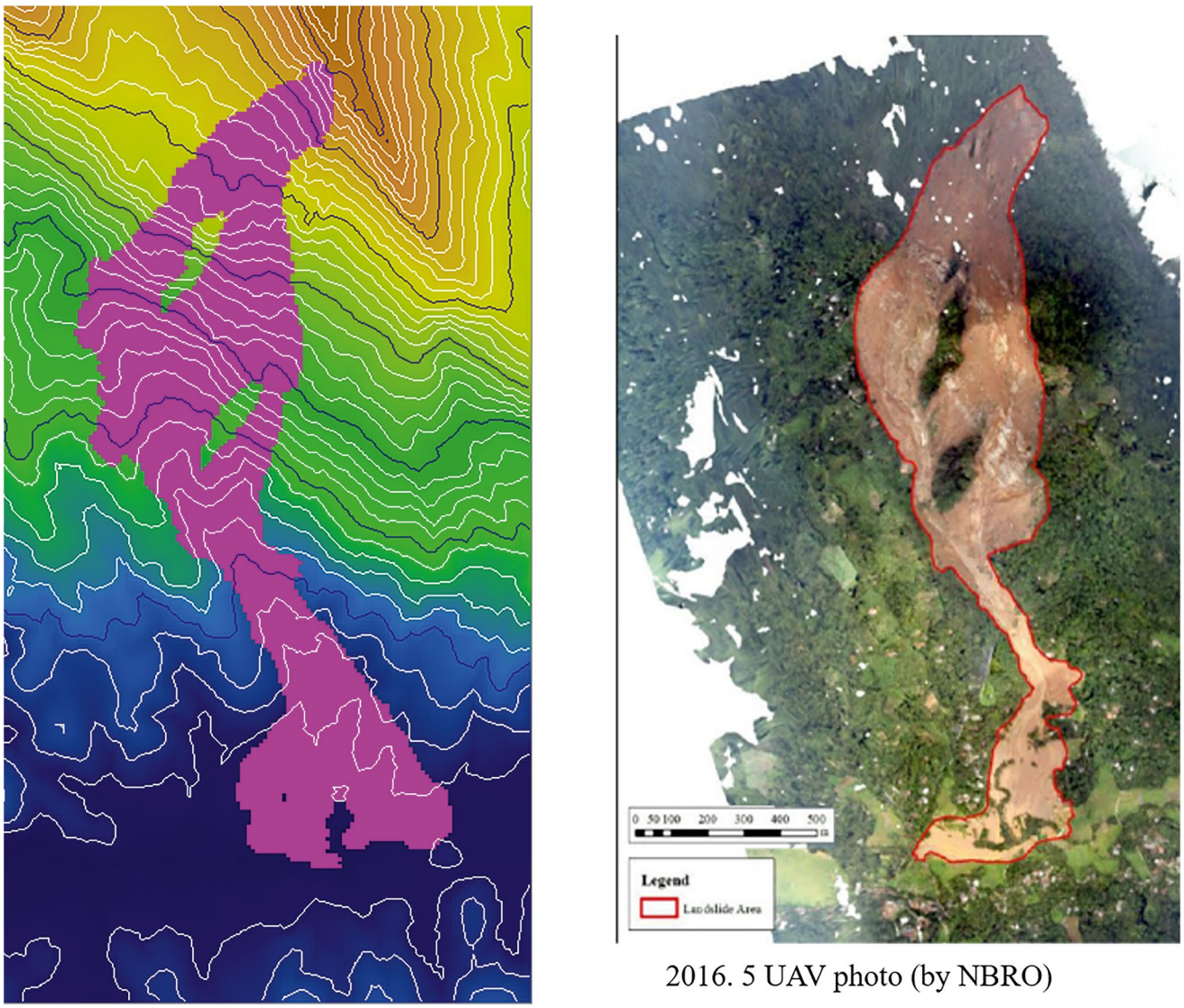


Fig. 4 Simulation of the 2016 Aranayake landslide together with UAV photo

The central row is the landslide hazard map. The time is shown in the Sri Lanka time. The graph starts at 6:30 May 14, 2016 and lasts for 90 h. Three vertical pink lines correspond to the A-line: 16:30 May 16, 2016, the B-line: 18:30 May 16, 2016, and the C-line: 16:30 May 17, 2016, respectively. Time A shows that the first small landslide occurred, Time B shows that the second landslide occurred, and Time C shows that the 2016 Aranayake large and long-travelling landslide occurred and killed 127 people. The real Aranayake landslide is reported to have occurred at around 4 PM on 17 May 2016 (Dang et al. 2019).

The AR system seemed to be effective in this study. We wished to investigate landslide hazards when a heavier rain comes to Aranayake. The most well-known large-scale landslide disaster caused by long rains in Japan is the 2–4 September 2011 Typhoon Talas landslide disaster in the Kii Peninsula. 373 houses were destroyed, and 94 persons were killed. Accumulated rainfall for 3 days was 1800 mm. The rainfall record in Kazaya, which was near large-scale landslides, and the MSSG rainfall near Kazeya are shown in Fig. 7.

Three times (D, E, F) are shown crossing two rainfall data. Time is shown from 1:00 on 31 August 2011 for 120 h. MSSG rainfall is smaller than the rainfall data monitored at Kazeya AMeDAS (Automated Meteorological Data Acquisition System) rain station. AMEDAS data presents only one point location. Aerial rainfall data are needed for the aerial rainfall and landslide hazard map. We used

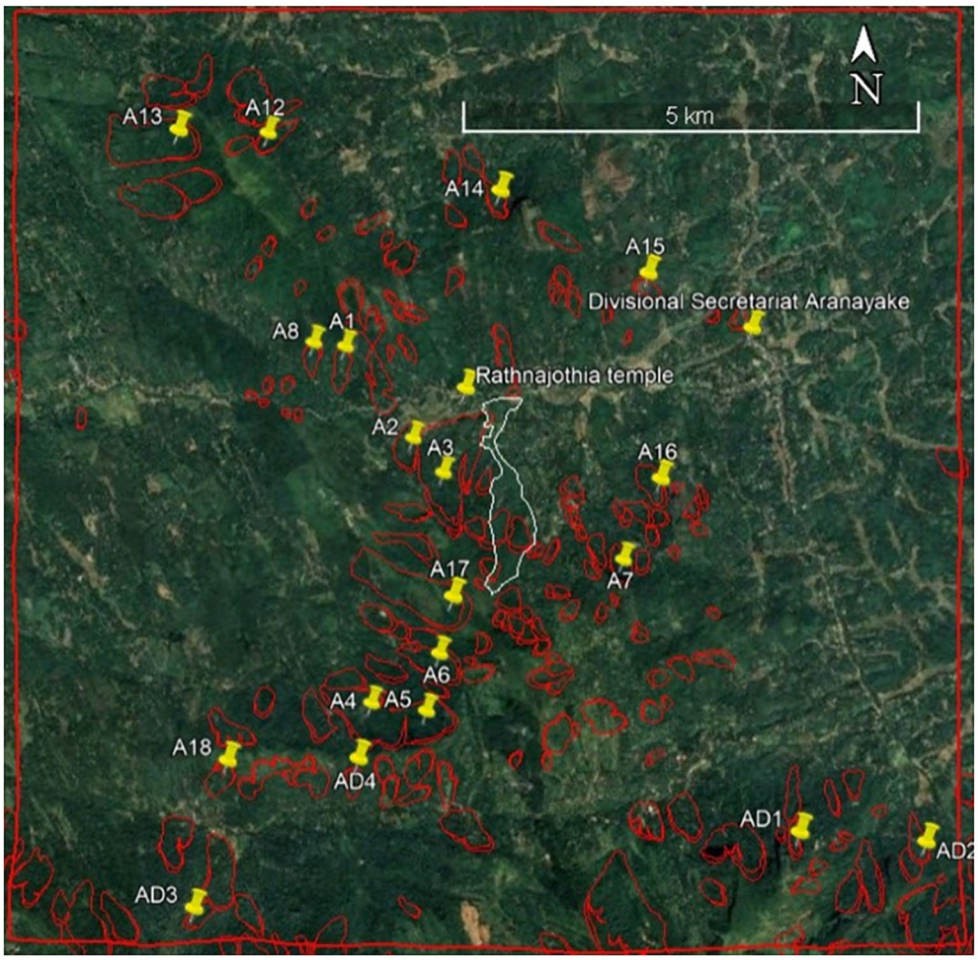


Fig. 5 Landslide mapping in the center of Aranayake area (10 km × 10 km) by Miyagi T

MSSG rainfall, though it is smaller than the monitored rainfall. Bringing the MSSG rainfall for 10 km × 10 km from the Kii Peninsula to the Aranayake area, Fig. 7 was obtained. One small landslide occurred at the time of D (02:30 Sep 03, 2011). At the time of E (13:30 Sep 03, 2011), a middle-size landslide and the 2016 Aranayake landslide occurred. At the time of F (21:30 Sep 03, 2011), four more landslides occurred.

Landslide hazard is affected by the ground condition and the rainfall condition. When we have various MSSG rainfall

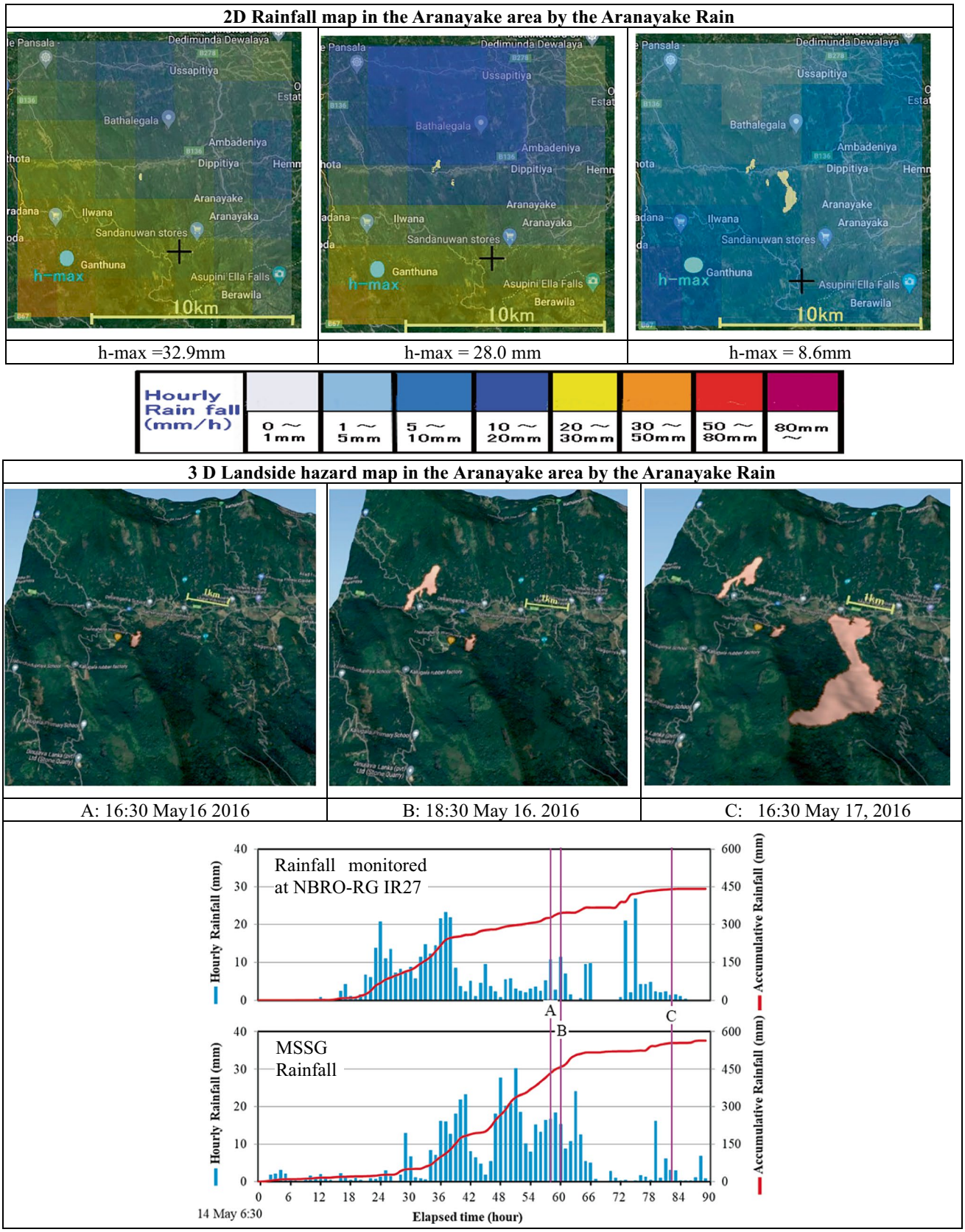


Fig. 6 AR rainfall and landslide hazard map in the Aranayake landslide area which was caused by 14–15 May 2016 rainfall

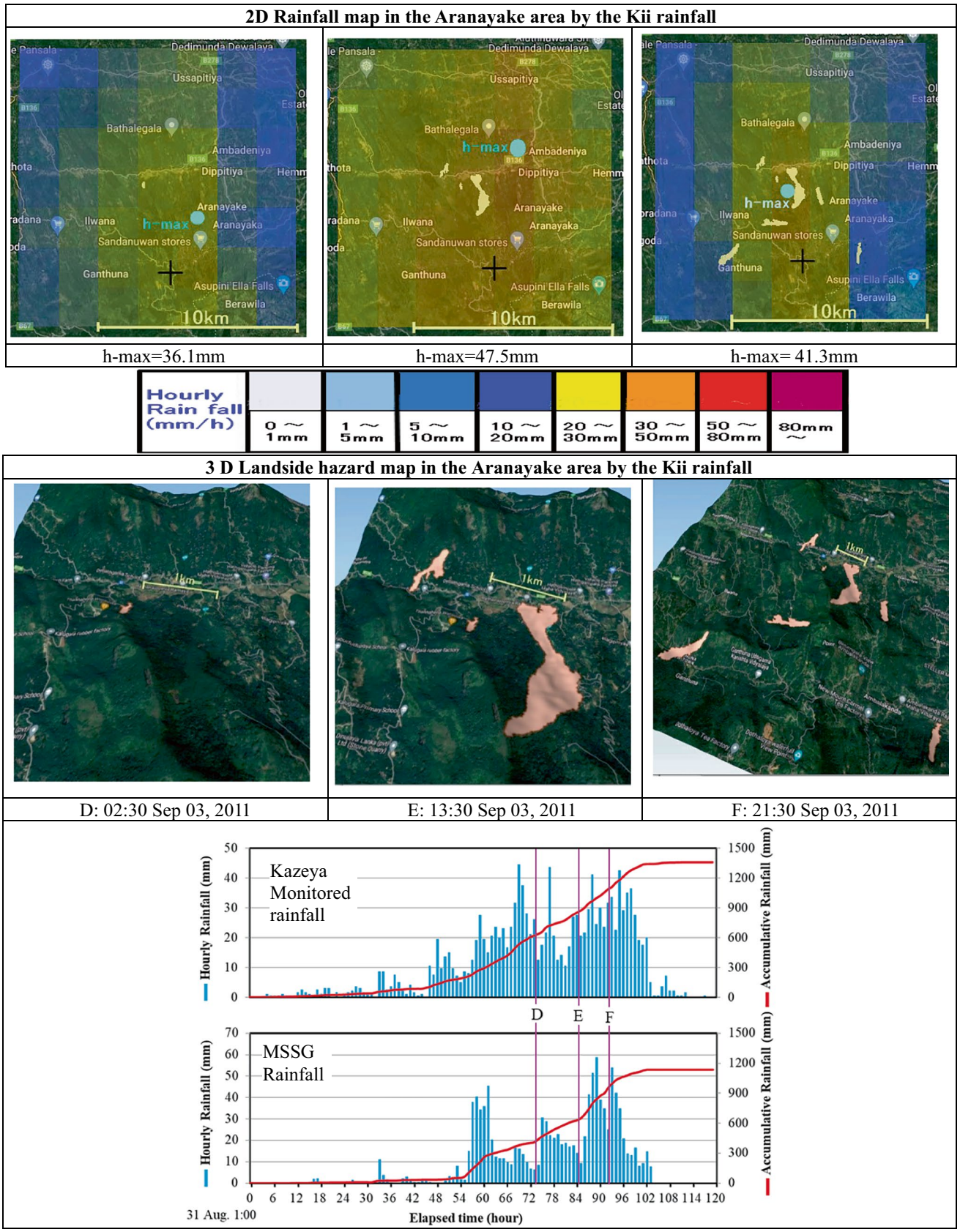


Fig. 7 AR rainfall and landslide hazard map in the Aranayake landslide area, in case of bringing the MSSG rainfall for 10 km × 10 km from the Kii Penisula in Japan on 2–3 September 2011

patterns for 20 km × 20 km in some areas, and apply them for other specific areas, it will be useful to know possible landslide hazard in advance.

3 Earthquakes and Microearthquake Monitoring in Sri Lanka

Earthquakes in Sri Lanka are monitored by the Geological Survey and Mines Bureau (GSMB). The analysing method is a local (Richter) magnitude based on the vertical component. It is expressed as MLv. GSMB reported 11 earthquakes greater than 3.0 MLv from 2013–2023 (Sassa et al. 2023a, b). Within those 11 earthquakes, 5 occurred from 2013 to 2022, and 6 occurred in 2023. Namely more than half of the earthquakes in 10 years from 2013–2023 took place in a single year 2023. GSMB reported 14 earthquakes more than 2.0 MLv in 2023–2024, and their epicenters are shown in Fig. 8. The largest earthquake was M4.6 on 10 September 2023. Namely, seismic activities in Sri Lanka have recently increased.

When the ICL investigated the 2016 Aranayake landslides in 2017, earthquakes were not serious matters in Sri Lanka.

Objectives of the joint ICL-NBRO focused only on rain-induced rapid and long-travelling landslides. However, in 2021–2022 earthquakes and especially microtremors were increasingly reported in Sri Lanka. Then, we came to focus earthquakes as a triggering factor of landslides from the end of 2022.

The ICL investigated the 2006 Leyte landslide in the Philippines killing over 1000 people, which was triggered by a microearthquake (Magnitude Ms = 2.6) in 22 km west of the source area of the landslide. This disaster is an excellent example showing that a Ms = 2.6 earthquake in around 20 km apart from the source area caused this catastrophic landslide. If nearby earthquakes occur a few km from potential landslide sites, even a much smaller earthquake may trigger a catastrophic landslide. Then, the ICL decided to monitor the microearthquakes in landslide areas in Sri Lanka in 2022 and developed an ICL-type seismograph which consists of an accelerometer and a velocity meter for nearby microearthquakes, and to detect ground tilt using the static component of the accelerometer to study the risk of landslides triggered by earthquakes or nearby microearthquakes.

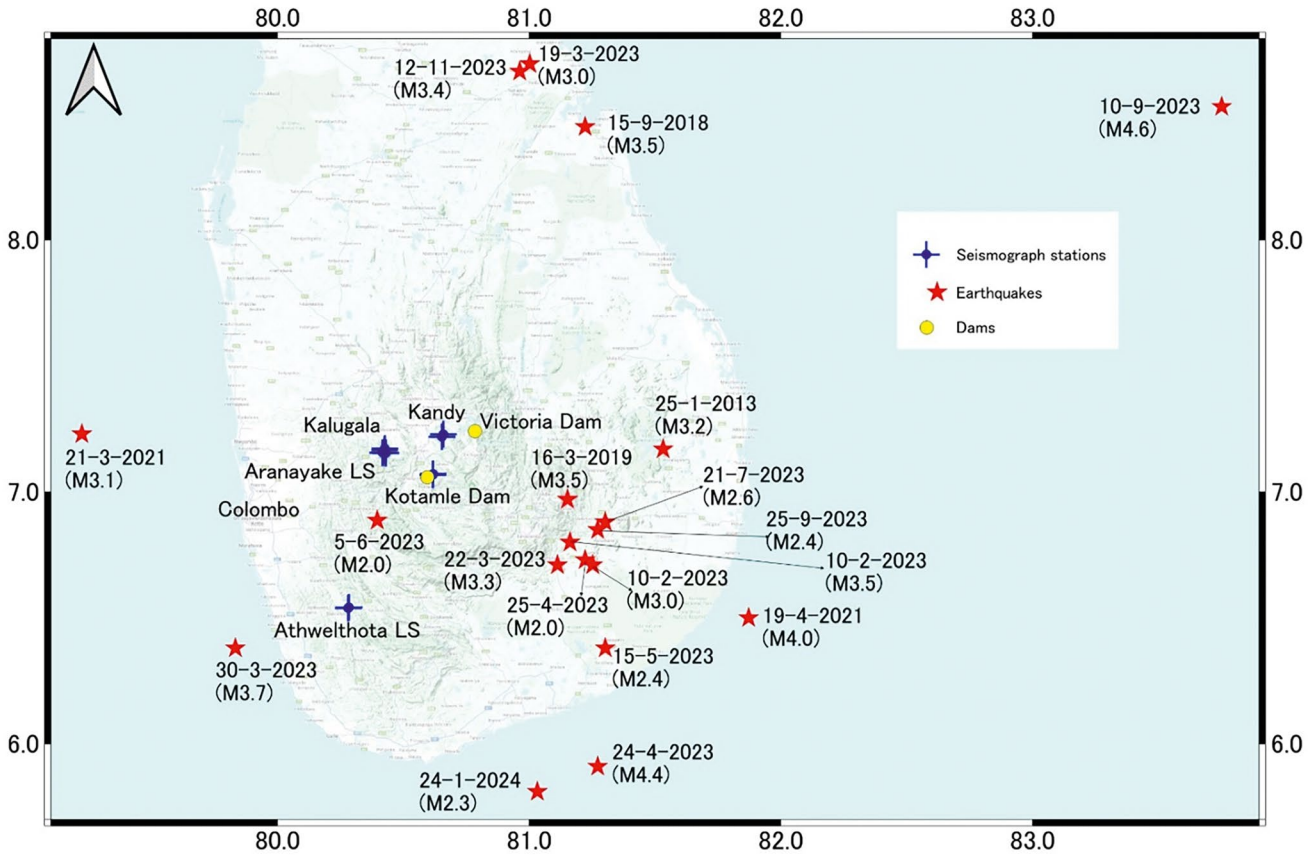


Fig. 8 Recent earthquakes in Sri Lanka from 2013–2024 (GSMB) (Earthquakes greater than MLv = 3 from 2013–2023 and greater than MLv = 2 from 2023–2024)



Fig. 9 ICL-type seismograph consists a velocity seismometer (KINKEI-KVS300) and an acceleration seismometer (Analog Devices-ADXL335)

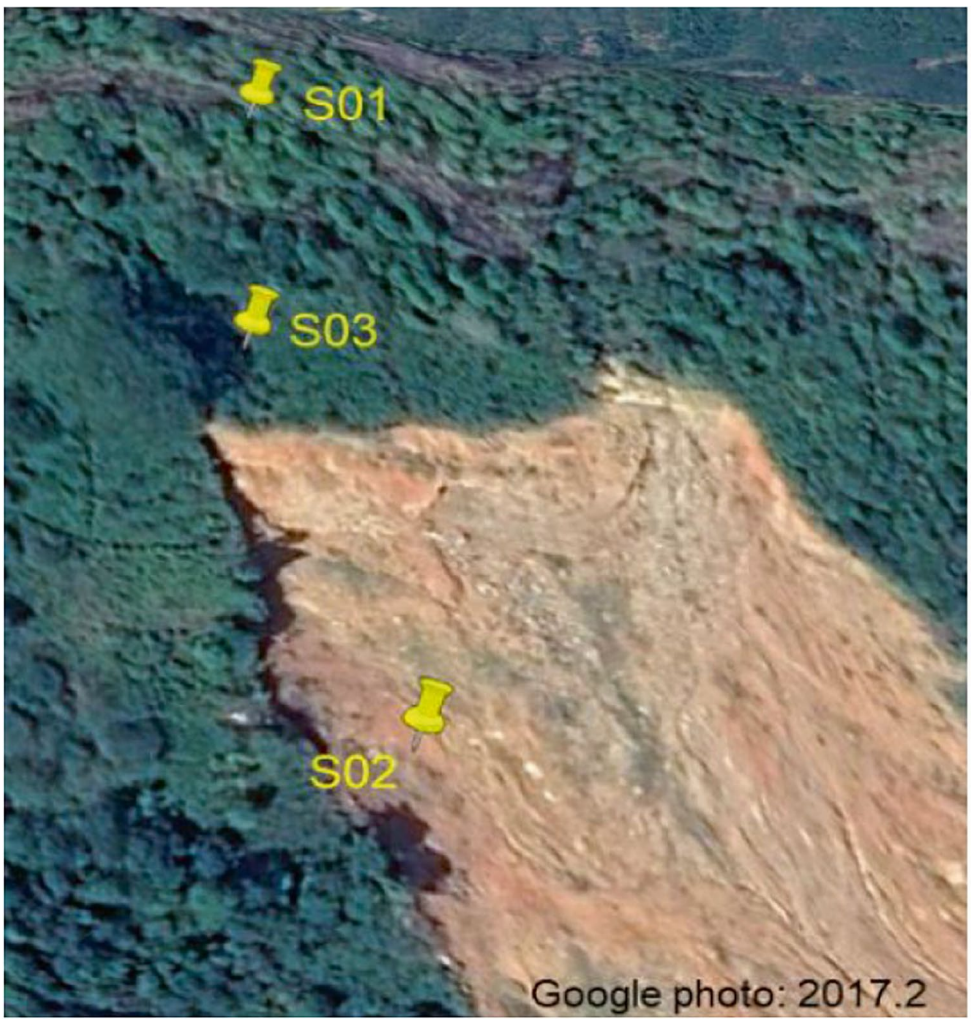


Fig. 10 Installation of the monitoring system in the Aranayake landslide

The ICL developed and produced the ICL-type seismograph in 2022. Figure 9 shows the system installed on an unstable soil layer above the heads carp of the Aranayake landslide (Matsunami et al. 2024). Figure 10 shows three locations of seismographs plotted on a Google photo (2017.2). Namely, S01 is installed on the bed rock, which is outcropped on the mountain ridge. S02 is installed on a thin debris deposit within the landslide source area, and S03 is located on the unstable soil layer above the head scarp of the 2016 Aranayake landslide.

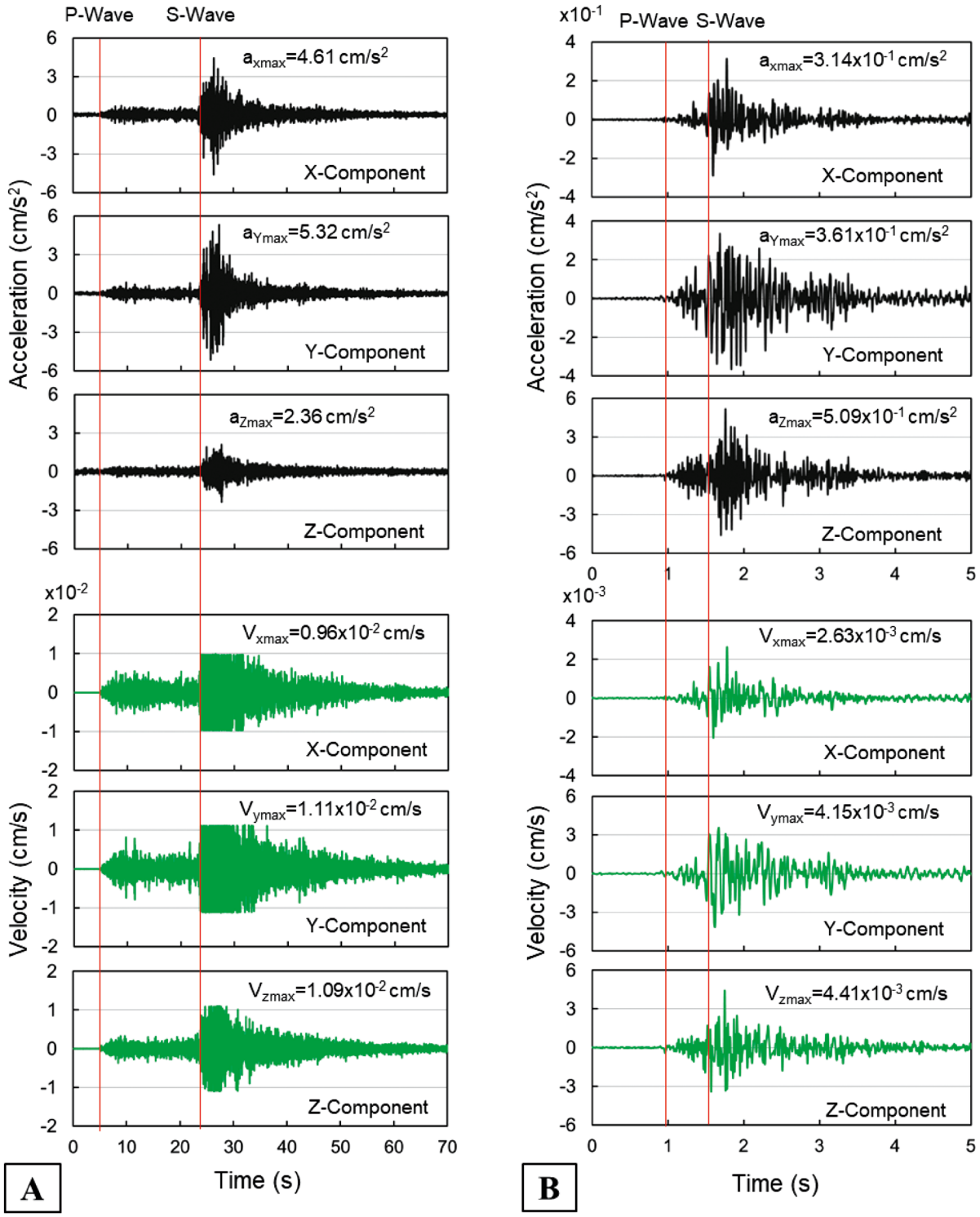
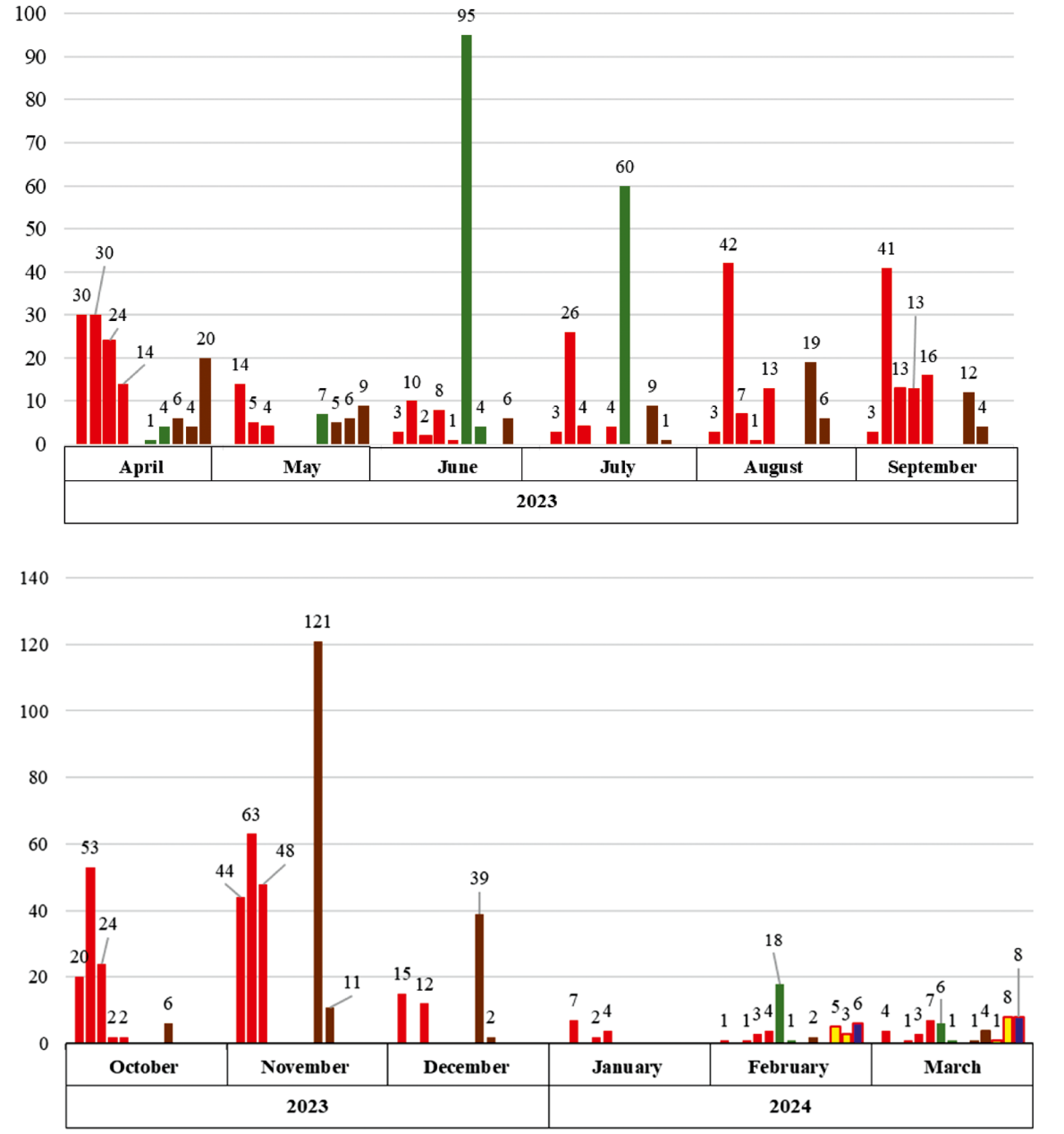


Fig. 11 The Monitored 2023.4.24 Hambantota-offshore earthquake and a microearthquake by Sensor (S03) of the Aranayake landslide site. (**a**) Time series data of acceleration and velocity of the 2023.4.24 earthquake by Sensor S03 (2023/04/24 00:45:31 IST). (**b**) Time series data of acceleration and velocity of a microearthquake by Sensor S03 (2023/04/20 18:01:50 IST)

Figure 11 shows the monitored results of S03 on the unstable ground (potential retrogressive landslide mass). The left figures show the seismic records of the Hambantota-offshore earthquakes (Ms = 4.4), the upper-left graph shows the data of acceleration-type seismometer, and the lower-left graph shows the data of velocity-type seismometer. The velocity-type seismometer was saturated in the strong seismic wave.

The two graphs on the right show the records of more minor earthquakes. The record from the velocity-type seismometer was not saturated. P-S time of the Hambantota earthquake was around 20 s, P-S time of the nearby earthquake (right figure) was only 0.5 s. The epicenter of nearby microearthquakes would be around 4 km from the landslides (the position of the seismograph) using the equation Lay and Wallace (1995). Comparison



No.	Legend	Station	No.	Legend	Station
1		Aranayake Landslide - Bedrock Outcrop (Mountain top)	8		Athwelthota Landslide (1): Bedrock Outcrop
2		Aranayake Landslide Debris: (Landslide body)	9		Athwelthota Landslide (2): Unstable Soil
3		Aranayake Landslide Potential - Unstable Mass	11		Kothmale: Unstable Soil (Lower)
4		Kalugala Primary School (1): Unstable Soil	12		Kothmale: Unstable Soil (Top)
5		Kalugala Primary School (2): Bedrock Outcrop	14		Aranayake Potential Landslide - Middle
6		Kandy (1): Bedrock Outcrop	15		Aranayake Potential Landslide - Lower
7		Kandy (2) : Soil (Colluvium)			

Fig. 12 Number of monthly nearby microearthquakes from April 2023 to March 2024 (P-S time less than 5 s)

Table 1 ICL-type seismographs stations in Sri Lanka

No	Site name	Description
1	Aranayake landslide	Bedrock outcrop (mountain ridge)
2	Aranayake landslide	Landslide debris
3	Aranayake landslide	Potentially unstable mass
4	Kalugala primary school	Bedrock outcrop
5	Kalugala primary school	Unstable soil (cut slope)
6	Kandy	Bedrock outcrop
7	Kandy	Soil (colluvium)
8	Athwelthota landslide	Bedrock outcrop
9	Athwelthota landslide	Unstable soil
10	University of Peradeniya	Inside building
11	Kotmale dam slope	Lower landslide block
12	Kotmale dam slope	Upper landslide block
13	Aranayake test slope	Upper slope
14	Aranayake test slope	Middle slope
15	Aranayake test slope	Temple: Observation base

of recorded acceleration between the M = 4.4 Hambantota (Fig. 11a) and nearby microearthquakes (Fig. 11b) is around one order difference (X-component: 4.6 cm/s^2 and 0.3 cm/s^2, Y-Component:6.3 cm/s^2 and 0.4 cm/s^2, Z-component: 2.3 cm/s^2 and 0.5 cm/s^2). As seen in Fig. 12 later, microearthquakes in Aranayake landslides occur every month. The number of microearthquakes/month is often the order of 10.

The ICL distributed the seismographs in the 15 sites in Sri Lanka as shown in Table 1.

No. 10 is at University of Peradeniya. It is installed for education, training and testing.

Aranayake and Atwelthota are the 2016 and 2017 landslide sites.

The Kalugala Primary School sites are at the foot of the Aranayake mountain. One site within this school is above the excavated wall behind the school building, and one is on a bedrock.

Kandy is the previous landslide site. The Kotmale dam slope is selected to investigate the instability of the reservoir slope. The Aranayake Test slope was selected to investigate possible reactivation of the slope in/around the landslide source area in the future.

Figure 12 presents the number of monthly nearby microearthquakes from April 2023 to March 2024.

Nearby means that P-S time is less than 5 s. The distance between the sensor and the hypocenter, namely, around 8 times of the P-S time (Lay and Wallace 1995) less than 40 km.

No. 1–5 in red are installed in the Aranayake mountain. No. 6–7 in green in Kandy, and No. 8–9 in brown are located in the Atwelthota landslide site. In February 2024, we installed seismographs on slopes around the Kotmale dam reservoir (No. 11 and No. 12) and the Aranayake potential landslide (Test slope for landslide risk evaluation) (No. 14 and No. 15). As seen in the graph, many earthquakes are monitored in almost every month in the Aranayake mountain. The number of monthly earthquakes in the Aranayake (red color) is up to 63. In Atwelthota, nearby earthquakes are recorded in almost every month. Nearby earthquakes in Kandy are infrequent. However, 95 and 60 earthquakes were monitored in June and July 2023. The maximum monthly nearby earthquakes were observed in Atwlethota only in November 2023. The number of earthquakes in January–March was small. The reason is not known, though one possibility is low ground water level in winter if those earthquakes are caused by porewater pressure in the earthquake sources. We should observe earthquakes in the winter in 2025.

Figure 13 presents the frequency and velocity of the recorded microearthquakes from April 2023 to March 2024.

The monitored microearthquakes are up to 12 × 0.0001 cm/s = 0.012 cm/s. The ratio between acceleration and velocity in seismic shaking is around 100 times in the monitored data in the right figure of Fig. 11 where the acceleration was 3.1–5.1 × 10^{-1} cm/s^2, and the velocity was 2.6–4.4 × 10^{-3} cm/s. If this ratio between acceleration and velocity applies to any case, the earthquake with the velocity amplitude of 0.012 cm/s can correspond to the acceleration amplitude of 1.2 cm/s^2. Seismic acceleration caused by the MLv = 4.4 Hambantota earthquake was 2.4–5.3 cm/s^2. Namely the largest acceleration of the nearby microearthquakes monitored in Aranayake and Atwelthota represents around a half to a quarter (1.2/(2.4 ~ 5.3) of the acceleration by the Hambantota earthquake.

Examining the data up to the velocity of 10 (×0.001 cm/s) and excluding the data of more than 10 in Fig. 13, the general trend is that the lower the frequency, the stronger the earthquake. Probably the mechanism of microearthquakes less

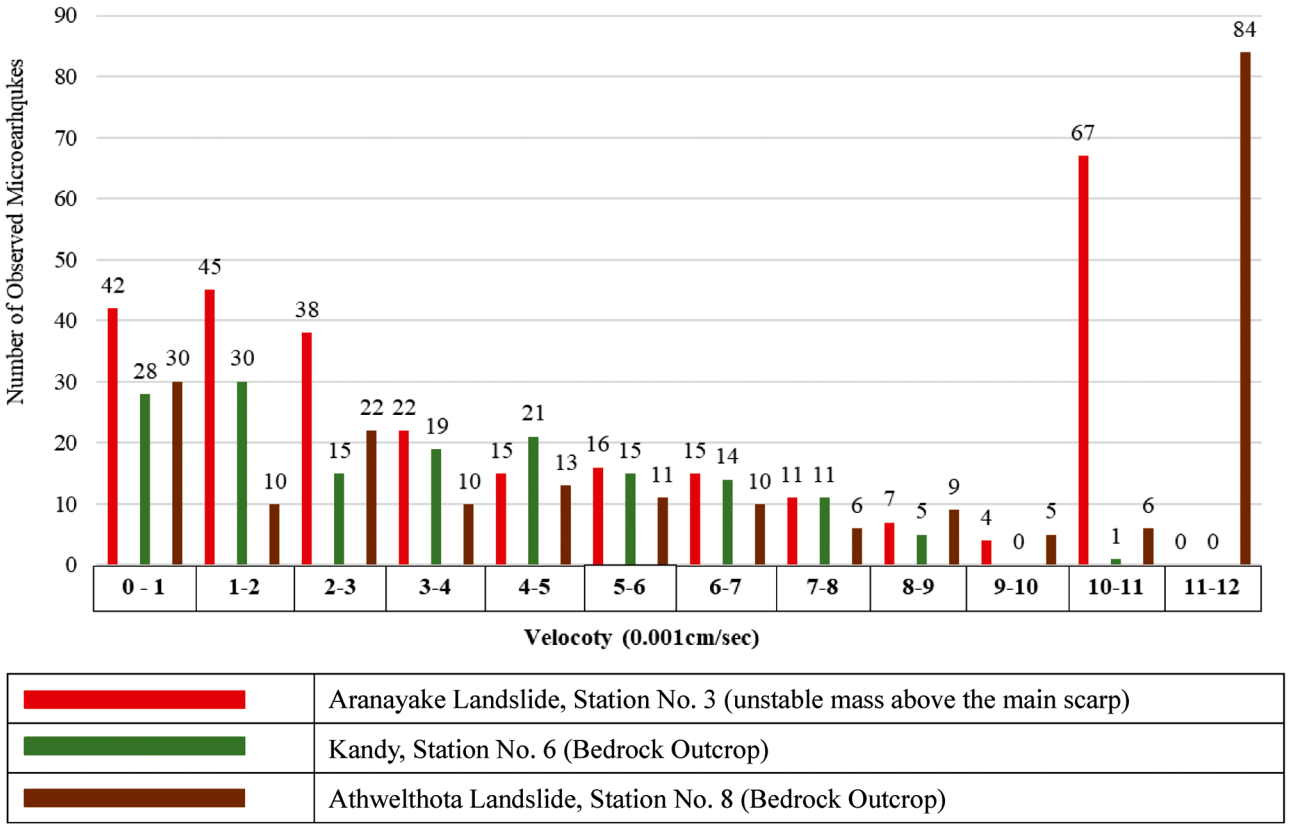


Fig. 13 Frequency and velocity of the recorded earthquakes from April 2023 to March 2024

than 0.01 cm/s and the earthquakes more than 0.01 cm/s could be different.

In order to examine the reason of the different trend in the Velocity-Frequency relationships between velocities less than 10 (×0.001 kine) and more than 10 (×0.001 kine), microearthquakes in more than 10 ranges are shown in 1/3 monthly time series in Fig. 14.

10–12 range microearthquakes are not observed in February–May. Most of 10–12 × (0.001 kine) range microearthquakes occurred in 5 months from August to December. The greatest number of microearthquakes occurred in November.

Microearthquakes are generated by the failure of rocks under the ground. The strength of rocks increases with depth because of the increased normal stress. The seismic source of

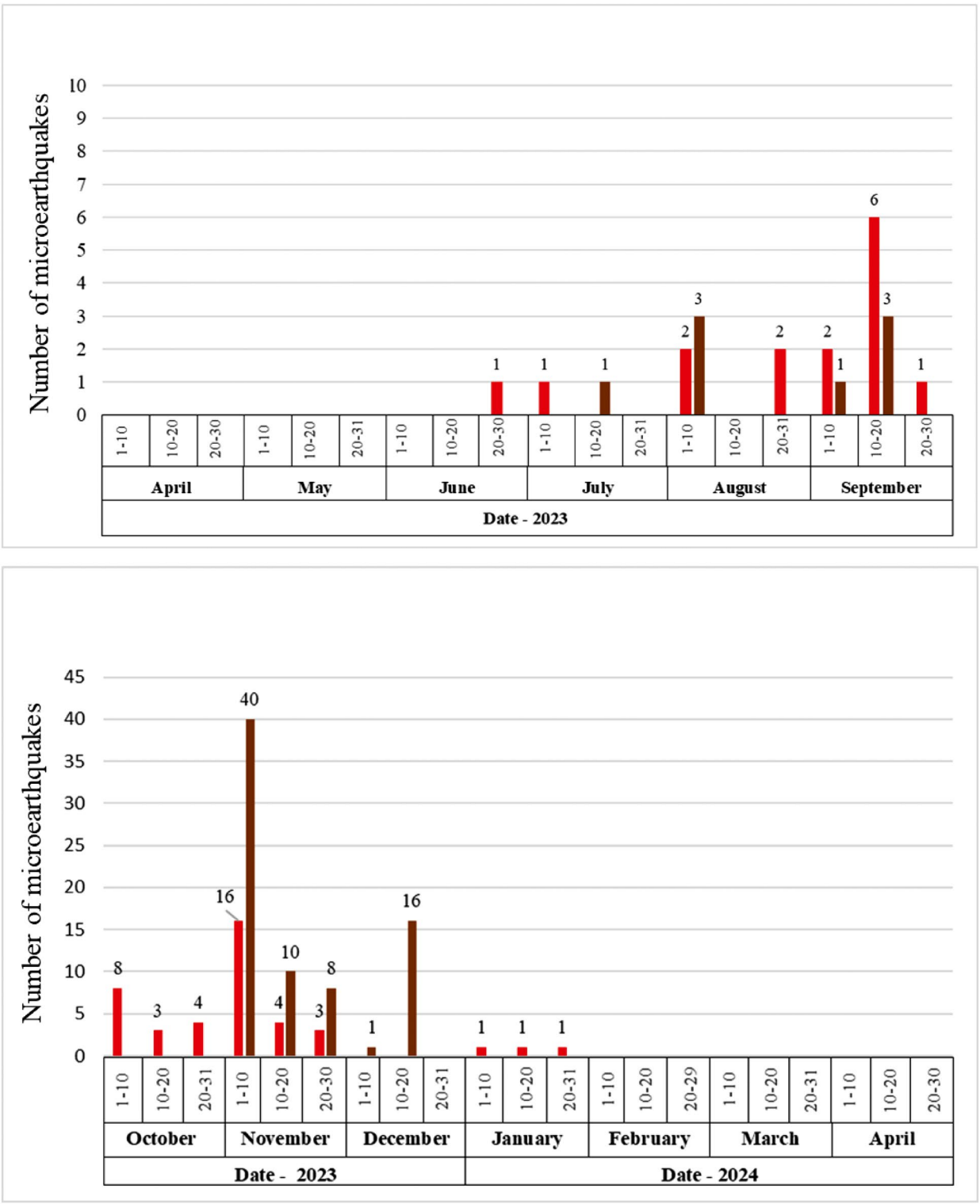


Fig. 14 Number of 1/3 monthly recorded microearthquakes in the range of 10–12 × 0.001 cm/s

larger earthquakes more than 10 Range would be deeper than the seismic sources less than 10 Range. One hypothesis is that pore water pressure in greater depth could be high in September–November, while pore water pressure is low in January to June.

Monitoring period was only 1 year and we could not decide the seismic source (hypocenters) of those monitored microearthquakes. When we can monitor microearthquakes in a longer period, and distribute more seismic sensors in suitable locations to decide the hypocenters, we may know the mechanism of microearthquakes.

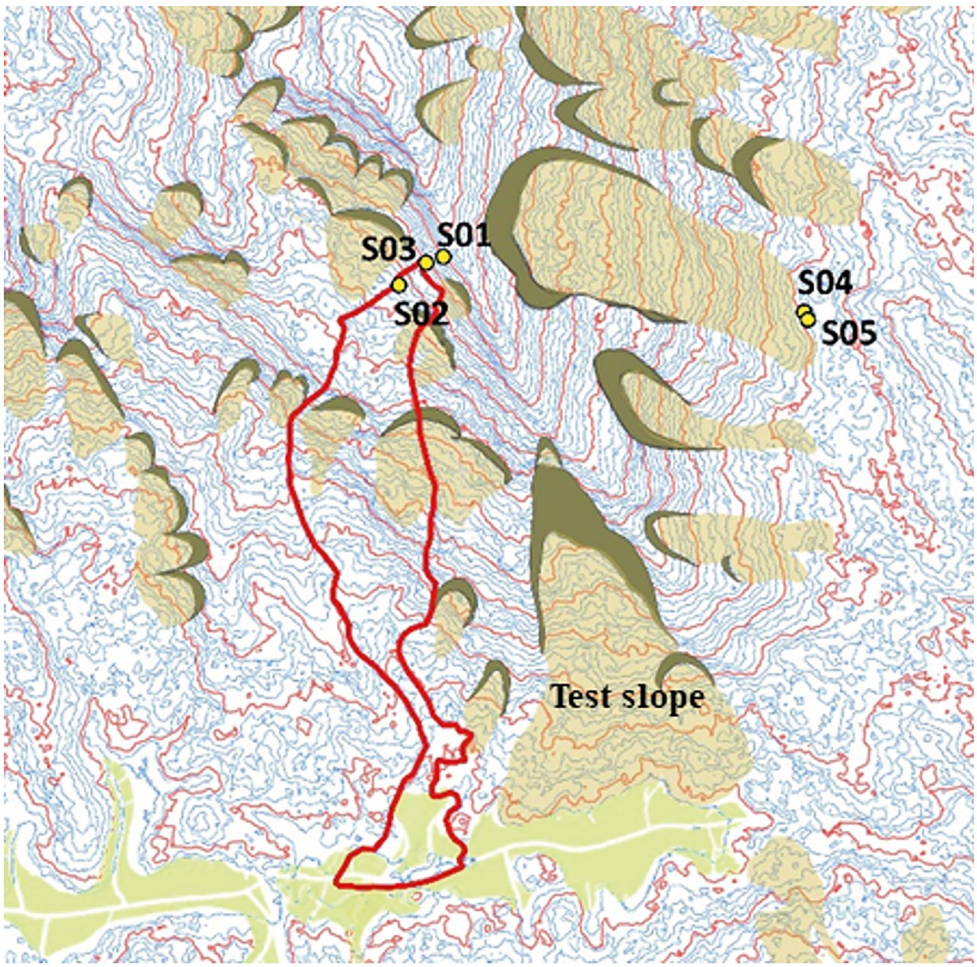


Fig. 15 The locations of the 2016 Aranauake landslides and the Aranayake Test slope. The mapping group identified previous landslides near the 2016 Aranayake landslide. Its moving area was delineated by the red line. Previous landslide bodies are marked by light-brown color. Its headscarpes are marked by dark-brounw color. We selected a very large previous landslide marcked as Test slope as a pilot study site for the forecasting of the future landslide. We installed two ICL-type seismographs and one rain gauge in this test slope. The test slope is a part of Aranayake mountain. The records of the seismographs installed at S01, S02, S03 present the very active microearthquakaes as shown in Figs. 12, 13, and 14

4 Case Study for the Landslide Risk by Post-Rainfall Earthquakes in Aranayake Test Slope

Sassa et al. (2023a, b) investigated the possibility of landslides triggered by small nearby earthquakes during or after rainfall when pore pressure within the ground is relatively high.

Figure 15 presents the locations of the 2016 Aranayake landslide and the Test slope.

The Test slope is the previous large-scale landslide close to the 2016 Aranayake landslide.

Most landslides occur in/around previous landslides (Miyagi et al. 2024). Geological conditions and triggering factors are suitable for the occurrence of landslides. The previous landslide caused an unstable (low safety factor) slope which will fail in the progress of weathering.

We have examined the landslide initiation and the motion in this Test slope using LS-RAPID.

In Fig. 16, the source area of the landslide is expected to be in the top part of previous landslides. Houses are shown as

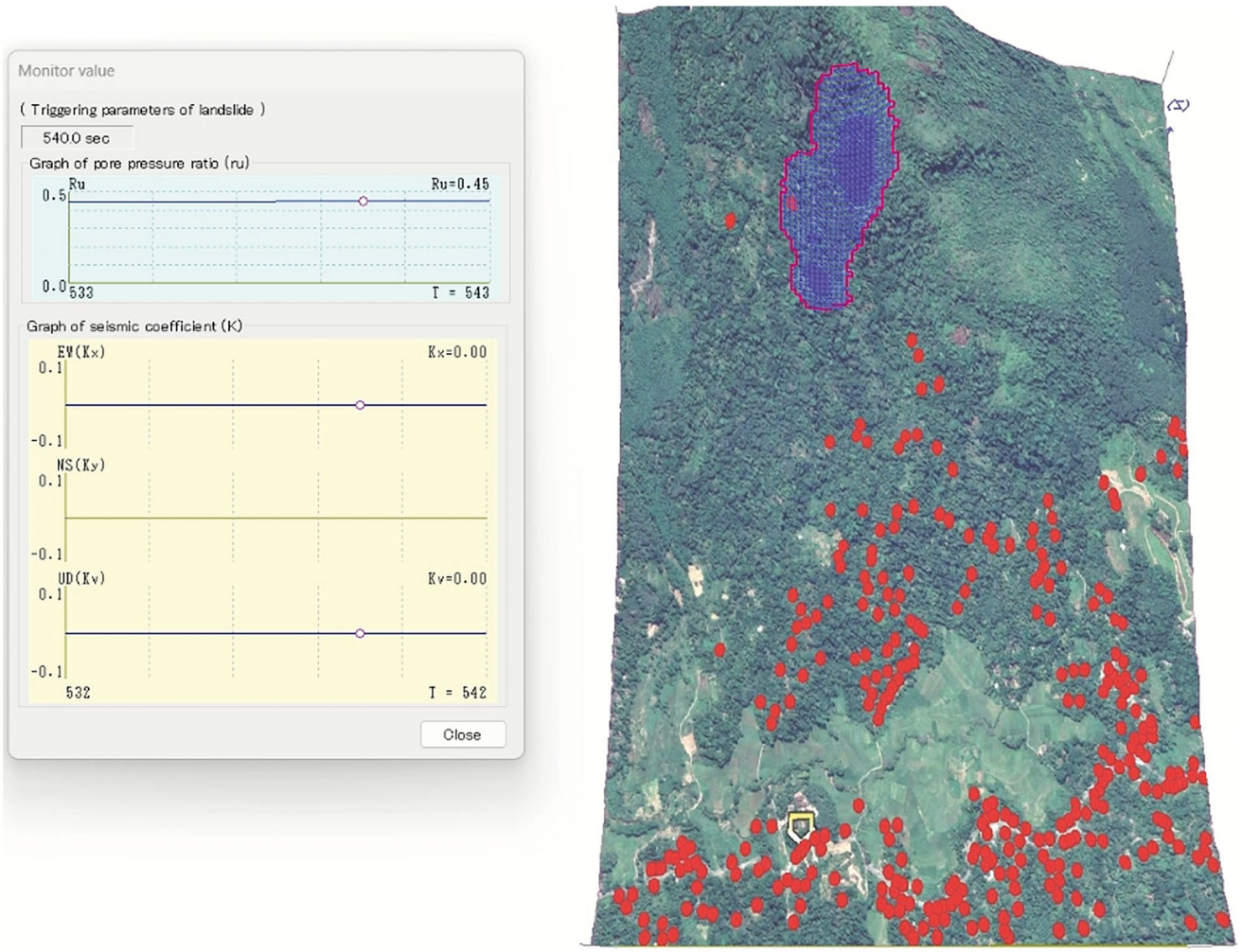


Fig. 16 LS-RAPID simulation for the Aranayake Test slope. Pore pressure ratio Ru was initially set as 0.45 and slowly increased to 0.46. Then, the seismic record of the Hambantota-offshore earthquake at S03 in the Aranayake with 3 components of stresses is amplified 12-fold, and loaded on the slope. The blue color area shows an estimated landslide block which was created by LS-RAPID and the red color plots show houses on the slope. The yellow color mark shows the location of a temple on the opposite side of the slope. It was selected as an observation base of this test slope, and a seismograph was installed (Seismic observation station No. 15 in Table 1) as a reference. The simulation results are shown in Fig. 17

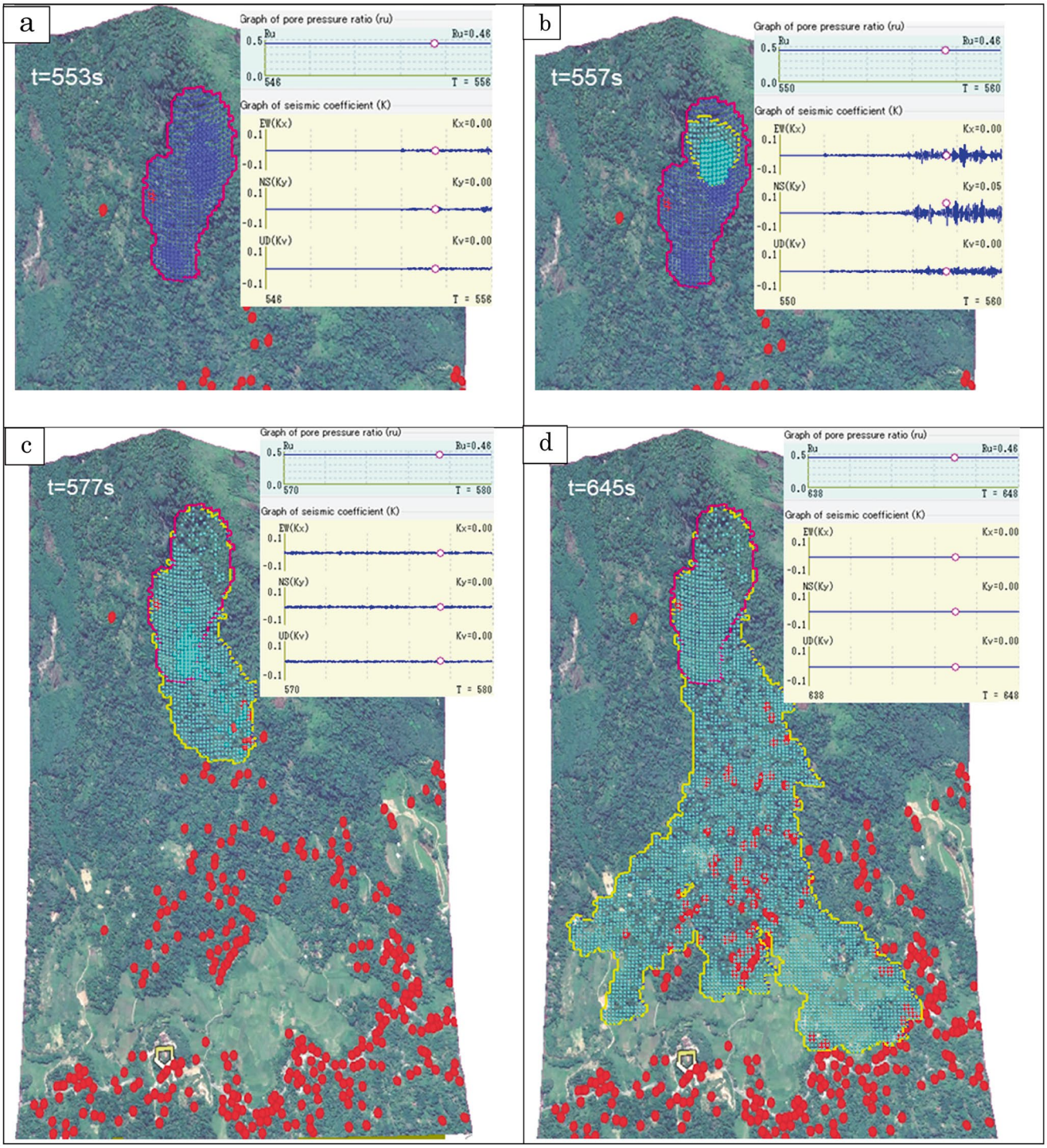


Fig. 17 Simulation results of the Aranayake test slope. Red line: Source area border. Dark blue balls: Unstable mass before motion. Right blue balls: Landslide mass during motion. Red dots: Houses. (**a**) Slope at the time during P-wave shaking: No failure in the slope (t = 553 s). (**b**) Slope at the time during S-wave shaking: Landslide started. (t = 557 s). (**c**) Slope after the major shaking: The whole landslide moved down to the lower slope (t = 577 s). (**d**) Slope after termination of motion. (t = 645 s)

red dots on the slope. Due to rainfall, the pore pressure ratio was assumed to be 0.46 when an earthquake occurred.

The seismic record of the Hambantota-offshore earthquake monitored by the sensor S03 in the Aranayake was amplified 12-fold. Then, the 12-fold stronger seismic wave of the Hambantota-offshore earthquake was loaded on the slope within the LS-RAPID model. In Fig. 17, the P-wave arrived at t = 553 s (a), the S-wave arrived and the initial failure occurred at t = 557 s (b), the failed mass moved on the lower slope deposit (c), and the enlarged landslide mass was expected to travel to destroy many houses and deposit at the toe of the slope and the flat area (d).

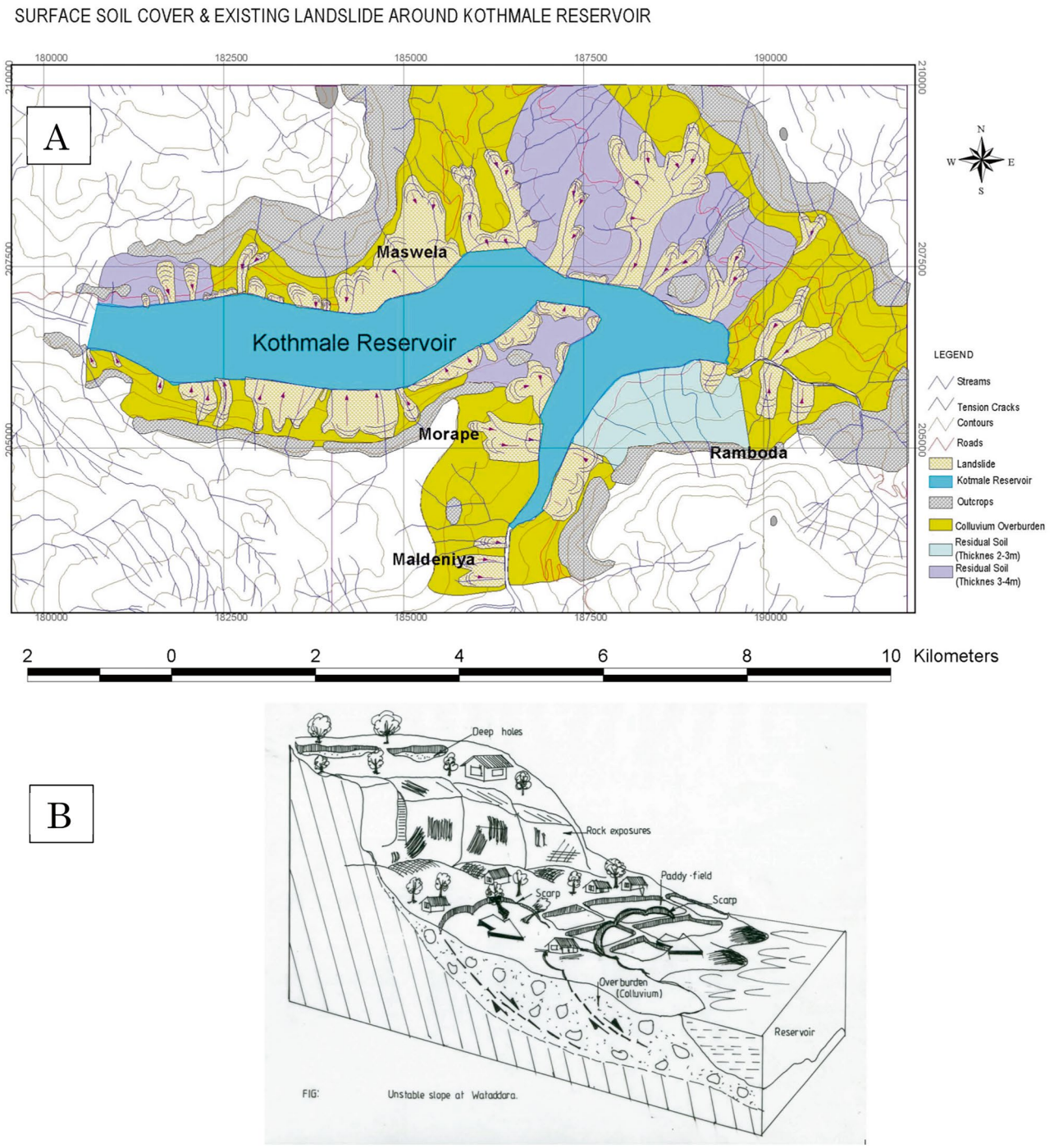


Fig. 18 Investigation of landslides around the Kotmale reservoir (Bandara and Bhandara 2012). (**a**) Plan of landslides and geological condition. (**b**) Sketch of one landslide around the Kotmale reservoir

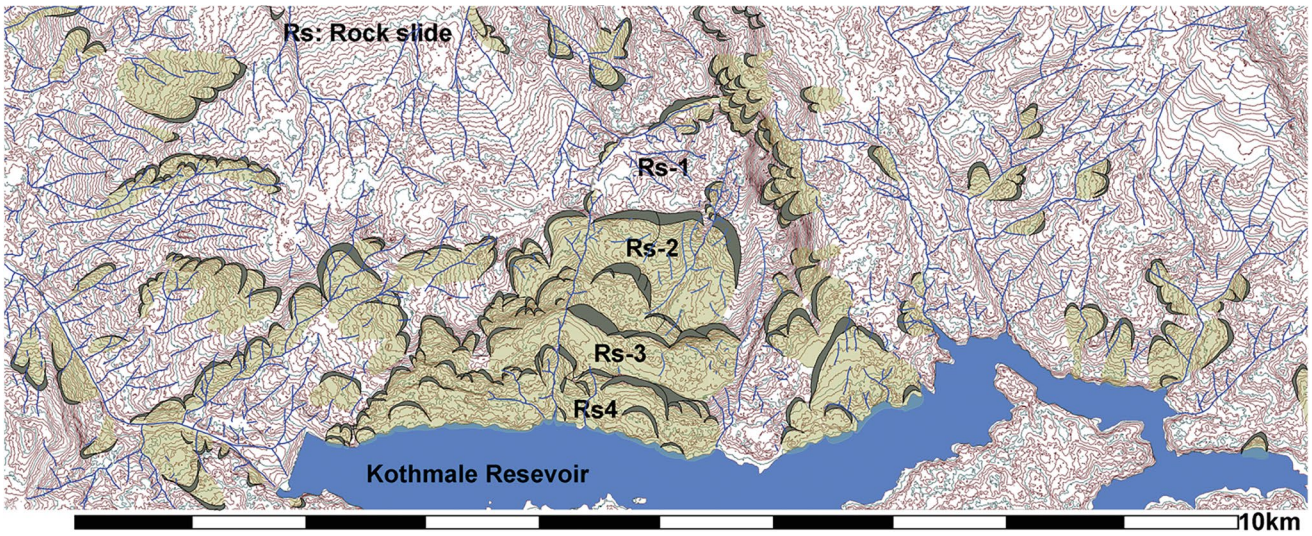


Fig. 19 Landslide topographic distribution map in Kotmale, Sri Lanka. Contour lines were generated from of AW3D 2.5 m data (Miyagi et al. 2024, P-LRT, Vol. 3–2)

5 Landslide Risk Around the Kotmale Reservoir

The Kotmale dam is located 21 km in the South-East direction from the Aranayake landslide. Both of the Kotmale dam and the Aranayake landslide are in the central mountainous region of Sri Lanka. The ICL team received the NBRO investigation report on the landslides around the Kotmale reservoir (Bandara and Bhandara 2012).

The report started with the introduction of the 1963 Vajont Dam Disaster in Italy. This disaster is also introduced in Wikipedia, https://en.wikipedia.org/wiki/Vajont_Dam.

The landslide mass of around 260 × 10^6 m^3 entered the reservoir, and the dam lake water flooded over the dam. This tsunami wave killed around 2000 people downstream.

Figure 18 is taken from the report of NBRO (Bandara and Bhandara 2012). A shows the landslide distribution near the reservoir. B illustrates of a landslide along the Kotmale reservoir. The top part of the slope is rock mass, and the toe of the landslide reaches the bottom of the dam reservoir. The report includes the fluctuation of the groundwater level monitored in 10 wells in the surrounding soil slopes of the reservoir from 2002–2004, the reservoir water level, and the monitoring result of 4 extensometers installed in landslides along the reservoir. The report was made in 2012 after the 2009–2011 field investigation by NBRO.

The report stated that the current mass movement and minor earth tremors around the Kotmale reservoir have been recorded since 1982.

The ICL-NBRO joint investigation team visited the Kotmale reservoir in 2023 and noticed large-scale retrogressive four-steps of rockslides from Rs-4 at the dam lake coast to the upper slope, Rs-3 and Rs-2 rockslides, and Rs-1, whose investigation is still at the preparation stage. The mapping group headed by Miyagi T made Fig. 19.

Sassa K and the landslide dynamic group first took an oblique view from Google Earth, drew the central investigation line, and planned to install 4 seismographs, with velocity type and acceleration type seismometers including the tilt meter function (S1–S4) along this investigation line as shown in Fig. 20. We installed two seismographs at S4 and S3 and started the monitoring from 2024.

Rock slides will slide along liner rock joints or faults or shear bands which are already made within the rock mass. A possible section of rock slides is illustrated in in the lower figure of Fig. 20. Two clear oblique planer planes (rock joints/faults/shear bands) are found, whose parts are steeper slopes between S1 and S2, and S2 and S3.

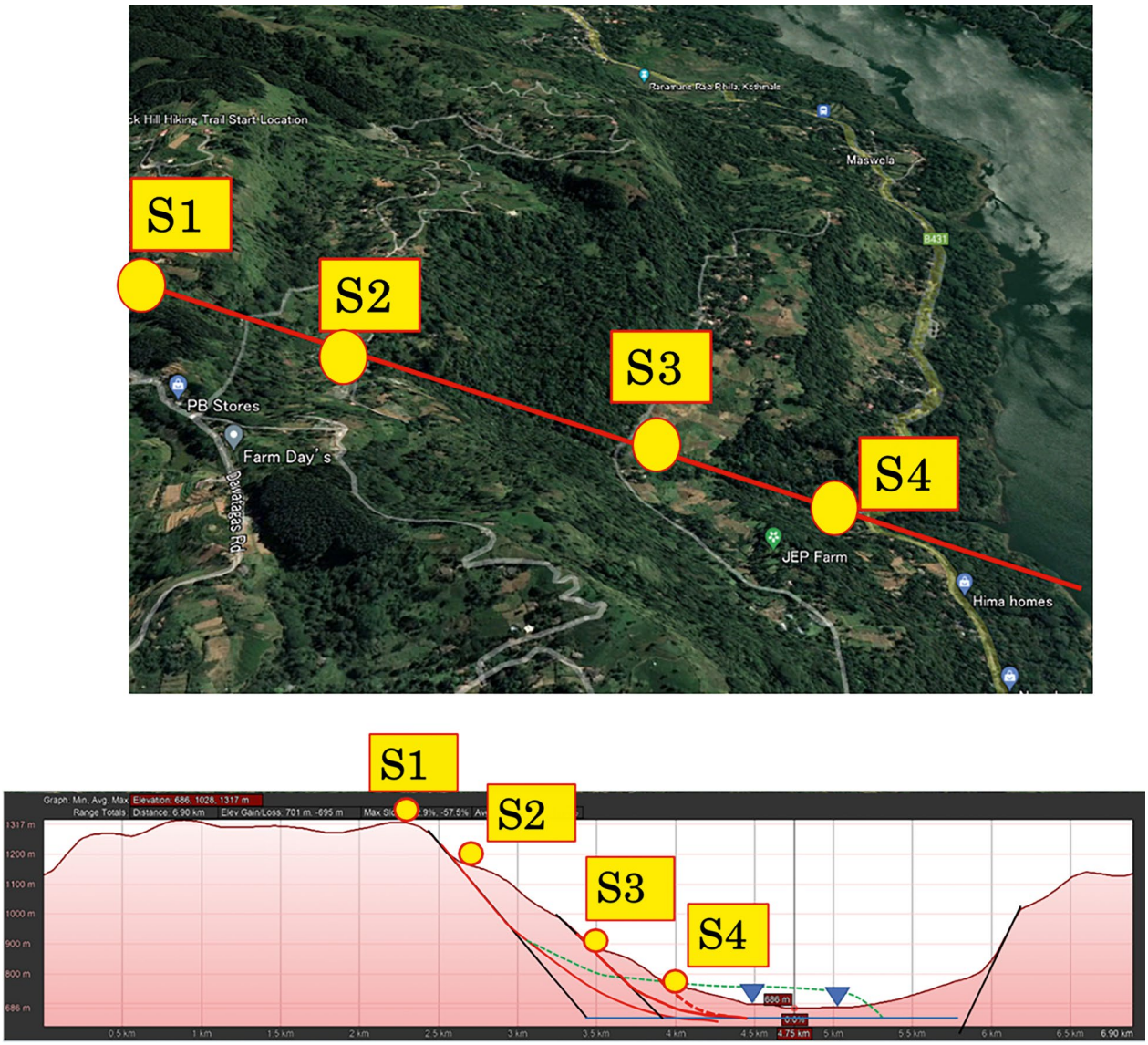


Fig. 20 Google photo of the Kotmale slope with the planned seismograph installation site for each of Landslide Blocks (Rs-1, Rs-2, Rs-3 and Rs-4) shown in Fig. 19. The lower figure: the ground surface of the slope was taken from AW3D Data. Underground rock joints and possible sliding surfaces are image illustration from the ground surface and 3D relief map (Fig. 24)

3D relief map (Fig. 24) is very helpful in understanding a series of four rockslides (Rs-1, 2, 3, 4) and to find steeper slopes along the rock joints/faults/shear bands made within the hard rock mass.

Additional note on Rs-4: The location of the point of seismograph S4 was initially planned on the slope below the road around the reservoir. However, the slope below the road was steep and covered by forests. The location is not suitable for the installation and periodical maintenance of seismograph. Then, the location was decided on the upper slope of the road to avoid the noise of roads and human disturbance, and the risk of theft.

Rs-4 is not a rock slide at present. The materials of Rs-4 were much disturbed and in a state of debris. Then, signs of deformation (cracks) are found along the road. The stability of Rs-4 is the essential for stability of Rs-3, Rs-2.

Several landslides (debris slides: Namely NOT rockslides) around the reservoir were reported, illustrated by Bandara and Bhandara (2012) as presented in Fig. 18b.

6 Landslide Disaster Risk Identification Under Frequent Nearby Small/Microearthquakes in Sri Lanka

The ICL-NBRO team installed 15 ICL-type seismographs (consisting of both velocity and acceleration type sensors) and monitored them from April 2023; the number of nearby

earthquakes with P-S time shorter than 5 s is more than ten/month in some months, as shown in Fig. 12. Therefore, the possibility of earthquake occurrence during or after rainfalls is not small. The magnitudes of the nearby earthquakes would be small. However, because of the short distance between hypocenters and landslides, seismic shaking is not so small that the order of 0.01 kine (cm/s) shaking is recorded. It is the order of 1 gal. 1 gal is the same order as the 2003 Hambantota earthquake (M = 4.4) shaking recorded in the Aranayake mountain, as shown in Fig. 11a.

6.1 Lesson Learned from a Case in the Philippines

The 2006 Leyte Landslide that destroyed the whole village and killed around 1000 people was triggered by Ms = 2.6 after the one-week rainfall (total rainfall was 674 mm for 9 days. The rainfall on the day (17 February 2006) of the earthquake and the landslide was only 2.6 mm).

Sassa et al. investigated this 2006 Leyte Landslide, took samples from the site, and conducted the physical simulation test using the undrained dynamic-loading ring shear test (Sassa et al. 2010). Figure 21 shows figures and a photo taken from the paper.

Figure 21a presents the rainfall record at Otikon Station, Libagon, Leyte, from 8 to 19 February 2006. The landslide was triggered by the small earthquake (Ms = 2.6) that took place 22 km west of the landslide source area.

Figure 21b shows the entire view of the landslides taken from a chartered helicopter by K. Sassa. The landslide covered the whole Guinsaugon village and killed around 1000 people.

Figure 21c shows the stress pass of the test simulating the landslide initiation and the post-failure motion obtained from the undrained dynamic-loading ring shear test. The apparatus used for this test is DPRI-6, which is capable to do tests under dynamic loading, up to 5 Hz, and high-speed shearing up to 224 cm/s at the center of the ring shear box. The details of this apparatus are reported by Sassa et al. (2004). The initial stress by gravity is not reproduced due to the capacity of DPRI-6, because the depth of the sliding surface of the landslides was 120–200 m. The sliding surface was assumed for the test to be 35 m deep and at an inclination of 25°. Then, corresponding normal stress and shear stress by gravity was loaded, and the pore pressure was increased due to the groundwater level increase by heavy rainfall. The white dot stress point corresponds to the water level at 5 m lower than the critical ground water level (reaching the critical failure line).

Figure 21d shows the seismic record monitored at the Masin, Leyte station. The seismic sharking stress (both normal stress and shear stress) with the same waveform of the acceleration (recorded at Masin) was loaded. The acceleration was estimated based on the distance between the Masin and the landslide, and the amplification was due to the elevation of the source area of the landslide and the P-Wave velocity contrast between the weathered landslide mass and the bedrock.

Figure 21c presents the normal stress and the shear stress by the self-weight of the landslide mass at T = 0. The normal stress (black) line and the shear stress (red) line fluctuated by seismic shaking.

Figure 21e, f illustrate the states of the volcanoclastic debris that was taken from the moved landslide mass. Time T1 denotes the initial state of debris. T2 shows the instant of failure, and T3 is during motion. A high normal stress was loaded at T1. The seismic sharking was given on the debris between T1 and T2. The seismic shaking stress was small compared to the stress by gravity (at T = 0), as seen in the stress fluctuation between T1 and T2. However, the given cyclic shear displacement should have destructed the grain of debris and the grain structure. Then, it shall cause the volume reduction of the grain structure (as illustrated in Fig. 21e). The sliding surface was estimated to be fully saturated during the prolonged rainfalls (more than 600 mm). The loaded normal stress which had been supported by grains changed to be supported by pore water. Because there was almost no volume reduction of water, the pore pressure was jumped to the level of the normal stress. The mobilized shear stress was reduced to a very low steady-state shear stress. The resulting apparent friction during motion was only 0.9 degrees (Fig. 21c). Then, the huge landslide mass moved into the village as a flood.

The lesson from the Leyte landslide is that Magnitude Ms = 2.6 earthquake, around 22 km apart from the landslide caused a catastrophic landslide. The seismic monitoring in the Aranayake landslide and the Kotmale slope has demonstrated that nearby earthquakes often occur throughout the year. The acceleration by nearby earthquakes is small at most 0.01 kine (cm/s) from April 2003 to March 2024. The value is approximately 1 gal (cm/s^2) in order. The acceleration caused by the Hambantota earthquakes (M = 4.4) 165 km from the Aranayake landslide was 2–5 gal in the Aranayake landslide (Fig. 11a). Hence, nearby earthquakes need to be carefully monitored for landslide disaster risk identification in Sri Lanka.

6.2 Microearthquake Monitoring in the Kotmale Reservoir

Nearby earthquakes have been monitored in the Kotmale slope since February 2024. Two examples of monitored earthquakes in the Kotmale slope are presented in Figs. 22 and 23.

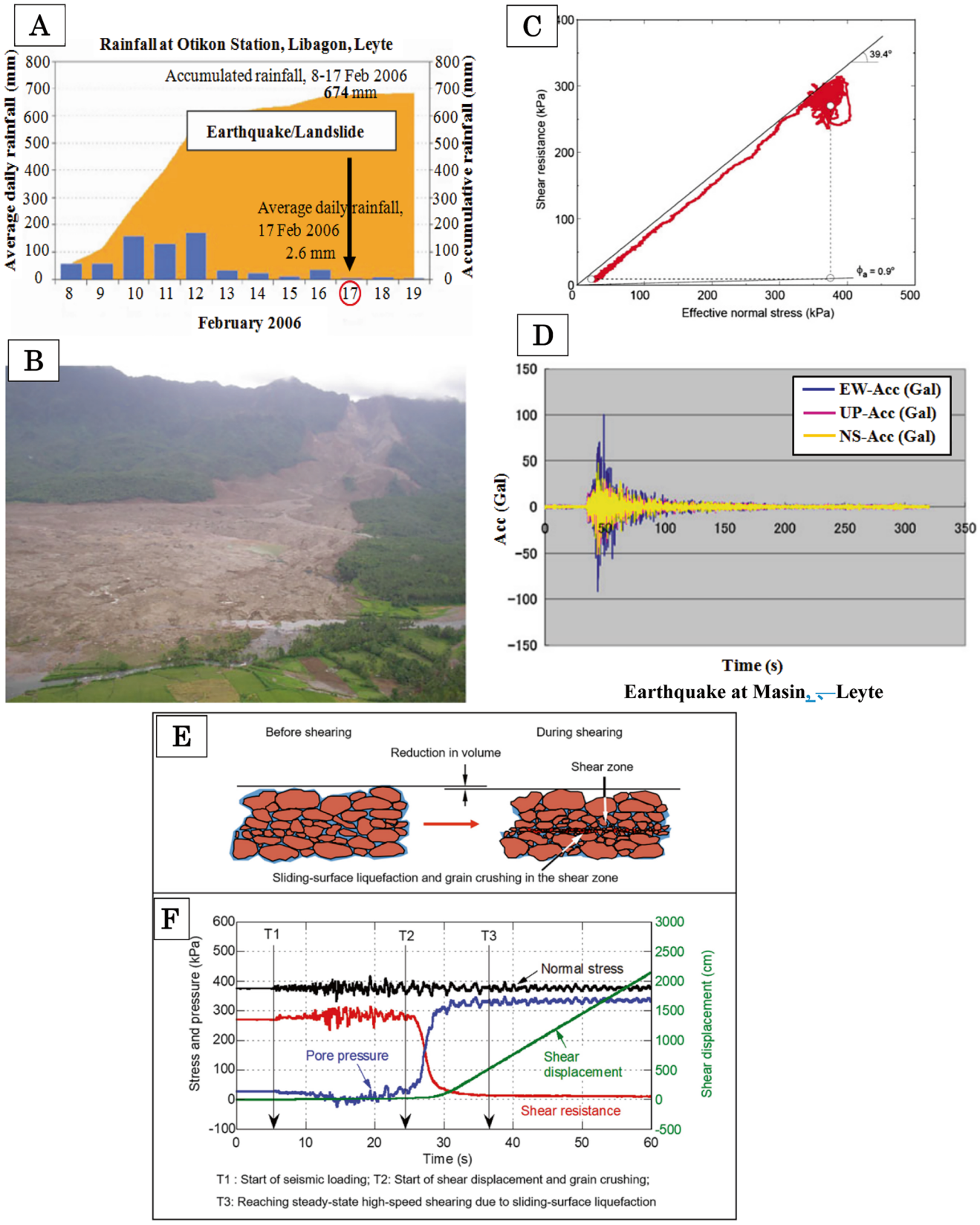


Fig. 21 Leyte landslide triggered by Ms = 2.6 earthquake after one weak rainfall, adopted from Landslides (Vol. 7–3, 2010) and P-LRT (Vol. 2–1, 2023). (**a**) Rainfall. (**b**) Photo of the Landslides (by K. Sassa), (**c**) Stress pass obtained by the undrained ring shear test, (**d**) seismic record (monitored at Maasin, Leyte), (**e**) Illustration of the sliding-surface liquefaction, (**f**) Time series data of the physical simulation test by the undrained ring shear test

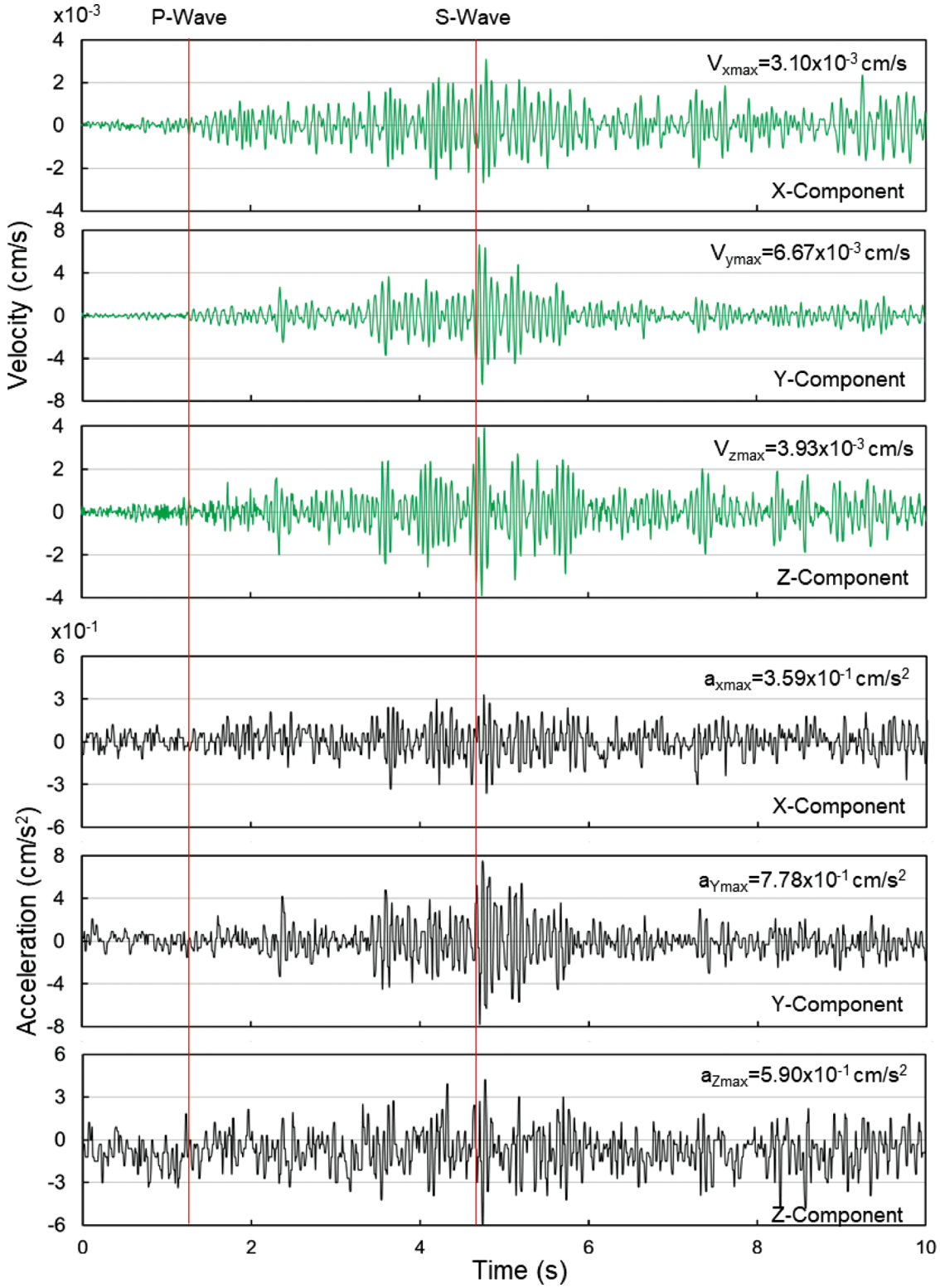


Fig. 22 Time series data of the microearthquake (P-S time = 3.4 s) recorded at ST 012 (Table 1) on 2 March 2024 in the upper landslide block S3 of the Kotmale dam (Fig. 20). The distance to the seismic source is around 25–30 km (Lay and Wallace 1995)

Figure 22 presents the time series data of the microearthquake (P-S time = 3.4 s) recorded at ST 012 (Table 1) in the upper landslide block S3 of the Kotmale dam (Fig. 20). The distance to the seismic source was around 25–30 km by referring to the equation by Lay and Wallace (1995):

$$D = (ts - tp) \times 8.0 \text{ for most of crustal events.}$$

The upper green color figure shows the Velocity measured by the velocity type seismometer which is suitable for micro-earthquake monitoring. The system cannot measure the strong earthquake as shown in Fig. 11a (lower figure). The value is saturated at 1 cm/s. This system is not resistant against careless strong shocks during the transportation.

The lower black color figure shows the Acceleration measured by the acceleration type seismometer which is suitable for greater seismic shaking and strong shocks.

Starting times of P-wave and S-wave are identified in the Y-component of the Velocity graph. From this graph, P-S time is 3.4 s. P-S time is not always easy to be identified in the acceleration-type seismometer record (black line) because the precision is not so high for small earthquakes. However, the maximum acceleration can be identified in the acceleration type seismometer as well as in the velocity type seismometer.

In Fig. 22, the largest velocity is 0.00667 cm/s (kine) in the Y-component. The largest acceleration is 0.778 cm/s^2 (gal) in the Y-component. The corresponding value of gal is around 100 times of kine.

Figure 23 shows the time series data of the microearthquake (P-S time = 0.1 s) recorded at ST011 (Table 1) in the lower landslide block S4 of the Kotmale dam (Fig. 20). The distance to the seismic source is less than 1 km (Lay and Wallace 1995).

The earthquake shown in Fig. 23 should be a much smaller earthquake than that shown in Fig. 22 in terms of the energy of earthquake (Magnitude). However, the distance to the seismic source was less than 1 km. Accordingly, the seismic acceleration loaded to the landslide mass was not so small compared to the earthquake shown in Fig. 22.

In Fig. 23, the largest velocity is 0.01085 cm/s (kine) in the Z-component. The largest acceleration is 0.64 cm/s^2 (gal) in the Z-component.

Comparing Figs. 22 and 23 events, the largest component in Fig. 22 is Y-component, in contrast, the largest component in Fig. 23 is Z-component. It means that the seismic source in Fig. 23 exists downward of the seismograph, whereas the seismic source in Fig. 22 exists in the East-West direction.

The maximum velocity in Fig. 23 (0.01085 kine) is greater than that in Fig. 22 (0.00667 kine). While the maximum acceleration in Fig. 23 (0.64 gal) in Z-direction is smaller than that in Fig. 22 (0.778 gal) in Y-c direction, both are almost the same order.

The shaking time of the earthquakes in Fig. 22 is longer than 10 s. By contrast, the shaking time of the earthquakes in Fig. 23 is less than 1 s.

Both recording results visualized the significance of the location of the hypocenter (Seismic source). Seismic sources in the Kotmale slope can be the zones of failures along active faults by tectonic stress, or failures along the developing sliding surfaces by gravitational stress. Porewater pressure also affects the strength of the slope materials.

6.3 Examination of Relief Map of the Kotmale Reservoir

Figure 24 is a relief map of the Kotmale slope made by Surfer software from AW3D data. This relief map presents the sharp bend of the Mahawelli river. This bending point is a joint of two crossing faults. Rock mass was disturbed around the joint. Other many lineaments are found. One of those lineaments is a valley along S1-S4. This valley is formed along an active fault system. Figure 20 suggests the potential sliding surfaces along possible two joint systems (one steep plane along the head scarps and one gentle plane) within the rock mass. The seismograph

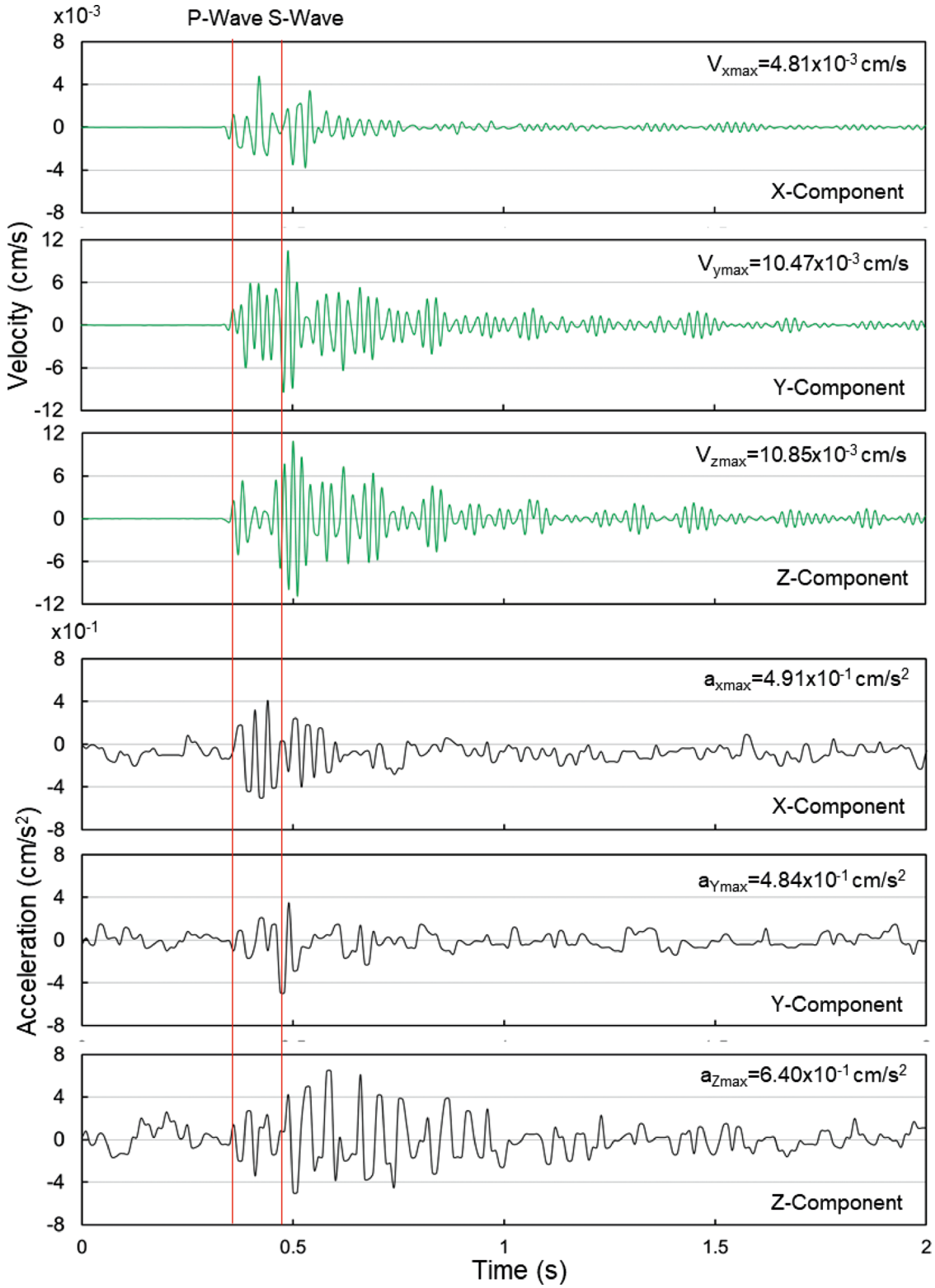


Fig. 23 Time series data of the microearthquake (P-S time = 0.1 s) recorded at ST 011 (Table 1) on 1 April 2024 in the lower landslide block S4 of the Kotmale dam (Fig. 20). The distance to the seismic source is less than 1 km (Lay and Wallace 1995)

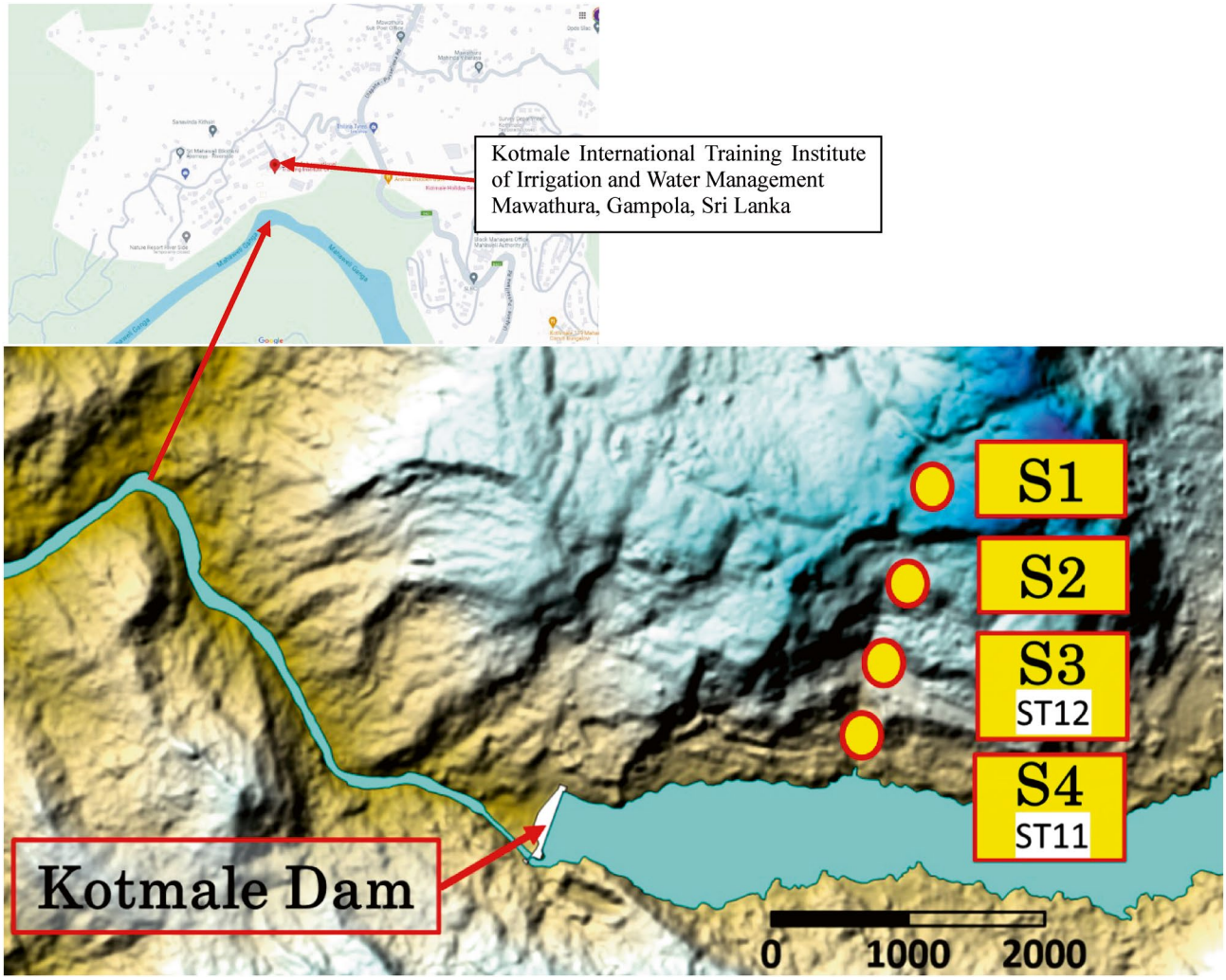


Fig. 24 Relief map of the Kotmale slope made by Surfer software from AW3D data. If the rock slide blocks move into the reservoir by the triggering earthquakes as illustrated in Fig. 17, water in the reservoirs will overtop the Kotmale dam and flow through this Mahawelli river—the longest river in Sri Lanka

installed at S4 received an earthquake (P-S time = 0.1 s. The seismic source will be less than 1 km). Z-component (vertical component) of this seismic record was the largest as shown in Fig. 23. The microearthquake observed at S4 can be related to an active fault forming this valley.

The Kotmale dam is shown in the white color. The size of the dam is much smaller compared to the size of the 4 series of rock slides (Fig. 24).

Blue color shows the dam reservoir and the Mahaweli Ganga river (the longest river in Sri Lanka). The river flows along the valley made by active fault systems and sharply bends its direction at the crossing point of two linear faults.

If a landslide-induced-tsunami generated by the rapid motion of rockslides into the Kotmale reservoir will overtop the Kotmale dam, the tsunami wave may flood over the village located in the corner of two linear faults. The Kotmale International Training Institute of Irrigation and Water Management and a post office, a temple and a few hundred houses located in this relatively flat area in the corner would be hit by this tsunami wave and flood.

7 Conclusion

When the ICL-NBRO joint project "Development of early warning technology of rain-induced rapid and long-travelling landslides in Sri Lanka" was proposed by the ICL and NBRO based on the ISDR-ICL Sendai Landslide Partnerships 2015–2025 in 2017, earthquakes in Sri Lanka were not the target of this project. However, earthquakes and microearthquakes (microtremors) have been a concern in Sri Lanka in the later stage. Then, with the supports of JICA, the ICL developed and produced 15 new seismographs that can monitor earthquakes and microearthquakes.

The monitoring results of those seismographs indicated that the earthquakes and nearby microearthquakes can be the triggers of a catastrophic landslides. Shear zones must be saturated for the initiation of catastrophic landslide. Therefore, rainfalls before the earthquakes are needed to trigger landslides. However, the slope in the waterfront, such as RS-4 Kotmale reservoir (Fig. 19) is always saturated near the water level of the reservoir. This fact shows a high risk.

Preparing for the risk of landslide disasters caused by nearby earthquakes requires monitoring nearby earthquakes for a longer period and installing the necessary number of seismographs to estimate the location of the hypocenters of these nearby earthquakes.

In addition to identifying landslide disaster risk caused by nearby microearthquakes (understanding disaster risk), an examination and planning of possible and effective measures is needed for the disaster risk preparedness (reducing disaster risk). This initiative matches well with the global promotion of understanding and reducing landslide risk.

The Kyoto Landslide Commitment 2020 for the global promotion of understanding and reducing landslide disaster risk (KLC2020) was established in 2020 as a successor of the ISDR-ICL Sendai Partnerships 2015–2025. 106 United Nations, International, and National organizations, including ICL, NBRO, and many involved organizations are signed partners of the KLC2020.

The ICL and the NBRO call for the KLC2020 partners and other organizations and individuals to support this risk reduction activities in identifying and planning for the landslide and tsunami disaster risk in a dam reservoir with potential large-scale landslides and/or rockslides around it.

Acknowledgement This research was partially supported by the Science and Technology Research Partnerships for Sustainable Development (SATREPS) project from 2019-2025, which was funded by the Japan Cooperation Agency (JICA) and the Japan Science and Technology Agency (JST).

The authors acknowledge the Kotmale dam officers for their support to the installation and monitoring of seismographs and also for providing the past seismic records monitored by the seismographs installed in the Kotmale dam. Dr. Jagath Gunatilake of the University of Peradeniya and Dr. Gamini Jayathissa of NBRO are deeply appreciated for their kind cooperation. Mr. Yuji Hayashi of Oriental Electronics, Inc. is appreciated for the data transfer and the maintenance of seismic monitoring equipment. Thanks go to Prof. Ryo Onishi of Tokyo Institute of Technology who contributed to the rainfall prediction, and Dr. Koichi Araki, Mr. Keisuke Takimoto and Mr. Yoichi Yamazaki of GODAI KAIHATSU Co., Ltd., Ishikawa, Japan who contributed to develop AR rainfall and landslide hazard map.

References

Araki K, Takimoto K, Yamazaki Y, Loi DH, Konagai K, Sassa K (2024) Time and site prediction of a potential large-scale landslides and the AR (augmented reality) presentation for early warning. Prog Landslide Res Technol 3(2) in print

Bandara KN, Bhandara RMS (2012) Investigation on instability of the area around Kotmale reservoir. NBRO Investigation Report, p 58

Dang K, Sassa K, Konagai K, Karunawardena A, Bandara RMS, Hirota K, Tan Q, Ha ND (2019) Recent rainfall-induced rapid and long-traveling landslide on 17 May 2016 in Aranayaka, Kagelle District, Sri Lanka. Landslides 16(1):155–164

Doan L, Dang K, Tien P, Sassa K (2024) Estimation of potential landslides in/around previous large-scale landslides and the critical pore pressure to initiate landslides by LS-RAPID. Prog Landslide Res Technol 3(2) in print

Konagai K, Karunawardena A, Bandara KN, Sassa K, Onishi R, Uzuoka R, Asano S, Sasahara K, Jayakody S, Ariyarathna I (2023) Early warning system against rainfall-induced landslides in Sri Lanka. Prog Landslide Res Technol 1(1) in print:217–235

Lay T, Wallace TC (1995) Modern global seismology. Academic Press, San Diego

Matsunami K, Sassa K, Weerasnghe R, Munasinghe T, Doan L (2024) Challenges of earthquake and micro-earthquake monitoring in Sri Lanka. Prog Landslide Res Technol 3(2) in print

Miyagi T, Doan L et al (2024) How to detect the previous large-scale landslide: source of future landslides by interpretation of ground topography from digital maps. Prog Landslide Res Technol 3(2) in print

Onishi R, Bandara HAAIS, Matsumoto K (2024) High-resolution rainfall simulations for early warning of long-traveling landslides in Sri Lanka. Prog Landslide Res Technol 3(2) in print

Sassa K (2015) ISDR-ICL Sendai Partnerships 2015–2025 for global promotion of understanding and reducing disaster risk. Landslides 12(4):631–640

Sassa K (2021) The Kyoto Landslide Commitment 2020: launched. Landslides 18(1):5–20

Sassa K, Fukuoka H, Wang G, Ishikawa N (2004) Undrained dynamic-loading ring-shear apparatus and its application to landslide dynamics. Landslides 1(1):7–19

Sassa K, Nagai O, Solidum R, Yamazaki Y, Ohta H (2010) An integrated model simulating the initiation and motion of earthquake and rain induced rapid landslides and its application to the 2006 Leyte landslide. Landsides 7(3):219–236

Sassa K, Matsunami K, Doan L, Miyag T, Thaldena N, Weerasinghe R, Konagai K, Karunawardena A (2023a) The 2023.4.24 Hambantota-offshore earthquake and microearthquakes in Sri Lanka and the landslide risk evaluation in a nearby slope by post-rainfall earthquakes. Landslides 20(8):1771–1779

Sassa K, Doan L, Dang K, Pl T (2023b) Siding-surface liquefaction and undrained steady-state shear strength. Prog Landslide Res Technol 2(1):11–95

Open Access This chapter is licensed under the terms of the Creative Commons Attribution 4.0 International License (http://creativecommons.org/licenses/by/4.0/), which permits use, sharing, adaptation, distribution and reproduction in any medium or format, as long as you give appropriate credit to the original author(s) and the source, provide a link to the Creative Commons license and indicate if changes were made.

The images or other third party material in this chapter are included in the chapter's Creative Commons license, unless indicated otherwise in a credit line to the material. If material is not included in the chapter's Creative Commons license and your intended use is not permitted by statutory regulation or exceeds the permitted use, you will need to obtain permission directly from the copyright holder.



Part III

IPL Projects, World Centres of Excellence on Landslide Risk Reduction, and Kyoto Landslide Commitment 2020

The 6th World Landslide Forum (WLF6), Florence, 2023

Veronica Tofani, Kyoji Sassa, Paolo Canuti,
Anna Elisa Bandecchi, Elisa Gargini, and Nicola Casagli

Abstract

The 6th World Landslide Forum "Landslides Science for sustainable development" (WLF6; https://wlf6.org) was held in Florence from November 14 to 17, 2023. The Forum was focused on Landslide Science for Sustainable Development, as a contribution to the Kyoto 2020 Commitment for global promotion of understanding and reducing landslide disaster risk (KLC2020). The Forum addressed key aspects related to landslide analysis, landslide monitoring and early warning, landslide modeling, landslide hazard and risk assessment, mitigation techniques, landslide triggering mechanism and climate change. The WLF6 was attended by more than 1200 participants from 61 countries. 853 abstracts were accepted, including 643 oral presentations and 210 e-posters. The 6th World Landslide Forum was awarded the Medal of the President of the Italian Republic, which is awarded for events of great scientific and cultural importance. Furthermore, the Forum was a sustainable event in line with the 2030 Agenda and the Sustainable Development Goals.

Keywords

Landslide · Risk Reduction · World Landslide Forum · KLC2020

V. Tofani (✉) · N. Casagli
Department of Earth Sciences, University of Florence, Florence, Italy

UNESCO Chair on Prevention and Sustainable Management of Geo-Hydrological Hazards, University of Florence, Florence, Italy
e-mail: veronica.tofani@unifi.it; nicola.casagli@unifi.it

K. Sassa
International Consortium on Landslides, Kyoto, Japan

P. Canuti
UNESCO Chair on Prevention and Sustainable Management of Geo-Hydrological Hazards, University of Florence, Florence, Italy

A. E. Bandecchi · E. Gargini
Civil Protection Center, University of Florence, Florence, Italy
e-mail: elisa.bandecchi@unifi.it; elisa.gargini@unifi.it

1 Introduction

The 6th World Landslide Forum "Landslides Science for sustainable development" (WLF6) (Fig. 1) was held from November 14 to 17, 2023 in Florence at the Palazzo dei Congressi. The WLF6 was focused on landslide science for sustainable development as a contribution to the Kyoto 2020 Commitment for global promotion of understanding and reducing landslide disaster risk (KLC2020) (Sassa 2021), to the Sendai Landslide Partnerships 2015–2025 (Sassa 2015), the Sendai Framework for Disaster Risk Reduction 2015–2030, the 2030 Agenda Sustainable Development Goals, the New Urban Agenda and the Paris Agreement (Casagli et al. 2022, 2023).

The Forum provided a platform for fruitful collaboration between landslide researchers and stakeholders to define common priority actions for landslide risk reduction at the global level. The Forum addressed key aspects related to landslide analysis, landslide monitoring and early warning, landslide modeling, landslide hazard and risk assessment, mitigation techniques, landslide triggering mechanism and climate change. The 6th World Landslide Forum was attended by a broad international audience interested in landslide disaster risk reduction: research and academic institutions; UN organizations; EU institutions and agencies; national governments and local authorities; non-governmental organizations with an interest in and activities related to disaster risk reduction; international and national civil protection and disaster relief organizations and agencies; and the private sector engaged in research, development and practical application of landslide risk reduction technologies and solutions. In particular, the WLF6 was attended by more than 1200 participants from 61 countries. 853 abstracts were accepted, including 643 oral presentations and 210 e-posters. During the Forum were organized 2 plenary sessions, 48 scientific parallel sessions, and 10 workshops and side events (Table 1).

© The Author(s) 2025

B. Abolmasov et al. (eds.), *Progress in Landslide Research and Technology, Volume 3 Issue 2, 2024*, Progress in Landslide Research and Technology, https://doi.org/10.1007/978-3-031-72736-8_17

Fig. 1 WLF6 logo

Table 1 WLF6 in figures

Participants	1202
Countries/Regions	61
Plenary sessions	2
Parallel sessions	48
Oral presentations	643
E-poster presentations	210
Workshops and side events	10
Exhibitors booths	27

The Forum was a sustainable event in line with the 2030 Agenda and the Sustainable Development Goals. The venue (Fig. 2), the Palazzo dei Congressi, is located in the city center of Florence, in a strategic position within walking distance of the city's main attractions. No printed material was provided to the participants. The detailed scientific program, the schedule and all general information were available on the congress app. The program and the proceedings of the

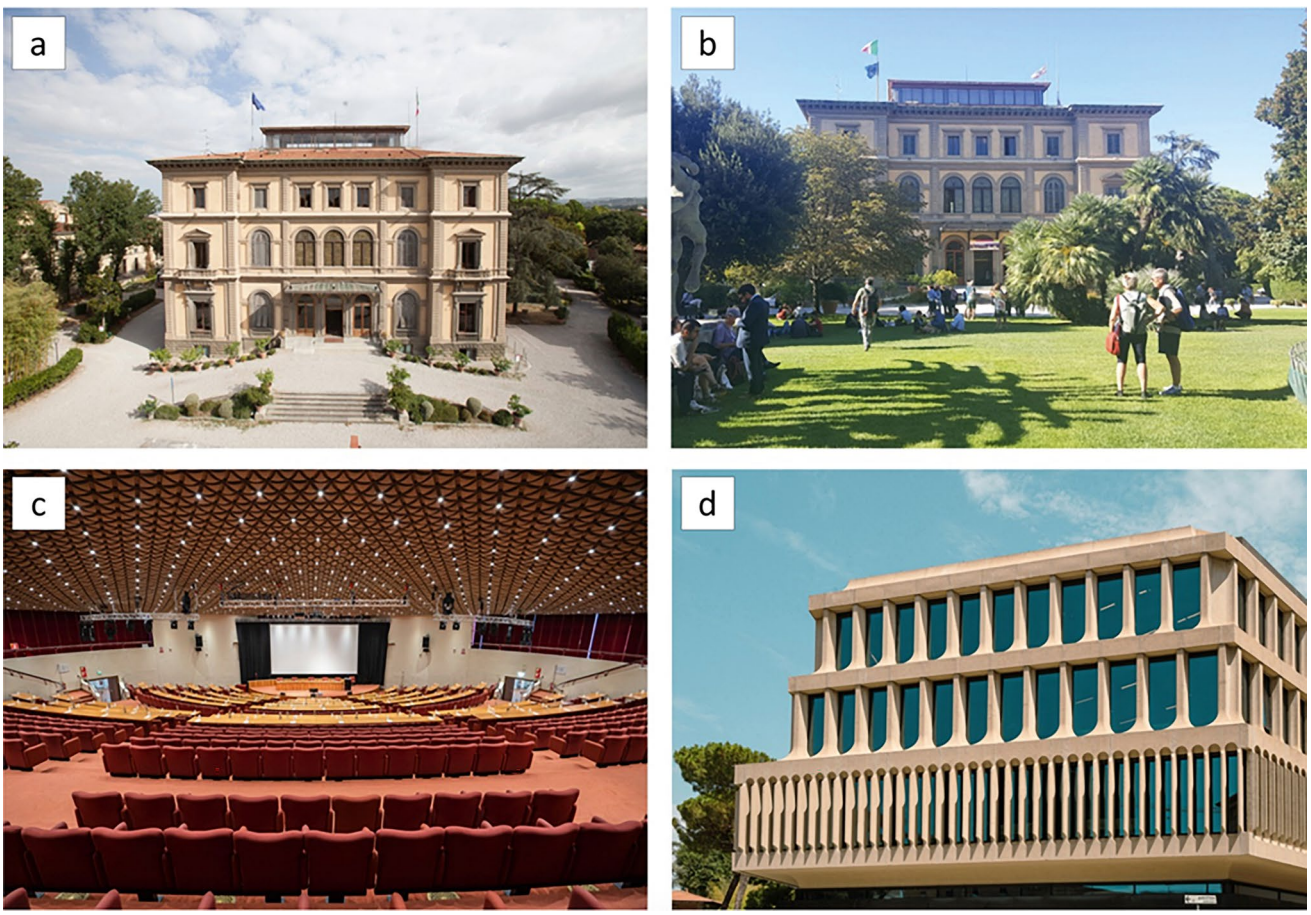


Fig. 2 Congress venue. (**a**) Palazzo dei Congressi, (**b**) Park in front of Palazzo dei Congressi, (**c**) Florence Auditorium for plenary sessions, (**d**) Palazzo degli Affari



Fig. 3 Medal of the President of the Italian Republic

Forum were distributed to the participants in electronic form and can be downloaded from the Forum's website (https://wlf6.org).

The 6th World Landslide Forum was awarded the Medal of the President of the Italian Republic, which is awarded for events of great scientific and cultural importance (Fig. 3).

2 Organizers, Organizing Committees, Patronage, Partners and Sponsors

Organizers

International Consortium on Landslides (ICL).

UNESCO Chair on Prevention and Sustainable Management of Geo-Hydrological Hazards, University of Florence, Italy.

Global Promotion Committee of International Programme on Landslides and KLC 2020 (GPC/IPL-KLC), including: United Nations Educational, Scientific and Cultural Organization (UNESCO), World Meteorological Organization (WMO), Food and Agriculture Organization (FAO), United Nations Office for Disaster Risk Reduction (UNDRR), United Nations University (UNU), International Science Council (ISC), World Federation of Engineering Organizations (WFEO), International Union of Geological Sciences (IUGS), International Union of Geodesy and Geophysics (IUGG).

Forum Chair

Nicola Casagli, Professor, University of Florence; President of ICL.

Forum Co-chairs

Kyoji Sassa, Professor Emeritus, Kyoto University; Secretary General of ICL).

Paolo Canuti, UNESCO Chair Holder, UNESCO Chair on Prevention and Sustainable Management of Geo-Hydrological Hazards, University of Florence.

Secretary general

Veronica Tofani, Associate Professor, University of Florence, Vice President of ICL.

Secretariat General

It was composed of 16 members from the University of Florence: Domenico Armignacco, Anna Elisa Bandecchi, Tommaso Carlà, Pierluigi Confuorto, Matteo Del Soldato, Elisa Gargini, Teresa Gracchi, Emanuele Intrieri, Silvia Massagni, Massimiliano Nocentini, Teresa Nolesini, Guglielmo Rossi, Melania Scacciati, Gabriele Scaduto, Carlo Tacconi Stefanelli, Luca Tanteri.

International scientific committee

It was composed of 24 members including ICL members and internationally recognized scientists in the field of landslide research and landslide risk reduction: Kyoji Sassa (Kyoto University, Japan; Secretary General of ICL), Matjaž Mikoš (University of Ljubljana, Slovenia), Shinji Sassa (Port and Airport Research Institute, Japan), Khang Dang (Research Promotion Officer, ICL), Veronica Tofani (University of Florence, Italy), Michel Jaboyedoff (University of Lausanne, Switzerland), Jan Klimes (Academy of Sciences, Czech Republic), Hans-Balder Havenith (Liege University, Belgium), Binod Tiwari (California State University, Fullerton, USA), Kazuo Konagai (University of Tokyo, Japan; Principal researcher of ICL Headquarters), Sabatino Cuomo (University of Salerno, Italy), Xuanmei Fan (Chengdu University, China), Paola Reichenbach (Research Institute for Geo-Hydrological Protection—National Research Council, Italy), Snježana-Mihalić Arbanas (University of Zagreb, Croatia), David Huntley (Geological Survey of Canada, Canada), Maneesha V. Ramesh (Amrita University, India), Vít Vilímek (Charles University in Prague, Czech Republic), Alexander Strom (Geodynamics Research Center LLC, Russia), Stefano Luigi Gariano (Research Institute for Geo-Hydrological Protection—National

Research Council, Italy), Dalia Kirschbaum (NASA Goddard Space Flight Center, USA), Zeljko Arbanas (University of Rijeka, Croatia), Fawu Wang (Tongji University, China), Faisal Fathani (University of Gadjah Mada, Indonesia), Beena Ajmera (Iowa State University, USA).

Local organizing committee Chair

Claudio Margottini, Italian Institute for Environmental Protection and Research, Italy.

Local organizing committee

It was composed of 42 members including the members of the ICL Italian network and staff from University of Florence: Federico Agliardi (University of Milano-Bicocca, Italy), Gioacchino Francesco Andriani (University of Bari, Italy), Matteo Berti (University of Bologna, Italy), Silvia Bianchini (University of Florence, Italy), Francesca Bozzano (Sapienza Università di Roma—Istituto Nazionale di Geofisica e Vulcanologia INGV, Italy), Marcello Buccolini (University of Chieti-Pescara, Italy), Domenico Calcaterra (Federico II University of Naples, Italy), Michele Calvello (University of Salerno, Italy), Giovanna Capparelli (University of Calabria, Italy), Filippo Catani (University of Padua, Italy), Corrado Cencetti (University of Perugia, Italy), Alessandro Chelli (University of Parma, Italy), Giovani Crosta (University of Milano-Bicocca, Italy), Alessandro Corsini (University of Modena and Reggio Emilia, Italy), Sabatino Cuomo (University of Salerno, Italy), Carlo Esposito (Sapienza Università di Roma, Italy), Riccardo Fanti (University of Florence, Italy), Anna Maria Ferrero (University of Turin, Italy), Paolo Frattini (University of Milano-Bicocca, Italy), Giandomenico Fubelli (University of Turin, Italy), Antonio Galgaro (University of Padova, Italy), Stefano Luigi Gariano (Research Institute for Geo-Hydrological Protection—National Research Council, Italy), Monica Ghirotti (University of Ferrara, Italy), Giovanni Gigli (University of Florence, Italy), Francesco Maria Guadagno (University of Sannio, Italy), Giuseppe Mandrone (University of Turin, Italy), Claudia Meisina (University of Pavia, Italy), Sandro Moretti (University of Florence, Italy), Mario Parise (University of Bari, Italy), Dario Peduto (University of Salerno, Italy), Antonella Peresan (National Institute of Oceanography and Applied Geophysics, Italy), Federico Raspini (University of Florence, Italy), Paola Revellino (University of Sannio, Italy), Gabriele Scarascia Mugnozza (Sapienza Università di Roma, Italy), Nicola Sciarra (University of Chieti-Pescara, Italy), Andrea Segalini (University of Parma, Italy), Samuele Segoni (University of Florence, Italy), Vincenzo Simeone (Politecnico di Bari, Italy), Daniele Spizzichino (Italian Institute for Environmental Protection and Research, Italy), Paola Reichenbach (Research Institute for Geo-Hydrological Protection—National Research Council, Italy), Damiano Vacha (University of Turin, Italy), Pasquale Versace (University of Calabria, Italy).

Medal and Patronage

The WLF6 has received the Medal of the President of the Italian Republic (Fig. 3) the patronage from five Italian Ministries (Fig. 4):

- Ministero delle Infrastrutture e dei Trasporti,
- Ministero dell'Interno,
- Ministero dell'Agricoltura della Sovranità Alimentare e delle Foreste,
- Ministero dell'Ambiente e della Sicurezza Energetica,
- Ministro per la Protezione Civile e le Politiche del Mare—Presidenza del Consiglio dei Ministri,

and the patronage from 37 public institutions (Fig. 4): Dipartimento della Protezione Civile—Presidenza del Consiglio Dei Ministri, Dipartimento Casa Italia—Presidenza Del Consiglio Dei Ministri, Dipartimento per la Trasformazione Digitale—Presidenza Del Consiglio Dei Ministri, Regione Toscana, Comune di Firenze, Città Metropolitana di Firenze, Anci Toscana, Università degli Studi di Firenze, Consiglio Nazionale dei Geologi (CNG), Consiglio Nazionale degli Ingegneri (CNI), Consiglio Nazionale degli Architetti Pianificatori Paesaggisti e Conservatori (CNAPPC), Consiglio Nazionale Geometri e Geometri Laureati, Consiglio dell'Ordine Nazionale dei Dottori Agronomi e dei Dottori Forestali (CONAF), Corpo Nazionale Soccorso Alpino e Speleologico (CNSAS), Consiglio Nazionale delle Ricerche (CNR), Istituto Superiore per la Protezione e la Ricerca Ambientale (ISPRA), Istituto Nazionale di Geofisica e Vulcanologia (INGV), Istituto Nazionale di Fisica Nucleare (INFN), Agenzia Spaziale Italiana (ASI), Istituto Nazionale di Oceanografia e di Geofisica Sperimentale (OGS), Area Science Park, Centro Euro-Mediterraneo sui Cambiamenti Climatici (CMCC), Consorzio Cineca, Rai Cultura, Fondazione Earth And Water Agenda (EWA), Autorità di Bacino Distrettuale del Fiume Po, Autorità di Bacino Distrettuale Appennino Settentrionale, Autorità di Bacino Distrettuale Appennino Centrale, Autorità di Bacino Distrettuale Appennino Meridionale, Associazione Nazionale Consorzi Gestione e Tutela del Territorio e Acque Irrigue (ANBI-Toscana), Confindustria Firenze, Camera di Commercio di Firenze.

Partners

The Forum has received the partnership from 19 national and international associations (Fig. 5): International Consortium on Geo-Disaster Reduction (ICGDR), Global Alliance of Disaster Research Institutes (GADRI), International Association of Geomorphologists (IAG/AIG), RETURN—Multi-Risk Science for Resilient Communities Under a Changing Climate, Landaware, Alert Geomaterials,

Fig. 4 WLF6 Patronage



International Association for Engineering Geology and the Environment—Gruppo Nazionale Italiano (IAEG-Italia), Associazione Italiana di Geologia Applicata e Ambientale (AIGAA), Associazione Italiana di Geografia Fisica e Geomorfologia (AIGEO), Gruppo Italiano della Associazione Internazionale degli Idrogeologi (IAH-Italy), Società Geologica Italiana (SGI), Associazione Geotecnica Italiana (AGI), Società Italiana di Geologia Ambientale (SIGEA), Associazione Italiana per lo Studio del Quaternario (AIQUA), Associazione Italiana di Ingegneria Agraria (AIIA), Società Idrologica Italiana (SII), Sezione Italiana European Association of Geoscientists and Engineers—

Fig. 5 WLF6 partners



Society Of Exploration Geophysicists (EAGE-SEG), Gruppo Italiano di Idraulica (GII), Legambiente.

Sponsors and Exhibitors

There were 21 WLF6 sponsors (Fig. 6): Hexagon (Platinum Sponsor); LiSALab—Ellegi s.r.l. (Gold Sponsor); ESA, MicroGeo s.r.l., Rete Ferroviaria Italiana s.p.a., TRE Altamira (Silver Sponsors); ANBI Toscana, CAE, CNR, EcorisQ, e-GEOS, Geobrugg, Hortus, IAEG, INGV, Maccaferri, NHAZCA, OGS, Planetek Italia, Spektra, Winet s.r.l. (Bronze Sponsors).

At the WLF6 Technical Exhibition there were 27 exhibitors: the 21 sponsors and CSG, Georisk Engineering, ISPRA, METER, Sistematica s.p.a., Studio Pandolfi (Fig. 6).



Fig. 6 WLF6 Sponsors and exhibitors

3 Programme

The Forum was scheduled for November 14–17, 2023 (Table 2).

November 13 was dedicated to the ICL/IPL meeting. The Opening Plenary Session took place on November 14 (Table 3).

Parallel Scientific Sessions were held from November 15 to 17, organized in the following scientific themes:

- Theme 1: Kyoto Landslide Commitment for sustainable development (Coordinators: Kyoji Sassa, Matjaž Mikoš, Shinji Sassa, Khang Dang).

Table 2 WLF6 programme at a glance

Day	Morning 8:30–13:00	Afternoon 14:30–18:00	Evening
Mon. 13th		ICL/IPL Meeting	
Tue. 14th	Opening Ceremony and High-Level Panel Discussion	Keynote Lectures and Awards Ceremony	Welcome Cocktail
Wed. 15th	Parallel Sessions	Parallel Sessions	
Thu. 16th	Parallel Sessions	Parallel Sessions	Banquet
Fri. 17th	Parallel Sessions	Parallel Sessions and Closing Ceremony	

- Theme 2: Remote sensing, monitoring, and early warning (Coordinators: Veronica Tofani, Michel Jaboyedoff, Jan Klimeš, Hans-Balder Havenith).
- Theme 3: Testing, modeling, and mitigation technique (Coordinators: Binod Tiwari, Kazuo Konagai, Sabatino Cuomo, Xuanmei Fan).
- Theme 4: Mapping, hazard, risk assessment and management (Coordinators: Paola Reichenbach, Snježana Mihalić Arbanas, David Huntley, Maneesha V. Ramesh).
- Theme 5: Climate change, extreme weather, earthquakes, and landslides (Coordinators: Vít Vilímek, Alexander Strom, Stefano Luigi Gariano, Dalia Kirschbaum).
- Theme 6: Progress in landslide science and applications (Coordinators: Zeljko Arbanas, Fawu Wang, Faisal Fathani, Beena Ajmera).

For each theme, several sessions were proposed. In total, 48 scientific sessions were organized, 643 oral presentations were delivered, and 210 e-posters were presented; the final list of the sessions with number of oral and e-poster presentations is reported in Table 4. The scientific sessions, to which only a few contributions were received, were cancelled and the contributions were moved to other sessions.

The WLF6 Proceedings can be freely downloaded from: https://wlf6.org/wp-content/uploads/2023/12/WLF6_ABSTRACT-BOOK_FINAL.pdf.

Ten workshops and side events were organized during the Forum, from November 13 to November 18 (Sect. 5).

The Closing Plenary Session took place on November 17 in the afternoon (Table 5).

During the KLC2020 General Conference 2023 and Panel Discussion (Fig. 7), the Florence Declaration on risk reduction has been adopted. The declaration is a further commitment to KLC2020, in order to share information and best practices, support research and development of new technologies, and build capacity at all levels to improve landslide preparedness and response.

The full text of the Florence Declaration is reproduced in Fig. 8 and it is also available at: https://wlf6.org/florence-declaration/.

In the afternoon session four Forum lectures were delivered from Olivier Dewitte, Xuanmei Fan, Jonathan Godt and Giovanni Battista Crosta (Fig. 9).

Table 3 WLF6 opening plenary session

9:00–10:30	**OPENING CEREMONY** Chairs: **Kyoji Sassa**—ICL Secretary General and **Veronica Tofani**—ICL Vice President and WLF6 Secretary General
9:00–9:10	**Opening address from the primary organizers** **Nicola Casagli**—ICL President and Chair of the 6th WLF **Paolo Canuti**—UNESCO Chairholder prevention and sustainable mitigation of geo-hydrological hazard
9:10–9:35	**Greetings from United Nations organizations** **Tshilidzi Marwala**—Under-Secretary-General of the United Nations / Rector of the United Nations University **Mami Mizutori**—UN Special Representative of the Secretary-General for Disaster Risk Reduction **Qu Dongyu**—Director-General of the Food and Agriculture Organization FAO **Elena Manaenkova**—Deputy Secretary-General of the World Meteorological Organization WMO **Lidia Brito**—Assistant Director-General for Natural Sciences of United Nations Educational, Scientific and Cultural Organization UNESCO
9:35–9:55	**Greetings from scientific organizations** **Motoko Kotani**—Vice-President for Science and Society of the International Science Council ISC **Mustafa B. Shehu**—President of the World Federation of Engineering Organizations WFEO **John Ludden**—President of the International Union of Geological Sciences IUGS **Chris Rizos**—President of the International Union of Geodesy and Geophysics IUGG
9:55–10:30	**Welcome messages from host organizations in Italy** **Marco Pierini**—Vice Rector of Florence University **Nello Musumeci**—Minister for Civil Protection **Anna Maria Bernini**—Minister of University and Research **Gilberto Pichetto Fratin**—Minister of Environment
10:30–11:00	**COFFEE BREAK**
11:00–13:00	**KLC2020 GENERAL CONFERENCE 2023 & HIGH-LEVEL PANEL DISCUSSION** Chairs: **John Ludden**—IUGS President
11:00–11:10	**Opening of the KLC2020 General Conference 2023** **John Ludden**—IUGS President and Chair of KLC2020 General Conference 2023
11:10–11:30	**Signing ceremony of new KLC2020 signatories** **Kyoji Sassa**—Secretary General of KLC2020 *Introduction of new KLC2020 partners:* **Zhimin Wu**—Director, Forestry Division at FAO **John Ludden**—President, International Union of Geological Sciences (IUGS) **Fawu Wang**—Professor, Tongji University, China **Jian Guo**—Professor, Tsinghua University, China **Huiming Tang**—Vice-President, China University of Geosciences, China **Rajendra Ratnoo**—Director, National Institute of Disaster Management (NIDM), India **Kaoru Takara**—President, National Research Institute for Earth Science and Disaster Resilience (NIED), Japan **Taichi Minamitani**—Director, Disaster Risk Reduction Team 1, Global Environment Department, Japan International Cooperation Agency (JICA), Japan **Shinji Sassa**—Head, Soil Dynamics Group, National Institute of Maritime, Port and Aviation Technology, Japan **Katsuo Sasahara**—Professor, Kochi University, Japan **Ryosuke Seko**—Director, Chuo Kaihatu Cooperation, Japan **Yoshiyuki Yagiura**—President, Kiso-Jiban Consultants Co., Ltd., Japan **Julijana Bojadjieva**—Macedonian Association for Geotechnics, North Macedonia **Jagath Gunatilake**—Director, Engineering Geology Research Group (EGRG), University of Peradeniya, Sri Lanka **Jonathan Chambers**—United Kingdom Research and Innovation as represented by the British Geological Survey, UK **Beena Ajmera**—Iowa State University, USA
11:30–12:45	**High-Level Panel discussion "KLC2020 Review and way forward"** Chairs: **Matjaž Mikoš and Qunli Han**—Global Promotion Committee of IPL and KLC2020 Panelists from KLC2020 partners: **Thomas Hofer**—Senior Forestry Officer at FAO **Yuki Matsuoka**—Head UNDRR office in Japan **Soichiro Yasukawa**—Chief of Disaster Risk Reduction Unit at UNESCO **Satoru Nishikawa**—International Institute of Disaster Science **Alexander Rudloff**—Secretary General of IUGG **Hiroshi Kitazato**—Treasurer of IUGS **Fabrizio Curcio**—Department of Civil Protection Italian Government **Stefano Laporta**—ISPRA, Geological Survey of Italy **Nicola Casagli**—ICL President and Chair of the 6th WLF *Explanation of the Florence Declaration*
12:45–12:50	**Adoption of the Florence Declaration on Landslide Risk Reduction** **John Ludden**—IUGS President and Chair of KLC2020 General Conference 2023

(continued)

Table 3 (continued)

12:50–13:00	**Joint photo of the panelists and the new KLC2020 signatories**
13:00–14:00	**LUNCH BREAK**
14:00–16:00	**WLF6 PLENARY LECTURES** **Chairs: Fausto Guzzetti—National Research Council and Vít Vilímek—ICL Vice-President**
14:00–14:30	**Olivier Dewitte—Royal Museum for Central Africa** **Landslides in tropical environments: insight from the East African Rift**
14:30–15:00	**Xuanmei Fan—Chengdu University of Technology** **Mechanisms and prediction of earthquake and climate change induced cascading hazards**
15:00–15:30	**Jonathan Godt—USGS** **New US National Strategy for Landslide Loss Reduction**
15:30–16:00	**Giovanni B. Crosta—Università degli Studi di Milano Bicocca** **Landslides impact on structures and infrastructures**
16:00–16:30	**COFFEE BREAK**
16:30–18:00	**RECOGNITION AND AWARDS CEREMONY** **Chairs: Peter Bobrowsky—Chair IPL Awards Committee and Irasema Alcántara Ayala—Chair IPL Evaluation Committee**
16:30–17:00	**World Centers of Excellence on Landslide Risk Reduction** • Institute of Cold Regions Science and Engineering, Northeast Forestry University, China • Croatian Landslide Group, Croatia • Charles University, Czech Republic • National Institute of Disaster Management (NIDM), India • Amrita Vishwa Vidyapeetham, Amritapuri campus, India • Universitas Gadjah Mada, Indonesia • University of Calabria (UNICAL), Italy • UNESCO Chair on Prevention and Sustainable Management of Geo-Hydrological Hazards, University of Florence, Italy • CERI—Centre for Research on Prediction, Prevention, and Mitigation of Geological Risks, Italy • Institute of Geography, National Autonomous University of Mexico (UNAM), Mexico • JSC "Hydroproject Institute", Russia • Laboratory of Engineering Geodynamics, Department of Engineering and Ecological Geology, Faculty of Geology, Moscow State University, Russia • University of Belgrade, Faculty of Mining and Geology, Belgrade, Serbia • University of Ljubljana -Faculty of Civil and Geodetic Engineering (UL FGG) and the UNESCO Chair on Water-related Disaster Risk Reduction (WR DRR), Ljubljana, Slovenia • Engineering Geology Research Group (EGRG), Department of Geology, University of Peradeniya, Sri Lanka • British Geological Survey, U.K.
17:00–17:30	**Varnes Medals** **Charles Ng**—Hong Kong University of Science and Technology—*2022 Medal* **Edward N. Bromhead**—formerly Kingston University UK—*2022 Medal* **Irasema Alcántara-Ayala**—National Autonomous University of Mexico—*2023 Medal*
17:30–17:40	**IPL-KLC Award for Success** **Maneesha V. Ramesh**—*2021-2023 Award*
17:40–17:50	**Hiroshi Fukuoka IPL Award** **Vít Vilímek** and **Jan Klimeš**—Charles University—*2021-2023 Award*
17:50–18:00	**Oldrich Hungr Awards** **Clarence Choi**—University of Hong Kong—*2022 Award* **Tommaso Carlà**—University of Florence—*2023 Award*
18:00–19:00	**WELCOME COCKTAIL**

Table 4 WLF6 scientific sessions, number of oral and e-poster presentations

Theme and session number—Title	Conveners	Presentations	
		Oral	E-poster
1.1—International programme on landslides and global and international activities for KLC2020	K. Sassa, M. Mikoš, I. Alcantara-Ayala, Q. Han, K. Konagai, C. Margottini, S. Mihalić Arbanas	23	3
1.3—Cascading multi-hazard risks: submarine landslides, tsunamis, and impacts on infrastructures	S. Sassa, D. Tappin, F. Løvholt	14	2
1.4—Landslides and society: cultural, educational, ethical and social aspects in sustainable landslide risk reduction	M. Mikoš, I. Alcántara-Ayala, B. Ajmera, P.T. Bobrowsky, G. Di Capua, C. Margottini, S. Peppoloni	15	9
1.7—Cultural heritage threatened by landslides: from earth observation and in situ investigation to sustainable mitigation measures	C. Margottini, W. Frodella, D. Spizzichino, J.I. Gallego Revilla, S. Morelli, R. Bonì, R.M. Mateos Ruiz	9	8

(continued)

Table 4 (continued)

Theme and session number—Title	Conveners	Presentations	
		Oral	E-poster
1.9—Landslides and other ground failures triggered by the february 6, 2023 M 7.7 and M 7.6 Turkey-Kahramanmaras earthquakes	C. Gokceoglu, J. Wasowski, T. Gorum, K. Onder Çetin, C. Margottini	5	0
2.1—Case studies and state of the art on landslide monitoring	P. Marr, T. Glade, C. Massey, D. Kirschbaum, R.W.M. Cheung	26	14
2.2—Integrated application of deformation monitoring techniques and process analyses of deep-seated landslides	C. Fey, C. Rechberger, C. Crippa, L. Vick	14	7
2.3—Proactive risk management based on innovative monitoring methods	D. Giordan, L.H. Blikra, G.B. Crosta, J.-P. Malet, N.J. Rosser	7	1
2.4—Multiplatform and multisensor applications for landslides characterization and monitoring	G. Rossi, S. Karantanellis, L. Loiotine, C. Tacconi Stefanelli, F. Mugnai, M. Mulas	14	5
2.5—Geophysical imaging, close-range sensing and geomodelling of landslide processes	H.-B. Havenith, V. Pazzi, S. Martino, A.-S. Mreyen, R. Schlögel	11	4
2.7—Investigation of mass movements in alpine environments with remote sensing methods	F. Agliardi, B. Dini, M. Jacquemart, A. Manconi, A. Mondini	12	8
2.8—Earth observation data for landslide prediction and risk assessment	M.T. Brunetti, G. Amarnath, S. Peruccacci, T. Stanley, L. Brocca	7	0
2.9—Past, present and future of satellite interferometry for landslides	M. Del Soldato, L. Solari, G. Bru, Q. Meng, R.M. Palau Berastegui	21	3
2.10—Soil moisture and rainfall measured through remote sensing for monitoring and predicting landslides	M. Bordoni, L. Ciabatta, E. Volpe, T. Stanley	7	2
2.11—Enhancements in landslide data analysis for improved understanding, forecasting and early warning systems	K. Sasahara, M. Hendry, E. Intrieri, R. Macciotta Pulisci, D. Elwood,	13	5
2.12—Landslide early warning systems: innovations and applications	S. Segoni, M. Stähli, N. Satyam, A. Patton, L. Piciullo, G. Devoli	21	10
3.1—Recent advancement in laboratory and in-situ testing methods for landslide and slope analyses	B. Tiwari, B. Ajmera	15	5
3.2—Natural field laboratories on landslides	S. Martino, D. Bakun-Mazor, C. Colombero, M. Ziegler	11	1
3.3—Recent advancement on slope stability and deformation analysis	B. Tiwari, B. Ajmera	14	1
3.4—Physical and numerical modelling of Landslide-Structure-Interaction (LSI)	S. Cuomo, M. Martinelli, V. Thakur, C. Choi	14	2
3.5—Rock falls and rock avalanches	G. Crosta, F. Bourrier, A. Giacomini, S. Pudasaini	18	7
3.6—Landslides prediction: advanced techniques and alternative data sources for uncertainty assessment and reduction	D.J. Peres, F. Marra, E. Leonarduzzi, C. Zhao, B. Mirus	12	2
3.7—Advancements in landslide and debris flow mitigation using geosynthetics and other solutions	K. Konagai, B. Tiwari, J. Jokela, D. Cazzuffi, S. Cuomo, Z. Arbanas	10	0
3.9—Geotechnical mitigation of landslide hazard through nature-based solutions (nbs)	M. Uzielli, V. Capobianco, F. Preti, L. Borselli	10	0
4.1—Regional and global landslide inventories: parameters and principles of compilation	A. Dufresne, X. Fan, A. Strom	12	5
4.2—Spatial landslide assessments and beyond: new challenges in mapping, modelling, validation and scenario building	T. Glade, H. Petschko, S. Steger, B. Carvalho Vieira, S. Pereira	28	14
4.3—Weak points in landslide susceptibility modelling	T. Bornaetxea, A. Braun, I. Marchesini	17	4
4.4—Shallow landslides: monitoring, modeling, predicting	M. Bordoni, R.J. Marin, S. Moreiras, J. Dou	10	5
4.5—Rockfall data: collection methods, analysis and use for hazard and risk assessments	M. Rossi, S. Melzner	15	9
4.6—Landslides in urban environments	R.M. Mateos Ruiz, R. Sarro, E. Poyiadji, M. Jemec-Auflič	16	5
4.8—Landslide impacts, vulnerability and quantitative risk assessments of people, communities, structures, and infrastructure	D. Peduto, O. Mavrouli, M. Winter, P. Salvati	29	10
4.9—Land use and slope management practices with landslide occurrence: past, recent and future challenges and adaptation strategies	C. Meisina, T. Glade, F. Catani, Y. Bamutaze	11	0

(continued)

Table 4 (continued)

Theme and session number—Title	Conveners	Presentations	
		Oral	E-poster
4.10—Landslide risk management: the challenges of transdisciplinary research in data-scarce environments	M. Micu, O. Dewitte, O. Ivanik, T. Shevchenko, J. Uwihirwe, V. Zumpano	7	0
4.11—Assessing geohazards of submarine landslides: where are we? and what are we missing?	S. Ceramicola, M. Urlaub, N. Scarselli, L. Chiocci, G. Ercilla	8	6
5.1—Landslides and climate change: processes, trends, challenges and perspectives	C. Camera, G. Rianna, M. Böhme, A. Reder, G.M. Stock	7	9
5.2—Landslides in the cold regions and extremes	C. Morin, M. Jacquemart, J. Blahůt, G. Magnarini, D. Dräbing, S. McColl	15	3
5.3—Towards a holistic understanding of landslide-induced disaster cascades in the Himalayas	S. Sen, U. Ozturk, R. Shukla, K. Cook, S. Srikrishna	7	2
5.4—Wildfire, erosion and landslide in the framework of global warming: civil protection and land management aimed at mitigation of effects on slopes induced by extreme events	G. Mandrone, D. Peduto	10	1
5.5—Advances in earthquake-induced landslide research	P. Frattini, H.-B. Havenith, G. Forte, O. Marc, S. Martino	23	3
5.6—Landslides, earth dam and levee failures during recent extreme precipitation events	D. Pradel, N.H. Jafari, M. Pando, K.S Hughes Merz, A. Morales	6	0
5.7—Timescales in evolving landscapes affecting landslide hazard and risk	Y. Zhang, D. Yue, M. Winter, T. Dijkstra, G. Chen	11	6
6.1—Advances in understanding and modelling the internal and surface deformation of landslides	L. Guerriero, L. Borgatti, D. Di Martire, M. Francioni, D. Stead	22	8
6.4—Machine learning applications in landslide science	F. Catani, X. Fan, B. Pradhan, C. Van Westen, A.P. Yunus	18	6
6.5—Hydrological monitoring, modelling, and analysis of rainfall-induced landslides	B. Mirus, L. Piciullo, E. Leonarduzzi, M. V. Ramesh, W.L. Liang, P. De Vita	9	4
6.6—Advances in understanding, quantifying and modeling the contribution of plants to slope stability	E.B. Masi, W. Wu, M. Bordoni, M. Moscariello, J.P. Galve	7	3
6.7—4D high-resolution topographic surveys to support the analysis of slope instability processes in high-steep slope agricultural and forested landscapes	S. Cucchiaro, E. Arnone, A. Beinat, P. Tarolli	6	0
6.8—Landslides in subaerial and subaqueous volcanic environments	F. Di Traglia, L. Borselli, I. Manzella, L.N. Schaefer, M. Urlaub	9	0
6.9—Landslide studies in Italy: state of the art and future perspectives	P. Revellino, D. Calcaterra, V. Tofani, A. Cevasco, M. Francioni	18	5

Table 5 WLF6 closing plenary session

16:00–17:00	**CLOSING CEREMONY** Chairs: **Snježana Mihalić Arbanas**—Chair ICL Network Committee and **Faisal Fathani**—ICL Vice-President
16:00–16:10	**Bestow of WLF6 PhD Award** for the best oral presentation held by a PhD student
16:10–16:30	**Speech by the WLF6 Forum Chair and Certificates to new ICL Members** **Nicola Casagli**—ICL President and Chair of the 6th WLF
16:30–16:50	**Speech by the new ICL President and Introduction of the new ICL officers** **Željko Arbanas**—ICL Incoming President
16:50–17:00	**Welcome Address to WLF7** **Jia-Jyun Dong and Chih-Chung Chung**—Chair and Organizer of the 7th World Landslide Forum

During the recognition and awards ceremony, the following institutions were recognized as World Centers of Excellence on Landslide Risk Reduction for their great efforts and important results in this field: Institute of Cold Regions Science and Engineering, Northeast Forestry University, China; Croatian Landslide Group, Croatia; Charles University, Czech Republic; National Institute of Disaster Management (NIDM), India; Amrita Vishwa Vidyapeetham, Amritapuri campus, India; Universitas Gadjah Mada, Indonesia; University of Calabria (UNICAL), Italy; UNESCO Chair on Prevention and Sustainable Management of Geo-Hydrological Hazards, University of Florence, Italy; CERI—Centre for Research on Prediction, Prevention, and Mitigation of Geological Risks, Italy; Institute of Geography, National Autonomous University of Mexico (UNAM), Mexico; JSC "Hydroproject Institute", Russia; Laboratory of Engineering Geodynamics, Department of Engineering and Ecological Geology, Faculty of Geology, Moscow State University, Russia; University of Belgrade, Faculty of Mining and Geology, Belgrade, Serbia; University of Ljubljana -Faculty of Civil and Geodetic Engineering (UL FGG) and the UNESCO Chair on Water-



Fig. 7 Joint photo of the panelists and the new KLC2020 signatories

related Disaster Risk Reduction (WR DRR), Ljubljana, Slovenia; Engineering Geology Research Group (EGRG), Department of Geology, University of Peradeniya, Sri Lanka; British Geological Survey, U.K. (Fig. 10).

During the awards ceremony, the Varnes Medal, the Hungr Award, the Fukuoka Award and the IPL-KLC Award for Success were presented.

The Varnes Medal 2022 was awarded to Prof. Edward N. Bromhead (Fig. 11a) and Prof. Charles Ng (Fig. 11b), the Varnes Medal 2023 to Prof. Irasema Alcántara-Ayala (Fig. 11c).

The Hiroshi Fukuoka IPL Award went to Prof. Vít Vilímek and Prof. Jan Klimeš (Fig. 12).

The Oldrich-Hungr Awards for 2022 and 2023 were presented to Clarence Choi (Fig. 13a) and Tommaso Carlà (Fig. 13b), respectively, while the 2023 IPL-KLC Award for Success was presented to Maneesha V. Ramesh (Fig. 13c).



6th WORLD LANDSLIDE FORUM
2023 FLORENCE ITALY

2023 Florence Declaration on Landslide Risk Reduction

Preamble

We, the representatives of the global landslide community, gathered in Florence, Italy, for the 6th World Landslide Forum (WLF6) from 14 to 17 November 2023, have focused on Landslide Science for Sustainable Development by providing a common platform to foster cooperation among landslide scientists, engineers, practitioners, policymakers, and other stakeholders to define shared priority actions for landslide risk reduction at the global level. Additionally, we have addressed key aspects of landslide risk reduction, including monitoring and early warning, modelling, hazard and risk assessment, mitigation techniques, triggering mechanisms, relationships with climate change, landslide risk dialogue, and capacity building for social resilience as a part of intra-sectoral multi-hazard governance.

Landslides significantly threaten communities and individuals, causing loss of life and damage to property, infrastructure, economy, and cultural, natural and environmental heritage in all types of terrains and conditions. People most affected by landslide disasters are disproportionately the poor, the marginalized, and the vulnerable, especially women and children. Like other hazards, the adverse impact of landslides undermines efforts to achieve Sustainable Development Goals (SDGs) by 2030.

As climate change is expected to increasingly affect the frequency, magnitude, and extent of heavy rainfall, forest fires, snow and ice melt, and permafrost degradation, the potential for landslides is increased at local and regional levels. Likewise, population growth and development in mountainous, steep, and coastal areas, including infrastructure construction and urban expansion due to population shifts and growth, dramatically increase exposure to landslide hazards. Moreover, the combined effects of triggering factors, including rainfall, snow and ice melt, earthquakes, volcanic eruptions, and human activity can lead to major impacts from catastrophic landslides such as debris flows, rockfalls, rockslides, lahars, and megaslides.

Therefore, understanding landslide disaster risk requires an integrated multi-hazard and multi-sectoral approach that focuses on social and institutional vulnerability to formulate effective risk management policies. In the same way, landslide disaster risk can be effectively reduced through, *inter alia*, land use and urban planning, building codes, risk assessment, early warning systems, legal and policy developments, integrated research, insurance, and, most importantly, risk education and awareness at all levels, building together an effective landslide disaster risk governance.

The effectiveness of landslide disaster risk reduction actions depends on scientific, technological, and social developments to understand the components of disaster risk, including causes and

Fig. 8 Florence Declaration

triggering mechanisms, multi-hazard, cascading effects, vulnerability, exposure, public awareness, and community resilience. This goes hand in hand with capacity building and the production of freely available educational publications and tools, supported by multi-sector, bottom-up, and top-down collaboration between governments at all levels, civil society, and scientific communities, to reduce landslide disaster risk.

In view of the former considerations, the WLF6 community COMMITS to support efforts that:

1) foster understanding and reduce the risk of landslide disasters worldwide;
2) share information and best practices, support research and development of new technologies, and build capacity at all levels to improve preparedness and response to a landslide disaster;
3) pursue and support the further implementation of the Kyoto 2020 Commitment for Global Promotion of Understanding and Reducing Landslide Disaster Risk (KLC2020) by continuing to reduce the risk and impact of landslides on the environment and society, and working with all stakeholders to make further progress in the coming years;
4) work together to raise awareness of the risks posed by landslides and promote the implementation of effective mitigation and adaptation measures, including early warning systems, safe land use planning, sustainable land management practices, risk education and awareness;
5) initiate and promote the process to organize the 7th World Landslide Forum (WLF7) in 2026 by mobilizing a medium and long-term global alliance to accelerate and incentivize landslide risk reduction actions as defined in KLC2020; and
6) submit the 2023 Florence Declaration on Landslide Risk Reduction to UNDRR for endorsement as a further commitment from the global landslide community to the Sendai Framework for Disaster Risk Reduction 2015-2030.

We CALL on:

a) new competent global, regional, national, and local institutions and entities to join and support the KLC2020 initiative as an engagement to the Sendai Landslide Partnerships 2015-2025, the Sendai Framework for Disaster Risk Reduction 2015-2030, the 2030 Agenda Sustainable Development Goals, the New Urban Agenda, and the Paris Climate Agreement;
b) landslide scientists, researchers, engineers, practitioners, policy makers, and other stakeholders to contribute to the open access book series Progress in Landslide Research and Technology, the Landslide journal and other ICL publications;
c) all stakeholders to join us in this effort and recognize the critical role of understanding and reducing landslide disaster risk in creating a safer and more sustainable future for all; and
d) related governmental, non-governmental, and international programs and initiatives from the natural, engineering, human, social, and economic sciences, both public and private, to further promote science and technology and their applications for landslide disaster risk reduction by supporting and joining KLC2020.

Adopted in Florence, Italy, 14 November 2023

Fig. 8 (continued)



Fig. 9 Plenary lecturers Prof. Olivier Dewitte (**a**), Prof. Xuanmei Fan (**b**), Prof. Jonathan Godt (**c**) and Prof. Giovanni B. Crosta (**d**)



Fig. 10 Joint photo of the World Centers of Excellence on Landslide Risk Reduction

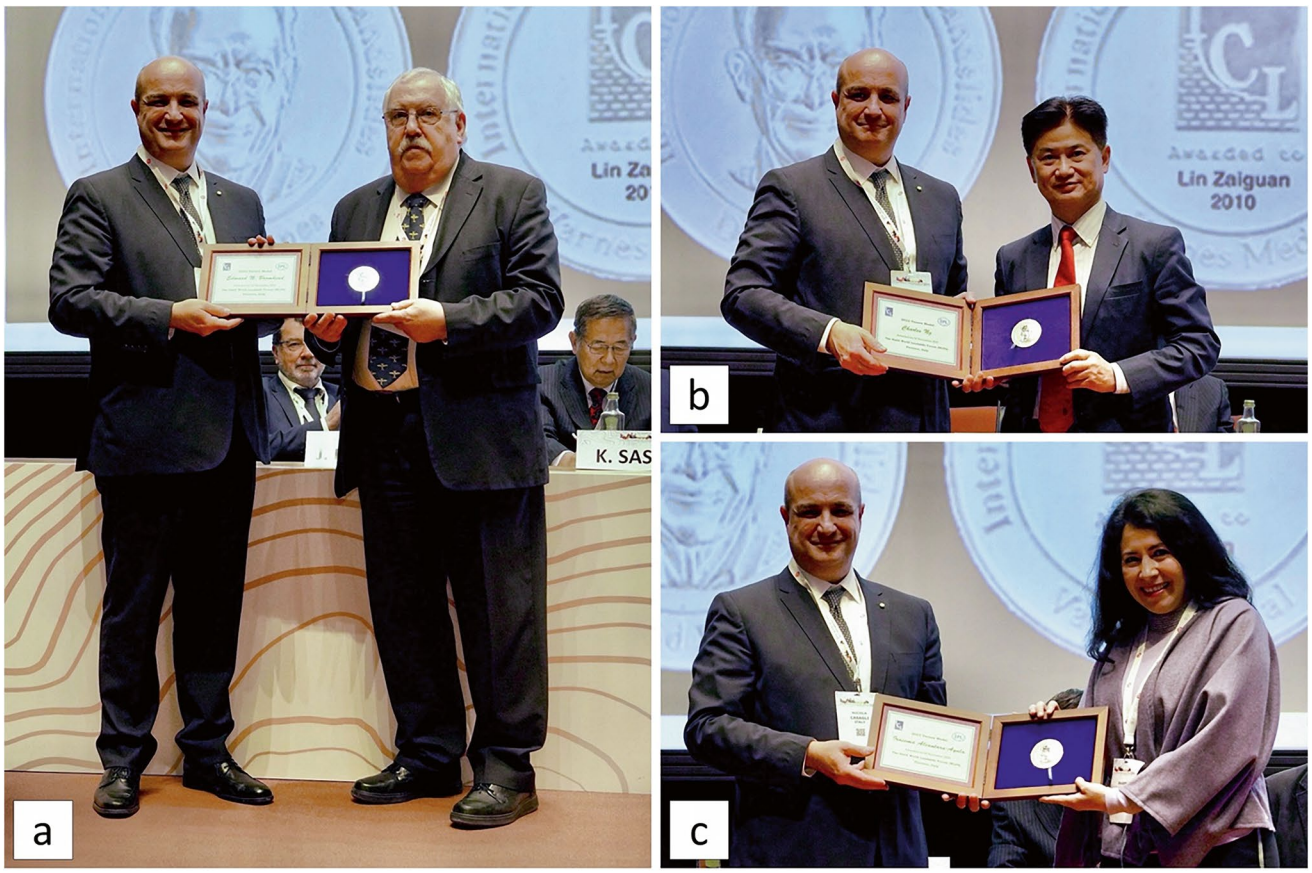


Fig. 11 Varnes Medal 2022 awarded to Prof. Bromhead (**a**) and Prof. Ng (**b**); Varnes Medal 2023 awarded to Prof. Alcántara-Ayala (**c**)

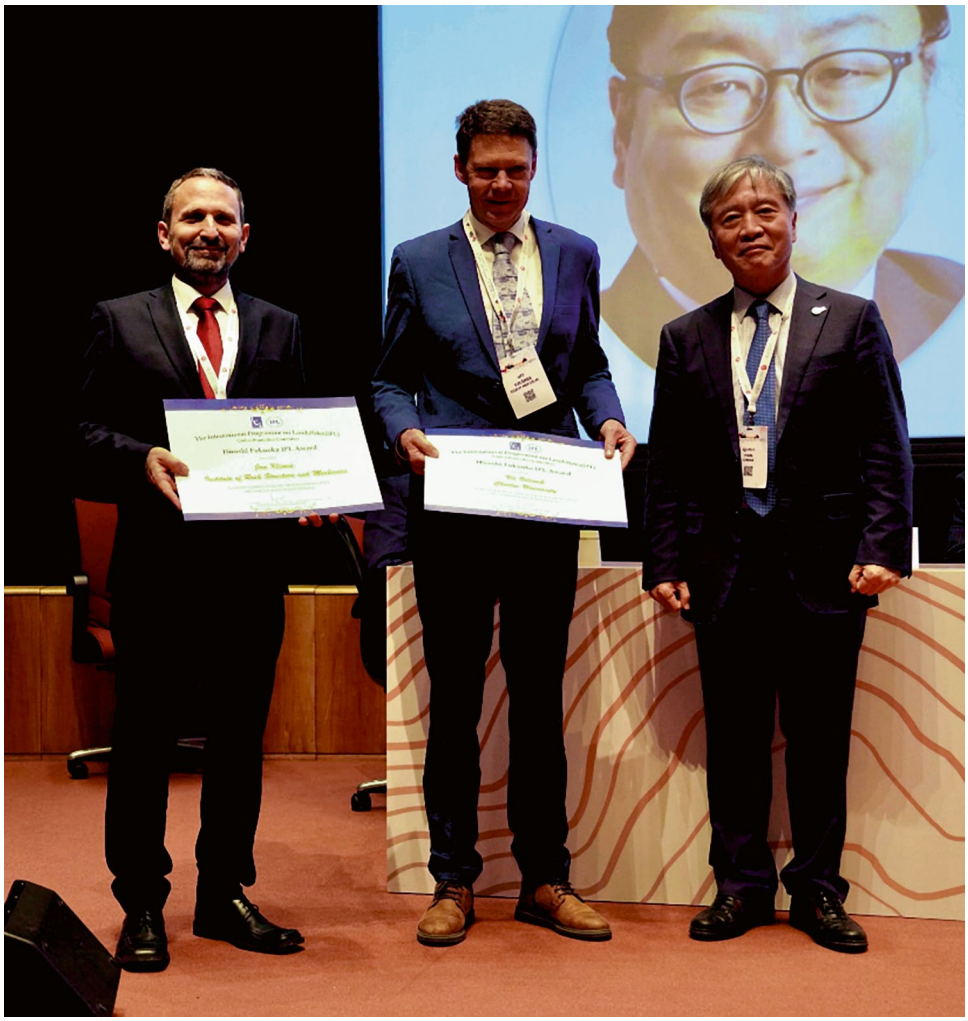


Fig. 12 Presentation of the Hiroshi Fukuoka IPL Award to Prof. Klimeš and Prof. Vilímek



Fig. 13 Presentation of the Oldrich-Hungr Awards to Clarence Choi (**a**) for 2022 and to Tommaso Carlà (**b**) for 2023; presentation of the 2023 IPL-KLC Award for Success to Maneesha V. Ramesh (**c**)

Table 6 WLF6 registered participants

Country/Region	Participants	Country/Region	Participants
Albania	1	Malaysia	1
Algeria	3	Marocco	1
Armenia	1	Mexico	2
Australia	3	Nepal	5
Austria	29	Netherlands	7
Belgium	9	New Zealand	8
Brazil	6	North Macedonia	1
Republic of Cameroon	1	Norway	32
Canada	18	Philippines	3
Chile	4	Poland	23
People's Republic of China	97	Portugal	7
Chinese Taipei	40	Puerto Rico	1
Colombia	6	Republic of Cyprus	2
Congo	4	Romania	4
Croatia	15	Russian Federation	1
Czech Republic	16	Rwanda	1
Denmark	1	Serbia	1
Ecuador	1	Slovakia	3
Egypt	1	Slovenia	5
El Salvador	1	South Korea	14
France	21	Spain	18
Georgia	4	Sri Lanka	11
Germany	39	Sweden	2
Greece	12	Switzerland	32
Hungary	1	Thailand	2
Iceland	3	Turkey	7
India	25	Uganda	1
Indonesia	1	United Kingdom	18
Iran	1	United States	37
Italy	524	Uzbekistan	1
Japan	63	Total Participants	1202

4 Participants

A total of 1202 participants from 61 countries from 5 continents attended the Forum (Tables 1 and 6).

The country/region with the highest number of participants is Italy, followed by People's Republic of China and Japan. 257 PhD students attended the Forum. During the closing plenary session, the Best PhD award presentation was bestowed to Yaser Peiro for the presentation entitled "The application of a PB slope stability model for the conservation of cultural heritage: the case study of the archaeological site of Pietrabbondante".

5 Workshops and Side Events

During the Forum, one exhibition and nine workshops and side events were organized.

Exhibition "The story of the Vajont landslide told through the photographs of Edoardo Semenza"

The "Vajont disaster" of October 9, 1963, a paradigm of a man-made catastrophe, was documented by the extraordinary photographs taken by Prof. Edoardo Semenza before and immediately after the event (Fig. 14).

Semenza was an engineering geologist and one of Italy's leading landslide researchers. He discovered the presence of an ancient landslide mass on the southern side of the Vajont valley, upstream of the reservoir under construction, years before the first mobilization. His discovery was immediately considered by the designers and project managers of the dam as a hypothesis to be verified by further research and investigation. Unfortunately, his work could not prevent the disaster.

The exhibition, organized on the occasion of the sixtieth anniversary of the Vajont disaster, aimed to raise awareness of the fundamental role that knowledge of geology plays in respecting and protecting the environment.

RETURN Project workshop

(November 15, 8:30–13:00)

The Forum hosted a workshop organized by Fondazione RETURN entitled "Multi-risk science for resilient communities under a changing climate—ground instabilities: from back learning to forward scenarios in a multihazard resilience perspective".



Fig. 14 Exhibition on the Vajont landslide

The RETURN project (multi-Risk sciEnce for resilienT commUnities undeR a changiNg climate project) aims to provide multihazard scenarios related to ground instabilities that can be used to plan countermeasures to increase the resilience of urban areas, infrastructures and communities towards greater sustainability.

The workshop was open to the participants of the RETURN project registered at WLF6 and was organized to communicate the ongoing results and to discuss among the researchers involved in the project how to apply the tools identified so far to the reconstruction of scenarios.

TRE ALTAMIRA side event

(November 15, lunch break 13:00–14:00)

TRE ALTAMIRA organized the side event entitled "Advancing geohazard monitoring: leveraging satellite radar data from wide area analysis to targeted local studies".

Spaceborne radar interferometry is becoming a key tool for wide-area mapping of ground deformation and for monitoring programs. The expanding array of satellite data sources has opened up unprecedented opportunities for interferometric applications, prompting a shift from a static view of the Earth's surface to a continuous stream of space-based ground motion measurements.

The workshop aimed to demonstrate the potential of satellite interferometric data as a powerful tool for monitoring and risk management. Through a series of compelling case studies, speakers demonstrated how these data can raise awareness among local and regional authorities of the critical need for proactive geohazard mitigation.

Ferrovie dello Stato Group side event

(November 15, lunch break 13:00–14:00)

The Forum hosted a side event organized by the Ferrovie dello Stato Group entitled "Sustainable and resilient rail and road infrastructures: landslide management and climate adaptation—when the infrastructural network generates connections".

The Ferrovie dello Stato Group promotes territorial studies, as well as the research, design and implementation of measures to manage the extensive interaction of landslide phenomena with transport infrastructures.

The "Resilience Transformation Roadmap" aims to improve the resilience of infrastructure by (i) defining climate adaptation guidelines with decision support tools; (ii) strengthening sensor networks and developing monitoring systems to cope with extreme events; (iii) forecasting models for the occurrence of extreme events.

LiSALab side event

(November 16, lunch break 13:00–14:00)

LiSALab organized the side event entitled "2003–2023—twenty years of GbInSAR natural hazard and landslide monitoring: worldwide examples and case studies".

The workshop aimed at reviewing the past 20 years, during which three experienced users described their experiences in monitoring natural hazards, particularly landslides, through the operational use of GbInSAR technology, including in emergency scenarios.

The first presentation focused on monitoring natural hazards such as volcanoes or during emergencies. The second presentation showed the application of this technology in environmentally challenging conditions, such as those found in Nordic environments, with low temperatures and high latitudes. The third presentation discussed the application of this tool in the Alpine region.

Studio Pandolfi workshop

(November 16, lunch break 13:00–14:00)

Studio Pandolfi promoted the workshop entitled "Innovative monitoring and modelling for rock slopes' stability: the Carrara marble quarries".

The Carrara marble quarries are known for their excellence in stone quarrying due to several factors: the concentration of quarries in a limited geographical area which have been cultivated for over two thousand years, the innovative technologies used, and the significant scientific research carried out over the years by numerous research institutions.

The workshop was the first in a series of technical-scientific events. It aimed at promoting the exchange and sharing of knowledge and best practices in ornamental stone quarrying.

LARAM School side event

(November 16, lunch break 13:00–14:00)

The Forum hosted the LARAM School side event entitled "LARAM Alumni Event—from 2006, to today, towards the future".

After attending the LARAM School, organized by the University of Salerno (Italy), many lecturers and students from different annual courses have met at various scientific events, including recurring conferences such as the World Landslide Forums, the International Symposiums on Landslides and the assemblies of the European Geosciences Union.

The workshop aimed to bring together LARAM alumni who are still active in the field, holding prestigious positions in academic institutes or other institutions after attending the LARAM course and therefore facing landslide problems and challenges daily.

Hexagon side event

(November 17, lunch break 13:00–14:00)

The Forum hosted a side event organized by Hexagon entitled "Total Monitoring: use cases, new tools and challenges in natural hazard monitoring".

Hexagon is a global leader in digital reality solutions, that combine sensors, software and autonomous technologies. The core of Hexagon Geosystems is represented by IDS GeoRadar, Geopraevent and Leica Geosystems, which offer technologically advanced solutions that combine monitoring technologies to provide real-time insight into movement. This is the result of the combined experience of several thousand monitoring projects in over one hundred countries.

During the event, participants were introduced to "Total Monitoring", a concept of using a combination of technologies to provide reliable information about movement in the monitored area and the most advanced technologies to improve early warning and situational awareness.

GeoSciences IR workshop

(November 17, 14:30–16:00)

The GeoSciences IR project organized a workshop on "New technologies for landslide monitoring and mapping".

GeoSciences IR is a project funded by the NextGenerationEU program, with the aim of creating a research infrastructure for the Italian Network of Regional Geological Surveys. The project involves 16 partners from academic and research institutions.

The GeoSciences IR event at WLF6 aimed to present innovative landslide monitoring techniques, methods for landslide mapping and inventory updating, landslide risk analysis and mitigation measures implemented in the project.



Fig. 15 A group of participants to the Florence walking tour

"Here be landslides: Florence from Romans up to now" side event

(November 13, 9:30–17:30; November 18, 9:30–13:00)

On November 13 and 18, some researchers from the University of Florence acted as local guides for a three-hours walking tour of Florence's most impressive monuments, anecdotes and places (Fig. 15).

Following the historical footsteps of Leonardo Da Vinci and the powerful Medici family, a non-technical and interactive tour showed the deep connection between the local geology and the history of Florence, from its foundation to the present days, highlighting some of the most remarkable monuments and palaces built since medieval time: their very stones can tell a fascinating story, often forgotten by Florentines, and show hidden scars from ancient and recent hazardous events such as floods and landslides.

References

Casagli N, Canuti P, Sassa K, Tofani V (2022) The Sixth World Landslide Forum (WLF6) on November 14-17th, 2023, Florence, Italy. Landslides 19(10):2539–2545

Casagli N, Canuti P, Sassa K, Tofani V (2023) The Sixth World Landslide Forum (WLF6): call for abstracts. Landslides 20(2):707–716

Sassa K (2015) ISDR-ICL Sendai Partnerships 2015–2025 for global promotion of understanding and reducing landslide disaster risk. Landslides 12(4):631–640

Sassa K (2021) The Kyoto Landslide Commitment 2020: launched. Landslides 18(1):5–20

Open Access This chapter is licensed under the terms of the Creative Commons Attribution 4.0 International License (http://creativecommons.org/licenses/by/4.0/), which permits use, sharing, adaptation, distribution and reproduction in any medium or format, as long as you give appropriate credit to the original author(s) and the source, provide a link to the Creative Commons license and indicate if changes were made.

The images or other third party material in this chapter are included in the chapter's Creative Commons license, unless indicated otherwise in a credit line to the material. If material is not included in the chapter's Creative Commons license and your intended use is not permitted by statutory regulation or exceeds the permitted use, you will need to obtain permission directly from the copyright holder.



How to Detect the Previous Large-Scale Landslide: Source of Future Landslides by Interpretation of Ground Topography from Digital Maps

Toyohiko Miyagi and Doan Huy Loi

Abstract

Large-scale landslides often occur in the same place as previous landslides. Determining the location of potential future landslides is crucial and helpful for reducing landslide risk. In this paper, we compared the landslide topography distribution map and the 2011 landslide disasters in the Kii Peninsula to determine the overlap of new landslides in 2011 and past landslides. We found that over 60% of large-scale landslides took place in areas where previous landslides had been identified in the landslide topography distribution map. Following this finding, we created the landslide distribution maps for four regions in Sri Lanka from AW3D data to assess the risk of large-scale landslides.

Keywords

Large-scale landslide · Digital maps · Sri Lanka · Landslide topography

1 The Basic Steps of Landslide Topography Detection and Some Difficulties by DTM

Definition of Landslide Topography and Focus on Its Detection

The topographic area formed by landslide activity is called "Landslide topography". In a broad sense, landslide is a general term that refers to slope movement.

There are various opinions on the definition of "landslide" itself. However, in a large-scale landslide topography with a slippery surface (hereinafter referred to as a landslide topography), even if a landslide-like failure occurs on the part of the slope, the land that has been moved, deformed, or altered is subject to a landslide. It has the characteristic of remaining on slopes as.' 'This becomes the material for the next slope movement to occur.

With this feature, identifying the area of landslide topography is highly effective in considering slope disaster prevention.

Landslides are a phenomenon of deformation of the ground surface. Therefore, by carefully observing the topography, it is possible to determine where and how landslide topography formed by landslide action exists.

Whether the tool for topographical interpretation is aerial photography, which has been used for a long time, or digital 3D information, which has become popular in recent years, if the material to be observed is accurate and 3D data, it is possible to understand the earth's surface. You will be able to understand the situation accurately.

Technology for sensing terrain has developed dramatically, particularly in the last five years. However, various difficulties are involved in determining whether this development has led to the ability to understand the existence of landslide terrain easily.

Aerial Photographs Interpretation and Landslide Topography Distribution Map

The existence of landslide terrain is thought to be widely known. It is well known that slopes move slowly, significantly deforming houses, roads, and river channels, and sometimes moving significantly, causing devastating disasters. So, if you ask me, "Has sufficient consideration been given to understanding the landslide topography and considering the relationship between the slope disaster at hand?' 'I have to say that this is somewhat insufficient. Japan has spent 20 years since 1985 understanding the distribution of LSLS

T. Miyagi (✉)
International Consortium on Landslides (ICL), Kyoto, Japan

D. H. Loi
International Consortium on Landslides (ICL), Kyoto, Japan

Institute of Transport Science and Technology, Hanoi, Vietnam

© The Author(s) 2025

B. Abolmasov et al. (eds.), *Progress in Landslide Research and Technology, Volume 3 Issue 2, 2024*, Progress in Landslide Research and Technology, https://doi.org/10.1007/978-3-031-72736-8_18

across the country. Since 2005, the distribution information on large-scale landslides has been compiled into a GIS database and made available to the general public.

Efforts to understand the distribution of landslide topography in Japan began around 1977. Initially, there was extremely little awareness of "land formed by landslide activity' 'itself. However, as stereoscopic interpretation of aerial photographs became a routine practice, it began to be pointed out that landslide topography was widely distributed.

Furthermore, it has been pointed out that large-scale landslides frequently reactivate during national infrastructure development, such as dams and highways. As stated in the title of this report, large-scale landslides can now be considered both previous large-scale landslides and sources of future landslides.

2 Detection of Landslide Topography Using a Digital Map

If contour lines accurately reproduce the shape of the earth's surface, would anyone be able to easily determine them, even if they have never studied topography? Although this is only empirical knowledge, the answer is no. Various types of 3D information are visualized, such as shaded maps, anaglyphs, and three-dimensional maps, and this is similar. Needless to say, it is impossible to understand the phenomenon without a prerequisite understanding that landslide areas are like this.

ABCs of Large-Scale Landslide Judgment

Varnes (1978) is a classic example of a large-scale landslide. He focused on the fact that large-scale landslides occurred at various locations during the construction of highway networks in the United States and examined the causes of these disasters by combining aerial photo interpretation, aircraft observation, and field surveys. He shows a sketch of a typical landslide (Fig. 1). Based on this diagram we will briefly explain what morphological characteristics a landslide has and how they can be understood using contour lines aerial photographs, and various 3D information.

As shown in Fig. 1, the landslide area can be distinguished from the surrounding non-landslide slope by clear slope conversion lines at the steep slopes of the sliding cliffs and in the sedimentary regions. In particular, the cliff at the top of the landslide area is a large steep slope. If the type of landslide slumps, this sliding cliff continues with the underground slip surface. The main sliding scarp immediately after the deformation is the easiest to recognize among the sliding landforms. The area surrounded by the main cliff and side cliffs is the upper half of the landslide body. In the upper half of the moving body, microtopography such as secondary cliffs and parallel cracks to the direction of movement are distributed. As shown in the figure, the soil mass that has been moved by arc sliding (backward rotation) is often subdivided into large blocks, resulting in microtopography such as secondary cliffs, which may slope toward the main cliff. Ponds and marshes can sometimes be seen on slopes with reverse slopes. The lower half of the moving body (foot) spreads downward from the area where the side cliffs disappear. This is because a part of the soil mass moved by the circular sliding surface overflowed below the sliding surface area. This part was caused by overflowing flow during the process of slumping landslide, and the fracture has progressed relatively. The earth and sand at the tip of the moving body progress in fragmentation and tend to spread, and the microtopography characteristic of landslide topography easily disappears. Landslide terrain has its own built-in reactivation potential. The possibility of reactivation needs to be estimated and evaluated based on the characteristics of the landslide topography. From this point of view, the characteristics shown in Fig. 1 are probably the result of the vivid

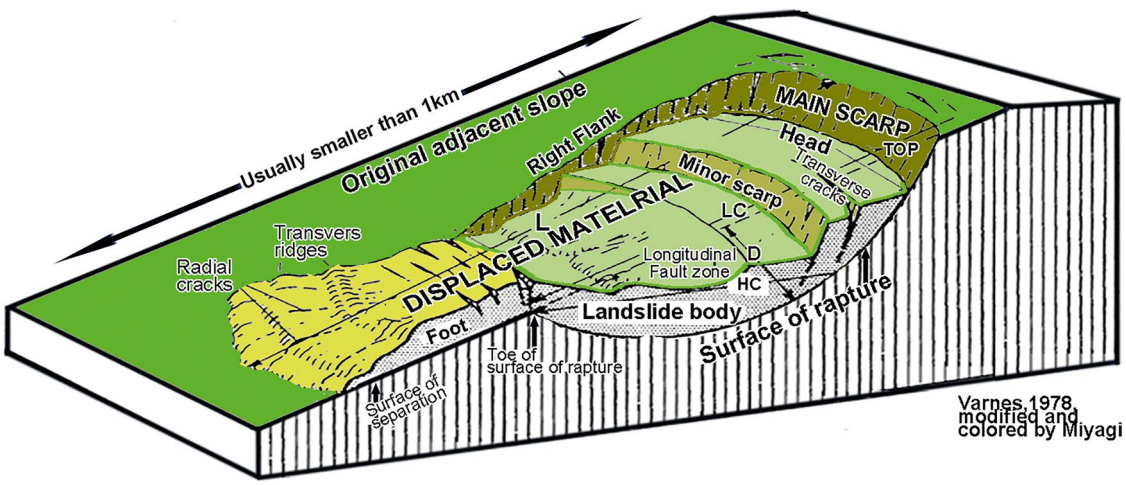


Fig. 1 Microtopographic features immediately after changes in landslide tendency (additions and coloring to the figure from Varnes 1978)

changes seen immediately after large-scale landslide activity. Landslide topography caused by a landslide is subject to constant weathering and erosion immediately after its formation, waiting for an opportunity, such as a rise in the groundwater level due to heavy rain or strong seismic motion to trigger the next landslide reactivation. River erosion and human-induced topographical changes also have a significant impact. The landslide area may become partially unstable due to these processes. This is the reason why landslide changes occur intermittently.

If landslide topography is mapped as a result of landslide movement, a huge number of locations will be identified, as will be discussed later in this paper. However, it is unlikely that these landslide features have the same potential for reactivation. In the future, it will be necessary to identify areas with a high risk of reactivation from among the vast landscape of landslides.

What Kind of Digital Data Complies with LSLS Detection?

There are always issues to remember when creating contour lines and mapping landslide topography. DTM is generally considered to represent topography. For example, the last pulse of point cloud data using LiDAR used to obtain high-precision grid data is data that indicates the shape of the ground. In recent years, it has become common to acquire and analyze this LiDAR data when understanding the fine structure of landslide topography. However, the accuracy of DTM changes depending on the density of the point cloud. For example, the authors created data on Japanese mangrove forests and their forest floor microtopography (Makabe et al. 2015; Unome 2020); when the tree crown coverage exceeds 85%, the point cloud density becomes as high as 100+/m^2. Even if high-precision equipment is used, the point cloud density reaching the ground surface will drop to less than 1/m^2, and it may not be possible to guarantee accuracy that meets the survey objectives.

In addition, when DSM based on photogrammetry data such as AW3D (JAXA/RESTEC/NTT data) is used as primary data, the vegetation cover-based DTM obtained by DSM has an accuracy of analogy of topographical amount depending on the degree of vegetation cover. May change significantly. The accuracy characteristics of data sources should always be kept in mind. To be clear, the relationship between DSM and the DTM that is generated based on it is similar to the relationship between aerial photographs and contour maps. If the plant cover is so dense that the ground cannot be seen, it is common to subtract the tree height from the DSM and convert it into DTM data. In this case, when comparing the DSM obtained at the ridge, valley wall slope, and valley floor, there is no difference in altitude between the DSM and DTM because the valley floor generally lacks forest cover. On the other hand, other slopes have bark grafting, so the tree height will be subtracted from the DSM. As a result, there is a possibility that the representation of the actual terrain in DTM may be biased.

Additionally, it is necessary to pay attention to the relationship between grid size and landslide topography representation. The left side of Fig. 2 is a three-dimensional topographic map (Ikeda 2021; Miyagi et al. 2024) constructed from 5 m and 10 m DTM data based on the 1 m DTM acquired in Japan. Grid size greatly affects the amount of calculation. The right side of Fig. 2 is the author's interpretation of the landslide topography depicted in the three-dimensional topographic map on the left (Miyagi et al. 2024). The microtopography that can be read varies greatly depending on the density of point cloud data. The 1 m grid allows a detailed understanding of the fine structure of the landslide topography. With a 10 m grid, visibility is significantly reduced. In Fig. 2c, areas where the characteristic microtopography has become unclear are indicated by white lines. Even with this accuracy, the part corresponding to the main cliff can be easily identified.

Points to Note When Landslide Topography Mapping

Landslide topography can be understood and mapped by aerial photo interpretation, contour lines created using DEM, or three-dimensional topographic maps. However, each data has its own strengths and weaknesses, so it is necessary to understand the characteristics of the data itself before using it. Furthermore, it is also true that the knowledge of the observers who map the landslides by observing the landslide topography forms the basis of their interpretation. This report compares the results of landslide topography interpretation and mapping work conducted in Sri Lanka with the locations where slope disasters have occurred. It was found that there was a corresponding response between the two. The following shows the possibility of understanding the likelihood of the next landslide disaster occurring by understanding the landslide topography resulting from landslide activity.

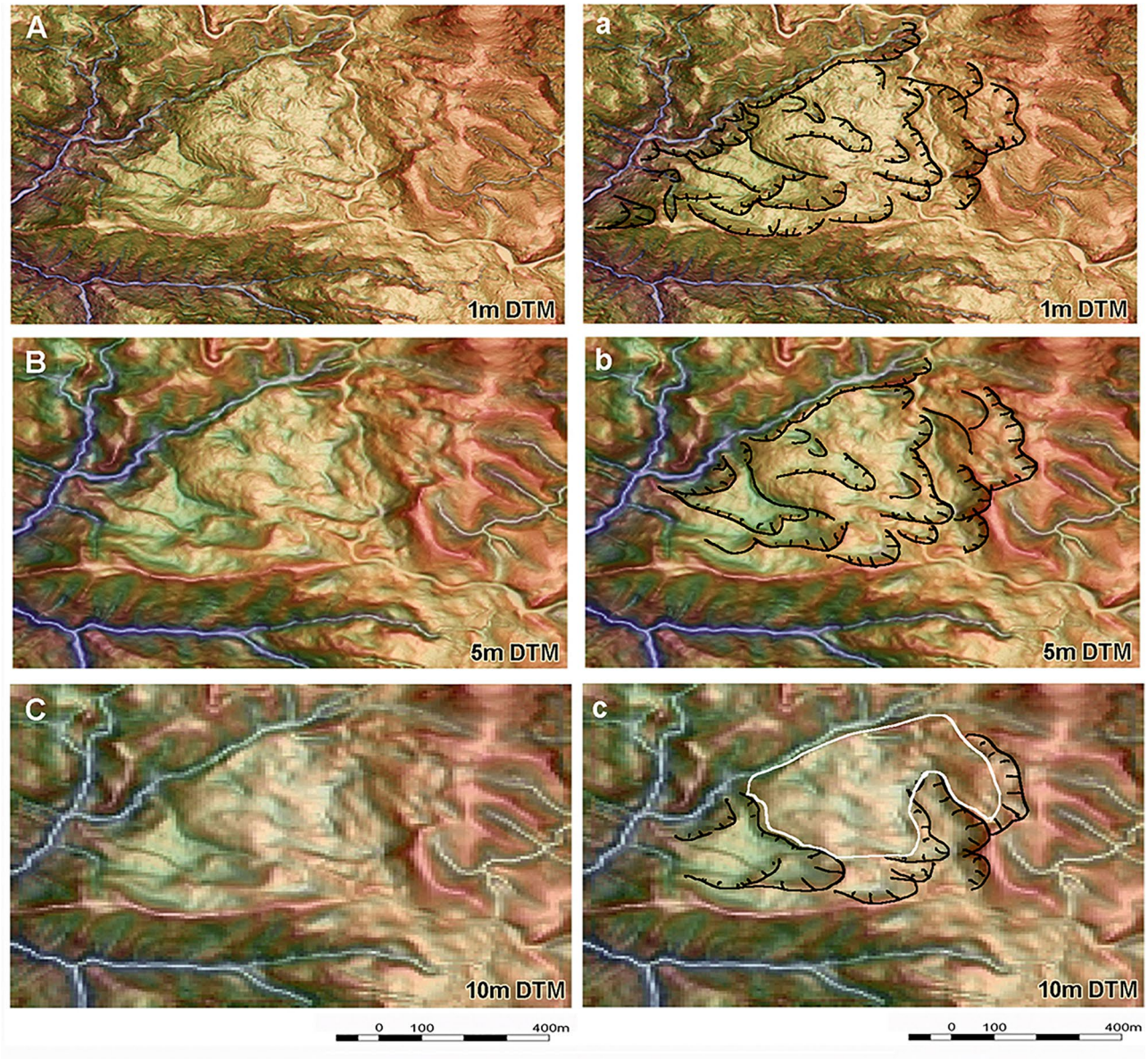


Fig. 2 Extraction of landslide topography (especially cliff topography) using a three-dimensional topographic map created using DTM

3 Large-Scale Landslides Follow Past Landslides: A Case Study in the Kii Peninsula

Detaining the location of future landslides is crucial to reducing the risk. A detailed and trustworthy landslide map would be beneficial. Landslides often occur in the same place as previous landslides (Temme et al. 2020). Japan spent tremendous effort mapping the distribution of landslides throughout the country. Fortunately, the data has been published and is now available for download on the website: https://dil-opac.bosai.go.jp/publication/nied_tech_note/landslidemap/gis.html.

NIED published the landslide distribution map in Kii Peninsula, Japan, in 2005. It was developed by interpreting monochrome aerial photographs taken in the 1970s at a scale of 1:40,000 using a simple stereoscope. The landslide topography distribution map did not interpret small-scale landslides.

The Kii Peninsula, a steep mountainous area, is commonly damaged when typhoons hit Japan due to its susceptibility to heavy rainfall (Hefryan et al. 2016). The 2011 Kii Peninsula landslide in Japan was a catastrophic event triggered by record-breaking rainfall due to Typhoon 12, also known as Typhoon Talas (Saito and Matsuyama 2012). This typhoon hit the Kii Peninsula in September 2011, causing over 3000 landslides (Tien et al. 2018). The

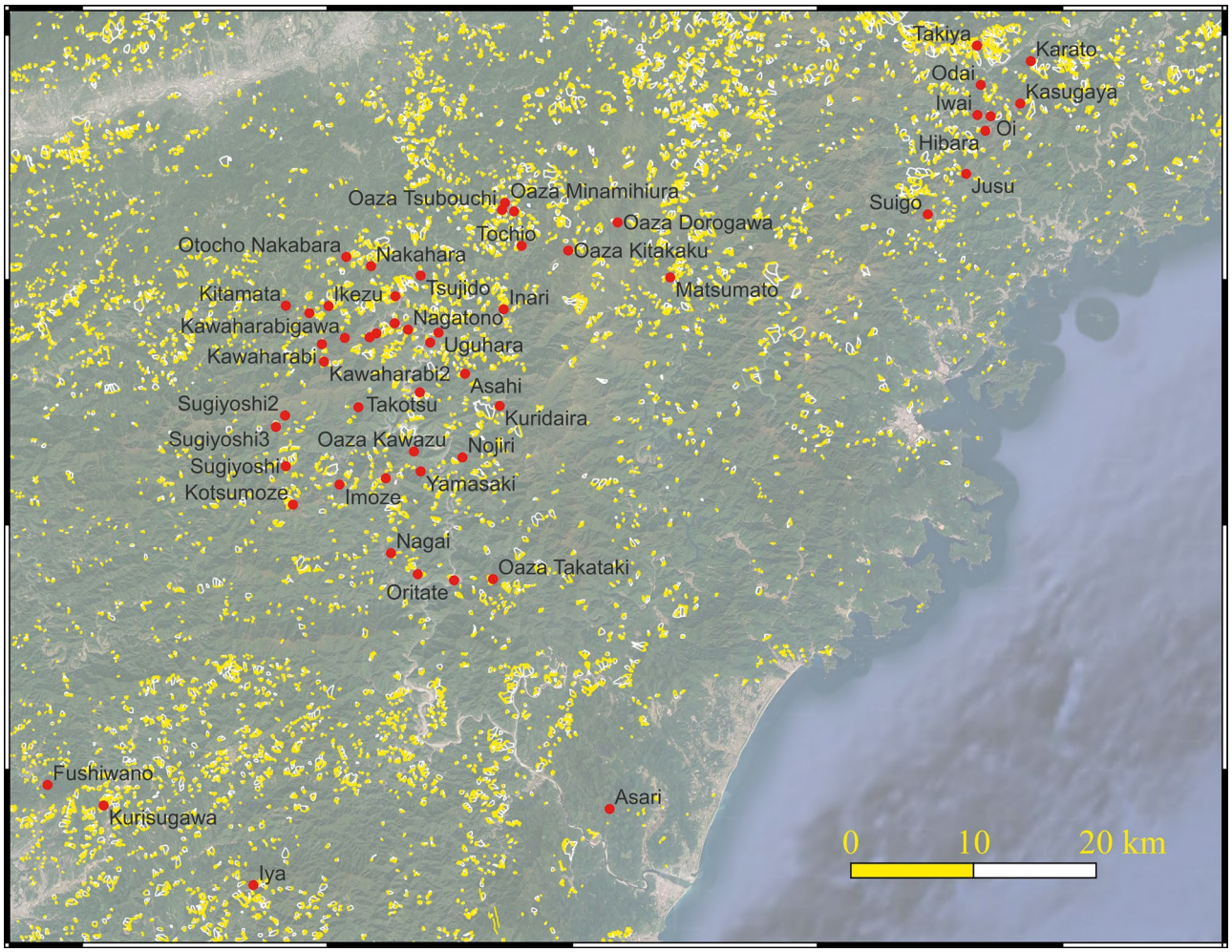


Fig. 3 Landslide distribution map and location of large landslides in the 2011 disaster in the Kii Peninsula (Landslide distribution was mapped by NIED)

total amount of sediment-related disasters caused by Typhoon Talas was approximately 100 million m^3 (Hefryan et al. 2016).

Figure 3 shows the location of 54 large-scale landslides in 2011 and the landslide distribution map published in 2005. The landslide location was based on the report of the Geospatial Information Authority of Japan and a comparison of Google Earth photos before and after the 2011 event. The number of landslides overlapping the previous landslide was 36. The rate was 36/54 = 66.7%.

Examples of 2011 Landslides Follow Past Landslides

In this section, we briefly introduce some large-scale landslides from 2011.

The Kuridaira landslide in Japan was the largest in the Kii Peninsula in 2011, at 34.075°N, 135.837°E. It is about 680 m long, 600 m wide, 74 m thick, and has a volume of 14 × 106 m^3 (Chigira et al. 2013). The landslide mass moved to the river, forming a landslide dam up to 100 m high (Tien et al. 2018). The Kuridaira landslide took place in the two former landslides areas. The head scrap on the left side is the same as that of the mapped landslide, while the right one is located upper than the mapped one. Figure 4a clearly indicates that the largest landslide in the 2011 event was identified.

The Akatani landslide (Fig. 4b) was another significant event that occurred at 16:21:30 on September 4, 2011 (Yamada et al. 2016). It was located at 34.126°N, 135.725°E, about 902 m in length, 400 m in width, 56 m in maximum depth, and 8.2 × 106 m^3 in volume (Chigira et al. 2013). A dam was formed due to the landslide displaced mass. In this example, the mapped landslide was smaller actual landslide. The reason may be due to the retrogression of the landslide; the landslide may have occurred at the lower part of the Akatano landslide, and after that, failure was expanded to upslope. The Akatani 2 landslide and a mapped one have almost the same shape.

The Akatani East landslide was located at 34.134°N, 135.741°E, about 1.4 km away from the Akatani landslide. It

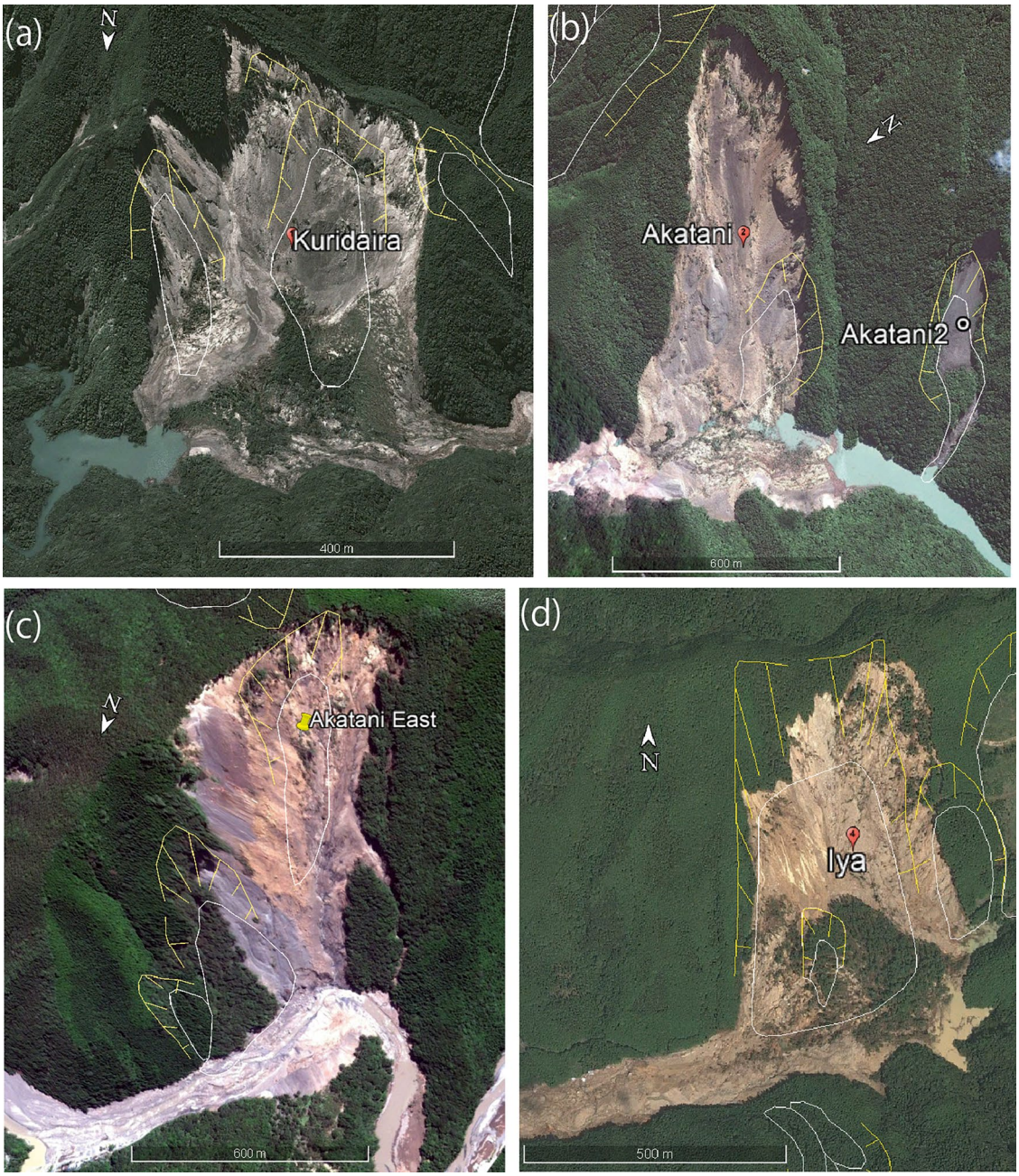


Fig. 4 Overview of (**a**) Kuridara landslide, (**b**) Akatani landslide, (**c**) Akatani East landslide, (**d**) Iya landslide

had a length of around 820 m, a thickness of 22 m, a width of 480 m, and a volume of 2.1 × 106 m^3 (Chigira et al. 2013). Although the Akatani East landslide is much larger than the mapped landslide, the head scarps are in the same place. It's possible that the left toe of the current landslide is a constituent of a previous landslide (Fig. 4c).

The Iya landslide was located at 34.134°N and 135.741°E and occurred at the top of the slope. The landslide mass flowed downstream along the Iya River, and the landslide dam was formed. The landslide was about 680 m in length, 400 m in width, 70 m in maximum depth, and 5.2 × 106 m^3 in volume (Chigira et al. 2013). Google Earth image after landslide shows that the Iya landslide shape and location are similar to a mapped landslide (Fig. 4c).

One example of a long-traveling landslide is the Otocho Nakabara landslide. The Othocho Nakabara landslide was located at 34.182°N, 135.696°E and was 310 m in length and 173 m in width. The landslide occurred on the ridge top and moved more than 1 km to the downslope (Fig. 5). The head scrap and the size of the mapped landslide were the same as the Othocho Nakabara landslide.

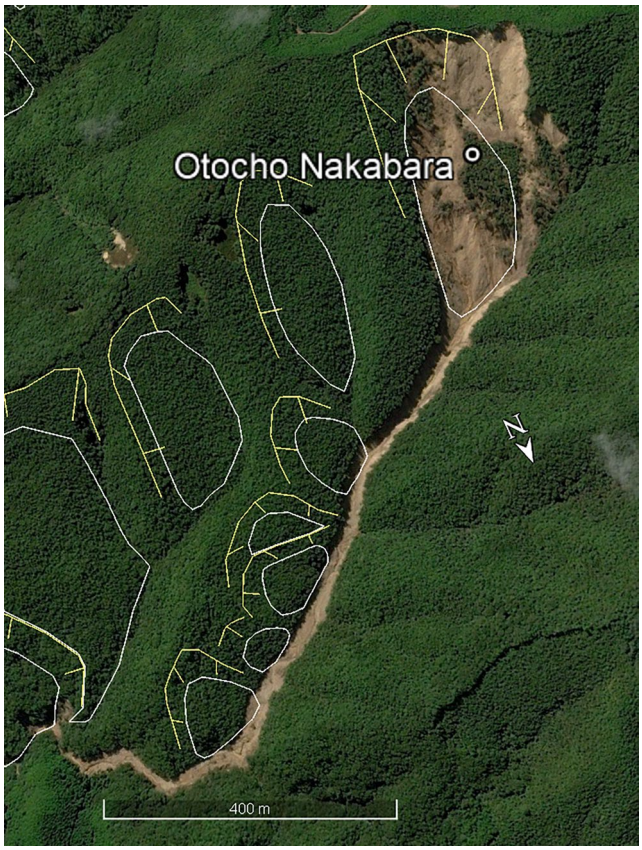


Fig. 5 A long-travelling landslide in Othocho Nakabara. The Google Earth image was taken in September 2011

The yellow line is the head scarp, the white polygon is the landslide body. The Google Earth images were taken in September 2011.

Figure 6 shows three landslides in the Tsubouchi area. The largest block is Tsubouchi 2, which is about 360 m wide, 255 m long, and 1.2×106 m^3 in volume (Chigira et al. 2013). All three landslides were determined in the 2005 landslide distribution map.

4 Landslide Topographic Distribution Map in Sri Lanka

Landslides commonly trigger disasters in Sri Lanka. They are often triggered by heavy rainfall during the monsoon seasons.

The Aranayake landslide was a significant disaster in Sri Lanka in 2016. The landslide occurred in Aranayake, Kegalle District, Sri Lanka, on May 17, 2016. The landslide was triggered by heavy rainfall. From May 14 to 17, the rainfall reached 446.5 mm, and the landslide moved a distance of approximately 2 km (Dang et al. 2019). It resulted in the death of about 127 people and destroyed 75 houses.

The 2017 floods and landslides in Sri Lanka were a significant disaster that profoundly impacted the country. According to the Disaster Management Center, the 2017 disaster affected 631,346 people of 164,264 families, resulting in 203 deaths and 96 missing persons.

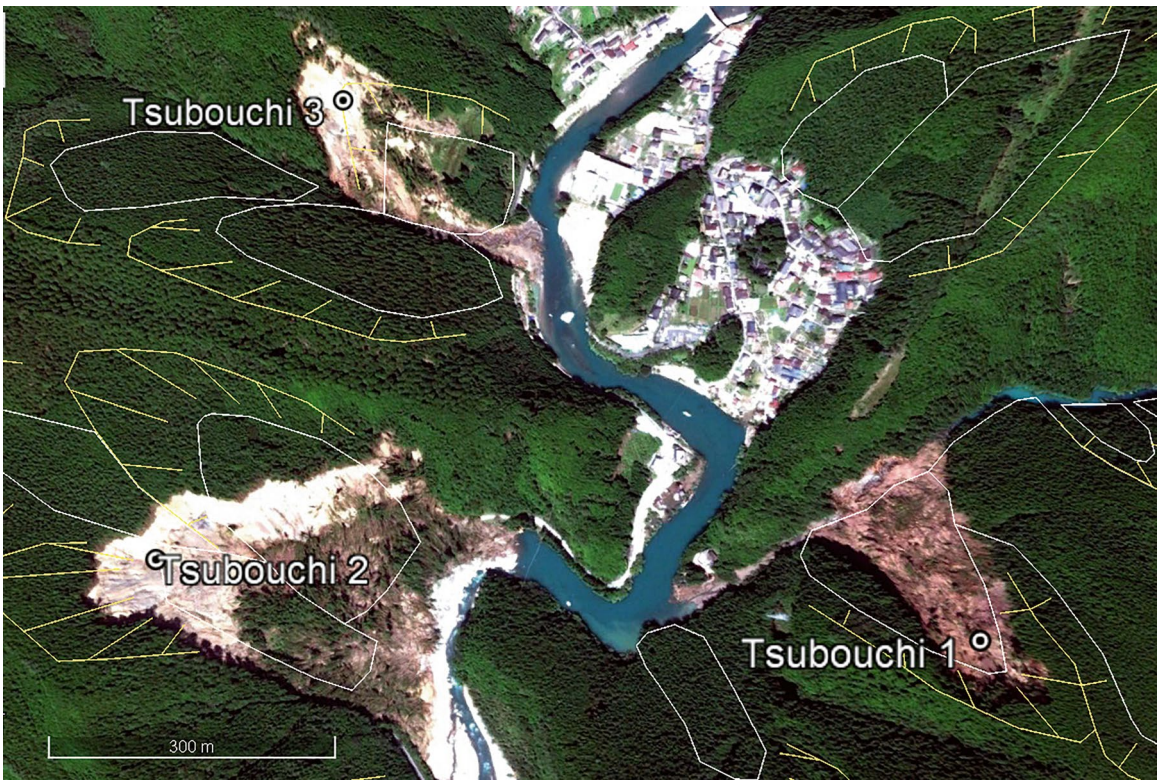


Fig. 6 Overview of three landslides in Tsubouchi. The Google Earth image was taken in September 2011

These events highlight the significant impact of landslides on the people and infrastructure of Sri Lanka. Efforts are ongoing to manage and mitigate the effects of these disasters.

National Building Research Organization (NBRO), Sri Lanka and the International Consortium on Landslides (ICL) applied the SATREPS Project (Science and Technology Research Partnerships for Sustainable Development), "Development of Early Warning Technology of Rain-Induced Rapid and Long-Travelling Landslides in Sri Lanka" to understand and reduce the landslide risk. SATREPS Project is funded by the Japan International Cooperation Agency (JICA) and the Japan Science and Technology Agency (JST). During this project, we purchased AW3D data to study the landslide topography in Sri Lanka.

Figure 7 shows an example of mapping the landslide topography in the Kalutara district. The landslide occurred in 2017 killed 8 people and damaged 16 houses. A 5 m contour map (Fig. 7a) was generated from a 2.5 m resolution AW3D taken after the 2017 event, showing the significantly changed contour in the landslide area. Based on the contour changing, the landslide topography was mapped in Fig. 7b. The relief map created with Surfer software using AW3D data indicates the landslide area. Figure 7d shows a landslide which has 150 m width at the middle, a UAV photo of a landslide which has a 150 m width in the middle and a 670 m in length.

Mapping Results

During this project, we conducted landslide distribution maps in Aranayake, Kandy, Athelthota and Kotmale. We introduced some maps of four areas in Figs. 8, 9, 10 and 11.

Contour lines were generated with 5-m spacing from AW3D 2.5 m DSM data for the Kandy area in the central

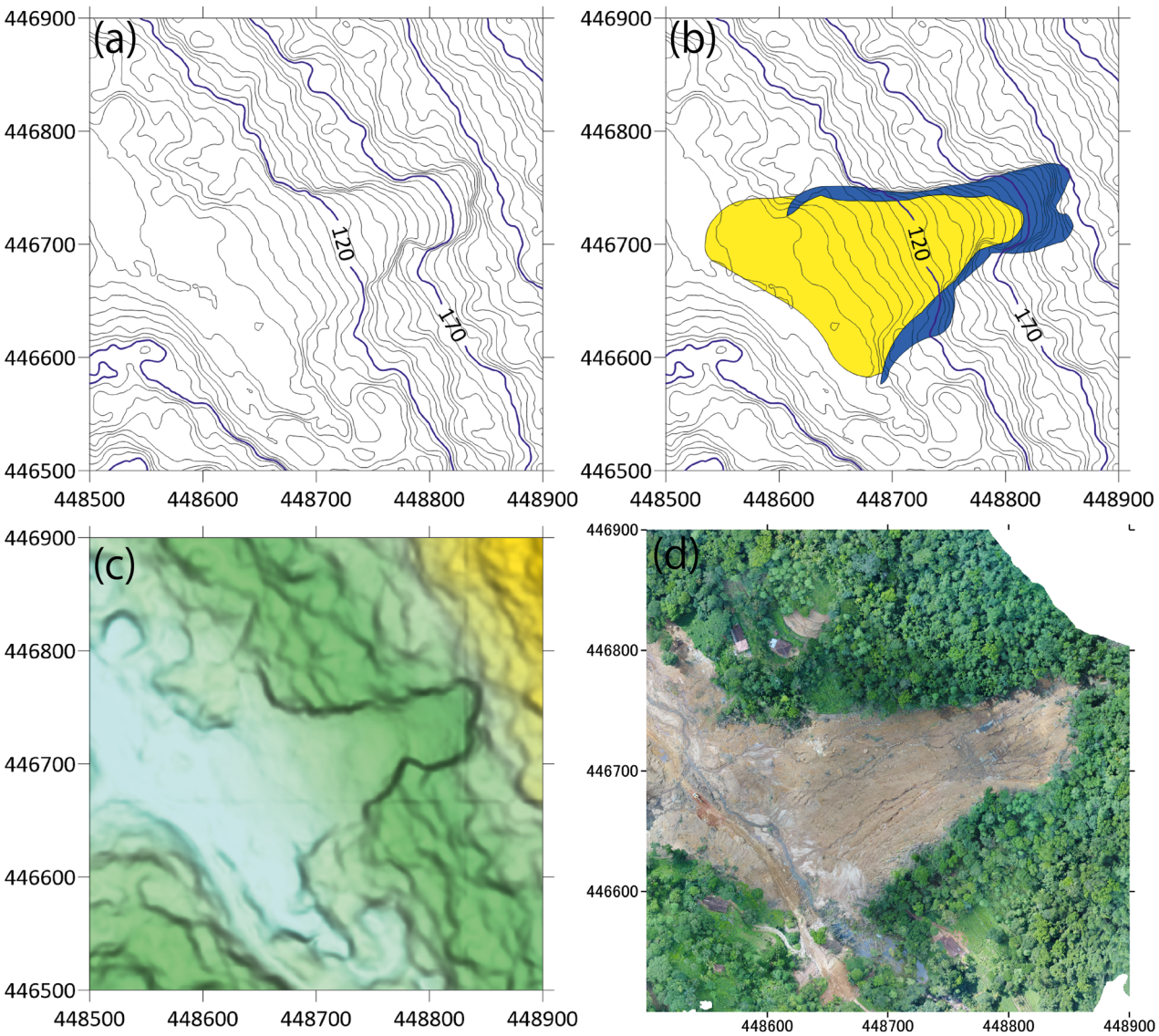


Fig. 7 (**a**) Example of contour lines generated from the AW3D data, (**b**) landslide topographic map from contour map (blue polygon is landslide scarp, yellow polygon is landslide body), (**c**) Relief map created from AW3D data, (**d**) UAV photo of landslide area

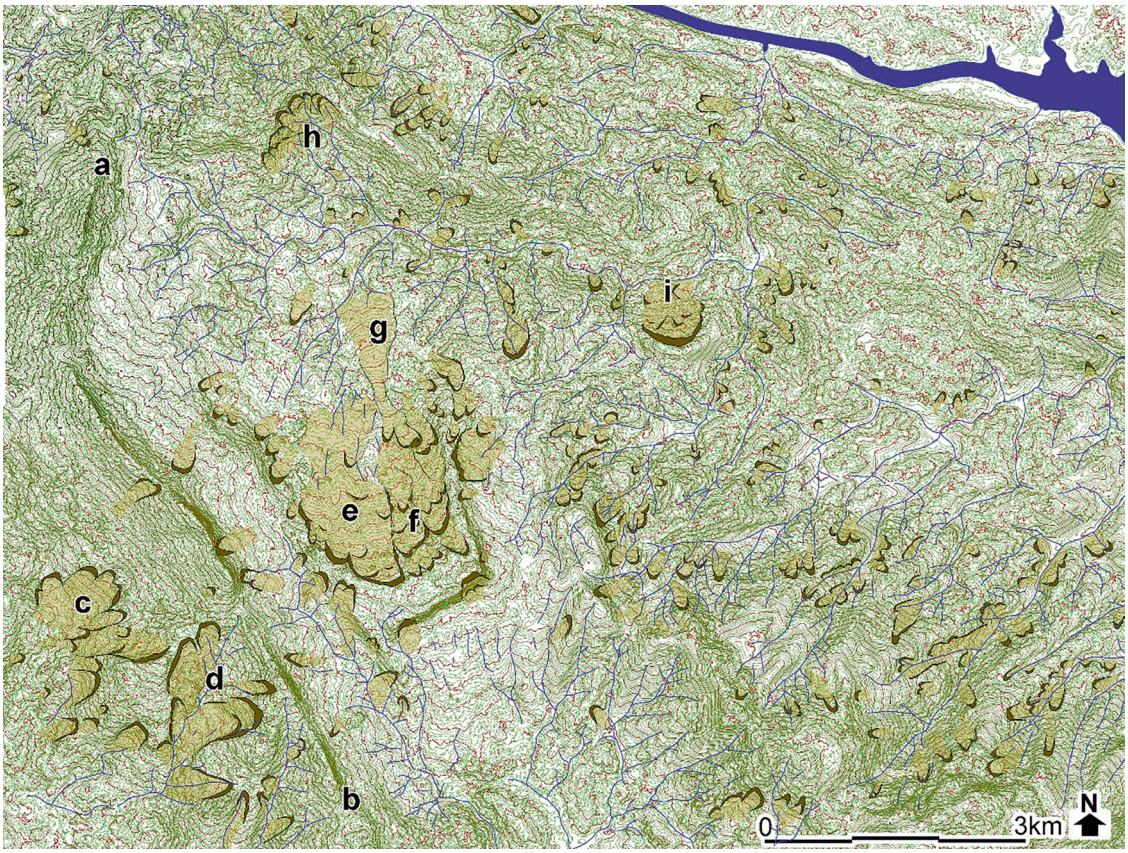


Fig. 8 Landslide topographic distribution map near Kandy in the central highlands of Sri Lanka (Miyagi et al. 2024)

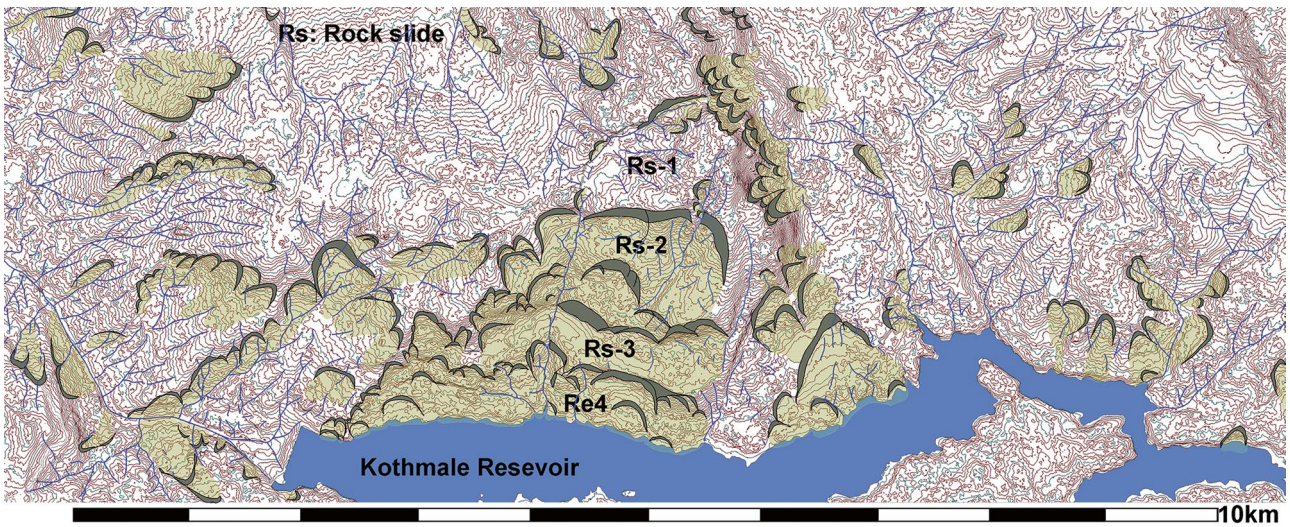


Fig. 9 Landslide topographic distribution map in Kotmale, Sri Lanka and contour characteristics of AW3D 2.5 m data

highlands of Sri Lanka. These lines helped identify the water system, ridgeline, and landslide topography, including the main slip cliff and moving body. Figure 8 displays the western part (a-b) with a steep ridge extending in the south-north direction. Only a few small landslides can be seen on the northeast side of this steep ridge. At the foot of this ridge is a gentle slope resembling a cliff cone. Large-scale landslide topography (0.4~1 km in width) can be seen at the upper end of the water system (c, d, e, f, g, h, and i). The lower end of f is further subdivided, and debris-flowing topography (g) can

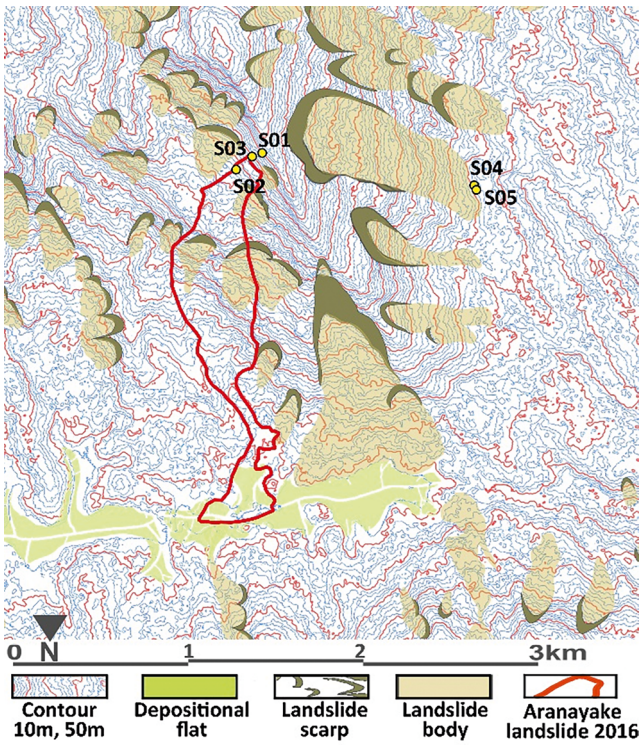


Fig. 10 Landslide topographic distribution map in Aranayake, Sri Lanka and contour characteristics of AW3D 2.5 m data S01 to S05: seismometers

be confirmed. Low mountains and hills surround the river at the northern end of the figure, but landslide topography covers some areas such as h and i.

The Kotmale Dam is a notable hydroelectric and irrigation infrastructure in Kotmale, Sri Lanka. It provides electricity and water to the region's people. Therefore, preparing for landslide risk in this dam area is necessary. Figure 9 shows the landslide topographic distribution map in Kotmale. Four large rock slides named Rs-1 to Rs-4 are located near the dam. Retrogression may occur when failure starts from the rockslide Rs-4 and progresses to Rs-3, Rs-2, and Rs-1, forming a massive landslide. If this scenario becomes true, the landslide tsunamis will have a significant effect on the dam and also on residents downstream.

Figure 10 shows the landslide topographic characteristics mapped in the Aranayake area using a 10-m contour map. The red polygon is the 2016 Aranayake landslide. There are numerous potential future landslides near the disaster in 2016. Earthquake events and microtremors have been increasingly reported in Sri Lanka since 2021. The 2006 Leyte landslide in the Philippines was triggered by a minor earthquake and caused extensive damage to the region, claiming over a thousand lives. In 2023, to cope with the escalating seismic activities in Sri Lanka, the ICL and NBRO installed five velocity-type seismometers (S01 to S05 in Fig. 10) to monitor microearthquakes in the Aranayake area.

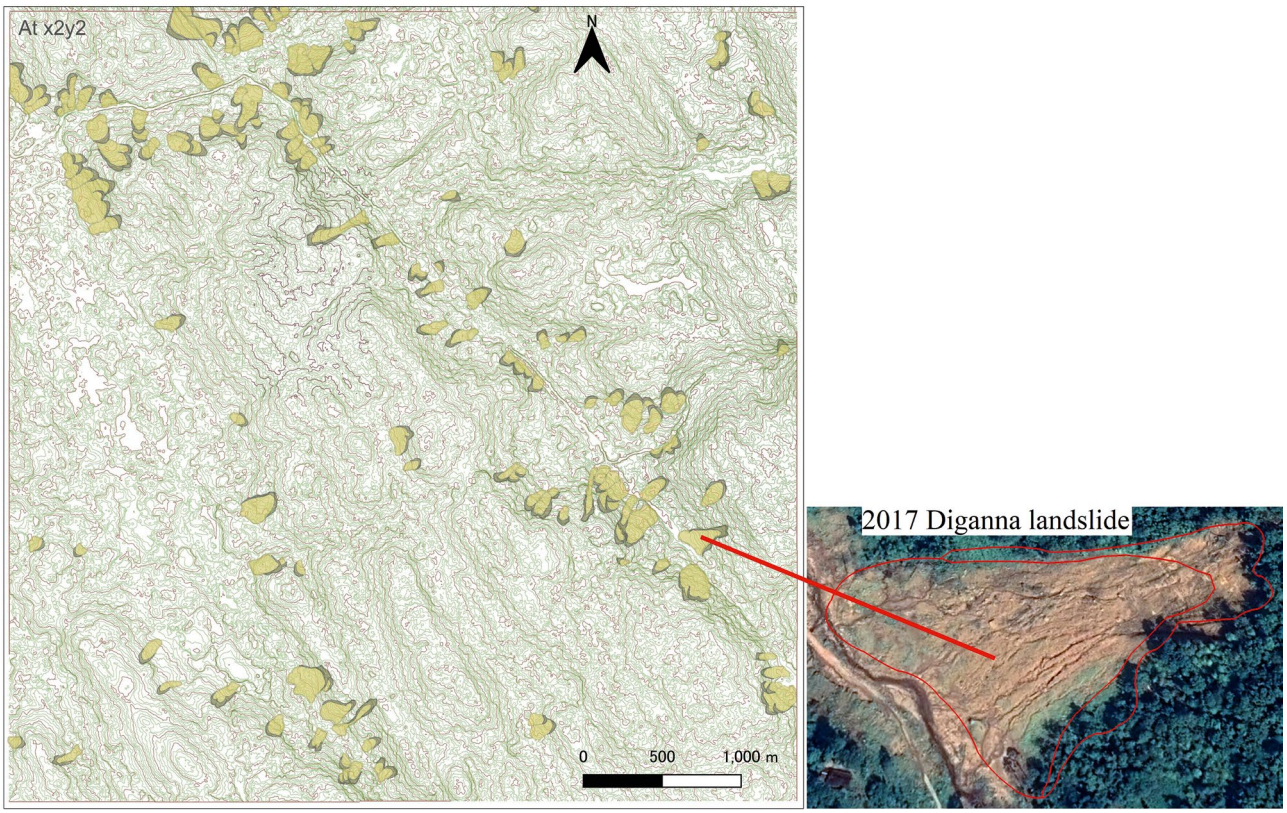


Fig. 11 Landslide topographic distribution map in Palindanuwara, Kalutara, Sri Lanka and contour characteristics of AW3D 2.5 m data

The risk assessment of post-rainfall earthquake-induced landslide in a slope near the 2016 landslide was conducted and reported in Sassa et al. 2023.

Palindanuwara area has experienced significant landslides, particularly during periods of heavy rainfall. Two notable landslides occurred in May 2017. The Diganna and Athelthota landslides caused extensive damage to the community's people and infrastructure, resulting in 18 fatalities. The landslide topography distribution map in Palinnuwara is shown in Fig. 11. There are many potential landslides in a 25 km^2 area. Most of them are medium and large-scale landslides. The right figure illustrates the overlap of the landslide shape in the Google Earth photo of the 2017 Diganna landslide. The location of the mapped landslide is precisely the same as the actual landslide.

5 Conclusion

In this paper, we first present how to determine landslide topography using AW3D data. Then, we compare the published landslide distribution map with the 2011 landslide disaster in the Kii Peninsula. The comparison results highlight that more than 60% of large-scale landslides occurred in the same places as previous landslides. Although this finding is specific to the Kii Peninsula, we believe it will have similar results in other landslide regions. Based on this finding, we create the landslide topography distribution maps for four landslide-prone areas in Sri Lanka. Those maps may reduce the risk of large-scale landslides in Sri Lanka.

Acknowledgement In compiling this report, I would like to express my sincere gratitude to JICA/JST SATREPS officials and collaborators from Japan and Sri Lanka.

References

Chigira M, Tsou C-Y, Matsushi Y, Hiraishi N, Matsuzawa M (2013) Topographic precursors and geological structures of deep-seated catastrophic landslides caused by typhoon Talas. Geomorphology 201:479–493

Dang K, Sassa K, Konagai K, Asiri K, Bandara RMS, Hirota K, Tan Q, Ha ND (2019) Recent rainfall-induced rapid and long-traveling landslide on 17 May 2016 in Aranayaka, Kagelle District, Sri Lanka. Landslides 16:155–164. https://doi.org/10.1007/s10346-018-1089-7

Geospatial information Authority of Japan. https://www.gsi.go.jp/BOUSAI/h23-taihu12-index.html. Lass access on April 10, 2024

Hefryan SK, Ishikawa Y, Gomi T, Shiraki K, Wakahara T (2016) Analysis of landslide dams formation based on topographical characteristics in Kii Peninsula, Japan. INTERPRAEVENT 2016 – Extended Abstracts, 114-115

Ikeda K (2021) Three dimensional microtopography map for interpretation the detail structure of landslide area. In: Committee of evaluation study team, Japan Landslide Society (sd.) Guidebook of the slope disaster risk evaluation. Asakura shoten, pp 74–92. In Japanese

Makabe S, Miyagi T, Daimaru H, Unome H (2015) Classification of the reflectivity of extra high resolution laser data by SAKURA system in mangrove habitat, Amami Island, Japan. Restoration Stud 7:15–23. In Japanese

Miyagi T, Ikeda K, Ishikawa H, Doan L, Thanh NK, Tien PV, Li Y, Zhang F (2024) Interpretation and mapping for the Prediction of Site Risk of Landslide Disasters: From Aerial Photography to Detection by DTMs. Open Access Book, Springer (Accepted version)

NIED Landslide topography distribution map https://dil-opac.bosai.go.jp/publication/nied_tech_note/landslidemap/gis.html. Lass access on April 10, 2024.

Saito H, Matsuyama H (2012) Catastrophic Landslide Disasters Triggered by Record-Breaking Rainfall in Japan: Their Accurate Detection with Normalized Soil Water Index in the Kii Peninsula for the Year 2011. SLOA 8:81–84. https://doi.org/10.2151/sola.2012-021

Temme A, Guzzetti F, Samia J, Mirus BB (2020) The future of landslides' past—a framework for assessing consecutive landsliding systems. Landslides 17:1519–1528. https://doi.org/10.1007/s10346-020-01405-7

Tien PV, Sassa K, Takara K, Fukuoka H, Khang D, Shibasaki T, Setiawan H, Ha ND, Loi DH (2018) Formation process of two massive dams following rainfall-induced deep-seated rapid landslide failures in the Kii Peninsula of Japan. Landslides 15(9):1761–1778

Unome S (2020) Current status of airbone LiDAR system with a case study in Amami Oshima island and the introduction of the latest LiDAR technology. Mangrove Sci 11:27–35. In Japanese

Varnes DJ (1978) Slope movement types and processes: Landslide analysis and control. Highway Res Board Special Rep. 176:11–33

Yamada M, Mangeney A, Matsushi Y, Moretti L (2016) Estimation of dynamic friction of the Akatani landslide from seismic waveform inversion and numerical simulation. Geophys J Int 206(3):1479–1486. https://doi.org/10.1093/gji/ggw216

Open Access This chapter is licensed under the terms of the Creative Commons Attribution 4.0 International License (http://creativecommons.org/licenses/by/4.0/), which permits use, sharing, adaptation, distribution and reproduction in any medium or format, as long as you give appropriate credit to the original author(s) and the source, provide a link to the Creative Commons license and indicate if changes were made.

The images or other third party material in this chapter are included in the chapter's Creative Commons license, unless indicated otherwise in a credit line to the material. If material is not included in the chapter's Creative Commons license and your intended use is not permitted by statutory regulation or exceeds the permitted use, you will need to obtain permission directly from the copyright holder.



LS-RAPID Estimation of the Critical Pore Pressure Able to Initiate (Activate) Landslides Within the Existing Large-Scale Landslides

Doan Huy Loi, Pham Van Tien, Khang Dang, and Kyoji Sassa

Abstract

Landslides have the potential to cause severe damage to infrastructure and can lead to loss of life. It is crucial to take preventive measures to mitigate landslide risks. Landslides in Sri Lanka are a common natural disaster, often triggered by heavy rainfall during the monsoon season.

The National Building Research Organization of Sri Lanka (NBRO) and the International Consortium on Landslides (ICL) commenced a 5-year research project in 2020 named "Development of Early Warning Technology of Rain-induced Rapid and Long-travelling Landslides (Project RRLL)," which was supported by JICA (Japan International Cooperation Agency) and JST (Japan Science and Technology Agency). The project's main objective is to create essential technologies for an early warning system that can predict landslides caused by heavy rainfall. One of the key technologies is use of the LS-RAPID to simulate the landslides initiation and motion. First, this article presents two case studies in Japan, and Sri Lanka to show the ability of LS-RAPID to reproduce rainfall-induced landslides. Then, LS-RAPID was applied to estimate the potential activation in previous large-scale landslides and the critical pore pressure needed to initiate landslides in the Aranayake area, Sri Lanka.

Keywords

Potential landslides · Previous large-scale landslides · LS-RAPID · Sri Lanka

1 Introduction

Landslides cause billions of dollars in damages and thousands of fatalities annually, making them a devastating natural disaster (NASA 2024). For example, the deadly Petrópolis catastrophe occurred on 15 February 2022, resulting from flash floods and landslides. The disaster claimed the lives of 231 people (Alcântara et al. 2023). On February 6th, 2024, a landslide took place in the town of Maco, Davao de Oro, Philippines, resulting in the loss of at least 98 lives (Petley 2024; Wikipedia 2024). Landslide risk assessment is crucial for disaster prevention.

This paper introduces a method to estimate the potential landslides activation within previous large-scale landslides and the critical pore pressure to initiate such activation. Figure 1 illustrates the flow chart of a trial method to create the hazard mapping for Sri Lanka. This method was developed under the SATREPS (Science and Technology Research Partnerships for Sustainable Development) project "Development of Early Warning Technology of Rain-Induced Rapid and Long-Travelling Landslides in Sri Lanka (RRLLs)." There are four main techniques used in this method: landslide interpretation, Geotechnical model (LS-RAPID), high-resolution rainfall prediction model (Multi-Scale Simulator for the Geoenvironment—MSSG), and Augmented reality (AR) system. The landslide interpretation was presented by Miyagi et al. (2024a). The detailed information and application of MSSG in Sri Lanka can be found in Onishi et al. (2024). The AR system was reported by Araki et al. (2024). We focused on the LS-RAPID model and its applications (red dashed border rectangle in Fig. 1). First, the basic information about LS-RAPID is introduced.

D. H. Loi (✉)
International Consortium on Landslides, Kyoto, Japan

Institute of Transport Science and Technology, Hanoi, Vietnam

P. Van Tien
Institute of Geological Sciences, Vietnam Academy of Science and Technology, Hanoi, Vietnam

K. Dang
International Consortium on Landslides, Kyoto, Japan

VNU University of Science, Hanoi, Vietnam

K. Sassa
International Consortium on Landslides, Kyoto, Japan

© The Author(s) 2025

B. Abolmasov et al. (eds.), *Progress in Landslide Research and Technology, Volume 3 Issue 2, 2024*, Progress in Landslide Research and Technology, https://doi.org/10.1007/978-3-031-72736-8_19

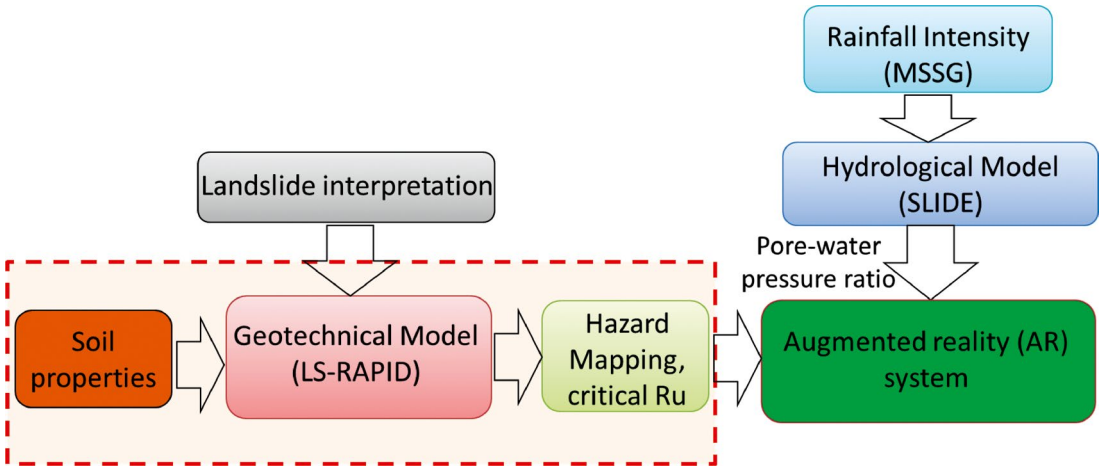


Fig. 1 Flow chart of hazard mapping

Then, two case studies of large-scale landslides caused by the prolonged rainfall were reported to explain the model's ability and reliability. The 2011 Kii Peninsula landslide was selected since it is notable evidence that heavy rainfall caused numerous larger-scale landslides within the existing landslides. The 2016 Aranayake landslide stands as one of the most fatal landslides in the history of Sri Lanka.

To date, the LS-RAPID model has only been applied to actual disasters or small-scale susceptibility assessments. The present paper aims to estimate the potential larger-scale landslides and their critical pore pressure for a wide area in Aranayake, Sri Lanka by using LS-RAPID.

2 LS-RAPID Model

LS-RAPID is an integrated model that simulates the initiation and motion of landslides triggered by earthquakes, rainfalls, or the combined effects of both (Sassa et al. 2010). LS-RAPID is the commercial software; the free trial version can be downloaded from https://soft.godai.co.jp/En/Soft/Product/Products/LS-RAPID/. The manual and video tutorials published by Ajmera et al. in 2023 provided a complete walk-through of the LS-RAPID program. The pore water pressure ratio (R_u) was considered as the triggering factor for rainfall-triggered landslides. The pore pressure ratio when the slope starts failure is critical. This software is helpful for engineers and scientists who are studying landslides. Using LS-RAPID, they can better understand the risks posed by landslides and develop strategies to mitigate them.

The LS-RAPID method is widely used to investigate landslides globally. It is often combined with laboratory tests to get detailed soil strength data. Some studies use estimation parameters. Figure 2 shows the location of 46 case studies that were analyzed using LS-RAPID. It was applied in ten countries: Canada, China, Croatia, India, Indonesia, Italy, Japan, Philippines, Sri Lanka, and Vietnam. The case studies include earthquake-induced landslides and rainfall-induced landslides and combining both effects.

The three primary purposes of the LS-RAPID model are to reproduce landslide disasters, assess susceptibility, and map hazards (Fig. 2b). Two disasters: the 2011 Kii Peninsula landslides in Japan and the 2016 Aranayaka landslide in Sri Lanka will be reported in the next section. The most important part of this paper is estimation of potential landslides activation within the previous large-scale landslides and the critical pore pressure to initiate landslides in Aranayake for hazard mapping.

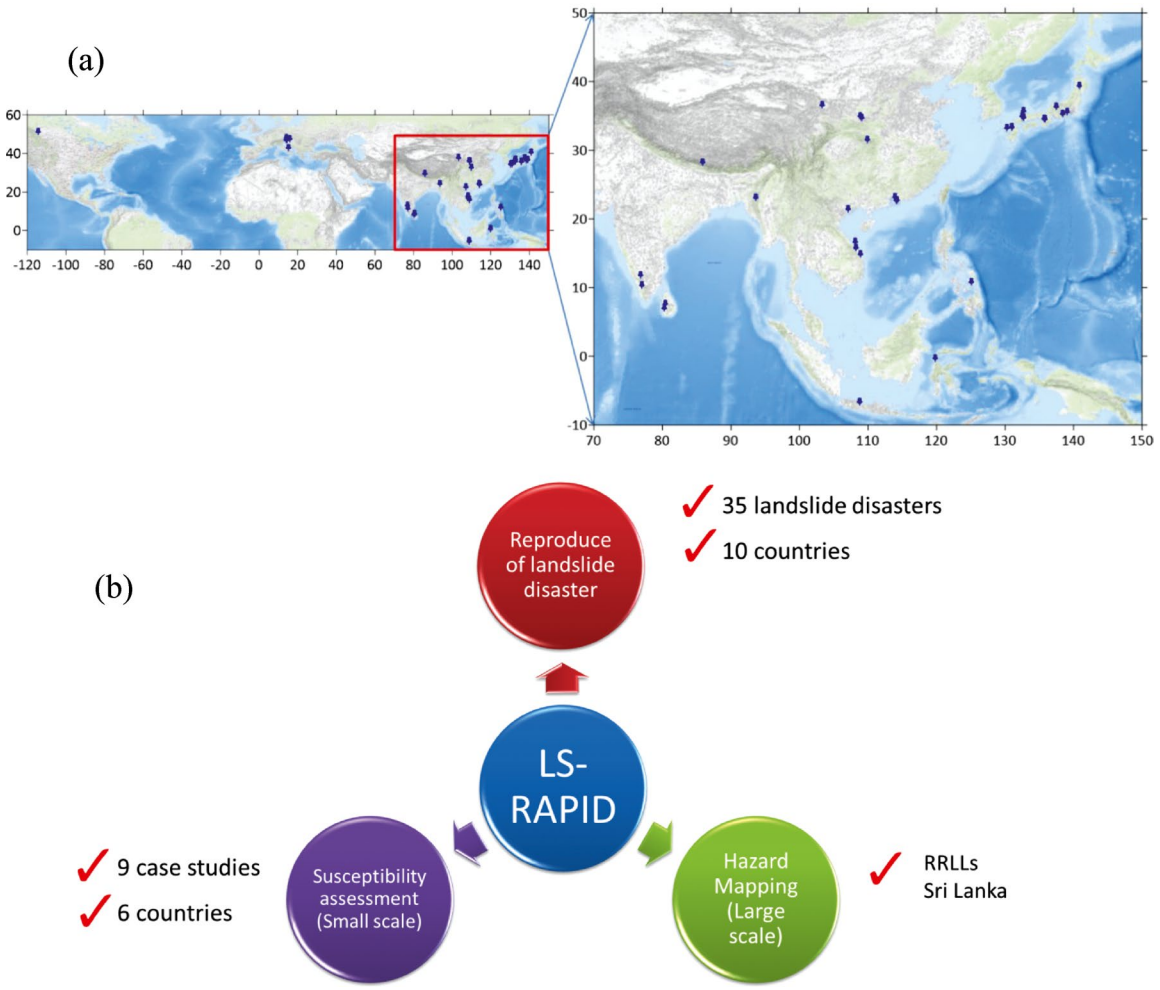


Fig. 2 (**a**) Location of LS-RAPID applications (**b**) three functions of LS-RAPID

3 Previous Case Studies

3.1 The 2011 Kii Peninsula Large-Scale Landslides in Japan Caused by Long Rainfalls

Introduction

From 2nd to 4th September 2011, Typhoon Talas brought extreme rainfalls, resulting in the largest historical flooding and landslide disaster, causing 94 fatalities, destroying 373 houses, and partially damaging 2924 houses in Kii Peninsula, Japan (FDMA 2012; Chigira et al. 2013). Heavy rainfall exceeded 1800 mm, triggering more than 3000 landslides in Mie, Nara and Wakayama Prefectures in Kii Peninsula, Japan (Tien et al. 2018). The total volume of sediments was about 100 Mm^3, while large-scale deep-seated landslides took place in 72 locations. Landslides blocked river streams to form natural lakes at 17 locations. The 2011 event became the second most severe sediment-related disaster in the Peninsula after the 1889 flooding and sediment disaster that claimed 1492 lives and forced 2500 people to move out of the Totsukawa village to a new place in Hokkaido (Inoue and Doshida 2012; Chigira et al. 2015; Tien 2018). Located in the centre of the Kii peninsula, a small area in the Totsukawa village that severely suffered from large landslides is one of the main study areas in this research (Fig. 3). This study area lies at the boundary between Totsukawa village, Yoshino district and Gojo city of Nara Prefecture in the upper reaches of the Kumano River. The study area is typical for geological and topographical settings and landslide characteristics. Locations of several large landslides, i.e., Kuridaira, Akatani, Akatani-East, Nagatono, Ui, and Uguhara, are presented in Fig. 3a. Aerial photograph of the Kuridaira landslide and Google image of large landslides around Akatani valleys are presented in Fig. 3b, c. The description of several largest landslides in the Totsukawa village is presented in Table 1.

The Kuridaira landslide was the biggest block, with a width of 600 m, a length of 750 m and a sliding depth of 100 m. The Akatani landslide was 350 m wide in the middle

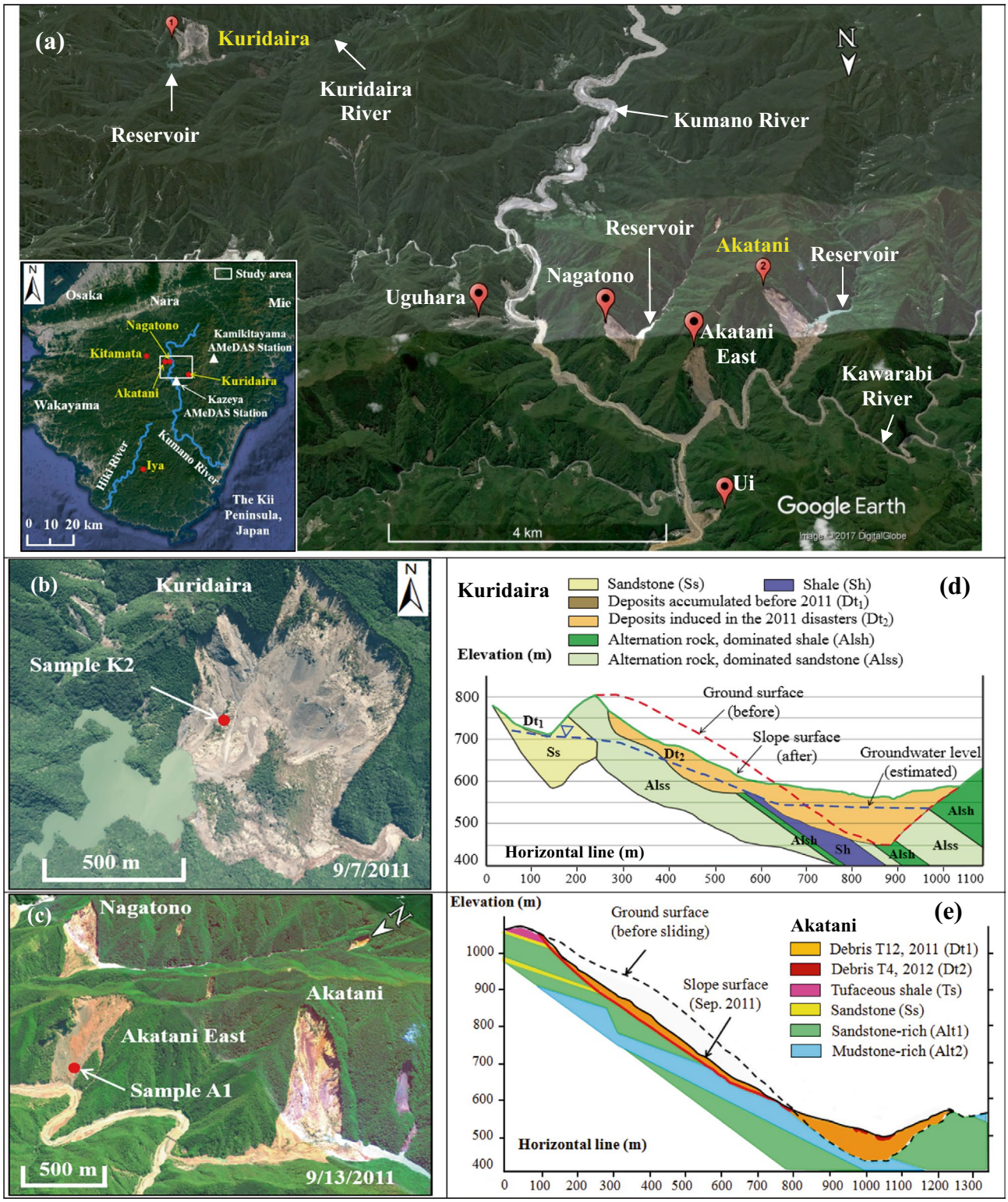


Fig. 3 (**a**) Location of the study area and large landslides in Totsukawa village, (**b**) the Kuridaira landslide (by the Kii Mountain District Sabo Office), (**c**) Google Earth image of large landslides in Akatani and Nagatono valleys, and (**d**, **e**) geological profiles of Kuridaira and Akatani landslide dams, respectively (Sassa et al. 2023)

slope, 900 m long and 67 m deep (Tien et al. 2018). The massive volumes of Kuridaira and Akatani landslides of 24.0 and 10.2 Mm^3 blocked the river valleys to form natural dams up to 100 m high in a catchment area of 8.7 km^2 and 85 m high in a catchment of 13.2 km^2, respectively. The Kuridaira and Akatani reservoir dams are located on the left- and right-bank tributaries of the Kumano River. The source areas of the Kuridaira and Akatani landslides consisted of broken for-

mations and fractured wedge-shaped discontinuities of sedimentary rocks in the Hidakagawa Group of the Cretaceous Shimanto Belt (Chigira et al. 2013; Tien et al. 2018). The Kuridaira landslide is mainly characterized by composed mixed materials of sandstone and shale (Fig. 3d). The Akatani landslide is composed of mixed material of sandstone and mudstone (Fig. 3e). The large-scale landslides took place at midnight on September 3 and early morning on September 4, 2011 mainly, when rainfall accumulated at high values. In the Typhoon Talas, a historical largest accumulative precipitation of 1800 mm was monitored at the Kamikitayama AMeDAS Station between August 31 and September 4. The accumulative rainfall recorded at the Kazeya Station, which is located nearest to the Totsukawa village, was 1359 mm in the same period. The maximum daily rainfall reached 661.0 and 591.5 mm at the Kamikitayama and Kazeya Stations on September 3, respectively (Fig. 4). The rainfall data shows that heavy rainfall during the typhoon was the main triggering factor of the Kii Peninsula landslides.

Table 1 Description of largest landslides around the Totsukawa village (Tien 2018)

Description/Areas	Kuridaira	Akatani	Akatani East	Nagatono
Landslide area (m^2)	548,500	423,700	221,400	220,700
Volume of collapsed sediment (Mm^3)	24.0	10.2	2.1	6.8
Slope angle (degree)	31	34	29	34
Slope height (m)	410	610	450	400
Width (m)	600	300–500	330	310
Length (m)	800	1000	750	610
Maximum depth (m)	100	67	22	46
Formation	Hidakagawa Group in the Shimanto Belt			
Lithology	Broken formations and mixed rocks			

Integrated Simulation of Rainfall-Induced Landslides by Ring Shear Apparatus and LS-RAPID Model

The mechanisms of the rainfall-induced Kuridaira and Akatani landslides were investigated through a series of pore water pressure (PWP) tests with ring shear apparatus ICL-2 at an undrained capability of 3.0 MPa in the normal stress. The entire process of landslide initiation and motion was reproduced using the LS-RAPID computer model. Soil samples of the sliding surfaces of the landslides were first col-

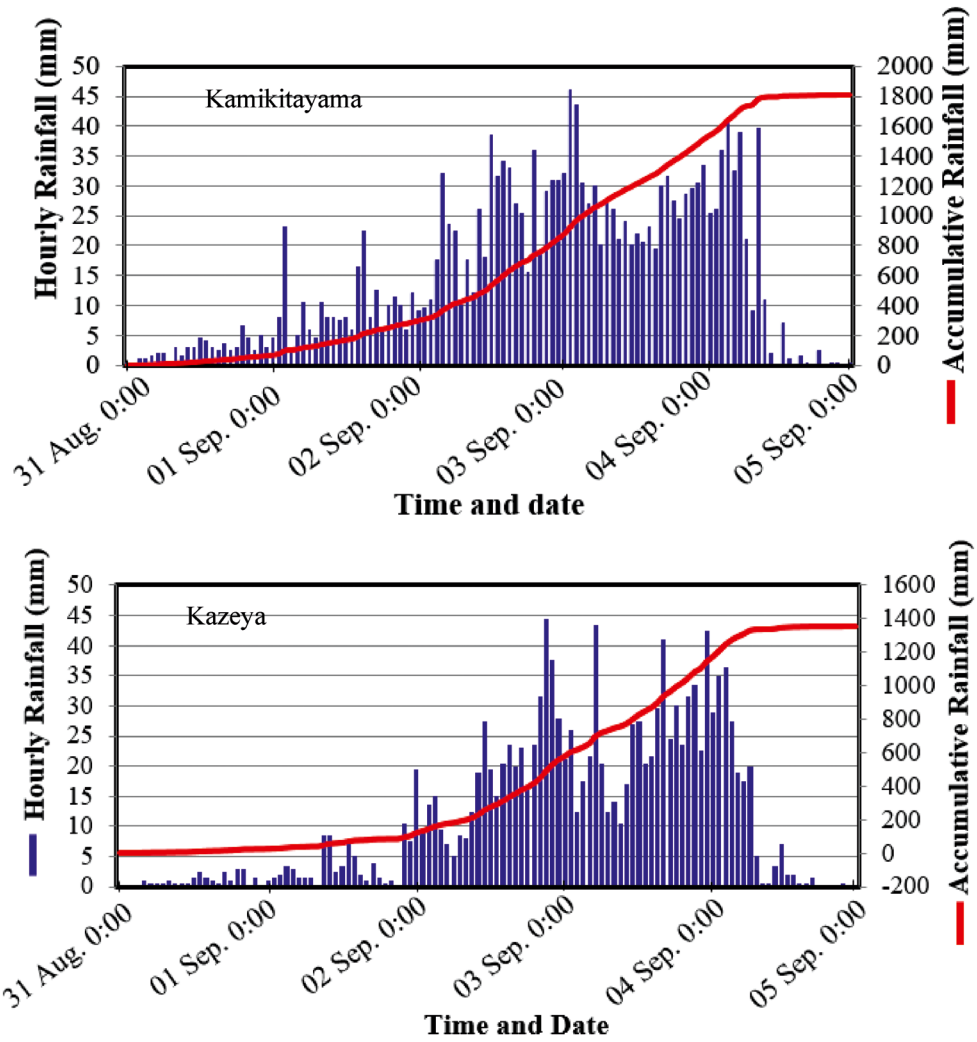


Fig. 4 Rainfall data at Kamikitayama and Kazeya AMeDAS Stations in the Typhoon Talas (JMA 2011)

lected in the site surveys. Then, PWP control tests on landslide samples were conducted to indirectly investigating the sliding mechanism under rainfall conditions. The rainfall-induced landslide simulation by ring shear apparatus was not only important to examine the failure mechanisms of soil samples, but it also provided significant information on the pore water pressure ratio that triggered the failures (Sassa et al. 2014). Finally, the landslide initiation and motion processes were simulated by LS-RAPID software that employed geotechnical parameters of soil samples of the sliding surface measured in the ring shear tests.

Ring shear tests on shale sample (K2) of the Kuridaira slope and sandstone-rich material (A1) of the Akatani slope were presented in Fig. 5. In the tests, the fully saturated samples were consolidated to normal stress of 1000 kPa and shear stress of 600 kPa and 620 kPa for samples K2 and A1 in drained condition. These initial stresses (black line) were close to the actual stress conditions of the Kuridaira and Akatani landslide samples along their sliding surface with slope angles of 31° and 34°, respectively. The pore water pressure increment was then produced to simulate the increasing of groundwater level under rainfall. The rates for the PWP increment (blue line) were 1.0 and 0.5 kPa/s for samples K2 and A1. As shown in Fig. 5, the failure of samples K2 and A1 occurred at the PWP values of about 340 and 370 kPa, which correspond to the pore water pressure ratios (r_u) of 0.34 and 0.37, respectively. The parameter r_u represents the ratio of the increasing pore water pressure value at the point of failure to the normal stress. The pore water pressure ratio indirectly indicates the high pore water pressure values due to rainfall that initiated the Kuridaira and Akatani landslides. The friction angles at the peak and the mobilized apparent friction angles were correspondingly 42.7° and 3.4° for sample K2 and 42.4° and 5.5° for sample A1. The steady-state shear resistance of samples K2 and A1 was 60.0 and 94.5 kPa. The high-speed movement was observed due to a significant loss of shear resistance resulting from a rapid generation of excess pore water pressure in the tests.

The 3D computer simulation of the Kuridaira and Akatani landslide triggered by rainfall was performed by using the LS-RAPID model. The model utilized topographical data of the two landslides before and after the sliding. Soil parame-

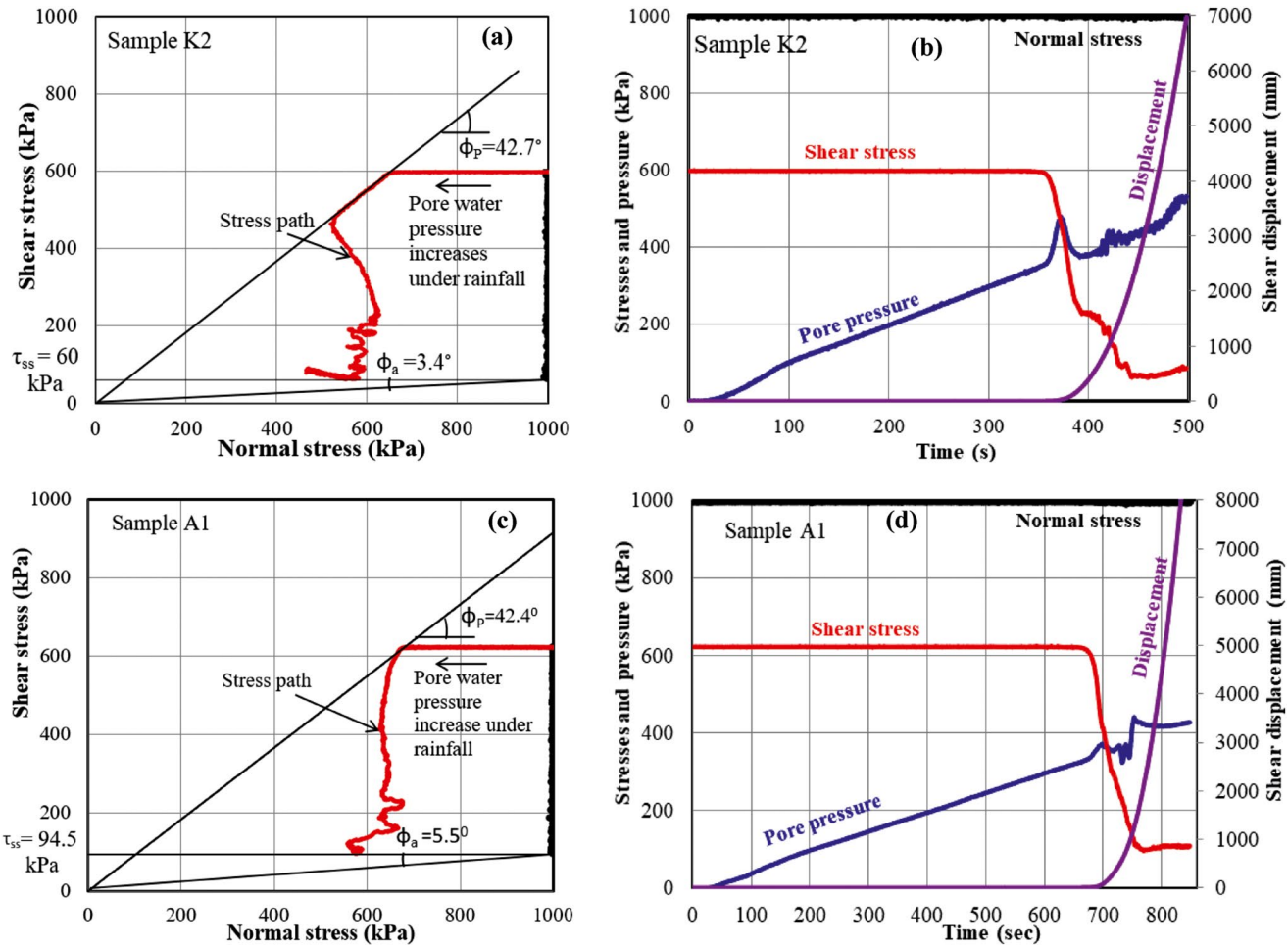


Fig. 5 Results of pore-water pressure control tests on samples K2 and A1: (**a**, **c**) stress path and (**b**, **d**) time series

Table 2 Soil parameters employed in the computer model (Tien et al. 2018)

Soil parameters	Kuridaira sample K2	Akatani sample A1	Source
Total unit weight of the soil mass (γ_t, kN/m^3)	19.5	20.2	Test data
Unit weight of water (γ_w, kN/m^3)	9.81	9.81	Assumed
Pore pressure generation rate (B_{ss})	0.25–0.85	0.25–0.9	Estimated
Lateral pressure ratio ($k = \sigma_h/\sigma_v$)	0.35–0.35	0.35–0.42	Estimated
Friction angle during motion (φ_m, °)	41.5	39.5	Test data
Peak friction angle (φ_p, °)	44.1	42.1	Test data
Steady state shear resistance (τ_{ss}, kPa)	25–95	94.5–150	Test data
Shear displacement at the start of strength reduction (D_L, mm)	3	5	Test data
Shear displacement at the end of strength reduction (D_U, mm)	1500	1500	Test data
Triggering factor of pore pressure ratio (r_u)	0.33	0.36	Test data

ters measured in the ring shear tests were input into the model. Notably, a pore pressure ratio (r_u) indirectly simulated the pore water increment under the groundwater rise due to rainfall, which was employed as the landslide triggering factor. The pore pressure ratios of 0.34 and 0.37 measured in the PWP tests were first used for the Kuridaira and Akatani landslides, respectively. Critical pore pressure ratios were then estimated in testing models and decided based on the model calibration and validation. The critical values corresponded to 0.33 and 0.36 for the Kuridaira and Akatani landslides. Details of soil parameters for the simulation of the two rainfall-induced landslides in the Kii Peninsula are listed in Table 2.

The results presenting the initiation and motion process of the Kuridaira and Akatani landslides are shown in Fig. 11. The pore pressure ratios gradually increased to the critical values within 10 s. These ratios were kept constant for a modelling duration of 150 seconds. The evolution process of the Kuridaira and Akatani landslides triggered by heavy rainfall, which was characterized by the four main stages, is shown in Fig. 6. Unstable and moving parts are depicted in the red ball zones. In the stable condition (stage I), the slopes were still stable if the Ru ratios were lower than critical values (Fig. 6a). In stage II, the Kuridaira and Akatani slopes failed to initiate down movement when the pore pressure ratios reached the critical values of 0.33 and 0.36. The local failures initiated from the middle areas of both Kuridaira and Akatani slopes (Fig. 6b). The slope failures then exacerbated and extensively expanded to surrounding areas due to the loss of support at the base and the dynamic loading impacts from the upper zones. This transient motion process corresponds to stage III in the model (Fig. 6c). In the final period, a large volume of the landslide materials accumulated at the stream valleys and completely blocked the rivers to form natural lakes (Fig. 6d).

3.2 The 2016 Aranayaka Landslide in Sri Lanka

The following analysis of the Aranayaka landslide is primarily based on a comprehensive study conducted by Dang K et al. published in 2019. For a deeper understanding of the event and its analysis, readers are encouraged to consult the original work.

On May 17, 2016, an extensive landslide triggered by unprecedented rainfall associated with a slow-moving tropical cyclone devastated Aranayaka in the Kegalle district of Sri Lanka (Fig. 7). This event resulted in 127 deaths and destroyed 75 homes, making it one of the deadliest landslides in recent Sri Lankan history. Over the 3 days leading up to the landslide, the area recorded a total rainfall of 446.5 mm, significantly exceeding average precipitation and saturating the soil to critical level.

To understand the mechanisms behind this catastrophic landslide, our research focused on analyzing the soil properties from the original landslide site. Two soil samples were collected for analysis: one from a weathered soil layer of the granitic gneiss on the landslide's left flank, and another from a deeply weathered granitic gneiss at the central depression of the landslide site. These samples underwent rigorous ring-shear testing to measure their shear resistance and behavior under stress.

The ring shear testing revealed that the first sample, taken from the weathered soil, exhibited high shear resistance, suggesting it was less likely to have initiated the slide (Fig. 8). In contrast, the second sample from the granitic gneiss showed significantly lower shear resistance, indicating that it likely constituted the primary slip surface material (Fig. 10). These differences in material properties were crucial in understanding the landslide's initiation and progression.

Subsequently, the study employed computer simulations to model the landslide's dynamics using the LS-RAPID software, incorporating the soil parameters obtained from the ring-shear tests and estimating pore-water pressure from rainfall data (Fig. 9). The simulation results closely mirrored the actual event, both in terms of the landslide's timing and its path of movement (Fig. 10). This alignment between the simulated and actual outcomes underscores the potential of such modeling techniques in predicting similar disasters.

The Aranayaka landslide serves as a critical case study for understanding the risks associated with rainfall-induced

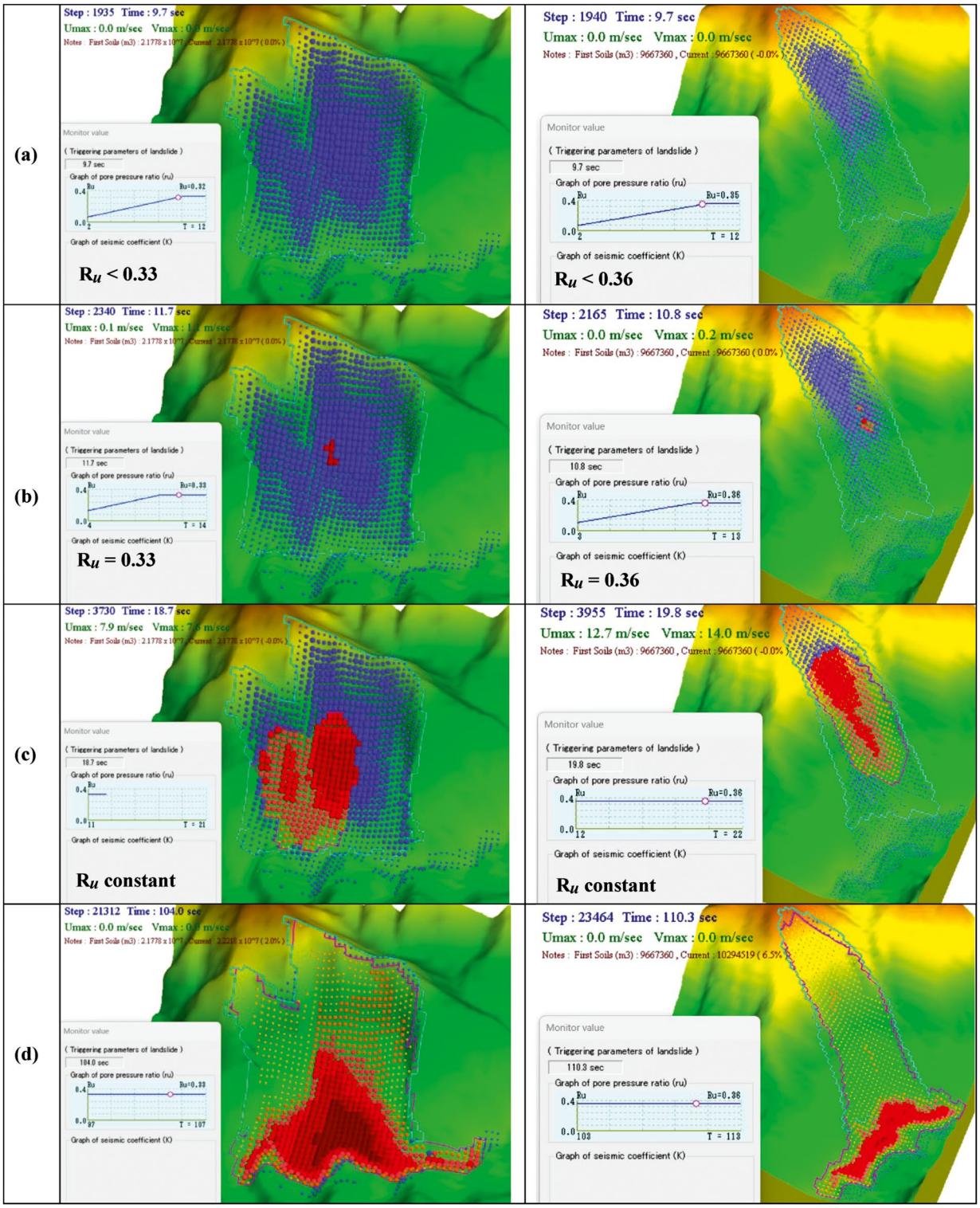


Fig. 6 Modeling results of the rainfall-induced landslides with LS-RAPID: Kuridaira (left) and Akatani (right)

landslides in Sri Lanka. This research not only highlights the importance of geological and hydrological factors in landslide dynamics but also validates the effectiveness of integrating empirical soil data with advanced simulation tools. By refining our predictive capabilities, we can enhance early warning systems and develop more effective landslide mitigation strategies, thereby reducing the potential impact on vulnerable communities.

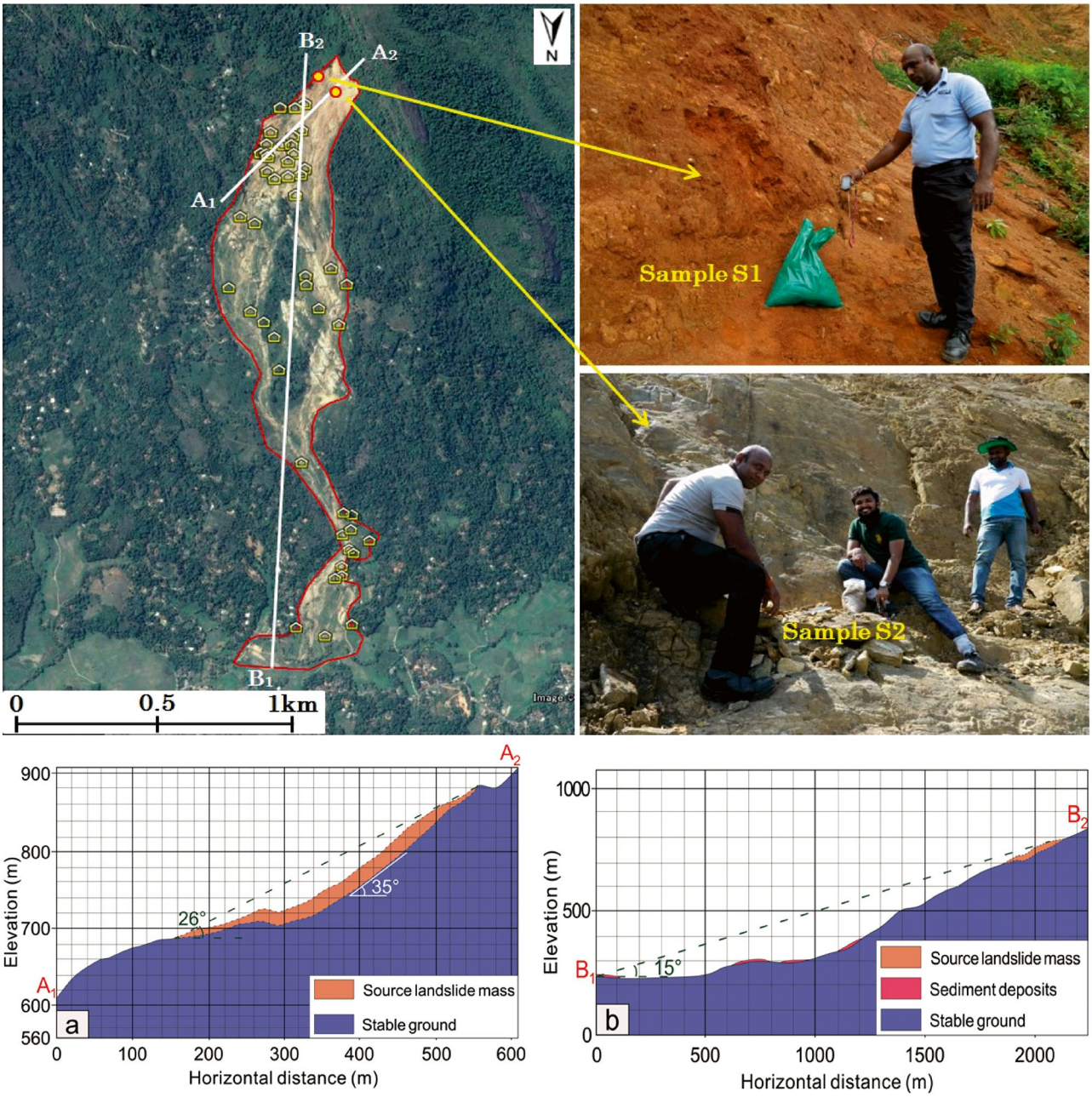


Fig. 7 View of the Aranayaka Landslide: Sampling sites and cross sections (from Dang et al. 2019)

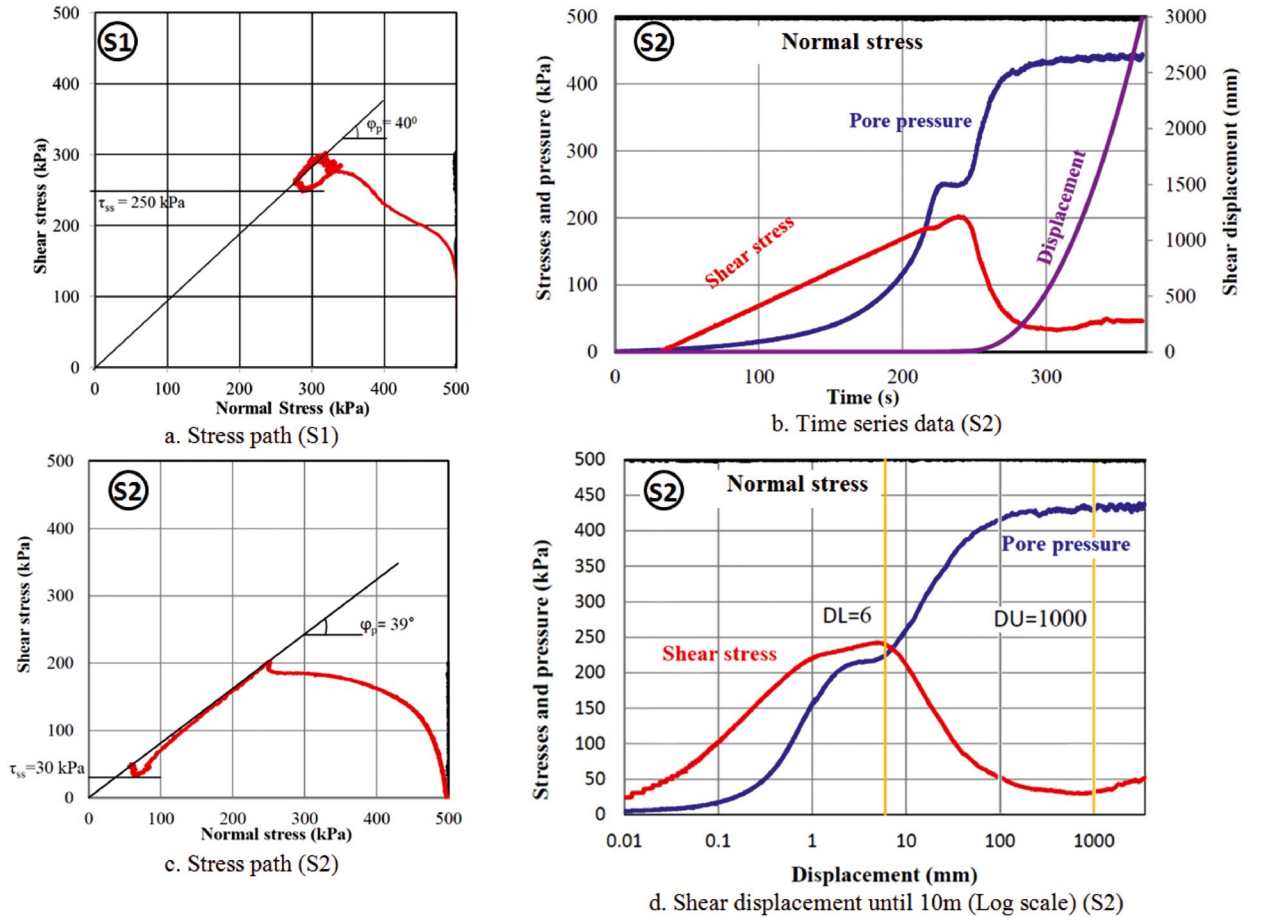


Fig. 8 Ring-shear test results on Aranayaka landslide soil samples S1 and S2 under initial normal stress of 500 kPa. (**a**) stress path of undrained shear displacement-controlled test for sample S1 at a constant shear rate of 0.05 mm/s; (**b**) time series data for sample S2; (**c**) stress path for sample S2; (**d**) shear displacement during undrained monotonic stress-controlled test on sample S2 (Dang et al. 2019)

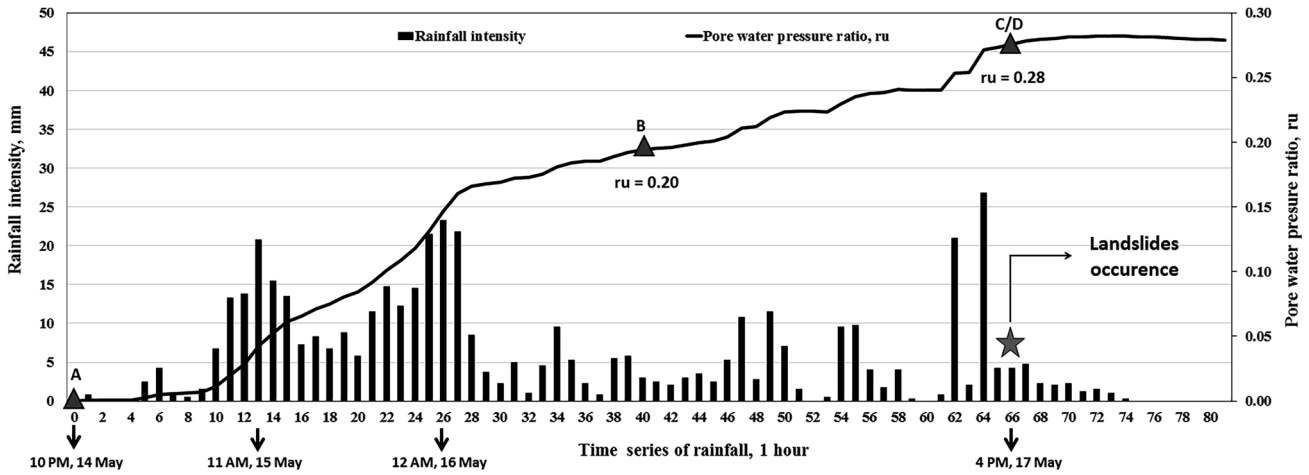


Fig. 9 Rainfall data and pore water pressure ratios in the Aranayaka landslide area, 14–17 May 2016. Note: Points A, B, C, and D correlate with simulation results depicted in Fig. 15 (Dang et al. 2019)

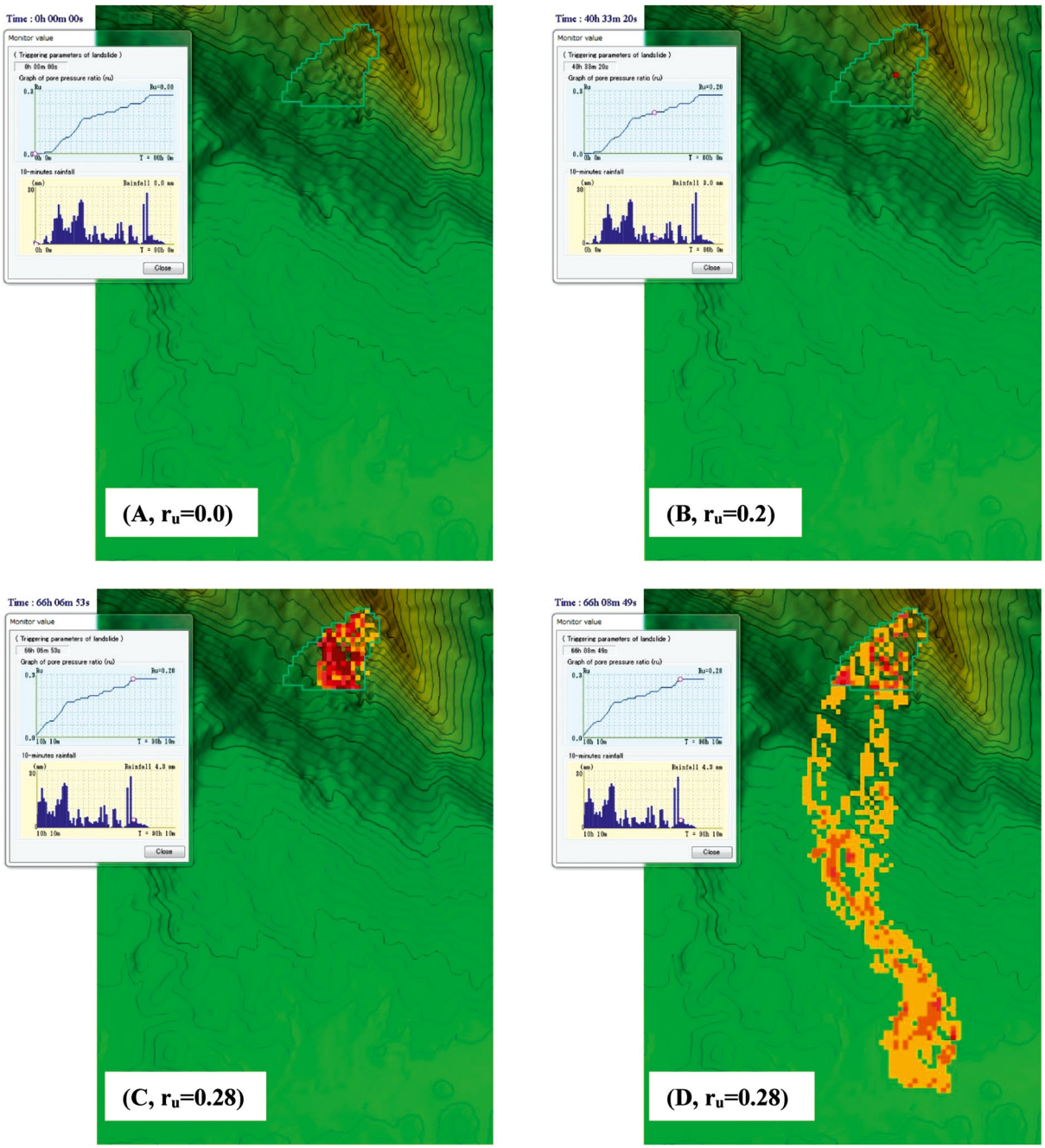


Fig. 10 Computer simulation results of the Aranayaka Landslide Movement (Dang et al. 2019)

4 Estimation of the Critical Pore Pressure Able to Initiate (Activate) Landslides Within the Existing Large-Scale Landslides

4.1 Source of Potential Future Landslides

During the Sri Lanka SATREPS project, the landslide topographic distributions were mapped for four areas in Sri Lanka. In this paper, we only briefly introduce how to map the landslide in the past using the AW3D data. The details can be found in Miyagi et al. (2024a, b). Figure 11 shows an example of a previous landslide that was mapped from a contour map. Figure 12 shows the landslide topographic landslide distribution map in Aranayake, Sri Lanka.

Determining the location of potential future landslides is difficult, but it is crucial for landslide preparedness. Landslides tend to occur in areas where they have happened before (Temme et al. 2020). The 2014 Oso landslide, one of the deadliest in US history, occurred on the same site as a 2006 landslide (Iverson et al. 2015). In 2020, Temme et al.

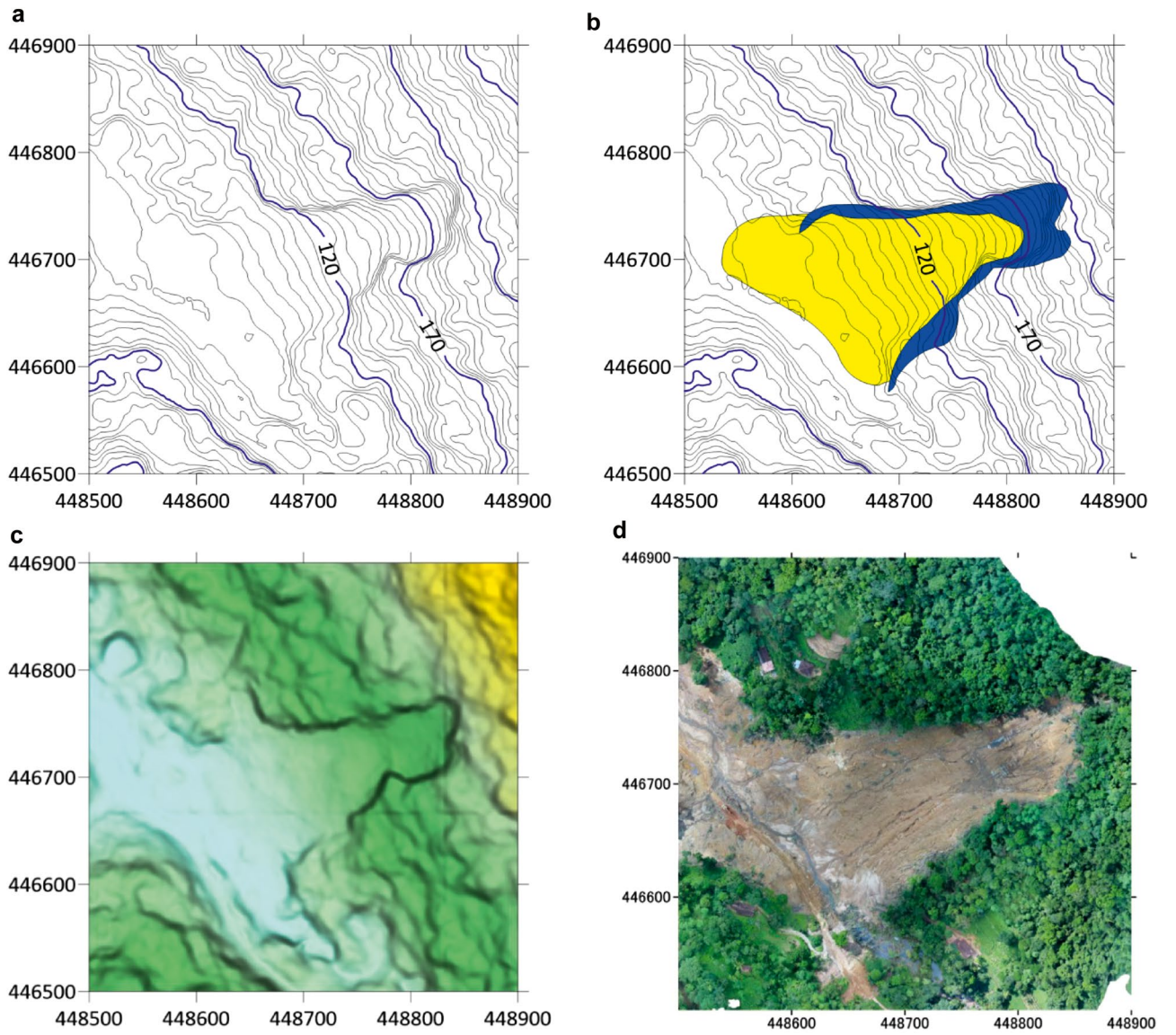


Fig. 11 (**a**) Example of contour lines generated from the AW3D data, (**b**) landslide topographic map from contour map (blue polygon is landslide scarp, yellow polygon is landslide body), (**c**) Relief map created from AW3D data, (Miyagi et al. 2024a) (**d**) UAV photo of landslide area (NBRO, 2017)

reported that about 30% of 3000 landslides (mainly shallow) mapped between 1939 and 2014 in the Collazzone region, Italy overlap or touch earlier ones. Overlapping landslides were larger than others (Samia et al. 2017). Therefore, considering only large-scale landslides, the overlap ratio is much greater than 30%. For example, Miyagi et al. (2024a) found that more than 60% of 54 large-scale landslides in 2011 in the Kii Peninsula, Japan, overlapped or touched earlier landslides mapped using aerial photos. Figure 13 shows that the Otocho Nakabara landslide occurred in 2011, following the mapped landslide published by NIED in 2005.

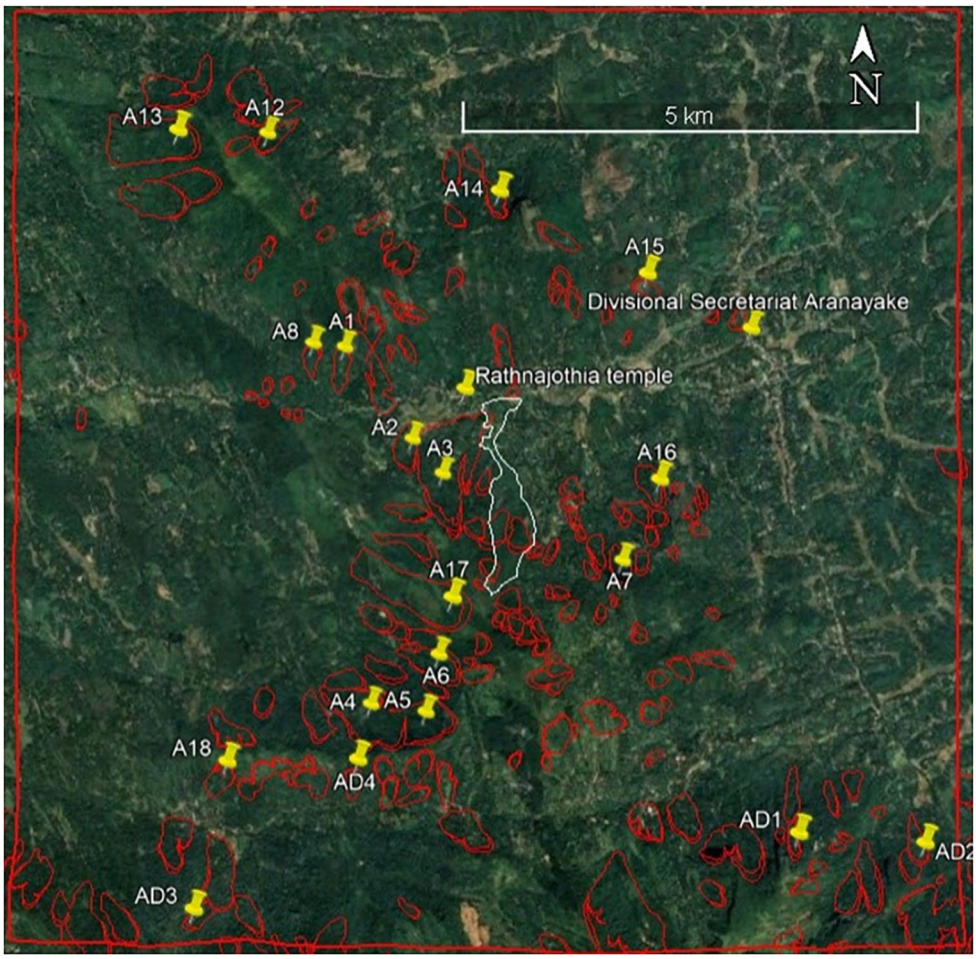


Fig. 12 Landslide topographic distribution map in Aranayake, Sri Lanka

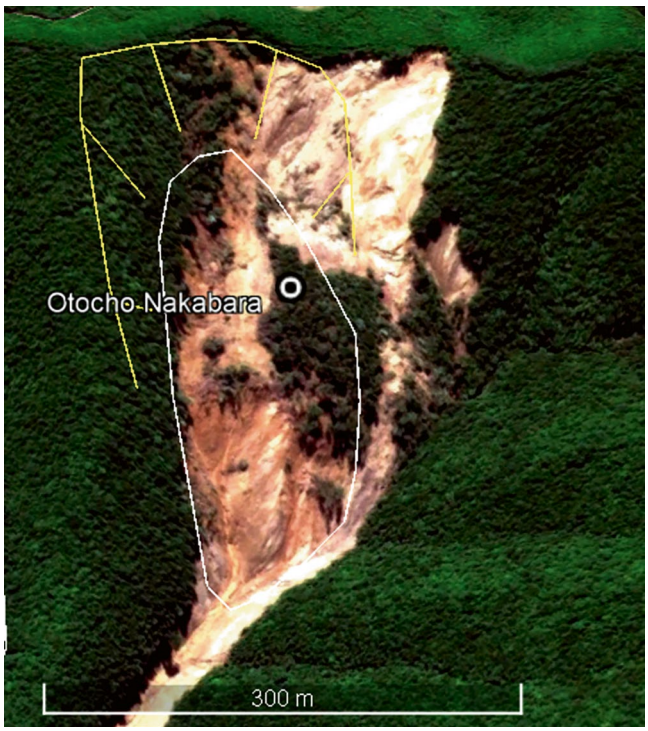


Fig. 13 The 2011 Otocho Nakabara landslide and landslide topography feature published by NIED in 2005

4.2 Estimation of Potential Landslides Using LS-RAPID

Overview of the Simulation

Figure 14 summarizes the steps in estimating potential landslides using LS-RAPID. The first step involves establishing the topography using AW3D data, which provides a detailed three-dimensional representation of the terrain. Once the topography has been established, the next step is to determine the sliding surface for the landslide. This is accomplished using the ellipsoidal parameters, which provide a mathematical representation of the shape of the sliding surface.

Before we start the simulation, we need to configure various settings within LS-RAPID. This includes inputting triggering factors such as changing pore water pressure ratio, earthquake waveform, or both, and soil parameters.

The final step is determining the critical Ru and the landslide moving area.

Preparation of the Topography Data Using AW3D Data

AW3D data consists of the Digital DSM (Digital Surface Model) and DTM (Digital Terrain Model) in tiff format with a resolution of 2.5 m. However, in LS-RAPID, we use 10 m grid data, and then the original data is exported to the data

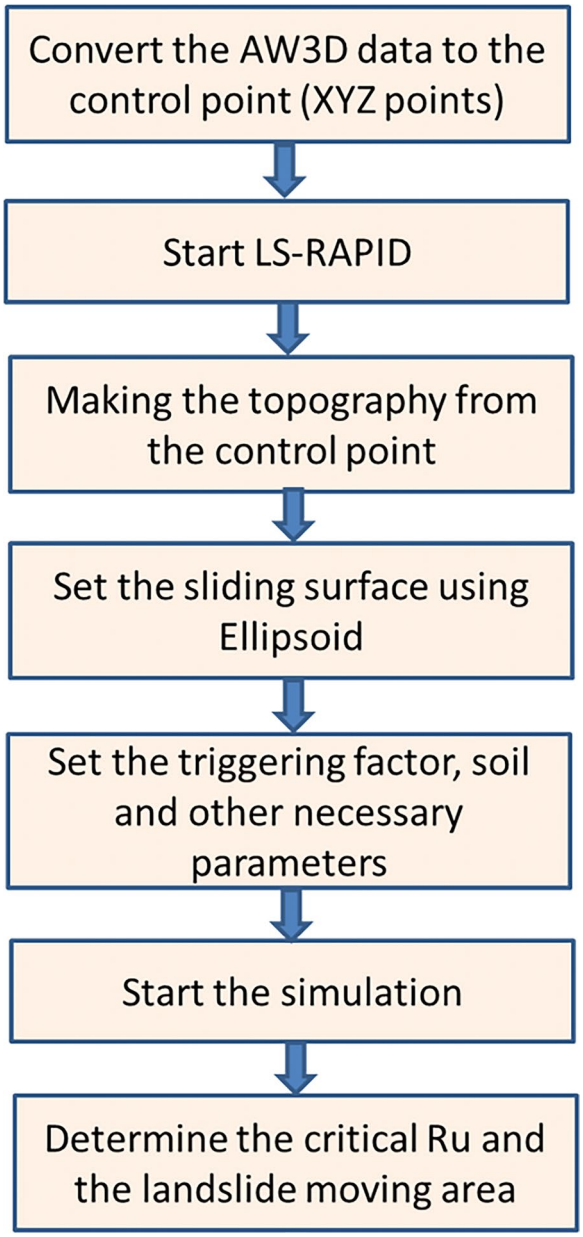


Fig. 14 Flowchart for estimating potential landslides using LS-RAPID

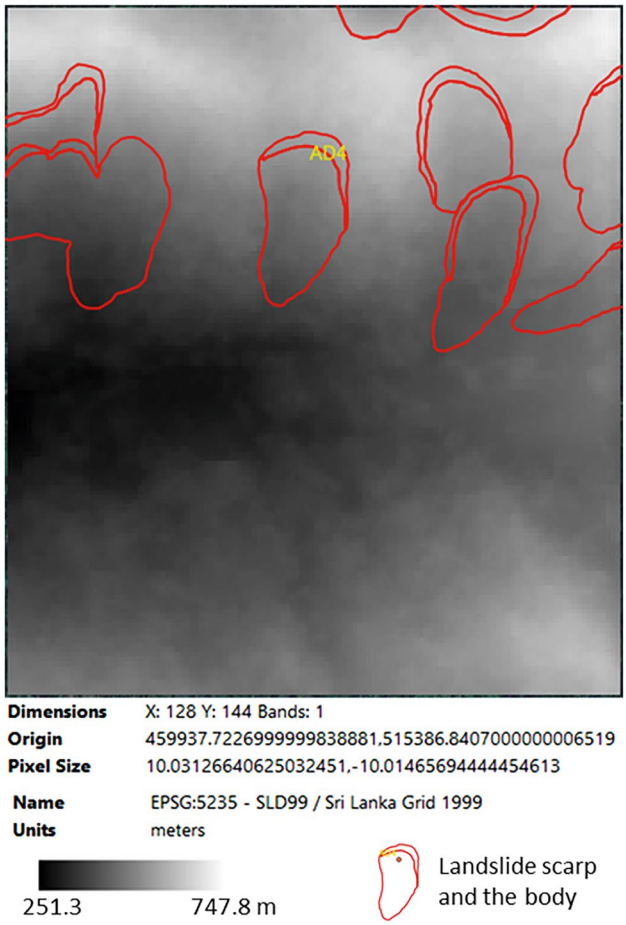


Fig. 15 Example of AW3D data overlapping on the landslide distribution map

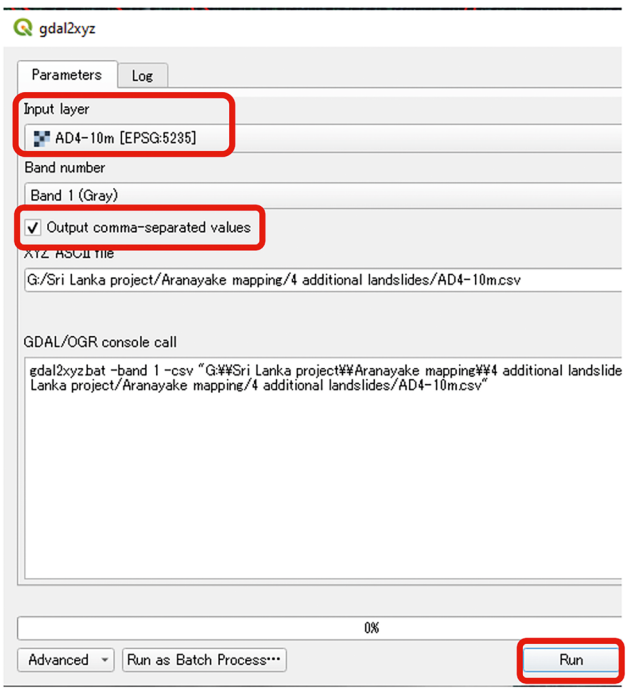


Fig. 16 Screenshot of converting the grid data to the control point

with a pixel size of 10 m. Figure 15 shows the example of AW3D data for a potential landslide named AD4. The area for a landslide is about 1 to 4 km^2 to ensure it is wide enough for landslide analysis. The coordinate reference system is EPSG: 5235-SLD99/Sri Lanka Grid 1999.

To convert the grid data to a control point file that contains (x, y, z) coordinates, the "gdal2xyz" tool is utilized. This tool is available in QGIS, and can be accessed from the Processing Toolbox. Once the tool is opened it will be prompted to select the input file which contains the grid data (Fig. 16). After selecting the input file, the "output comma-separated values" is clicked. Then, click on the "Run" button to start the conversion process.

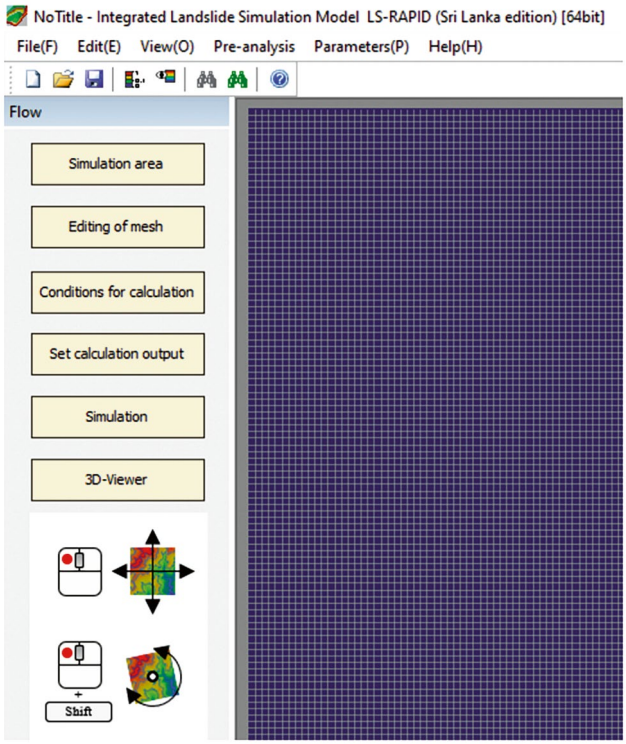


Fig. 17 Screenshot of LS-RAPID 64-bit

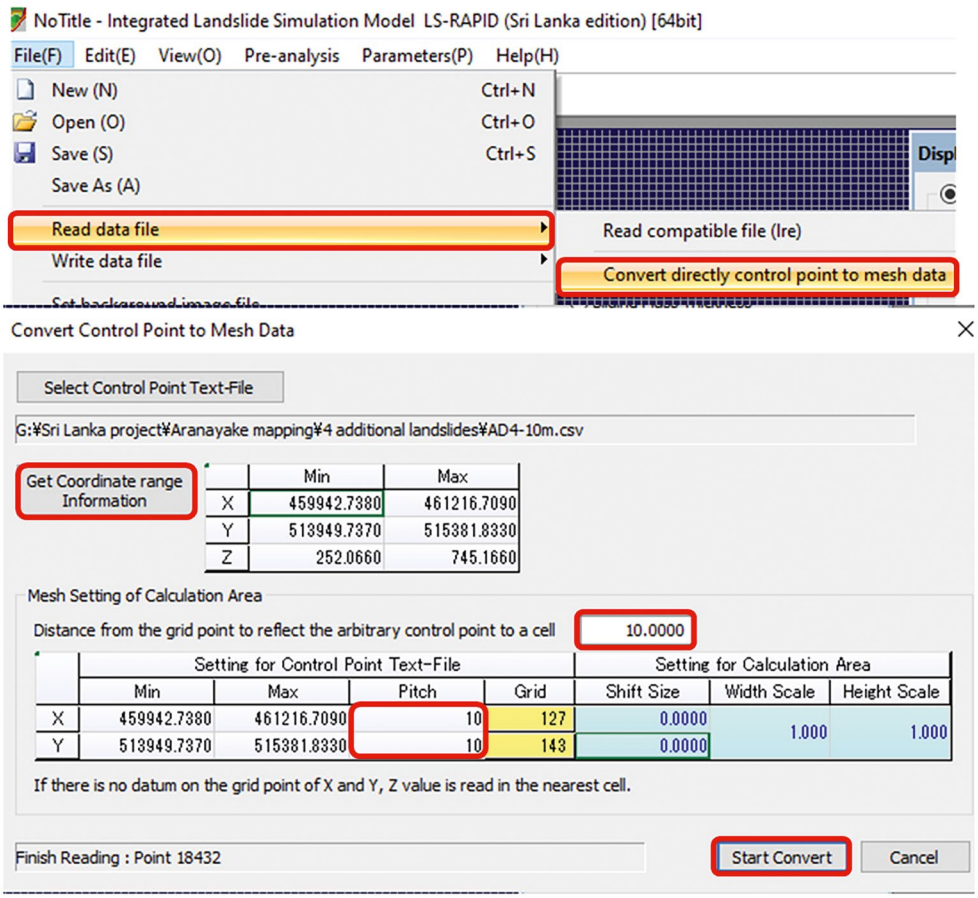
Preparation of Slope Surface

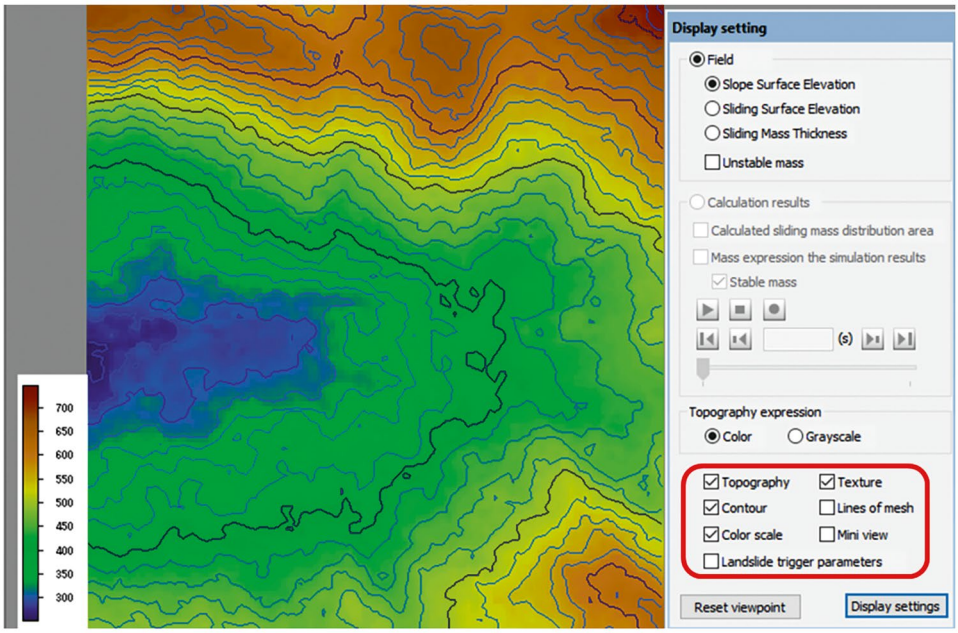
The 2024 LS-RAPID 64-bit was used to estimate the critical pore water pressure and landslide moving area. The 64-bit version can simulate a wider area than the 32-bit version.

Upon starting LS-RAPID, no information about the topography is available (Fig. 17). The steps to generate the slope surface elevation are illustrated in Fig. 17. From the "File" menu, select the "Read data file" option, then click "Convert directly control point to mesh data," and the screenshot of the window is present in the lower part of Fig. 18. To obtain the minimum and maximum values of the x, y, and z coordinates, click on the "Get coordinate range Information" button. Then, we input the grip cell in "Pith" and the "Distance from the grip point to reflect the arbitrary control point in the cell" and click on the "Run" button to start the conversion process. The topography is shown in Fig. 19. We can choose the "color" or "grayscale" option. The contour and color scale is possible to express. The "Texture" option is used to show the background image. The background image was exported from QGIS, including the landslide topography feature overlapping the Google Earth photo.

The left side of Fig. 20 shows the necessary steps to select and display a background image. First, click the "File" option and select "Set background image file." Next, use the

Fig. 18 Screenshot of converting the control point to topography data





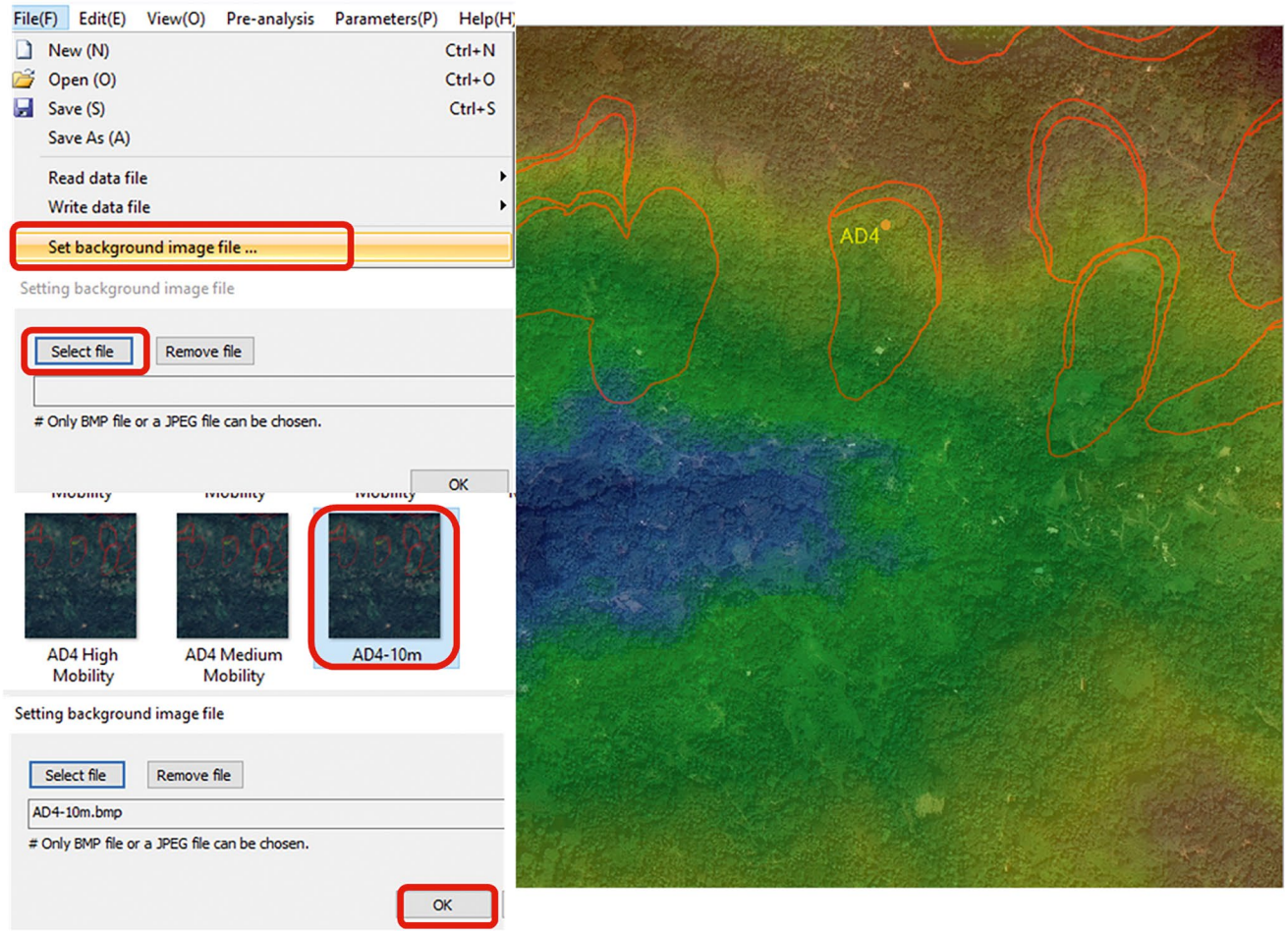


Fig. 19 Slope surface elevation model in LS-RAPID

Fig. 20 Screenshot of setting background image file

"Select File" button to navigate to and choose the BMP or JPEG file associated with the background image. It is important to note that the coordinates of the corners of the background image are the same as those of the simulation area. After selecting the file, click the "Open" button to finalize the process. The result is present on the right side of Fig. 20.

Creating Possible Sliding Surfaces

We can estimate the possible sliding surface of future landslides based on the shape of previous landslides.

To set the ellipsoidal parameters, click the "Edit" Menu and choose the "Ellipsoid Sliding Surface setting" option.

Select a central longitudinal section of the landslide body (AD4 in this example) to get started. This can be done by inputting the coordinates of the start and end points. After inputting coordinates, the corresponding section will appear in the figure on the right side of the window, as shown in Fig. 21. Then, two points, A and B, which the sliding surface passes through, are selected.. Point A is located in the head scarp of the previous landslide. Point B depends on the size of the landslide and topography. We focus on large-scale landslides and normally select point B, which is near the center of the previous landslide body and more than 100 m from point A. It is very difficult to estimate the correct size of a future landslide without a detailed investigation. Different people may create potential landslides of different sizes and shapes. After selecting points A and B, we need to input the coordinates for the center of the ellipsoid on the longitudinal section. The ellipsoid will be shown below the table. The bottom part of the right side of Fig. 26 is the coordinates for ellipsoid passes along the cross-section. Point C and the centre of the ellipsoid on the crossing section depend on the previous landslide's left and right borders. After setting it, we can check the landslide dimension. In this example, the max-

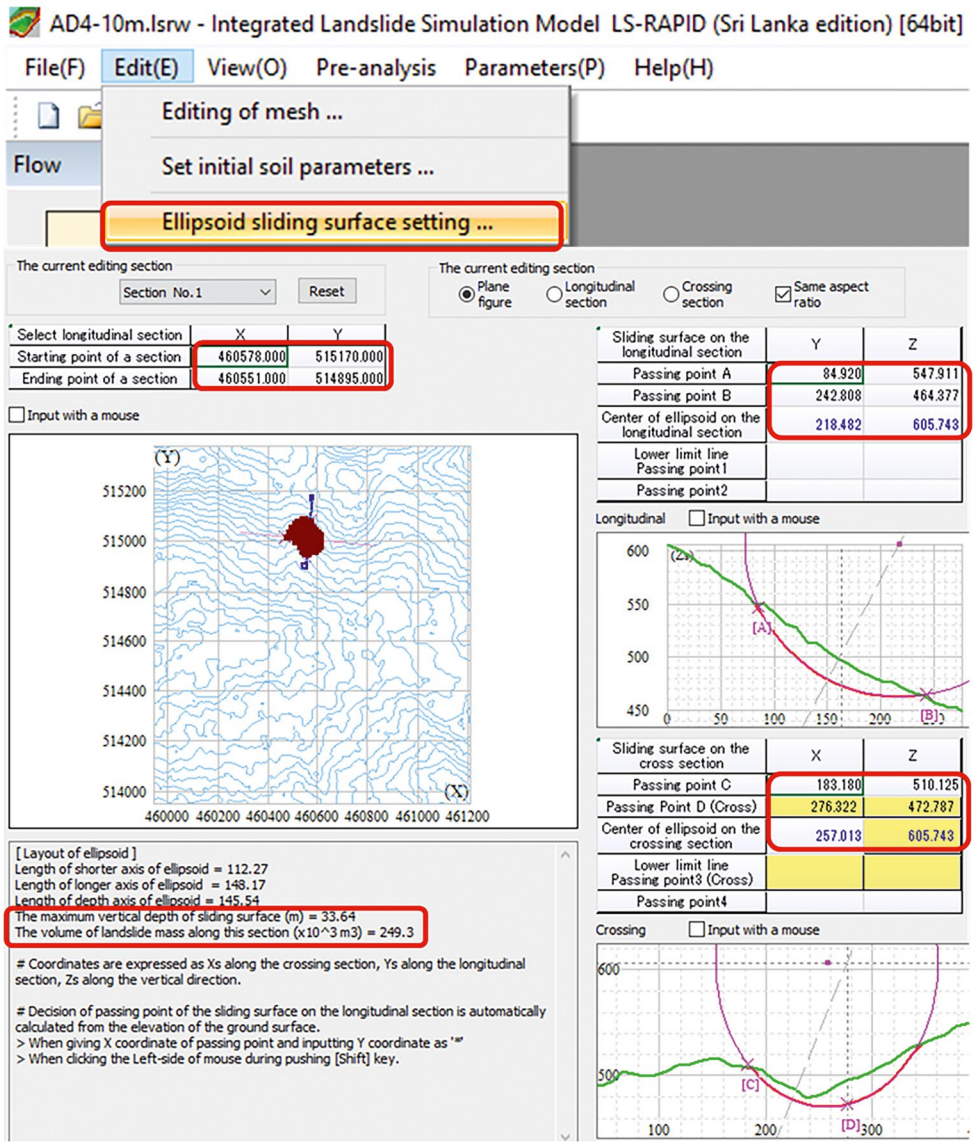


Fig. 21 Screenshot of the ellipsoid sliding surface setting

imum vertical depth of the sliding surface and the landslide volume are 33.64 m and 249.3 × 10^3 m^3, respectively.

The LS-RAPID 32-bit (version 2.5) and 64-bit added a planar sliding surface function. This function is used when the landslide has planar sliding or when reducing the landslide depth. Users need to input the coordinates of points 1, 2, and 4 (Fig. 21). Compared to Fig. 21, the landslide depth and volume were reduced to 27.57 m and 201 × 10^3 m^3, respectively (Fig. 22).

The sub-section is applied if a landslide consists of more than one block. The maximum number of sections is 10. Figure 23 shows an example of three blocks for one landslide area. The example includes both the planar and ellipsoid sliding surfaces.

Estimate and Set Soil Parameters, Triggering Factor

Soil parameters are often obtained from ring shear tests to reproduce past landslides. However, collecting samples and conducting ring shear tests for numerous potential landslides is expensive and challenging. In addition, some landslides have a complex geology, consisting of many layers and areas, resulting in complicated soil parameter settings. To simplify hazard mapping, we propose a method that includes three regions in the simulation area: source area and upper and lower moving areas. Figure 24 compares the simulation results of the simple method (3 areas), complicated setting (8 areas), and UAV photo of the 2017 Aranayake landslide. The landslide traveling distance in Fig. 24a is shorter than in Figs. 24b, c. However, it also reaches the flat area. Therefore, the simple method can produce acceptable simulation results. Based on the landslide depth (D), we dive into three classes: shallow landslide (D < 15 m), moderate landslide (15 m < D < 30 m), and deep landslide (D > 30 m). Two cases, medium mobility, and high mobility, are simulated. Table 3 presents an example of soil parameters for moderate landslides. The details of how to input the soil parameter can be found in Ajmera et al. in 2023.

This paper focuses on rainfall-triggered landslides. The simulation process necessitates a time series of R_u values. Notably, the same Ru values are employed across all cells within the simulation area. The R_u time series is visually presented in Fig. 25. The pore water pressure has increased from 0 to 1.0 within a time frame of 1200 s.

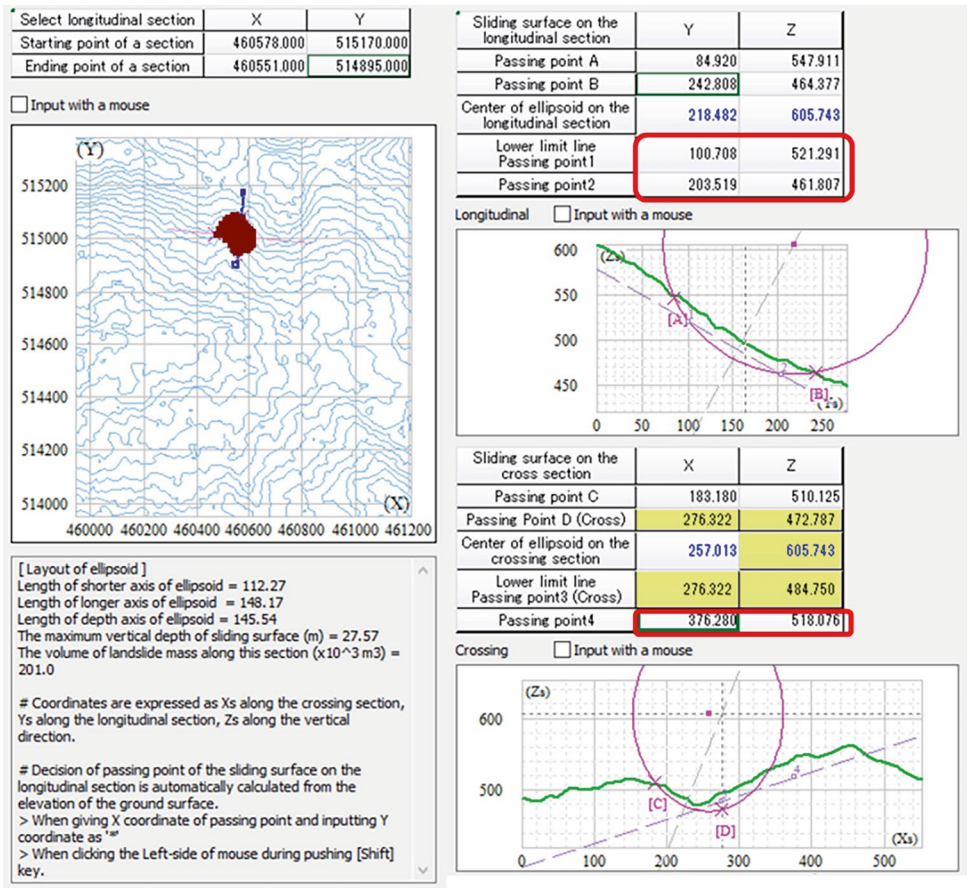


Fig. 22 Screenshot of the planar sliding setting

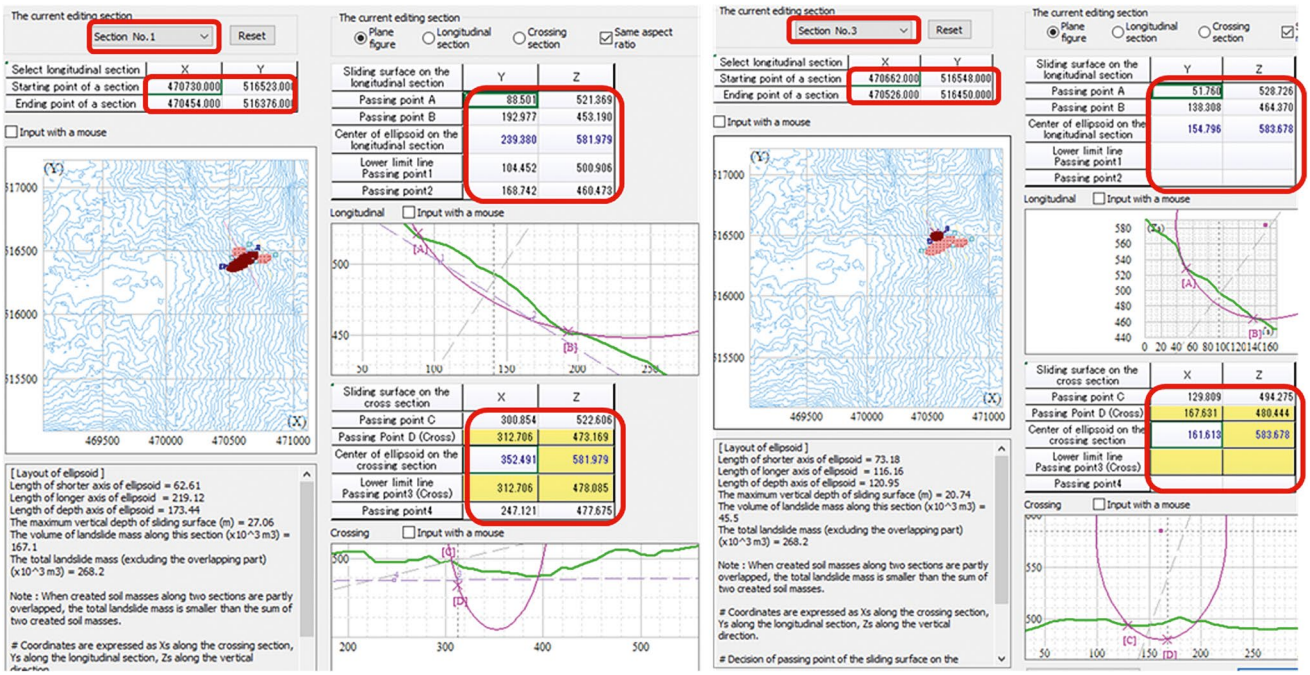


Fig. 23 Screenshot of the ellipsoid sliding surface setting for three landslide blocks

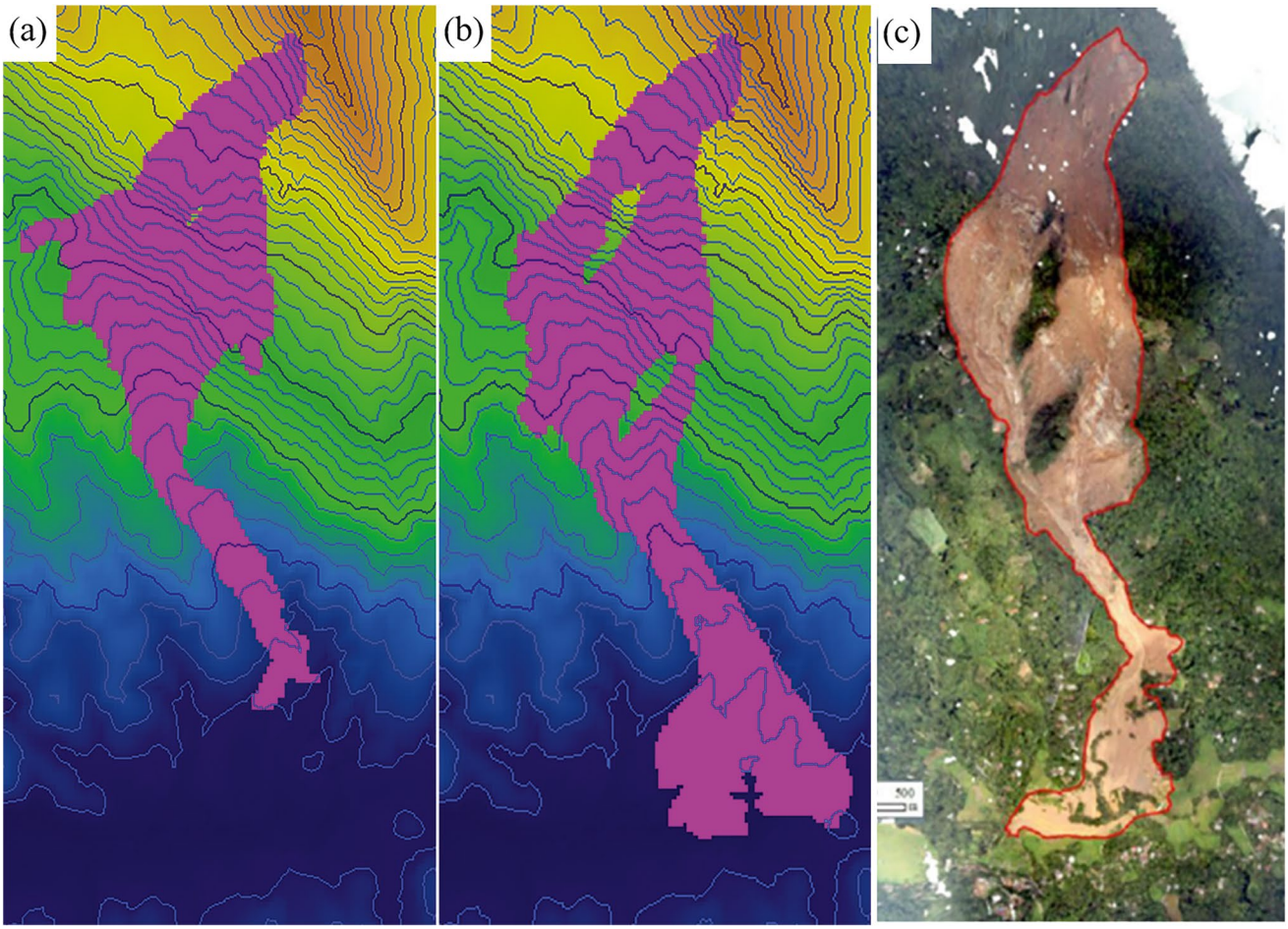


Fig. 24 LS-RAPID simulation results for 2016 Aranayake landslide and UAV photo (NBRO)

Table 3 Example of soil parameter for LS-RAPID

	Medium mobility			High mobility		
Landslide depth	(1) Source area	(2) Moving area (upper)	(3) Moving area (lower)	(1) Source area	(2) Moving area (upper)	(3) Moving area (lower)
15 m < D < 30 m	K = 0.5	K = 0.7	K = 0.85	K = 0.5	K = 0.7	K = 0.9
	φi = 0.6	φi = 0.6	φi = 0.6	φi = 0.6	φi = 0.6	φi = 0.6
	φm = 0.7	φm = 0.7	φm = 0.7	φm = 0.7	φm = 0.7	φm = 0.7
	τss = 30-50	τss = 20-30	τss = 20-30	τss = 30-50	τss = 15-20	τss = 5-10
	Bss = 0.90	Bss = 0.90	Bss = 0.90	Bss = 0.90	Bss = 0.95	Bss = 0.95
	φp = 0.8-0.9	φp = 0.8-0.9	φp = 0.8-0.9	φp = 0.8-0.9	φp = 0.8-0.9	φp = 0.8-0.9
	Cp = 70	Cp = 30	Cp = 30	Cp = 70	Cp = 30	Cp = 30
	γ = 19	γ = 19	γ = 19	γ = 19	γ = 19	γ = 19
	DL = 5	DL = 5	DL = 5	DL = 5	DL = 5	DL = 5
	DU = 200	DU = 200	DU = 200	DU = 200	DU = 200	DU = 200

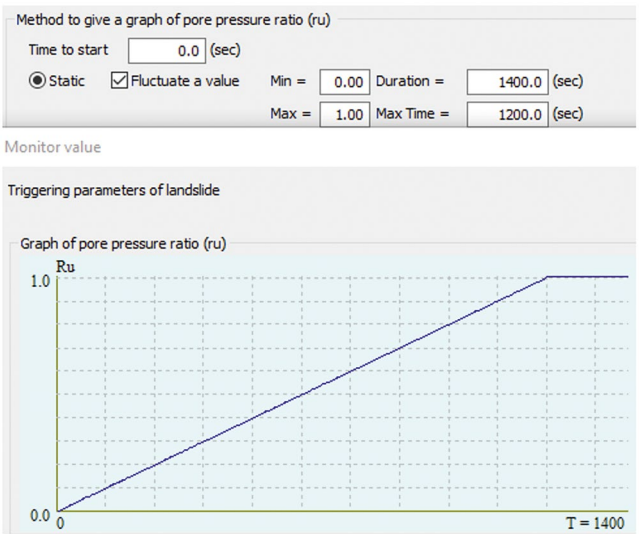


Fig. 25 Screenshot of setting triggering factor

Critical Pore Water Pressure and Landslide Runout Distance

As the simulation progresses, the R_u value gradually increases. The critical R_u value is the value at which the landslide starts moving (Fig. 26). The simulations provide the extent of the landslide runout for each potential landslide, as illustrated in Fig. 27.

The critical pore water pressure determines when landslides occur, and the landside runout distance is used to estimate their potential impact. Both data are crucial to landslide risk assessment and hazard mitigation. Those results provide valuable data for an early warning system that leverages Augmented Reality (AR) technology to facilitate the evacuation of large-scale landslides triggered by heavy rain. The detail of AR technology was published by Araki et al. in 2024.

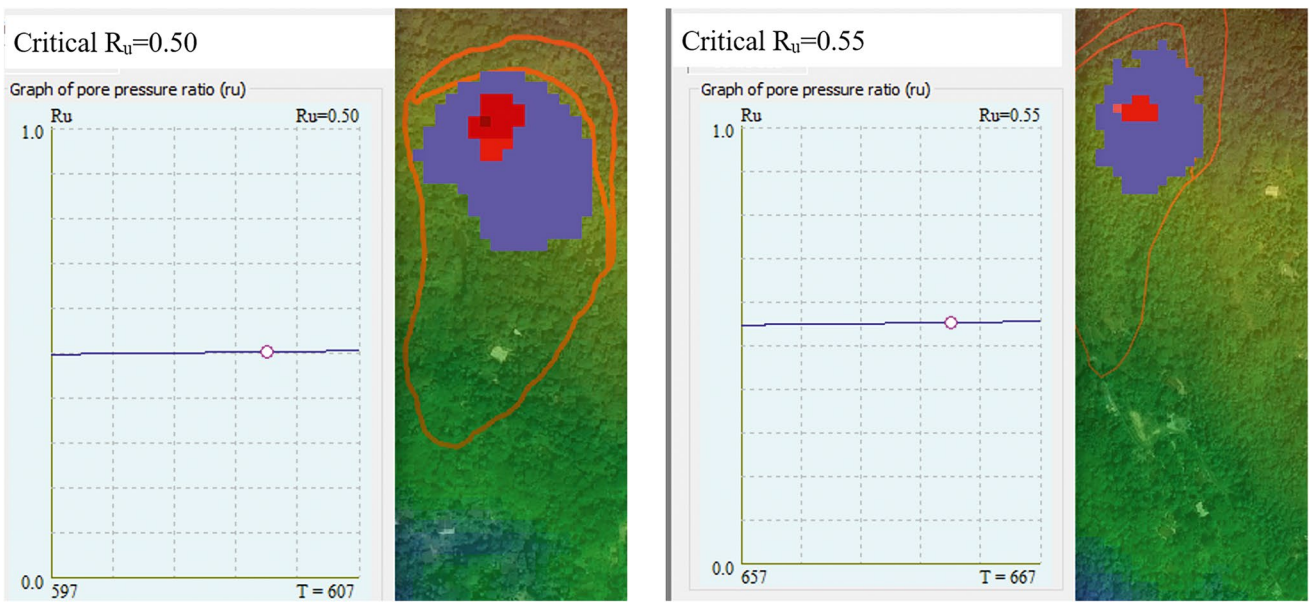


Fig. 26 Critical pore water pressure from LS-RAPID model, Left (R_u = 0.50), Right (R_u = 0.55)

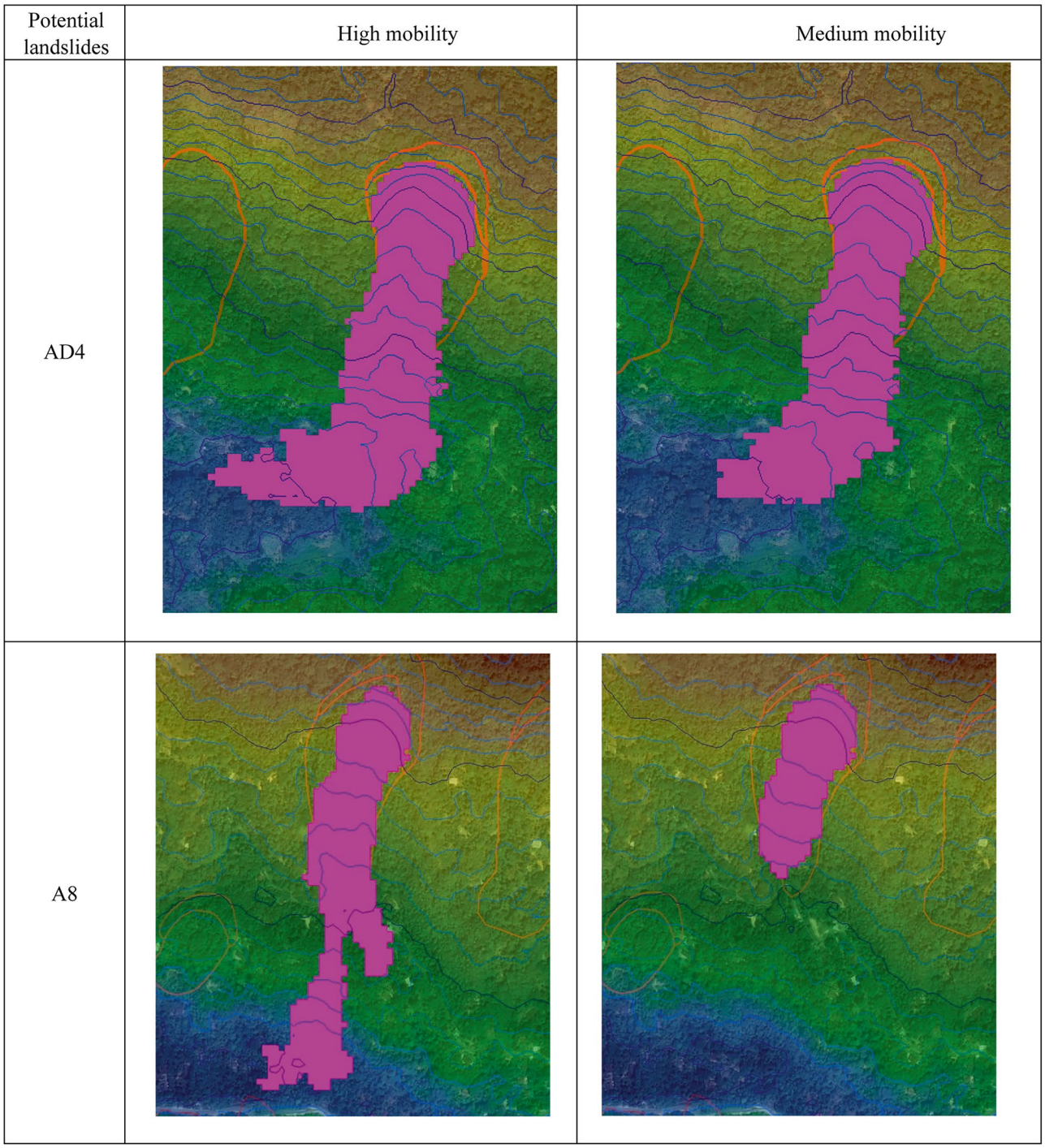


Fig. 27 Landslide simulation results. In the upper figure, the landslide runout distances are similar for both high and medium mobility. In the lower figure, the landslide runout distance of high mobility is much longer than that of medium mobility

5 Conclusion

Determining the location of future landslides is a complex task that requires a detailed investigation. The 2011 Kii disaster is evidence to suggest a hypothesis that the potential large-scale landslides could follow past landslides. From this hypothesis, the landslide topography distribution maps that show the location of past landslides were created for Sri Lanka during the project "Development of early warning technology of rain-induced rapid and long-traveling landslides in Sri Lanka." The maps were used to determine the potential large-scale landslide in Aranayake.

After determining the location of potential landslides, we tried to calculate the critical pore water pressure ratio and landslide runout distance using the LS-RAPID model. Those

data are crucial aspects of landslide risk assessment and hazard mitigation.

We are aware that our research may have some limitations. The first is applying the soil parameter estimates from the 2016 Aranyake landslide to a wide area. The second is to set the dimensions of landslides based on our experience. Further data collection would be needed to identify landslide disaster risk accurately.

Acknowledgements This study was supported by a SATREPS "Science and Technology Research Partnership for Sustainable Development" project named "Development of Early Warning Technology of Rain-Induced Rapid and Long Travelling Landslides" from 2019 to 2025.

We acknowledge Professor Toyohiko Miyagi and Ms. Li Yuxin for their great efforts in creating the landslide topography distribution map in the Aranayake area.

The authors would like to thank GODAI KAIHATSU Co., Ltd. especially for developing of LS-RAPID 64-bit.

References

Ajmera B, Ahari HE, Loi DH, Setiawan H, Dang K, Sassa K (2023) LS-RAPID manual with video tutorials. In: Sassa K, Konagai K, Tiwari B, Arbanas Ž, Sassa S (eds) Progress in landslide research and technology, 1(1), 2022

Alcântara E, Marengo JA, Mantovani J, Londe LR, San RLY, Park E, Lin YN, Wang J, Mendes T, Cunha AP, Pampuch L, Seluchi M, Simões S, Cuartas LA, Goncalves D, Massi K, Alvalá R, Moraes O, Filho CS, Mendes R, Nobre C (2023) Deadly disasters in southeastern South America: flash floods and landslides of February 2022 in Petrópolis, Rio de Janeiro. Nat Hazards Earth Syst Sci 23:1157–1175. https://doi.org/10.5194/nhess-23-1157-2023

Araki K, Takimoto K, Yamazaki Y, Loi DH, Konagai K, Sassa K (2024) Time and site prediction of a potential large-scale landslides and the AR (augmented reality) presentation for early warning. Prog Landslide Res Technol 3(2) in print

Chigira M, Tsou C-Y, Matsushi Y, Hiraishi N, Matsuzawa M (2013) Topographic precursors and geological structures of deep-seated catastrophic landslides caused by typhoon Talas. Geomorphology 201:479–493

Chigira M, Hiraishi N, Ching-Ying T, Matsushi Y (2015) Catastrophic landslides and their precursory deep-seated gravitational slope deformation induced by the river rejuvenation in the Kii Mountains, Central Japan. In: Lollino G et al (eds) Engineering geology for society and territory, vol 2. Springer, Cham. https://doi.org/10.1007/978-3-319-09057-3_95

Dang K, Sassa K, Konagai K, Karunawardena A, Bandara RMS, Hirota K, Tan Q, Ha ND (2019) Recent rainfall-induced rapid and long-traveling landslide on 17 May 2016 in Aranayaka, Kagelle District, Sri Lanka. Landslides 16(1):155–164

FDMA (2012) Report No. 20 released by the Fire and Disaster Management Agency on 28 September 2012, 10 pages (in Japanese)

Inoue K, Doshida S (2012) Comparison of distribution of disasters occurring in 1889 and 2011 on Kii Peninsula. J Jpn Soc Erosion Control Eng 65(302):42–46

Iverson RM, George DL, Allstadt K, Reid ME, Collins BD, Vallance JW, Schilling SP, Godt JW, Cannon CM, Magirl CS, Baum RL, Coe JA, Schulz WH, Bower JB (2015) Landslide mobility and hazards: implications of the 2014 Oso disaster. Earth Planet Sci Lett 412:197–208

JMA (2011) Hourly rainfall data at Kitayama Station. Japan Meteorological Agency. http://www.data.jma.go.jp/gmd/risk/obsdl/index.php

Miyagi T, Ikeda K, Ishikawa H, Doan L, Thanh NK, Tien PV, Li Y, Zhang F (2024a) Interpretation and mapping for the prediction of site risk of landslide disasters: from aerial photography to detection by DTMs. Landslide Res Technol 3(1):15–61

Miyagi T, Loi DH (2024b) How to detect the previous large-scale landslide: source of future landslides by interpretation of ground topography from digital maps. Prog Landslide Res Technol 3(2) in print

NASA. https://appliedsciences.nasa.gov/what-we-do/disasters/landslides. Last access on 8 May 2024

Onishi R, Bandara HAAIS, Matsumoto K (2024) High-resolution rainfall simulations for early warning of long-traveling landslides in Sri Lanka. Prog Landslide Res Technol 3(2) in print

Petley D (2024) The 6 February 2024 landslide at Masara in The Philippines. Landslide Blog. https://eos.org/thelandslideblog/masara-landslide-1. Last access on 20 May 2024

Samia J, Temme A, Bregt A, Wallinga J, Guzzetti F, Ardizzone F, Rossi M (2017) Do landslides follow landslides? Insights in path dependency from a multi-temporal landslide inventory. Landslides 14:547–558. https://doi.org/10.1007/s10346-016-0739-x

Sassa K, Nagai O, Solidum R, Yamazaki Y, Ohta H (2010) An integrated model simulating the initiation and motion of earthquake and rain induced rapid landslides and its application to the 2006 Leyte landslide. Landslides 7:219–236

Sassa K, He B, Dang K, Nagai O, Takara K (2014) Plenary: progress in landslide dynamics. In: Sassa K, Canuti P, Yin Y (eds) International programme on landslides in landslide science for a safer geoenvironment, vol 1. Springer, pp 37–67

Sassa K, Doan L, Dang K, Tien P (2023) Siding-surface liquefaction and undrained steady-state shear strength. Prog Landslide Res Technol 2(1):11–95

Temme A, Guzzetti F, Samia J, Mirus BB (2020) The future of landslides' past—a framework for assessing consecutive landsliding systems. Landslides 17:1519–1528. https://doi.org/10.1007/s10346-020-01405-7

Tien PV (2018) Mechanisms and hazard assessment of rainfall-induced landslide dams. Ph.D. Thesis, Kyoto University

Tien P.V, Sassa K, Takara K, Fukuoka H, Khang D, Shibasaki T, Setiawan H, Ha N.D, and Loi D.H (2018) Formation process of two massive dams following rainfall-induced deep-seated rapid landslide failures in the Kii Peninsula of Japan. Landslides, 15(9), 1761–1778

Wikipedia. https://en.wikipedia.org/wiki/2024_Maco_landslide. Last access on 8 May 2024

Open Access This chapter is licensed under the terms of the Creative Commons Attribution 4.0 International License (http://creativecommons.org/licenses/by/4.0/), which permits use, sharing, adaptation, distribution and reproduction in any medium or format, as long as you give appropriate credit to the original author(s) and the source, provide a link to the Creative Commons license and indicate if changes were made.

The images or other third party material in this chapter are included in the chapter's Creative Commons license, unless indicated otherwise in a credit line to the material. If material is not included in the chapter's Creative Commons license and your intended use is not permitted by statutory regulation or exceeds the permitted use, you will need to obtain permission directly from the copyright holder.



Part IV

ICL Landslide Teaching Tools

MaPLoRds: Mobile Application for Local Road Network Risk Assessment

Biljana Abolmasov, Ranka Stanković, Nikola Vulović, Miloš Marjanović, Uroš Đurić, and Nikola Gudžić

Abstract

MaPLoRds is a software system developed to enable local municipality users to assess the resilience of their local road network from natural hazards in climate-changing conditions. The system analyzes the characteristics of the road network, vulnerability, and climate-related hazards, to evaluate the network's resilience. A tool for mobile devices (mobile application) is developed to facilitate the data collection in the field and a web application is developed for data analysis, resilience, and priority assessment based on the methodology. The bilingual glossary, in Serbian and English, is produced for the developed version of the application, introducing key terms and phrases that are required for the MaPLoRds interface, both for mobile and web application. The system is developed according to the highest industry standards and by Platform Security and Personal Data Protection rules. Personal Data of the users (e.g., password) are stored in encrypted form in the central database, while all other non-sensitive data are not encrypted. In this paper, the MaPLoRds mobile application is available on https://maplords.rgf.bg.ac.rs

Keywords

Local roads · Landslides · Mobile application

B. Abolmasov (✉) · R. Stanković · M. Marjanović · N. Gudžić
Faculty of Mining and Geology, University of Belgrade, Belgrade, Serbia
e-mail: biljana.abolmasov@rgf.bg.ac.rs; ranka.stankovic@rgf.bg.ac.rs; milos.marjanovic@rgf.bg.ac.rs; nikola.gudzic@rgf.bg.ac.rs

U. Đurić
Faculty for Civil Engineering, University of Belgrade, Belgrade, Serbia
e-mail: udjuric@grf.bg.ac.rs

N. Vulović
ENVI Software Solutions, Belgrade, Serbia

1 Introduction

The local road transport network is the weakest link in natural disaster emergencies, especially in climate-changing conditions (Abolmasov et al. 2023b). Improving the national road network resilience (Abolmasov et al. 2023a) is important but without complementary activities on the local level, natural disasters may still impact many people and services. Particularly vulnerable are people living in remote settlements, which might be completely cut off during a severe hazard event, which might prevent their timely evacuation, or halt their supply chain and essential services. In such a case, a resilient national road nearby is not as useful as it would be if the entire system was to endure the hazard impact.

The need to follow resilience standards applied to national road infrastructure therefore must be recognized and implemented at the local road level, as well (Marjanović et al. 2019; Abolmasov et al. 2024). The primary obstacle to achieving full (national and local road) climate resilience is understaffed and underequipped authorities that oversee road management. One approach would be to resolve these issues systematically but slowly, by hiring, training, and equipping authorities in charge. Alternatively, the problem could be reduced by developing methodologies that offer automated, ready-to-use outputs, requiring minimal interaction with the operative staff. MaPLoRds has shown such capabilities and confirmed them on practical examples for the City of Kraljevo and the Aleksandrovac Municipality (Abolmasov et al. 2024).

The generated maps and reports could be directly used in investment planning simulation, enabling decision-makers to identify which road links are of the highest priority, and what type of investment is suitable and cost-effective. In this paper, the MaPLoRds mobile application is presented, and the online version is available at https://maplords.rgf.bg.ac.rs

© The Author(s) 2025

B. Abolmasov et al. (eds.), *Progress in Landslide Research and Technology, Volume 3 Issue 2, 2024*, Progress in Landslide Research and Technology, https://doi.org/10.1007/978-3-031-72736-8_20

2 What Is MaPLoRds

MaPLoRds is a software system developed to enable users to assess the resilience of their local road network from natural hazards in climate-changing conditions. It is an essential tool for applying a methodology developed to enhance the climate resilience of the local road network. The system analyzes the characteristics of the road network, vulnerability, and climate-related hazards, to evaluate the network's resilience. MaPLoRds features user-friendly interfaces and visualization tools to support the decision-making process. The MaPLoRds system consists of both a mobile and a web application. The system uses open data from Geographic Information Systems (GIS) and open maps. This data is available for use both in the field, through mobile devices, and in the office, using a web application. The mobile and web application is primarily in Serbian but also includes English. The application includes a list of important words and phrases in both Serbian and English, which is useful for understanding the app's interface. However, the application can support other languages too. All the different languages are stored in a central place and can be easily added to the application when needed.

3 MaPLoRds System Development

The MaPLoRds mobile application is developed using Net MAUI (https://dotnet.microsoft.com/en-us/apps/maui) as a Multiplatform App User Interface and C# programming language. The web services that are used for communication between mobile application and back-office (central) database are developed using ASP.NET Core Web API. The web application, allowing for several modules with features such as data visualization, validation of data, and consistency check-ups, is developed as a web application using ASP.NET Core (Core6, MVC app).

The system's initial list of roles includes the following: System Administrator (responsible for user and role management), Power-user for all LSGs, Power-user for a specific LSG, Field Specialist, and Public users (with restricted access to available data on the site—read-only mode). The user assigned the role of Field Specialist is intended to use the mobile application with rights to create observations, fill in data forms, capture photos, and submit data to the central database.

The database management system used is PostgreSQL 14.4 (https://www.postgresql.org/)) with pgAdmin 14 tools (https://www.pgadmin.org/). The GIS database support is using PostGIS (https://postgis.net/). Geospatial data sharing is implemented by GIS web services relying on GeoServer 2.21 (https://geoserver.org/), also an open-source tool. More precisely, Geospatial Information System Web RESTfull API—Services that follow the Open Geospatial Consortium (OGC) standards for web services: Web Mapping Services (WMS) and Web Feature Services (WFS) are used. The database name is maplords_db.

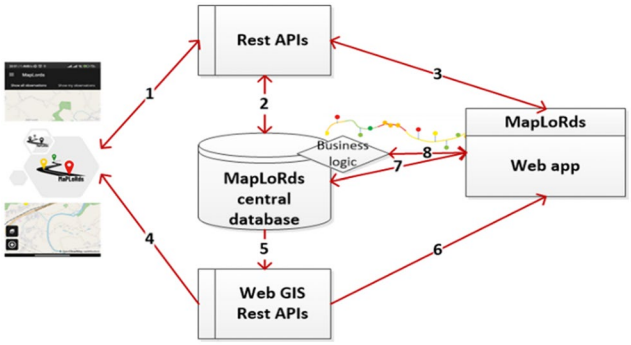


Fig. 1 Components of MaPLoRds system

The main components of the system and data flow interaction are presented in Fig. 1. On the left side is a mobile application for data collecting in the field. Data are stored in the local database, whereupon synchronization requests and via available internet connection alphanumeric data (1) are sent via Rest API for storage in the MaPLoRds database (2). A Set of Rest APIs is also used to exchange alphanumeric data (3) with MaPLoRds Web Application. WebGIS Rest APIs are used to read data (5) from a central database and to serve the WMS layer for mobile application (4), as well as for web application (6). Business logic is implemented in the business layer over the central database as a set of procedures that perform all required calculations (score calculations) and deductions (priority class assignment) (8), whose results are retrieved by web application together with other required data (7).

4 MaPLoRds Mobile Application

How to Start?

The installation "apk" file is available at http://maplords.rgf.bg.ac.rs/data. The final version of the application is published on official Google Play (https://play.google.com/) and for IOS on App Store repositories. After installation, the Field user authorized for data collection can start with his registration. Verification of the registration is to be provided by the Power-user.

A User-friendly interface guides the user to report an observed issue that will be called observation (using a button on a map). The users are offered the chance to choose the type of hazards on the road by image clicks for easier selection, upon which several forms follow with further data collection requirements.

The user of the mobile application has the following options for data collection:

- self-registration module, user login, password change,
- collection of new observation data,
- search, view, and filter collected data (with the option to see own data and data of other users in the same LSG),
- editing of collected data, except geolocation and date/time.

After finishing all required data entries, a pin location on the map is generated. The click-on pin opens the form with the saved data. In case a new issue needs to be reported on an existing issue from the past, both entries (old and new) will be saved to the database, but the old entry will be marked as inactive.

Mobile application is enabled to work in online and offline mode. Frequently, internet connectivity may not be accessible on location. In such cases, offline mode operation enables the collection of necessary field data and its storage in a local database on a mobile device. Once an internet connection is re-established, the status or datasets will be updated, transferred, and synchronized with the backend database.

MaPLoRds General Panels

The first application panel is the Login panel, see Fig. 2. The new user needs to access the user registration form and click on the Register link. The existing user uses his own, already-generated, username and password to log in.

Upon clicking on the Register link, the new user will be prompted to fill in the information displayed which includes their first and last name, telephone number (optional), select municipality (LSG), username, and password. The checkbox "I have read and accept privacy, terms and conditions" with appropriate links to documents must be checked before proceeding with application use.

Before login, the account must be approved by the System Administrator. The whole procedure of registering is explained in a quick tutorial that is available for download at https://maplords.rgf.bg.ac.rs/data/tutorial/QuickTutorial.pdf. In addition to the registration button, the Login panel also includes a Request button for resetting a forgotten password. Registration fields are Full name (first and last name); E-mail; Municipality (LSG); Username; and Password.



Fig. 2 Login panel (with registration link)

Data Collection

The reporting of climate-related hazard problems on road infrastructure will be facilitated by a user-friendly interface that includes a background map. Users will be able to select one or more types of occurrences (landslide, rockfall, flood, flash flood) on the road by choosing from offered images, making the selection process easy. They will then be prompted to fill out several forms for data collection, including data on traffic and estimated investments.

After completing all required data entries, a pin on the map will be generated. Clicking on the pin will open a form with saved data. If a new observation is reported for a location that has an existing observation, both entries (old and new) will be saved in the database. The ordinal number (observation_id field) of the new entry will be increased by

one, so the old entries have smaller ordinal numbers. After successful login user can preview and enter new observations, change profile, modify settings, and read the Privacy Policy and Terms of Use.

The preferred and default functionality of the application is to use online maps. However, in areas where the internet is not available, the user can select to work with offline maps that are prepared and available on the project server. The download of maps per selected Local Self Government (LSG) is automated, so the system will then automatically calculate and record the current user's location, along with the corresponding date and time, and save the collected data. It is assumed that in real time the user is present at the road location road being observed. The system will later automatically align recorded observation points with road links, by using distance measurement to match the point with the road links accurately.

After clicking the Add new button or icon (+), a panel is displayed, and then the user can select a hazard data entry by clicking on one of the four pictures offered (see Fig. 3). Four types of hazards are available, namely, landslide, rockfall, flood, and flash flood. Each hazard type has a distinct color scheme. The data entry forms also include a camera button to take photos, which is present in the panels for hazards, traffic, and infrastructure data. After selecting a button corresponding to the identified hazard type, the user can access the appropriate data entry form. Upon completing the data entry for one hazard, the user will be redirected to the previous panel to record additional hazards for the same observation, if applicable.

Panel for Hazards—Landslides an Rockfall Example

The landslide panel is distinguished by a dark red color scheme and allows users to insert data specific to the chosen type of landslide hazard. The panel begins with a schematic presentation of all quantitative values to guide users as they complete the form. In the dimension data section, users can enter values for length, width, depth, and area. Required—obligatory values are indicated by a red asterisk (*) in the caption label. The form is designed to adapt to the required data, so if a user selects "no" for "visible scarp", no additional quantitative data will be needed, and a corresponding text box will not be visible. However, if the user selects "yes" for "visible scarp", two text boxes for height and volumes will appear. Logical constraints are also included in the form, such as if the landslide activity is described as "once in a few years", it cannot be categorized as "active" (by definition).

Categorical variables can be selected in either a single-choice or multiple-choice format. Single-choice format allows the user to select only one option from the offered choices, whereas multiple-choice options allow the user to select zero or more options.

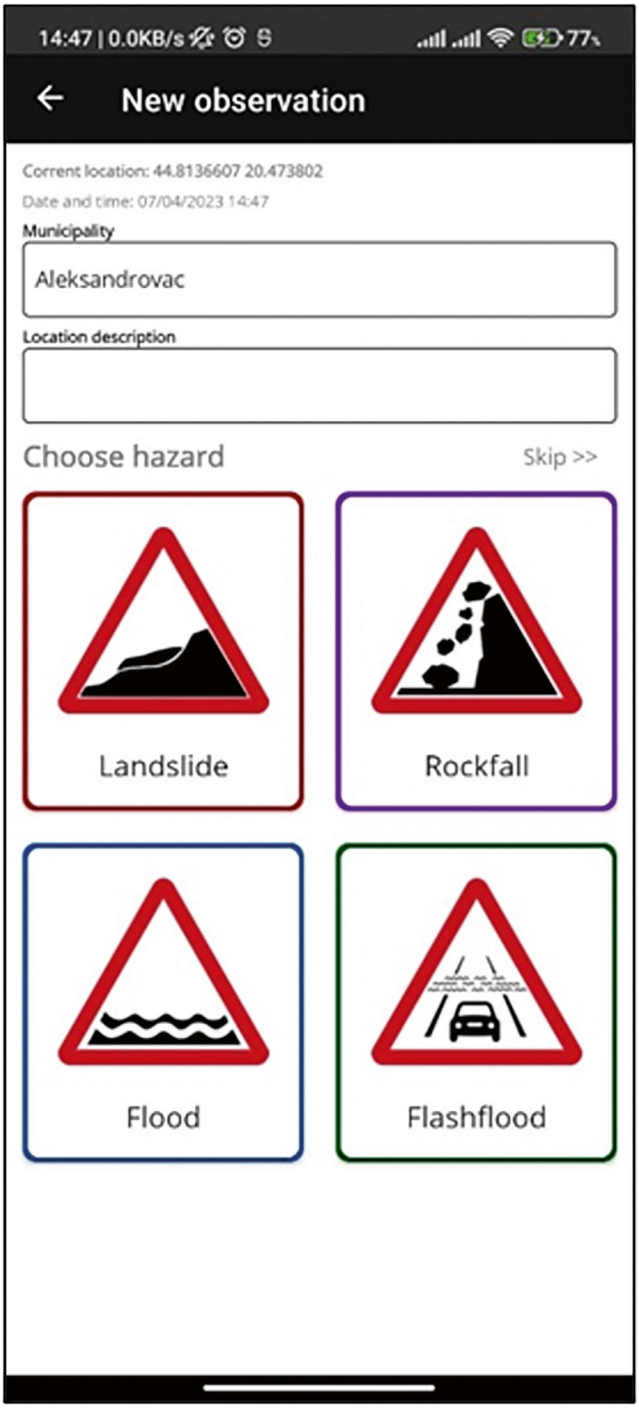


Fig. 3 New observation, panel for hazard selection

To enable single-choice selection, option buttons can be used, as presented in Fig. 4. For the frequency of landslide occurrence, the user can choose from options such as "once in a few years", "once in a year" or "more than once in a year". Option buttons are designed to be easily selectable on mobile devices, and the selected option is identified by a checkmark (tick mark). For multi-value selection, checkboxes are used. For example, in the case of landslide triggers,



Fig. 4 Panel for basic landslide data

the user can select one or more options from the list of offered choices, including "rainfall", "earthquake", "snowmelt", "erosion of the base" and "human activity (undercutting, overloading…)". The final section of the panel is dedicated to the status of the activity of the landslide, as well as for the information on remediation if available. The remediation date is recorded in a text field, which allows for the inclusion of partial dates such as "2015, end of the year", "2016, May" or "2016-05-25". Note that it is very important that the first 4 characters denote the year of the remediation.

After finishing with landslide data entry, the user can:

- Add new hazards (using the NEW button) (save and go to the home panel),
- Return to the first screen (BACK button) (without saving of current data go to the home panel),
- Take a picture (using the CAMERA button), save it (it is automatically linked to the observation),
- Finish with hazards and go to the Traffic form (using the NEXT button, go to the traffic panel in),
- Abandon any entry on the current form and skip to the next (traffic) panel by clicking on the SKIP icon,
- Finish with Traffic and go to the Infrastructure form (using the NEXT button).

The Rockfall panel has a purple color scheme (Fig. 5). When selecting the rockfall hazard type, the user can enter relevant data for the rockfall event. The rockfall panel begins with a schematic presentation of all quantitative values to guide the user when filling in the form. A similar approach for option buttons and multiple-choice checkboxes is used in landslides. The same conditional functionality of buttons and fields, as well as logical consistency check, is applied as in the landslide case. In the dimension data section, the user can enter values for the runout, release height, and block volume. Required—obligatory values are indicated by a red asterisk mark (*) in the caption label. For multi-value selection in rockfall triggers, checkboxes are used, allowing the user to select one or more options from the offered list. The available options to be checked for rockfall triggers include "rainfall", "earthquake"," icing", "plant roots", "snowmelt" and "human activity (undercutting, overloading…)". Similar to the landslide triggers, for this panel as well at least one selected option is required from the list. The final section of the panel is dedicated to the status of the rockfall activity, as well as to the information on remediation if available. The remediation date is recorded in a text field, which allows for the inclusion of partial dates such as "end of 2015" or "May 2016".

After finishing with rockfall data entry, the user can:

- Add new hazards (using NEW button) (save and go to the home panel),
- Return to the first screen (BACK button) (without saving current data go to the home panel))
- Finish with hazards and go to Traffic form (using NEXT button go to traffic panel))

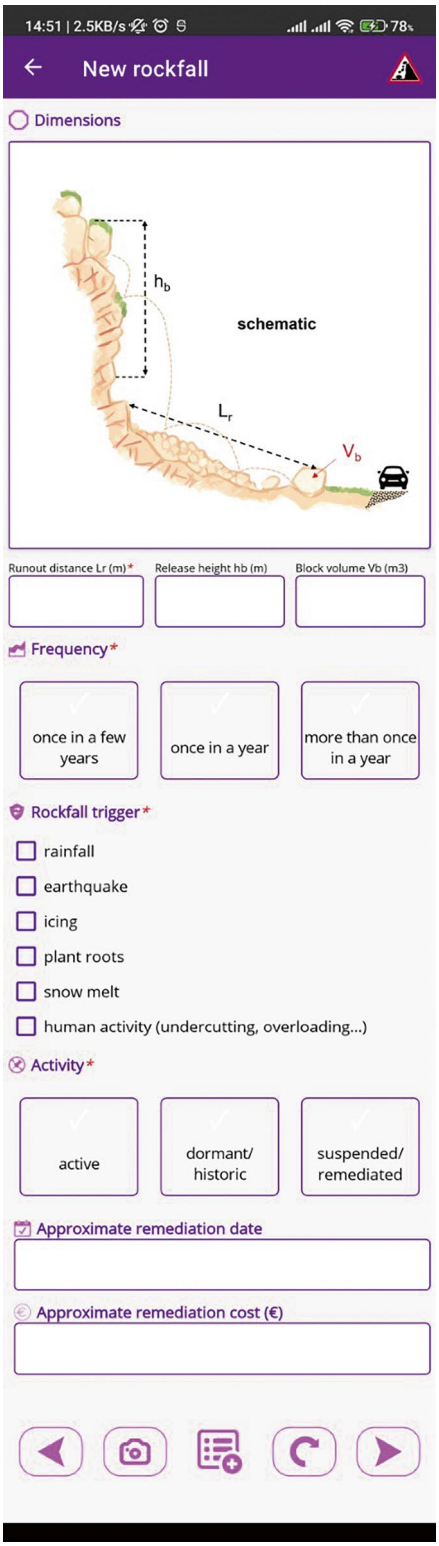


Fig. 5 Basic panel for rockfall hazard

- Open the camera, take a picture, and save it (it is automatically linked to the observation),
- Abandon any entry on the current form and skip to the next (traffic) panel by clicking on the NEXT button.

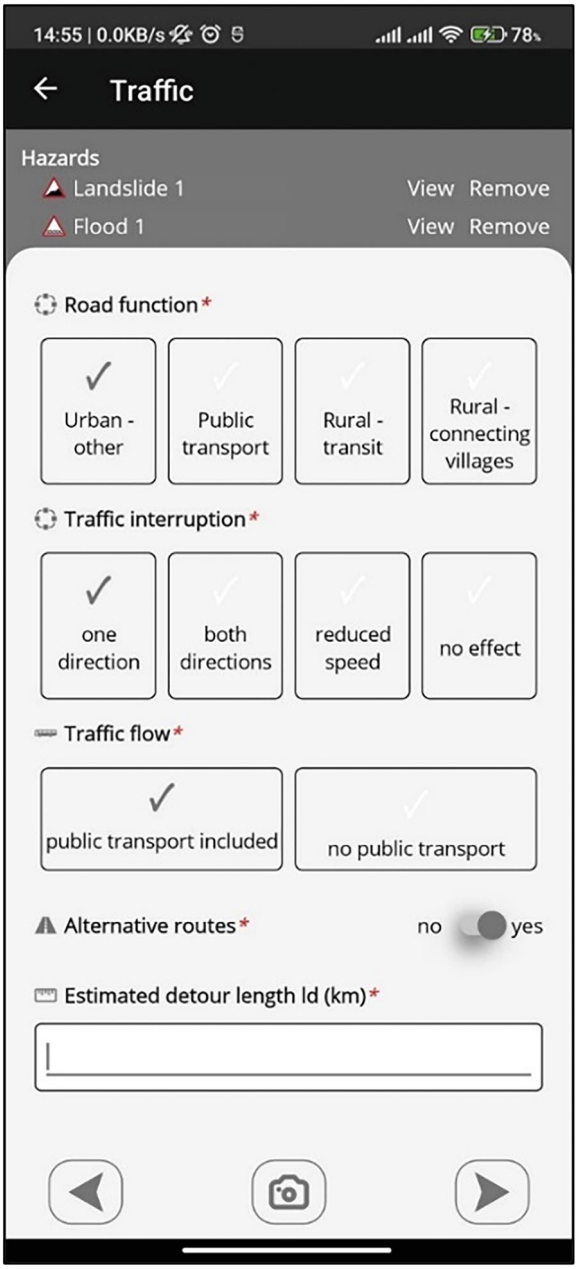


Fig. 6 Panel for traffic information

Adding Traffic Information

Once all hazard information has been added, the traffic information panel becomes available. To provide a better overview of the recorded hazard data, a list of all previously recorded hazards is displayed at the top of the panel, with links for viewing and removing functionality if necessary (as shown in Fig. 6).

For the traffic interruption type, one of the following options can be selected: “single lane”, “both lanes”, “reduced speed”, or “no effect”.

For traffic flow type, one of the following options can be selected: public transport included or no public transport.

The alternative routes parameter is implemented as a "no/yes" switch. If the user selects "yes" then the estimated length of the alternative route is required.

After finishing with traffic data entry, the user can:

- Return to the hazard screen (BACK button) (without saving current data go to the home panel)
- Open the camera, take a picture, and save it (it is automatically linked to the observation),
- Abandon any entry on the current form and skip to the next (traffic) panel by clicking on
- Finish with Traffic and go to the Infrastructure form (using the NEXT button).

Adding Infrastructure Information

The Affected Road part of the panel is divided into three logical parts:

- **Road:** "pavement, asphalt layers"; "pavement, concrete layer"; "pavement, cobbled stone"; "pavement, all layers"; "embankment, damage of embankment"; "drainage, cleaning or repair of light drainage elements";
- **Structure:** "bridge, light surface repair"; "bridge, structure repair"; "bridge, new bridge"; "retaining wall, wall repair"; "retaining wall, new wall (sections)"; "drainage, repair of culverts";
- **Other:** "third party utilities, interruption of existing roadside infrastructure"; "earthworks, removal of the soil"; "scaling, rock scaling"; "households, endangered households"; "casualties, dead or injured", "endangered stream".

The quantitative value for Road width (designation B) is required (obligatory) data. An extensive list of boxes is presented to explain the interface, but usually, only a few of these boxes will be visible (Fig. 7). Specifically, depending on the selected options for the Affected Road, only relevant quantitative values will become visible. To specify the type of Surface course, the user can select one option from the list provided, which includes: "dirt", "gravel", "macadam", "cobbled stone", "concrete", and "asphalt". Clicking the NEXT button will take you to a multimedia panel while selecting the BACK button will return you to the transport panel. To obtain more information, the user can click on the "i" button.

Uploading Images/Photos

As already explained at the panel for new observation, the CAMERA button can be used for taking pictures from any of the panels. In addition, users have the option to take pictures outside of the application and later link them to the observation entry by uploading them on the screen. Photos from the fields will be automatically sent to the server along with other data (as one batch) to record the visual evidence of the observation. Later, users can use the web application to describe the photos.

Data Preview

On the Home panel, users have the option to select the data preview feature, which displays a list of observations. After choosing a particular observation from the list, its details are presented (Fig. 8). It is worth noting that a location can be observed multiple times during the designated period, and all data is recorded and available for preview. However, the most recent data will be displayed at the top and used for scoring. Examples of editing options for different data groups are presented in Fig. 6. Once all the necessary data has been provided, the observation data can be uploaded to the server. If photos are included in the data, they will be exported automatically as well. The user has the option to select specific observations for export or choose to export all observations at once. It is important to note that a successful export requires the mobile device to be connected to the internet. After a successful upload, the exported data is removed from the list of observations for upload.

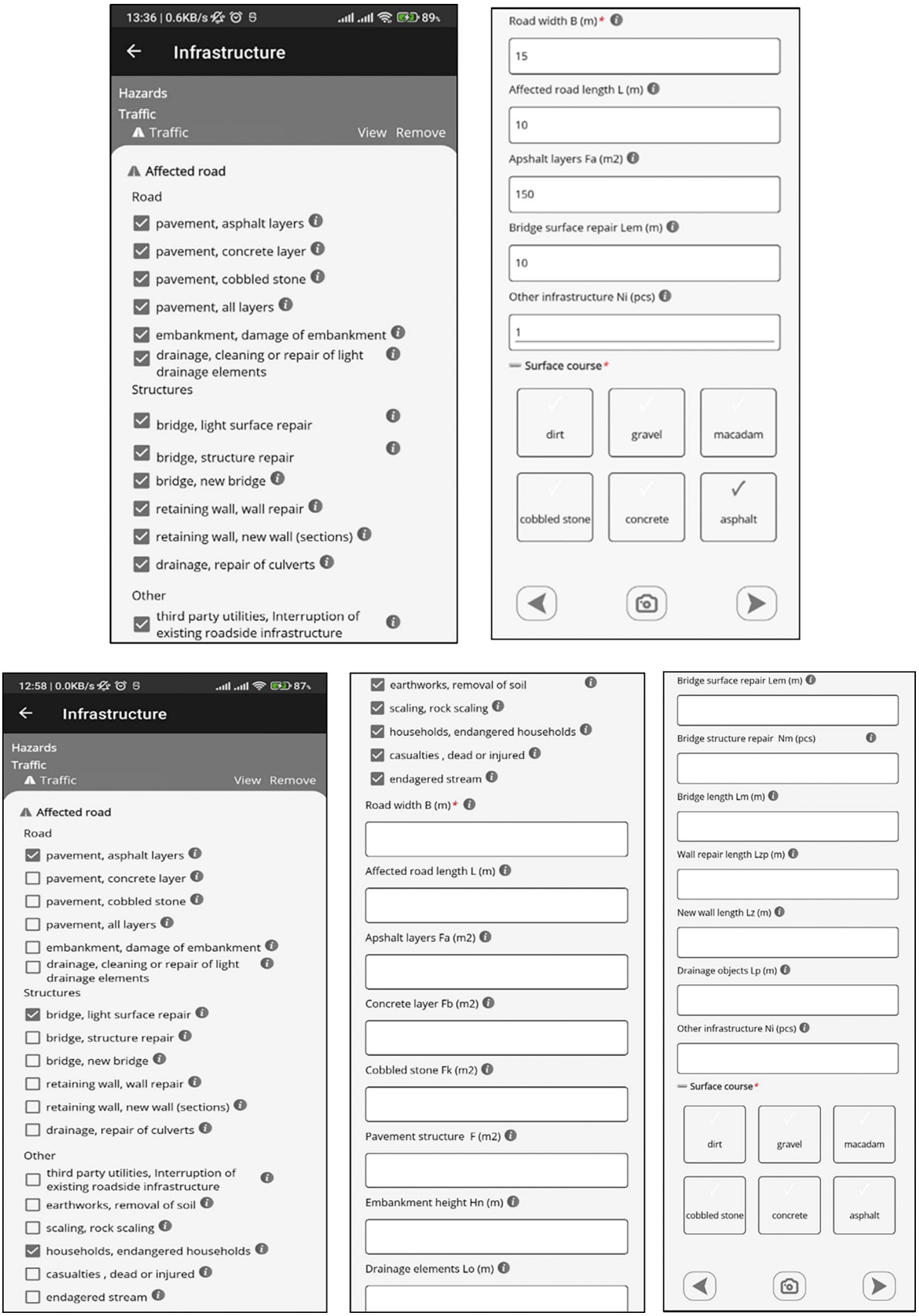


Fig. 7 New infrastructure panel

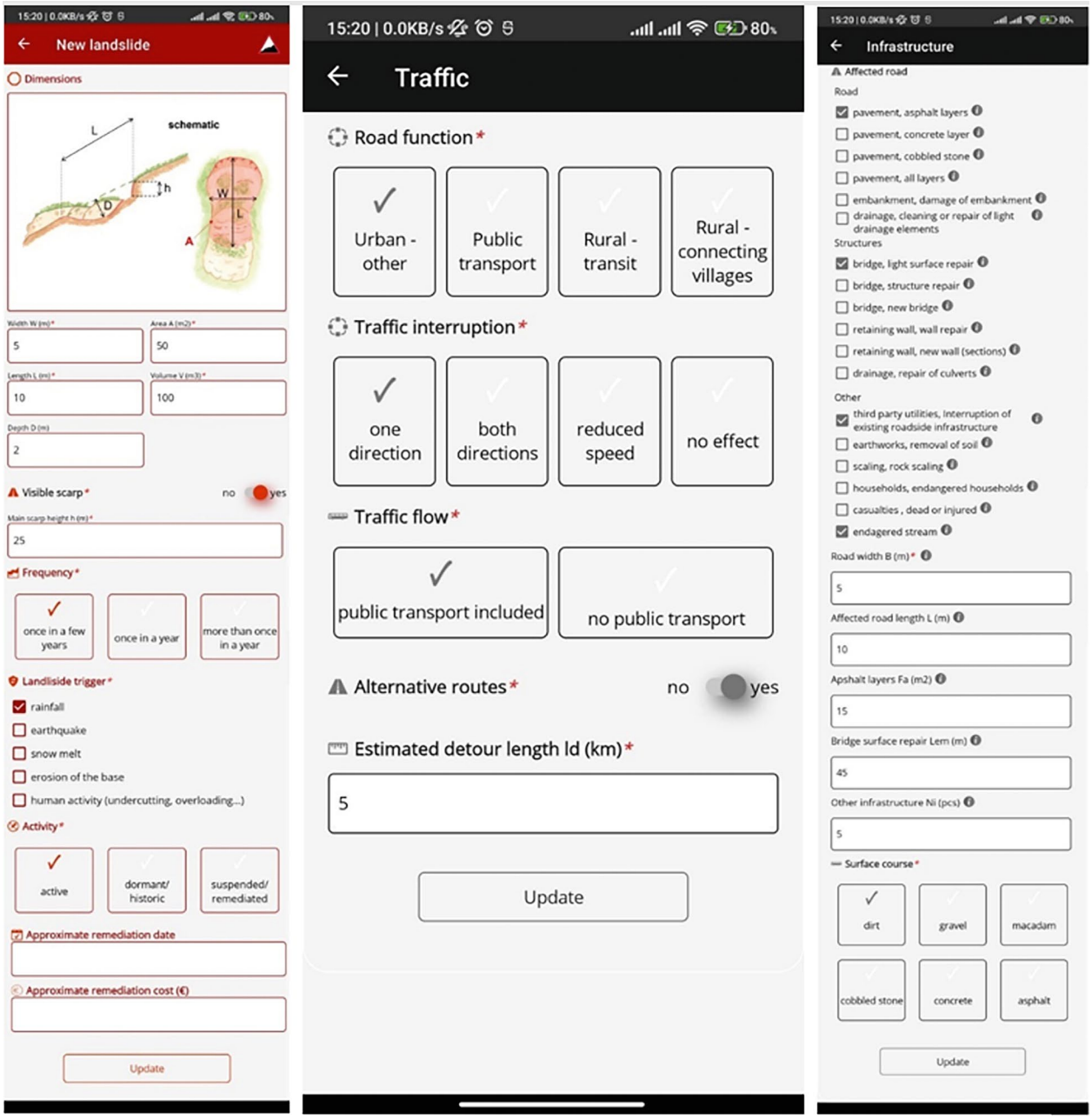


Fig. 8 Editing/updating (examples)

5 Conclusion

This work examines a strategy for increasing climate resilience on local road infrastructure in the Republic of Serbia, under the World Bank project framework. The development of the MaPLoRds mobile application (for Android and iOS) and web GIS application enables users to perform continuous data collection related to road hazard events. A tool for mobile devices (MaPLoRds mobile application) is developed primarily to facilitate data collection in the field. The tools are simple to use, intuitive, and with a user-friendly interface for utilization by engineers in the LSGs administration. The mobile application MaPLoRds has been successfully tested and collecting of data is still in progress for two municipalities in Serbia—City of Kraljevo and Aleksandrovac Municipality. It is expected to introduce MaPLoRds mobile and web applications for more local-municipal roads exposed to climate-related hazards. This work is also contributing to ICL/WCoE activities within the framework to open access data/support/application on landslide risk reduction.

Acknowledgments This research is conducted in the framework of the World Bank Project: "Improving Resilience and Safety of the Local Road Transport Network in the Republic of Serbia" realized by ARUP d.o.o. Belgrade Office and University of Belgrade, Faculty of Mining and Geology.

References

Abolmasov B, Stanković R, Marjanović M, Vulović N, Đurić U (2023a) CliRtheRoads: an integrated approach to landslide risk management on roads in Serbia. In: Alcántara-Ayala I et al (eds), Progress in landslide research and technology, vol 2(Issue 2), 2023, Progress in Landslide Research and Technology. pp 403–409. https://doi.org/10.1007/978-3-031-44296-4_23

Abolmasov B, Marjanović M, Đurić U, Krušić J (2023b) An integrated approach to landslides risk management for local and national authorities. In: Alcántara-Ayala I et al (eds.) Progress in landslide research and technology, vol 2(Issue 2), 2023, Progress in Landslide Research and Technology, pp 355–360. https://doi.org/10.1007/978-3-031-44296-4_20

Abolmasov B, Marjanović M, Stanković R, Đurić U, Vulović N (2024) Increasing the local road network resilience from natural hazards in municipalities in Serbia. Prog Landslide Res Technol 3(1):2024. https://doi.org/10.1007/978-3-031-55120-8. (In Press)

Marjanović M, Abolmasov B, Milenković S, Đurić U, Krušić J, Samardžić PM (2019) Multihazard exposure assessment on the Valjevo City Road Network. In: Pourghasemi HR, Gokceoglu C (eds) Spatial modeling in GIS and R for Earth and environmental sciences. Elsevier, pp 671–688. ISBN 978-0-12-815226-3. https://doi.org/10.1016/B978-0-12-815226-3.00031-4f

Open Access This chapter is licensed under the terms of the Creative Commons Attribution 4.0 International License (http://creativecommons.org/licenses/by/4.0/), which permits use, sharing, adaptation, distribution and reproduction in any medium or format, as long as you give appropriate credit to the original author(s) and the source, provide a link to the Creative Commons license and indicate if changes were made.

The images or other third party material in this chapter are included in the chapter's Creative Commons license, unless indicated otherwise in a credit line to the material. If material is not included in the chapter's Creative Commons license and your intended use is not permitted by statutory regulation or exceeds the permitted use, you will need to obtain permission directly from the copyright holder.



Simple Method of Risk Assessment for Landslides: A Case Study of the JICA Project in Honduras

Kiyoharu Hirota, Kosuke Uzawa, and Takeshi Kuwano

Abstract

This paper describes a simple method of risk assessment for landslides. The study area is landslide-prone in the northern part of Tegucigalpa, the capital of Honduras. In creating a landslide risk map from a landslide hazard map, the authors used a matrix diagram as a risk analysis method to classify risks by focusing on the relationship between the degree of landslide hazard and the number of houses free from landslides. The authors will introduce the activities involved in the process leading up to risk assessment and a simple method from creating a landslide survey sheet to creating a landslide risk map. It is a part of the activities of the Japan International Cooperation Agency.

Keywords

Landslide · Risk assessment · Risk matrix diagram

1 Introduction

While a landslide hazard map can be prepared by identifying the locations of landslides and their nature and condition, creating a landslide risk map is complex. It necessitates a quantitative evaluation of the probability of landslide occurrence, a process that relies on reliable data and poses significant challenges.

K. Hirota (✉) · K. Uzawa
International Consulting Department, Kokusai Kogyo Co., Ltd., Tokyo, Japan
e-mail: kiyoharu_hirota@kk-grp.jp; Kosuke_Uzawai@kk-grp.jp

T. Kuwano
Earth System Science Co., Ltd., Tokyo, Japan
e-mail: kuwano-takeshi@ess-jpn.co.jp

Under these circumstances, the authors considered how to create a landslide hazard map and assess landslide risk using a straightforward method.

This paper introduces the activities of the "Project for Control and Mitigation of Slope Disasters in the Central District in Republic of Honduras" of the Japan International Cooperation Agency (hereinafter referred to as JICA) as a case study. It lists the following items and describes the method and content of the study.

1. Creation of a landslide stability survey sheet,
2. Creation of a landslide hazard map and house survey based on the map,
3. Creation of a risk matrix diagram,
4. Creation of a landslide risk map, and
5. Proposal of a risk assessment process in the community.

The following content is based on the content presented at the 6th World Landslide Forum in Florence (WLF6).

2 Background

Honduras was affected by Hurricane Mitch, which struck Central America, including neighboring countries, from October 22 to November 5, 1998. In Tegucigalpa (Fig. 1), landslides and floods caused extensive damage, including many deaths. Based on this background, creating a landslide hazard map was necessary to serve as the basis for landslide prevention works. Even in situations where landslide experts are not always available, it is necessary to be able to create landslide hazard maps as quickly as possible. JICA experts created a landslide inventory map of Tegucigalpa during the 2012–2013 JST-JICA "Disaster Geology Research Focusing on Landslides in Tegucigalpa Metropolitan Area" (Grupo de Mapeo de Deslizamientos de Tierra de Tegucigalpa, 2014, Fig. 2). In this study, training on the basics of landslide topography interpretation and methods for creating landslide

© The Author(s) 2025

B. Abolmasov et al. (eds.), *Progress in Landslide Research and Technology, Volume 3 Issue 2, 2024*, Progress in Landslide Research and Technology, https://doi.org/10.1007/978-3-031-72736-8_21

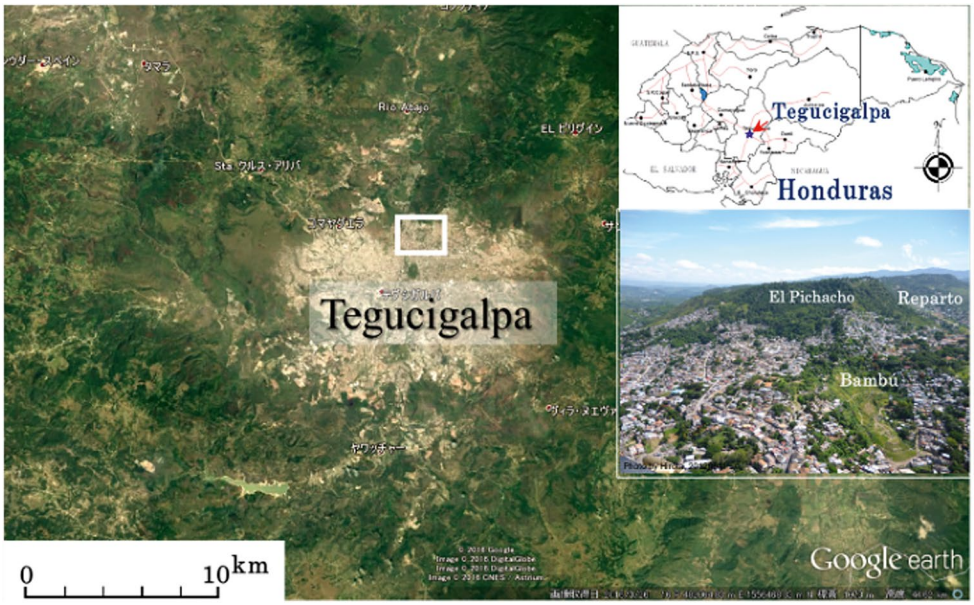


Fig. 1 Tegucigalpa, Honduras (modified from Google earth image)

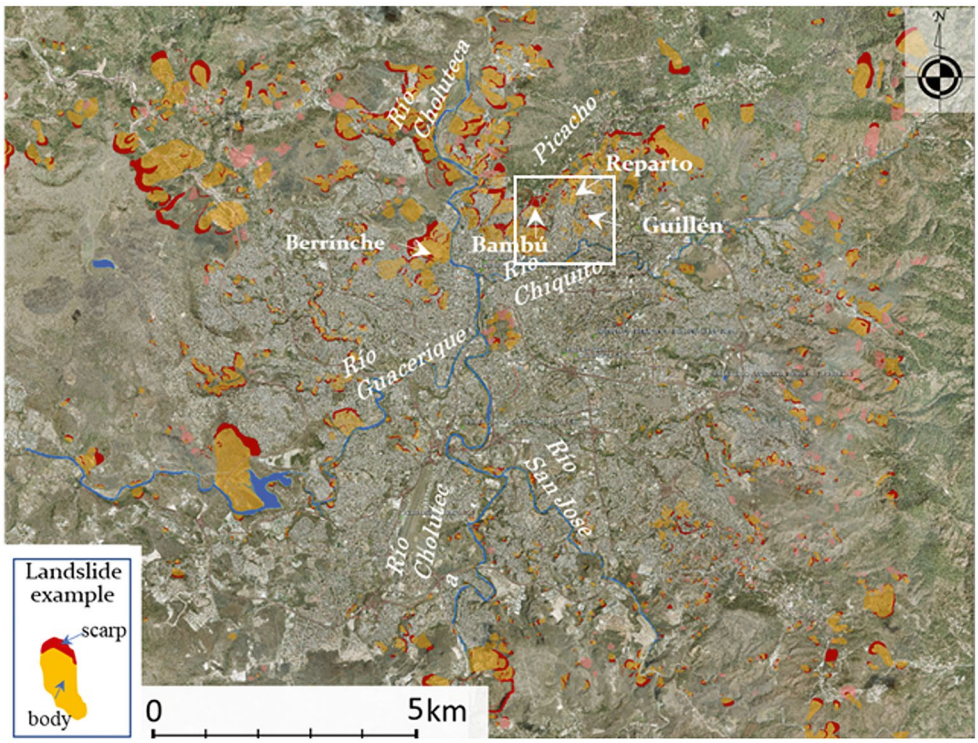


Fig. 2 Landslide Inventory Map of Tegucigalpa (White square, Target area, modified from Grupo de Mapeo de Deslizamientos de Tierra de Tegucigalpa (2014))

hazard maps was given to counterparts (hereinafter referred to as C/P) on the host country (Honduras) side (Yamagishi 2014; Sato et al. 2015). In addition, in the JICA project, the authors are assisting C/P in creating hazard maps. Landslide susceptibility maps have been created by C/P in the El Edén and Nueva Santa Rosa areas of Tegucigalpa (Kuwano et al. 2016; Torres et al. 2016; Hirota et al. 2017; Torres and Garcia-Urquia 2021). This susceptibility map categorizes landslide activity (stability) into three categories and is a precursor to creating of hazard maps, which continues into today's technical support activities (Kuwano et al. 2021; Hirota et al. 2021a, b). The area within the white square in Figs. 1 and 2 is the area where this risk assessment was conducted.

The main geology of the area targeted for landslide risk assessment consists of sedimentary rocks of sandstone (Ss) and tuff (Tuff), which are covered by Ignimbrite, with a Quaternary conglomerate layer (Cgl) distributed. Tuff is

composed of several different layers. At a minimum, the pumice tuff and two other tuffs have many cracks, and the upper part is easily weathered and softened. The area has collapsed over a wide area and is covered by Detritus (Dt) and Debris flow (Df), making the area vulnerable to disasters. River deposit (Rd) is deposited on the riverbed (Fig. 3). The horizon prone to landslides is Tf. The boundary between Ss and Tf is a geological discontinuity, making it slide easily.

3 Methods

Figure 4 shows the technology transfer procedure. The main flow of the methodology is to carry out "Preparation" to "Educational Program" almost simultaneously. In "Preparation," commercially available maps, topographical maps, and geologic maps are purchased. The results of the previous project so far include aerial photographs (taken by JICA in February 2013), processed local aerial photographs,

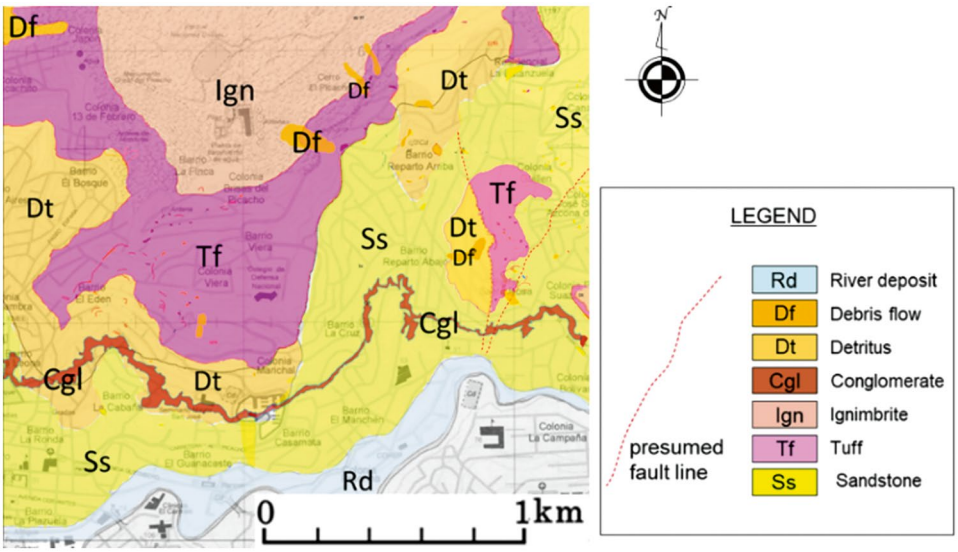


Fig. 3 Geologic map of the study area in the northern part of Tegucigalpa, Honduras, Base Map: TEGUCIGALPA, HONDURAS 1: 12,000 E952 EDITION 2-NIMA

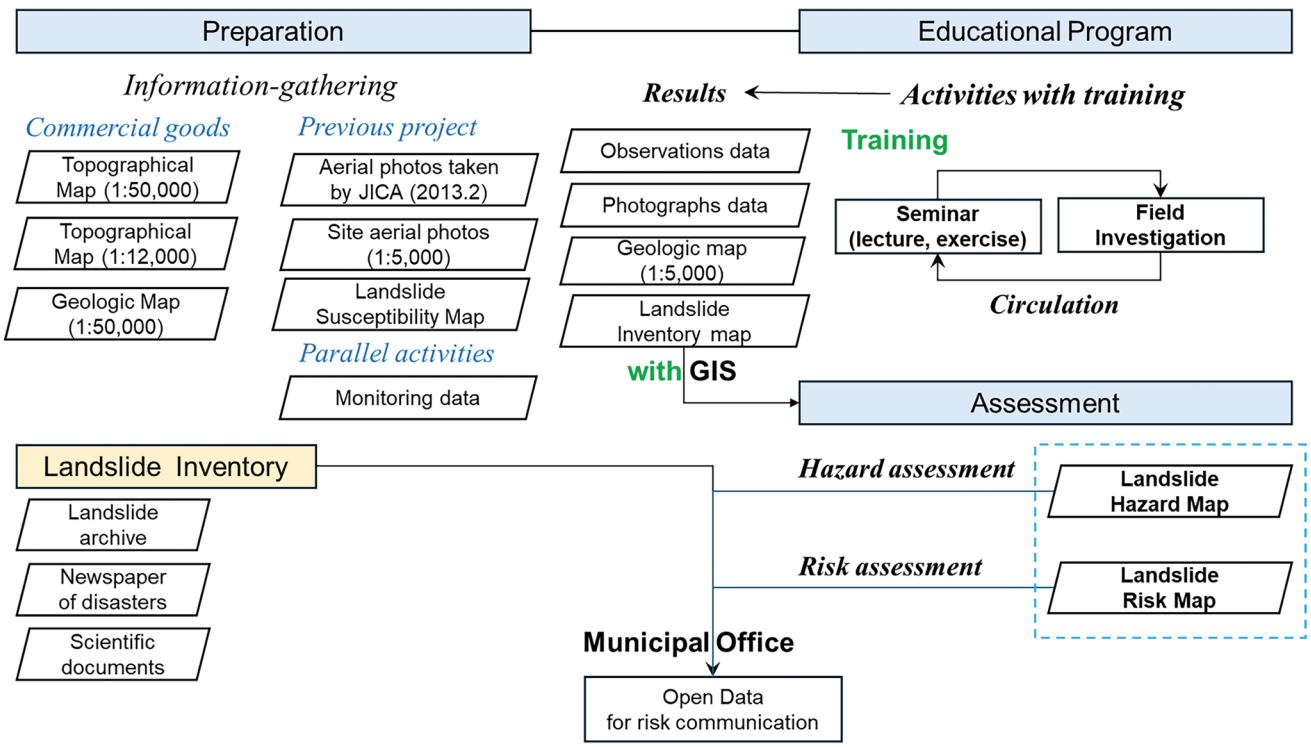


Fig. 4 Flow chart of landslide hazard mapping system including educational program and assessment (modified from Hirota et al. 2017, the dashed box indicates the scope of the JICA project)

and landslide susceptibility maps. Additionally, the working group will review the latest landslide data.

These materials are used as teaching materials for the "Educational Program" which include seminars and exercises on creating landslide inventory maps. The results of the training are utilized in field investigation. This is a cyclical training that is conducted from seminar to field work as needed. The output of the educational program includes the creation of observation data, photographic data, regional geologic maps, and landslide inventory maps.

Observation data is mainly evaluated by assigning points to each landslide based on observed factors on the Landslide Survey Sheet. Using these findings, the "Assessment" section creates landslide hazard maps and landslide risk maps to be used in risk assessment. The results of these activities will be managed and made public by the Municipal Office (AMDC in Tegucigalpa), and will be updated annually as part of ongoing risk assessments. "Assessment" is carried out in the order of Hazard Assessment and Risk Assessment.

In the process of "Educational Program," GIS training was provided to C/P using GIS information. The "Educational Program" basically includes lectures, exercises, and on-site surveys to ensure that the lecture content becomes firmly established (Fig. 5).

Indoors (classrooms, etc.) include lectures (seminars) on landslides based on geology and topography, exercises such as topographic interpretation, during the field training, C/P conduct landslide surveys to prepare survey sheets with JICA experts on site. The following points should be noted at the site for investigation of landslides (Fig. 6). Examples are Point of view-1as Scarp, Point of view-2 as Building tilt, Point of view-3 as Puddles and wastewater.

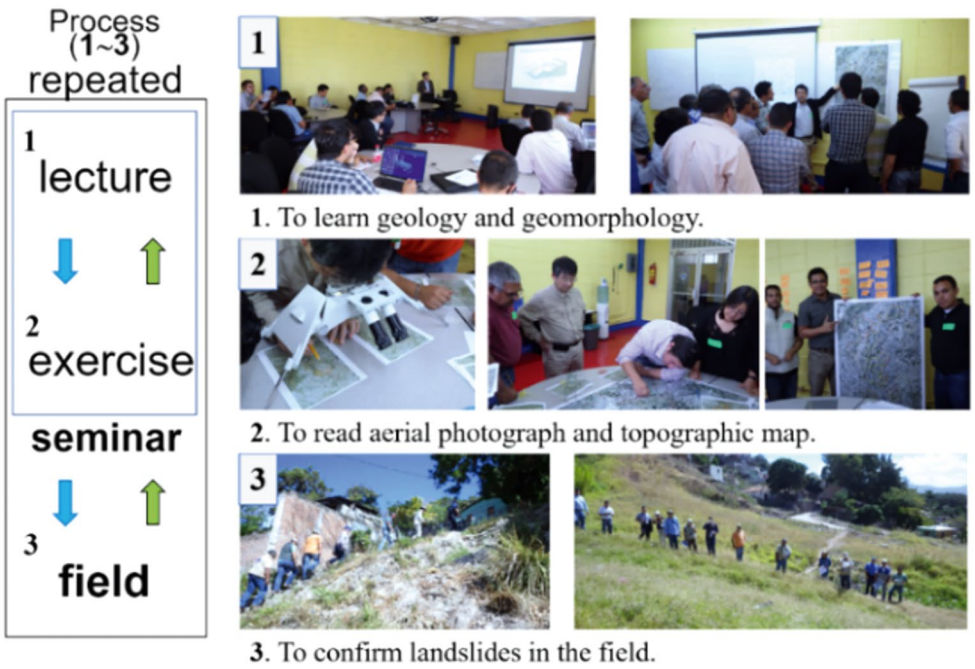


Fig. 5 Educational process



Fig. 6 Examples of "the point of view" at field

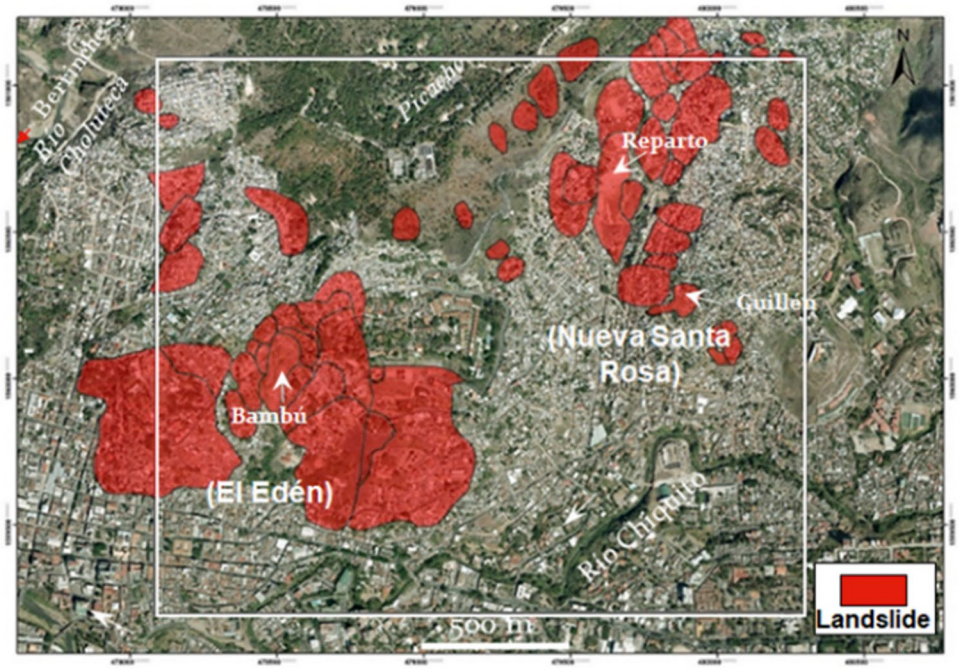


Fig. 7 Landslide inventory map in Tegcigalpa, modified from Grupo de Mapeo de Deslizamientos de Tierra de Tegucigalpa (2014)

3.1 Creating landslide inventory map

Based on the Landslide Inventory Map (see Fig. 2), landslide within the survey area are compiled on GIS (Fig. 7). After creation, the shapes of landslides are confirmed and corrected through field surveys.

When creating a landslide hazard map based on a landslide inventory map, the educational program provides training on how to express the edited landslide impact area as a polygon (Fig. 8).

The risk impact range A includes the polygon B (target of hazard evaluation) and polygon C (polygon B′ movement range). Take the distance to the range of polygon C in the sliding direction and add the same distance as the landslide polygon length (L). However, L(L′) must be 250 m or less, and if L exceeds 250 m, L′ is 250 m.

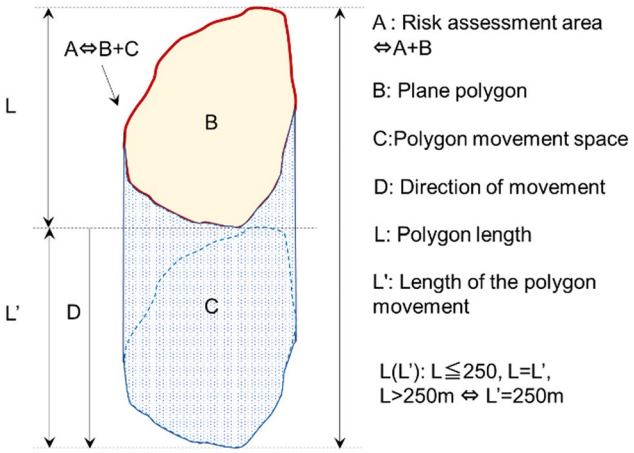


Fig. 8 Area affected by landslide

3.2 Creating a landslide survey sheet

The survey sheet will be learned through the "Educational process" several times to determine the items and points to be assigned. "ITEM" factors are selected based on repeated field surveys and are appropriate for the survey area. "CATEGORY"s are broadly divided into five categories, and the three basic categories are "Topographic conditions," "Geological conditions," and "Hydrological conditions" (Fig. 9).

Topographic conditions (40 points)

Landslide Scarp (20 points): Easy to see displacements.
Surface anomalies (20 points): Easy to see changes.

Geological Conditions (20 points)

Rocks Type (5 points): Collluvium, Weathered (altered) rock, Moderate soils, Hard (solid) rock.
Fractured rocks (15 points): High fracture density, Moderately fractured, Low fracture density, No rocks.

Hydrological conditions (20 points)

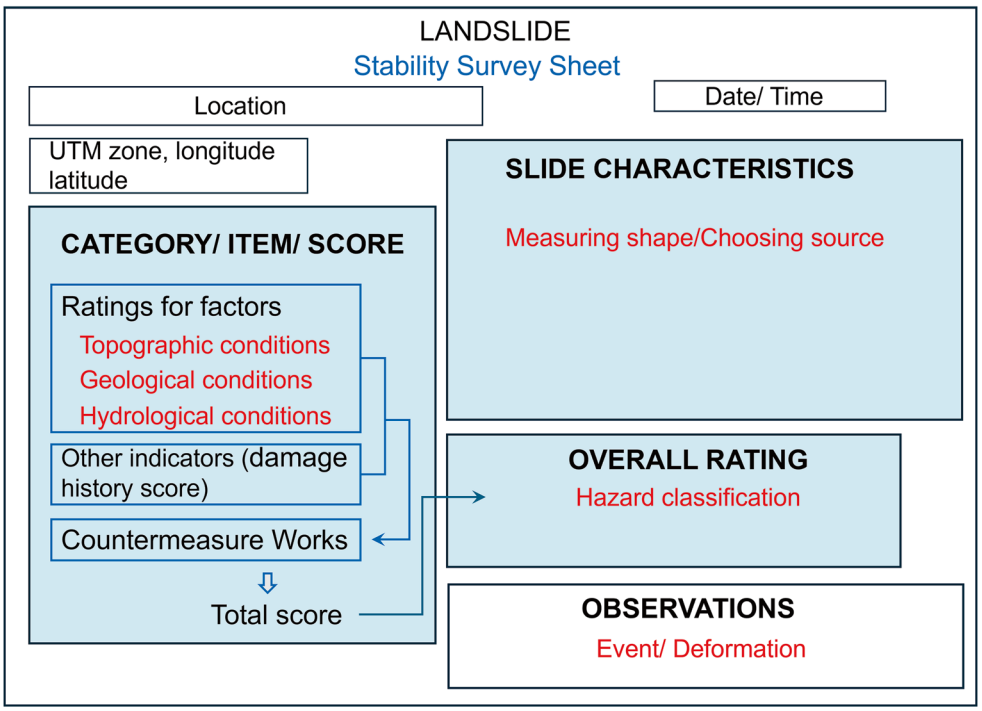


Fig. 9 Component of the landslide survey sheet

Many springs/many water leaks, Few springs/few water leaks, Traces of water, Without the presence of water.

In addition, there are two other items that are closely related to landslide stability.

Other indicators (20 points): Tilted-Electric poles/trees, Depormed steps, Deformed pipes, and Fissures/cracks in buildings. The observed phenomena are rated on a scale of zero to three.

Countermeasure works(0 to −50 points subtracted from the total): Points are measures (incomplete) in progress as minus twenty (−20), measures (completed) as minus fifty (−50). In the case there are not measures at the check site, point is nothing (0).

The "CATEGORY/ITEM/SCORE" part consists of the elements shown in Fig. 10. "Topographic conditions," "Geological conditions," "Hydrological conditions," and "Other indicators (damage history score)" through on-site observation are rated on a scale of 0 to 100. The assigned points are lowered considering the conditions of countermeasure works. The landslide evaluation during the survey is obtained as a total score.

Based on this, the "Orvall rating" divides the diagnosis into three categories: Countermeasure work is necessary (Hazard Level III), No urgent countermeasure necessary (Hazard Level II), and Countermeasures are not necessary(Hazard Level I). These classifications are used to create hazard maps.

CATEGORY		ITEM		SCORE		
Topographic conditions	Landslide Scarp	Clearly exists		20		
		It exists, but partially and not clearly		15		
		It exists, but not clear		10		
	Surface anomalies	New and big cracks, steps and subsidence		20		
		Small and old cracks, steps and subsidence		15		
		Slight deformation of the terrain		10		
		No abnormalities		0		
Geological Conditions	Rocks Type	Colluvium		5		
		Weathered (altered) rock		4		
		Moderate soils		3		
		Hard (solid) rock		2		
	Fractured rocks	High fracture density		15		
		Moderately fractured		10		
		Low fracture density		5		
		No rocks		0		
Hydrological conditions		Many springs / many water leaks		20		
		Few springs / few water leaks		10		
		Traces of water		5		
		Without the presence of water		0		
Other Indicators	* ☐ Tilted-Electric poles /trees		3 or more correspondences	20		
	☐ Deformed steps		2 correspondences	15		
	☐ Deformed pipe		1 correspondence	10		
	☐ Fissures / cracks in buildings		no correspondence	0		
Countermeasure Works		There are no countermeasures on the site		0		
		There is a work of countermeasure (incomplete)		-20		
		There is a countermeasure (complete)		-50		
	* check the options that apply		TOTAL AMOUNT (TA) =			
	Fill in field					
	Automatic calculation		NOTE:			
			In case TA <0, then TA = 0			

Fig. 10 CATEGORY/ITEM/SCORE part of the survey sheet

4 Results

1. **Landslide survey sheet.**

The landslide survey sheet created in the educational program was revised through repeated field surveys. The one shown in Fig. 11 is V3.1, and by checking the blue box in the Score field, the score will be automatically displayed in the light blue area. If all items are checked, the total amount will be displayed and automatically ranked in the overall rating. Photographs of areas where displacement was observed at the site were attached as documents to the survey sheet.

2. **Preparation of landslide hazard map and house survey based on the map.**

A landslide hazard map was created based on the results table of the various landslide surveys. The landslide polygons in the hazard map were used to survey houses (Fig. 12).

Because it is difficult to access individual buildings in densely populated areas, GIS personnel used GIS data to count the number of buildings based on the relative positions of their roofs.

3. **Creating a risk matrix diagram.**

The vertical axis elements are divided into three categories according to the damage level, and the horizontal axis elements are divided into three categories according to the risk level, and these are combined to create a matrix diagram (Tables 1 and 2).

Diagram horizontal axis element (hazard level)

Diagram vertical axis element (Degree of damage)

Create a Landslide Risk Matrix based on the above (Fig. 13).

Area A (red zone): Unacceptably high social-risk area.
Area B (yellow zone): Socially acceptable, given a good reason.
Area C (green zone): Socially acceptable risk area.

LANDSLIDE

FIELD EVALUATION FORM TO MAKE A MAP OF RISKS TO MASS MOVEMENTS

Location:			
Inspector:		Organization:	

Date/Time:

UTM zone:	
Latitude:	
longitude:	

CATEGORY		ITEM		SCORE		
Topographic conditions	Landslide Scarp	Clearly exists		20		
		It exists, but partially and not clearly		15		
		It exists, but not clear		10		
	Surface anomalies	New and big cracks, steps and subsidence		20		
		Small and old cracks, steps and subsidence		15		
		Slight deformation of the terrain		10		
		No abnormalities		0		
Geological Conditions	Rocks Type	Colluvium		5		
		Weathered (altered) rock		4		
		Moderate soils		3		
		Hard (solid) rock		2		
	Fractured rocks	High fracture density		15		
		Moderately fractured		10		
		Low fracture density		5		
		No rocks		0		
Hydrological conditions		Many springs / many water leaks		20		
		Few springs / few water leaks		10		
		Traces of water		5		
		Without the presence of water		0		
Other Indicators	* ☐ Tilted-Electric poles /trees		3 or more correspondences	20		
	☐ Deformed steps		2 correspondences	15		
	☐ Deformed pipe		1 correspondence	10		
	☐ Fissures / cracks in buildings		no correspondence	0		
Countermeasure Works		There are no countermeasures on the site		0		
		There is a work of countermeasure (incomplete)		-20		
		There is a countermeasure (complete)		-50		

* check the options that apply

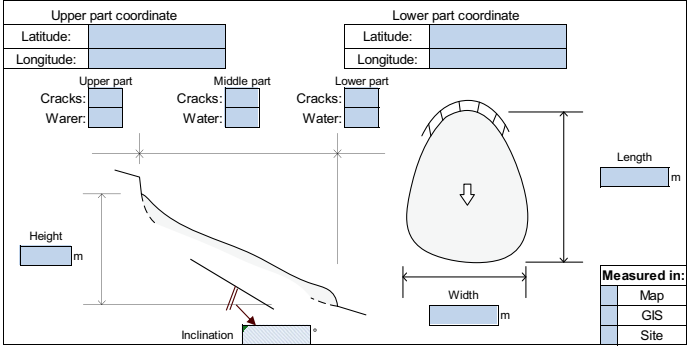
Fill in field

Automatic calculation

TOTAL AMOUNT (TA) =

NOTE:
In case TA <0, then TA = 0

SLIDING CHARACTERISTICS:



OVERALL RATING:

	Diagnosis	Rank	
1	Countermeasures work is necessary	TA >= 70	-
2	No urgent countermeasure necessary, periodic inspections needed	50 <= TA < 70	-
3	Countermeasures are not necessary	TA < 50	-

OBSERVATIONS:

v3.1 (2019.11.28)

Fig. 11 Landslide survey sheet

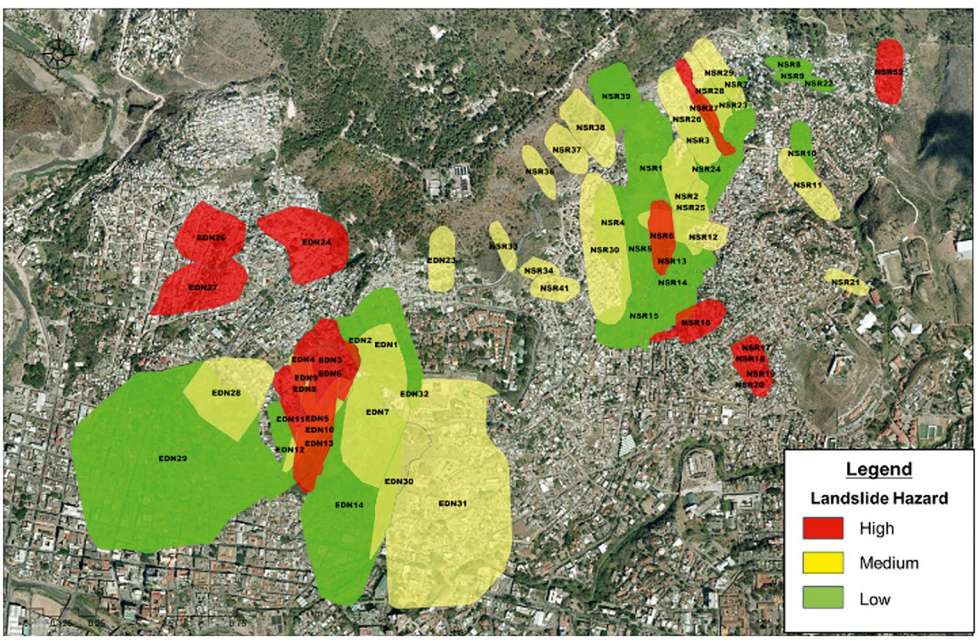


Fig. 12 Landslide hazard map

Table 1 Hazard level for landslide score rank

Hazard level: follow the hazard assessment category according to the survey sheets				
Level	Qualitative expression		Landslide Scoring	
III	High	h	1	ST ≧ 70
II	Medium	m	2	50 ≦ ST < 70
I	Low	l	3	ST < 50

Table 2 Estimated damage classification table

Degree of damage: according to number of houses			
	Elements to evaluate		
Level	Qualitative expression		Number of houses
3	Sector	Many	100~
2	Neighborhood	Medium	10~99
1	Scattered	Few	1~9

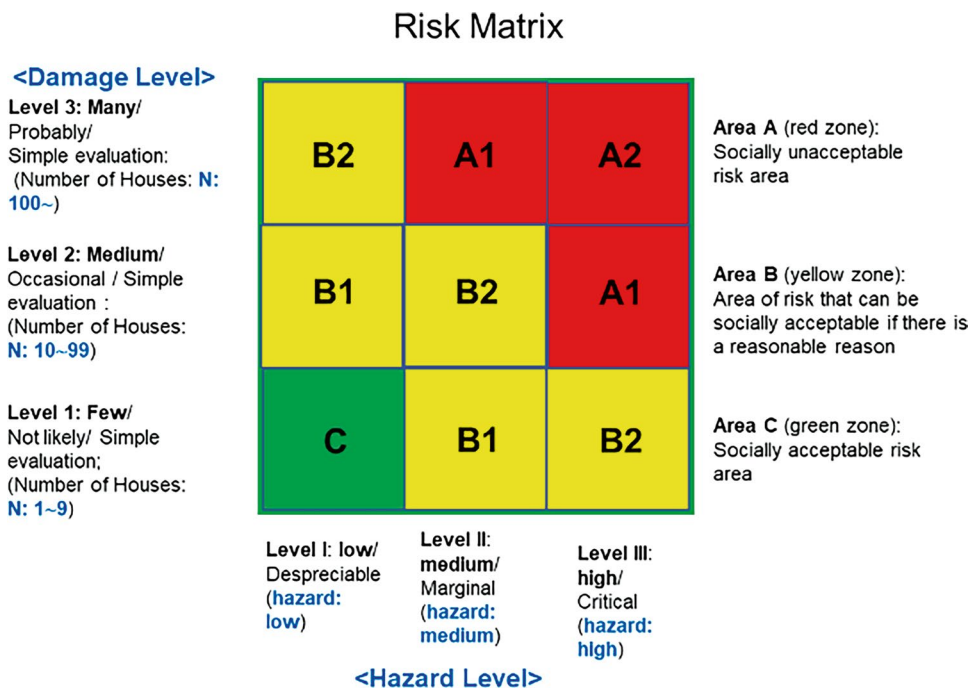


Fig. 13 Matrix diagram for risk assessment (A2 > A1 > B2 > B1 > C: in descending order of risk)

4. **Creation of landslide risk map**

Landslide risk maps are created based on landslide hazard maps (Table 3 and Fig. 14). Classifications of A1, A2, B1, and B2 are determined by a combination of Hazard and Risk levels (Fig. 13 and Table 4).

[Risk classification]

Surveys were conducted for risk assessment in each region where hazard assessment was conducted. The definitions of the survey items and the implementation method are described below, and the survey results are summarized in the table below (Table 4).

Number: The number assigned to each landslide.

Score: Score evaluated using the simplified hazard/risk assessment checklist.

Hazard category: Hazard classification (high, medium, low) obtained from the Simplified Hazard and Risk Assessment Check Table.

Area: The polygon area calculated by the GIS.

All buildings: Number of house-polygon centroids within each impact area.

Public facilities: "Churches," "Schools," "Clinics," "Community Facilities," "Waiting Stations," "Government Facilities," "Antennas," "Kindergartens," "Police Stations," "High Schools," and "Universities" were considered public buildings. The number of public buildings is a fraction of the total number of buildings. A field survey was conducted to confirm the type of public buildings.

Table 3 Risk classification

Risk	Risk area		Colour
High	A	A2	Red
		A1	Light red
Medium	B	B2	Yellow
		B1	Light yellow
Low	C		Green

5. **Proposing a risk assessment process in the community.**

Figure 15 proposes a process for continuing risk assessment in the study area (e.g., community unit). First, set goals. The goal is "Strengthening of Risk Assessment Capacity for Landslide Disasters." The items are as follows, in order: In a risk assessment, it needs to plan and set what to do at each stage of PRE, ACT, and POST (Preparation, Activities, and Results and Discussion, respectively). These planning items

Fig. 14 Landslide risk map

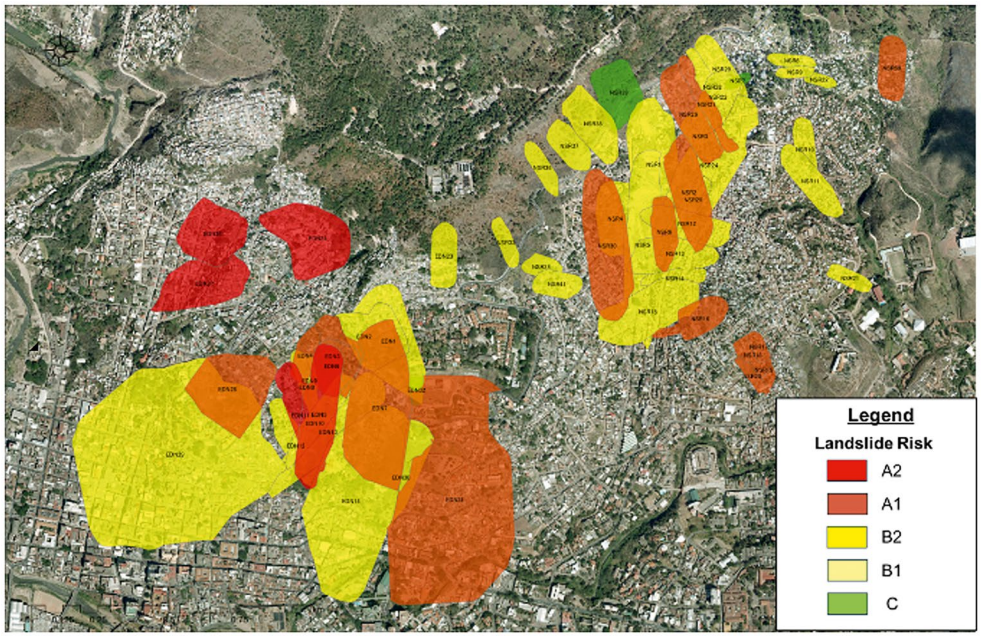


Table 4 List of hazard and risk assessment results for landslide (part of list)

No.	Score	Hazard category	Area (m^2)	All buildings	Public facilities	Risk category	Risk Rank
EDN1	39	Low	65,990	139		High	B2
EDN2	45	Low	38,445	81		Medium	B1
EDN3	85	High	40,938	54		Medium	A1
EDN4	75	High	13,491	33		Medium	A1
EDN5	85	High	55,140	105		High	A2
EDN6	70	High	27,741	18		Medium	A1
EDN7	50	Medium	108,221	156		High	A1
EDN8	50	Medium	13,399	20		Medium	B2
EDN9	50	Medium	9,747	12		Medium	B2
EDN10	55	Medium	26,041	65		Medium	B2
EDN11	70	High	37,977	139	1	High	A2
EDN12	40	Low	28,368	26		Medium	B1
EDN13	45	Low	62,616	150		High	B2

should be handled appropriately depending on the region and period of activity.

After setting GOAL, decide which community to target, carry out activities in the order from PRE onwards, and finally accumulate the results and data of the activities carried out in order. The information accumulated in this way can be used when setting similar or similar goals.

PRE: Preparation

- Creation of a geologic map, Landslide Inventory, and hazard map.
- Creating an evacuation timeline in the event of a disaster (information sharing).

ACT: Activities

- Evacuation behavior training based on the evacuation timeline.
- Understanding landslide disaster locations.
- Creation of landslide risk map (hazard map base map).

POST: Result and Discussion

- Verification of risk map and timeline.
- Judging the good and bad points after using the materials.
- Update evacuation timeline/create individual timeline.
- Update of landslide disaster risk map.

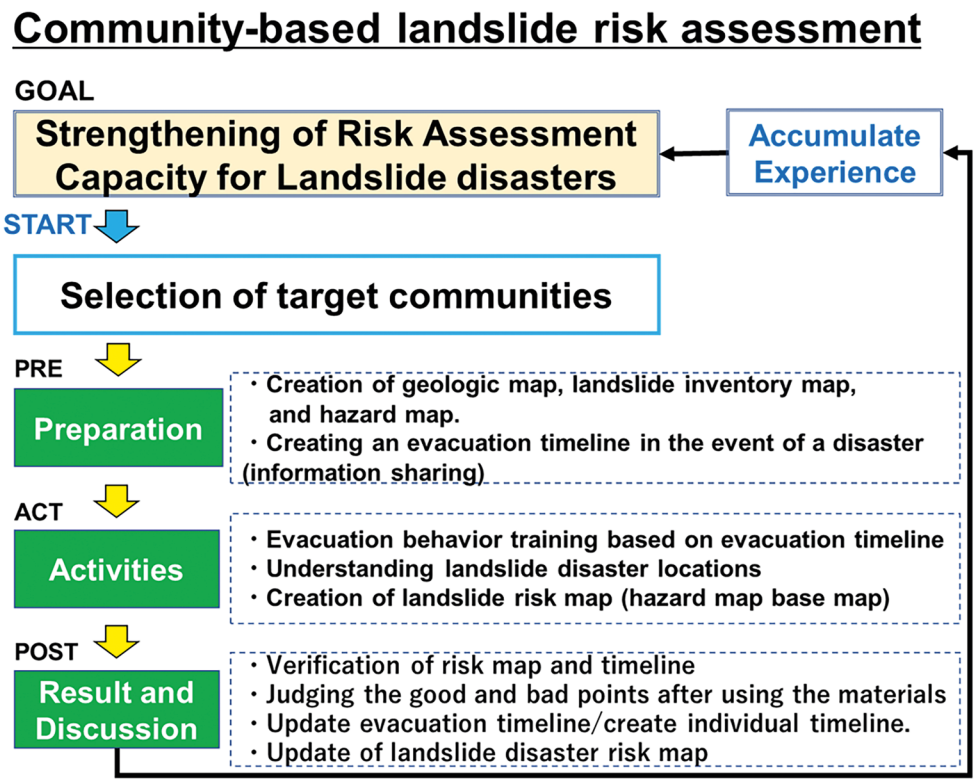


Fig. 15 Risk assessment cycle

5 Discussion

1. **Landslide survey sheet**
   The points for each element were 40 points for Topographic conditions, 20 points for Geological conditions, 20 for Hydrological conditions, and 20 for "Other indicators," giving a total of 100 points. As these factors differ depending on the area to be surveyed, the evaluation is categorized into "Countermeasure work is necessary (Hazard Level III)," "No urgent countermeasure necessary (Hazard Level II)," and "Countermeasures are not necessary (Hazard Level I)" under diagnosis in the overall rating of the survey sheet.
   In this case, all data from the landslide survey sheets must be analyzed totally to select the appropriate number of points for each boundary among hazard area.
2. **Creation of landslide hazard map and house survey based on the map.**
   Regarding the housing survey, there are currently apartment complexes, and it is difficult to distinguish whether each house is an individual household. Therefore, the author believes that the appropriate method is to count the number of houses using GIS images.
3. **Creating a risk matrix diagram.**
   When creating a landslide risk map using a risk matrix, it is difficult to determine how to assign risk levels to landslide polygons. When creating a risk matrix diagram, it is considered that if the degree of hazard is plotted on the horizontal axis, it is easier to manage risk by plotting the frequency of precipitation on the vertical axis. However, since no data shows the probability of landslide disasters depending on the amount of precipitation, the number of houses within each landslide polygon affected by a landslide was used. Damage level classification based on the number of houses should be considered for each region.
4. **Creation of landslide risk map.**
   A landslide risk map was created by classifying the landslides according to the matrix used for risk analysis. Creating landslide risk maps is difficult because the relationships between the factors that cause landslides, such as the amount of precipitation and landslide occurrence, and the relationship between earthquake scale and landslide occurrence locations need to be clarified. In the future, in areas where landslides occur frequently, it is desirable to accumulate and analyze data on the relationship between precipitation and slope disasters, for example. This allows us to discuss the frequency of landslide occurrence in relation to precipitation.
5. **Proposing a risk assessment process in the community.**
   The authors considered a model that could continue as a regional risk communication method regarding the risk assessment process. However, they still need to put this into practice, and they will use better methods in future activities, especially reviewing the items raised in the PRE-POST process to create an appropriate method for risk communication.

6 Conclusion

Through a JICA project in Honduras, the authors devised a simple hazard evaluation method and a method for creating hazard/risk maps based on the evaluation results. Based on the technology transfer methodology, engineers who are not normally involved in landslides can now perform landslide hazard assessments and create hazard maps and risk maps. Possible reasons for this are as follows.

1. The structure of the survey sheet was easy to understand as it organized geological, topographical,, and hydrological conditions and other items for checking the status of countermeasure works. Moreover, the working group themselves came up with the observation items.
2. In risk assessment, information on hazard levels and damage levels could be expressed in an easy-to-understand manner on a matrix.
3. Repeated lectures, exercises, and field surveys to explain points of focus regarding slope instability. In addition, the working group repeatedly practiced activities related to the series of steps from hazard assessment to risk map creation.
4. The authors allowed the working group to present their research and decisions orally in the seminar, which is thought to have enabled them to acquire skills more reliably.

Acknowledgments We would like to thank everyone involved in the project in Honduras, especially AMDC, UNAH, and COPECO, for their cooperation in the seminars and on-site training. We appreciate the Output 3 working group members for making survey sheets for every field survey and Ms. Vilma Marina Mejia and Mr. Alejandro Flores for supporting our activities while carrying on the project. We would also like to thank the JICA Honduras Office and Headquarters staff for their tremendous support for the project.

References

Grupo de Mapeo de Deslizamientos de Tierra de Tegucigalpa (2014) Manual para elaboración de mapa de inventarios de Deslizamientos de tierra. Caso de aplicación: ciudad de Tegucigalpa (ISBN 978-99926-701-1). 80 p

Hirota K, Yamagishi H, Yagi H, Kuwano T (2017) Technical cooperation for development of landslide hazard mapping system: a case study of capacity building through a JICA project in Tegucigalpa, Honduras. J Jpn Landslide Soc 54(4):22–27. (in Japanese with English abstract)

Hirota K, Ruiz M, Kuwano T (2021a) Preliminary report of simple hazard mapping methods for slope stability in Tegucigalpa, Honduras. E-Proceedings of The Fifth World Landslide Forum, pp 25–32. 02-06 November 2021 KICC, Kyoto, Japan, ICL

Hirota K, Rosa C, Hasegawa K (2021b) Slope stability around the northern part of the Tegucigalpa Basin, Honduras: a case of landslide process at residential development areas. Understanding and reducing landslide disaster risk, Zěliko Arbanas. In: Bobrowsky PT, Konagai K, Sassa K, Takara K (eds) Specific topics in landslide science and applications, vol 6. Springer, pp 369–376

Kuwano T, Hara T, Tsukamoto S, Inaoka M, Suzuki T (2016) JICA landslide projects for strengthening and capacity building of the control and mitigation in Honduras, Memory of Second Central American and Caribbean Landslide Congress, 18-20 July 2016. Tegucigalpa, Honduras, pp 7–12

Kuwano T, Hara T, Aoki H, Hirota K, Hasegawa K, Uzawa K (2021) Slope disaster and countermeasures in Honduras. E-Proceedings of The Fifth World Landslide Forum, pp 46–56. 02-06 November 2021 KICC, Kyoto, Japan, ICL

Sato G et al (2015) Investigation and mitigation of landslides in Republic of Honduras as Japan's International cooperation program. J Jpn Landslide Soc 52(4):1–7. (in Japanese with English abstract)

Torres L, Garcia-Urquia E (2021) AHP method applied to landslide susceptibility mapping in pilot sites of Tegucigalpa, 2016. E-Proceedings of the 5th World Landslide Forum, pp 33–39. 02-06 November 2021 KICC, Kiyoto, Japan, ICL

Torres L, Sevilla N, Hirota K, Yamagishi H, Tsukamoto S (2016) How to make a database of landslides in Tegucigalpa, Honduras. Second Central American and Caribbean Landslide Congress, pp 29–34

Yamagishi H (2014) Integrated disaster prevention maps and landslide hazard maps using GIS: examples of Shikoku and Central America Honduras. J Jpn Landslide Soc 51(2):24–29. (in Japanese)

Open Access This chapter is licensed under the terms of the Creative Commons Attribution 4.0 International License (http://creativecommons.org/licenses/by/4.0/), which permits use, sharing, adaptation, distribution and reproduction in any medium or format, as long as you give appropriate credit to the original author(s) and the source, provide a link to the Creative Commons license and indicate if changes were made.

The images or other third party material in this chapter are included in the chapter's Creative Commons license, unless indicated otherwise in a credit line to the material. If material is not included in the chapter's Creative Commons license and your intended use is not permitted by statutory regulation or exceeds the permitted use, you will need to obtain permission directly from the copyright holder.



Part V

Technical Notes and Case Studies

Assessing Landslide Disaster Risk Reduction and Resilience: Case Studies and Insights, India

Surya Parkash, Ravinder Singh, and Shubham Badola

Abstract

The purpose of this paper is to highlight the issues of landslide disaster risk reduction in India by presenting real case studies of landslide incidences happened in the past. It also focuses upon the resilience measures and policies required for reducing landslide risk. This study highlights and give insight on the few important case studies of past landslides/mass-movement incidences such as Phuktal landslide dammed reservoir, Kargil-Ladakh (2015), Idukki-Kerala (2018), landslide at Noney district-Manipur (2022), Rock-ice avalanche and debris flow, Chamoli (2021), land subsidence in Joshimath-Uttarakhand (2022), South Lhonak Glacial Lake Outburst Floods-Sikkim (2023) etc. These disaster events are influenced by the intrinsic factors (i.e., geo-tectonic, drainage/hydrology, land uses) and extrinsic factors (i.e., climate change, anthropogenic activities, climate variability, natural and socio-economic development).

The landslide disaster events induced by geo-tectonics, heavy rainfall, Glacial Lake Outburst Floods (GLOFs), anthropogenic activities etc. have been causing severe losses and damages to lives and properties in different regions of India. The extreme weather events and climate change increases the frequency of disaster events in hilly regions of India. As a result, the necessity for stringent policies and strategies (e.g., landuse, construction practices, enact/revise regulations etc.) for reducing disaster risks was extremely felt. Simultaneously, the advancement of innovative technology and tools such as Deep Learning (DL), data mining, Artificial Intelligence (AI), Machine Learning (ML), Internet of Things (IOT) are required to generate reliable, field validated models of multi-hazards based early warning, risk assessment, mitigation, response etc., which may reduce impacts of future disasters and its occurrences.

Keywords

Landslide · Climate change · Flash floods · GLOFs · Landuse practices · Regulations

1 Introduction

India is vulnerable to a range of mass movements that cause significant harm, including property and human casualties. Approximately 12.6% (i.e., 0.42 million square kilometers) of the country's total geographical area is vulnerable to landslide hazards, according to the Geological Survey of India (GSI). Landslides and mass-movement related events can occur in 21 States and 4 Union Territories due to the mountainous North-Western Himalayan area, the Eastern and Western Ghats, and the Sub-Himalayan topography of the North-East.

The massive increase in urbanization in many of these mountainous locations and its rising impact on socio-economic aspects along with the recent land subsidence events have drawn worldwide attention to landslide studies. The triggers of the landslides in the Indian Himalayan region are attributed either to natural (earthquakes and rainfall) or to anthropogenic (slope cuts, deforestation, blasting) activities.

Recently on 7th March 2024, Indonesia Sumatra island has been affected by torrential rains which triggers flash floods and landslides on Sumatra Island that claimed loss of lives-property and leaving several others missing. There is increase in vulnerability of local population to natural catastrophes and geo-hazards, such as landslides, avalanches, flash floods, earthquakes and GLOF combined with geo-

S. Parkash (✉) · S. Badola
National Institute of Disaster Management (NIDM), New Delhi, India
e-mail: surya.nidm@nic.in

R. Singh
G20, Ministry of External Affairs (MEA), New Delhi, India

© The Author(s) 2025

B. Abolmasov et al. (eds.), *Progress in Landslide Research and Technology, Volume 3 Issue 2, 2024*, Progress in Landslide Research and Technology, https://doi.org/10.1007/978-3-031-72736-8_22

tectonically active regions. Among these calamities, landslides have been recognized as one of the major geo-hazards with capacity to wreak havoc across a huge geographic area. Regular patterns of climate change, global warming, human interventions, and unplanned developmental activities are all causes of landslides.

The primary goal of this chapter is to highlight the socio-economic issues faced during geo-hydro-meteorological events investigated during the field study and emphasize on challenges to reduce the risks in future.

The focus also encompasses an investigation of resilience strategies and essential policies aimed at mitigating landslide risks. This study aims to offer valuable insights into the intricate mechanisms underlying landslide occurrences, leading to extreme weather events. Moreover, due to climate change and increasing impacts of extreme weather events in mountainous areas, the objective is to emphasize the pressing need for robust policies and innovative technological solutions, such as deep learning, machine learning and artificial intelligence, to develop risk assessment models and reliable early warning systems. Ultimately, this research will make a meaningful contribution towards minimizing the devastating consequences of future disaster events on lives and properties across India.

The methodology adopted in this paper entails a thorough investigation into various real-life instances of extreme weather events occurring in India based on field study and emphasize on present scenario of Disaster Risk Reduction (DRR) to improvise it further. This study includes the case study of Phuktal landslide dammed reservoir in Kargil-Ladakh (2015), the Idukki-Kerala landslide (2018), the landslide in Noney district-Manipur (2022), the Rock-ice avalanche and debris flow in Chamoli (2021), land subsidence in Joshimath-Uttarakhand (2022), and the South Lhonak GLOF in Sikkim (2023), among others.

Furthermore, it underscores the importance of implementing stringent policies and strategies, such as regulations regarding land use and construction practices, to mitigate the risks associated with disasters. The research includes specific recommendations for individual events, as well as common recommendations for all phases of disaster management tailored to the diverse geographical regions of India.

2 Past Events

This study highlights and give insight on the few important events of past landslides/mass-movement incidences (Fig. 1) such as Phuktal landslide dammed reservoir, Kargil-Ladakh (2015), Idukki-Kerala (2018), landslide at Noney district-Manipur (2022), Rock-Ice Avalanche and debris flow,

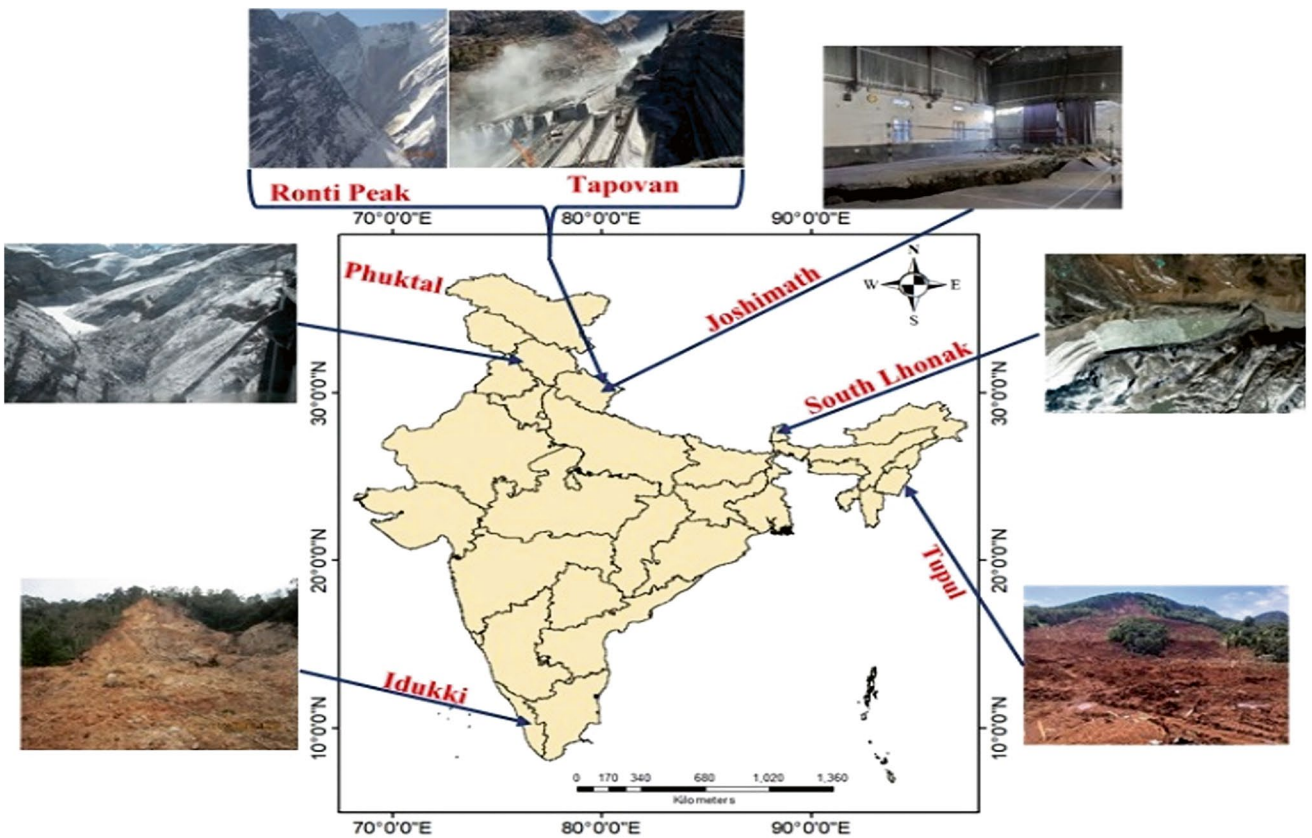


Fig. 1 Location of Important past landslide/mass-movement incidences

Chamoli (2021), land subsidence in Joshimath-Uttarakhand (2022), South Lhonak GLOF-Sikkim (2023) etc. These disaster events are influenced by the intrinsic factors (i.e., geo-tectonic, drainage/hydrology, land uses) and extrinsic factors (i.e., climatic change, natural climatic fluctuation, socio-economic development, and human activity).

2.1 Phuktal Landslide Dammed Reservoir, Kargil-Ladakh (2015)

An artificial landslide dammed reservoir was formed due to incidence of landslide probably happened near 31st December 2014 in the left bank of river Phuktal (Fig. 2) about 90 km from Padum (District Kargil) that blocked the course of the river Phuktal. In the event of an unexpected rupture of the landslide dam, the lives, property, and infrastructure located downstream were therefore seriously threatened by the reservoir of the landslide dam. The landslide dam is located (330 17′ 25.3″ N, 770 17′ 06.8″ E) in far remote area of district Kargil, Ladakh and had poor connectivity and logistical difficulties due to tough terrain and climatic conditions. This stretch was blocked and covered by heavy snow during winter season.



Fig. 2 Landslide dam blocking the river Phuktal

2.1.1 Area

The incident location is in the Zanskar area of Ladakh, which includes upper Indus River basin, portions of the Himalayan and Karakoram mountain ranges. Due to its unique topography, climatic condition and lack of vegetation it is designated as Cold Desert. Due to the closure of Panjila Pass, since the Zanskar area receives a lot of snowfall and is isolated from rest of the nation from November through June. Temperature during the short spell of summer range between 3 and 35 °C and minimum −20 to −35 °C in winter. Temperature profile of Zanskar region during operation Phuktal is shown in Fig. 3 and is a testimony to the hostile operational conditions.

The Phuktal River is a tributary of Zanskar River and reaches Indus (Sindhu) River close to Nimmo hamlet in District Leh. Its catchment area is around 5600 km^2 at the place of landslides. Up to the river's confluence with the Indus, its entire drainage area is around 15,800 km^2. A few kilometers below this confluence lies the Nimoo-Bazgo Hydel Power Project.

2.1.2 Causes

A massive landslide occurred on 31st December 2015, from the left bank of the Tsarab Chu, forming a 50 m high, 60 m wide, and 500–600 m long dam. It submerged approximately 270 hectares of land, with the landslide area comprising mainly limestone and shale rock (i.e. Zanskar supergroup). The debris, including large boulders, slid due to gravity

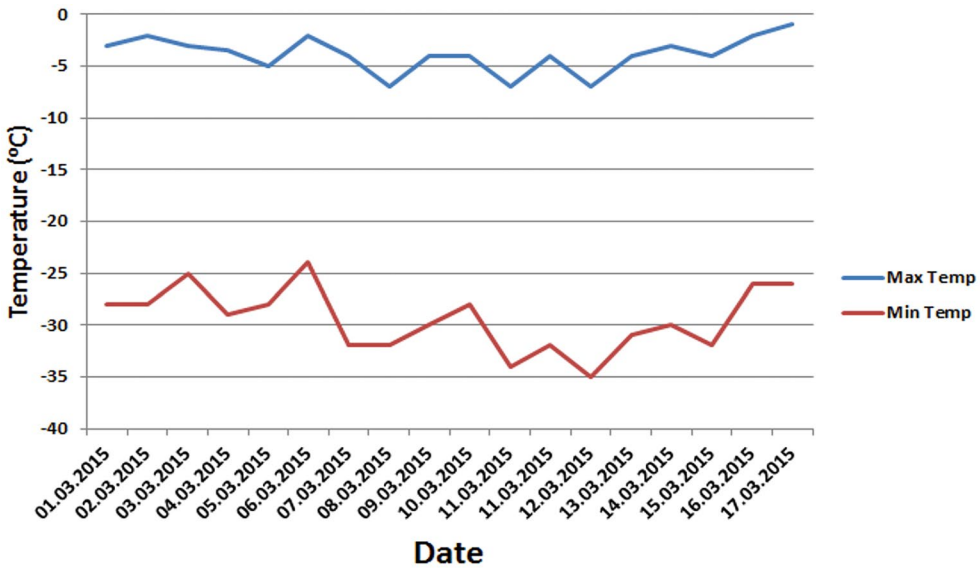


Fig. 3 Temperature profile of Zanskar region

along jointed valleys, blocking the narrow section. Causative factors include steep slopes, tectonic movements, high weathering, and unique hydrological conditions. The rock mass has 3–4 sets of joints, with bedding joints dipping 40°–60° northeast. The debris consists of 60%–70% finer material and 30% large boulders, likely cemented by calcium leaching from limestone weathering.

2.1.3 Damage

In case of sudden breach of dam the extreme climatic situation resulted unguided, unconfined debris and mud flow which posed direct impact on the downstream population, infrastructure (Nimmo Bazgo dam) and hydrological region. The mountain slopes in the upstream and downstream area are very steep and large volume of weathered and scree deposit rest on them. This material in due course of time may slide into the river by deep cutting and scouring of banks during flash floods which may pose threat to life and livestock, Phuktal Gompa, Padam town, small villages, Border Roads Organisation (BRO) camp, low lying bridges, Nimoo-Bazgo dam, habits downstream of Nimoo-Bazgo dam.

2.1.4 Recommendations

- A mechanism needs to be established at the State Government level, so that an automatic activation of operation starts without losing crucial time.
- Accessibility and evacuation in remote areas becomes a major challenge during disaster. Therefore, capacity building and training of local administration, mainly first responders must be strengthened to deal with any disaster situation in well-coordinated manner.
- The State Government, Indian Army, Air Force, and stakeholders should collaborate on a dynamic action plan, with regularly updating through joint meetings at the state level.
- The concerned State Government should take initiative revise and update their Disaster Management Plan incorporating GLOF and Landslide Lake Outburst Flood (LLOF) in detail. A functional operational structure needs to be established by the State concerned to deal with probable danger of sudden outburst of artificial dam.

2.1.5 Conclusion

The Multi-disciplinary team having vast experience was formed by National Disaster Management Authority (NDMA), to regularly review the activity at site with help of Army/ Air Force and Civil Administration, despite high altitude constraints and inclement weather condition. Revising the proposed action plan after field inspection in consultation with stakeholders helped in challenging task of controlled release of water from landslide dam. Additionally, modeling the dam break scenario using ASTER DEM aided the State Administration in organizing evacuation plans effectively.

Although, on 7th May 2015, breach of landslide dammed reservoir was happened through the channel created by controlled blasting and causes small flash flood in the downstream. This flash flood resulted into loss of few foot bridges and damage to school building and BRO bridge but no loss of human life reported due to alertness and evacuation of people in the downstream. After the event, the Standard Operating Procedure (SOPs) on "Averting Threats Emanating from Glacial Lake Outburst Floods (GLOF) and Landslide Lake Outburst Flood (LLOFs) in Himalayan Region" was released by NDMA and circulated to all concerned stakeholders to prevent such events in future.

2.2 Idukki Landslides, Kerala (2018)

According to IMD statistics (Fig. 4), there was 15% "excess" rainfall in June 2018 compared to 18% "excess" rainfall in July 2018. The first period of "exceptionally high" rainfall fell between June 8 and June 30, 2018. During this period, 59 landslide incidents were reported in the Kerala districts of Kozhikode, Wayanad, Kannur, Malappuram, Palakkad, and Idukki.

On July 11, 2018, the second round of intense rainfall began, and it lasted until August 19, 2018. With massive rainfall of 164% over average (758.6 mm vs. a normal of 287.6 mm) and extremely destructive landslides in nearly every district of Kerala, the period from August 1 to August 19 was the most severe. The region experienced its worst disaster since 1924 due to heavy rainfall in late August,

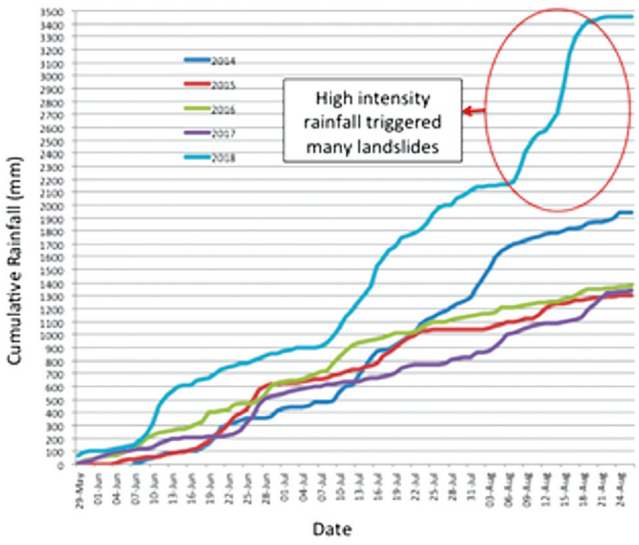


Fig. 4 Cumulative rainfall in Idukki District for the previous 5 years (2014–2018) during the SW monsoon period (29 May to 26 August) (Source: Kanungo et al. 2020)

resulting in reservoir overflow, flash floods, and numerous landslides across 13 out of 14 districts in Kerala. Idukki district was severely impacted, with over 500 landslides on Revenue land and more than 1000 within forest areas, as reported by the media.

In the Wayanad district, there have been over 250 recorded landslides, along with a significant number of subsidence and abortive landslides. Subdivisions in Kozhikode, Malappuram, and Palakkad have also reported high rates of landslides. Many landslides have also been reported in Kannur, Pathanamthitta and Kottayam districts (Source: Kanungo et al. 2020). Following are the major landslide sites visited in Idukki district of Kerala during the field visits as given in Table 1.

2.2.1 Area

The research region is located between longitudes 76° 37′ and 77° 25′ East and latitudes 9° 15′ and 10° 2′ North. With a total area of 4358 km^2, it is home to 14 2000-m peaks, including Anamudi, the highest peak in South India. With plantations and urban communities making up the remaining portion, the land is nearly half forest. Because of the ideal topography and changes in land usage, landslides occur often. Numerous landslides and floods caused by severe rains in 2018 had an impact on livelihoods, infrastructure, agriculture, and human life. With an average of almost 3000 mm of precipitation every year, Kerala state got 2346.6 mm of rain between June and August 2018. Excessive rains in Kerala caused 4728 landslides, with Idukki suffering the most damage with 2219 landslides. Over 1.4 million people were forced to flee their homes and 483 individuals lost their lives as a result of landslides that mostly happened in the Western Ghats region, particularly in environmentally sensitive areas.

2.2.2 Causes

The affected region comprises of highly weathered gneissic rocks with high-grade metamorphic rocks that are prone to weathering. A thick layer of lateritic red soil, sandy, and boulders cover the rocks. Because of the clay-rich lateritic soil's ability to hold water, the slope experiences considerable pressure. Planar failure during heavy rainfall is facilitated by the gneissic rock's dip slope relationship. Toe cutting by streams, a lack of slope protection, anthropogenic activities close to drainage systems, a lack of catch water drains, and unplanned construction without safety precautions are important factors that cause landslides. Buildings piled high on slopes cause landslide damming, which modifies river channels and reactivates old landslide zones.

2.2.3 Recommendations

Based on observations made during field visits to several places damaged by landslides and the lessons so learned in Kerala's Idukki district, the following recommendations are offered (Source: Kanungo et al. 2020):

- Filling in cracks using locally available soil material, properly compacted, and sealing the surfaces of the fissures with a local clay or bentonite clay slurry.
- Utilizing sand, rubble, and stones that have been carried and placed on slopes and riverbeds, respectively, for landslide mitigation rehabilitation projects and other tasks.
- To give toe support and prevent the landslide phenomena, slopes surrounding buildings or any other infrastructure,

Table 1 Major landslides happened in Idukki District, Kerala (2018)

S.N.	Place	Village	Description
1	Puliyanmala Thodupuzha Road	Idukki and Arakkulam	Major landslides on road sides and road damage
2	Cheruthony Bridge	Idukki	Damages on both sides of the approach road due to heavy water flow from the Cheruthony dam opening
3	Perumkala	Idukki	Major landslide; 4 deaths happened
4	Chittadikavala	Upputhodu	Major landslide; 3 death cases and 1 missing reported
5	Keerithodu	Kanjikkuzhy	Major landslide
6	Ponmudy S Valavu	Konnathady	Major landslide; 2 death cases and 3 missing cases reported
7	Panniyar Hydro Electric Project	Konnathady	Heavy rain and flood caused power house damage
8	Panniyarkutty	Konnathady	Major landslide; destroyed completely
9	Near Viswadeepthi School, Adimaly	Mannamkandom	5 Acre agricultural land completely destroyed
10	Koompanpara	Mannamkandom	One house completely destroyed and 5 family members died, 2 injured due to heavy landslide
11	60th Mile	Anaviratty	5 Acre agricultural land completely destroyed
12	2nd Mile	Pallivasal	Major landslide; 3 persons injured
13	Arts College Munnar	Munnar	Major landslide; major portion of Govt. Arts College was destroyed
14	Periyavara Bridge	Munnar	Approach road and bridge destroyed due to heavy flow of water
15	Devikulam (Near PHC)	KDH	3 houses were completely destroyed due to major landslide; 2 died and 1 injured

including those created by road cuttings, should be secured by retaining walls and other suitable structures.
- Channelizing surface water, catch water drains and culverts on roadways must be built with a discharge capacity that matches the water flow in the catchment region.
- It is imperative to forbid encroachment into regions flooded by floods or the riverbed.
- Restrictions must be placed on human settlements below, above, or in the influence zone of old or active landslide areas; existing settlements in these areas must be moved to safer locations; bridge piers and the embankments of river banks near the bridges must be protected from erosion with appropriate retaining structures.
- Building and resort development permits should only be granted following careful examination of the hill slopes from an instability perspective.
- Defined high-risk and high-priority zones for the protection of critical infrastructure and installations (roadways, buildings, hydroelectric power plants, bridges, etc.).
- Training of engineers and geologists from concerned line Departments engaged in infrastructure developments must be prepare to standard technical Detailed Project Reports (DPRs) for landslide risk mitigation and slope protection.

2.2.4 Conclusion

The 2018 monsoon season in Kerala brought about significant rainfall, resulting in severe landslides across multiple districts. The high incidence of landslides was exacerbated by factors such as weathered geological formations and anthropogenic activities. Recommendations include proactive measures such as crack filling, utilizing local materials for mitigation, and proper infrastructure planning to minimize future landslide risks. Additionally, strict regulations on construction and settlement in landslide-prone areas, along with enhanced training for relevant professionals, are vital steps towards effective mitigation and protection of lives and infrastructure.

2.3 Landslide Incident at Noney, Manipur (2022)

A massive landslide (Fig. 5) occurred on June 30, 2022, at wee hours (i.e.00:30 h), on Tupul Yard Railway construction site in district Noney, Manipur, as a result of heavy rains. In this incident 80 people got trapped under debris, out of which 58 died, 18 were wounded and 3 reported missing (DIPR, 23rd July 2022).

The incident site is traversed by many lineaments, running from North-East to South-West (Fig. 6a). Singh et al. (2022) created the longitudinal profile of this area using a

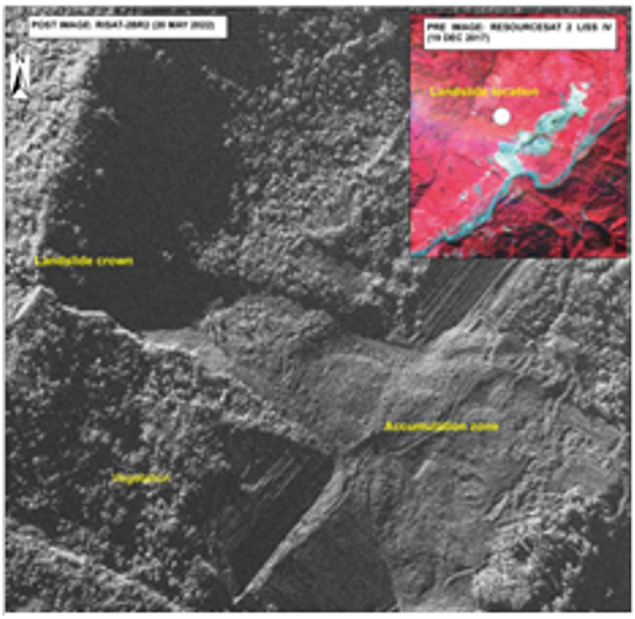


Fig. 5 Satellite image of the location of Tupul Landslide near under construction railway station (Source NRSC-ISRO 2023)

12.5 m ALOS PALSAR DEM to illustrate the terrain along the slide. The profile (Fig. 6b) clearly shows that the mass was located on a concave slope, with steeper slopes in the area above the railway station. When the breakdown occurred, the fast-moving material (Fig. 6c) rotated and collapsed down the slope, causing the landslide. The debris mass descended at an average slope angle of 25° for around 500 m. Additionally, the fast-moving waste material obstructed the Ijai River's path, creating a dam lake scenario (Fig. 6d).

2.3.1 Area

The landslide is located 50 km from Imphaland, over the Ijai River, to the northeast of Tupul Bazaar. Near the event site, the Disang and Barail groups are divided by the Churachandpur-Mao thrust. The region is tectonically active, with many thrusts, faults, and lineaments (Fig. 12).

In addition, the Barail group is made up of the Langka, Noney, Dalang, Pen, and Leimatak faults, which are many strike-slip faults moving in an North-South orientation. The Churachandpur-Mao thrust, which divides the Disang and Barail groups, is located quite close to the Noney Fault (Fig. 7). The Noney Fault is located relatively close to the Tupul landslide area along with the river flows (Singh et al. 2022). A major quake with a magnitude of M6.7 struck this fault in 2016, with the junction of the Noney and Dalong faults serving as the epicenter (Fig. 12). The debris mass descended at an average slope angle of 25° for around 500 m and obstructing the Ijai River's path, creating a dam lake scenario.

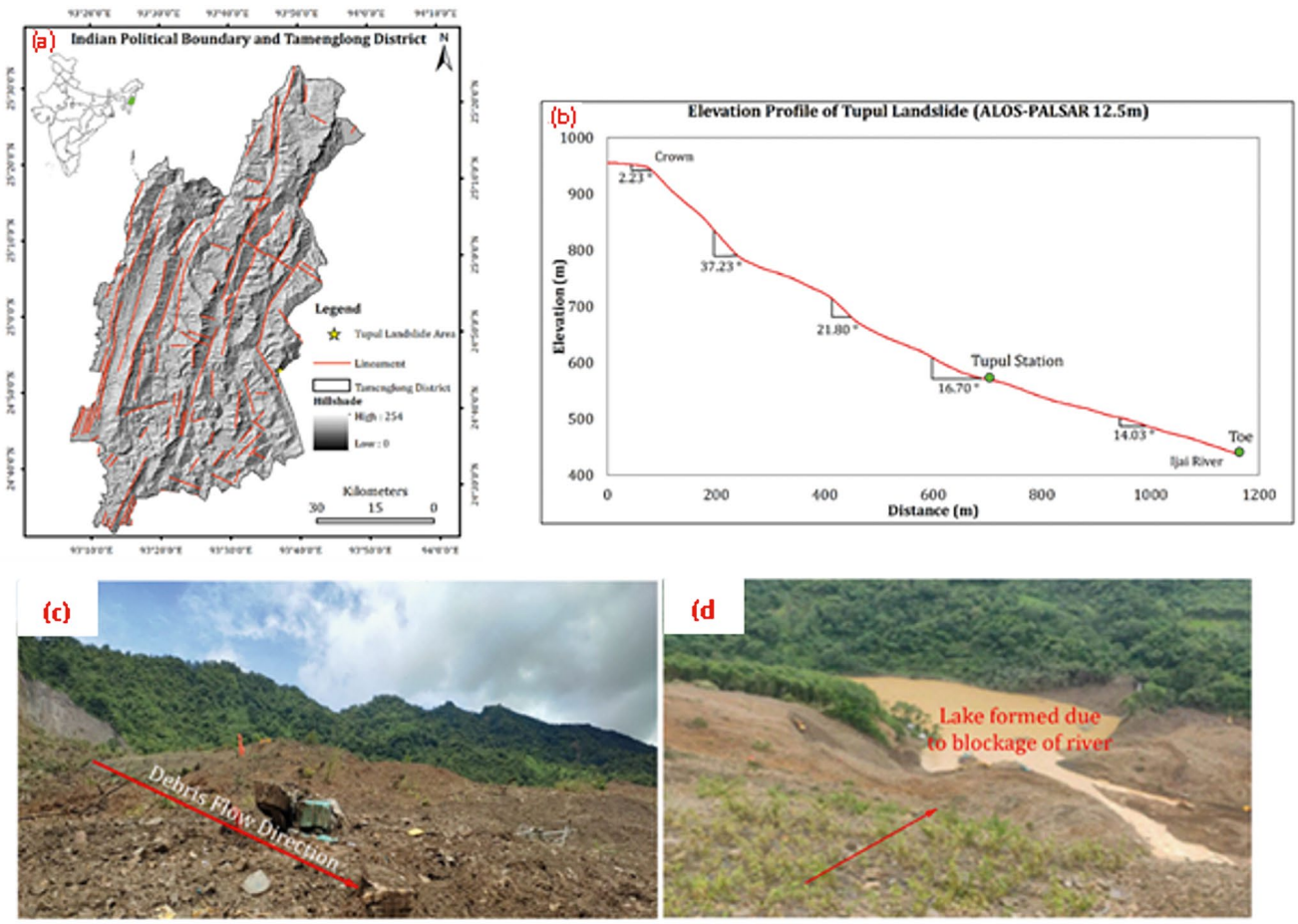


Fig. 6 (**a**) Lineament map of Tamenglong, (**b**) Elevation profile of Tupul landslide, (**c**) Debris deposition of landslide, (**d**) Formation of lake due to river blockage (Source: Singh et al. 2022)

2.3.2 Cause

There are numerous reasons contribute to the landslides in the Tupul region such as unstable geology, intense precipitation, uncontrolled slope cutting, and seismic activity. The area, is close to the Indian-Eurasian plate border, and prone to earthquakes (seismic zone-V); notable ones occurred in 2016.The location is in the Oligocene Barail group, which is extremely porous and readily saturated with water during periods of heavy rain, thus weaking slopes. In addition, the bulk of strike-slip faults, including the Noney, Pen, Dalang, Leimatak, and Kadi faults, cross the Barail group. The area had exceptional rainfall in May 2022 (375.60 mm) and June 2022 (329.9 mm) at Noney District, according to data collected at the closest station which was around 60% more than the previously recorded rainfall (e-pao.net 2022). Furthermore, instability was made worse by the unplanned slicing of slopes during railway construction. All of these factors coupled together to cause a devastating landslide that buried infrastructure and claimed lives.

2.3.3 Recommendations

To prevent future disasters, authorities must prioritize afforestation, monitor landslide-prone areas, foster collaboration between government and academia, implement mitigation measures, and educate communities on early warning systems and evacuation plans. Key measures to minimize damage include:

- Once the initiatives are funded, there should be collaboration between the researchers, academicians, Government authorities and other concerned stakeholders.
- Fault monitoring and identification are necessary for the geographical forecast of possible landslide zones.
- Identifying potential landslide zones and setting up early warning systems with real-time monitoring.
- The nature-based solutions and bio-engineering methods could be used in the near future to prevent such large-scale landslides.
- Appropriate mitigation measures should be put in place in hilly locations where landslides occur often.

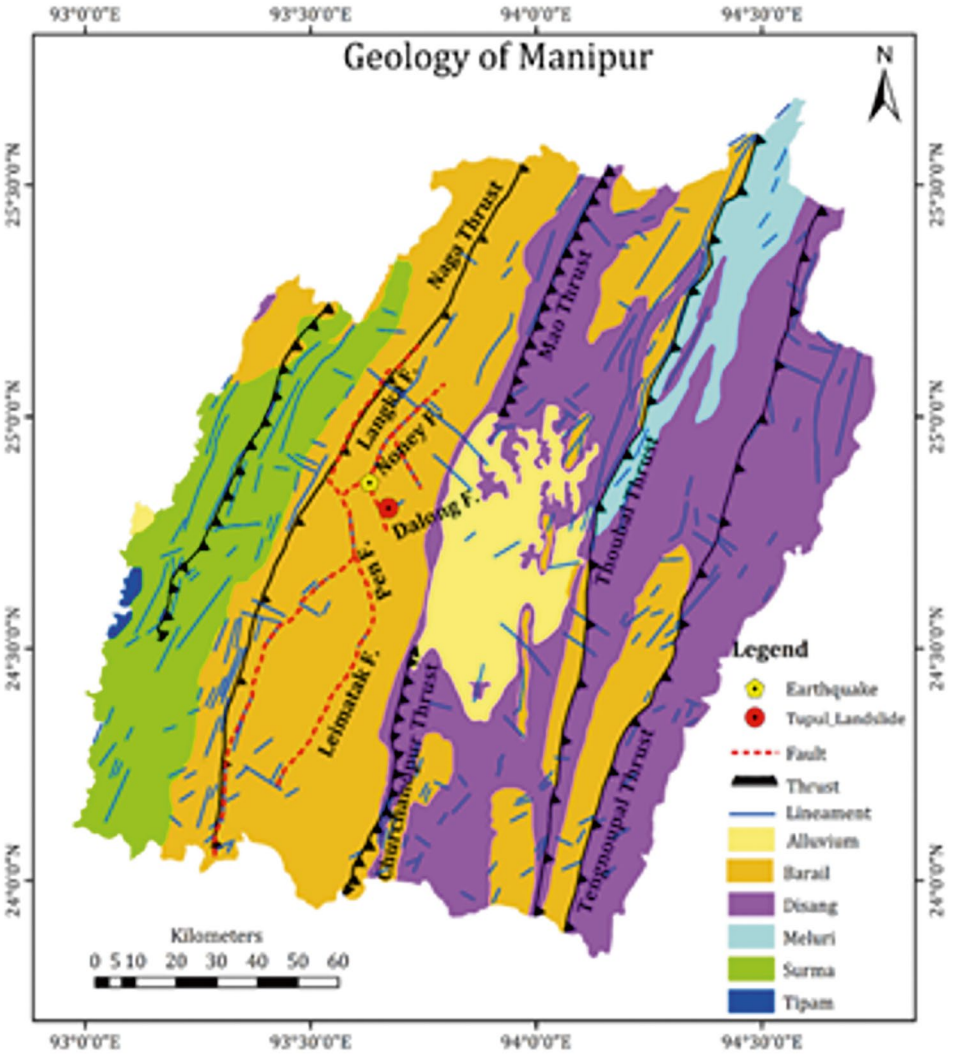


Fig. 7 The geological map depicted in the picture displays the regions' thrusts and faults, the position of the Tupul landslide, and epicentre of the 2016, 6.7 M earthquake (Source: Singh et al. 2022)

- The government should use a bottom-up strategy to educate the public and put non-structural solutions (e.g., early warning systems, evacuation plans etc.) in place in order to lessen the damage caused by landslides.

2.3.4 Conclusion

A fatal landslide at the Tupul railway yard building site in Manipur serves as a clear evidence of the destructive power of natural disasters amplified by human activity. A similar mishap occurred in Dima Hasao, Assam during May 2022, where a landslides event damaged the railway and road connectivity. The destruction of infrastructure and human life highlights how vital it is to take preventative action now, to lessen future hazards. The complicated interaction of man-made and natural causes like this, in the occurrence of slope failure more scientific based field study need to be carried out in collaboration of different stake holders. Communities and government agencies must prioritize afforestation, monitor fault lines, work together efficiently, adopt mitigation measures, and raise public awareness through early warning systems and education in order to avert repeat catastrophes. By implementing a comprehensive strategy that incorporates community engagement, government action, and scientific research, we may endeavor to lessen the susceptibility of hilly areas to landslides and protect lives and livelihoods.

2.4 Rock-Ice Avalanche and Debris Flow, Chamoli-Joshimath (2021)

Flash floods occurred in the Rishiganga and Dhauliganga rivers on Sunday, February 7, 2021, at around 10:08:45 a.m. as a result of a significant debris flow caused by a rock avalanche at the Raungti mountain (6063 m, 30° 22′ 27.38″ N, 79° 43′ 52.03″ E) (Fig. 8). In the middle Garhwal Himalaya, a massive rock mass collapse and the dislodgment of a glacieret resulted in an air blast and dust clouds i.e. Nanda Devi

Ranges (NDMA 2022). A significant debris flow occurred in the Raunthi Gadhera, Rishiganga, and Dhauliganga river valley in Chamoli, resulting in a landslide dam formation at crash zone and debris-dammed lake in the Rishiganga River, with massive debris entering surrounding rivers (Siddique et al. 2022). Apart from harm to the homes, highways, bridges (including five suspension bridges), and the Raini and Tapovan hydroelectric power plants, this incident claimed lives of 204 people and around 186 livestock. In addition, there were negative effects on connectivity, water, and power for 13 settlements.

2.4.1 Area

Physically, the region is made up of glaciated terrain with extremely rough mountainous topography that includes valleys with steep slopes, tiny spurs, and ridges that are sharp, angular, and serrated. The Mana Formation (~Joshimath Formation) rocks, which include migmatite, kyanite-sillimanite bearing schist, and gneiss with pegmatite and quartz veins with lenticular bands of quartzite and marble, represent the source area and likely location of a rock, snow, or ice avalanche. Rocks in the area trend NW-SE regionally, with very minor dips towards NE (Fig. 9). The Geological Survey of India (GSI) has identified a number of NE-SW trending faults in the region in addition to the Main Central Thrust (MCT). Three regular sets of joints, which included foliation joints, were found in the exposed rocks of the Raunthi River valley and Rishiganga. The Raunthi is a compound valley type glacier formed by two tributary glaciers, extended between 4250 m and 6500 m Mean Sea Level (MSL) laying on 12° surface slope (Martha et al. 2021).



Fig. 8 The location of the rock-ice avalanche at Raunthi Glacier, Chamoli

2.4.2 Cause

From February 4 to 6, 2021, very light to light rainfall was recorded in the Chamoli district of Uttarakhand, with the maximum amount on February 5, which is equivalent to the 24-h total rainfall between February 4 and February 5, at 08:30 IST. According to the NDMA study, the main cause of slope failure is rockfall associated with glacieret ice avalanche. This is regulated by three sets of joints that enable the inverted triangle-type wedge collapse of the rock mass and the dislodgement of glacieret over it. The ice-capped failed rock mass dropped from 5474 m to 3732 m and traveled 2.9 km on a sharp incline. The failing mass (rock and ice) collided with the terminal moraine deposit, pulverizing and displacing boulders off the travel path. The failure's energy melted snow and ice, pulverized rock, causing downstream debris flow, and an air blast, uprooting trees in Raunthi Gadhera, Rishiganga, and Dhauliganga valleys (NDMA 2022).

2.4.3 Damage

Debris flow has swept away and destroyed the hydroelectric power projects of the Rishiganga hydro project (13 MW), NTPC hydropower project (520 MW) (Fig. 10), and BRO

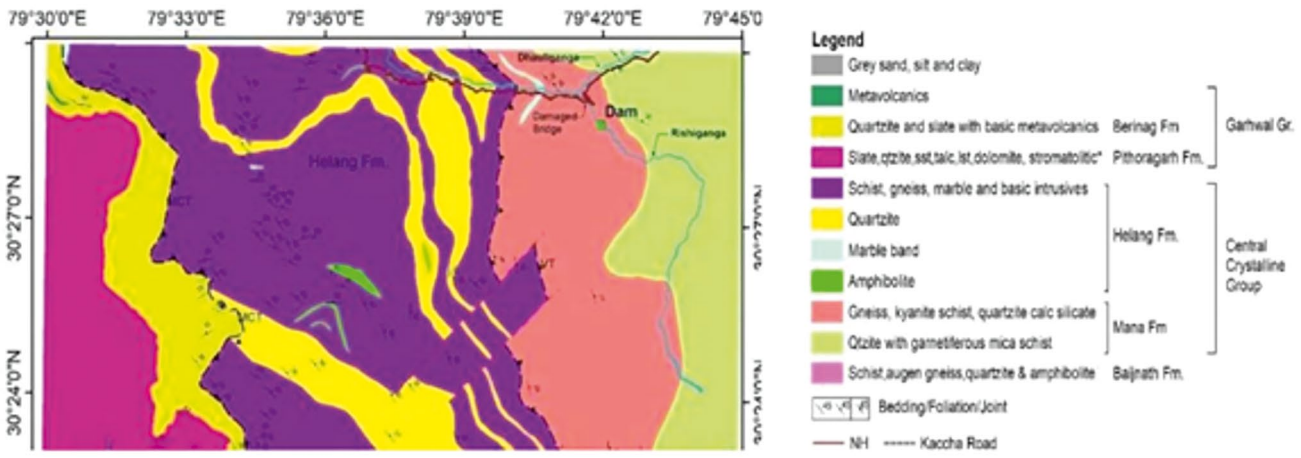


Fig. 9 Geological map of the impacted locations in the Rishiganga-Dhauliganga valley (Source: https://bhukosh.gsi.gov.in/Bhukosh/Public)



Fig. 10 Damage barrage of NTPC Tapovan-Vishnugad HEP

Bridges. Thirteen villages faced utility supply line damage, leading to electricity and water loss, while approximately 204 people are reported dead or missing. Also, Raunthi Gadhera debris flow blocked Rishiganga River, forming an artificial lake due to debris damming.

2.4.4 Recommendations

Comprehensive studies and assessments, along with the implementation of monitoring systems, legal frameworks, and capacity-building initiatives, are imperative for effectively managing multi-hazard risks, enhancing resilience, and integrating climate adaptation measures in the Himalayan region. Therefore, following measures could be useful for future:

- Research on risk assessment for multiple disasters and cascade events utilizing high-resolution satellite data and field surveys is required.
- Environment Impact Assessment (EIA) along with Disaster Impact Assessment (DIA) study of every hydroelectric project (HEP) and developmental projects to be done considering ecological sensitivity of the region.
- Keeping climate-related risk monitoring, management, and adaptation front and center in studies, research, initiatives, etc.
- Weather monitoring systems and Automatic Weather Stations (AWS) should be established at suitable locations with complete remote capabilities and automatic data transfer.
- Training programmes and capacity enhancement programmes to be organised for the scientific/technical experts and other stakeholders.
- Develop legal framework based on NDMA documents and guidelines on GLOF (October, 2020) and National Landslide Risk Management Strategy (Singh and Parkash 2019) for unstable areas, including Mountain Zone Regulation and Building Bye-laws.
- The appropriate department's integration and coherence of the district disaster management plans (DDMP) with the DRR, the climate change action plan, and the sustainable development goals (SDG).

2.4.5 Conclusion

The Himalayan glaciers and mountains are currently feeling the consequences of global warming and climate change. Therefore, it is essential that best practices from both domestic and foreign sources be shared and learnt from in order to lessen the harm caused by possible risks and threats in the Indian Himalayan areas. In India, Chamoli incident was the first time that rock and ice avalanche with cascading impact of debris flow occurred in Himalayan region. However, in the past, similar type of rock falls and glacier avalanche catastrophes occurred in the Russian Caucasus, Nepal, Canada, and the European Alps. Furthermore, it is recommended that all hydroelectric projects (HEPs) follow recommendations and standards and implement all necessary safety measures at every stage of operation, including design, feasibility studies, construction, and operation.

2.5 Land Subsidence, Joshimath, Chamoli (2022)

Based on earlier assessments (Heim and Gansser 1939; Mishra Report 1976), the town of Joshimath was mostly constructed atop debris from past landslides and lacked sufficient in-situ rockmass stability. The scientific literature has

extensively documented its history of slope failures. Due to its location in Seismic Zone-V and close proximity to the Main Central Thrust (MCT). Because of this, the town is susceptible to displacements, deformations, and ground distresses. On March 29, 1999, a large earthquake with a magnitude of 6.6 occurred. Although the problem of developing fissures was reported in many houses from past few years but recently in January 2023 reports were received from multiple sources concerning the emergence and spread of fissures in the earth, buildings, and roads starting on January 2, 2023. Additionally, on January 3, 2023, there was information about sediments being flushed out of the water at various locations within the Jaypee Residence Colony, Joshimath (Shankar et al. 2023a, b).

2.5.1 Area

Strategically significant, Joshimath Tehsil in District Chamoli is a well-liked hill station and pilgrimage site. With an average altitude of around 1830 meters above sea level, it is situated between 30° 30′ N and 30° 35′ N and 79° 30′ E and 79° 40′ E. This region is bordered to the northeast by the North-West to South-East trending Pindari Thrust and to the southwest by the Main Central Thrust. It is a section of the Higher Himalayan Crystalline, which is mostly composed of high-grade gneisses and schists. Geomorphologically speaking, area consists of a weakly weathered overburden landslide mass from both glacial and fluvio-glacial deposits, along with subsurface drainages, steep slopes, silty sandy matrix under wet conditions, unfavorable morphology, excessive rainfall, and an area that is seismically active and located in seismic zone-V.

About 1500 mm of rain falls on average each year, with the summer monsoon season accounting for 80% of the total with occasional cloudbursts. The ridge trend North-West to South-East is the source of several drainage. The majority of the slopes are concave in character, indicating the presence of an ancient landslide zone and slope mass depletion (also indicated by the slopes' curvi-linear base). There has been significant glacial and periglacial activity in the late Quaternary. The presence of ancient drainages inside the current overburden mass might be one of its components.

2.5.2 Cause

Possible causes of ground distress, deformation, and displacement include excessive pore water pressure from water infiltration due to precipitation or human activities such as drainage discharges, ground failure resulting in cracks in various building elements due to unstable and unplanned construction on old landslide masses without proper drainage and adherence to building regulations, sudden water outflows possibly caused by increased sub-surface drainage pressure or blockages, piping erosion along sub-surface drains leading to soil loss, subsidence, and ground cracks. Frequent seismic activity in Seismic Zone-V causing overburden loosening, cracks, and slope instabilities, neglect of hazard susceptibility maps and failure to implement landslide management guidelines and recommendations, and tourism and population rise causing adverse effects on the natural ecosystem, including deforestation and groundwater over-exploitation.

2.5.3 Damage

Although no human causality but about 161 buildings in Ravigram, 134 buildings in Gandhinagar, 80 buildings in Manohar bagh, 56 buildings in Singdhar, 51 buildings in Parsari, 38 buildings in Sunil, 31 buildings in Upper Bazar, 28 buildings in Marwari and 24 buildings in Lower Bazar have developed cracks to different degrees (Figs. 11 and 12). The number has increased as the time is passed due to delay in proactive measures being taken at concerned departmental levels.

2.5.4 Recommendations

- Explore the possibility of slope stabilization through various prevention and mitigation techniques to recover the ground. Hydroseeding and plantation for landslide mitigation and livelihood.
- Comprehensive Drainage System with sewer line connections to households.
- Rehabilitation structures should be constructed based on multi-hazard resistant approach at a safer location.
- Assessment of all those hot spot areas in the state where cracks, have been reported in the recent past and are likely to suffer similar consequences.
- Development of large-scale Multi-Hazard zonation map of Joshimath and other similar town of the state including Nainital and Mussoorie.
- Timely treatment of failed or unstable slopes.
- Implementation of National Guidelines, Codes, Standards, Procedures, Manuals and Strategies for disaster risk reduction and resilience may be strictly followed up.
- Roles, Responsibilities and Accountability of each stakeholder in generating new risks or management of existing risks, may be fixed more strongly in a concrete manner.

2.5.5 Conclusion

The Mishra Commission (1976) warned against construction in Joshimath due to its unstable geological foundation and glacieret loose material. However, Joshimath has being urbanised due to tourism and unplanned developmental activities. Field observations reveal exposed jointed gneisses, signs of subsidence, displaced boulders, and cracks, indicating high landslide susceptibility in Joshimath.



Fig. 11 Wide cracks in the retaining wall due to land settlement and gushing water through water drain in JP Colony



Fig. 12 Leaning of Hotel Malari Inn over Hotel Mount View

Similarly, other Himalayan towns such as Thathri-Doda (Jammu & Kashmir), Shimla (Himachal Pradesh), Nainital (Uttarakhand), Gangtok (Sikkim), Aizawl (Mizoram) etc. are highly vulnerable towards building collapse and land-sinking due to heavy unplanned anthropogenic activities. Urgent action is needed to prevent future disasters through comprehensive scientific investigations and integrated approaches. Public awareness and capacity development activities of government agencies and other stakeholders are crucial for mitigating risks in the Himalayan region along with implementation of building-bye laws and regulations.

2.6 South Lhonak GLOF, Sikkim (2023)

In the intermittent night of 3rd October 2023, an unexpected melting of glacier ice and landslide in South Lhonak Lake (27°54′20″N and 88°10′20″ E) (Fig. 13) triggered glacial lake outburst flood (GLOF) (Fig. 14) in the Teesta river basin, resulting in the destruction of the Teesta 3–1200 MW Urja Limited Hydro-electric dam at Chungthang dam and Teesta 5–500 MW National Hydroelectric Power Corporation (NHPC) gates badly damaged. Total of 88,400 people were affected, 104 dead and 77 persons are missing (Srivastava et al. 2023). Both the direct and indirect effects of global warming and climate change are to blame for this disaster.



Fig. 13 South Lhonak Lake (Before and After)



Fig. 14 South Lhonak Lake breaching site and Landslide Dammed Reservoir in River Teesta

2.6.1 Area

Situated in the East district of Sikkim, India, the South Lhonak Lake site is measured in latitude (27°54′0″N to 27°55′20″N) and longitude (88°9′20″E to 88°12′5″E). The region is geologically part of the Central Crystalline Gneissic Complex of Proterozoic age, namely the Kanchenjunga Gneiss Formation. This formation is made up of mica schist with well-developed joint planes, garnet biotite gneiss, and bent migmatite. Terrain is rugged, marked by gullies, deep streams, and landslide zones, with dendritic drainage pattern and occasional waterfalls (Joshi et al. 2024).

2.6.2 Cause

According to the Indian Metrological Department (IMD) rainfall data, from 1st March to 4th April 2023, the Sikkim State exceptionally received 260 mm of rainfall; which was 68% more than usual (Petley 2023). The geography of the region ranges from gentle to steep sloping surface. A quick, unexpected loose snow avalanche occurred on April 4, 2023, from higher levels. From the moment of trigger till it descended, the avalanche rapidly expanded and carried a large amount of snow with it. Generally, loose snow avalanches happen during or shortly after a period of warmth that lead due flash flood in no time.

2.6.3 Damage

On the early morning of October 4th 2023, a sudden and significant increase in water flow within the Teesta River catchment resulted in 40 casualties, with 70 individuals still reported as missing. This catastrophic event has led to the destruction of 15 bridges, the disruption of water pipelines and sewage lines, and the destruction of 2002 residential houses across multiple districts and huge damage to hydropower project (Fig. 15) along with cut off of road network from boarder areas.

2.6.4 Recommendation

Glacier bodies of the Himalayas which are in the remote part needs to be looked upon so as to prevent any such incidents in near future. Therefore, following points should be considered in order to minimize losses:

- Community to be trained at advance level for rescuing in poor weather condition.
- Enforcing the industry's stringent safety regulations.
- Required to give the local population basic nursing training.
- Detailed survey for placing the real time monitoring equipment so it does not get destroyed either due to fast winds or debris of event.



Fig. 15 Teesta 3 (1200 MW) Hydro-Electric Project of Urja Limited (Before and After) (Source: SANDRP 2023)

- Use of advance technology and satellite based early warning systems for remote areas.

2.6.5 Conclusion

The Himalayas pose significant challenges for disaster management due to their diverse array of natural hazards, rugged terrain, and unpredictable weather. Incidents like the April 4, 2023 avalanche underscore the difficulties in rescue operations in poor weather conditions. Globally, safety violations contribute to tragedies, despite warnings, human negligence persists, necessitating community preparedness and adherence to safety protocols. While hazards are inevitable, proactive risk management and government regulation of tour operators can mitigate their impact. Local residents often act as first responders, highlighting the importance of basic rescue training. Learning from past mistakes and anticipating future challenges are essential for minimizing the human toll of disasters.

3 Common Recommendations

Recommendations suggested above are as per the disaster events occurred, ground situation, requirements/need etc. Whereas, there are common recommendations to avoid these future disaster risks of landslides and associated mass-movements in the Indian Himalayan region at each phases of disaster given as under: -

Pre-Phase:

- Identify highly vulnerable areas in glaciers and inaccessible regions with the help of remote sensing for the safety of our vital infrastructures and installations of early warning systems in the downstream.
- Real time monitoring and prediction of landslides and mass-movement by judicious application of advance technology and tools such as AI, ML, IOT etc.
- Study on multi-Hazards Risk Vulnerability Assessment (m-HRVA) with field validated models need to be done.
- State Government and concerned stakeholders should take initiative to revise and update their Disaster Management Plan (DMP) incorporating LLOF and GLOF.
- Before allowing construction of structures on hills, careful geotechnical analysis of the hill slopes from the perspectives of instability and carrying capacity should be done.
- Illegal constructions and encroachment in the flood plains and riverine areas must be prohibited and rehabilitated.
- Existing human settlements must be relocated to safer regions, and human settlements below, above, or in the impact zone of old or active landslide zones must be prohibited.
- To provide toe support, retaining walls and other suitable structures should be used to safeguard road-cut slopes and slopes surrounding important buildings or infrastructure.
- Awareness programmes should be initiate to aware villagers and local persons about sustainable land use practices to avoid Jhum cultivation.
- Training programmes and capacity enhancement programmes to be organised for the scientific/ technical experts and other stakeholders on different aspects of landslide risk reduction and mitigation.
- Provide the basic first-aid and nursing training to the local people to deal with landslide injured person.
- Environment Impact Assessment (EIA) along with Disaster Impact Assessment (DIA) study of every hydro-electric project (HEP) and developmental projects to be done considering ecological sensitivity of the region.
- Coherence and integration of disaster management plans with climate change action plan and sustainable development goals and its implementation at ground level.
- Revision and implementation of National Guidelines, Codes, Standards, Procedures, and Strategies for disaster risk reduction and resilience may be strictly followed up.
- Roles, responsibilities and accountability of each stakeholder in generating new risks or management of existing risks, may be fixed more strongly in a concrete manner.
- By combining further scientific and technical know-how with local understanding, disaster risk reduction and climate change adaption may be improved.

During Phase:

- Concerned State Government, and other stakeholders should jointly develop a comprehensive action plan for providing necessary support. The action plan must be updated time to time with joint sitting of all stakeholders at State level.
- Immediate rescue and shifting of the persons residing in affected and vulnerable zone is required.
- Immediate steps should be taken to drain the existing water pools on slope. These depressions should be filled with local material to avoid standing water on slope. Filling of ground cracks with impervious material and leveling is important to avoid pouring of water into the slope.

Post-Phase:

- Accessibility and evacuation in remote areas becomes a major challenge during disaster. Therefore, capacity building and training of local administration, mainly first responders must be strengthened to deal with any disaster situation in well-coordinated manner.
- The nature-based solutions and bio-engineering methods could be used to prevent landslides as per site conditions.
- Encourage public-private partnership to increase DRR investment by promoting build back better approach in rehabilitation and reconstructions. There is need to enforce the stringent safety policies, regulations, quality control and audits in DRR.

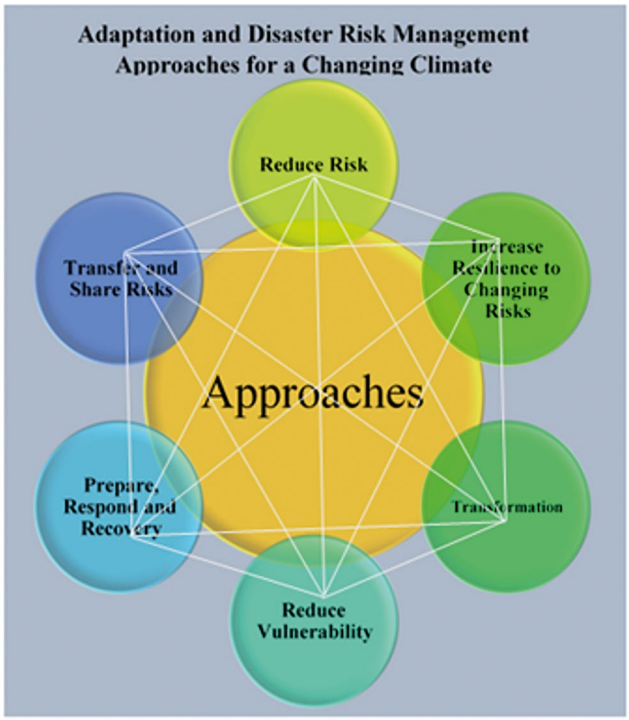


Fig. 16 Strategies for catastrophe risk reduction and management in a changing climate include adaptation and risk management

4 Discussion and Conclusion

Landslide losses are linked to geophysical, meteorological (hydro-meteorological), and climate change occurrences, which are more common in industrialized nations. Small island developing states (SIDS), landlocked developing countries (LLDC), least developing countries (LDC), and developing nations all have greater death rates and economic losses as a percentage of Gross Domestic Product (GDP).

The main factor contributing to the long-term rise in economic losses from weather- and climate-related disasters has been people's and economic assets' increased exposure. Although a role for climate change cannot be ruled out, long-term trends in economic catastrophe losses adjusted for income and population expansions have not been linked to climate change.

The Special Report of the Intergovernmental Panel on Climate Change (2012) on "Managing the Risks of Extreme Events and Disasters to Advance Climate Change Adaptation" (Fig. 16) states that the frequency and amplitude of extreme weather and climate events have grown, but so have the populations and assets that are at danger, which has an impact on the risk of disasters. Future variations in exposure, susceptibility, and temperature extremes brought on by human climate change and natural climate variability change, and socio-economic development can alter the impacts of climate extremes on natural and human systems and the potential for disasters.

Severe weather occurrences will have a stronger effect on industries including water, forestry, health, tourism, agriculture, and food security that are more closely related to the climate. For instance, there is strong certainty that climate change has the potential to have a significant impact on water management systems, even if it is currently impossible to confidently estimate precise changes at the catchment size. However, climate change is in many instances only one of the drivers of future changes, and is not necessarily the most important driver at the local scale. Climate change related events can also produce large impacts on human, environment and infrastructure, such as loss of life, property and hydro-electric project at Chungthang in Sikkim due to Lhonak GLOF incident.

All above given case study provide insight of past disaster events has clearly indicated that present and future mass-movement related incidences such as landslides, snow avalanche, GLOF, flash floods etc. are triggered and alter by interplay of natural factors, anthropogenic activities and cli-

mate change extremes. Recent incident of South Lhonak GLOF event happened on 4th October 2023 is a clear example of impact of extreme weather and climate change on cryosphere dynamics. However, there is lack of data and records to prove impact of climate change and global warming in aggravating disaster events. An iterative process of monitoring, research, assessment, learning, and innovation in the setting of climatic extremes can reduce the risk of disaster and promote adaptive management.

The melting glaciers and thinning of ice-mass balance pose a threat of water insecurity and food security around the Indian Himalayan Regions (IHR) nations such as India, Nepal, Bhutan, Afghanistan etc. Therefore, appropriate actions to be taken to minimize the carbon emission by adopting sustainable measures such as energy transition, utilization of renewable energy sources, reduce waste, conservation of water bodies and natural ecosystem etc.

The effects of climate extremes on human and natural systems, as well as the likelihood of disasters, may change in the future due to variations in exposure, susceptibility, and temperature extremes brought on by anthropogenic climate change, natural climate variability, and socio-economic growth. Resilient and sustainable pathways may be significantly impacted by the linkages between disaster risk reduction, adaptation, and mitigation of climate change. Interactions between the adaptation and mitigation goals will manifest locally yet have global ramifications. Risk reduction and risk transfer initiatives can typically support holistic approaches to effective risk management. Effective adaptation and disaster risk reduction depend on early and appropriate risk communication in form of early warning system. The Early Warning for All (EW4All) program, introduced by UN Secretary-General Antonio Guterres in March 2022, calls for early warning systems to safeguard every person on Earth by 2027.

Now, there is immense necessity for stringent policies and strategies (e.g., land-use planning, construction practices, regulations etc.) for reducing disaster risks was extremely felt. Simultaneously, the advancement of innovative technology and tools such as artificial intelligence (AI), machine learning (ML) (Badola et al. 2023), data mining, Internet of Things (IOT) are required to generate reliable, field validated models of multi-hazards based early warning, risk assessment, mitigation, response etc. will reduce impacts of future disasters and its occurrences.

Acknowledgments Authors would like to thanks ICL for providing the opportunity of writing the chapter on the emerging issues and challenges caused by landslides and its associated hazards. There is no funding source for the present study and sole work is done by the authors during field study.

References

Badola S, Mishra VN, Parkash S (2023) Landslide susceptibility mapping using XGBoost machine learning method. In: 2023 International Conference on Machine Intelligence for GeoAnalytics and Remote Sensing (MIGARS), vol 1, pp 1–4. IEEE.

Directorate of Information & Public Relations (DIPR): Landslide Early Warning System (LEWS) to be made operational by 2025, DIPR Manipur, 28th July 2022

E-pao.net (2022) Survey report of Tupul landslide trigerred on 29th 30th June 2022.

Heim AA, Gansser A (1939) Central Himalaya: Geological observations of the Swiss Expedition, 1936. Hindustan Publishing Corporation, India

IPCC (2012) Field CB, Barros V, Stocker TF, Qin D, Dokken DJ, Ebi KL, Mastrandrea MD, Mach KJ, Plattner G-K, Allen SK, Tignor M, Midgley PM (eds). Cambridge University Press, pp 582

Joshi M, Kumar K, Rajeevan K, Barfal SS (2024) Tragedies due to human folly: a learnt lesson from year 2023 Sikkim avalanche. Q Sci Adv 13:100162

Kanungo DP, Singh R, Dash RK (2020) Field observations and lessons learnt from the 2018 landslide disasters in Idukki District, Kerala, India. Curr Sci 119(11):1797–1806

M C Mishra Commission (1976) Preventing landslide in Joshimath, Chamoli, order no. A.O. 142/28-5/44/76

Martha TR, Roy P, Jain N, Vinod Kumar K, Reddy PS, Nalini J, Sharma SVSP, Shukla AK, Rao KHVD, Narender B, Rao PVN, Muralikrishnan S (2021) Rock avalanche induced flash flood on 07 February 2021 in Uttarakhand, India—a photogeological reconstruction of the event. Landslides 18(8):2881–2893

NDMA (2022) Detailed Report on Study of causes and impacts of the Uttarakhand Disaster on 7th February 2021 in Raunthi Gadhera, Rishiganga and Dhauliganga valley – Measures to reduce disaster risks, April 2022, pp 1–60

NRSC-ISRO (2023) Landslide Atlas of India - Mapping, Monitoring and R&D studies using Remote Sensing data, National Remote Sensing Centre-ISRO, 2023, pp 39

Petley D (2023) India: The likely causes of the 4 October 2023 Sikkim flood disaster. PreventionWeb

SANDRP (2023) Glacial Lake Flood destroys Teesta-3 Dam in Sikkim, brings wide-spread destruction

Shankar H, Chauhan P, Singh D, Ravi Bhandari CM, Bhatt AR, Kannaujiya S, Singh RP (2023a) Multi-temporal InSAR and Sentinel-1 for assessing land surface movement of Joshimath town, India. Geomatics Nat Hazard Risk 14(1)

Shankar H, Chauhan P, Singh D, Bhandari R, Bhatt CM, Roy A, Kannaujiya S, Singh RP (2023b) Multi-temporal InSAR and Sentinel-1 for assessing land surface movement of Joshimath town, India. Geomatics Nat Hazards Risk 14(1):2253972

Siddique T, Haris PM, Pradhan SP (2022) Unraveling the geological and meteorological interplay during the 2021 Chamoli disaster, India. Nat Hazards Res 2(2):75–83

Singh R, Parkash S (2019) Need of National Landslide Risk Management Strategy for Reducing Landslide risk in India. J Disaster Dev 8(1&2):44–64. ISSN: 0973-6700

Singh A, Adaphro A, Niraj KC, Nitesh DCS, Shukla DP (2022) Analysing the causes and lessons learned from Tupul landslide, Noney district, Manipur, Research Square, pp 1–11

Srivastava S, Sarkar-Swaisgood M, Baker T, Hong S, Maruichi D (2023) Climate catastrophe in the Sikkim Himalayas: Twin track resilience strategy. News and Press Release UN ESCAP, 23 Oct., 2023

Open Access This chapter is licensed under the terms of the Creative Commons Attribution 4.0 International License (http://creativecommons.org/licenses/by/4.0/), which permits use, sharing, adaptation, distribution and reproduction in any medium or format, as long as you give appropriate credit to the original author(s) and the source, provide a link to the Creative Commons license and indicate if changes were made.

The images or other third party material in this chapter are included in the chapter's Creative Commons license, unless indicated otherwise in a credit line to the material. If material is not included in the chapter's Creative Commons license and your intended use is not permitted by statutory regulation or exceeds the permitted use, you will need to obtain permission directly from the copyright holder.



A Web-GIS for the Analysis of Scientific Literature on Earthquake-Triggered Landslides

Federica Fiorucci, Luca Schilirò, Mauro Rossi, Federica Polpetta, Carolina Fortunato, and Paola Reichenbach

Abstract

Earthquake-triggered landslides (EQTLs) are a widespread phenomenon which frequently occur after significant seismic events, causing additional damage and casualties. Over the past two decades, the topic of earthquake-triggered landslides has seen a significant increase in attention from the scientific community. This growing interest is evident through the multitude of articles appearing in international, peer-reviewed journals. In this study, we report the main features of a web-GIS database containing the most relevant scientific articles on EQTLs (i.e., more than 800 articles published between 1984 and 2021). After a description of the structure and utilization method of the Web-GIS, we provide a synthetic analysis of the collected articles, to provide an overview of publication trends on EQTLs theme worldwide.

Keywords

Web-GIS · Landslide · Earthquake · Bibliographic data

F. Fiorucci (✉) · M. Rossi · P. Reichenbach
CNR IRPI – Istituto di Ricerca per la Protezione Idrogeologica, Consiglio Nazionale delle Ricerche, Perugia, Italy
e-mail: federica.fiorucci@cnr.it; mauro-rossi@cnr.it; paola.reichenbach@cnr.it

L. Schilirò · F. Polpetta
CNR IGAG – Istituto di Geologia Ambientale e Geoingegneria, Consiglio Nazionale delle Ricerche, Rome, Italy
e-mail: luca.schiliro@cnr.it; federica.polpetta@cnr.it

C. Fortunato
Istituto di Geologia Ambientale e Geoingegneria, CNR, Rome, Italy

1 Introduction

Earthquakes pose significant threats globally, causing substantial damage and loss of life. Earthquake-triggered landslides (EQTLs) contribute to about 70% of earthquake-related fatalities not directly linked to ground shaking (Marano et al. 2010). These landslides often disrupt transportation networks (Martino et al. 2019), impeding rescue and recovery efforts, and may block river channels, leading to downstream floods and long-term changes in drainage-basin characteristics (Koi et al. 2008).

Considering the importance that this topic is assuming within the scientific community, significant information on EQTLs literature were recently collected through a systematic search on the Clarivate™ Web of Science™ Core Collection platform of the main scientific articles published in international peer-reviewed journals (Schilirò et al. 2023). The gathered information was then organized to be accessible and available through a web-GIS.

A web-GIS involves the integration of Geographic Information System (GIS) functionality with web-based technologies, making spatial data and mapping capabilities accessible through a web browser. Such a combination has facilitated the accessibility of GIS to the general public in a simple and effective manner (Green and Bossomaier 2004), allowing the retrieval and exploitation of geospatial information without the need for specialized desktop GIS software. Web-GIS technology plays a crucial role in the field of data information and distribution, offering a range of benefits for individuals, organizations, and communities, such as accessibility that ensures relevant data can be reached by a diverse audience, including professionals, decision-makers, and the public. Its user-friendly interface makes it easier for individuals with varying levels of GIS expertise to interact with and interpret spatial data.

© The Author(s) 2025

B. Abolmasov et al. (eds.), *Progress in Landslide Research and Technology, Volume 3 Issue 2, 2024*, Progress in Landslide Research and Technology, https://doi.org/10.1007/978-3-031-72736-8_23

Given the importance of EQTLs in earthquake hazard assessment, and the need for a user-friendly tool to access this information, this paper describes a web-GIS database designed to consult and geographically organise information gathered from the scientific literature on EQTLs.

2 Methods

The implementation of the web-GIS platform was performed in two steps. The first involves data collection and selection of the articles on EQTLs, as described in detail by Schilirò et al. (2023). The second pertains to the organization and structuring of the data required for the preparation of the web-GIS.

To select the main articles published on EQTLs in peer-reviewed international journals, we used the Clarivate™ Web of Science™ Core Collection platform (WoSCC). We used as search parameters on WoSCC a combination of significant keywords (e.g., *landslide*, *slope failure*, *earthquake*, *seismic*, *triggered*, *induced)* and Boolean search criteria applied to the "title", "abstract", and "keywords" of the articles (Reichenbach et al. 2018). The search allowed to collect 810 articles from 1984 to 2021, that were integrated with other sources of information (i.e., ISC Event Bibliography http://www.isc.ac.uk/event_bibliography/index.php last access: February 15, 2024). Each article was verified to confirm the relevance for the topic.

The articles collected and organized in a database was classified into four categories considering the following main topics:

- regional landslide analysis: articles concerning the analysis of EQTLs over wide areas;
- single-landslide analysis: articles concerning the analysis of single slope failures;
- other: articles describing various activities related to EQTLs, such as data presentation (e.g., Fortunato et al. 2012; Tanyaş et al. 2017; Villani et al. 2018; Rodríguez-Peces et al. 2020), collection of historical information and review of significant articles (e.g., Keefer 1984, 2002; Bird and Bommer 2004; Wasowski et al. 2011; Fan et al. 2019);
- not applicable: articles concerning topics and activities only partially related to EQTLs.

The articles included in the "regional landslide analysis" and "single-landslide analysis" categories were further subdivided in sub-topics related to the type of scientific activity described in the paper, such as mapping, characterization, modelling (Schilirò et al. 2023). Also the "Not applicable" category was divided in sub-topics with respect to elements/processes representing the main theme of the article, but that is somehow related to EQTLs, such as: dating of historical-Holocene earthquakes through landslide deposits, analysis of tsunamis and floods induced by EQTLs, investigation of EQTLs processes in the framework of landscape evolution assessment.

After this step, we developed a dedicated web-GIS database (https://nixus.irpi.cnr.it/en/map/a-web-gis-database-of-the-scientific-articles-on-e/qdjango/54/ last access: February 15, 2024) designed to search, visualize and analyze different information (e.g., bibliometric information, addressed topics and earthquakes) in a geographic framework. The geographical data contained in the literature database, such as country and earthquake information, was used to aggregate the articles.

The implementation of the web-GIS utilized G3W-SUITE (https://g3wsuite.it/en/g3w-suite-publish-qgis-projects/ last access: February 15, 2024), a modular client–server application, integrating the QGIS Python Application Programming Interface. This framework enables to publish and manage QGIS cartographic projects. The web-GIS incorporates two geographic layers and two tables. The first layer represents earthquakes, geolocated according to their epicenter coordinates (latitude and longitude). The second layer corresponds to countries, derived from the "world_boundaries" shapefile (https://public.opendatasoft.com/explore/dataset/world-administrative-boundaries/export last access: February 15, 2024). The two tables ("articles for earthquake" and "articles for country") establish a one-to-many relationship with their respective geographic layers.

The user-friendly interface of the web-GIS comprises different panels. In the left panel, users can explore and utilize the following information and tools:

- Metadata: it provides summary data about the web-GIS. In particular, the panel includes sub-panels reporting general information (i.e., title of the web-GIS, fees, access constraints, reference person name and his/her contact), spatial extension of the exposed data, the adopted reference system as EPSG code, and the list of the layers, that are iconized differently if they are tables or geographic primitives;
- Charts: the chart tool allows aggregating geographical information. In this web-GIS, the Chart tool displays two graphs describing the number of articles per country and the number of articles per earthquake;
- Search: it employs a search tool enabling alphanumeric queries on available layers (i.e., "earthquakes" and "world_boundaries"). To facilitate the query building, the "Fields" name and its value are suggested by drop-down windows;
- Web Map Service (WMS): it allows users to customize the view using WMS services;

- Map: it contains a list of available layers (i.e., "articles_earthquake", "earthquake", "articles_country", "world_boundaries") and their corresponding legends. By right-clicking on the layer name, users can visualize the attribute table.

The right panel provides commands for zooming in and out, measuring distances and areas, uploading new layers, and it includes a snapshot tool. Users can also execute queries (by selecting the "i" icon, *query layer*) on specific earthquakes or countries to visualize associated information.

3 Results

The web-GIS shows a map featuring world boundaries and earthquake epicentres (Fig. 1). On the map, world boundaries are categorized according to the number of papers, with darker grey representing regions with a higher number of articles on EQTLs. Earthquakes are shown using two combined information: the number of articles (dot size) and the magnitude (dot colour).

Both the tables "article for country" and "article for earthquake" provide information on: country, publication year, authors, title, journal, topic, sub-topic/s, and earthquake data (code, name, and date). It is also reported a "doi_link" field which allows the direct access to the paper using the button *open* (Fig. 2). Further refinement of the selection is possible by using the *search* tool, which performs a generic search and a selection over the entire display fields; for instance, it is possible to make a sub-selection of the selected articles with respect to a specific topic or sub-topic.

One of the advantages of the web-GIS application is the typical, user-friendly interface, which makes it easier for people with different levels of GIS skill to handle spatial data. In the here-described web-GIS, the "charts" tool provides an overview of the collected articles contained in the map through the "articles for earthquake" bar chart diagram and the "articles for country" bar chart diagram. Zooming in a specific area (Fig. 3a) of the map and switching to a filtered data using the specific button, bar chart diagram can be refined (Fig. 3b and c) according to the geometry in the displayed extension.

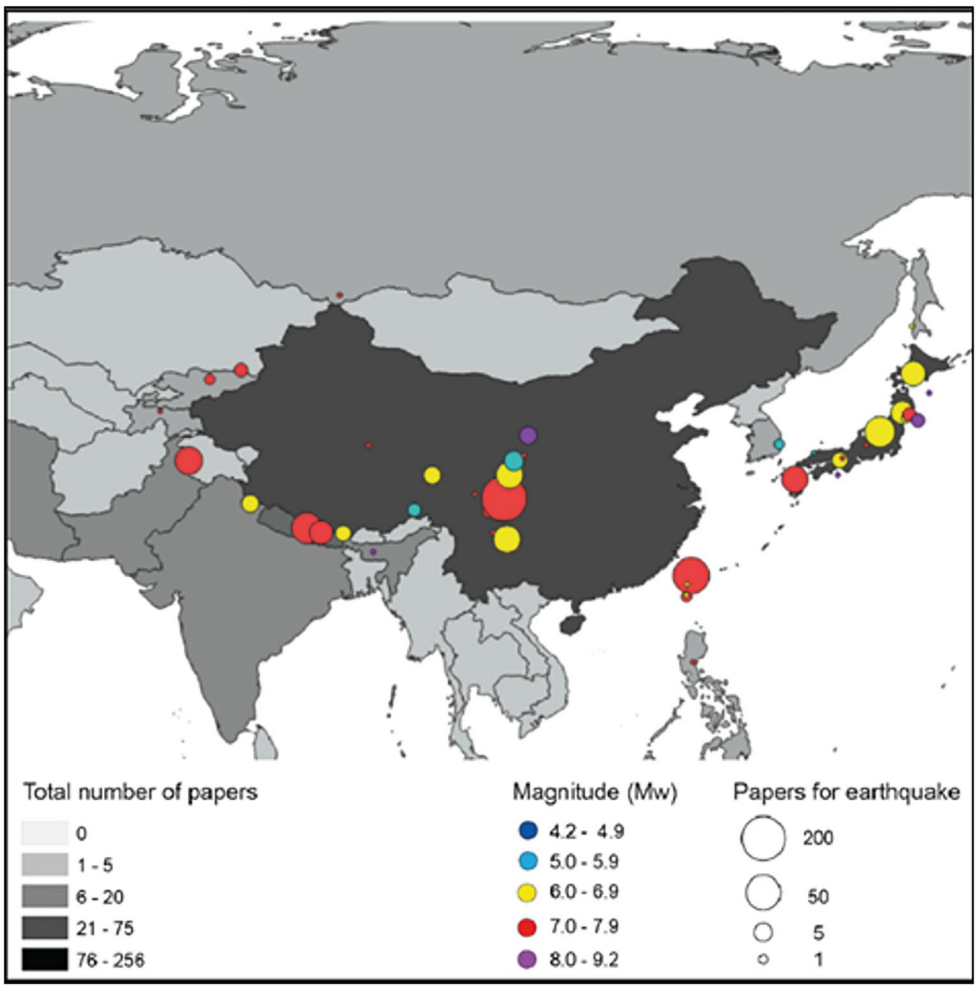


Fig. 1 Example of web-GIS view reporting the spatial distribution of earthquakes in east Asia

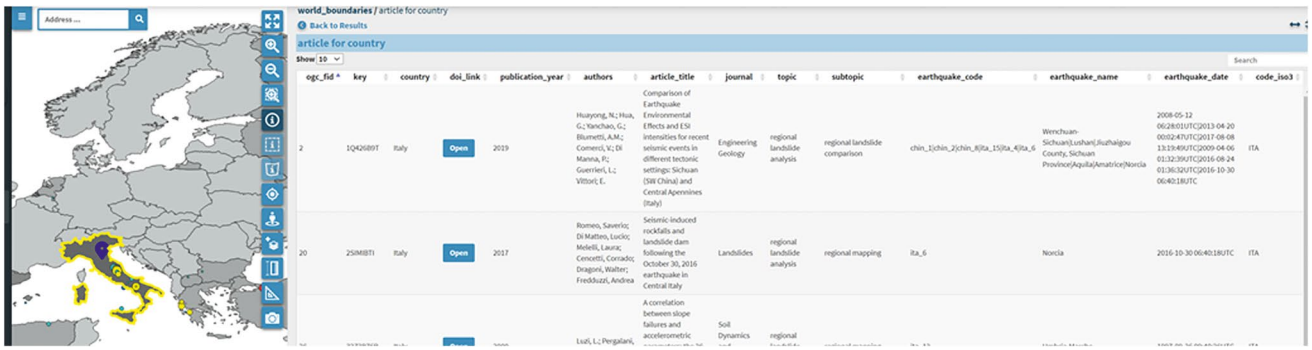


Fig. 2 Example of the table "article for country" generated by the web-GIS through the selection of a specific country. In this case, the table reports the list of articles related to EQTLs occurred in Italy

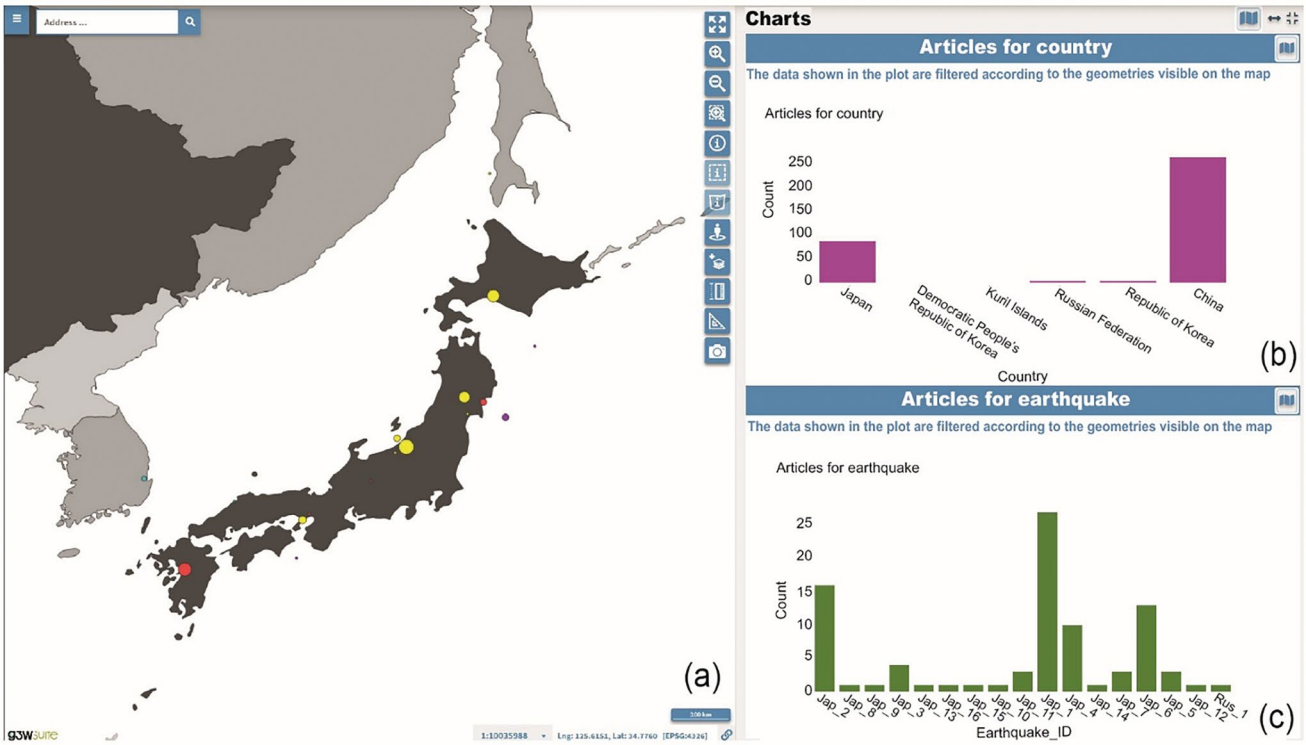


Fig. 3 Map and bar chart diagrams available on the web-GIS. (**a**) Zoom of an area around Japan (**b**) bar chart diagram reporting the number of articles for country and (**c**) for earthquake of the filtered data according to the geometry in the bounding box

The worldwide chart bar diagram reveals that the higher of publications illustrate events that occurred in China. Specifically, the "articles for earthquake" diagram indicates that the 2008 Wenchuan is the most studied event with 180 articles, while the "articles for country" diagram shows additional 76 articles dealing with other Chinese earthquakes, for a total of 264 articles out of 810 (32.6%). Japan is the second country, but with a significant lower number of articles (87), followed by Taiwan (63) and Italy (53). The analysis of the database reveals that 59 out of 63 Taiwan articles deal with the 1999 Chi-Chi earthquake, while the articles describing Italian events are distributed among 19 earthquakes.

4 Conclusions

In this article, we present a web-GIS implemented to examine a database of scientific articles published in the last four decades on the EQTL theme. In the database are recorded 810 papers and the information collected for each article can be used for different types of spatial or textual queries. The web-GIS facilitates the preparation of interactive and visually appealing maps and charts, enhancing an efficient distribution, accessibility, and utilization of the scientific literature across various domains. In addition, the user-friendly inter-

face, facilitate the search for people with varying levels of GIS skill.

This brief description of the web-GIS highlights the potentiality of the tool for performing cross-correlated searches. In fact, it is possible to focus the bibliographic search on specific topics for a given earthquake or country.

4.1 Code Availability

The web-GIS described in the article can be accessed at: https://nixus.irpi.cnr.it/en/map/a-web-gis-database-of-the-scientific-articles-on-e/qdjango/54/ (last access: February, 15 2024).

Acknowledgments This research was carried out in the framework of the FRA.SI project—Multi-scale integrated methodologies for seismically induced landslides hazard zonation in Italy (Metodologie integrate multi-scala per la zonazione della pericolosità da frana sismo-indotta in Italia) funded by the Italian Ministry of Ecological Transition (Ministero della Transizione Ecologica, grant no. DD 449/2018).

References

Bird JF, Bommer JJ (2004) Earthquake losses due to ground failure. Eng Geol 75:147–179. https://doi.org/10.1016/j.enggeo.2004.05.006

Fan X, Scaringi G, Korup O, West AJ, Westen CJ, Tanyas H, Hovius N, Hales TC, Jibson RW, Allstadt KE, Zhang L, Evans SG, Xu C, Li G, Pei X, Xu Q, Huang R (2019) Earthquake-induced chains of geologic hazards: patterns, mechanisms, and impacts. Rev Geophys 57:421–503. https://doi.org/10.1029/2018RG000626

Fortunato C, Martino S, Prestininzi A, Romeo RW (2012) Nuova versione del catalogo italiano degli effetti deformativi indotti da forti terremoti (CEDIT). Ital J Eng Geol Environ 2:63–74. https://doi.org/10.4408/IJEGE.2012-02.0-05

Green D, Bossomaier T (2004) Online GIS and spatial metadata, 1st edn. CRC Press, New York

Keefer DK (1984) Landslides caused by earthquakes. Geol Soc Am Bull 95:406–421

Keefer DK (2002) Investigating landslides caused by earthquakes – a historical review. Surv Geophys 23:473–510. https://doi.org/10.1023/A:1021274710840

Koi T, Hotta N, Ishigaki I, Matuzaki N, Uchiyama Y, Suzuki M (2008) Prolonged impact of earthquake-induced landslides on sediment yield in a mountain watershed: The Tanzawa region, Japan. Geomorphology 101(4):692–702. https://doi.org/10.1016/j.geomorph.2008.03.007

Marano KD, Wald DJ, Allen TI (2010) Global earthquake casualties due to secondary effects: a quantitative analysis for improving rapid loss analyses. Nat Hazards 52:319–328. https://doi.org/10.1007/s11069-009-9372-5

Martino S, Bozzano F, Caporossi P, D'angiò D, Della Seta M, Esposito C, Varone C et al (2019) Impact of landslides on transportation routes during the 2016–2017 Central Italy seismic sequence. Landslides 16:1221–1241. https://doi.org/10.1007/s10346-019-01162-2

Reichenbach P, Rossi M, Malamud BD, Mihir M, Guzzetti F (2018) A review of statistically-based landslide susceptibility models. Earth Sci Rev 180:60–91. https://doi.org/10.1016/j.earscirev.2018.03.001

Rodríguez-Peces MJ, Román-Herrera JC, Peláez JA, Delgado J, Tsige M, Martino S, Garrido J (2020) Unbiased logic-tree data for earthquake-induced landslide hazard maps for low-to-moderate magnitude events. Data in Brief 31:105940. https://doi.org/10.1016/j.dib.2020.105940

Schilirò L, Rossi M, Polpetta F, Fiorucci F, Fortunato C, Reichenbach P (2023) A web-based GIS (web-GIS) database of the scientific articles on earthquake-triggered landslides. Nat Hazards Earth Syst Sci 23:1789–1804. https://doi.org/10.5194/nhess-23-1789-2023

Tanyaş H, van Westen CJ, Allstadt KE, Anna Nowicki JM, Görüm T, Jibson RW, Godt JW, Sato HP, Schmitt RJ, Marc O, Hovius N (2017) Presentation and analysis of a worldwide database of earthquake-induced landslide inventories J Geophys Res-Earth. 122:1991–2015. https://doi.org/10.1002/2017JF004236

Villani F, Civico R, Pucci S, Pizzimenti L, Nappi R, De Martini PM (2018) Open EMERGEO working group, 2018. A database of the coseismic effects following the 30 October 2016 Norcia earthquake in Central Italy. Scientific Data 5:180049. https://doi.org/10.1038/sdata.2018.49

Wasowski J, Keefer DK, Lee CT (2011) Toward the next generation of research on earthquake-induced landslides: Current issues and future challenges. Eng Geol 122:1–8. https://doi.org/10.1016/j.enggeo.2011.06.001

Open Access This chapter is licensed under the terms of the Creative Commons Attribution 4.0 International License (http://creativecommons.org/licenses/by/4.0/), which permits use, sharing, adaptation, distribution and reproduction in any medium or format, as long as you give appropriate credit to the original author(s) and the source, provide a link to the Creative Commons license and indicate if changes were made.

The images or other third party material in this chapter are included in the chapter's Creative Commons license, unless indicated otherwise in a credit line to the material. If material is not included in the chapter's Creative Commons license and your intended use is not permitted by statutory regulation or exceeds the permitted use, you will need to obtain permission directly from the copyright holder.



Time and Site Prediction of a Potential Large-Scale Landslides and the AR (Augmented Reality) Presentation for Early Warning

Koichi Araki, Keisuke Takimoto, Yoichi Yamazaki, Doan Huy Loi, Kazuo Konagai, and Kyoji Sassa

Abstract

To protect oneself from large-scale landslides, it is crucial to promote evacuation actions by notifying the predicted occurrence time and location of the landslide. This paper reports on an early warning information delivery system called AR presentation for early warning, targeting large-scale landslides induced by heavy rain. The AR presentation for early warning previously registers the landslide occurrence time and the landslide runout extent obtained from simulations. It then determines whether a landslide will occur based on predicted rainfall and displays the predicted landslide occurrence time and landslide runout extent on web browsers using Augmented Reality technology. Using the large-scale landslide in Aranayaka as a case study, it was confirmed through AR presentation for early warning that this landslide occurred 12 h after the predicted start time.

Keywords

AR presentation · Early warning · Large-scale landslide

1 Introduction

In Sri Lanka, large-scale landslides induced by heavy rainfall, such as those in Aranayaka (JICA Survey Team 2016) and Athwalthota (National Building Research Organization 2017), have occurred. To protect against such large-scale landslides, it is crucial to predict the timing and location of landslide occurrences. Additionally, it is important to inform and warn residents about these predicted landslide timings and locations, prompting evacuation actions.

This paper reports on an early warning information delivery system developed using Augmented Reality technology, aimed at facilitating evacuation actions for large-scale landslides triggered by heavy rain. We call our system as "AR Presentation for Early Warning". This system displays the predicted timing and location of landslides on web browsers. Residents can check the predicted timing and location of the landslides through the web browsers on PCs and mobile devices such as smartphones and tablets. Furthermore, our system presents the predicted landslide locations in both 2D and 3D.

2 AR Presentation for Early Warning

2.1 Overview

AR presentation for early warning displays landslide runout extents based on the predicted pore water pressure ratio values (predicted Ru values) calculated from rainfall predicted by the Multi-Scale Simulator for the Geoenvironment (MSSG) (Onishi et al. 2022), and the critical pore water pressure ratio values (critical Ru values) obtained from simulations. Figure 1 shows an overview diagram of our system. Our system consists of Preliminary Analysis, Forecasting and Augmented Reality components. In the Preliminary Analysis, the landslide simulation software LS-RAPID (Sassa et al. 2010) is used to obtain the landslide runout extents and critical Ru values for landslide terrains. In the Forecasting, the predicted Ru values are calculated based on the predicted rainfall from MSSG and compared with the critical Ru values of the landslide terrains. If there is a landslide terrain where the predicted Ru value exceeds the critical Ru value, the time when the critical Ru value is exceeded, and the landslide runout extent of the landslide terrain are

K. Araki (✉) · K. Takimoto · Y. Yamazaki
GODAI KAIHATSU Co., Ltd., Ishikawa, Japan
e-mail: kouichi.araki@godai.co.jp; takimoto@godai.co.jp; yamazaki@godai.co.jp

D. H. Loi · K. Konagai · K. Sassa
International Consortium on Landslides, Kyoto, Japan

© The Author(s) 2025

B. Abolmasov et al. (eds.), *Progress in Landslide Research and Technology, Volume 3 Issue 2, 2024*, Progress in Landslide Research and Technology, https://doi.org/10.1007/978-3-031-72736-8_24

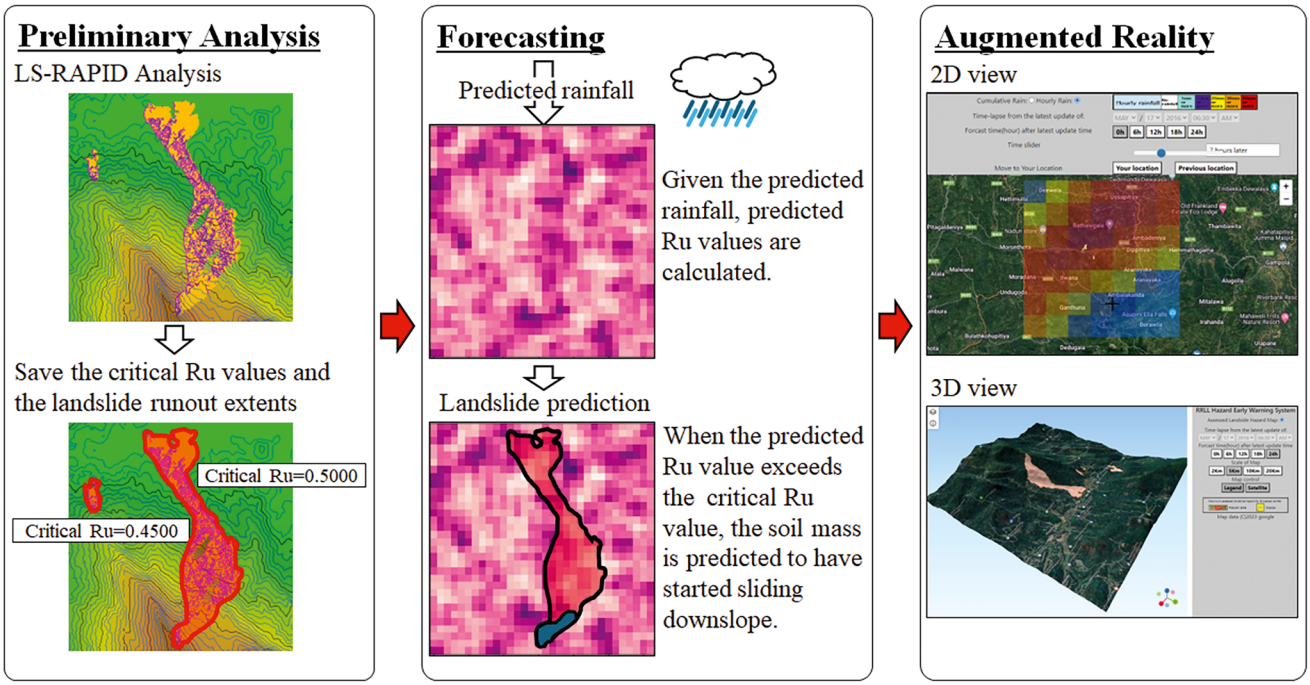


Fig. 1 Overview of the AR presentation for early warning

recorded. The Augmented Reality processes the display of the predicted rainfall and the landslide runout extents in both 2D and 3D. The 2D display shows the landslide runout extents and the predicted rainfall from MSSG. The 3D display shows the landslide runout extents.

2.2 Preliminary Analysis

To obtain the critical Ru values and the landslide runout extents for each landslide terrain, simulations are conducted using LS-RAPID. The landslide terrains suspected of being triggered by heavy rainfall are selected. Firstly, soil parameters, elevation data and areas where sediment movement occurs (source area) are set in LS-RAPID (Fig. 2). The time series of Ru values required for the simulation is used the same across all landslide terrains. Figure 3 shows this time series of Ru values. As the simulation time steps progress, the Ru value increases, and the Ru value at the point when landslide movement begins is the critical Ru value. The critical Ru values and the landslide runout extents for each landslide terrains are obtained by the simulations (Fig. 4). For comparison with the predicted Ru value in the Forecasting and for displaying the landslide runout extent in the Augmented Reality, the critical Ru values and landslide runout extents are registered (Fig. 5).

2.3 Forecasting

In the Forecasting, the predicted Ru values are calculated from the Ru values within source areas in Ru grids which are calculated from the predicted rainfall from MSSG and topographic data and so on. Then, these predicted Ru values are compared with the critical Ru values registered in the Preliminary Analysis to determine whether a landslide will occur.

Figure 6 shows the process flow of the Forecasting. Using the predicted rainfall for the next 24 h from MSSG, the past 48 h of rainfall, topographic data and soil parameters, the Ru grids are calculated hourly for the next 24 h. The SLIDE model (Liao et al. 2010) is used to compute the Ru grids. Equation 1 shows the formula for the SLIDE model.

$$\begin{cases} m_1 = 0 \\ O_t = K_t \times \sin\beta \times m_t \times H \times \cos\beta \times \Delta t \\ \Delta m_t = \dfrac{\left(I_t - O_t\right)}{n \times H\left(1 - S_r\right)} \\ m_{t+1} = m_t + \Delta m_t \end{cases} \quad (1)$$

where t is time, m_t is the ratio between the depth of unconfined aquifer and the thickness of the soil layer, O_t is the water outlet of a finite portion of a slope of finite length, K_t is the significance of global drainage capability due to both

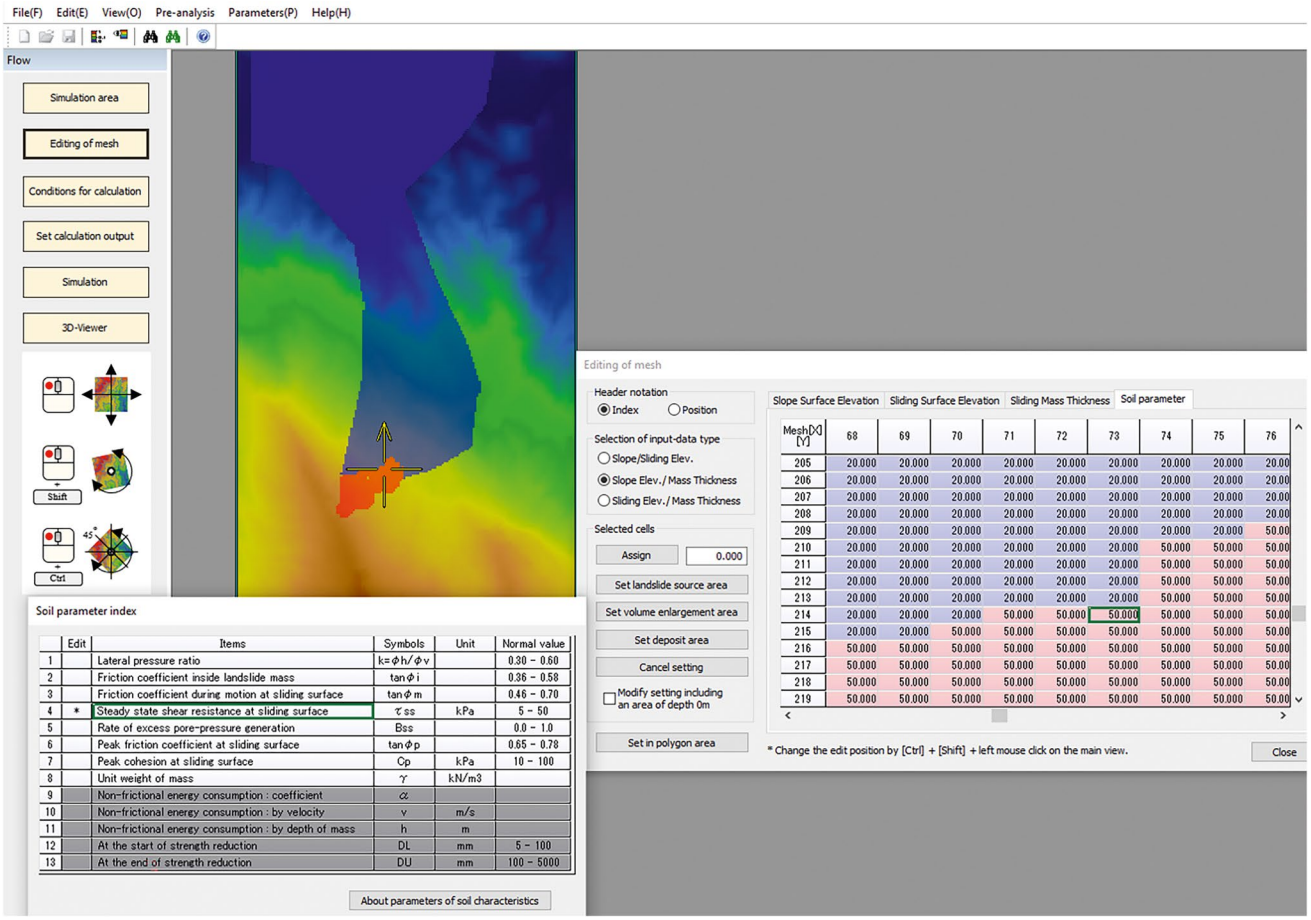


Fig. 2 Input parameter setting screen in LS-RAPID

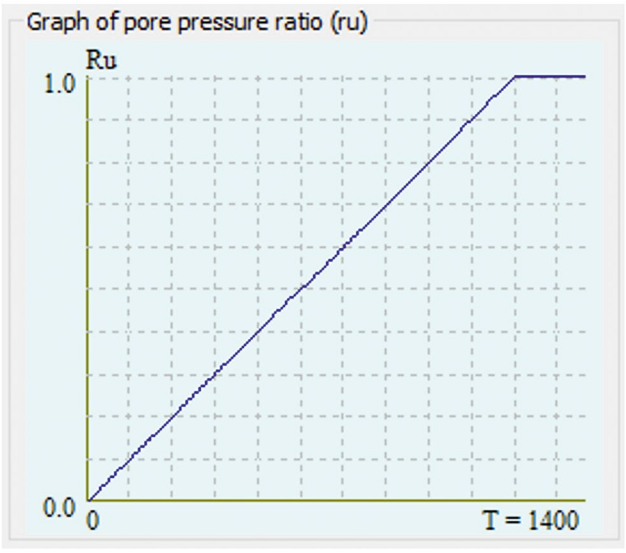


Fig. 3 Ru values used in Preliminary Analysis. The X-axis represents time, with each grid equaling 120 s. The Y-axis represents Ru values, with each grid equaling 0.1

intrinsic soil permeability and the presence of numerous preferential down-flow ways, β is slope angle, H is landslide depth, I_t is rainfall intensity, n is porosity, S_r is degree of saturation. Equation 2 shows the formula for the calculation of the Ru values in the Ru grids (Huy et al. 2018).

$$Ru = \frac{U}{\sigma} = \frac{m_t \times \gamma_w}{\gamma} \tag{2}$$

where U is the pore-water pressure, σ is the weight of soil mass, γ_w is the unit weight of water, γ is the unit weight of soil mass.

In each Ru grid, the average Ru values within the source area of each landslide terrain is calculated. These average Ru values are the predicted Ru values. The predicted Ru values compare with the critical Ru value of each landslide terrain. If the predicted Ru value exceeds the critical Ru value of a landslide terrain, it is determined that the landslide may occur in that landslide terrain. Note that, if the predicted Ru value falls below the Ru value specified by the user, the landslide runout extent is reset.

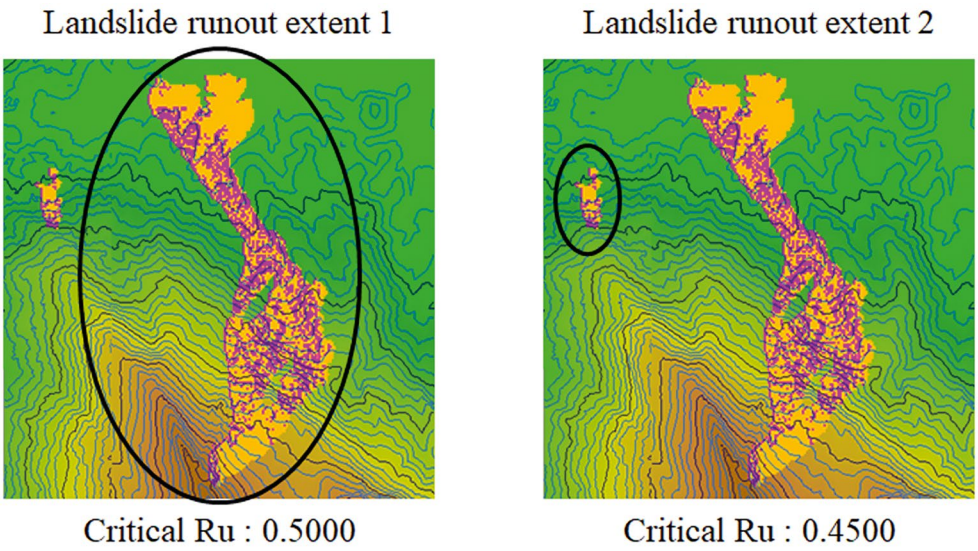


Fig. 4 Critical Ru values in landslide terrains

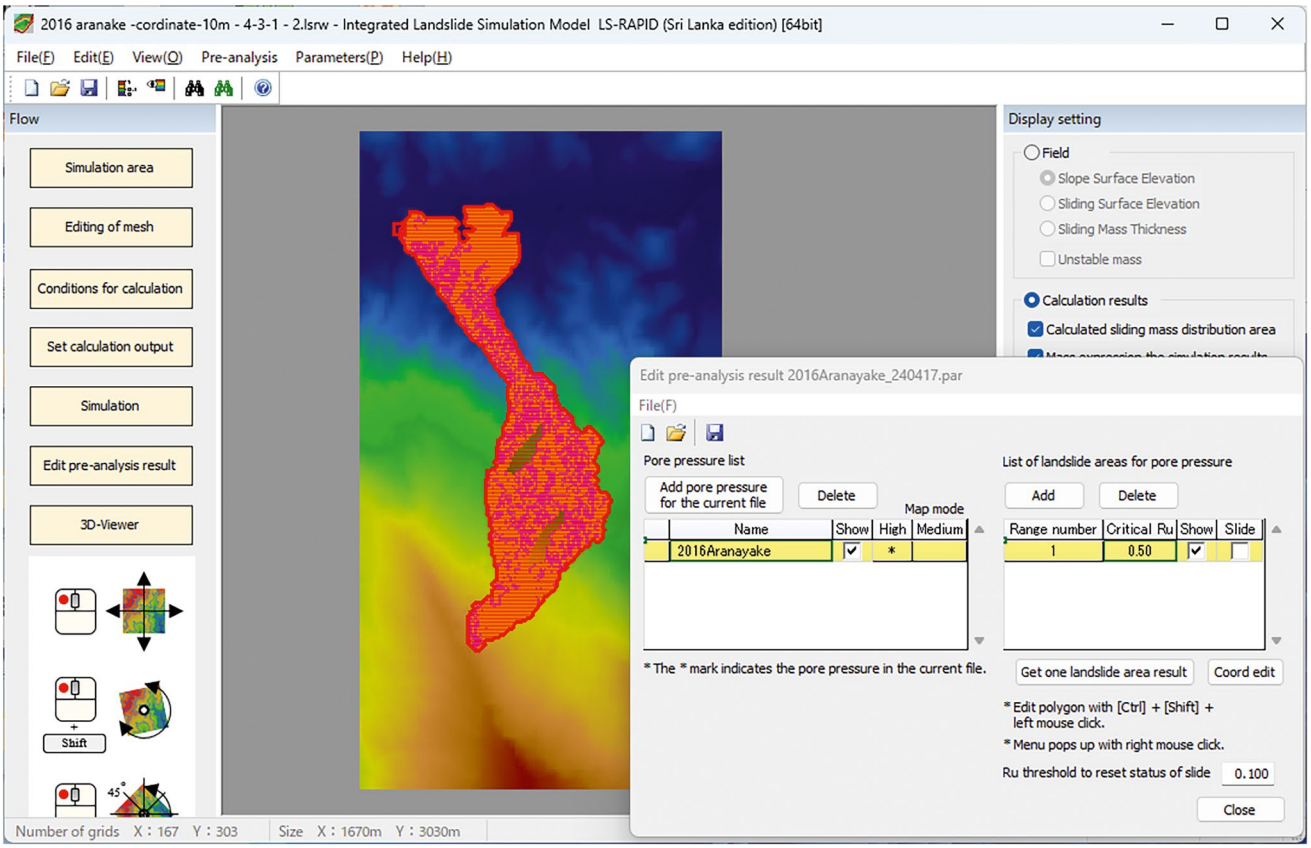


Fig. 5 Setting screen for critical Ru values and landslide runout extents

2.4 Augmented Reality

The Augmented Reality performs processing to display the predicted rainfall from MSSG and the landslide runout extents in web browsers. Figure 7 shows an example of the 2D display. In the 2D display, both the predicted rainfall and the landslide runout extents are shown. The background image is a satellite photo, and the display time can be changed using the time slider or the buttons on web site. The landslide runout extents are displayed at the time specified when the critical Ru value is exceeded. For small mobile devices, a different design from the PC version is used for better visibility. Additionally, if GPS of the mobile devices is enabled on the mobile device, the current location can be displayed.

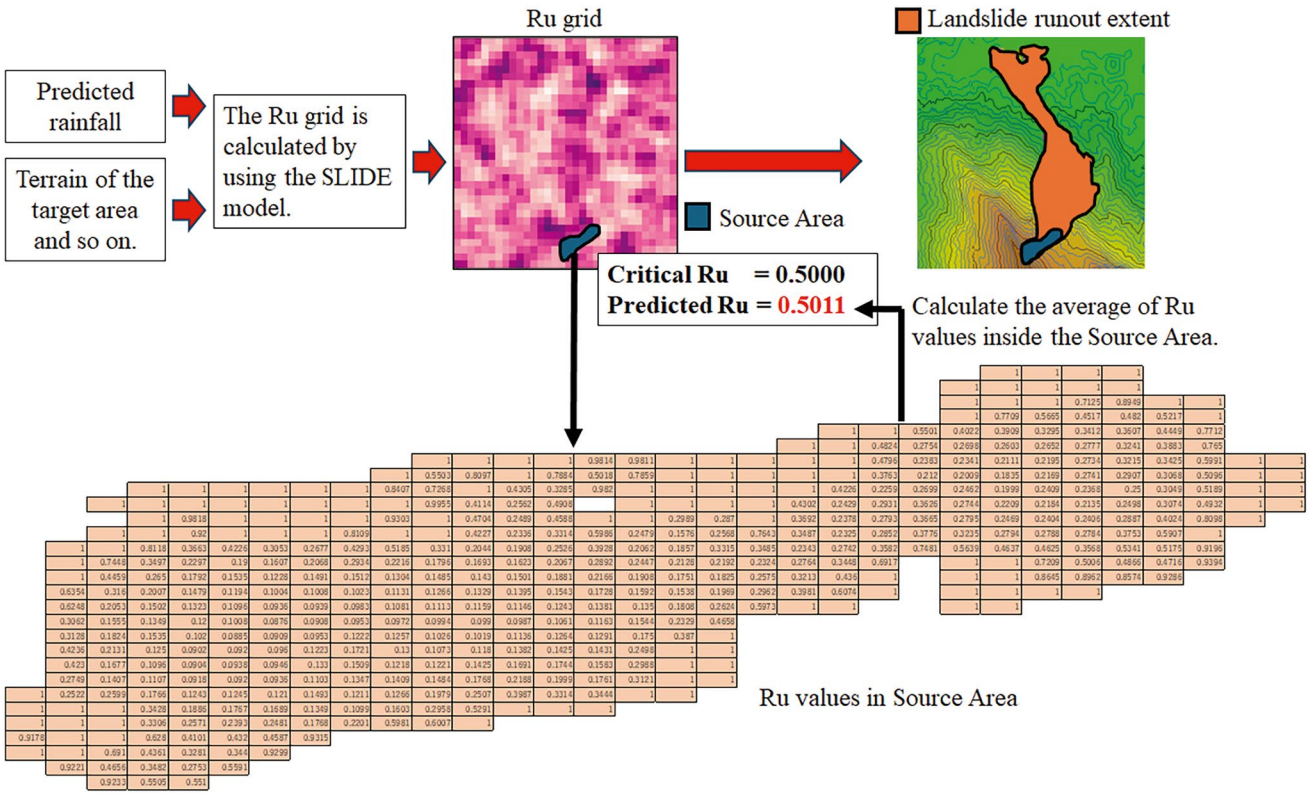


Fig. 6 Forecasting process flow

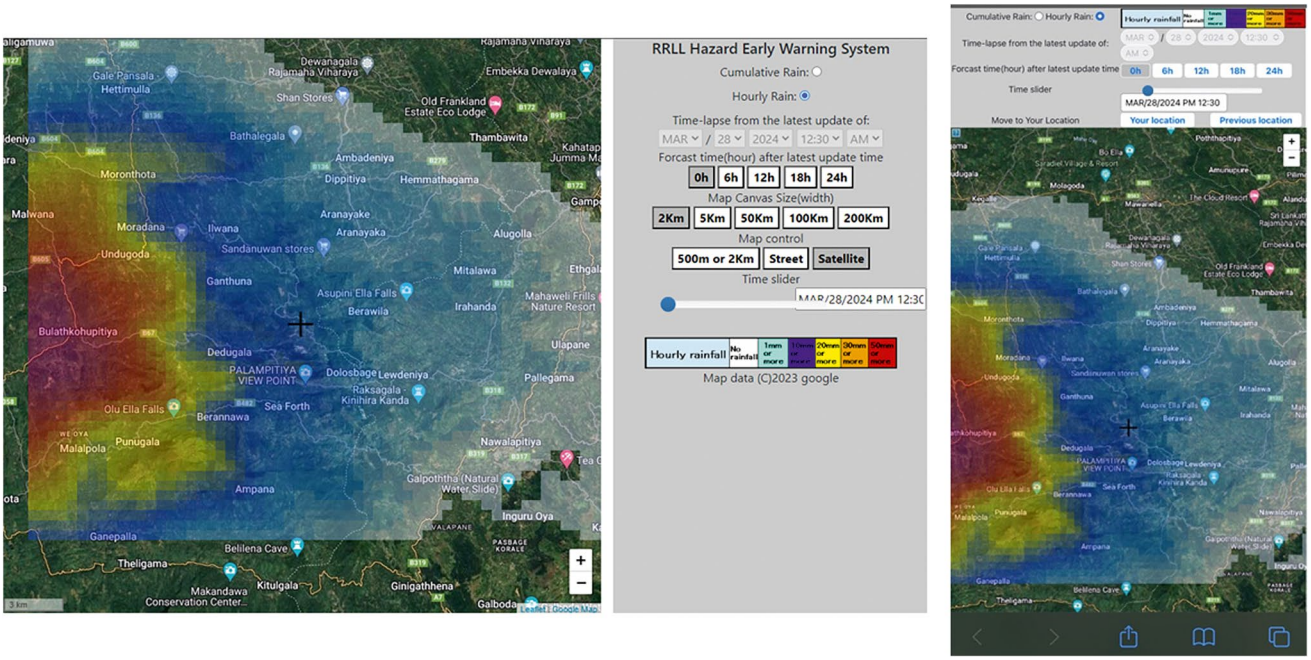


Fig. 7 Example of 2D display. The left image shows the display on PCs. The right image shows the display on a mobile device. The legend for predicted rainfall is light blue for 1–10 mm, blue for 10–20 mm, yellow for 20–30 mm, orange for 30–50 mm, and red for over 50 mm

Figure 8 shows an example of a 3D display. In the 3D display, the landslide runout extents are shown with a satellite photo as the background image. The landslide runout extents are displayed at the time specified when the critical Ru value is exceeded. Note that the 3D display can only be viewed from PCs due to the performance limitations of mobile devices.

3 Implementation

The AR presentation for early warning was implemented using two workstations and multiple servers. Figure 9 shows the implementation diagram for the AR presentation for early warning. The first workstation (blue box in Fig. 9) hosts the Simulation Server and the Landslide Judge Server.

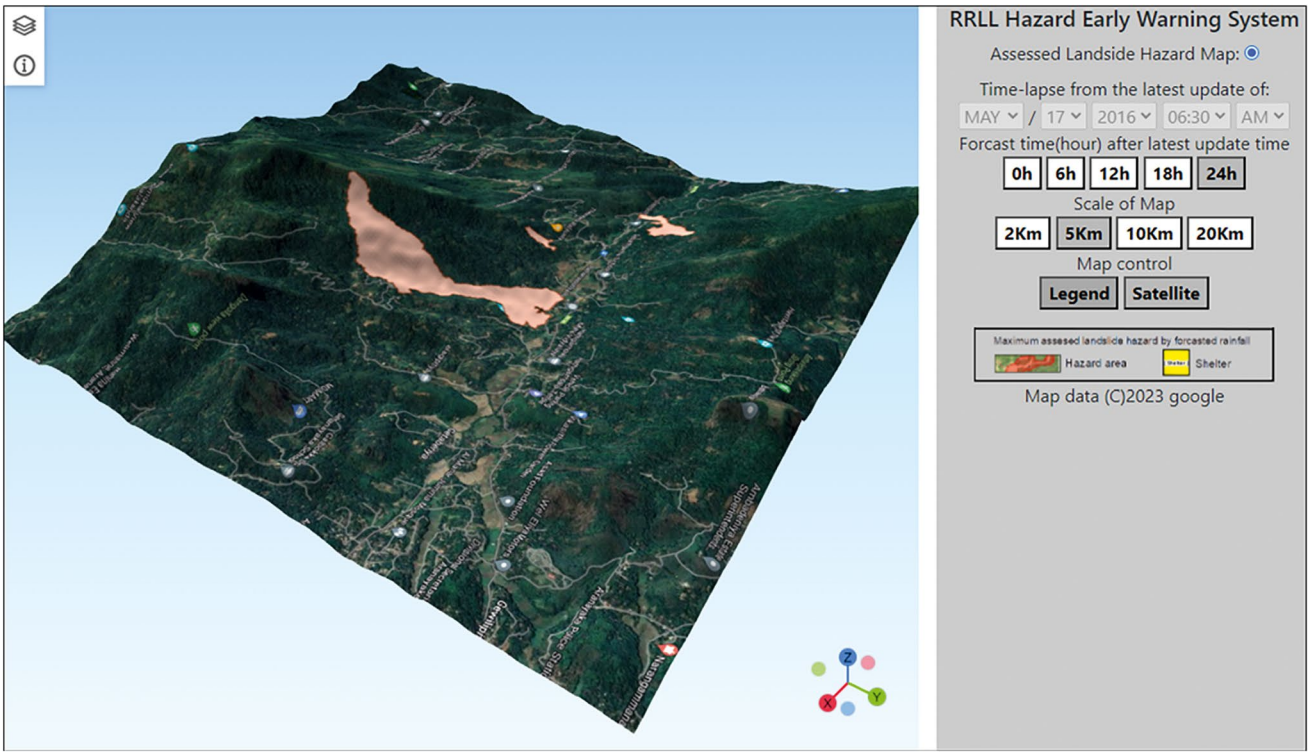


Fig. 8 Example of 3D display. The pink areas indicate the landslide runout extents

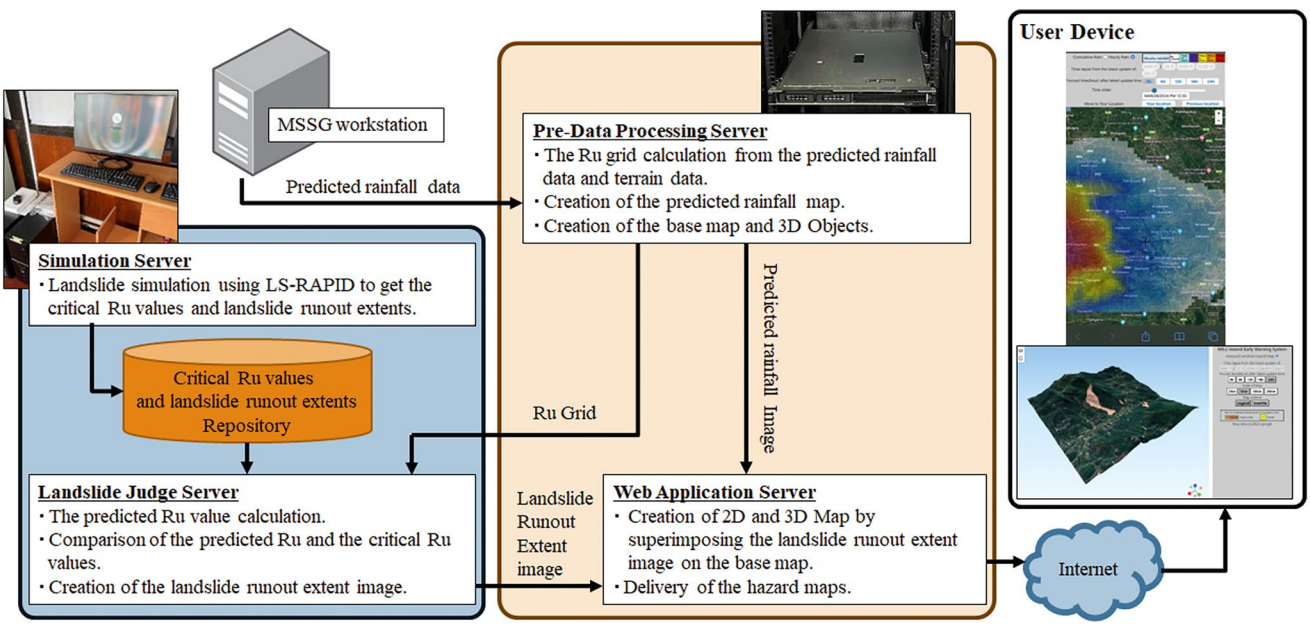


Fig. 9 Implementation diagram of AR presentation for early warning

Table 1 Workstation specification

Item	The workstation where the Simulation Server and the Landslide Judge Server are running.	The workstation where the Pre-Data Processing Server and the Web Application Server are running.
CPU	Intel(R) Xeon(R) Silver 4210 (2.2GHz)	Intel(R) Pentium(R) Gold G6405T CPU (3.5GHz)
Memory size	364GB	32GB

The second workstation (orange box in Fig. 9) hosts the Pre-Data Processing Server and the Web Application Server. Table 1 shows the specification of our workstations.

The Simulation Server conducts LS-RAPID simulations to obtain the critical Ru values and the landslide runout extents for each landslide terrain. Then, the critical Ru values and landslide runout extents obtained from the simulations are stored in the repository within the workstation.

The Pre-Data Processing Server receives the predicted rainfall data transmitted from the MSSG workstation via FTP. The received predicted rainfall data, which is in GrADS format, covers a 24-h forecast at hourly intervals. Next, the Ru grids are calculated using the SLIDE model and then sent to the Landslide Judge Server. The Pre-Data Processing Server also creates GeoTIFF images of the predicted rainfall for display in web browsers and sets up background maps using Google's Map Tile (Google 2018) and creates 3D objects.

The Landslide Judge Server calculates the predicted Ru value from the Ru grids. The predicted Ru values are compared with the critical Ru values stored in the repository. If the predicted Ru value exceeds the critical Ru value, the image of the landslide runout extent is generated and sent to the Web Application Server.

The Web Application Server displays the images of the predicted rainfall and the images of the landslide runout extent in web browsers. For 2D and 3D displays, Leaflet (Leaflet 2011) and Qgis2threejs (Qgis2threejs Plugin 2013) are used, respectively. This server first adds location information to the images of the landslide runout extent. In 2D display, this server overlays the images of the predicted rainfall, the images of the landslide runout extent and the background map. For 3D display, this server creates the composite image of the landslide runout extent and the background maps, uses elevation data to render the terrain in 3D, and overlays the 3D objects.

4 Example

An example of AR Presentation for Early Warning is shown on the large-scale landslide occurred in Aranayaka. As a preliminary analysis, this landslide was simulated using LS-RAPID. As the result of the simulation, the critical Ru value of the landslide was 0.5000. The predicted rainfall used in the Forecasting was set from 6:30 on May 14, 2016 to 5:30 on May 18, 2016, covering the time when this landslide occurred (around 16:00 on May 17, 2016). The predicted rainfall covered the area of 126 km north to south and 128 km east to west, including the site of this landslide and was provided in 2 km grid. The SLIDE model was used to calculate the Ru grid, and the predicted Ru value for this landslide was computed. As a result, 10 h after the start of the forecast (at 16:30 on May 17, 2016), the predicted Ru value reached 0.5011, exceeding the critical Ru value. Therefore, it was determined that the landslide would occur at 16:30 on May 17, 2016.

Figure 10 shows the landslide runout extent for this landslide. The left figure represents the actual landslide runout extent (Dang et al. 2019), while the right figure shows the result 12 h after 6:30 on May 17, 2016, displayed in 3D by the AR presentation for early warning. Since the web browser displays at 6-h intervals, setting the display time to 12 h later allows the landslide runout extent in Aranayaka to be shown. Thus, users can be informed that there is a possibility of a landslide occurring 12 h later. The landslide runout extent marked with a yellow circle represents the simulated landslide runout extent of this landslide. The landslide runout extent shown in the AR presentation for early warning generally matches the actual landslide runout extent.

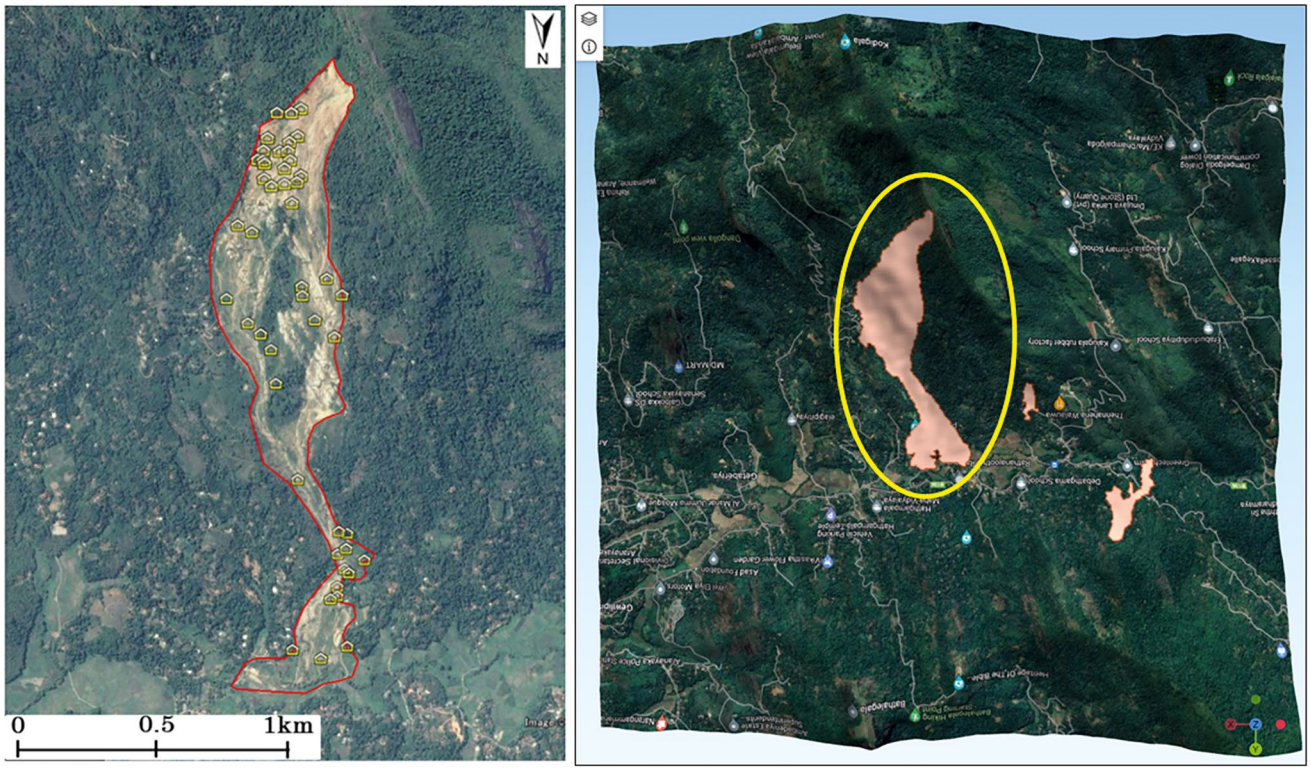


Fig. 10 The landslide runout extent of the major landslide in Aranayaka. The left figure shows the actual landslide runout extent in Aranayaka (Dang et al. 2019). The right figure displays the landslide runout extent through AR presentation for early warning. The yellow circle indicates the simulated landslide runout extent in Aranayaka

5 Conclusion

The AR presentation for early warning introduced in this paper is an early warning information delivery system using Augmented Reality technology, targeting large-scale landslides induced by heavy rain. In the AR presentation for early warning, the time and extent of landslide runout obtain from the simulations are registered. Next, it determines whether landslide will occur based on the predicted rainfall. If the decision indicates that landslide will occur, the time and the landslide runout extent are displayed on web browsers on PCs and mobile devices. Using the large-scale landslide in Aranayaka as a case study, the AR presentation for early warning confirmed that the landslide occurred 12 h after the forecast start time.

By utilizing our system, residents can confirm the occurrence time and location of large-scale landslides and can take evacuation actions. Additionally, by overlaying information layers required by stakeholders, further utilization of this system is anticipated.

Acknowledgments We would like to express our gratitude for the funding provided by the Japan-Sri Lanka SATREPS project titled "Development of early warning technology of rain induced rapid and long traveling landslide in Sri Lanka." We also extend our thanks to the staff of the National Building Research Organization (NBRO) in Sri Lanka for their support in implementing the system locally.

References

Dang K, Saasa K, Konagai K, Karunawardena A, Bandara RMS, Hirota K, Tan Q, Ha ND (2019) Recent rainfall-induced rapid and long-traveling landslide on 17 May 2016 in Aranayaka, Kagelle, District, Sri Lanka. Landslide 16:155–164

Google, Google Maps Platform (2018). https://developers.google.com/maps/documentation/tile. Last accessed: 19 April 2024

Huy L D, Sassa K, Fukuoka H, Sato Y, Takara K, Setiawan H, Pham T, Dang K (2018) TXT-tool 3.081-1.4: initiation mechanism of rapid and long run-out landslide and simulation of Hiroshima landslide disasters using the integrated simulation model (LS-RAPID), Landslide Dynamics: ISDR-ICL Landslide Interactive Teaching Tools, pp 149–168

JICA Survey Team (2016) 22nd May 2016, aerial survey report on inundation damages and sediment disasters

Leaflet (2011). https://leafletjs.com. Last accessed: 19 April 2024

Liao Z, Hong Y, Wang J, Fukuoka H, Sassa K, Karnawati D, Fathani F (2010) Prototyping an experimental early warning system for rainfall-induced landslides in Indonesia using satellite remote sensing and geospatial datasets. Landslides 7:317–324

National Building Research Organization (2017) Landslide Disaster 2017 May Damage & Loss Assessment

Onishi R, Hirai J, Kolomenskiy D, Yasuda Y (2022) Real-time high-resolution prediction of orographic rainfall for early warning of landslides. Progress Landslide Res Technol 1(1):237–248

Qgis2threejs Plugin (2013). https://minorua.github.io/Qgis2threejs/docs/. Last accessed: 19 April 2024

Sassa K, Nagai O, Solidum R, Yamazaki Y, Ohta H (2010) An integrated model simulating the initiation and motion of earthquake and rain induced rapid landslides and its application to the 2006 Leyte landslide. Landslides 7:219–236

Open Access This chapter is licensed under the terms of the Creative Commons Attribution 4.0 International License (http://creativecommons.org/licenses/by/4.0/), which permits use, sharing, adaptation, distribution and reproduction in any medium or format, as long as you give appropriate credit to the original author(s) and the source, provide a link to the Creative Commons license and indicate if changes were made.

The images or other third party material in this chapter are included in the chapter's Creative Commons license, unless indicated otherwise in a credit line to the material. If material is not included in the chapter's Creative Commons license and your intended use is not permitted by statutory regulation or exceeds the permitted use, you will need to obtain permission directly from the copyright holder.



Part VI

World Landslide Reports

Characteristics of Landslides Affecting Road Networks in Ethiopia: Evidence from 25 Years Research, Practice and Documentation

Kifle Woldearegay

Abstract

Over the last four decades, Ethiopia has been involved in massive road constructions which pass through complex geological, geotechnical, hydrological and terrain conditions of the country. The sustainability and functionality of these roads is, however, hugely affected by interrelated geohazards. This paper presents on the characteristics of landslides that have been affecting road networks in Ethiopia with data from research, practice and documentation over 25 years period (1997–2022). The study involved: (1) field inventory and characterization of 158 landslide-affected road sections, (2) investigations of the geological, geohydrological and geotechnical conditions, (3) monitoring groundwater levels and spring discharges, (4) measurement of flood levels of rivers/streams close to landslides, (5) in-situ and laboratory tests of the engineering properties of soils and rocks, (6) assessments on the association of the landslides with gully erosion, construction, and other factors, and (7) assessments on the performances of mitigation measures implemented. Results revealed that debris/earth slides are the dominant types of failures, with some debris/earth flows. Failures occurred in unconsolidated sediments with certain conditions: (a) concave terrains with slope angles 12°–38°, (b) variable depths of failures: maximum values 2.5–13.5 m, (c) shallow groundwater systems: water level fluctuated between 0 and 3.5 m below surface, and (d) active stream/river incisions at downslope sides of the roads. Broadly, the landslide-road-landscape interactions could be categorized into three: (a) failure of the upslope part of the road, (b) failure of the downslope part of the road, and (c) failure of the whole road section (upslope, road and downslope). Though different mitigation measures were implemented in 125 sites, the measures were unsuccessful in 70 sites (56%). In all the landslide-affected road sections, no comprehensive geological/geotechnical site investigations and slope stability analysis were carried out and the landslide-road-landscape interactions were poorly understood. With the expected increase in road/railway network development, limited capacity, climate change and fragile nature of the Ethiopian landscapes, landslides and associated problems are expected to pose major risks unless due attention is given to these interrelated geohazards. This calls for further collaborative research, innovations, and capacity building to address landslides and related geohazards in Ethiopia and in other developing countries with similar conditions.

Keywords

Failure mechanisms · Landslide mitigation · Landscape-road–landslide interactions · Slope stability · Transport infrastructure

1 Introduction

Despite advances in better understanding of the initiations of landslides and in techniques of slope instability hazard assessments (Hansen 1984), landslides remain among the major natural disasters throughout the world (Varnes 1978, 1984). The Sendai Framework for Disaster Risk Reduction 2015–2030 (SFDRR) (adopted by the United Nations World Conference on Disaster Risk Reduction) outlines four priorities for action to prevent new and reduce existing disaster risks (UNISDR 2015): (1) understanding disaster risk, (2) strengthening disaster risk governance to manage disaster risk, (3) investing in disaster reduction for resilience, and (4) enhancing disaster preparedness for effective response, and to "Build Back Better" in recovery, rehabilitation and reconstruction.

Landslides continue to prevail in both the developed and developing countries, with larger casualties in developing

K. Woldearegay (✉)
School of Earth Science, Mekelle University, Mekelle, Ethiopia
e-mail: kifle.woldearegay@mu.edu.et

© The Author(s) 2025

B. Abolmasov et al. (eds.), *Progress in Landslide Research and Technology, Volume 3 Issue 2, 2024*, Progress in Landslide Research and Technology, https://doi.org/10.1007/978-3-031-72736-8_25

nations but with severe economic losses in the industrialized world (Guzzetti et al. 1999). On the African continent, in spite of their socio-economic and environmental impacts, landslides are only rarely studied and systematic landslide hazard investigations in sub-Sahara Africa are particularly rare (e.g. Van Den et al. 2009).

Ethiopia is one of the African countries which is affected by landslides and associated hazards. Though no comprehensive inventory is done so far, various studies (e.g. Gezahegn 1998; Ayalew 1999; Temesgen et al. 1999, 2001; Nyssen et al. 2002; Ayalew and Yamagishi 2000, 2003; Woldearegay et al. 2004; Ayenew and Barbieri 2005; Ayalew et al. 2009; Woldearegay 2013; Hearn 2018) show the prevalence of landslides of different types and sizes that have been affecting lives (human and animal), infrastructures, agricultural lands and the natural environment. Roads are among the infrastructures affected by such hazards. Ethiopia has expanded its road network from 6400 km in 1951 (Ibrahim 2011) to 155,830.1 km in 2021 (MoTL 2022). The country plans to further expand its road network to 245,942 km by 2030 (MoTL 2022). The Ethiopian Roads Authority and the regional governments have identified transport infrastructure damages due to interrelated hazards (landslides, siltations, floodings, erosions, etc.) and their cascading effects as top priorities for further interventions to enhance the sustainability and functionality of road networks. Hearn (2018) has stressed on the significance of landslides hazards to the maintenance and serviceability of the road network in Ethiopia, and the need for risk-based approach to cost-effective slope management. Though landslides are caused by various factors, some factors are common for most of the landslides sensitive areas and could be classified into (Glade and Crozier 2005): (a) preconditions: inherent static factors that act as catalysts to allow other factors to act more effectively, (b) preparatory factors which make the slope susceptible to movement without actually initiating it, and (c) triggering factors which finally initiate the movement. In the design of mitigation measures and management of roads understanding the failure mechanisms and influencing factors is critical. Hunt et al. (2008) have developed a comprehensive model on the failure mechanisms/failure processes with roads, with Lao as an example.

As part of long-term research and database development, and hence for better understanding of landslides (scales, effects, processes) in Ethiopia, we have been engaged in research and documentation of landslides and associated hazards since 1997. These landslides have affected lives (human and animal), transport infrastructures (such as roads, railways, pipelines, power lines, etc.), agricultural lands, dwelling/residential areas, and the environment in the different terrains (highlands, rift escarpments and some hilly areas in the lowlands) of the country. This paper presents evidence only on 158 landslide-affected road sections (landslide areal sizes greater than 5000 m^2), mainly on: (a) characteristics of landslides, factors contributing to slope instabilities, and road-landscape-landslide interactions, (b) the performances of mitigation measures implemented, and (c) gaps and recommendations for further research, industry practice and capacity building in landslide science and technology in the country.

2 Materials and Methods

2.1 Study Site

Location The locations of landslides which affected road networks, with areal sizes greater than 5000 m^2, considered in this study are shown in Fig. 1.

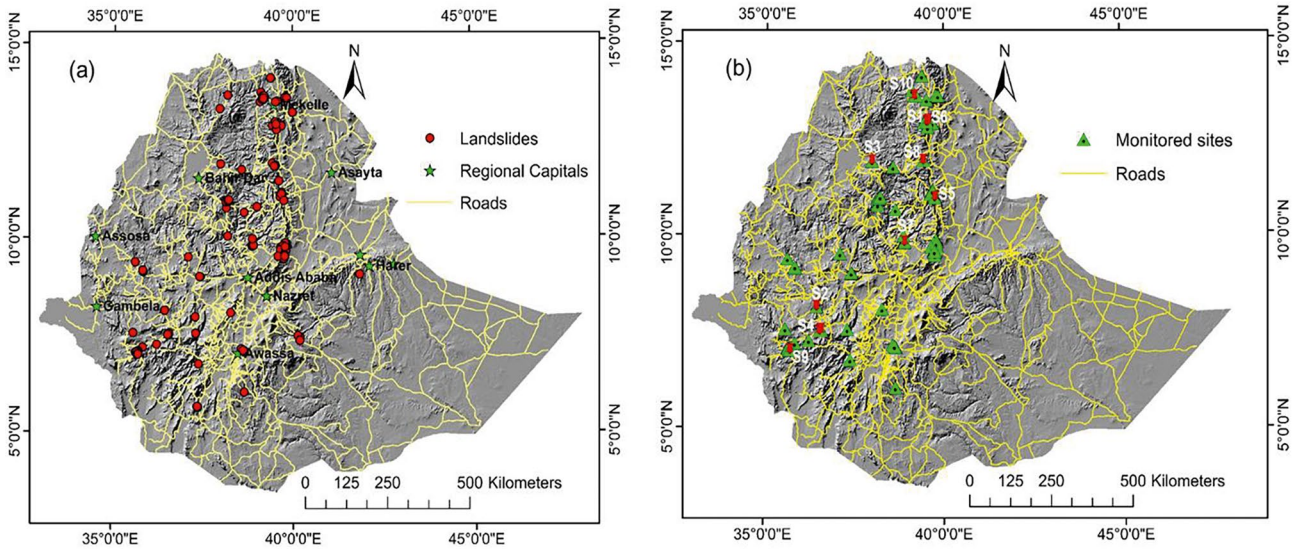


Fig. 1 Locations of inventoried landslides affecting road networks (**a**) and monitored sites (groundwater levels and spring discharges) (**b**) in Ethiopia

Topography and Drainage Different geomorphic and geological processes have created highly variable terrain conditions in Ethiopia: hilly and mountainous highlands with deeply incised rivers/valleys; highly rugged rift escarpments; gentle/flat rift valley floors; and flat lowland areas. Dominantly the altitude of the country ranges from about 1000 m to 3500 m; with some as high as 4620 m above sea level (Mount Ras Dashen) and as low as about 100 m below sea level (in the Denakil depression, Afar). Many rivers originate in the highlands and flow through deep gorges/rivers, draining extensive areas of the country.

Climate Climatic data of Ethiopia for the years 1996–2020 (ENMSA 2021) show that: (a) mean annual rainfall varies from about 2000 mm in the south western highlands to less than 300 mm in the south eastern and north eastern lowlands, (b) temperatures range from about −15 °C in the highlands to about 25 °C in the lowlands, and (c) the major precipitation is in the months of June to September, with minor rainfall in the months of February to May.

Deforestation, Erosion and Land Restoration Ethiopia is among the African countries which is highly affected by deforestation and erosion processes including stream/river incisions and gully erosion (e.g. Virgo and Munro 1978; Hurni and Perich 1992; Nyssen et al. 2004; Billi and Dramis 2003). As part of land restoration and climate change adaptation efforts various soil and water conservation (SWC) measures (both physical and biological) have been implemented in Ethiopia (Tuinhof et al. 2012).

Geology and Tectonics The major rocks in Ethiopia include (Fig. 2): (a) Metamorphic rocks (mainly metasediments and metavolcanics) and associated intrusive rocks (Mohr 1983), (b) Paleozoic sediments which include glacial tillites and post-glacial sediments (siltstone/sandstone units) (Mohr 1962, 1967, 1983; Kazmin 1972), (c) Mesozoic sediments

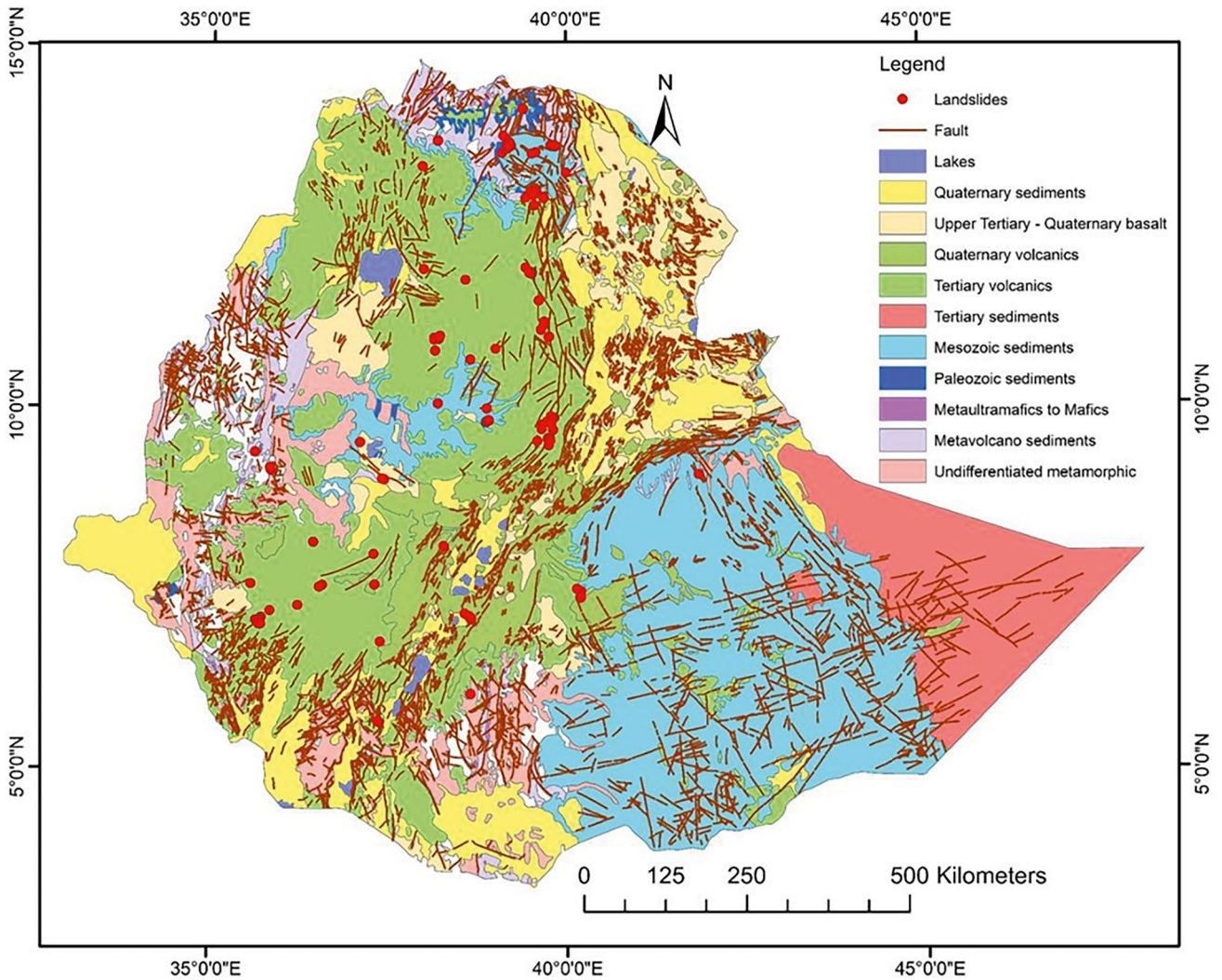


Fig. 2 Locations of inventoried landslides affecting road networks with simplified geology of Ethiopia (modified after Mengesha et al. 1996)

which include sandstone, shale and limestone units (Assefa 1981, 1991; Russo et al. 1999), (d) Cenozoic volcanics (basalt flows of the trap series) which are often associated with pyroclastic and lacustrine deposits (Mohr and Zanettin 1988), (e) Trachytes and Intrusive rocks (like dolerites) (Mohr 1962), and (f) rift floor volcanics (Mohr 1971). These different rock formations are often affected by different types of geological structures (joints, faults, shear zones, etc). Unconsolidated sediments which include colluvial/debris, residuals, and alluvials are common.

2.2 Methods

This study involved: (1) document review, (2) field inventory and characterizations of landslides, (3) investigations of the geological, geohydrological and geotechnical conditions of the sites, (4) monitoring groundwater levels and springs discharges, (5) measurement of flood levels of rivers/streams close to landslides, (6) in-situ and laboratory test of the engineering properties of soils and rocks, (7) assessments on the association of the landslides with gully erosion, construction (excavation or loading), and other factors, and (8) assessments on the performances of mitigation measures implemented in the different sites. The methods used is detailed below.

Field Inventory and Characterization of Landslides Though several road sections were affected by landslides of different types and sizes (such as rockfalls, debris/earth slides/flows) (e.g. Ayalew 1999; Nyssen et al. 2002; Hearn 2018), this study focused on 158 landslides that have affected road sections but with areal sizes greater than 5000 m^2. These different landslide-affected sites were assessed at different times over 25 years period (1997–2022). Each of the landslides were described following the work of Varnes (1978). Different parameters were assessed including slope angle, dimensions (length, width, height, depth), and slope shape of the landslide-affected areas. The slope angle at source areas of the sites were estimated using: field measurements (using Theodolites); 20 or 40 m elevation contours (Ethiopian Mapping Authority 1996); and topographic survey data from design documents of the Ethiopian Roads Authority. The slope shapes of the sites were described based on the nine hillslope forms (Parsons 1988). The depths of failures were estimated using different methods: examinations of scars of recent landslides; sub-surface data (test pits, trenches, road cuts, hand-dug groundwater wells); and resistivity geophysical methods and drilling logs in some sites with greater thicknesses of unconsolidated sediments.

Investigations of the Geological and Geotechnical Conditions These were evaluated using field and lab-based investigations which included: surface mapping, test-pits, trenches, some resistivity geophysical methods, and in-situ tests (strength, permeability). The engineering properties of rocks in each of the landslide affected sites were characterized based on evaluations of discontinuities, intact rock strength, and degree of weathering. Rock discontinuities were described with respect to their spacing, aperture, roughness, persistence, block size and infill materials following ISRM (1981) standards. In 85 sites in-situ intact rock strength of fresh (grade I) to slightly weathered (grade II) rocks (BS 5930 1981) were determined using Schmidt hammer tests. In 65 sites in-situ saturated hydraulic conductivity tests were conducted on soils and highly weathered rocks using the inverse auger-hole test method (Kessler and Oosterbaan 1974). Moreover, laboratory tests were carried out on unconsolidated sediment samples (n = 361) collected from the landslide-affected sites. Grain-size distribution analysis, Atterberg tests, moisture content and free swell tests were carried out in different periods and at different institutions in Ethiopia (Mekelle University, Addis Ababa University, Water Works Design and Supervision Enterprise).

Assessments of Groundwater Levels, Springs Discharges and Surface Water Conditions Several researchers (e.g. Anderson and Kemp 1991; Terlien 1996) have stressed the importance of hydrological evaluations in landslide studies. Fluctuations in the groundwater regime can lead or predispose slopes to failure due to the matric suction decrease in unsaturated soils or the pore pressure increase in saturated ones (Pirone et al. 2015). The overall hydrology of the landslide-affected sites were evaluated based on: hydraulic properties of unconsolidated sediments; degree of weathering and fracturing of rocks; distribution (lateral and vertical) of the major soil and rock units; and assessment of overall recharge-storage-discharge conditions of the sites. Measurements of groundwater levels were carried out in 108 sites using meter tapes; with some sites using meter tapes with probes. Measurements were done within the landslide zone or adjacent to it (within 100 m distance from the affected areas). The duration of groundwater level measurements were mostly one time. In a number of sites continuous monthly measurements were also carried out for: 1 year (n = 22), 2 years (n = 13) and 3 years (n = 5). Spring discharges were measured in 47 sites using bucket method which is recommended for discharges less than 4 l/s (Inversin 1986). Any seepage zones, ponding/stagnating water, piping erosion, sinkholes, etc. were assessed in all the sites through field observations. The one time hydrological measurements/assessments were carried out in the months of August to December; periods with higher groundwater levels, spring discharges and seepages.

Assessments on Erosion/Undercutting and Floodings Modification of slope geometry through natural or artificial processes could influence the stability of slopes (Varnes 1978; Selby 1993). Any features of erosions or river/stream undercuttings were documented and characterized including their dimensions (length, width, depth). The maximum flood levels of streams/rivers close to the landslide-affected sites (n = 36) were assessed using the past flood marks. Moreover, any effects of unmanaged water from culverts, roadside ditches and bridges on erosion and associated slope instabilities were assessed.

Assessments on Construction Related Effects Road constructions could affect slope processes in a number of ways, among others: destabilization of side-cast material and hillsides downslope (Montgomery 1994), and removal of vegetation (Psomiadis et al. 2020). Field assessments were carried out for any processes such as loading/placement of excavated materials, unloading/excavations, etc and their possible effects on landslide processes.

Assessments on Soil and Water Management Interventions Any traditional or introduced practices that change the hydrological conditions of the areas were assessed for each site including: soil and water conservation (SWC), drainages (surface and sub-surface), diversion/channeling water into and/or from landside prone areas, etc.

Assessments on the Performances of Mitigation Measures The performances of the implemented mitigation measures were assessed using field observations and compared with their design objectives. These field assessments included: types, dimensions, and status (functionality, any damage, etc.) of the mitigation measures.

Discussions with Local Communities To gather some evidence on past landslide history and/or any changes in factors which could influence landslide processes (deforestation, construction activity, gully erosion, etc.), discussions were carried out with elders and others who have better knowledge of the landslide-affected areas.

3 Results and Discussion

3.1 Engineering Properties of Rocks and Soils

3.1.1 Properties of Rocks

From review of previous studies, field observations and laboratory investigations over the years, the properties of the major rocks in Ethiopia is summarized below.

Metamorphic rocks–include (Mohr (1983): (1) metasediments which are foliated, jointed slates/phyllites with some calcareous sediments, and (2) metavolcanics which are of igneous origins (intermediate and basic lavas) and are characterized by jointed schist. At shallow depths (due to weathering/fracturing) the metasediments have low to moderate permeability while metavolcanics have moderate to high permeability.

Lower (Enticho) Sandstone—Yellow to white, fine to medium grained, slightly to moderately weathered, horizontally bedded, jointed sandstone with sand-silt matrix and poorly sorted pebbles and boulders (Kazmin 1972; Beyth 1972a, b; Bosellini et al. 1997). This unit is generally characterized by moderate to high permeability.

Paleozoic Glacial Tillites—Grey to black sand-silt-clay matrix, interbedded with thin layers of silty limestone, and with poorly sorted pebbles and boulders (Mohr 1962, 1967, 1983; Kazmin 1972; Beyth 1972a, b; Woldearegay 2005). The glacial tillites have generally low to moderate permeability. In slopes, these rocks retard the vertical flow and promote lateral movement of water towards the slope.

Post-Glacial Sediments—Poorly cemented clay, silt and fine sand, horizontally bedded, jointed sandstone (Woldearegay 2005). At shallow depths (due to weathering) these have low to moderate permeability. In slopes, these masses retard the vertical flow and promote lateral movement of water towards slope faces/downslope areas.

Adigrat Sandstone—Medium to coarse-grained, slightly to moderately weathered, horizontally bedded, jointed sandstone with some shale and laterite bands as intercalations (Bosellini et al. 1997; Abay and Meisina 2015; Woldearegay 2005). These rocks are associated with vertical/sub-vertical joints and tensional fractures as well as horizontal/sub-horizontal bedding planes. Due to their often ridge forming nature they act as recharge zones to downslope areas.

Gohatsion Formation (Abay Beds)—Mainly exposed along the Blue Nile gorge and are composed of limestones, calcareous sandstones, shales, and gypsum beds (Assefa 1981, 1991; Wolela 1997; Russo et al. 1999; Ayalew and Yamagishi 2000, 2003; Hearn 2018). The shale components, due to their low hydraulic conductivity, retard the vertical flow and promote lateral movement of water towards the slope faces/downslope areas.

Antalo Limestone—Yellow to white, slightly to moderately jointed limestone with intercalations of calcareous clay (marl) (Bosellini et al. 1997; Wolela (1997). The hard limestones are mostly well jointed and are represented by high permeability while the shale components, due to their low permeability retard the vertical flow and promote lateral movement of water towards slope faces/downslope areas (Woldearegay 2005; Abay and Meisina 2015).

Agulae Shale—Gray, green and black, thinly bedded, moderately to highly weathered shale (marly), which is

interlaminated with thin limestone beds and with some gypsum beds (Bosellini et al. 1997; Nyssen et al. 2002; Woldearegay 2005; Ayalew et al. 2009; Abay and Meisina 2015; Hearn 2018). Due to their low hydraulic conductivity, the shales retard the vertical flow and promote movement of water towards the slope faces/downslope areas.

Upper (Ambaradom) Sandstone—Fine to medium grained, white to pink coloured, thickly bedded, slightly to moderately weathered sandstone, which is interbedded with thin layers of siltstone/ claystone. These rocks form vertical/sub-vertical joints and horizontal/sub-horizontal bedding planes and are generally characterized by moderate to high permeability (Woldearegay 2005). Due to their ridge forming nature these act as recharge to the downslope areas.

Basalt Flows—These rocks include (Mohr and Zanettin 1988; Ayenew and Barbieri 2005; Woldearegay 2005) dark coloured, fine to coarse grained igneous rocks which are associated with soft sediments (volcanic ash and/or lacustrine deposits) as discontinuous interbeds. Horizontal/sub-horizontal flow structures form rock sequences which range from well-developed columnar joints to less fractured/massive layers and with some paleosols. The basalts have variable hydraulic characteristics: more fractured (high permeability) to less fractured (low permeability). The soft sediments (found as interbeds) have generally low permeability and hence retard the vertical flow and promote lateral movements of water towards slope faces/ downslope areas.

Volcanic Plugs and Doleritic Intrusions—These rocks occur in localized areas and include dolerites/diorites and volcanic plugs (Mohr 1962). In steep terrains they are affected by vertical/sub-vertical tensional fractures and act as recharge to downslope areas.

Rift Floor Volcanics—These have variable properties which range from fractured basalt flows to volcaniclastic and pyroclastic deposits (Mohr 1971; Bonini et al. 2005; Hayward and Ebinger 1996). These rocks are affected by faults, joints and collapse structures. The rift floor volcanic rocks have highly variable permeabilities which range from high (for hard and fractured ones) to low (for soft formations, mainly pyroclastic deposits).

Strength of rocks: The different rocks were found to have variable strengths (Table 1): relatively higher UCS values were recorded in Basalt flows, Antalo limestone and Metavolcanics while lower values were measured in Metasedments.

Table 1 Unconfined Compressive Strength (UCS) values of rocks as obtained from Schmidt Hammer Test (L-type) and laboratory tests

	UCS (MPa) (Schmidt hammer test)		UCS (MPa) (Laboratory test)	
Rock type	n	Range	n	Range
Basalt flows	127	54–128	34	58.4–86.2
Antalo Limestone	85	73–132	28	67.5–84.5
Adigrat Sandstone	62	55–104	19	50.2–66.7
Enticho Sandstone	31	38–78	15	41.3–69.8
Metavolcanics	25	67–125	13	49.5–73.6
Metasediments	21	31–56	11	36.2–52.3

n = number of tests

3.1.2 Engineering Properties of Soils

The unconsolidated sediments affected by landslides in the different sites were colluvials/debris and residual soils derived from different rock types. Results of the laboratory tests (Table 2) and in-situ permeability tests revealed the following.

Grain-size, Plasticity and Free Swell As can be noted from Table 2, higher liquid limit, plastic limit, plasticity index, and free swell values were found in soils derived from shales followed by those derived from basalt flows. On the other hand, colluvial soils were found to be dominated by heterogeneous masses (gravel percentages up to 20%) with relatively lower plasticity and free swell properties.

Permeability Results of the in-situ hydraulic conductivity tests of residual soils revealed different permeability values:

(a) soils derived from Agulae shales: $3.6*10^{-5}$ to $6.3*10^{-6}$ cm/s; (b) soils derived from Antalo limestone: $3.4*10^{-3}$ to $8.2*10^{-5}$ cm/s; and (c) soils derived from volcanic rocks (basalt flows of the trap series): $5.2*10^{-4}$ to $7.6*10^{-6}$ cm/s.

Table 2 Results of laboratory tests on engineering properties of unconsolidated sediments from landslide-affected sites

Soil property	RLS (n = 63)	RSH (n = 48)	RVO (n = 138)	COL (n = 112)
Moisture content (%)	14–70.5	18.2–45.8	21.5–86.5	18.5–72.4
LL (%)	25–72	32.5–86.4	28.5–79.2	17.5–56.5
PL (%)	11–24.6	14.5–32.8	13.5–30.6	8.4–29.3
PI (%)	14.5-46.5	20.5–50.5	16.5–47.5	10.8–36.7
Free swell (%)	13–81	21–96	18.5–86.2	10.2–46.4
% gravel	0–8	0–7	0–12.5	0–20
% sand	5–81	8–63	8–65	18–65
% fines (silt And clay)	6–76	26–81	11–72	25–52

Note: LL = liquid limit; PL = Plastic limit; PI=Plasticity index. RLS = Residual soils derived from limestone; RSH = Residual soils derived from shale; RVO = Residual soils derived from volcanics (basalt flows of the trap series); COL = Colluvials; n = number of tests

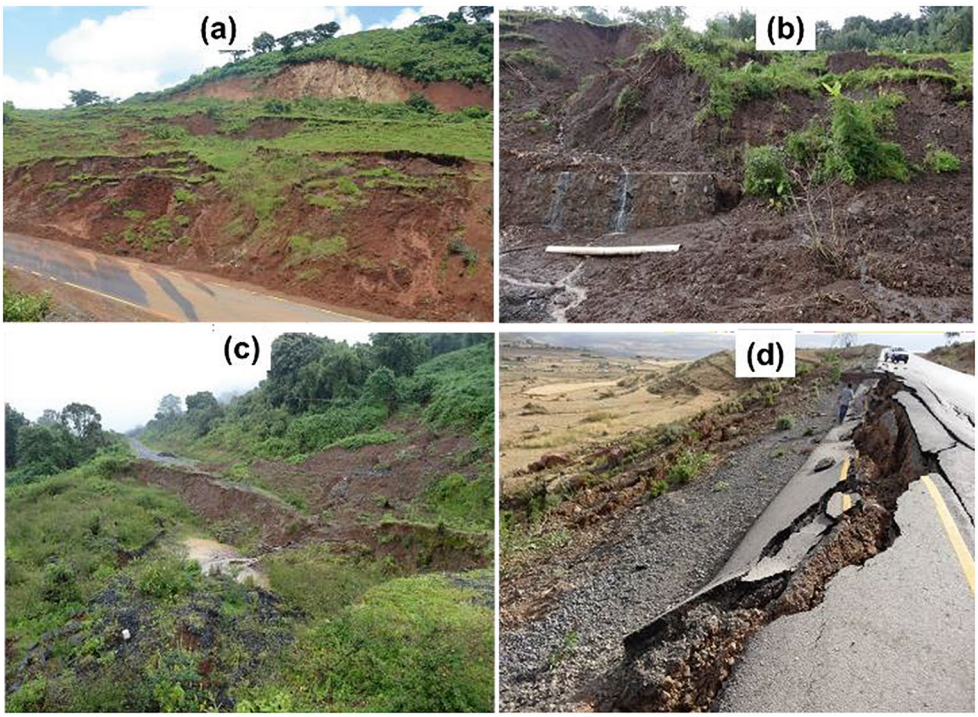


Fig. 3 Examples of landslides affecting road networks in Ethiopia: (**a**) debris/earth slides with failure in the upslope section of road, (**b**) debris/earth slides/flows which overrode retaining structures, (**c**) failures that affected the whole road (including upslope and downslope), and (**d**) failure in downslope sections that progressed upslope and affected the road

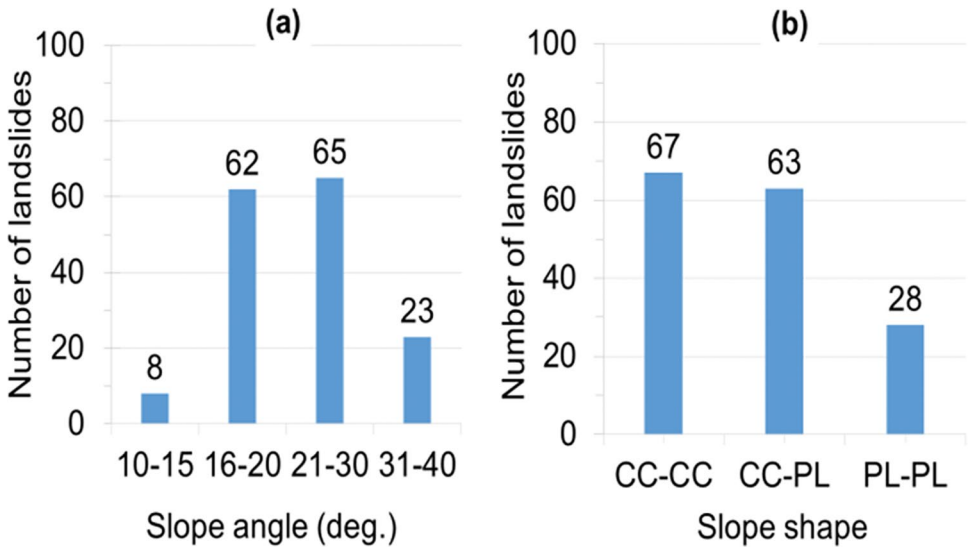


Fig. 4 Terrain conditions of the landslide-affected sites: (**a**) slope angles versus number of landslides, and (**b**) slope shapes versus number of landslides. CC-CC (concave plan-concave profile), CC-PL (concave plan-planar profile), PL-PL (planar plan-planar profile) (Parsons 1988)

3.2 Characteristics of Landslides

The inventoried landslides were mainly debris/earth slides (n = 151) and debris/earth flows (n = 7) (e.g. Fig. 3). Landslides occurred during/following rainfalls. Failures were rotational to quasi-rotational (n = 115) and translational (n = 36) types. The landslides occurred in areas underlain by Antalo limestone, Shales and Volcanic rocks (Basalt flows) of the trap series. The depths of failures were found to vary along the slope profile: maximum values between 2.5 m and 13.5 m (mean: 8.6 m). The areal sizes of the landslides were in the range 5000–37,550 m^2.

In relation to terrain conditions, failures occurred in: slope angles 12–38°; and variable slope shapes: concave (n = 121; 76.6%) and planar (n = 37; 23.4%) (Fig. 4). The landslides on relatively gentle slope angles were associated with steep road cuts (measured: upto 60°) and failures progressed upslope beyond the road reserves.

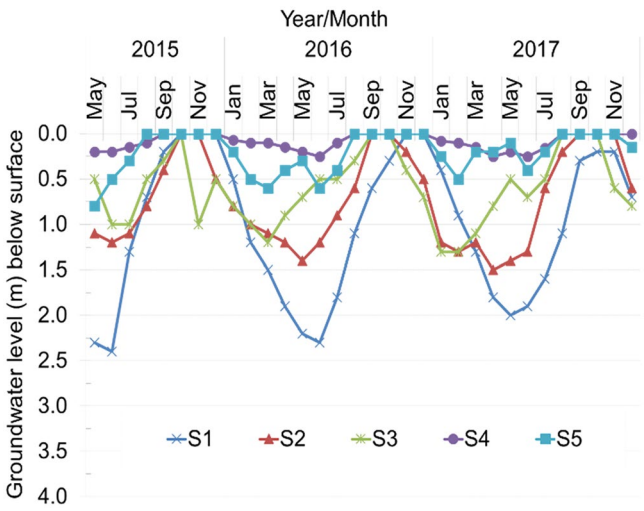


Fig. 5 Variability in groundwater levels in wells in landslide-affected sites (Fig. 1b): S1 (Adigura), S2 (Jimma), S3 (Debretabor), S4 (Wacha), S5 (Kombolcha) landslides. In the five sites groundwater level has reached at surface or close to surface in the months of August to December. Site S3 has shown a slight increase in groundwater level in the months March to May due to small rains. Site S4 has shown little fluctuation in groundwater level year-round due to greater recharge from upslope areas

3.3 Hydrological Conditions of the Landslide-Affected Sites

Evaluation of the hydrological conditions of the road sections affected by landslides revealed the following.

Groundwater Levels in Wells The water level in wells in the different sites (n = 108) varied between 0 and 3.5 m below surface. Maximum raise in water levels were recorded following the main rainy seasons (September to December) while lower water levels were measured during dry seasons (April to June) (e.g. Fig. 5). In some sites, with higher recharges from upslope areas, groundwater levels in the slopes had shown little variation year-round during the monitoring periods (e.g. S4 in Fig. 5).

Springs Discharges and Water Use The measured discharges of the springs in the different sites (n = 47) varied between 1.8 to 3.6 l/s. In each site several numbers of springs (up to four) were observed. In 28 sites water from springs caused damage to roads and in 12 sites water was used for domestic and irrigation purposes.

Ponding/Stagnating Water In 52 sites, ponding/stagnating water (with variable volumes) were observed at the middle and upper sections of the landslides. The estimated volume of ponded/stagnated water varied from 4 to 45 m^3; one site has created a large pond with storage capacity about 1800 m^3. In all the inventoried landslides, seepages and piping (subsurface erosion) features were observed at the contact zones between unconsolidated sediments and underlying weathered rocks.

Stream/River Erosion and Scouring In 36 sites stream/river incisions were observed close to the landslides which affected road sections; failures have progressed upslope from the rivers/streams to the roads. Results of the flood level measurements in 36 sites revealed that flooding have affected the slopes through scouring and saturation of the toe of the sliding masses. As a result, some of the mitigation measures (retaining structures, etc.) were found to be scoured by river/stream flow (e.g. Fig. 6). Water from road hydraulic systems (roadside ditches, culverts, and bridges) have also caused stream/river erosion and undercutting; contributing to further instability of slopes which further affected the roads.

3.4 Failure Models/Scenarios

In relation to landslide-road-landscape interactions, the inventoried landslides could be categorized into three failure models/scenarios: upslope, downslope, and whole road section instabilities as discussed below.

Failure of Upslope Road Section Such scenarios occurred in 21 sites (33%) and affected the upslope sections with the subgrade and downslope areas unaffected. Though failures were on unconsolidated sediments in the upslope part of the road, several problems were observed both at upslope, road and downslope areas: (a) landslides have blocked roads in 16 sites, (b) landslides progressed upslope into farmlands and dwelling houses beyond the road reserve, and (c) sediments from the landslide mass have caused siltations/blockages of road hydraulic systems (culverts and roadside ditches, etc.).

Failure of Downslope Road Section Such failures were recorded in 87 sites (55%) but progressed to the roads with observed problems of road cracking, subsidence, settlements and partial sliding of roads. In areas affected by such failure modes several conditions were observed in a number of sites: (a) more steeper slopes at downslope areas as compared to their upslope (n = 45), (b) more heterogeneous soil masses in the downslope areas including placed/dumped materials from road excavations (n = 35), (c) stream/river incisions by floods (n = 28), and (d) partial blockages of streams/rivers by the landslide masses (n = 17).

Failure of the Whole Road Section (Upslope, Road and Downslope) Such scenarios were observed in 38 sites (24%) and failure involved the whole road section. In the majority of the sites with such failure cases, the roads passed through larger landslide zones. Two cases were

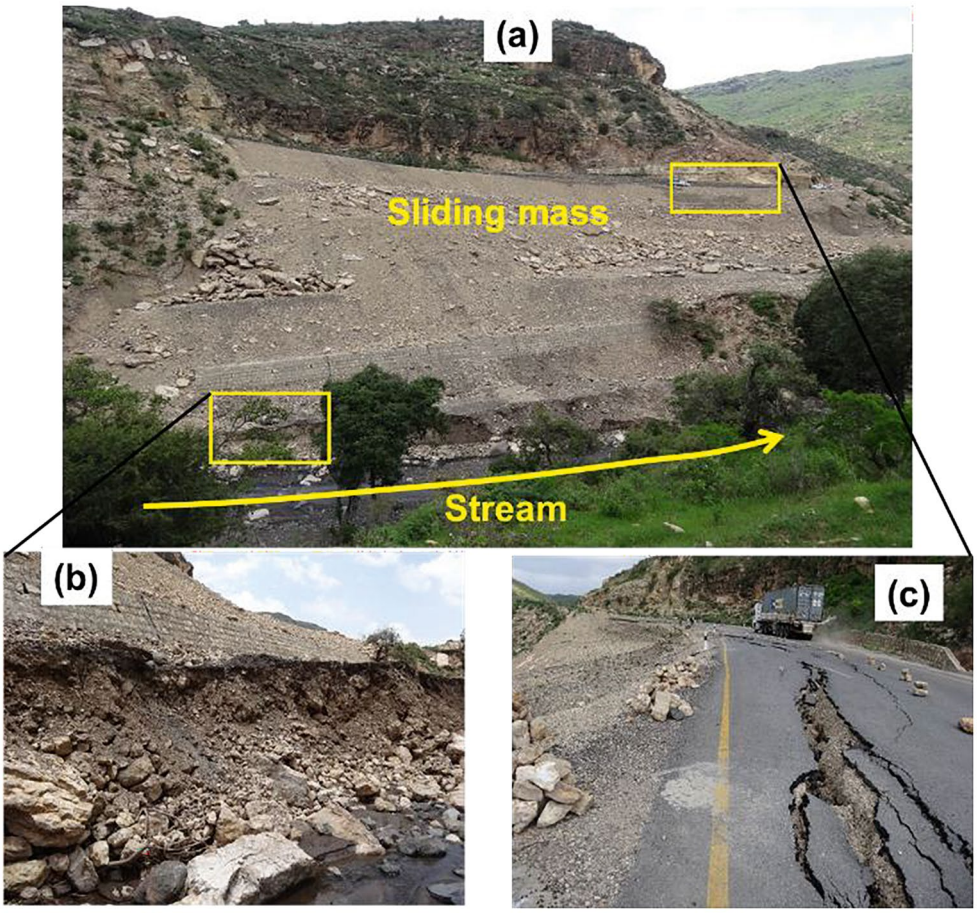


Fig. 6 Example of landslide in northern Ethiopia (along Hiwane-Mehoni road) (S6: Fig. 1a): (**a**) view of the landslide area, (**b**) mitigation measures (retaining structures) affected by stream erosion/scouring, and (**c**) cracking of rehabilitated asphalt road due to the landslide

observed under this scenario: (a) both upslope and downslope sections affected by landslides with part of the sub-grade unaffected (mostly on hard formation) (n = 21), and (b) the whole road section (upslope, road and downslope) affected by landslides (n = 17). Stream/river incisions (by flood) and road blockages (by landslides) were observed in 12 and 16 sites respectively. Many of the problems observed in upslope as well as downslope failure scenarios were also observed in failures that involved the whole road section.

3.5 Types and Effectiveness of Mitigation/ Stabilization Measures

Evaluations of 125 sites show that one or combinations of different landslide mitigation measures were implemented which included: backfilling, retaining structures, drainages, and other methods (biological measures, benches, etc.). The inventoried measures and the observed problems are summarized below.

Backfilling with Selected Materials Such measures were implemented in 65 sites affected by failures of the downslope road sections (e.g. Fig. 7a). Subsidence, settlement, cracking and sliding of parts of the roads were observed in areas treated with such measures. Though implemented and acted as temporary solutions to ease traffic, backfilling practices were observed to aggravate slope instabilities. This could be due to combinations of: (a) addition of load over sliding masses, and (b) blockages of sub-surface flow of water (compaction effect) and hence water pressure build-up within the slopes.

Retaining Structures One or combinations of different types of retaining structures were implemented in several sites: gabion (n = 44; 35%), masonry (n = 50; 40%), concrete (n = 31; 25%). Some of the observed problems with retaining structures included the following:

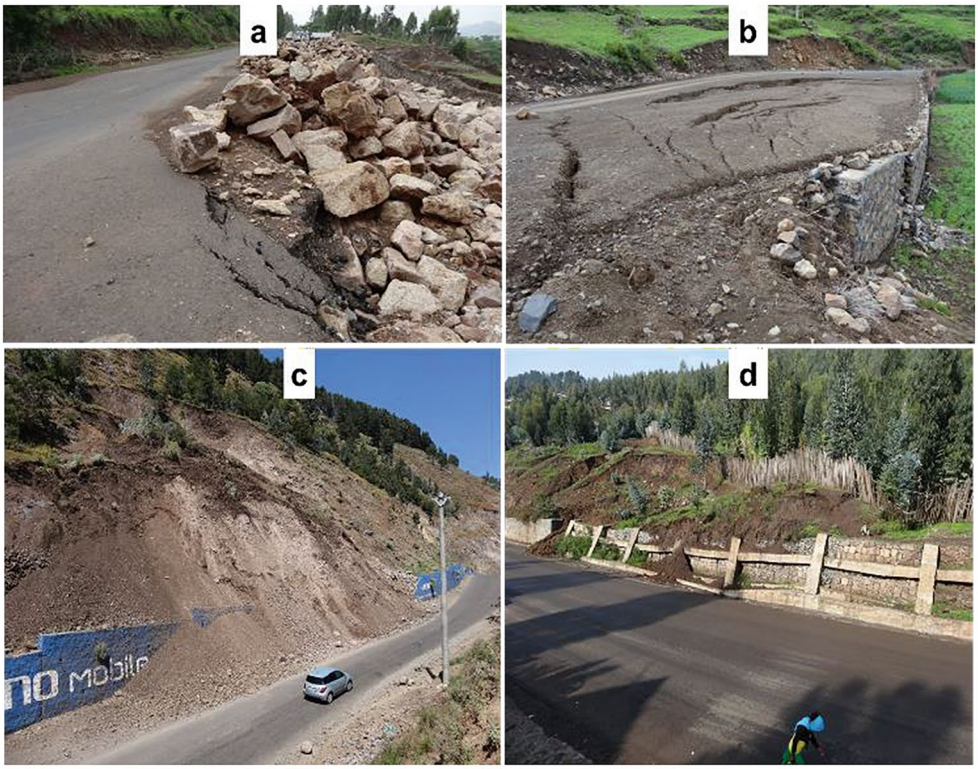


Fig. 7 Examples of problems with mitigation measures implemented in the different sites: (**a**) backfilling with selected materials; (**b**) retaining structure (masonry) damaged by landslides; (**c**) and (**d**) debris/earth slides which overrode retaining structures

- *Foundation depths of retaining structures*—retaining structures were not properly keyed to stable stratum and were placed over sliding masses. These lead to further instability of the slopes due to additional loading and blockages of sub-surface water flow.
- *Undercutting/scouring*—retaining structures were found to be affected by erosion/scouring with flood water in natural streams/rivers (e.g. Fig. 6) as well as unmanaged water from road hydraulic systems (roadside ditches, culverts and bridges).
- *Override slides*—in some sites landslides have occurred in the upslope of roads and the displaced unconsolidated sediments overrode retaining structures (e.g. Fig. 7c, d).

Drainages Surface and sub-surface drainages were implemented in 123 and 36 sites respectively. Some of the problems with drainages included one or combinations of:

(a) improper installation of sub-surface drainage systems as water bearing zones were not properly intercepted,
(b) blockages of filters installed for sub-surface drainages, and
(c) blockage of sub-surface flow due to compaction of permeable zones (mostly the interface between soil and underlying rock). In some sites surface drainages were not properly implemented and/or wrongly used. Ponding of water in sliding areas, and/or constructions of trenches which enhance recharge of water in the landslide affected sites were some of the observed problems.

Other Mitigation Measures Integrated with some biological measures, benches were implemented in 13 sites. Major problems with biological measures were (1) management challenges of the planted grasses/trees because of free-grazing practice in most parts of Ethiopia, (2) limited availability of species varieties and selection problems of locally suitable grasses/trees for slope protection, and (3) ownership issues with the planted grasses/trees.

Overall Performance of Mitigation Measures Though different mitigation measures were implemented in 125 landslide-affected road sections, the performances of the measures were successful (n = 25; 20%), partially successful (n = 30; 24%), and unsuccessful (n = 70; 56%). In some sites mitigation measures were implemented up to five times in four years (e.g. Fig. 8).

3.6 Landslides and Roads: Reciprocal Interactions and Effects

The inventoried landslides were found to cause a number of problems:

- ***Damage on roads***—a total of 20.5 km road (asphalt and all weather gravel) was damaged by the 158 landslides.

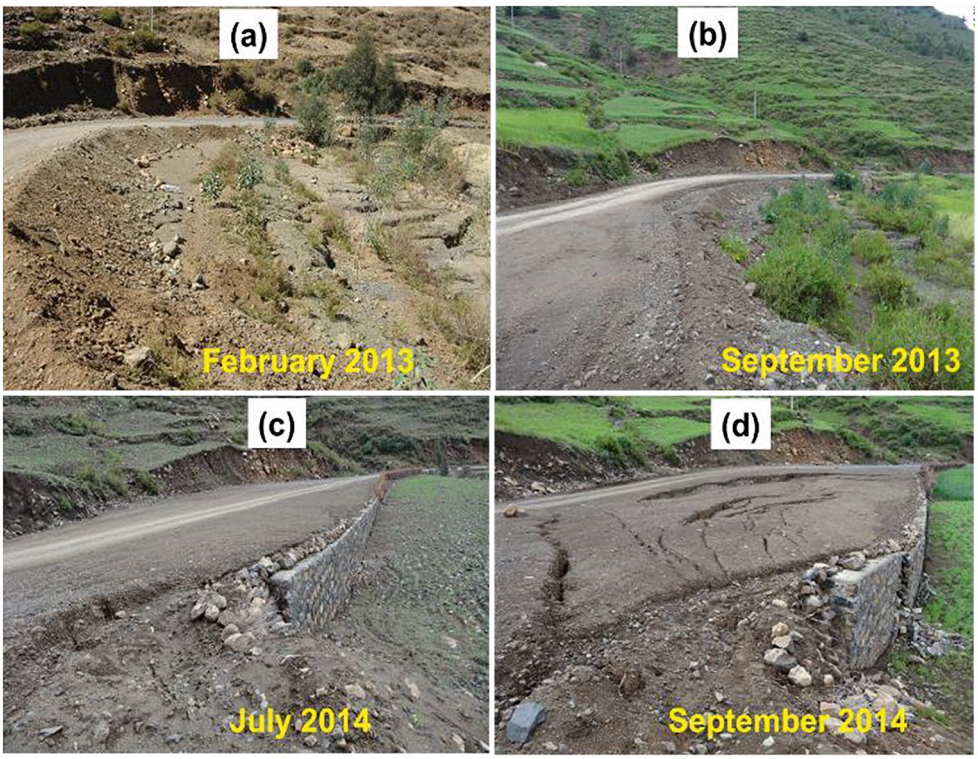


Fig. 8 Typical example of the repeated maintenance measures implemented in northern Ethiopia (S1: Adigura landslide; Fig. 1b)

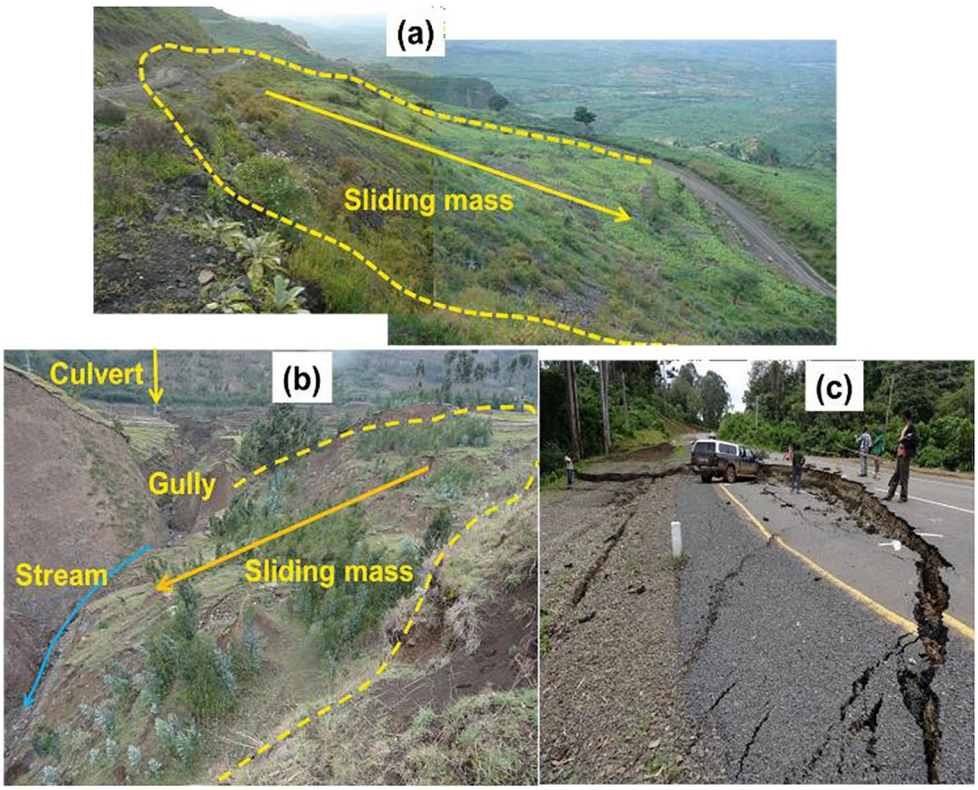


Fig. 9 Examples on the effects and interactions between landslides and roads: (**a**) panoramic view of landslide initiated by road construction which affected farm lands and roads along Lemi-Alemketema route (S7: Fig. 1b), (**b**) unmanaged water from culvert which caused downstream gully erosion and associated landslides along Woldia-Gashena road (S8: Fig. 1b), and (c) car accident due to landslides

- ***Maintenance costs***—in all the landslide affected sites maintenances were reported from single to multiple times.
- ***Damage on farmlands, dwelling houses, and other infrastructures***—landslides that were initiated as a result of road constructions have affected the upslope and/or downslope areas (e.g. Fig. 9a).

- ***Hazards from unmanaged water from road hydraulic systems*—**in 136 sites water from culverts and roadside ditches have caused scouring/gully erosions at downstream areas. In 25 sites unmanaged water from culverts have contributed to initiations of landslides that affected downstream areas (e.g. Fig. 9b): some of these failures progressed upslope and affected the roads.
- ***Hampering traffic and causing car accidents***—road blockages were reported in 36 sites which lasted from few hours (sites close to towns) to three days (in remote areas). Car accidents were found to be common in many of the damaged roads due to landslides (Woldearegay 2014; Hearn 2018) (e.g. Fig. 9c). In 18 sites blockages of roads for days have hampered socio-economic activities including access to health services.
- ***Siltations/blockages of hydraulic structures*—**culverts, roadside ditches, etc. were blocked in 121 sites due to siltations from landslide masses. These caused other cascading problems such as floodings, erosion/scouring, etc. of roads and downstream areas (farmlands, other infrastructures).

4 Conclusions and Recommendations

This study was based on data gathered over 25 years period (1997–2022) through research, practice and documentation on 158 landslides (areal sizes greater than 5000 m^2) which affected road networks in Ethiopia. The following conclusions and recommendations are made for further landslide practice, research, innovations and capacity building.

Scale, Occurrences and Effects of Landslides on Infrastructures Due to the absence of comprehensive inventory of landslides and their effects on infrastructures, there is little understanding on the scale and effects of such hazards in Ethiopia. In recent years some studies (e.g. Hearn 2018) have started to report on the effects of landslides on road networks. The evidence presented in this paper shows that the occurrences and effects of landslides on roads and other infrastructures in Ethiopia is much greater than what is perceived and reported so far. The data presented in this paper is not based on comprehensive inventory but rather from isolated observations and documentations over the years.

Types and Causes of Landslides The landslides were dominantly on unconsolidated sediments underlain by Limestones, Shales and Basalt flows. Failures were found to be associated with certain terrain conditions: slope angles in the range 12 to 38°, and in concave areas with some on planar terrains. The landslide-affected areas were found to be associated with geohydrological systems that favour water pressure build-up within the slopes due to: (a) presence of permeable zones at the interface between unconsolidated sediments and the underlying weathered rocks, (b) low permeability nature of the underlying rocks which enhance lateral flow of water towards slope faces and downstream areas, and (c) road construction activities which contribute to compaction and blockages of sub-surface flows within the slopes. Stream/river incisions, road excavations, and placement of excavated materials on downslope areas and other potentially unstable terrains have also contributed to instability of the slopes.

Landslide-Road-Landscape Interactions The interactions between landscapes, roads and landslides were found to be complex and with reciprocal effects. Some of the processes/factors contributing to slope instabilities include: (a) slope modifications due to road excavations, placement of excavated materials on marginally stable terrains, etc., (b) changes in slope hydrology (surface and sub-surface) such as blockages of sub-surface water flow (due to compaction/loading) and creating concentrated surface runoff (in roadside ditches, culverts), and (c) cascading effects of landslides on roads, other infrastructures, agricultural lands, dowelling houses, environment, etc. There is a need to properly understand the reciprocal effects and interactions between landslides, roads and landscapes.

Need for Comprehensive Geological, Hydrological and Geotechnical Site Investigations In all the studied sites no adequate geological and geotechnical site investigations were carried out during road design and constructions. In all the sites data on sub-surface condition including engineering properties of soils and rocks, groundwater conditions, depths and geometry of failures were poorly understood. Though landslides were triggered following heavy rainfalls, many of the failures occurred during upgrading of the roads: widening of roads is often done towards the outer shoulders. Moreover, many of landslides were associated with old landslides; hence the need to understand the history of the route and its interaction with the engineering environment beyond the road corridor. There is, therefore, a need for comprehensive geological and geotechnical site investigations that involve surface and sub-surface methods including geophysical investigations, drillings and groundwater level monitoring.

Need for Comprehensive Landslide Inventory, Capacity Building and Research So far no comprehensive inventory of landslides and their effects have been made in Ethiopia. Landslides and associated hazards are expected to increase due to: (a) the rugged and complex terrains (highlands, rift escarpments, and rift valleys) with complex geological, tectonic hydrological conditions, (b) the expected increase in transport infrastructure development, (c) population pressure

and associated increase in settlement of people in landslide-prone terrains, and (d) climate change. There is, therefore, a critical need for: (1) better understanding of landslide processes through comprehensive inventory of past failures, (2) assessments of performances of implemented mitigation measures/practices, (3) enhancing the capacity of institutions and professionals to address landslide issues, and (4) promoting research and innovations in landslide science and technology in Ethiopia and in other developing countries with similar conditions.

Towards Multi-purpose/Benefit Oriented Landslide Mitigation Measures The designs and constructions of landslide mitigation measures should be based on clear understanding of the causes and geometry of failures and through proper stability analysis of slopes. It is critical that retaining structures are keyed to stable stratum, with clear understanding on the geometry of failures and magnitude of the stresses. Though drainage (surface and subsurface) is an important mitigation method it is advisable to go beyond drainage and move towards integrating the concept of "water management" in landslide mitigation; an opportunity to use water and enhance stability of slopes.

Acknowledgements Prof. Kyoji Sassa is highly acknowledged for his support and encouragement to be engaged with and contribute to landslide research in Ethiopia. The following organizations have provided support to this research and documentation: Mekelle University; Ethiopian Roads Authority; Ethiopian Geological Survey; Addis Ababa University; Ethiopian Science and Technology; Jimma University; Austrian Development Cooperation; International Council for Science Union-Regional Office for Africa; and Tigray Bureau of Road, Transport and Construction. The content of this paper is the responsibility of the author and does not necessarily represent the official views of the organizations and individuals who supported this work. The anonymous reviewers for this paper are highly acknowledged for their constructive comments and suggestions.

Declaration of Conflicting Interest The author declared no conflict of interest with respect to the research, authorship, and/or publication of this article.

References

Abay A, Meisina C (2015) Engineering-geological properties of carbonates and shale: their implications for dam construction in Mekelle, Northern Ethiopia. Momona Ethiopian J Sci (MEJS) 7(1):64–84. Mekelle University, ISSN:2220-184

Anderson MG, Kemp MJ (1991) Towards an improved specification of slope hydrology in the analysis of slope instability problems in the tropics. Progress Phys Geography 15(1):29–52

Assefa G (1981) Gohatsion formation. A new Lias-Malm lithostratigraphic unit from the Abay river basin, Ethiopia. Geos 2:63–88

Assefa G (1991) Litho-stratigraphy and environment of deposition of the late Jurassic-early Cretaceous sequence of the central part of north-western Plateau. Ethiopia N Jb Geol Paleontol Abh 183(3):255–282

Ayalew L (1999) The effect of seasonal rainfall on landslides in the highlands of Ethiopia. Bull Eng Geol Environ 58:9–19

Ayalew L, Yamagishi H (2000) Slope failures in the Blue Nile basin, as seen from landscape evolution perspective. J Geomorphol:611–622

Ayalew L, Yamagishi H (2003) Slope failures in the Blue Nile basin, as seen from landscape evolution perspective. Geomorphology 1361, Elsevier Science Publ., Amsterdam, pp 1–22

Ayalew L, Moeller D, Reik G (2009) Geotechnical aspects and stability of road cuts in the Blue Nile Basin, Ethiopia. Geotech Geol Eng 27(6):713–728

Ayenew T, Barbieri G (2005) Inventory of landslides and susceptibility mapping in the Dessie area, northern Ethiopia. Eng Geol 77:1–15. https://doi.org/10.1016/j.enggeo.2004.07.002

Beyth M (1972a) Paleozoic sedimentary basin of Mekele Outlier, Northern Ethiopia. Am Assoc Petr Geol Bull 56:2426–2439

Beyth M (1972b) The geology of central and western Tigre. PhD Thesis, University of Bon, Germany, 155 pp

Billi P, Dramis F (2003) Geomorphological investigations on gully erosion in the Rift valley and the northern highlands of Ethiopia. Catena 50:353–368

Bonini M, Corti G, Innocenti F, Manetti P, Mazzarini F, Abebe T, Pecskay Z (2005) Evolution of the Main Ethiopian Rift in the frame of Afar and Kenya rifts propagation. Tectonics 24:1–24. https://doi.org/10.1029/2004TC001680

Bosellini A, Russo A, Fantozzi PL, Assefa G, Tadesse S (1997) The Mesozoic succession of the Mekele Outlier (Tigrai Province, Ethiopia). Mem Sci Geol 49:95–116

BS 5930 (1981) Code Practice for Site Investigations. British Standards Institution (BSI), London, 147 pp

ENMSA (Ethiopian National Meteorology Service Agency) (2021) Hydrometeorological data of Ethiopia for the years 1996-2020. Addis Ababa, Ethiopia

Ethiopian Mapping Authority (1996) Topographic maps of Ethiopia (scale: 1:50000). Addis Ababa

Gezahegn A (1998) Slope instability assessment in the Blue Nile Gorge, Ethiopia. In: Moore D, Hungr O (eds) Proceedings of the 8th International IAEG Congress. Vancouver, Balkema, Rotterdam, pp 1437–1442

Glade T, Crozier MJ (2005) The nature of landslide hazard impact. In: Glade T, Anderson M, Crozier MJ (eds) Landslide hazard and risk. Wiley, Chichester. https://doi.org/10.1002/9780470012659.ch2

Guzzetti F, Carrara A, Cardinali M, Reichenbach P (1999) Landslide hazard evaluation: a review of current techniques and their application in a multi-scale study, Central Italy. Geomorphology 31:181–216

Hansen A (1984) Landslide hazard analysis. In: Brundsen D, Prior DB (eds) Slope instability. Wiley, New York, pp 523–602

Hayward NJ, Ebinger CJ (1996) Variations in the along-axis segmentation of the Afar Rift system. Tectonics 15:244–257. https://doi.org/10.1029/95TC02292

Hearn GJ (2018) Slope hazards on the Ethiopian road network. Quarterly J Eng Geol Hydrogeol. https://doi.org/10.1144/qjegh2018-058

Hunt T, Hearn G, Chonephetsarath X, Howell J (2008) Slope Maintenance Manual. Ministry of Public Works and Transport, Lao PDR – Scott Wilson Ltd in association with Lao Consulting Group, Vientiane. http://www.gov.uk/dfid-research-outputs/seacap-21-slope-maintenance-manual

Hurni H, Perich I (1992) Towards a Tigray Environmental and Economic Strategy (TREES). Group for Development and Environment, Institute of Geography, University of Berne, Switzerland, 32 pp

Ibrahim W (2011) Road Sector Development and Economic Growth in Ethiopia. EDRI Working Paper 4. Addis Ababa, Ethiopia: Ethiopian Development Research Institute, 41 pp. https://elibrary.acbfpact.

org/acbf/collect/acbf/index/assoc/HASH0154/75c72727/64f4e457/ff92.dir/EDRI0006.pdf
Inversin AR (1986) Micro-hydropower source book. A practical guide to design and implementation in developing countries. NRECA (National Rural Electric Cooperative Association) International Foundation, Washington DC. 285 pp
ISRM (1981) Rock characterization, testing and monitoring. In: Brown ET (ed) ISRM Suggested methods. Pergamon Press, New York, 211 p
Kazmin V (1972) Geology of Ethiopia; explanatory note to the geological map of Ethiopia, 1:2,000,000. Ministry of Mines, Addis Ababa, Ethiopia, 14 pp
Kessler J, Oosterbaan R (1974) Determining hydraulic conductivities of soils. In: Drainage principles and applications. International Institute for Land Reclamation and Improvement, Wageningen, The Netherlands, vol 16(III), pp 253–296
Mengesha T, Tadiwos C, Workineh H (1996) Geological map of Ethiopia. Bulletin of the Ethiopian Institute of Geological Survey, 3. Scale 1:200000, Addis Ababa, Ethiopia
Mohr PA (1962) In: The geology of Ethiopia. II Poligrafico, Asmara
Mohr PA (1967) Review of the geology of the Siemen Mountains. Bull Geophys Observatory Addis Ababa Univ Ethiopia 10:79–93
Mohr PA (1971) The geology of Ethiopia. Addis Ababa University Press
Mohr PA (1983) Ethiopian flood basalt province. Nature 303:577–583
Mohr P, Zanettin B (1988) The Ethiopian flood basalt province. In: McDougall JD (ed) Continental flood basalts. Kluwer Acad. Publ, Dordrecht, pp 63–110
Montgomery DR (1994) Road surface drainage, channel initiation, and slope instability. Water Resources Res 30(6):1925–1932. https://doi.org/10.1029/94WR00538
MoTL (Ministry of Transport and Logistics) (2022) Ethiopian transport master plan road network for the years 2022-2052, Addis Ababa, Ethiopia. 186 pp. https://ethiotransport.gov.et/userfiles/media/default/Masterplan/road-network.pdf
Nyssen J, Poesen J, Moeyersons J, Luyten E, Veyret-Picot M, Deckers J, Haile M, Govers G (2002) Impact of road building on gully erosion risk: a case study from the northern Ethiopian highlands. Earth Surf Process Landforms 27:1267–1283
Nyssen J, Poesen J, Moeyersons J, Deckers J, Haile M, Land A (2004) Human impact on the environment in the Ethiopian and Eritrean highlands – a state of the art. Earth-Sci Rev 64:273–320
Parsons AJ (1988) Hillslope form. Routledge, London, 212 pp
Pirone M, Papa R, Nicotera MV, Urciuoli G (2015) Soil water balance in an unsaturated pyroclastic slope for evaluation of soil hydraulic behaviour and boundary conditions. J Hydrol 528:63–83
Psomiadis E, Papazachariou A, Konstantinos XS, Alexiou DS, Charalampopoulos I (2020) Landslide mapping and susceptibility assessment using geospatial analysis and earth observation data. Land 9:133. https://doi.org/10.3390/land9050133
Russo A, Fantozzi P, Tadesse S (1999) Geological map of Mekelle Outlier (Western Sheet), 1: 100000 scale. Cooperazione Italiana, Roma
Selby MJ (1993) Hillslope materials and processes, 2nd edn. Oxford University Press, New York, 451 pp
Temesgen B, Umer M, Asrat A, Berakhi O, Ayele A, Francisco D, Demssie M (1999) Landslide hazard on the slope of Dabicho ridge, Wondogenet area: the case of June 18, 1996 event. SINET: Ethiopia J Sci 22(1):127–140
Temesgen B, Umer M, Korme T (2001) Natural hazard assessment using GIS and remote sensing methods, with particular reference to the landslides in the Wondogenet area, Ethiopia. Phys Chem Earth 26(9):665–675
Terlien MTJ (1996) Modeling spatial and temporal variations in rainfall-triggered landslides. The integration of hydrological models, slope stability models and geographic information systems for the hazard zonation of rainfall-triggered landslides with examples from Manizales (Colombia). PhD Thesis. ITC publication No. 32, 254 pp
Tuinhof A, Van Steenbergen F, Vos P, Tolk L (2012) Soil and water conservation at scale, Tigray, Ethiopia. Chapter of book "Profit from Storage: the costs and benefits of water buffering (3R)", pp 86–90
UNISDR (United Nations International Strategy for Disaster Reduction) (2015) Sendai framework for disaster risk reduction 2015–2030. UNISDR, Geneva. https://www.undrr.org/publication/sendai-framework-disaster-risk-reduction-2015-2030
Van Den ME, Moeyersons J, Nyssen J, Abraha A, Poesen J, Haile M, Deckers J (2009) Spatial patterns of old, deep- seated landslides: a case-study in the northern Ethiopian highlands. Geomorphology 105:239–252. https://doi.org/10.1016/j.geomorph.2008.09.027
Varnes DJ (1978) Slope movement types and processes. In: Schuster RL, Krizek RJ (eds) Landslides: analysis and control. National Academy of Sciences, Transportation Research Board, Washington DC, Special Report 176, 11–35
Varnes DJ (1984) Landslide hazard zonation: a review of principles and practice. Commission on landslides of the IAEG, UNESCO, Natural Hazards, No 3, 61 pp
Virgo K, Munro R (1978) Soil and erosion features of the central Plateau region of Tigray, Northern Ethiopia. Geoderma 20:131–157
Woldearegay K (2005) Rainfall-triggered landslides in the northern highlands of Ethiopia: characterization, GIS-based prediction and mitigation. PhD Thesis. Graz University of Technology, Austria
Woldearegay K (2013) Review of the occurrences and influencing factors of landslides In the highlands of Ethiopia: with implications for infrastructural development. Momona Ethiopian J Sci (MEJS) 5(1):3–31, pp. 1–7. Mekelle, Ethiopia: Department of Earth Sciences, Mekelle University
Woldearegay K (2014) Landslide-related road failures in Ethiopia. Abstract. National workshop on natural hazard monitoring and risk management, Institute of Geophysics Space Science and Astronomy, November 6–7, 2014, Addis Ababa University, Ethiopia
Woldearegay K, Riedmuller G, Schubert W, Mogessie A (2004) Controlling parameters and failure mechanisms of a large-scale landslide in northern Ethiopia. Felsbau 22(3):46–55
Wolela A (1997) Sedimentology, diagenesis and hydrocarbon potential of sandstones in hydrocarbon prospective Mesozoic rift basins (Ethi-o-pia, UK, USA). PhD Thesis, the Queen's University of Belfast, p 238

Open Access This chapter is licensed under the terms of the Creative Commons Attribution 4.0 International License (http://creativecommons.org/licenses/by/4.0/), which permits use, sharing, adaptation, distribution and reproduction in any medium or format, as long as you give appropriate credit to the original author(s) and the source, provide a link to the Creative Commons license and indicate if changes were made.

The images or other third party material in this chapter are included in the chapter's Creative Commons license, unless indicated otherwise in a credit line to the material. If material is not included in the chapter's Creative Commons license and your intended use is not permitted by statutory regulation or exceeds the permitted use, you will need to obtain permission directly from the copyright holder.



KLC2020 Official Promoters

The Kyoto Landslide Commitment 2020 (KLC2020)

Kyoto 2020 Commitment for Global Promotion of Understanding and Reducing Landslide Disaster Risk

A Commitment to the Sendai Landslide Partnerships 2015–2025, the Sendai Framework for Disaster Risk Reduction 2015–2030, the 2030 Agenda Sustainable Development Goals, the New Urban Agenda and the Paris Climate Agreement-

KLC2020 Official promoters are public and private organizations who promote the Kyoto Landslide Commitment 2020 and provide financial support for the implementation of the KLC2020 activities including the Open Access Book Series "Progress in Landslide Research and Technology."

Host organization

International Consortium on Landslides (ICL)/Željko Arbanas.

Public sectors: KLC2020 Official Promoters-public

International Unions/Associations, Governmental organizations, Universities and Research institutes

- The International Union of Geological Sciences (IUGS)/Hassina Mouri
- The International Union of Geodesy and Geophysics (IUGG)/Chris Rizos
- The International Association for the Engineering Geology and the Environment/Vassilis Marinos
- International Geosynthetics Society (IGS)/John Kraus
- Geological Survey of Canada, Natural Resources Canada, Canada/Sonia Talwar
- Faculty of Civil and Geodetic Engineering, University of Ljubljana, Slovenia/Matjaž Mikoš
- China University of Geosciences, Wuhan, China/Huiming Tang
- The State Key Laboratory of Geohazard Prevention and Geoenvironment Protection, Chengdu University of Technology, Sichuan, China/Qiang Xu
- Department of Civil Engineering, National Taiwan University, Chinese Taipei/Louis Ge
- Institute of Rock Structure and Mechanics, the Czech Academy of Sciences/Josef Stemberk
- Institute of Cold Regions Science and Engineering, Northeast Forestry University/Wei shan.

Private sectors: KLC2020 Official Promoters-private

Companies and corporation.

- Marui & Co. Ltd, Japan
- Nippon Koei Co., Ltd, Japan
- Ellegi srl, Italy
- Chuo Kaihatsu Corporation, Japan
- Godai Kaihatsu Corporation, Japan
- Kiso-Jiban Consultants Co., Ltd, Japan
- Kokusai Kogyo Co., Ltd., Japan
- OSASI Technos, Inc., Japan.

© The Author(s) 2025

B. Abolmasov et al. (eds.), *Progress in Landslide Research and Technology, Volume 3 Issue 2, 2024*, Progress in Landslide Research and Technology, https://doi.org/10.1007/978-3-031-72736-8

Geological Survey of Canada, Natural Resources Canada

GSC-Pacific Division

Geological Survey of Canada—Who We Are

The Geological Survey of Canada (GSC) is part of the Earth Sciences Sector of Natural Resources Canada. The GSC is Canada's oldest scientific agency and one of its first government organizations. It was founded in 1842 to help develop a viable Canadian mineral industry by establishing the general geological base on which the industry could plan detailed investigations. Throughout its long and colourful history, the GSC has played a leading role in exploring the nation.

Today, the GSC is Canada's national organization for geoscientific information and research. Its world-class expertise focuses on the sustainable development of Canada's mineral, energy and water resources; stewardship of Canada's environment; management of natural geological and related hazards; and technology innovation (Fig. A.1).

The GSC celebrated its 175th anniversary in 2017 which coincided with Canada's 150th anniversary of Confederation. The GSC co-leads the Canada-Nunavut Geoscience Office and works with dozens of universities and research institutes, industry organizations, other federal departments, provinces, territories and municipalities in Canada and across the world. In particular, we work closely with other geological survey organizations in Canada through the unique Intergovernmental Geoscience Accord.

Every year, we publish hundreds of maps, Open Files, peer-reviewed papers and other reports. Our scientists are recognized worldwide and sought after for their expert advice on locating mineral, energy and groundwater resources, reducing risk from natural hazards and reviewing environmental assessments.



Fig. A.1 Paleotsunami investigations in order to understand regional earthquake cycles and submarine landslide hazards

Strategic Priorities

The GSC has attempted to plot a course through this changing, uncertain world.

First, we identify three core areas of persistent scientific endeavour, which reflect stable, long-term needs of society:

- **Geological knowledge for Canada's onshore and offshore lands**
- **Geoscience for sustainable development**
- **Geoscience for keeping Canada safe.**

Next, we outline a new, fourth area of endeavour, Geoscience for society, which is the need to address the uncertainties of the changing world by expanding the reach and impact of geoscience knowledge in land-use decision making and in efforts to reduce the risk of disasters.

Finally, we recognize that our strength lies in a fifth area of endeavour, Our people, Our science, which we need to nurture to maintain a high-performing workforce

GSC-Pacific Division
GSC-Pacific Division, Vancouver, BC, Canada
e-mail: David.Huntley@nrcan-rncan.gc.ca

© The Author(s) 2025

B. Abolmasov et al. (eds.), *Progress in Landslide Research and Technology, Volume 3 Issue 2, 2024*, Progress in Landslide Research and Technology, https://doi.org/10.1007/978-3-031-72736-8

capable of world leading innovative geoscience for the benefit of Canada.

(a) Geological knowledge for Canada's onshore and offshore lands

Geoscientific knowledge is fundamental to managing our onshore and offshore lands and their abundant resources. With its 10 million km^2 of onshore land and an additional 7 million km^2 of ocean estate, Canada is a vast country and a core mission of the GSC is to map and understand the land and its resources. Our Geo-mapping for Energy and Minerals (GEM) program continues to advance our knowledge of the North and by 2020 will complete a first mapping of surface geology at a coarse scale.

In the offshore lands, our geoscience knowledge also serves to confirm the farthest extents of the Canadian territory. Our joint program with Global Affairs Canada and Fisheries and Oceans Canada to delineate the outer limits of the continental shelf in the Atlantic and Arctic Oceans will reach a critical milestone in 2019. The program will file its Arctic submission under the United Nations Convention on the Law of the Sea (UNCLOS) (Fig. A.2).

(b) Geoscience for sustainable development

Finding new resources remains a major challenge. Many near-surface deposits have been discovered in Canada, but significant mineral resources remain to be found in less accessible regions and at depths below the surface. Finding new resources requires systematic, intensive and innovative methods to assess the mineral potential in remote locations.

It requires searching beneath overburden cover, imaging the 3-D structure of the earth and understanding the geological processes that lead to concentration of minerals in certain locations (Fig. A.3).



Fig. A.2 The GSC studies the sea floor of the Arctic to understand its geology and geohazards. Here a small craft surveys the bottom of Southwind Fjord (Baffin Island, N Nunavut)



Fig. A.3 GSC geologists near the Heiberg Formation in northern Ellesmere Island (NU) as part of the geo-mapping for energy and minerals program. This formation is the primary host of major gas accumulations in the Canadian High Arctic

For the Energy sector, the greatest challenge is in the transition to a low-carbon economy. Although global fossil fuel use is likely to continue to grow over the foreseeable future, the trend will likely be at a decreasing rate. Canada has an abundant supply of conventional and unconventional (oil sands and shale) oil and gas, so development in frontier areas is likely to be slow. In addition, the government has placed a moratorium on exploration activity in the Arctic offshore lands.

(c) Geoscience for keeping Canada safe

The GSC will continue to work on understanding how landscapes will change, how infrastructure will be affected and how resilience to climate change can be built into new infrastructure. Climate change will likely have a significant impact on the water cycle. GSC research will shed light on the risk to potable water supplies, hydroelectric power generation, and hazards from floods and drought (Fig. A.4).

(d) Geoscience for society

The scientific knowledge required to assess cumulative effects is broad. The complex interactions between land use, water management and waste management require an integrated approach at a landscape scale. The GSC is a national provider of information on both land (surficial and solid geology) and water, including the integration of surface water and groundwater into the complete water cycle (Fig. A.5).

The GSC recognizes that this area of endeavour involves inherent complexities and that our goals in this area will be to some degree aspirational. However, we will investigate new ways of planning our programs, undertaking our field-



Fig. A.4 The GSC conducts climate change studies, here documenting the effects of fast melting permafrost leading to extreme coastal erosion on Pelly Island, NT



Fig. A.5 The GSC conducts geohazard studies to reduce risks to people and infrastructure, here installing equipment to monitor landslide activity above a critical railway corridor in central BC



Fig. A.6 Among many celebratory activities for the GSC's 175th anniversary in 2017, the GSC held a Rock and Fossil Exhibit, at its site at the Bedford Institute of Oceanography (Dartmouth, NS), as part of a 2-day open-house event, where more than 20,000 visitors participated

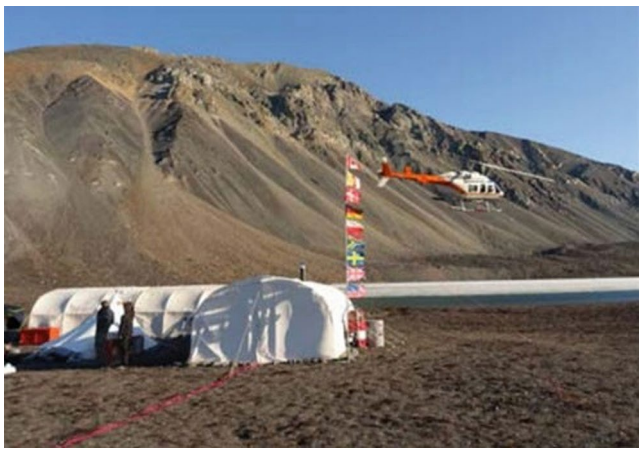


Fig. A.7 Joint Canadian/German (GSC/BGR) field mapping camp on northern Ellesmere Island, looking west as the fog covered sea ice of Yelverton Inlet, 2017

work, interacting with key stakeholders, and communicating our expert knowledge in ways that contribute positively to decision making about resource development.

(e) **Our people, Our science**

As a science organization within the federal government, the GSC's mandate is to conduct world-class science to inform public decision making. The Canadian government has articulated and adopted the principle of evidence-based decision making and reaffirmed the need for government science to be objective and non-partisan.To remain at the leading edge, our scientists need to work with a variety of partners. We need to reinforce the central role that the GSC plays in the Canadian geoscience community by building networks of collaboration, fully participating in national geoscience initiatives, and advocating for Canadian geoscience at the international level (Fig. A.6).

Moving Forward

Some of the objectives and goals that the GSC has set represent familiar territory for a national geoscience organization, but many others will pull us out of our comfort zone. We will take the time to better understand the challenges of delivering objective, nonpartisan science to support evidence-based decision making in Canada at a time of great technological and social change.

We will not be able to do this alone, so we look forward to strengthening our ties to other federal departments, provinces and territories, universities, Indigenous organizations, the private sector and civil society as a whole.

We ask all our stakeholders to contact us, to challenge us and, most importantly, to join with us to assure the future of Canada through thoughtful, respectful dialogue about the land we live on, its resources and its future (Fig. A.7).

Exploring Canada

Through its history, the GSC has been responsible for mapping the land mass of Canada, which supported the integration of the western provinces and northern territories into the country that we have today. The limit of Canada's offshore territory is still being extended today though surveys conducted by the GSC and the Canadian Hydrographic Service.

In more recent years, the GSC helped find the first economic diamond deposit in the Northwest Territories, leading to the expansion of diamond mining in Canada. These are only a few of the key GSC achievements that have built our knowledge of Canada's lands and provided the building blocks of its natural resource economy.

Today, exploration of this vast land is still reaping its natural resource rewards. The search for natural resources is difficult, akin to looking for a needle in a haystack.

The GSC's GEM program is exploring vast tracts of Canada's North, a land mass roughly equivalent to the combined areas of Quebec, Ontario and Manitoba, to find the "haystacks" with resource potential. This information is shared with the provinces and territories, as well as the private sector, so that the search for the "needles" can continue. The information is also critical to inform land-use planning.



In November 2016, the Royal Canadian Geographical Society (RCGS) awarded its prestigious Gold Medal to the GSC in recognition of the Survey's outstanding contribution to the development of Canada on the occasion of it's 175th anniversary.



Faculty of Civil and Geodetic Engineering, University of Ljubljana

Matjaž Mikoš

Summary

The Faculty of Civil and Geodetic Engineering of the University of Ljubljana (UL FGG) covering engineering disciplines, including water science and technology, has been involved in landslide risk reduction activities at the national level in Slovenia (former Yugoslavia, until 1991) for decades. In 2008, UL FGG became an ICL Full Member and has gradually developed its ICL engagement. UL FGG has been awarded the title of the World Centre of Excellence (WCoE) in Landslide Risk Reduction for five consecutive periods (2008–2011, 2011–2014, 2014–2017, 2017–2020, 2020–2023). Together with the Geological Survey of Slovenia, UL FGG hosted in 2017 the Fourth World Landslide Forum in Ljubljana, Slovenia.

UL FGG strongly supports diverse activities of the International Consortium on Landslides, Kyoto, Japan, and thus contributes to the 2030 Agenda for Sustainable Development, as well as to the Sendai Framework for Disaster Risk Reduction 2015–2030 (SF DDR). UL FGG was a signatory of the Sendai Landslide Partnerships 2015–2030, and is a dedicated official promoter of the Kyoto Landslide Commitment 2020, a SF DRR voluntary commitment by ICL.

In 2016, UL FGG started to host the University of Ljubljana UNESCO Chair on Water-related Disaster Risk Reduction (WRDRR), being still the only UNESCO Chair at this university, and one of a few in Slovenia. Among different activities, in 2022 the WRDRR Chair supported the launching of the regional platform called Resili-Enhance for enhancing the resilience to disasters for sustainable development. UL FGG also supports activities of the Slovenian National Committee for UNESCO Intergovernmental Hydrological Programme (IHP), now working on the IHP-IX programme (2022–2029).

UL FGG is actively involved in numerous international (bilateral) and national research projects in the field of hydrology and hydraulic engineering, including topics such as landslide research, landslide risk mitigation, natural risk dialogue, and capacity building for society resilience.

In the field of capacity building, UL FGG offers several courses for graduate and postgraduate students in landslide mechanics and dynamics, landslide stabilization and landslide risk mitigation. In this article, a short overview of the past and current activities of UL FGG as ICL Full Member and KLC2020 Official Promoter is shown.

World Centre of Excellence on Landslide

Risk Reduction and IPL projects

WCoE activities

The title of World Centre of Excellence (WCoE) on Landslide Risk Reduction is given to a governmental or non-governmental entity, which contributes to the landslide disaster risk reduction at a regional and/or global level in a specific unique field of expertise, as well as helps promoting International Programme on Landslides (IPL) and landslide research intellectually, practically and financially (https://www.landslides.org/ipl-info/world-centre-of-excellence/). UL FGG was granted the title of WCoE five consecutive times:

- WCoE 2008–2011 and 2011–2014: Mechanisms of landslides in over-consolidated clays and flysch.
- WCoE 2014–2017: Mechanisms of landslides and creep in over-consolidated clays and flysch.

M. Mikoš
Faculty of Civil and Geodetic Engineering,
University of Ljubljana, Ljubljana, Slovenia
e-mail: matjaz.mikos@fgg.uni-lj.si

© The Author(s) 2025

B. Abolmasov et al. (eds.), *Progress in Landslide Research and Technology, Volume 3 Issue 2, 2024*, Progress in Landslide Research and Technology, https://doi.org/10.1007/978-3-031-72736-8

- WCoE 2017–2020: Landslides in Weathered Flysch: from activation to deposition.
- WCoE 2020–2023: Landslides in Weathered Heterogenous Sedimentary Rock Masses such as Flysch.

The research efforts at UL FGG were focused on:

- Mechanisms of triggering such landslides (mud flows), estimation of debris-flow magnitudes triggered as shallow or deep-seated landslides (debris slides), and triggering of shallow rainfall-induced landslides using advanced statistical methods.
- Field and laboratory investigations of suction in over-consolidated clays and flysch, such as to improve the understanding of softening in stiff over–consolidated clays and marls, using soil matrix suction as an indicator for mudflow occurrence, and executing suction long-term monitoring of the Slano Blato landslide.
- Laboratory investigations of coarse debris-flow rheological parameters and soil–water characteristic curve of residual soil from a flysch rock mass.
- Mathematical modelling of debris flows (hazard assessment in deposition areas), using different numerical models and different digital terrain models.

The WCoE activities were financially supported by the Slovenian Research Agency through the Research Programme P2-0180 “Water Science and Technology, and Geotechnical Engineering: Tools and Methods for Process Analyses and Simulations, and Development of Technologies,” as well as by several national (Fig. A.8) and international (bilateral) research projects.

UL FGG and the Geological Survey of Slovenia jointly organized Fourth World Landslide Forum (WLF4), in Ljubljana between May 29 and June 2, 2017. With over 600 participants from 49 countries and 5 international organizations, WLF4 was promoting the culture of living with natural hazards.

IPL projects

An important ICL activity is IPL projects (https://www.landslides.org/projects/ipl-projects/). The IPL Evaluation Committee examines the submitted proposals of ICL members by carefully reading the written proposals and by listening to their presentations at annual ICL conferences. The initially accepted proposals by the IPL Evaluation Committee are discussed and then approved at the annual Board of Representatives meeting of ICL members (Annual Assembly). Finally, the IPL projects are approved annually

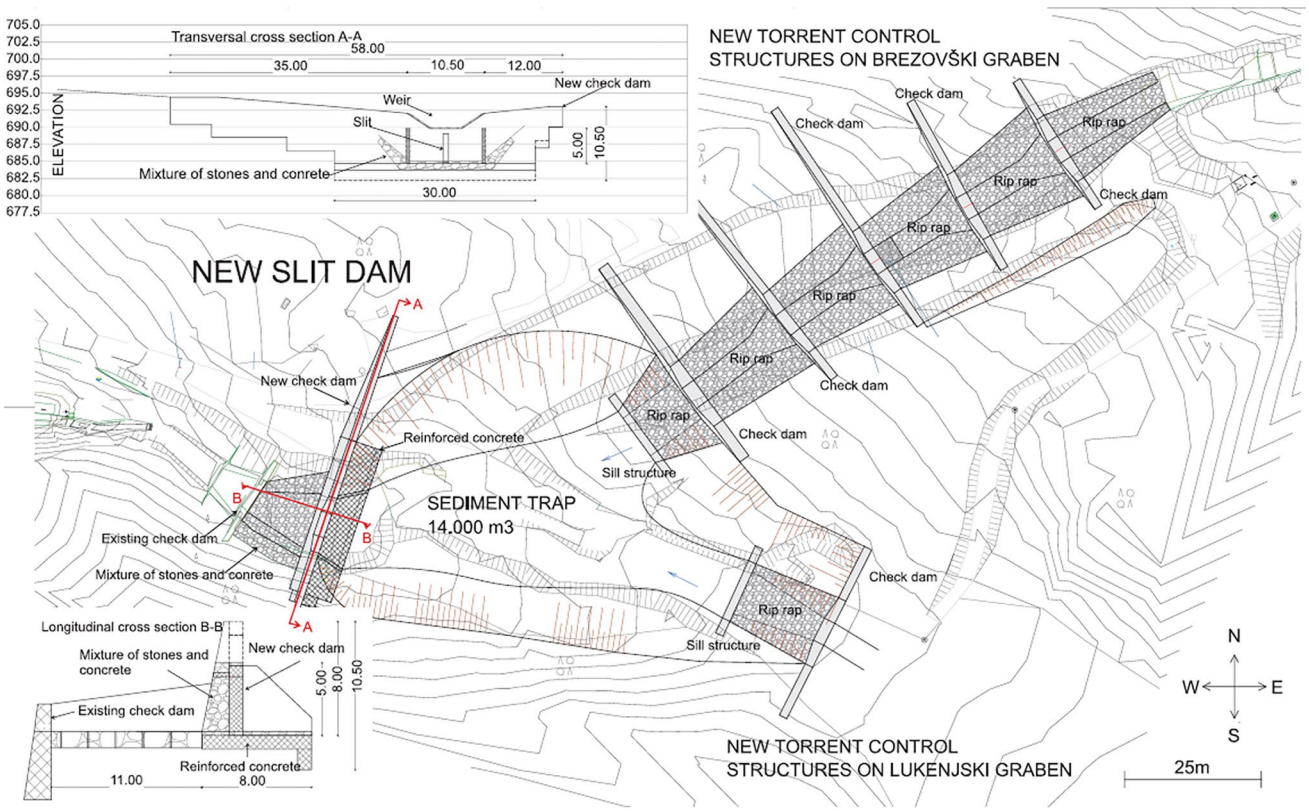


Fig. A.8 Technical countermeasures for future debris floods threatening the cabin station of the Krvavec ski area in N Slovenia. An extreme May 2018 debris flood case study in northern Slovenia: analysis, modelling, and mitigation. Landslides 17: 2373–2383, DOI 10.1007/s10346-019-01325-1

by the Global Promotion Committee IPL-KLC. UL FGG has successfully submitted several proposals for IPL projects and has been so far actively involved in the following ones:

- IPL-151 Soil matrix suction in active landslides in flysch—the Slano Blato landslide case (2010–2012).
- IPL-225 Recognition of potentially hazardous torrential fans using geomorphometric methods and simulating fan formation (2017–2020).
- IPL-226 Studying landslide movements from source areas to the zone of deposition using a deterministic approach (2017–2020)—coordinated by the Geological Survey of Slovenia.
- IPL-261 World-wide-web-based Landslide Observatory (W3bLO) (2022–2024)

ICL Thematic and Regional Networks

Following the ICL Strategic Plan 2012–2021, several thematic networks and regional networks have been established (for an overview, see https://www.landslides.org/projects/icl-networks/).

Landslide Monitoring and Warning Thematic Network—LaMaWaTheN

In 2012, UL FGG proposed the ICL landslide monitoring and warning thematic network—almost 10 ICL members joined the initiative. The general objective of the proposed network was to compare experiences in the field of landslide monitoring and installed early warning systems for active landslides in various regions of the world. Lately, we contributed to the network activities by preparing practice guidelines on monitoring and warning technology for debris flows.

The idea of the network was partially taken over by the web database ICL World Report on Landslides (https://www.landslides.org/projects/world-report-on-landslides/), created to be a platform to share landslide case studies among the global landslide community, with monitoring and warning systems being a part of the platform.

ICL Adriatic-Balkan Network—ICL ABN

Jointly with other ICL members from Croatia and Serbia, in 2013, UL FGG proposed to establish an ICL Adriatic-Balkan Regional Network. Various network activities were proposed, the most active being the organization of biennial regional symposia on landslide risk reduction in the Adriatic-Balkan Region (called ReSyLAB). UL FGG supported the First Symposium in Zagreb (Croatia, 2013), Second in Belgrade (Serbia, 2015), Third in Ljubljana (Slovenia, 2017), Fourth (Sarajevo, 2019), and Fifth in Rijeka (Croatia, 2022).

In the last decade, UL FGG has signed bilateral research projects with the ICL members in the region: "Adriatic-Balkan Regional Network: Landslide Risk Mitigation for Society and Environment" (2012–2013 with University of Belgrade, Serbia), "Study of landslides in flysch deposits: sliding mechanisms and geotechnical properties for landslide modelling and landslide mitigation SoLiFlyD" (2014–2015 with University of Rijeka, Croatia), and "Laboratory investigations and numerical modelling of landslides in flysch deposits in Croatia and Slovenia" (2016–2017 with the University of Rijeka, Croatia). This joint research has helped strengthen regional cooperation within the ICL ABN regional network.

Other ICL-Related International Activities

UL FGG served the ICL by taking different leading roles in the Consortium, i. e. UL FGG member served as Chair of IPL Evaluation Committee, twice as ICL Vice President, and was elected to Co-Chair and in 2021 to Chair of the IPL-KLC (https://www.landslides.org/ipl-info/ipl-klc-globalpromotion-committee/).

UL FGG has been strongly supporting the journal Landslides: Journal of the International Consortium on Landslides, published by Springer Nature (https://link.springer.com/journal/10346) since its launch in 2004. UL FGG works for the journal in the roles of reviewers and an associate editor, and regularly publishes its top research results in the journal, as well as disseminates information important for capacity building in landslide risk reduction—such as results of bibliometric studies on the journal Landslides and ICL books.

UL FGG also contributed to the two-volume set of Landslide Dynamics: ISDR-ICL Landslide Interactive Teaching Tools (LITT), namely to Vol. 1: Fundamentals, Mapping and Monitoring by practice guidelines on monitoring and warning technology for debris flows (https://www.springer.com/gp/book/9783319577739), and to Vol. 2: Testing, Risk Management and Country Practices (https://www.springer.com/gp/book/9783319577760) by a state-of-the-art overview on landslide disaster risk reduction in Slovenia, a study on two-dimensional debris-flow modelling and topographic data, and by study on intensity duration frequency curves for rainfall-induced shallow landslides and debris flows using copula functions.

UL FGG also contributed to the open-access book series "Progress in Landslide Research and Technology" Vol. 1 by a review article on the history of the International Programme on Landslides (IPL) (https://doi.org/10.1007/978-3-031-16898-7_3), an original article on the natural-hazard-related web observatory as a sustainable development tool (https://doi.org/10.1007/978-3-031-16898-7_5), and an original arti-

cle on landslide research and technology in patent documents (https://doi.org/10.1007/978-3-031-18471-0_3).

University of Ljubljana UNESCO Chair on Water-Related Disaster Risk Reduction (2016–2020 and 2020–2024)

Experiences and knowledge accumulated in the past decades at the Chair on Hydrology and Hydraulic Engineering at UL FGG in the field of (applied) hydrology in experimental basins, hydraulic engineering, landslide research, landslide risk reduction, and flood risk management, culminated in 2016 in the establishment of the UNESCO Chair on Water-related Disaster Risk Reduction (WRDRR Chair; www.unesco-floods.eu) at the University of Ljubljana. The UNESCO WRDRR Chair was positively evaluated by UNESCO in 2020 and prolonged for another 4 years (2020–2024). The Chair is associated to the university twinning and networking UNITWIN UNESCO—Kyoto University—ICL on "Landslide and Water-Related Disaster Risk Management".

The UNESCO WRDRR Chair is involved into numerous international (bilateral) and national research projects. Their results are timely reported in scientific literature (https://www.unesco-floods.eu/category/publications/).

In 2022, the UNESCO Chair supported launching of the ResiliEnhance Program for enhancing the resilience to disasters for sustainable development (https://unescochair-sprint.uniud.it/en/resilienhance-program/). The program is at the moment focused to Central and Eastern Europe, and supported by the Central Europe Initiative (CEI).

In 2022, the UNESCO Chair started to lead the University of Ljubljana project on Sustainable Development (2022–2025; www.unesco-floods.eu/ultra-pilot-projects/)to modernize university professional study programmes, especially in civil engineering, to increase students' competences for sustainable development, including disaster risk reduction and resilience building.

UL FGG supports activities of the Slovenian National Committee for UNESCO Intergovernmental Hydrological Programme (www.ncihp.si)—focus of the activities is the development of the IHP-IX Programme (2022–2029).

Conclusions

UL FGG as one of World Centres of Excellence in Landslide Risk Reduction, hosts the UNESCO Chair on Water-related Disaster Risk Reduction. UL FGG strongly supports ISDR-ICL Sendai Partnerships 2015–2025 for global promotion of understanding and reducing landslide disaster risk, and its extension to 2030 and beyond: the Kyoto 2020 Commitment for Global Promotion of Understanding and Reducing Landslide Disaster Risk that that was signed in November 2020. UL FGG is proud to be its Official Promoter, and will specifically work for its Actions 2, 5, 6, 9 and 10.

This review article is intentionally written without a list of references to described activities. For this purpose, listed websites and links may be used.

The author wants to thank colleagues from UL FGG and University of Ljubljana, and from the ICL community for the past and long-lasting excellent cooperation with a joint vision to reduce landslide disaster risk.

China University of Geosciences, Wuhan

Huiming Tang, Changdong Li, and Qinwen Tan

Introduction

China University of Geosciences, Wuhan (CUG), founded in 1952, is a key national university affiliated with the Ministry of Education. It is also listed in the National "211 Project", the "985 Innovation Platform for Advantageous Disciplines," and the "Double First-class Plan". CUG, featuring geosciences, is a comprehensive university that also offers a variety of degree programs in science, engineering, literature, management, economics, law, education, and arts. Its Geology and Geological Resources & Engineering have both been ranked as the national number one disciplines.

CUG has two campuses in Wuhan. The main campus is the Nanwang Mountain Campus, located in the heart of the Wuhan East Lake National Innovation Demonstration Zone, which is popularly known as China Optics Valley. The Future City Campus is located in the east of Wuhan and is 27 km from the main campus. These two picturesque campuses cover a combined area of 1,474,353 m^2. They are ideal places to study, work, and enjoy life. CUG owns a 4A-Level tourist attraction—the Yifu Museum. CUG also boasts four field training centers: Zhoukoudian in Beijing, Beidaihe in Hebei Province, Zigui in Hubei Province, and Badong in Hubei Province.

CUG has established a complete education system. As of December 2020, 30,239 full-time students, including 18,080 undergraduate students, 9302 master's students, 1916 doctoral students, and 941 international students, have enrolled in its subsidiary 23 schools and 86 research institutes. CUG currently has a faculty of 1858 full-time teachers, among which there are 539 professors (11 of which are members of the Chinese Academy of Sciences) and 984 associate professors.

CUG is focused on fostering high-quality talent. Among its over 300,000 graduates, many have gone on to become scientific and technological elites, statesmen, business leaders and athletes. And they have made great contributions to the nation and society, represented by former Premier WEN Jiabao and 39 members of the Chinese Academy of Sciences and Chinese Academy of Engineering.

CUG has strengthened exchanges and cooperation with international universities. It has signed friendly cooperation agreements with more than 100 universities from the United States, France, Australia, Russia, and other countries. CUG has actively carried out academic, scientific, and cultural exchanges with universities around the world. There are about 1000 international students from more than 100 countries studying at CUG. It also sponsors more than 900 teachers and students to study abroad or conduct international exchanges and invites more than 400 international experts to visit, lecture, and teach at CUG every year. In 2012, CUG initiated and co-established the International University Consortium in Earth Science (IUCES) with 11 other world-renowned universities. IUCES is committed to promoting the common development of geosciences education and scientific research through resource sharing, exchange, and cooperation among its member institutions. In addition, CUG has partnered with Bryant University from the USA, Alfred University from the USA, and Veliko Turnovo University from Bulgaria in establishing three Confucius institutes on their campuses (Fig. A.9).

H. Tang · C. Li · Q. Tan
China University of Geosciences, Wuhan, P.R. China
e-mail: tanghm@cug.edu.cn

© The Author(s) 2025

B. Abolmasov et al. (eds.), *Progress in Landslide Research and Technology, Volume 3 Issue 2, 2024*, Progress in Landslide Research and Technology, https://doi.org/10.1007/978-3-031-72736-8



Fig. A.9 Strategic plan of building a world-renowned research university in earth science

Strategic Plan of Building a World-Renowned Research University in Earth Sciences—A Beautiful China and a Habitable Earth: Towards 2030

CUG reviewed and approved Strategic Plan of Building a World-Renowned Research University in Earth Sciences on December 25 of 2019.

Themed "A Beautiful China & A Habitable Earth", the Plan depicts the blueprint of the second goal of the "three-step strategic goals", which is to build a world-renowned research university in Earth Sciences by 2030 based on the attained goal of developing CUG into a "high-level university with first-class Earth Sciences and coordinated development of multi-disciplines".

According to the Plan, our education missions are: Remaining true to CUG's core value of "seeking harmonious development between man and nature" we are committed to cultivating innovative talents who have lofty morality, solid foundation, and profound expertise and who pursue the unity of knowing and doing. We should provide personnel support and endeavor to innovate, apply and spread knowledge in order to provide theories, technologies, and approaches for the construction of a Beautiful China and a Habitable Earth. We should strive to optimize governance, reform culture, and fully invigorate the vitality of running a university. We should provide our service to the construction of an innovative country and to the promotion of a harmonious co-existence between man and nature. We should provide our service to the people and the governance of China. We should provide our service to the consolidation and development of the system of socialism with Chinese characteristics. We should provide our service to the reform and opening up and to the construction of socialist modernization.

According to the Plan, our endeavoring goals are: By 2030, we will have built a world-renowned research university in Earth Sciences, whose main indexes will have reached or nearly reached the level of other world-class universities. To upgrade CUG into a world-class university, we will endeavor to make the discipline of Earth Sciences rank top in the world and forge boldly ahead in competition to improve the quality of other disciplines of CUG. We will assemble a contingent of teachers and researchers with international competitiveness and influences to build a university with Chinese characteristics and superiority. We will build a world-class university that will be fully engaged in international exchange and cooperation and that will achieve educational, academic, cultural, and administrative excellence.

Outstanding Recent Achievements

In recent years, CUG has achieved significant progress in the research fields of geohazards, water resource, geochemistry, paleontology, geodetic surveying and lunar exploration program, etc. To keep to the theme of KLC2020, recent achievements on geohazards researches of CUG are focused and introduced.

(a) **Approval of National Observation and Research Station for Geohazards in the Three Gorges Reservoir Area, Hubei**

CUG was newly approved **National Observation and Research Station for Geohazards in the Three Gorges Reservoir Area, Hubei**.

This station, founded and administrated by Prof. Huiming Tang, is responsible to carry out field observations and scientific research on geohazards in condition of reservoir operation.

The central site of the station is located in Badong County of the Three Gorges Reservoir area (hereinafter abbreviated as the TGR area), and a larger monitoring network of multiple sites has been established, including the geohazard field test site for the Majiagou landslide, Zigui County, and systematic geophysical monitoring station for the whole TGR area, etc.

The Badong field site (also named Badong in-situ large-scale experimental station) is located in the Huangtupo landslide area, which has been recognized the largest reservoir landslide by volume in the TGR area. The field site consists of a tunnel complex and a series of monitoring systems (Fig. A.10). The tunnel complex, built in the Huangtupo riverside sliding mass #1, consists of a main tunnel with a length of 908 m and a width of 5 m, 5 branch tunnels (5–145 m long, 3.5 m wide), 2 test tunnels, and 35 observation windows. The test tunnels exposed the sliding zones of the landslide, facili-

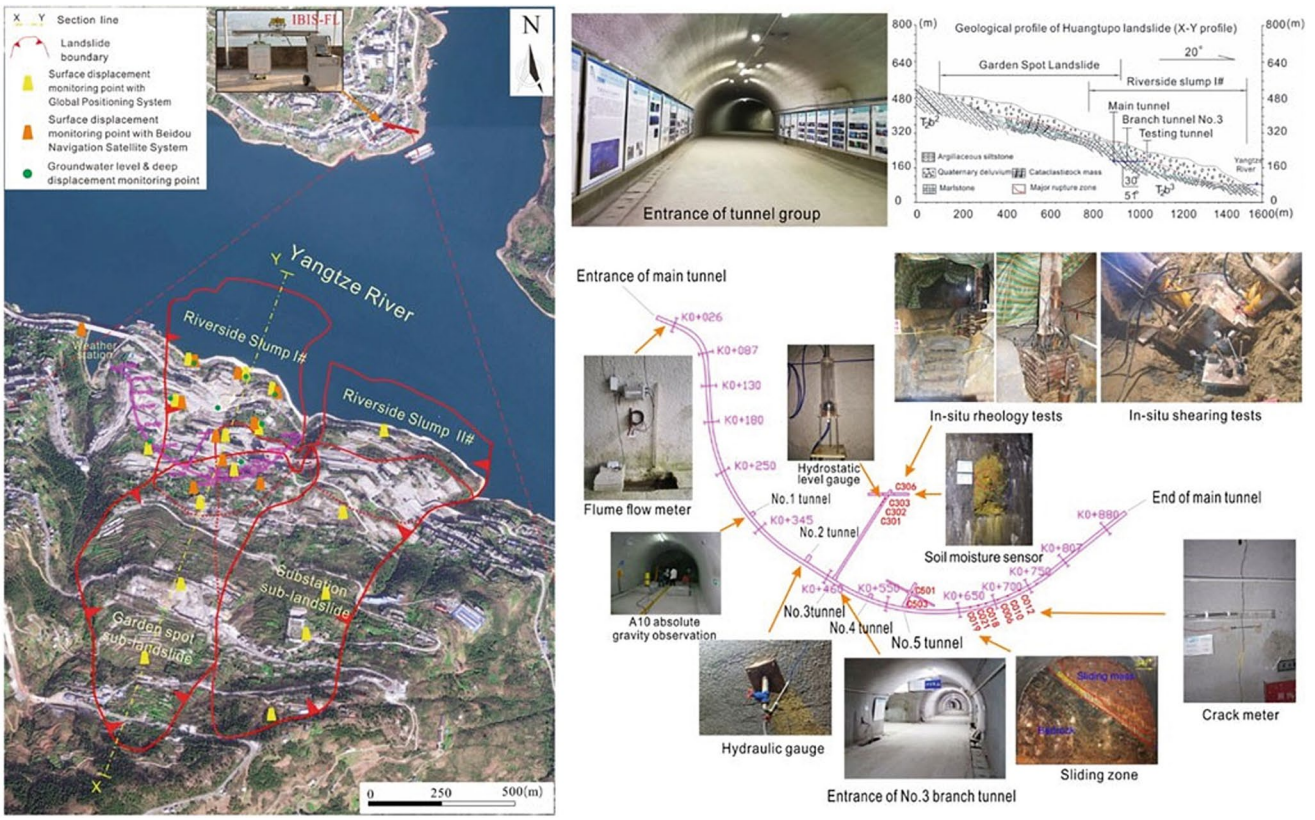


Fig. A.10 Badong in-situ large-scale experimental station of the National Observation and Research Station for Geohazards in the Three Gorges Reservoir Area, Hubei

tating their direct observation and the execution of scientific experiments, such as large-scale in-situ mechanical tests and deep deformation monitoring. The monitoring systems measure deformation as well as hydrologic, meteorological and hydro-chemical variables. The deformation system is composed of a slope surface displacement measurement unit and an underground displacement measurement unit. The slope surface displacement unit includes a number of GPS (Global Positioning System) and BDS (BeiDou Navigation Satellite System) measurement points, as well as an IBIS-FL (Interferometric Radar) monitoring system (Fig. A.12). The underground displacement unit includes nine deep inclinometer boreholes, a number of crack meters installed on the ground and the walls of tunnels, and many hydrostatic level gauges that measure the settlement of the tunnels in the sliding mass. The hydrologic system includes a number of devices that allow for observation of the water level of the Yangtze River, the ground water level and water discharge of the tunnels (Fig. A.12). A small meteorological station is located on the landslide and provides rainfall data. So far, multiple and massive data have been collected for the landslide area since the year 2012, when the field site was constructed; over 10,000 people with a variety of geology-related backgrounds from >20 countries have visited this experimental station.

(b) **Approval of the Basic research on the prediction and forecasting of major landslides program supported by the Major Program of NSFC**

CUG was approved the **Basic research on the prediction and forecasting of major landslides program** (2021–2025), supported by the Major Program of the National Natural Science Foundation of China. The program was designed for the prediction and forecasting of major landslides, with the concentration on the core scientific problems of landslide evolution process and physical-mechanical mechanism. Three key scientific problems, including correlation mechanism for landslide initiation, physical-mechanical mechanism for landslide initiation, and prediction and forecasting theory based on landslide evolution were proposed.

Five topics were set up to achieving those objectives. Topic 1 was proposing the initiation classification of major landslides based on large field test platform, with the adoption of field prototype test and other technical means. Topics 2–4 aimed to reveal the physical and mechanical mechanism of locked-segment dominated landslide, static liquefaction loess landslide and hydrodynamic pressure-driven landslide, and to establish the corresponding landslide initiation criteria, respectively. Topic 5 was responsible to established the

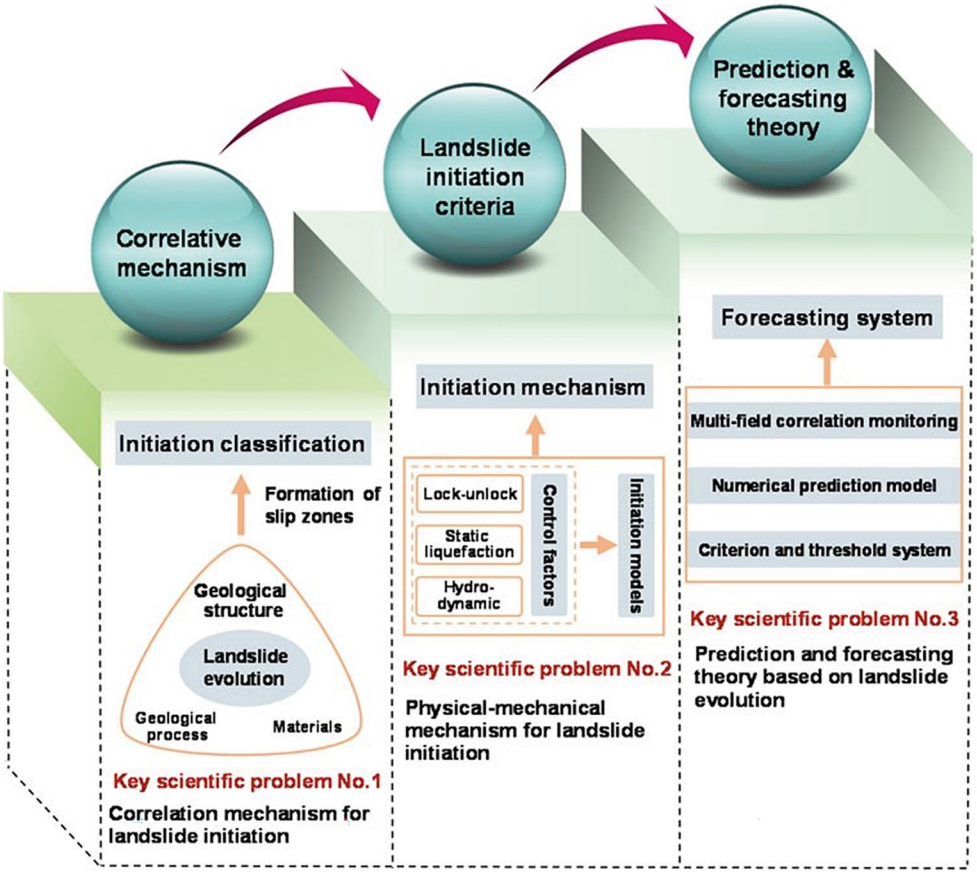


Fig. A.11 Scientific thought for the implement of research

prediction mode and real-time forecasting system. Ultimately, the landslide prediction and forecasting theory based on the evolution process and physical-mechanical mechanism would be put forward. The scientific thought for the implement of research is exhibited in Fig. A.11.

The implementation of the research is respected to lay the geological, mechanical and physical foundation for the above three types of landslide prediction, and to substantially promote the research on landslide prediction.

Figure A.12 shows the old Badong county, situated in the Huangtupo landslide area, and the exposures of the main rupture zones are now more than 50 m below the water surface of the Three Gorges Reservoir (Tang et al. 2015a). During the second relocation from 1982 to 2003, the county moved from Xinling town to the Huangtupo landslide area (Gong et al. 2021). A series of investigations were conducted during that period, and the new county area was further confirmed to be on the site of an ancient landslide then (Gong et al. 2021). Huangtupo landslide is developed in the Middle Triassic Badong Formation strata, within which interbedded strata structures are often observed, and many geohazards developed. The material composition of the Huangtupo landslide includes mudstone, pelitic siltstone, and argillaceous limestone (Tang et al. 2015b). Multiple slumps formed the complex mass at least 4000 years ago (Tang et al. 2015b). The elevation of the crown of the landslide is about 600 m asl., while its toe varies from 50 to 90 m, submerged in the Yangtze River. The composite landslide covers an area of 1.35 km^2, and its volume of nearly 70 million m^3 makes it the largest reservoir landslide in China (Tang et al. 2015b). Considering the risk of landslide reactivation by long-term reservoir operation and human activities, the drainage system and the anchored defense structures along its leading edge were constructed to control the landslide. Huangtupo demonstration base was designed and constructed in 2012, during the third relocation period from 2007 to 2017 (Gong et al. 2021). At that time, some Badong county residents still lived in the Huangtupo area, facing the unsure threat. The old giant landslide is in need of further research to ensure its safety as well as provide access for landslide hazard study. The demonstration base was in great request. With the building and development of the demonstration base, Over 10,000 people with various geology-related backgrounds from more than 20 countries have visited. A national observation station was also settled rely on the base in 2020.



Fig. A.12 Photo of old Badong County, showing the populated area built on the Huangtupo landslide (Tang et al. 2015a)

References

Tang H, Li C, Hu X, Wang L, Criss, R, Su A, Wu Y, Xiong C (2015a) Deformation response of the Huangtupo landslide to rainfall and the changing levels of the Three Gorges Reservoir. Bull Eng Geol Environ 74(3): 933–942

Tang H, Li C, Hu X, Su A, Wang L, Wu Y, Criss R, Xiong C, Li Y (2015b) Evolution characteristics of the Huangtupo landslide based on in situ tunneling and monitoring. Landslides 12(3):511–521

Gong W, Juang CH, Wasowski J (2021) Geohazards and human settlements: lessons learned from multiple relocation events in Badong, China—Engineering geologist's perspective. J Eng Geol 285:106051



The State Key Laboratory of Geohazard Prevention and Geoenvironment Protection

The State Key Laboratory of Geohazard Prevention and Geoenvironment Protection

Introduction

The State Key Laboratory of Geohazard Prevention and Geoenvironment Protection (herein abbreviated as SKLGP) (Chengdu University of Technology), Chengdu, Sichuan Province, China, is dedicated to the applied basic research on geohazard prevention and geoenvironment protection. Committed to meeting the needs of territorial disaster prevention and mitigation, to safeguarding the national major construction projects, SKLGP focuses on the research of generation background, formation mechanism, early identification, monitoring and warning of geohazards which are either induced by nature or human activities, as well as the theories and methods of project management, thereby forming a world-class research center, which combines the applied fundamental research, the development and promotion of advanced technologies, the education of high-caliber talents with international communication and cooperation, SKLGP provides support in a comprehensive way to achieve the national targets of geohazard prevention and geoenvironment protection.

With a unique system of academic thoughts and technical methods, SKLGP focuses on geology and combines the theoretical basis of geology with modern earth science, key zone theory and engineering. By doing so, SKLGP has developed a featured academic thought system with "geological process mechanism analysis—quantitative evaluation" and "system engineering geology". SKLGP has built a whole set of theories and methods, from field investigation, rock mass parameterization, simulation, and evaluation to early identification of potential risk, monitoring and early warning, risk prevention and mitigation, design and construction of projects, which is applicable, complete and targeted for geohazard prevention and geoenvironment protection, equipped with auxiliary facilities and software analysis system in addition.

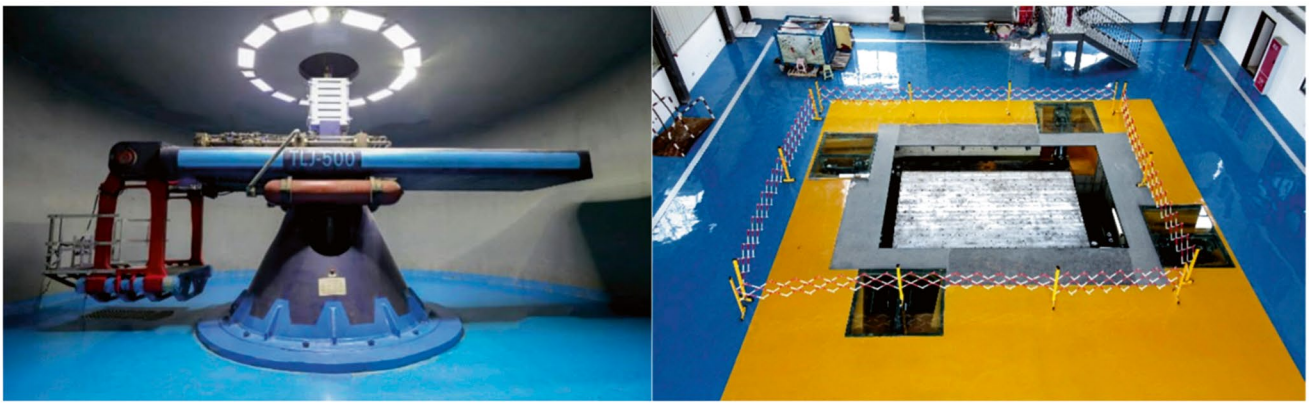
The State Key Laboratory of Geohazard Prevention and Geoenvironment Protection
The State Key Laboratory of Geohazard Prevention and Geoenvironment Protection, Chengdu City, Sichuan Province, P.R. China
e-mail: sklgp_cdut@126.com

© The Author(s) 2025

B. Abolmasov et al. (eds.), *Progress in Landslide Research and Technology, Volume 3 Issue 2, 2024*, Progress in Landslide Research and Technology, https://doi.org/10.1007/978-3-031-72736-8



The State Key Laboratory of Geohazard Prevention and Geoenvironment Protection, Chengdu University of Technology



Geotechnical Centrifuge Laboratory and Shaking Table Apparatus

We Are HIRING

SKLGP Positions Available!

Join the world first-class laboratory for geohazards!

It is more than a career.

Position:

* Scientific researcher
* Post doctor
* Professors, Associate Professors, Assistant Professors.
* Science Fund Program for Excellent Young Scientists (Overseas)
* National High-level Talent Recruitment Programs

Subjects: Geotechnical, Geology Engineering, Civil engineering, Geoscience, Remote sensing/GIS and all related subjects.

Basic Salary: 180,000–800,000 RMB per year

Additional benefits: settling-in allowance (150,000–500,000 RMB), research start-up funds (80,000–500,000 RMB), exceeding Expectations Bonus (depend on the research achievement, publications and etc.), national funding application (100,000–3,000,000 RMB), free accommodation

Research areas:

1. Evaluation and Prevention of Major Geohazards
2. Interaction between Human Activities and Geoenvironment and Disaster Mitigation
3. Regional Geoenvironment Evaluation and Protection
4. Geohazard Monitoring and Early Warning and Information Technology

How to apply:

The application should include:

1. a long-term CV that includes publications and research achievements,
2. 1–2 pages statement summarizing your expertise and present/future career goals,
3. names and contact details of two references.

The full application package should be sent electronically as a PDF document to:

Email: sklgp_cdut@126.com

Address: State Key laboratory of Geohazard Prevention and Geo-environment Protection, Sichuan, China

Don't hesitate to contact us for more details!

Tel: +86 84073193

Email: sklgp_cdut@126.com

iRALL School 2024

13th October to 27th October, 2024

"iRALL" The International Research Association on Large Landslides, is an international non-governmental, non-political, non-profit-making and unaffiliated institution for the promotion of knowledge about large landslides founded on 11 November 2015. The scientific committee consists of international experts in the field of large landslides. The secretariat of iRALL is located at the State Key Laboratory of Geohazard Prevention and Geoenvironment Protection (SKLGP), Chengdu University of Technology, Chengdu, China.

The objectives of iRALL are to promote:

- Cooperation and exchange of knowledge among scientists and engineers working on large landslides
- The dissemination of scientific knowledge of large landslides
- The mitigation of risks associated with large landslides and their consequences

Courses in the iRALL School 2024:

Module 1: Occurrence and mechanism of large landslides

Module 2: Field investigation and geophysical survey of large landslides

Module 3: Remote sensing and AI technology application of large landslides

Module 4: Numerical modelling of large landslide

Module 5: Risk analysis, prevention and mitigation for large landslides

Module 6: Co-seismic landslides and hazard-chain

Field excursion

Application and registration

The iRALL School is opened for 20 PhD students and for a maximum of 10 doctors/postdocs who have obtained their PhD degree not earlier than 2019.

Please click the following linkage to apply online. http://irall.sklgp.cdut.edu.cn/Application.htm

The deadline for applications is July 31st, 2024 and selection of participants will be announced by August 20th, 2024.



2023 iRALL School 2023

The First International Conference on Smart Informatics and Multi-hazard Reduction (SIMR 2024)

We are pleased to announce that the First International Conference of the Global Partnership for Smart Informatics and Multi-hazard Reduction (SIMR 2024) **will be held at Loughborough University, the United Kingdom, September 15–19, 2024.**

SIMR 2024 will create a multi-disciplinary forum for academic researchers and professionals to share research and practical experiences in developing and implementing multi-faceted approaches to address the global challenges created by increasing multi-hazard risk and climate change in a fast-changing world. It aims to foster international and interdisciplinary collaboration to advance scientific research and practice in harnessing data and informatics technologies to understand, assess and manage hazard risk for disaster risk reduction to achieve long-term resilience. This First SIMR conference will not only provide a platform for networking, skill development and information exchange, but more importantly, act as a catalyst for shaping the further development of smart informatics and multi-hazard risk reduction. Contributions from all relevant science, engineering, social and humanity disciplines are welcome.

In addition to scientific sessions, SIMR 2024 will offer training courses where participants can learn the latest high-performance hazard modelling and risk assessment skills. The conference will also include a field trip to the Peak District and enjoy the English countryside scenery.

15 Sep	16 Sep	17 Sep	18 Sep	19 Sep
Registration and Training courses	Opening Ceremony and Sessions	Sessions and Conference Dinner	Sessions	Field Trip

Organizers

- UNESCO Chair in Informatics and Multi-hazard Risk Reduction (IMRR), Loughborough University, UK
- State Key Laboratory of Geohazard Prevention and Geoenvironment Protection, Chengdu University of Technology, China
- School of Water Conservancy and Transportation, Zhengzhou University, China

Smart Informatics and Multi-hazard Reduction

GEODATA and AI

an up-coming high-impact Journal by Elsevier

Affiliated with The State Key Laboratory of Geohazard Prevention and Geoenvironment Protection (SKLGP)

Editor-in-chief	Kok-Kwang Phoon
Editors	Jianye Ching and Xuanmei Fan
Special editor	Limin Zhang
Managing editors	Zi-Jun Cao and Chong Tang

Aims and Scope:

Geodata and AI is an international journal that is focused on the development of machine learning and artificial intelligence for scientific discovery in geo-disciplines (research) and creation of novel digital service over the life cycle of natural or engineered geo-systems (practice). Geo-disciplines include geotechnical engineering, rock engineering, earthquake engineering, engineering geology, mining, geophysics, and geo-hazard. Geodata can be broadly defined as data produced by the characterization of the constituent ground and observation of the processes emerging from these disciplines. The heterogeneous spatial/temporal features and complex sampling characteristics (multi-source, uncertain, sparse, incomplete, potentially corrupted) of geodata are common in these disciplines with potential for data fusion. They are pivotal to the training of machine learning and artificial intelligence that are transformative business drivers when combined with other digital technologies.

The objectives of this international journal are to advance geodata science to address the challenges posed by geodata intrinsic and sampled features, to promote the compilation and sharing of geo-databases, to develop novel machine learning and artificial intelligence methods that are of significant value or even indispensable to actual projects, to establish benchmarks for competitive evaluation of algorithms, and to solve complex challenges such as risk

and resilience related to geo-disciplines. All aspects of a geodata-centric agenda that can transform research and/or practice are of interest:

- Geodata science
- Geo-databases
- Data fusion
- Physics-informed machine learning
- Data-driven site characterization
- Machine learning guided observational method
- Benchmarking
- Data-informed risk and resilience
- Trustworthy/explainable/interpretable AI
- Human-machine teaming
- Autonomous construction
- Smart infrastructure
- Building Information Modelling/Digital twin
- Privacy enhancing technologies

Timeline for Vol. 1, Issue 1

Submission of full paper: 1 Sep 2024
Final decision: 1 Feb 2025
Publication: Mar 2025

Please submit by email to Prof. Zijun Cao (zijuncao@swjtu.edu.cn) or Chong Tang (ceetc@dlut.edu.cn)

For more information, please contact the same email address.

Department of Civil Engineering, National Taiwan University

Department of Civil Engineering, National Taiwan University

Introduction

National Taiwan University (NTU) was originally established in 1928, when Taiwan was under Japanese rule, as Taihoku Imperial University. The current name dates back to 1945. As Taiwan's oldest and most prestigious university, we are also the largest comprehensive higher education institution (HEI) in the country. The academic freedom that we cherish and our excellent faculties attract both domestic and international students. Throughout our 90-year history, we have nurtured many talents, including leading academics and leaders in the public and private sectors. Our campus is vast, and spans across multiple locations, including Taipei, Yilan, Hsinchu, Yunlin, and mountainous areas in central Taiwan—accounting for nearly 1% of Taiwan's total land area. This provides teachers and students with an environment rich in biological and ecological diversity.

As the leading university in Taiwan, we are strongly committed to social responsibility as we strive to drive sustainable development and influence positive change in society. This was also reflected in the first University Impact Rankings launched in 2019 by Times Higher Education (THE), which measure the contributions of HEIs to the United Nations' Sustainable Development Goals (SDGs). We were ranked 70th in the world overall, and 1st in the world for SDG16: Peace, Justice, and Strong Institutions. Starting from creating a sustainable culture on campus, we aim awareness about sustainability throughout the university, through innovative teaching and research, environmental protection and recycling efforts, and a school administration that supports equality and wellbeing. Our sustainability efforts extend beyond our campus through industry-academia collaborations and service teams deployed to remote areas. In the near future, we will continue to reinforce the spirit of innovation and sustainability thinking among all faculty members and students. We will also continue our efforts to address economic, environmental, and social challenges through interdisciplinary collaboration, as we create connections between the local and the international community. The Department of Civil Engineering (Fig. A.13) can be regarded as the root of The College of Engineering. The early civil engineering education covers a wide range of professions. With the development and differentiation of various social industries, some fields have gradually separated and established specialized departments. We have also moved on, combining different fields and top-notch technology to remain as the leader of the tide.

Civil engineering is inseparable from the development of human civilization. From the beginning of civilization, all man-made structures have enchased and highlighted the value of civil engineering. NTU Civil Engineering is no exception. From the Department of Civil Engineering of the Imperial College of Taipei to the National Taiwan University Department of Civil Engineering today, the majority of Taiwan's significant constructions is and will always be our finest gallery.

In National Taiwan University, you will obtain high-quality guidance in and out of the classroom. Academic resources in the classroom and sports culture clubs, various student activities throughout the year, will bind you together with peers of the same dream. These friends may also be partners that can help you in future careers. If you are willing to take civil engineering as a career and take on the challenges and step forward as a team, then listen to your inner call, join us, and let us stride ahead hand in hand (Fig. A.14).

Department of Civil Engineering, National Taiwan University
Department of Civil Engineering, National Taiwan University, Taipei, Taiwan
e-mail: louisge@ntu.edu.tw

© The Author(s) 2025

B. Abolmasov et al. (eds.), *Progress in Landslide Research and Technology, Volume 3 Issue 2, 2024*, Progress in Landslide Research and Technology, https://doi.org/10.1007/978-3-031-72736-8



Fig. A.13 Quick facts of the Department of Civil Engineering



Fig. A.14 Life beyond Classroom

Outstanding Recent Achievements

Mitigating the Impacts of Natural Disasters via Cutting Edge Technology

Taiwan is located in the Circum-Pacific seismic belt, with many active faults and frequent typhoons. Due to the effects of climate change, extreme rainfall events that used to occur once in a century are now becoming more frequent, exacerbating the threat of landslides and debris flows. The prevention and mitigation of natural disasters such as earthquakes and flooding have therefore become a priority for the twenty-first century.

(a) **Earthquake Early Warning Systems: gain valuable response time**

For most natural disasters, potential losses to life and property can be mitigated through early warning and prevention. After the earthquake disaster of September 21st, 1999, building safety inspections needed to be conducted all across Taiwan. Our faculty and students with expertise in civil engineering and geology were quick to respond to this urgency, working closely with the National Center for Research on Earthquake Engineering to help the government improve the earthquake resistance standards and test specifications.



Fig. A.15 Taiwan Earthquake Loss Estimation System (TELES)

Moreover, they proposed a more elaborate system for earthquake damage and liquefaction assessment, and conducted a complete review and classification of the earthquake risk tolerance for all areas in Taiwan. The team also developed new disaster prevention technologies. One of the most significant contributions was to assist the public high (vocational) schools around Taiwan with assessments of the earthquake resistance and reinforcement needs of old buildings. In the numerous earthquakes that have since occurred, the effect of these reinforcements has become apparent. The stronger earthquake resistance of these buildings has improved safety for 2.65 million teachers and students around Taiwan (Fig. A.15).

Our school has also developed technology to monitor the status of bridges with high traffic volumes. This optical fiber monitoring system will emit a warning whenever poor conditions are recorded, prompting an early response from management that can prevent a disaster from happening. When bridges in remote areas are damaged, a lightweight bridge developed by NTU out of composite materials can be assembled by residents in short time. In this way, access to affected areas can be quickly restored, and disaster relief provided more efficiently. In the event of an earthquake, Taiwan's citizens will immediately receive an emergency alert by text message. This warning system, which was developed by Professor Wu, Yih-Min at our Department of Geosciences, analyzes the properties of a P-wave within 3 s after detecting the wave so that it can issue an alert to citizens more than 10 s before the S-wave, which is most likely to cause damage arrives. This early warning system is accurate and fast, giving people valuable seconds to escape to safety. Because it is also much cheaper to manufacture network of multiple sites has been established, including the geohazard field test site for the Majiagou landslide, Zigui County, and systematic geophysical monitoring station for the whole TGR area, etc. than previous seismographs, it could be rapidly rolled out to several hundred elementary and junior high schools, ensuring better protection of our country's younger generation. Moreover, this system has been successfully introduced in other earthquake-threatened countries, such as Indonesia, India, Vietnam, Nepal, and Mexico.

(b) **After the Flood: Rapid Mobilization and Improved Ability to Provide Relief**

Another critical area is flood disaster prevention. Also here, our faculty and students are actively involved in key activities ranging from early warning and response during the disaster, to raising the awareness of, and capability for, disaster prevention among citizens more generally. Our Center for Weather Climate and Disaster Research comprises experts in meteorology, hydrology, bioenvironmental engineering, and geology etc. This center helped New Taipei City and Keelung City establish an extreme weather and flood monitoring and warning system. Other projects include combining advanced deep learning with the analysis of radar data, which allows for closer monitoring of rainfall data in hydrologically sensitive areas. The improvement of flood models increases the accuracy of flood warnings and provides disaster prevention units with valuable information for them to rapidly formulate response strategies. From past experiences outside of Taiwan, we know that self-help and mutual support account for the largest share of the relief effort (90%) in the event of a disaster. In other words, even if flood warnings are effective, people in the affected area still need to be able to take own measures to protect themselves. At NTU, we actively participate in the community-level disaster relief preparations around the country, as well as in the training of disaster relief officers. Our experts provide citizens with the most up-to-date knowledge in disaster prevention, operate independent disaster relief systems, and evaluate the safety of shelters. These efforts contribute to the resilience and ability of local communities to mitigate impact, helping them recover more quickly. A plan for how to improve the disaster relief ability in the country proposed by our experts is another example of how we help make sure that the best disaster response capacity is in place. After improving the ability to respond to disasters, NTU's team also contributed to disaster prevention infrastructure around Taiwan, such as seismic isolation technology for buildings and equipment, or detention ponds in communities at risk. Our work and efforts in these areas help protect lives and property. As climate change continues to impact the world, we hope to leverage our technologies and expertise in these domains even further, and help strengthen the capacity to prevent and withstand natural disasters throughout the world.



Institute of Cold Regions Science and Engineering, Northeast Forestry University

Wei Shan and Ying Guo

Introduction

Institute of Cold Regions Science and Engineering of Northeast Forestry University (ICRSE-NEFU) is committed to the environmental geology and engineering geology of high latitude permafrost region and deep seasonal frozen area under the background of climate change, and attaches importance to the combination of basic research and applied research. With undergraduate, master, doctor, postdoctoral professional training system and standards, ICRSE-NEFU initiated "Geological environment risk research plan for permafrost degraded areas in Northeast China (GERRP)". With the support of the Chinese government, "Field scientific observation and research station of the Ministry of Education—Geological environment system of permafrost area in Northeast China (FSSE-PFNEC)" was established. Its observation stations cover all kinds of permafrost areas in Northeast China. At the same time, in order to develop and transfer technologies related to environmental governance and infrastructure construction in permafrost regions, "Provincial Collaborative Innovation Centre, Environment and road construction & maintenance in permafrost area of Northeast China (PCIC-PFER)" was established. Over the years, ICRSE-NEFU have continuously established cooperation with academic institutions and organizations at home and abroad, held various academic exchanges and regularly held "Academic Seminar on Engineering Geology and Environmental Geology in the Permafrost Along the Sino-Russian-Mongolian Economic Corridor", edited and published research cases of geoenvironmental disasters in permafrost regions in Northeast China, and shared the research results of GERRP. At present, the research results of GERRP are gradually enriched, some of them have highly academic value, and have been put into engineering practice. ICRSE-NEFU has gradually shown its unique research charm since it became an ICL member in 2002. In 2012, ICRSE-NEFU established a landslide research network in cold regions (ICL-CRLN), and then Research Center of Cold Regions Landslide was built.

Permafrost as one of the elements of the cryosphere, the change of thermodynamic stability of permafrost will directly affect the changes of hydrosphere, biosphere and lithosphere. Under the trend of global warming, the frequency and intensity of environmental and engineering geological disasters caused by permafrost degradation are getting higher and higher (Figs. A.16 and A.17). Taking the cold area in the southern boundary of the permafrost zone in Northeast China as study area, disasters such as ground subsidence, slope icing, landslides and other disasters caused by permafrost melting were studied. At the same time, we found melting permafrost also leads to seasonally high concentrations of greenhouse gases, triggering wildfires that may further accelerate permafrost degradation and environmental changes of terrestrial ecosystems and roads.

W. Shan · Y. Guo
Institute of Cold Regions Science and Engineering Northeast Forestry University, Harbin, China
e-mail: shanwei456@163.com

© The Author(s) 2025

B. Abolmasov et al. (eds.), *Progress in Landslide Research and Technology, Volume 3 Issue 2, 2024*, Progress in Landslide Research and Technology, https://doi.org/10.1007/978-3-031-72736-8

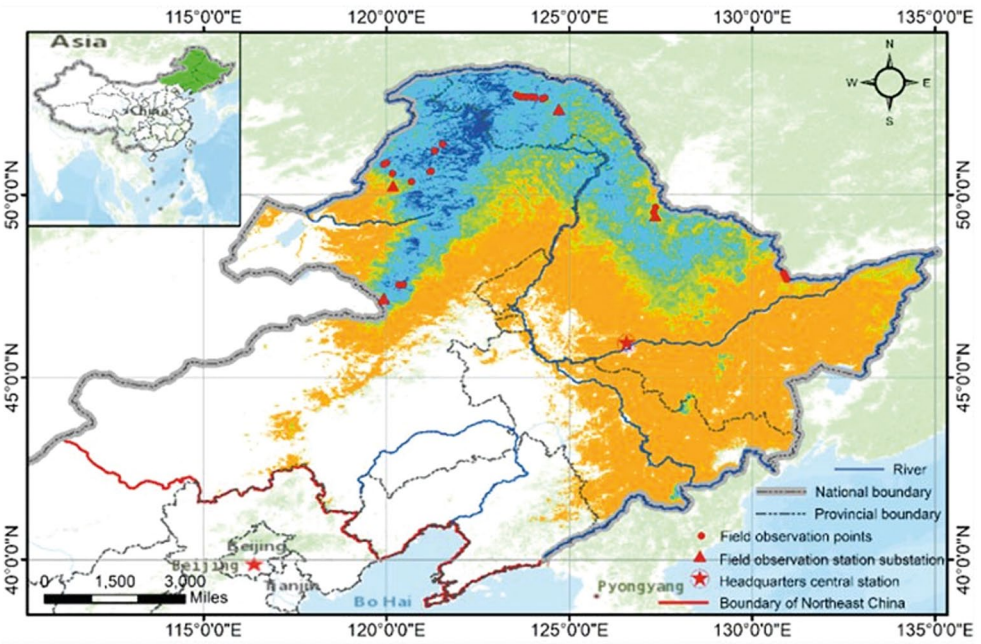


Fig. A.16 Permafrost distribution in NE of China (2014–2019)

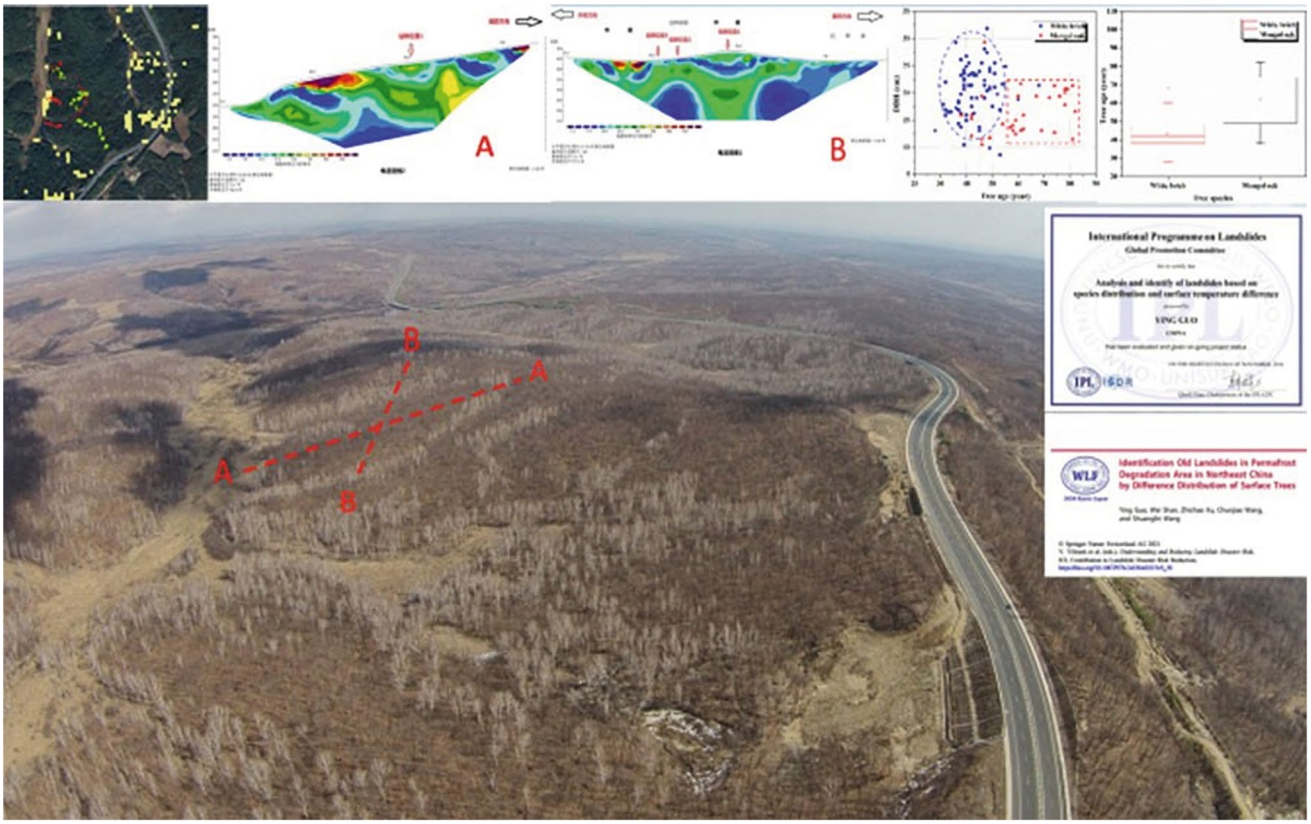


Fig. A.17 Different tree species and ages in the landslide area caused by permafrost degradation

Marui & Co. Ltd.

Taketoshi Marui and Yuji Ikari

Introduction

Marui & Co. Ltd. celebrated its 100th anniversary in 2020. Marui, as one of the leading manufacturers of testing apparatuses in Japan, has constantly been striving further to improve its service since its foundation in 1920, thus contributing to the sustainable development of our nation and society. Our main products cover various destructive and non-destructive testing apparatuses in geotechnical engineering, concrete engineering (mortar, aggregates, etc.), and ceramic engineering (Fig. A.18). Of particular note is that Marui has been helping manufacture ring-shear apparatuses (Fig. A.19) for the past half-century based on the leading-edge idea of Dr. Kyoji Sassa, Professor Emeritus at Kyoto University. Marui has delivered seven ring-shear apparatuses to the Disaster Prevention Research Institute, Kyoto University, and two to the International Consortium on Landslides. Also, the apparatuses were exported to the United States of America, China, Croatia, and Vietnam.

Since 2002, Marui has been a supporter of the International Consortium on Landslides (ICL) and has gradually been intensifying its contribution to the ICL's worldwide efforts for landslide risk reduction and international promotion of landslide research. According to NASA, more frequent and intense rainfall events due to climate change have been causing frequent landslides, particularly in mountains of Asian regions, including Japan, where waters can be stored in various ways. Summer monsoon rains, snow and glacier melt waters can destabilize steep mountainsides, triggering landslides, which are down-slope movements of rocks, soils, water, trees, etc. Marui, as an engineering supporter, commits deeply to various activities of research, particularly on triggering mechanisms of landslides.

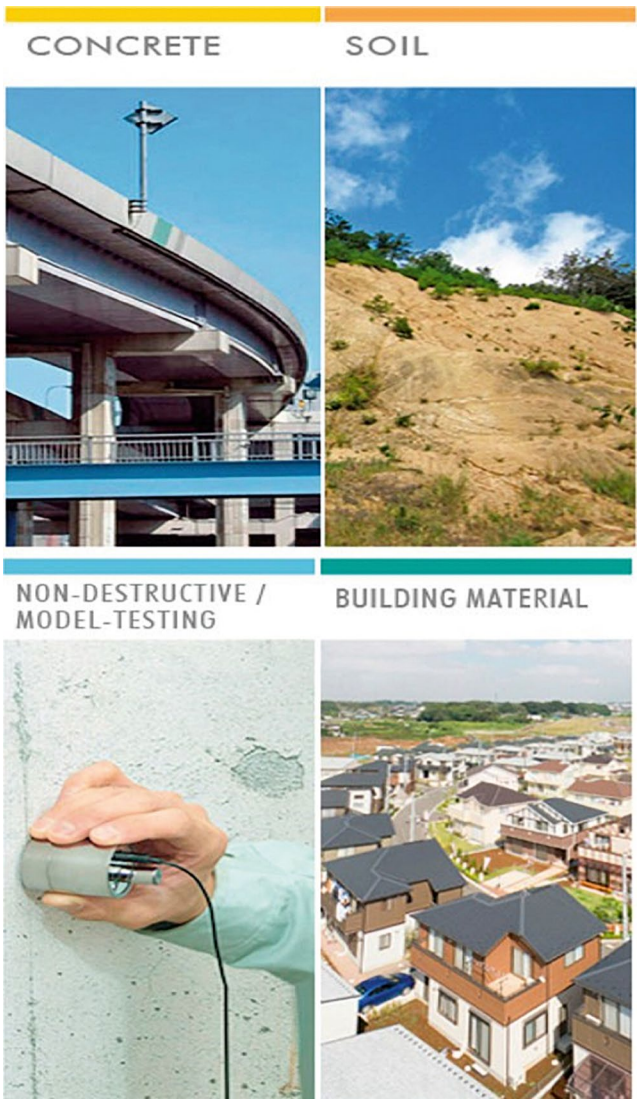


Fig. A.18 Products of testing apparatus such as non-destructive/model-testing for measuring intensity, physical property, durability, etc. for concrete, soil, building material, etc.

T. Marui · Y. Ikari
Marui & Co. Ltd., Osaka, Japan
e-mail: hp-mail@marui-group.co.jp;
http://marui-group.co.jp/en/index.html

© The Author(s) 2025

B. Abolmasov et al. (eds.), *Progress in Landslide Research and Technology, Volume 3 Issue 2, 2024*, Progress in Landslide Research and Technology, https://doi.org/10.1007/978-3-031-72736-8

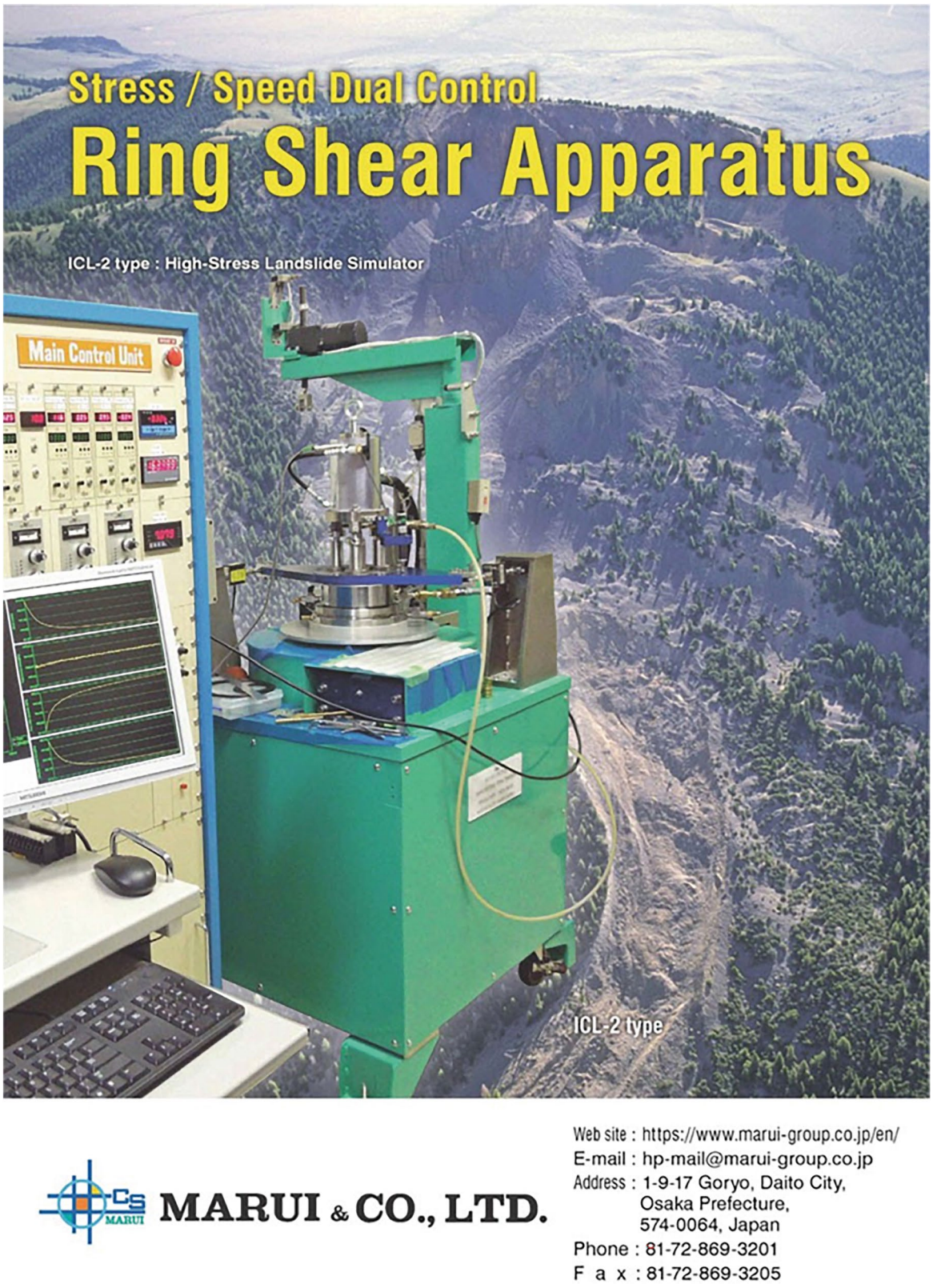


Fig. A.19 High-stress landslide simulator

In addition to the ring-shear apparatuses mentioned above, our company develops and sells soil and ground testing equipment. For example, our standard cyclic triaxial testing machine (Fig. A.20) is used by geological consultants, research laboratories, and educational institutions such as universities and technical colleges. Ground destruction phenomena, which often occur concurrently with earthquakes, significantly affect the seismic resistance of superstructures.



Compliant standards	JGS 0541 / JGS 0542
Dynamic vertical load	Pneumatic servo system: 1 kN
Static vertical load	Servo motor method: 5 kN
Side pressure load	Air regulator method: 1 MPa
Back pressure load	Air regulator method: 0.5 MPa
Dynamic control method	Load/displacement control: 0.05 to 1.0 Hz
Static control method	Displacement control: 0.005 to 5.0 mm/min
Three-axis room	・ Three-pillar fixed system ・ Specimen size: φ50 × H 100 mm
Measurement	・ Axial pressure (external): 5 kN ・ Axial pressure (internal): 1 kN ・ External displacement: 25 mm ・ Internal displacement: ± 2 mm x 2 ・ Side pressure: 1 MPa ・ Pore pressure: 1 MPa ・ Volume change: 50 cc

Fig. A.20 Cyclic triaxial testing machine

Cyclic triaxial tests are used to determine the constants required to judge the liquefaction potential and to determine the cyclic deformation characteristics of the ground required for seismic response analysis.

This equipment can perform not only liquefaction and deformation tests, but also static triaxial tests, isotropic consolidation tests, and anisotropic consolidation tests.

In addition, control and data recording can be processed entirely on a personal computer.

Marui & Co. Ltd. takes great pleasure in developing, manufacturing, and providing new products of high value, sharing the sense of s achievement with our customers and thus contributing to social development. The entire staff of Marui is determined to devote ceaseless effort to keep its organization optimized for its speedy and high-quality services, by the motto “Creativity and Revolution,” and strive hard to take a step further as a leading manufacturer of testing apparatuses, to answer our customer’s expectations for the twenty-second century to come.

Marui continuously contributes to the 2030 Agenda for Sustainable Development and the Sendai Framework for Disaster Risk Reduction 2015–2030. In line with this, Marui signed KLC2020 in 2019 and will strongly support its actions, especially KCL2020 Actions 3,4,5, and 9.

Nippon Koei Co., Ltd., Geohazard Management Division

Hiroaki Tauchi

Introduction

The Nippon Koei Group (NK) has been a leading international consultant providing engineering consulting services to over 5500 multi-disciplinary infrastructure and development projects in 160 countries worldwide. The landslide prevention specialist team (now called Geohazard Management Division) was established in 1966 to provide countermeasures against sediment disasters. Over the last 50 years, we have significantly improved the capacity of countries to respond and reduce risk from debris flows, slope instabilities, landslides, avalanches, and rock falls due to torrential rains, large-scale earthquakes, and volcanic eruptions that threaten a country's vital economic infrastructure lifelines, especially the road networks. At present, approximately 160 engineers provide a variety of technical consulting services to protect communities from disasters, as shown in Fig. A.21.

During disasters, we utilize remote sensing technologies such as 3D point clouds and interferometric SAR to create 3D models and gather surface and damage information to conduct a broad area survey, as shown in Fig. A.22. Based on this information, we provide experienced professional engineers to assess risk quickly and promptly respond with engineering design analyses and emergency and permanent measures based on our extensive experience and know-how. In order to efficiently plan and design disaster countermeasure works, we have implemented the automated design using visual programming. This automated design enables us to perform the 3D design of countermeasures quickly and calculate project costs, streamlining the overall process. Organizing design and construction information in 3D facilitates the construction process and allows for permanent maintenance by passing it on to the maintenance management phase as BIM (Building Information Modeling). As a result, the information necessary for effective maintenance is readily available and can be utilized throughout the project's lifespan.

H. Tauchi
Geohazard Management Division, Nippon Koei Co., Ltd., Tokyo, Japan

To maximize the effectiveness of infrastructures, we address efficient countermeasure plans, design, and research regarding cost reduction and cost-effectiveness using various numerical analyses such as the finite element method (FEM) and discrete element method (DEM), etc.

With climate change, the scale of disasters is enlarged and the frequency of disasters is increasing. This has resulted in more severe damage in more widespread and more urbanized areas, and more diverse and higher risks of disasters. In addition, in response to the SDG concept of "leaving no one behind," developing countries are lagging behind in hazard zoning and other efforts, which must be resolved. For this reason, NKG believes that it is important to assume that multiple types of disasters, such as floods, landslides and tsunamis, occur at the same time and in the same place. NKG provides risk mapping services using multi-hazard analysis as shown in Fig. A.23.

In Japan, we have worked hard to restore and recover from sediment-related disasters caused by earthquakes and heavy rainfalls that have frequently occurred in recent years (the 2011 Great East Japan Earthquake, the Northern Kyushu Flood in 2017, etc.). We have received letters of appreciation from national and local governments for our efforts.

Our major international projects include "The Project for Countermeasure Construction Against the Landslides on Sindhuli Road Section II, Nepal," "The project for the rehabilitation of Sindhuli road affected by the 2015 Gorkha Earthquake, Nepal," and "The project for landslide prevention for National Road 6 in Honduras"; all funded by the Japan International Cooperation Agency (JICA) grantsin-aid. Through these projects, we are contributing to the socio-economic development of each country by improving vulnerable locations in road networks against sediment disasters, promoting traffic safety, and providing logistics assistance for road users. In particular, the first of the three NK's projects mentioned above won the "3rd JAPAN Construction International Award" from the Ministry of Land, Infrastructure, Transport and Tourism as the project that has realized "high-quality infrastructures" through its excellent know-how, technical capabilities, and project management capabilities.

NK is an ICL member using its technology to reduce geohazard risk. Through various projects, NK continu-

© The Author(s) 2025

B. Abolmasov et al. (eds.), *Progress in Landslide Research and Technology, Volume 3 Issue 2, 2024*, Progress in Landslide Research and Technology, https://doi.org/10.1007/978-3-031-72736-8

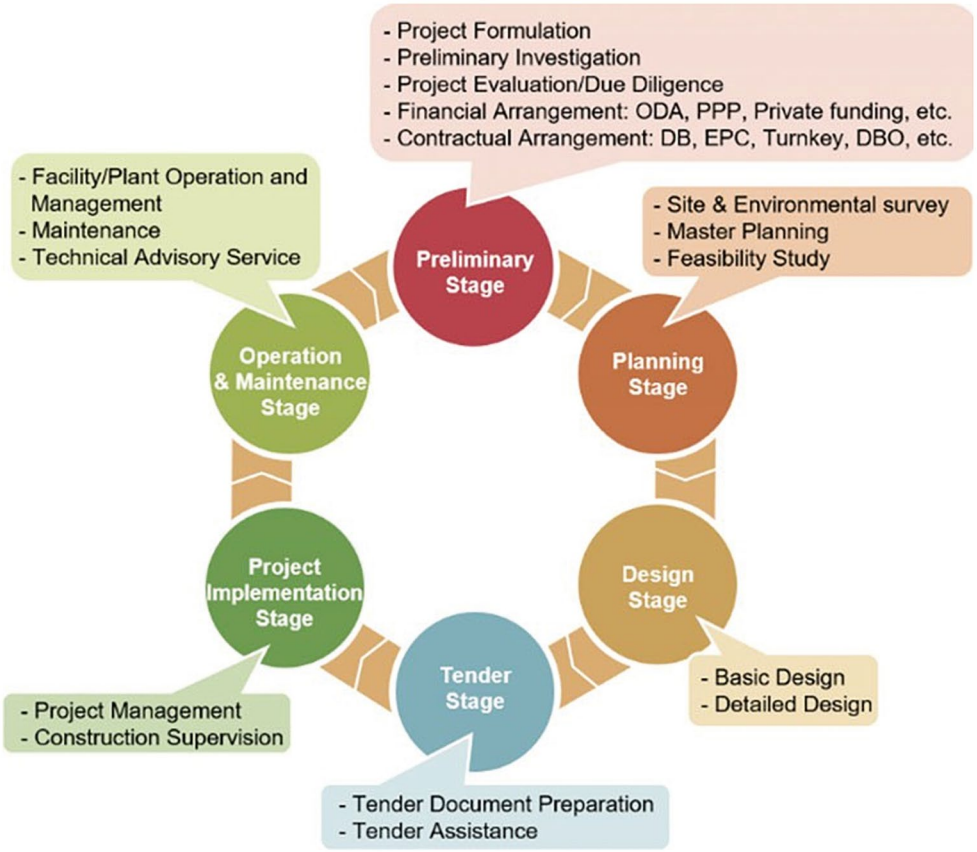


Fig. A.21 Our service for geohazard management



Fig. A.22 (Left) A landslide site, (Right) 3D point clouds

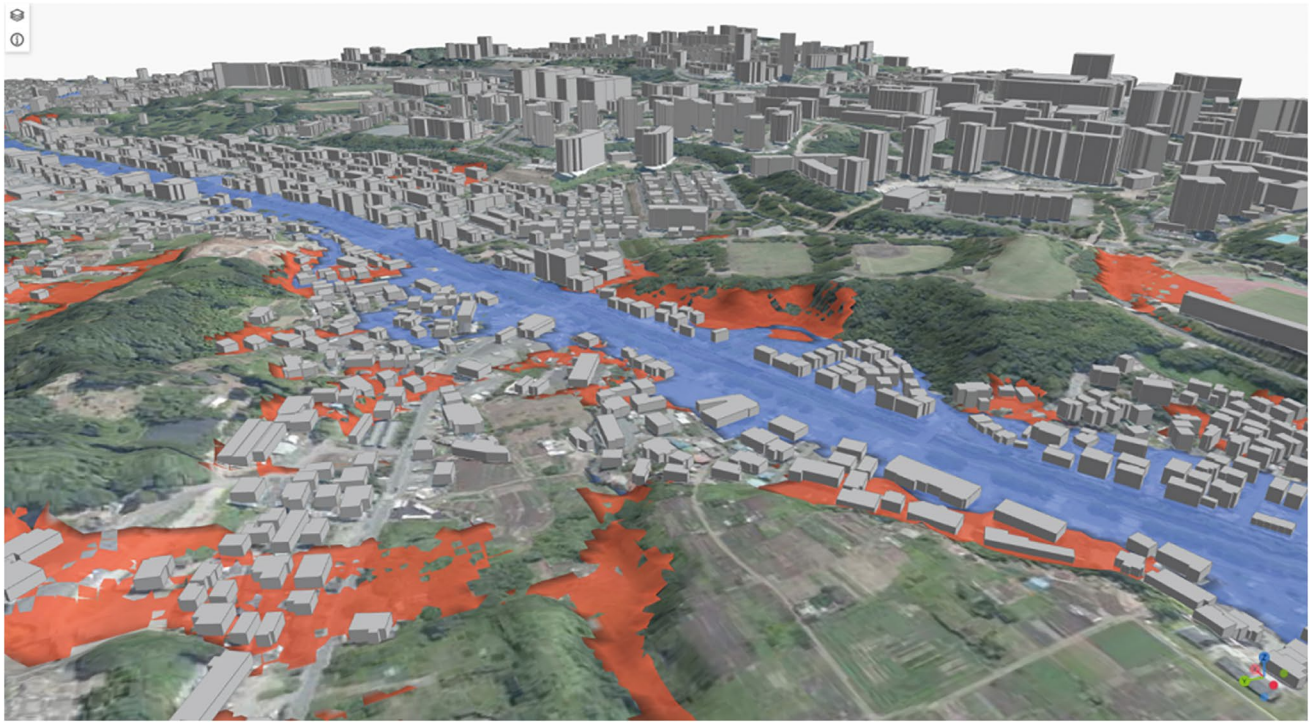


Fig. A.23 Visual programming and Automated design

ously contributes to the 2030 Agenda for Sustainable Development and the Sendai Framework for Disaster Reduction 2015–2030. Using our full capability with abundant experiences in Japan and Asia prone to natural disasters, we hope to contribute much more to reducing global sediment disasters, including landslides (Fig. A.24). In line with this, NK has signed the KLC 2020 and will strongly support its actions.

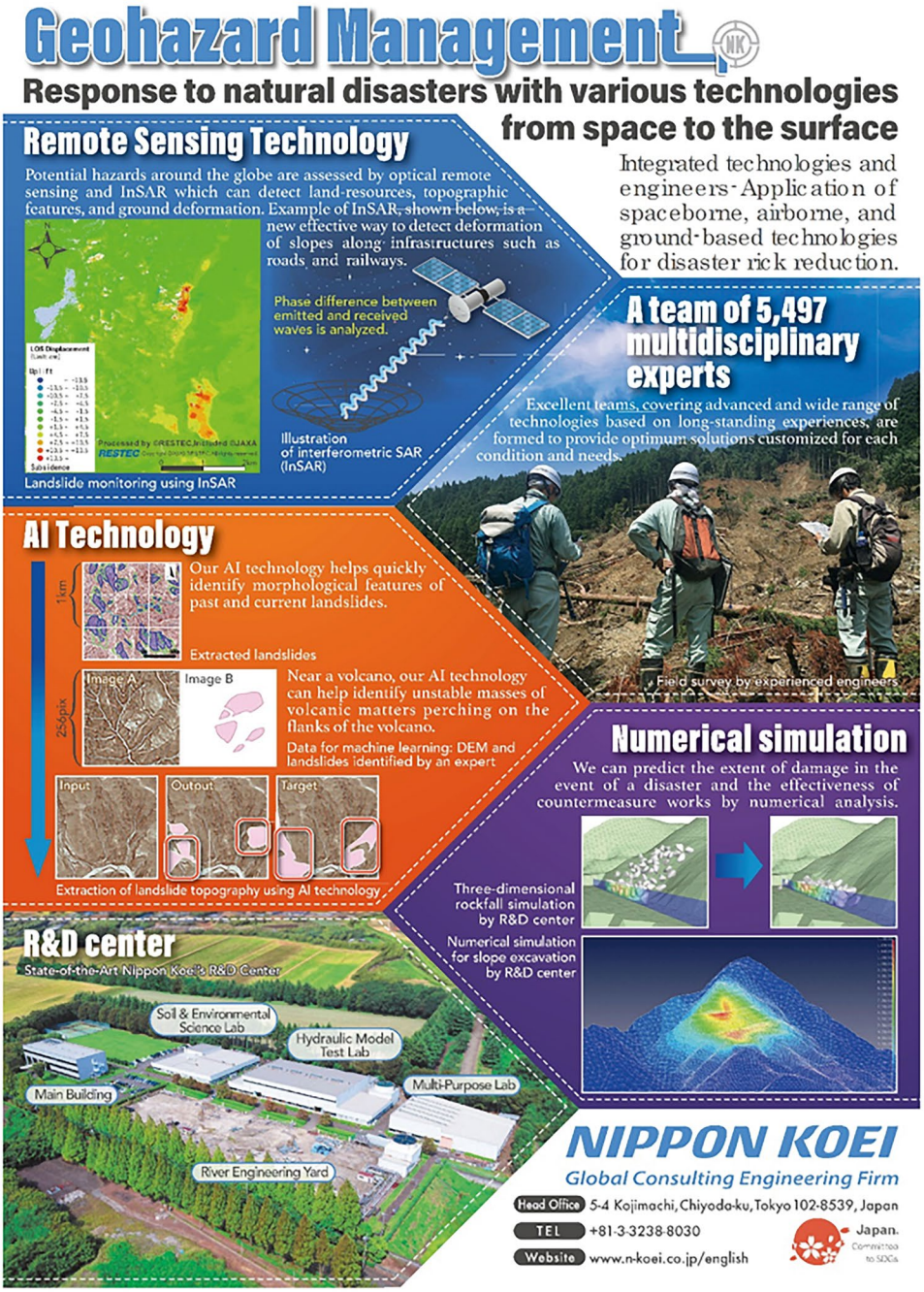


Fig. A.24 Introduction of our survey analysis technology for geohazard

Ellegi Srl



Ellegi Srl

Introduction

Ellegi srl provides worldwide monitoring services and produces Ground Based synthetic aperture radar (GBInsAR) for remote measurement of displacements and deformations on natural hazards and manmade buildings using its own designed and patented LiSALab system.

Its activities started in 2003 as a spin off project to exploit commercially the Ground Based Linear Synthetic Aperture Radars technology developed by European Commission's Ispra Joint Research Centre and based on the results of more than 10 years of research. Since then, Ellegi has industrialized and developed the core technology of the LiSALab system and latest LiSAmobile system represents the fifth generation of development.

In 2003 it was the first commercial company in the world to provide GBInSAR measurements of natural hazards and structure (Figs. A.25 and A.26).

Ellegi srl offers:

- Displacement fields measurement, control and monitoring of the deformation caused by natural hazards, like landslides, rockslides, sinkhole, volcanic deformation in every operative condition, including emergencies,
- Structural strain fields measurement, control, monitoring and diagnosis of the deformation affecting buildings, bridges, viaducts, dams.
- GBInSAR monitoring systems, installation, management and maintenance in order to provide information about natural hazards or anthropic activity, that can generate or cause slopes failures or buildings instabilities.

In all the above-mentioned activities Ellegi srl uses the GBInSAR LiSALab technology that represents a real "break-through".

E. Srl
Como, Italy

© The Author(s) 2025

B. Abolmasov et al. (eds.), *Progress in Landslide Research and Technology, Volume 3 Issue 2, 2024*, Progress in Landslide Research and Technology, https://doi.org/10.1007/978-3-031-72736-8

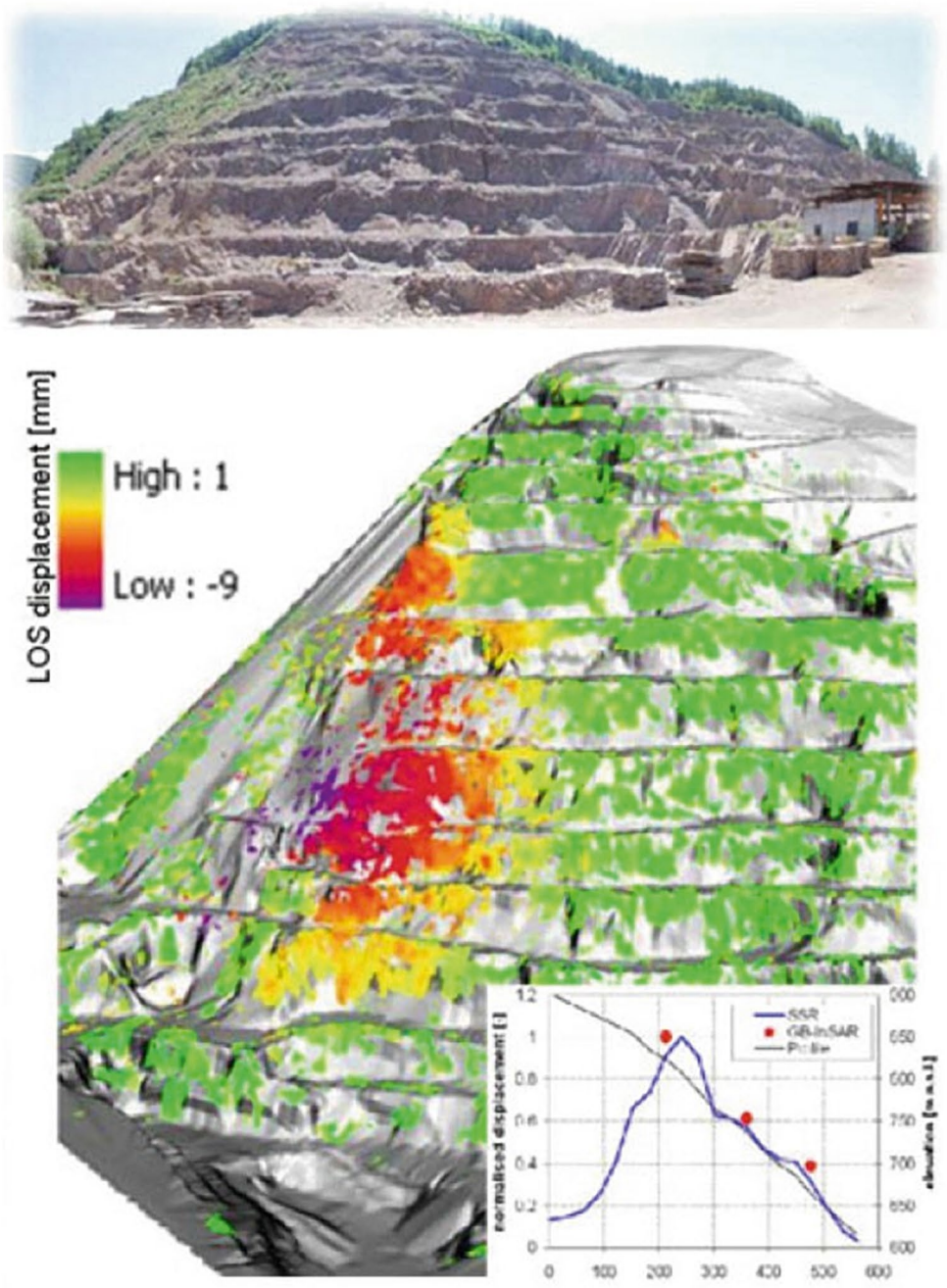


Fig. A.25 GBInSAR LiSALab technology quarry monitoring example and displacements' field comparison between the GBInSAR measurement and FEM model results

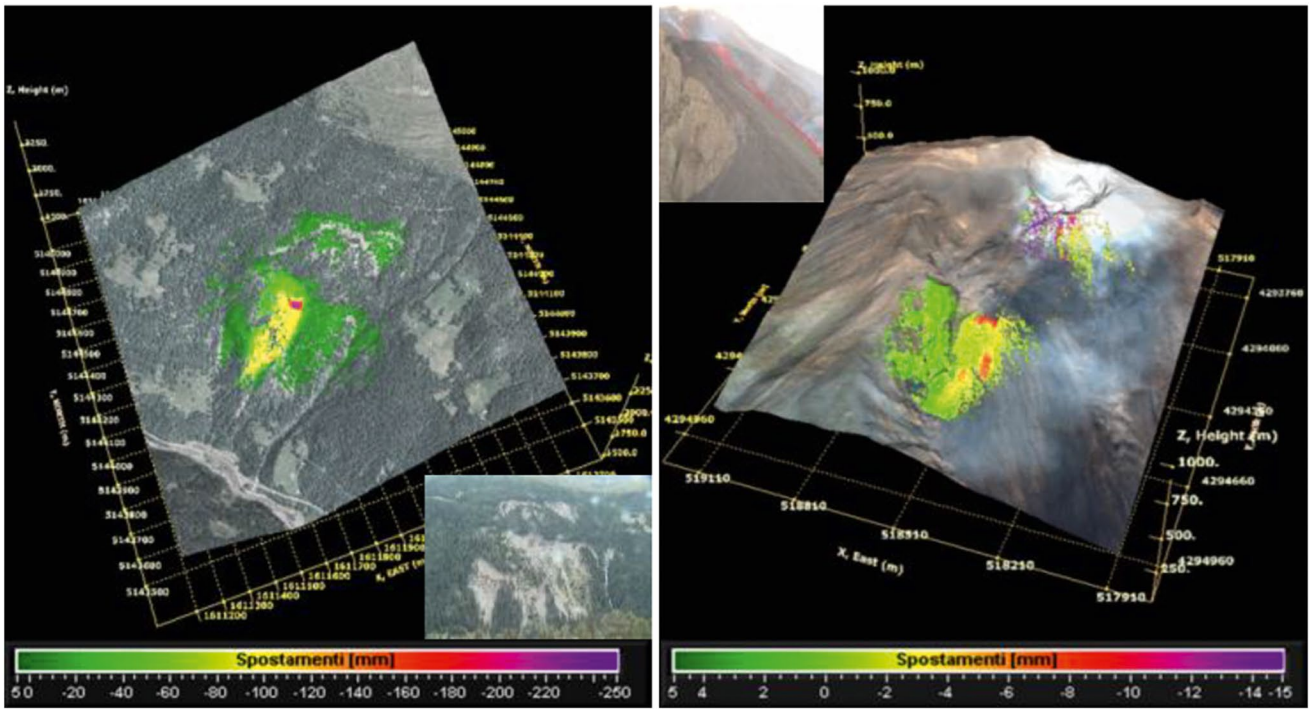


Fig. A.26 GBInSAR LiSALab technology result in monitoring a slope affected by a landslide (left) and a volcanic slope affected by deformation (right). Landslide or moving area mapping and boundaries identification is made easy by GBInSAR LiSALab technology

Chuo Kaihatsu Corporation

Lin Wang

Introduction

Chuo Kaihatsu Corporation (CKC) was founded in 1946, and has been aiming to become the "Only One" consultant for our customers. We engage in the hands-on work that will "Remain with the earth, Remain in people's hearts, and Lead to a prosperous future". We focus on road, river and dam engineering to flesh out industrial infrastructures specifically by means of geophysical/geotechnical/geological investigations, civil engineering surveys and project implementations. In recent years, we make significant efforts on earthquake disaster mitigation, sediment disaster prevention/mitigation and ICT information services. Many achievements of ours have already contributed to the mitigation of natural disasters such as landslides, earthquakes and slope failures in Japan, Asia and the Pacific Region. We aim to provide technological contributions so that a sustainable society will continue to develop in the future (Figs. A.27, A.28, A.29 and A.30).



Fig. A.27 Design for various structures

L. Wang
Chuo Kaihatsu Corporation, Tokyo, Japan
e-mail: wang@ckcnet.co.jp; https://www.ckcnet.co.jp/global;
https://www.ckcnet.co.jp/contactus/

© The Author(s) 2025

B. Abolmasov et al. (eds.), *Progress in Landslide Research and Technology, Volume 3 Issue 2, 2024*, Progress in Landslide Research and Technology, https://doi.org/10.1007/978-3-031-72736-8



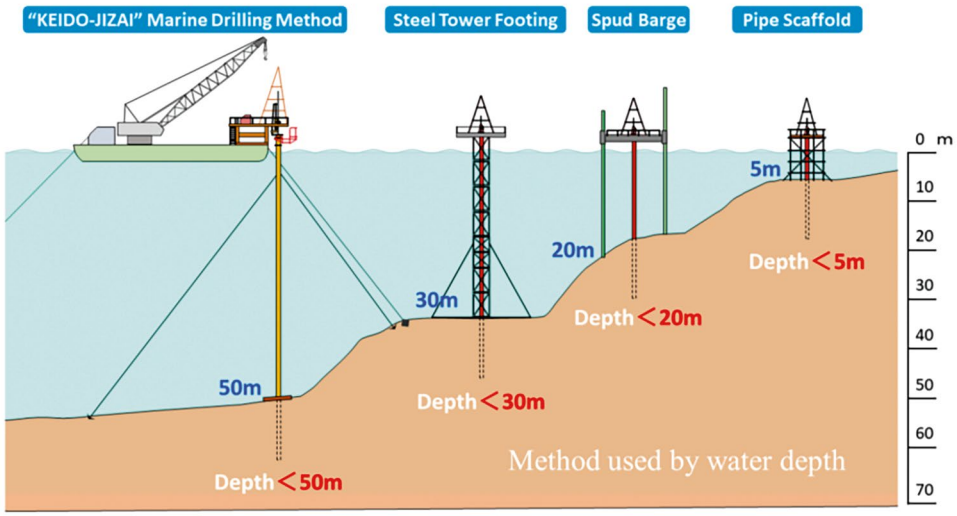


Fig. A.28 Deepwater drilling surveys

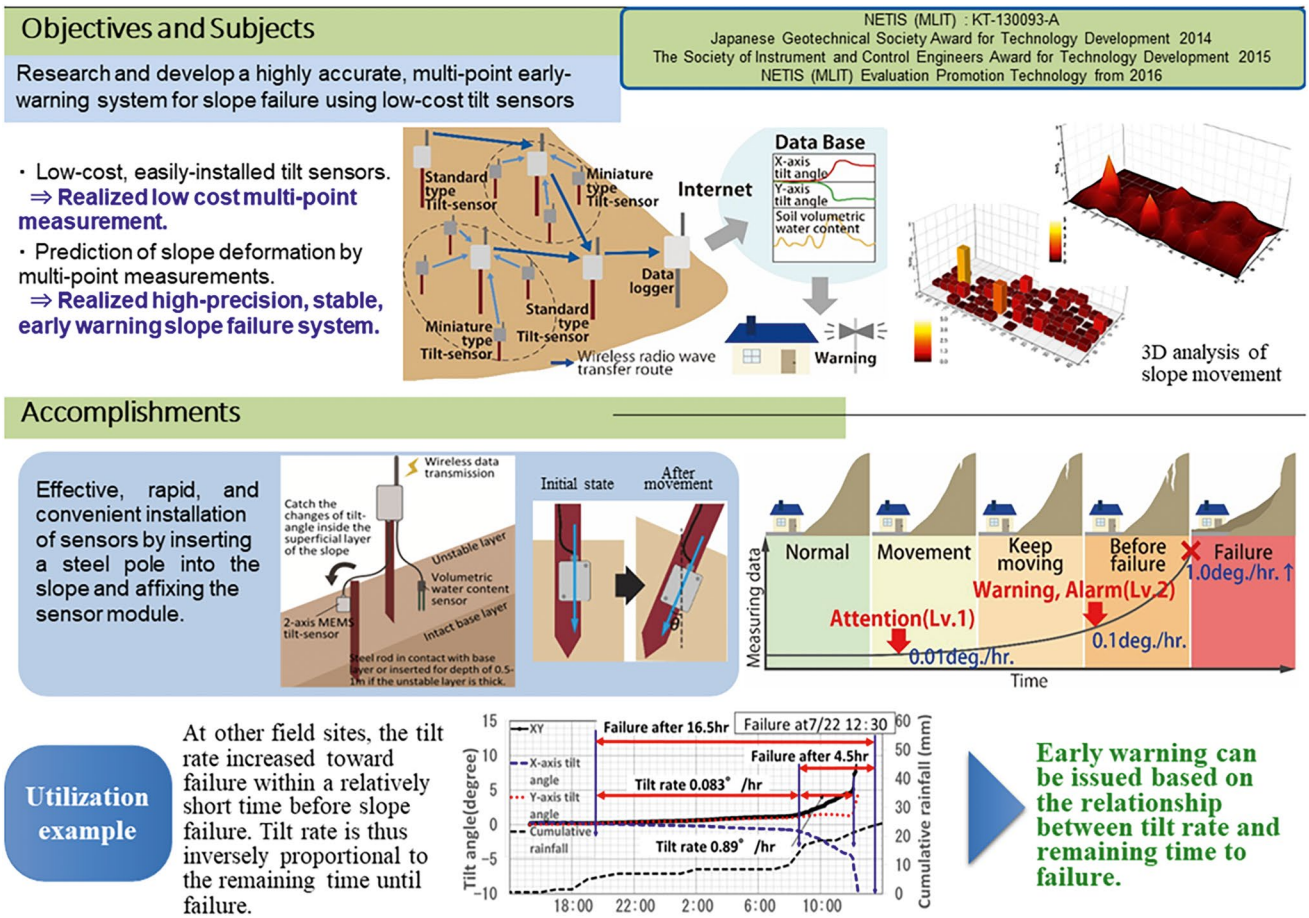


Fig. A.29 The early warning monitoring system of slope failure using multi-point tilt change and volumetric water content

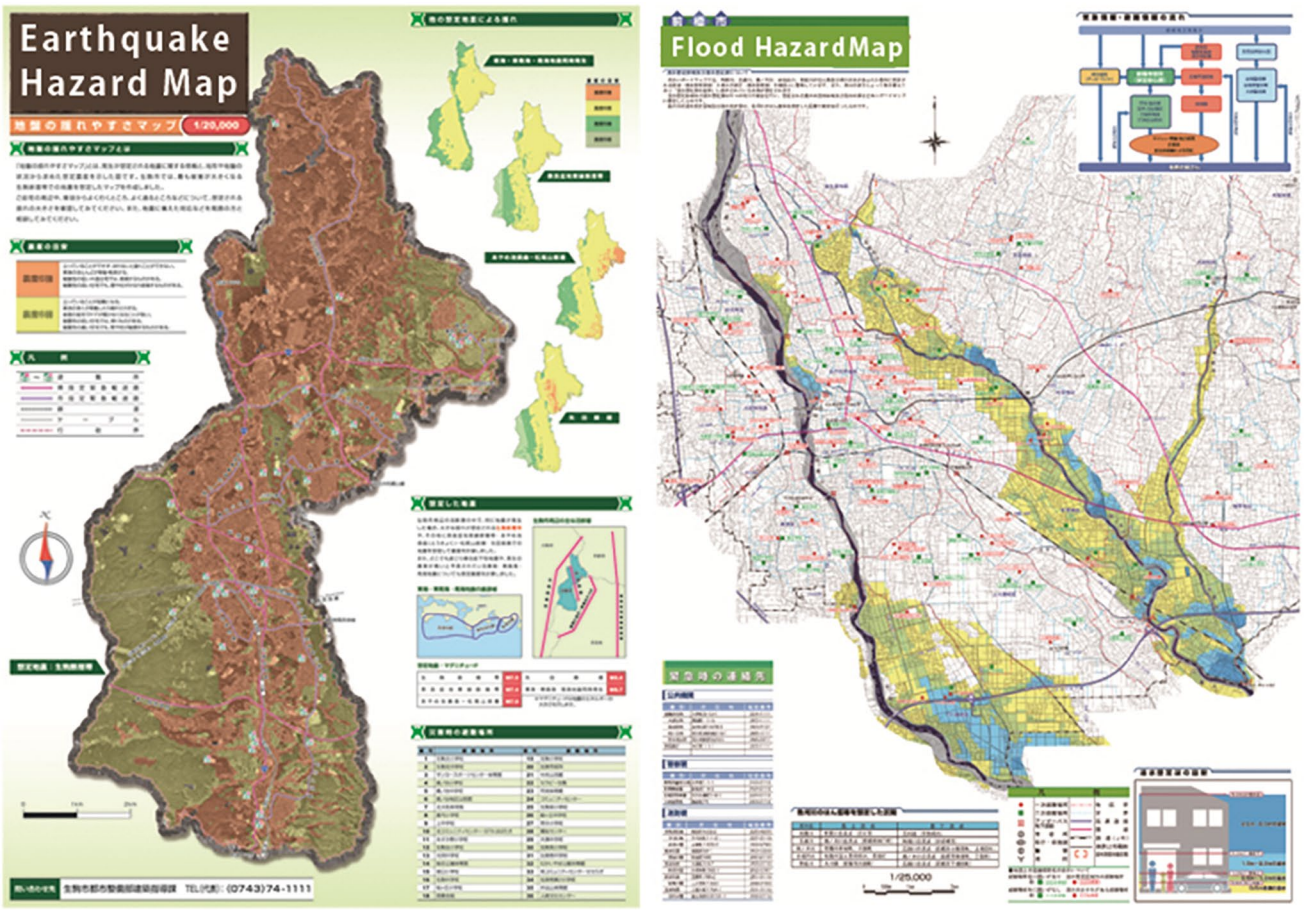


Fig. A.30 Making hazard map for sediment disaster, tsunami, flood, earthquake, liquefaction, etc.…

Godai Kaihatsu Corporation

Godai Kaihatsu Corporation

Introduction

Ever since its foundation in 1965, Godai Kaihatsu Co. Ltd. a civil engineering consulting firm, has long been providing a variety of software and measures particularly for natural disaster mitigation. With its rich expertise in both civil engineering and information technology (IT), the company has its primary goal to address real-world needs of disaster mitigation. All the staff of Godai Kaihatsu Co. Ltd. feels it more than happy that their cutting-edge technologies help mitigate natural disasters (Figs. A.31, A.32, A.33 and A.34).

Godai Kaihatsu Corporation
Godai Kaihatsu Corporation, Kanazawa, Ishikawa, Japan
e-mail: pp-sales@godai.co.jp; https://www.soft.godai.co.jp/soft/

© The Author(s) 2025

B. Abolmasov et al. (eds.), *Progress in Landslide Research and Technology, Volume 3 Issue 2, 2024*, Progress in Landslide Research and Technology, https://doi.org/10.1007/978-3-031-72736-8

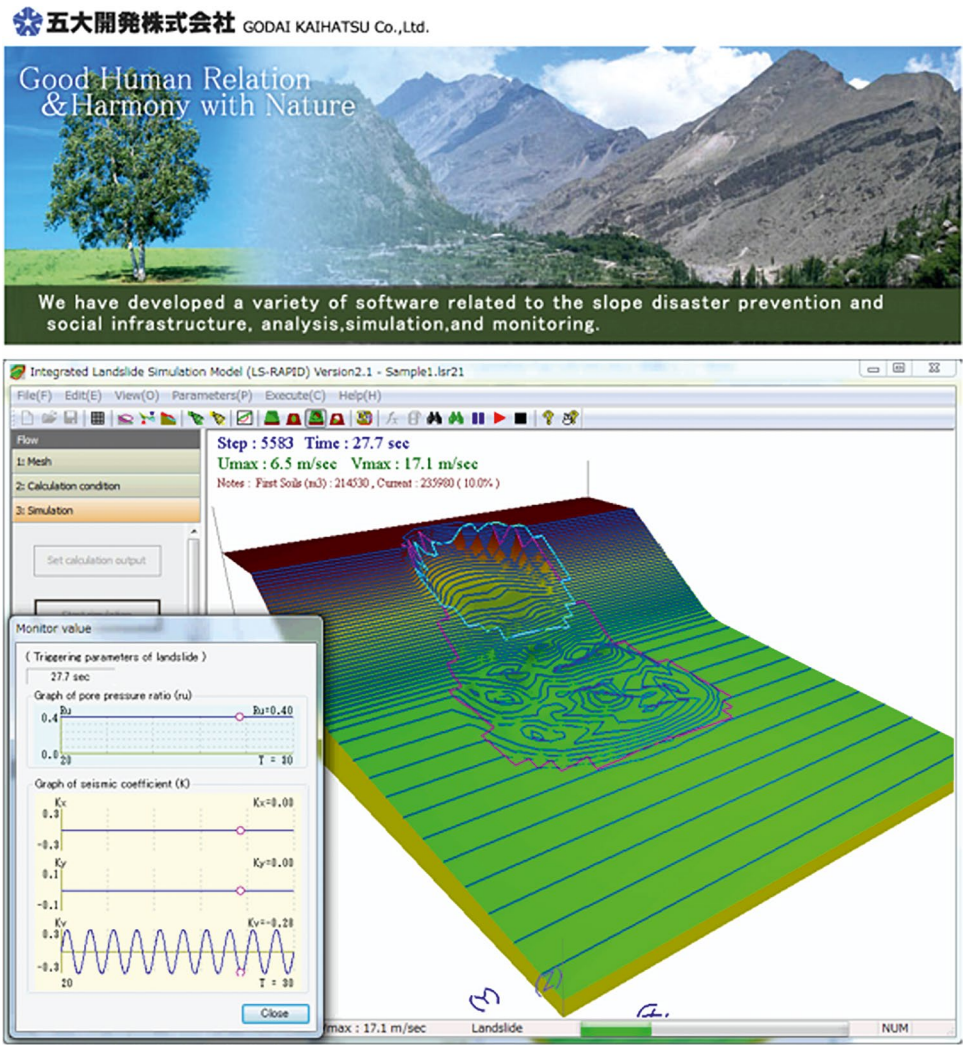


Fig. A.31 Integrated model simulating of earthquake and rain induced rapid landslides (LS-RAPID)

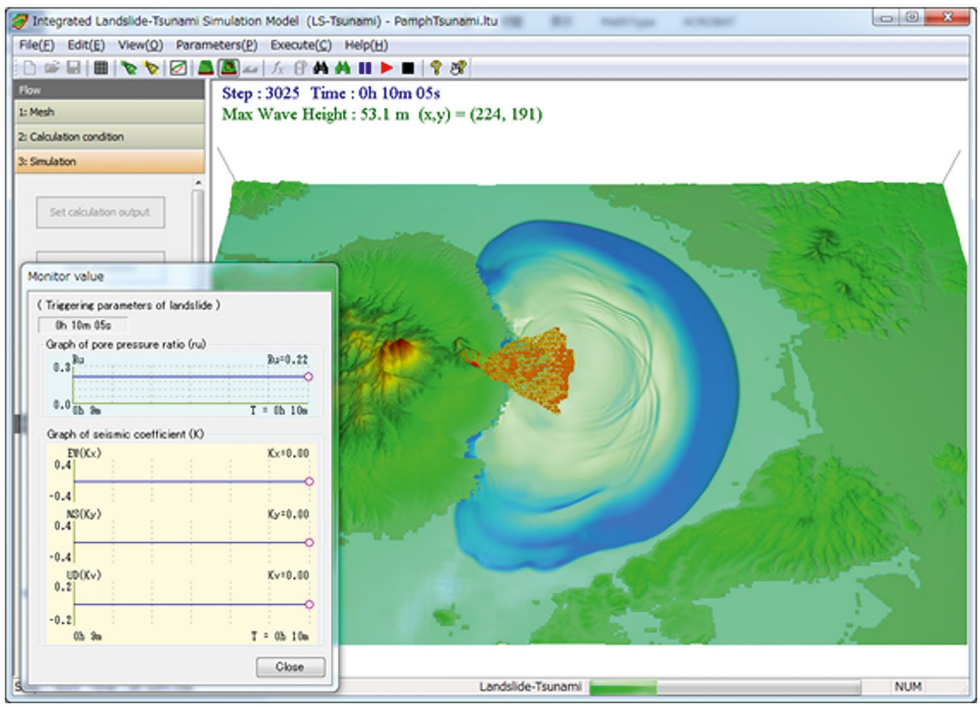


Fig. A.32 Tsunami model (LS-Tsunami)

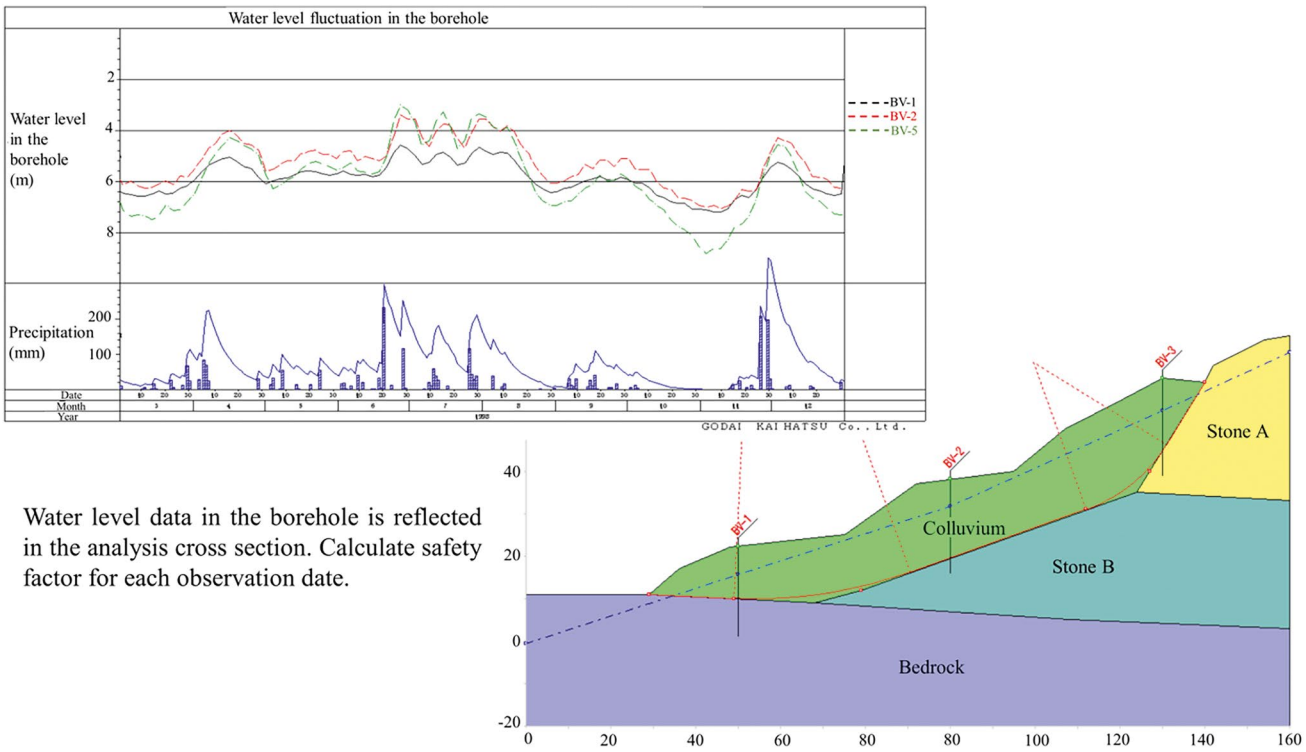


Fig. A.33 Power SSA PRO-Two-dimensional slope stability calculation of earthquake and rain induced landslide

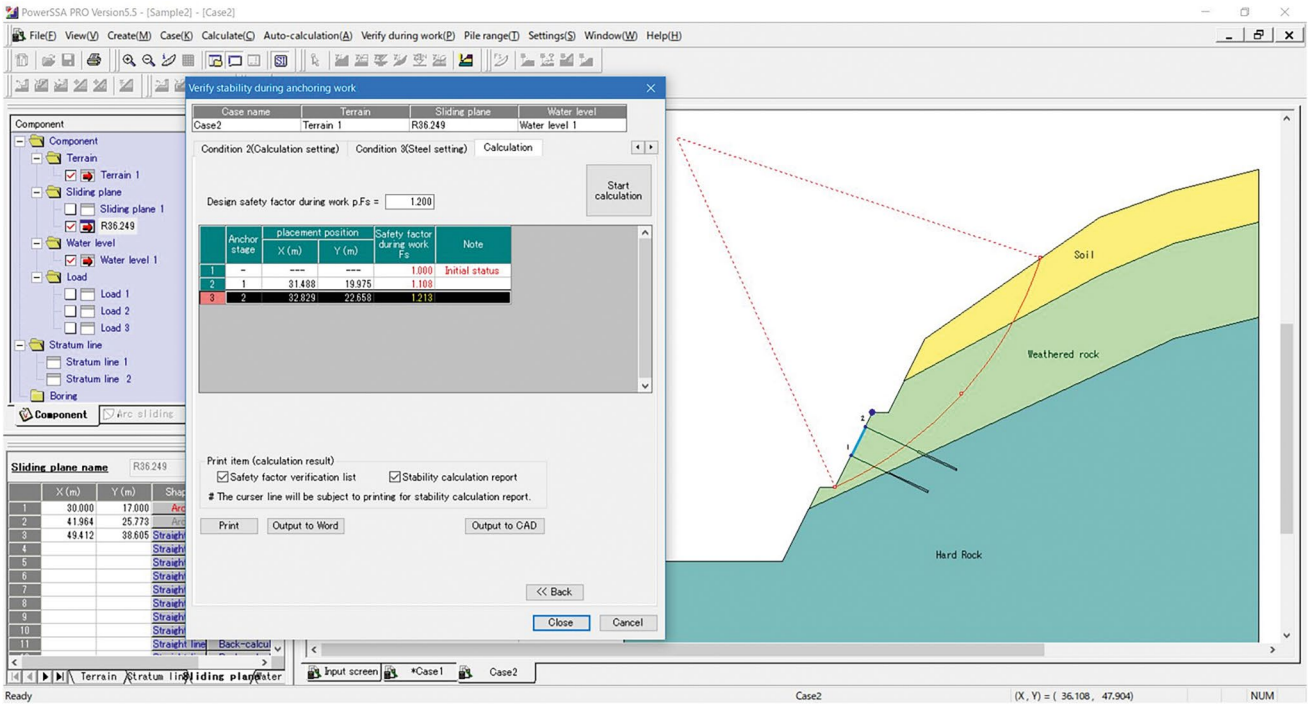


Fig. A.34 Anchor software-slope stability analysis for ground ancho

Kiso-Jiban Consultants Co. Ltd

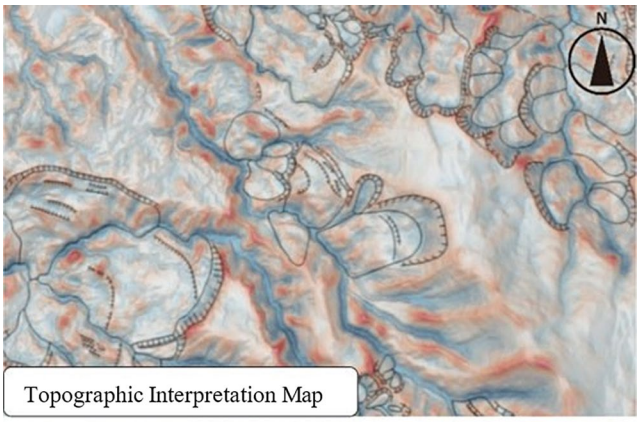
Kaoru Hanai and Junichiro Odaka

Introduction

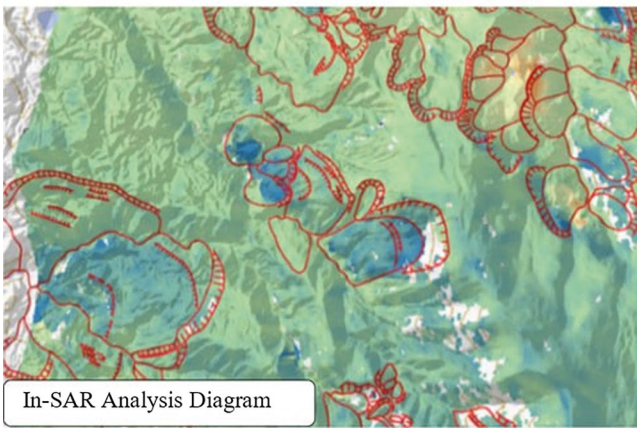
Since its establishment in 1953, Kiso-Jiban has been contributing on the development of social infrastructure as a "comprehensive construction consultant with strong geotechnical capabilities" in various situations, such as ground investigation, laboratory testing, analysis, civil structure design, etc. Kiso-Jiban has been working on the technological development for disaster prevention and mitigation against the recent exacerbation of natural disasters.

InSAR (Interferometric Synthetic Aperture Radar)

SAR is a technique that utilizes interference of radio waves for precise determination of distance. Kiso-Jiban has succeeded in estimation of both extent and rate of landslide movements by combining the topography interpretation and InSAR analysis.



Topographic Interpretation Map



In-SAR Analysis Diagram

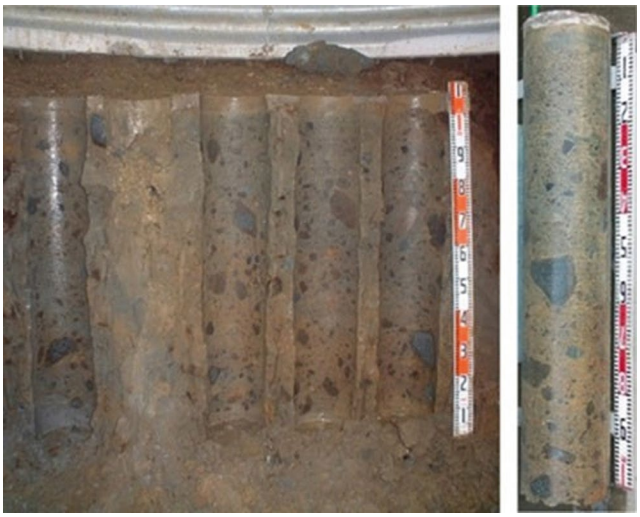
GP (Gel-Push) Sampling

GP Sampling can collect gravelly soil, etc., which is difficult to be collected by conventional samplers, by using a highly-concentrated water-soluble polymeric gel. GP Sampling was introduced in ISO 22475-1: 2021 revised in October 2021 as Category A, which provides the highest quality soil samples.

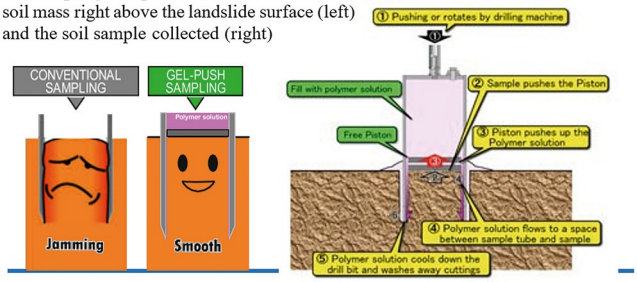
K. Hanai · J. Odaka
Kiso-Jiban Consultants Co. Ltd., Tokyo, Japan
e-mail: kisojiban-contactus@kiso.co.jp;
https://www.kisojiban.com/

© The Author(s) 2025

B. Abolmasov et al. (eds.), *Progress in Landslide Research and Technology, Volume 3 Issue 2, 2024*, Progress in Landslide Research and Technology, https://doi.org/10.1007/978-3-031-72736-8

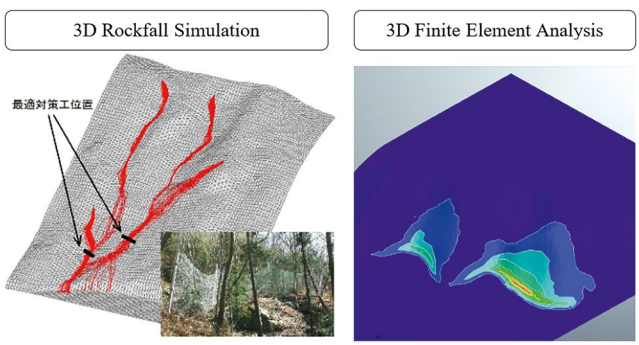


GP Sampling was performed in the disturbed soil mass right above the landslide surface (left) and the soil sample collected (right)



Slope Stability Analysis and Evaluation

Kiso-Jiban provides a wide range of numerical analyses related to slope stability evaluation. We have a wide range of analysis methods, from general two-dimensional limit equilibrium analysis to finite element analysis and analysis of rock masses with discontinuities, and we are challenging on the analysis that considers variability of ground and modelling uncertainty.



Inspection Technique for Disaster Danger Spots Using Mixed Reality (MR) Technology

MR (Mixed reality) is a technology that blends physical and digital worlds by superimposing 3D data and digital information on the real world as computer graphics.

Dangerous slopes with rockfall sources are spots where many unstable bedrocks and floating rocks exist. In many cases, approaching the inspection point on an outcrop is a difficult and dangerous task for investigators. Using MR technology makes it possible to realistically reproduce the outcrop situation at the site as a hologram. The outcrop situation can be safely inspected and confirmed without going to the site.



Kokusai Kogyo Co. Ltd

Kokusai Kogyo Co. Ltd.

Introduction

Kokusai Kogyo Co. Ltd. as a leading company of geospatial information technologies has long been providing public services with its comprehensive expertise to address real-world needs and cutting-edge measurement technologies. Kokusai Kogyo Co. Ltd. helps rebuild "Green Communities," which has been of our great concern in terms of "environment and energy," "disaster risk reduction" and "asset management". Kokusai Kogyo Co. Ltd. offers advanced and comprehensive analyses of geospatial information for developing new government policies, maintaining and operating social infrastructures safe and secure, and implementing low-carbon measures in cities. Influenced by the recent global climate change, extreme rainfall events have become more frequent worldwide and resultant hydro-meteorological hazards are creating more deaths and devastations particularly in many developing countries where effective advanced countermeasures are not readily available. Kokusai Kogyo Co. Ltd. is proud of its achievements in establishing resilient infrastructure systems and implementing effective monitoring/early warning systems in developing countries, which have long been helping reduce the risks from natural hazards (Figs. A.35, A.36, A.37 and A.38).

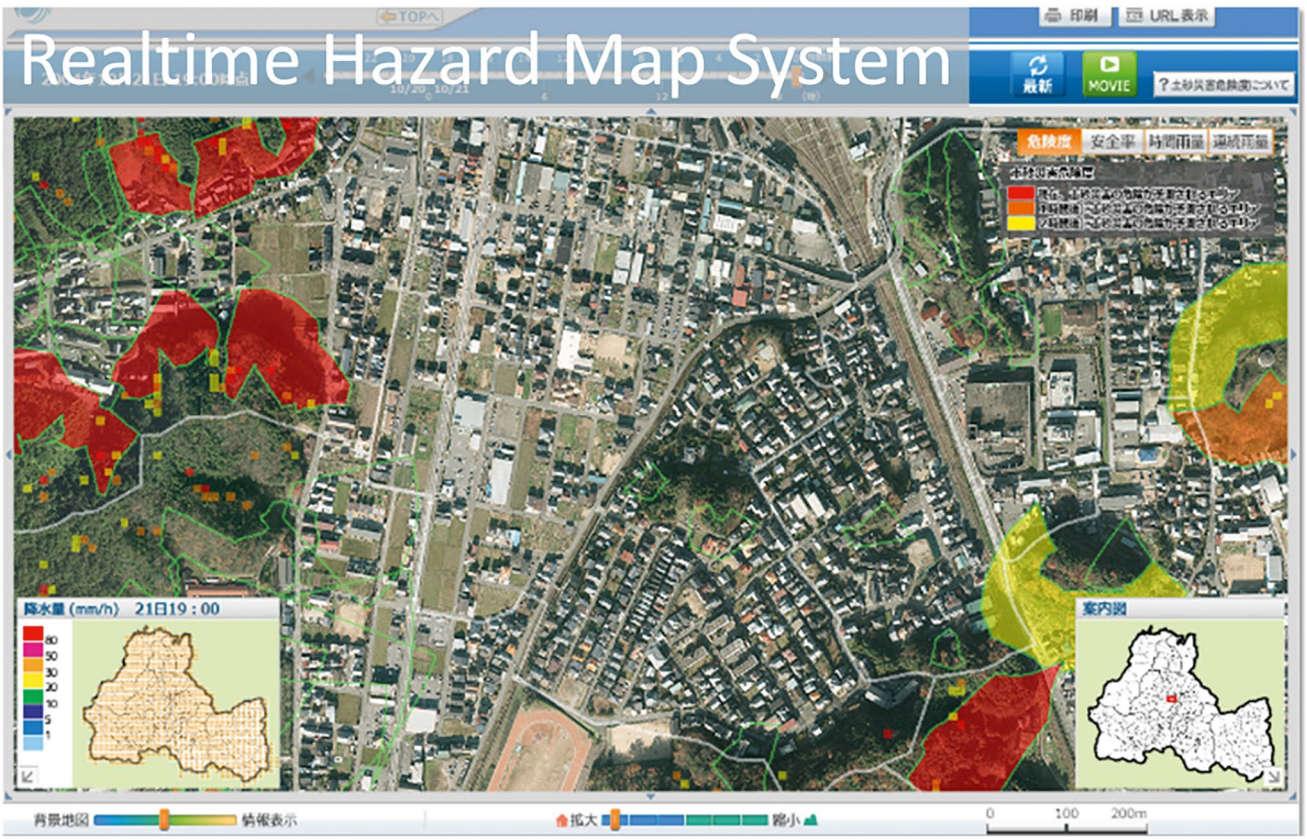


Fig. A.35 Our realtime hazard map reflects up-to-date information of soil natures and precipitations at landslide hazard sites, etc. that can constantly be changing, and evaluates area-wide hazard risk in real-time

© The Author(s) 2025

B. Abolmasov et al. (eds.), *Progress in Landslide Research and Technology, Volume 3 Issue 2, 2024*, Progress in Landslide Research and Technology, https://doi.org/10.1007/978-3-031-72736-8

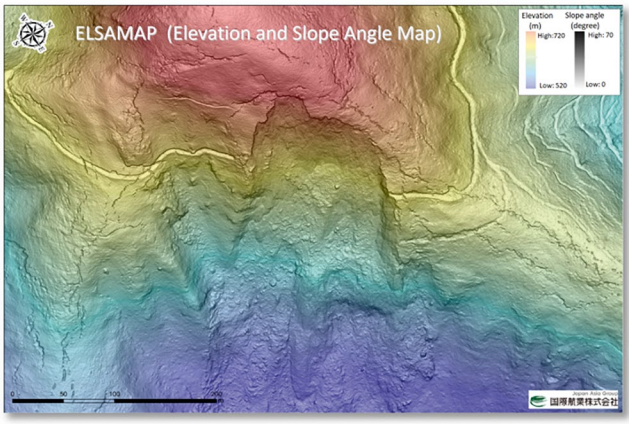


Fig. A.36 ELSAMAP is our cutting-edge 3D terrain visualization method allowing great geomorphological details to be visualized in one glance with gray-scaled slope inclinations and colored altitudes. ELSAMAP has been used to interpret micro-topographies, landslides and some other things

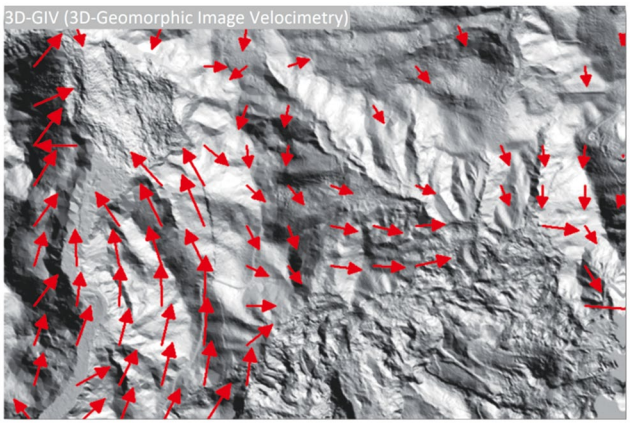


Fig. A.37 3D-GIV can help grasp the ground surface displacement caused by natural phenomena such as landslide by analyzing differences between digital geomorphic images obtained through ad hoc Airborne Laser Surveys



Fig. A.38 "Shamen-net" is a total monitoring system integrating GNSS and other monitoring device (Measurement precision: ± mm, on a real time basis)

OSASI Technos, Inc.

OSASI Technos, Inc.

Introduction

OSASI Technos, Inc. has been making its best efforts to develop its cutting-edge technologies for landslide early warning. Its unique compact and lightweight sensors making up the Landslide Early Warning System enable long-term monitoring of unstable landslide mass movements, precipitations, porewater pressure buildups, etc. in a remote mountainous area where commercial power is often unavailable. OSASI Technos, Inc. is also proud of its advanced technology to transfer observed data even in areas with poor telecom environments as proven in the successful implementations in South Asia. All staff members of OSASI Technos work together for mitigation of landslide disasters worldwide (Figs. A.39, A.40 and A.41).

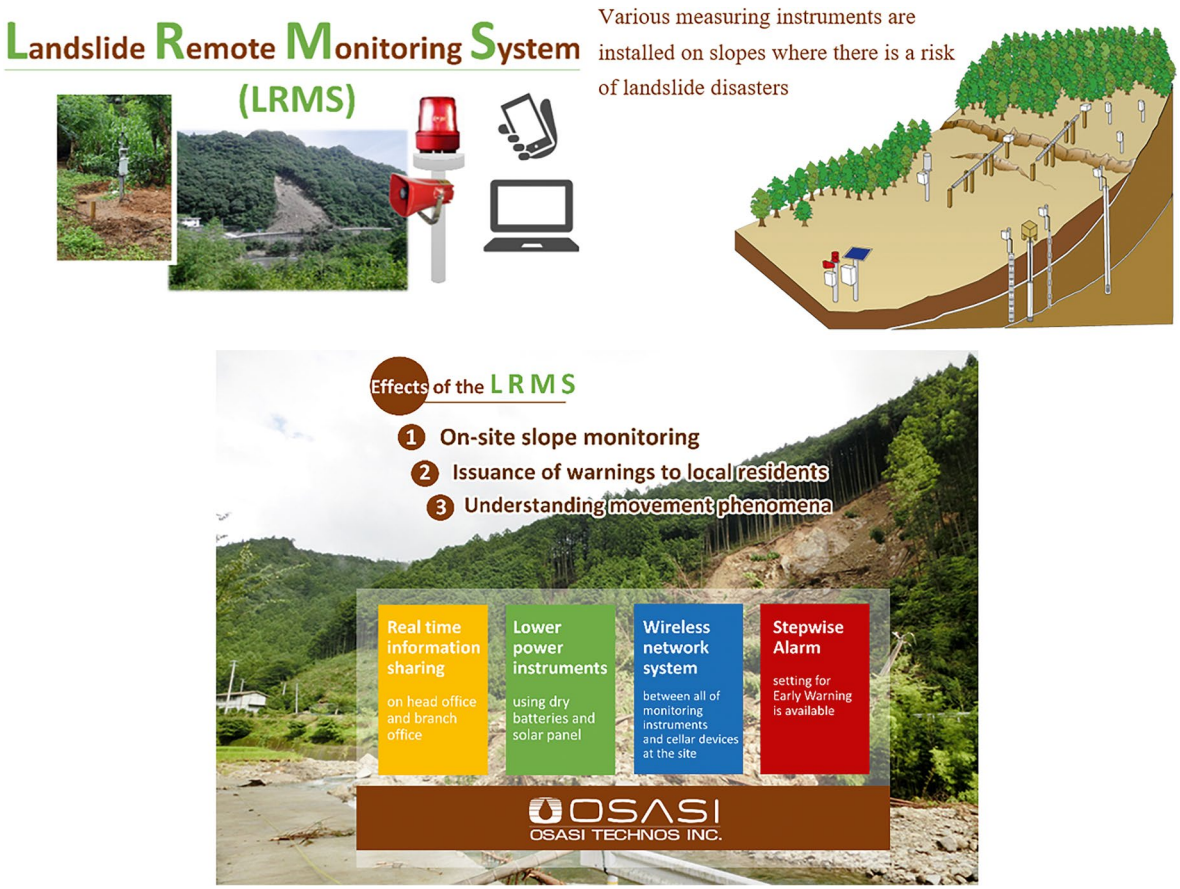
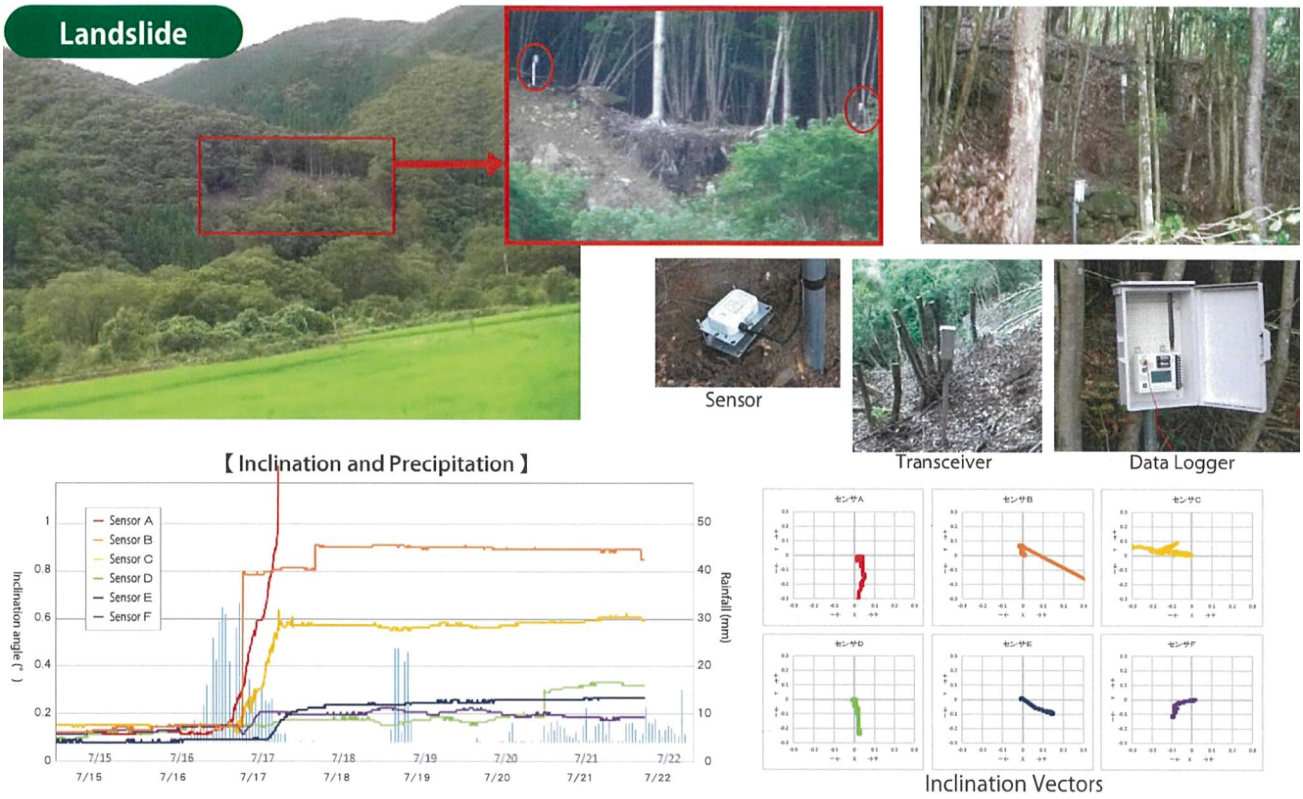


Fig. A.39 Landslide remote monitoring system

OSASI Technos, Inc.
OSASI Technos, Inc., Kochi, Kochi, Japan

© The Author(s) 2025

B. Abolmasov et al. (eds.), *Progress in Landslide Research and Technology, Volume 3 Issue 2, 2024*, Progress in Landslide Research and Technology, https://doi.org/10.1007/978-3-031-72736-8



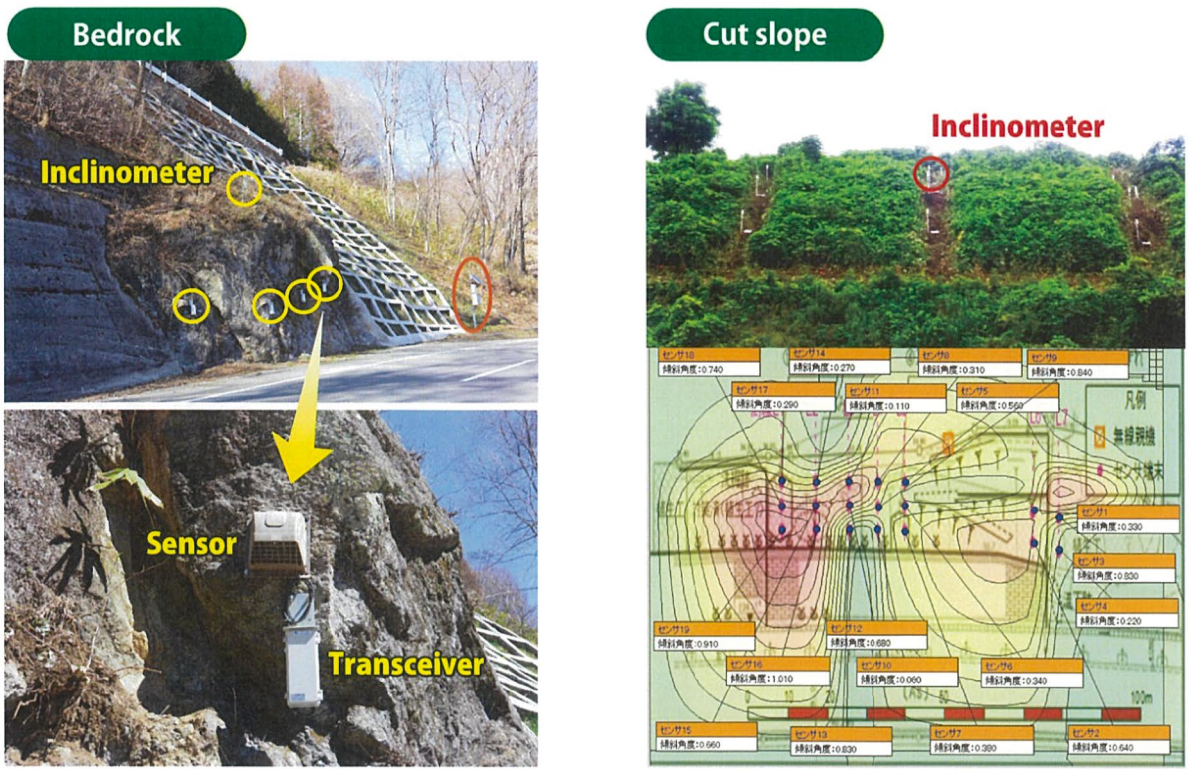
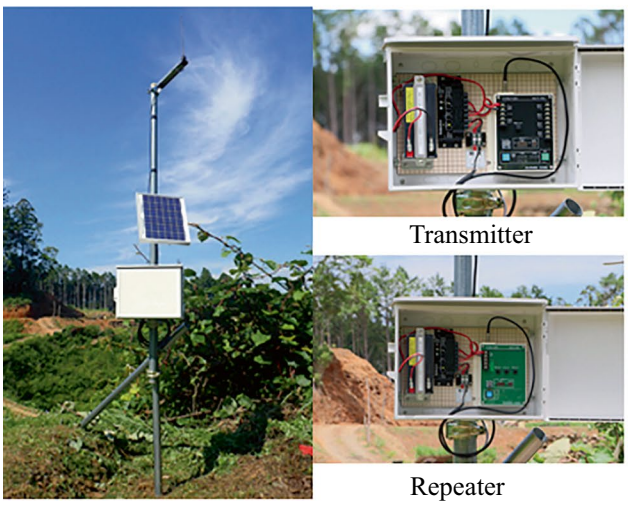


Fig. A.40 Inclination measure technology that enables surface deformation monitoring of slopes and bedrocks





Transmitter

Repeater

Wireless communication device for transmitting contact signals



Receiver

Wireless communication device for receiving contact signals

Features

- No need for cable wiring
- Compact and lightweight equipment for easy installation
- Regular monitoring of communication status (with retransmission)
- Transmitter operates for over 1 year on batteries
- Communication range of over 1000m (with clear line of sight)

Fig. A.41 An alarm wireless transmitter to prevent secondary disasters after landslides. This device transmits contact signals detected from debris flow sensors, extensometers, etc. using 429 MHz wireless communication

List of ICL Members

International Consortium on Landslides
An international non-government and non-profit scientific organization promoting landslide research and capacity building for the benefit of society and the environment.
President: Željko Arbanas (University of Rijeka, Croatia)
Vice Presidents: Nicola Casagi (University of Florence, Italy), Faisal Fathani (Gadjah Mada University, Indonesia), David Huntley (Geological Survey of Canada, Canada), Biljana Abolmasov (University of Belgrade, Serbia), Giovanna Capparelli (University of Calabria, Italy), Maneesha V. Ramesh (Amrita University, India) Executive Director: Kaoru Takara (National Research Institute for Earth Science and Disaster Resilience, Japan), Treasurer: Kyoji Sassa (Prof. Emeritus, Kyoto University, Japan)

Country/Region	ICL Full member
Bosnia and Herzegovina	The Geotechnical Society of Bosnia and Herzegovina
Brazil	Center for Scientific Support in Disasters – Federal University of Parana
Canada	Geological Survey of Canada
	University of Alberta
China	Northeast Forestry University, Institute of Cold Regions Science and Engineering
	China University of Geosciences
	Chinese Academy of Sciences, Institute of Mountain Hazards and Environment
	Tongji University
	Shanghai Jiao Tong University
	Tsinghua University
	The State Key Laboratory of Geohazard Prevention and Geoenvironment Protection (SKLGP), Chengdu University of Technology
	Civil Engineering and Development Department, Geotechnical Engineering Office, Hong Kong
	The Hong Kong University of Science and Technology
	The University of Hong Kong
Colombia	Universidad Nacional de Colombia
Croatia	Croatian Landslide Group from Faculty of Civil Engineering University of Rijeka and Faculty of Mining, Geology and Petroleum University of Zagreb
Czech Republic	Charles University, Faculty of Science
Egypt	The American University in Cairo
Germany	Technische Universitat Darmstadt, Institute and Laboratory of Geotechnics
Georgia	Department of Geology of National Environmental Agency of Georgia
India	Amrita Vishwa Vidyapeetham, Amrita University
	National Institute of Disaster Management, New Delhi
Indonesia	Gadjah Mada University, Center for Disaster Mitigation and Technological Innovation (GAMA-InaTEK)
	Parahyangan Catholic University
	Agency for Meteorology, Climatology, and Geophysics of the Republic of Indonesia (BMKG Indonesia)
Italy	UNESCO Chair for the prevention and the sustainable management of geo-hydrological hazards – University of Florence
	ISPRA-Italian Institute form Environmental Protection and Research
	University of Calabria, DIMES, CAMILAB
	Istituto di Ricerca per la Protezione Idrogeologica (IRPI), of the Italian National Research Council (CNR)
	Centro di Ricerca CERI – Sapienza Università di Roma
	National Institute of Oceanography and Applied Geophysics – OGS, Italy
	Department of Earth and Environmental Sciences, University Aldo Moro
Japan	Kyoto University, Disaster Prevention Research Institute
	Japan Landslide Society
	National Research Institute for Earth Science and Disaster Resilience

© The Author(s) 2025

B. Abolmasov et al. (eds.), *Progress in Landslide Research and Technology, Volume 3 Issue 2, 2024*, Progress in Landslide Research and Technology, https://doi.org/10.1007/978-3-031-72736-8

Korea	Korean Society of Forest Engineering	
	National Institute of Forest Science	
	Korea Authority of Land and Infrastructure Safety	
	Korea Institute of Civil Engineering and Building Technology	
Mexico	Institute of Geography, National Autonomous University of Mexico (UNAM)	
Russia	Moscow State University, Department of Engineering and Ecological Geology	
	JSC "Hydroproject Institute"	
Serbia	University of Belgrade, Faculty of Mining and Geology	
Slovakia	Comenius University, Faculty of Natural Sciences, Department of Engineering Geology	
Slovenia	University of Ljubljana, Faculty of Civil and Geodetic Engineering (ULFGG)	
	Geological Survey of Slovenia	
Sri Lanka	Central Engineering Consultancy Bureau (CECB)	
	National Building Research Organization	
	Engineering Geology Research Group (EGRG), Department of Geology, University of Peradeniya	
Chinese Taipei	Landslide group in National Central University from Graduate Institute of Applied Geology, Department of Civil Engineering, Center for Environmental Studies	
	National Taiwan University, Department of Civil Engineering	
Thailand	Ministry of Agriculture and Cooperatives, Land Development Department	
	Asian Disaster Preparedness Center (ADPC)	
Ukraine	Institute of Telecommunication and Global Information Space	
United Kingdom	British Geological Survey	
USA and Nepal	California State University, Fullerton and Tribhuvan University, Institute of Engineering	
Viet Nam	Institute of Transport Science and Technology	
	Vietnam Institute of Geosciences and Mineral Resources (VIGMR)	
Country/Region	**ICL Associate member**	
Belgium	Liege University, Georisk and Environment (G&E) group	
China	State Key Laboratory of Plateau Ecology and Agriculture (Qinghai University)	
Czech Republic	Czech Geological Survey	
	Institute of Rock Structure and Mechanics, Department of Engineering Geology	
India	Centre of Excellence in Disaster Mitigation and Management (CoEDMM) Indian Institute of Technology Roorkee	
Italy	University of Sannio, Department of Sciences and Technologies	
	Geotechnical Engineering Group (GEG), University of Salerno	
	Department of Earth and Environmental Sciences – University of Pavia	
	University of Chieti-Pescara, Department of Engineering and Geology	
	Federico II University of Naples, Department of Earth, Environmental and Resource Sciences	
	DIA – Università degli Studi di Parma	
	University of Urbino "Carlo Bo", Department of Pure and Applied Sciences	
	University of Turin	
Japan	Ehime University, Center for Disaster Management Informatics Research	
	Kochi University	
	National Institute of Maritime, Port and Aviation Technology	
North Macedonia	Macedonian Association for Geotechnics	
Russia	Russian State Geological Prospecting University n.a. Sergo Ordzhonikidze (MGRI-RSGPU)	
Slovenia	University of Ljubljana, Faculty of Natural Sciences and Engineering (UL NTF)	
Switzerland	Institute of Earth Sciences, Faculty of Geoscience and Environment/University of Lausanne	
USA	Iowa State University	
Country/Region	**ICL Supporter**	
China	Beijing Brilliant Sun Technology Co., Ltd	
Italy	IDS GeoRadar s.r.l.	
Japan	Marui & Co., Ltd., Osaka	Okuyama Boring Co., Ltd., Yokote
	Ohta Geo-Research Co., Ltd., Nishinomiya	Japan Conservation Engineers Co., Ltd., Tokyo
	Sabo Technical Center, Tokyo	GODAI Kaihatsu Corp., Kanazawa
	OYO Corporation, Tokyo	Kokusai Kogyo Co., Ltd., Tokyo
	OSASI Technos Inc., Kochi	NIPPON KOEI CO., LTD.
Chinese Taipei	Sinotech Engineering Consultants, Inc	

ICL Secretariat
Secretary General: Kyoji Sassa
International Consortium on Landslides, 138-1 Tanaka Asukai-cho, Sakyo-ku, Kyoto, 606-8226, Japan
Web: https://www.landslides.org/, E-mail: secretariat@landslides.org
Tel:+81 (75) 723 0640, Fax:+81(75) 950 0910